REPORT DOCUMENTATION PAGE		Form Approved OMB No. 0704-0188

1. REPORT DATE *(DD-MM-YYYY)*	2. REPORT TYPE Final Report	3. DATES COVERED *(From – To)* 1 August 2002 - 01-Feb-05

4. TITLE AND SUBTITLE

Flow Control Enabled Aircraft Design

5a. CONTRACT NUMBER
F61775-02-C4051

5b. GRANT NUMBER

5c. PROGRAM ELEMENT NUMBER

6. AUTHOR(S)

Dr. Rajendar Kumar Nangia

5d. PROJECT NUMBER

5d. TASK NUMBER

5e. WORK UNIT NUMBER

7. PERFORMING ORGANIZATION NAME(S) AND ADDRESS(ES)
Nangia Aero Research Associates
West Point, 78-Queens Road
Bristol BS8 1QX
United Kingdom

8. PERFORMING ORGANIZATION REPORT NUMBER

N/A

9. SPONSORING/MONITORING AGENCY NAME(S) AND ADDRESS(ES)
Air Vehicles Directorate
Air Force Research Laboratory
AFRL/VAAA, Bldg 45
2130 8th Street
WPAFB, OH 45433-7542

10. SPONSOR/MONITOR'S ACRONYM(S)

11. SPONSOR/MONITOR'S REPORT NUMBER(S)
SPC 02-4051

12. DISTRIBUTION/AVAILABILITY STATEMENT

Approved for public release; distribution is unlimited. (approval given by local Public Affairs Office)

14. ABSTRACT

This report results from a contract tasking Nangia Aero Research Associates as follows: Many future advanced aircraft concepts being considered by the Air Force fall outside the current aerodynamic design practice and will rely heavily on the use of flow control technology to optimize flight performance. Examples include SensorCraft, long range strike aircraft, ultra STOL transports, and hypersonic aircraft. To properly design and optimize the aerodynamic performance of these vehicle concepts high fidelity models and well-documented baseline configurations are desired. The key science issue is determining the correct mixture of passive shaping and active flow control in novel design situations, subject to the usual engineering constraints.

Specific Work to be Accomplished: The contractor will refine and employ high fidelity analytical models to assess vehicle performance for a generic sensor craft and supersonic strike aircraft. Sensitivities to wing configurations, high aspect ratio wings, wing junctions, wing tip configurations, scaling effects, wing geometry, inlet geometry, and flight Mach and altitude will be assessed. Numerical methods include previously developed (and largely validated) direct and inverse procedures, codes for subsonic, transonic and supersonic flows. The aim will be to assess active and passive flow control techniques and their relative merits.

15. SUBJECT TERMS
EOARD, Aircraft Design, Flow Control, Aerodynamics

16. SECURITY CLASSIFICATION OF:

a. REPORT UNCLAS	b. ABSTRACT UNCLAS	c. THIS PAGE UNCLAS	17. LIMITATION OF ABSTRACT UL	18, NUMBER OF PAGES 235	19a. NAME OF RESPONSIBLE PERSON Carl Tilmann

19b. TELEPHONE NUMBER *(Include area code)*
937-255-4077

Standard Form 298 (Rev. 8/98)
Prescribed by ANSI Std. Z39-18

PILOT DOCUMENT INTRODUCING ALL ASPECTS OF WORK ACCOMPLISHED UNDER USAF-EOARD CONTRACT SPC-024051

Dr. R. K. Nangia

SUMMARY & LIST OF REPORTS

This work follows previous work funded by USAF-EOARD under seeding Contract SPC-01-4087 which was reported as follows:

NANGIA, R.K., "Configuration & Aerodynamic Design Studies of Joined-Wing High Aspect Ratio Sensor Craft Concept", RKN/Aero/Report/2002-10, June 2002, (USAF-EOARD Contract SPC-01-4087).

During the course of the current USAF-EOARD Contract: SPC–02-4051, several aspects have been studied. The report has been issued in a total of six parts (essentially self-consistent entities) under the same major report number, **RKN/AERO/REPORT/2004-10, Issue 1, 2004.** The various parts are listed as follows:

Part 1 (This Document)

PILOT DOCUMENT INTRODUCING ALL ASPECTS OF WORK ACCOMPLISHED UNDER USAF-EOARD CONTRACT SPC-024051

Part 2

HIGH ASPECT RATIO UNCONVENTIONAL JOINED-WING CONFIGURATIONS INCORPORATING LAMINAR FLOW

Part 3

PLANFORM EFFECTS ON HIGH ASPECT RATIO UNCONVENTIONAL JOINED- & LAMBDA-WING CONFIGURATIONS INCORPORATING LAMINAR FLOW

Part 4

HIGH ASPECT RATIO LAMBDA-WING CONFIGURATIONS INCORPORATING LAMINAR FLOW

Part 5

INTEGRATION OF OVER-SURFACE SCARFED INTAKES ON AIRCRAFT WITH HIGH ASPECT RATIO WINGS (e.g. Sensor-Craft)

Part 6

TOWARDS DESIGN OF LONG-RANGE SUPERSONIC MILITARY AIRCRAFT

Important Note:

Several other papers and Publications arose during the work programme and these are listed in this document (Part 1).

**Consulting Engineers
Nangia Aero Research Associates
WestPoint, 78 Queens Road, Clifton
Bristol BS8 1QX, UK**

© *Dr. R.K. Nangia 2004*

The Investigation which is the subject of this report was initiated by
USAF - EOARD, 223/231 Old Marylebone Road, London, NW1 5TH, UK
and was carried out under the terms of Contract SPC-02-4051

DISTRIBUTION LIST

1	Mr. W. Donaldson	USAF-EOARD, London NW1 5TH, UK
1	Mr. C. Remillard	Chief, AFRL/VAAA; Bldg 45
		2130 8th Street, WPAFB, Ohio, USA 45433-7542
1	Mr. D. Multhopp	Technical Area Lead, AFRL/VAAA; Bldg 45
		2130 8th Street, WPAFB, Ohio, USA 45433-7542
2	Dr. C. P. Tilmann	Sr. Aerospace Engineer, AFRL/VAAA; Bldg 45
		2130 8th Street, WPAFB, Ohio, USA 45433-7542
1	Mr. William Fields	Tech Area Lead, AFRL/VAAA; Bldg 45
		2130 8th Street, WPAFB, Ohio, USA 45433-7542
1	Dr. K. P. Iwanski	Aerospace Engineer, AFRL/VAAA; Bldg 45
		2130 8th Street, WPAFB, Ohio, USA 45433-7542
1	Mr. Larry Leavitt	Head, Configuration Aerodynamics Branch
		NASA Langley Research Center, Mail Stop 499
		Hampton, VA 23681-2199
1	Dr. James Luckring	Configuration Aerodynamics Branch
		NASA Langley Research Center, Mail Stop 286
		Hampton, VA 23681-2199
1	Mr. John Perdzock	Head, SensorCraft Integrating Concept Office, AFRL/VAC; Bldg 45
		2130 8th Street, WPAFB, Ohio, USA 45433-7542
1	Dr. Maxwell Blair	AFRL/VASD; Bldg 146
		2210 Eighth Street
		Wright-Patterson AFB OH 45433-7531
1	Dr. Keith Numbers	AFRL/VAA, Long Range Strike Integrating Concept Office
1	Mr. D. Adamczak	Sr. Aerospace Engineer, AFRL/VAAA; Bldg 45
		2130 8th Street, WPAFB, Ohio, USA 45433-7542
1	Dr. Michael OL	Research Engineer, AFRL/VAAA Bldg 45
		2130 8th Street, WPAFB, Ohio, USA 45433-7542
2	Dr. R.K. Nangia	Nangia Aero Research Associates
		WestPoint, 78-Queens Road, Clifton
		BRISTOL BS8 1QX, UK.

CONTRACTUAL DECLARATIONS

"The Contractor, Dr. R. K. Nangia„ hereby delcares that, to the best of its knowledge and belief, the technical data delivered herewith under Contract No.SPC-024051 is complete, accurate, and complies with all requirements of the contract.

DATE: **March 2004**   **Name and Title of Authorized Official:**   **Dr R K Nangia**

"I certify that there were no subject inventions to declare as defined in FAR 52.227-13, during the performance of this contract."

DATE: **March 2004**   **Name and Title of Authorized Official:**   **Dr R K Nangia**

CONTENTS

ACKNOWLEDGEMENTS

A LIST OF TECHNICAL PAPERS & CONFERENCE PRESENTATIONS ARISING FROM THE WORK PROGRAMME

JOINED-WING SENSOR-CRAFT

1. NANGIA, R.K., PALMER, M.E. & TILMANN, C.P., "Towards Design of Unconventional High Aspect Ratio Joined-Wing Type Aircraft Configurations", RAeS Conference — "A 2020 Vision", April 2002, London UK.

2. NANGIA, R.K., PALMER, M.E., TILMANN, C.P., "On Design and Optimisation of Unconventional High Aspect-Ratio "Joined-Wing" Type Aircraft", CEAS Aerospace Aerodynamics Research Conference (Royal Aeronautical Society), 10 - 12 June 2002, Cambridge, UK   (PAPER 85)

3. NANGIA, R.K., PALMER, M.E. & TILMANN, C.P., "On Design of Unconventional High Aspect Ratio "Joined-Wing" Type Aircraft", Paper 25R2, ICAS-2002, Toronto, Canada, September 2002.

4. NANGIA, R.K., "Towards Designing High Aspect Ratio, High Altitude Joined-Wing Sensor-craft (HALE-UAV)", Paper (no.3) presented at the Bath UAV Aerodynamics Workshop (Sponsored by: USAF-EOARD, BAESYSTEMS & Bath University), November 2002.

5. NANGIA, R.K., "Designing Novel High Altitude Joined-Wing Sensor-craft (HALE-UAV)", Lecture presented to Royal Aeronautical Society, Bristol, 11th December 2002.

6. NANGIA, R.K., PALMER, M.E. & TILMANN, C.P., "Unconventional High Aspect Ratio Joined-Wing Aircraft With Aft- & Forward- Swept Wing-Tips",AIAA-2003-0605, January 2003, Reno NV, USA

7. NANGIA, R.K. PALMER, M.E., "Exploiting Unconventional Joined-Wing Concept for Subsonic High altitude Reconnaissance Aircraft", Paper 23, RTO-AVT-99 Conference, Brussels, April 2003.

8. NANGIA, R.K., PALMER, M.E. "Unconventional Joined-Wing Concept for Supersonic Aircraft", Paper 24, RTO-AVT-99 Conference, Brussels, April 2003.

9. NANGIA, R.K., PALMER, M.E. & TILMANN, C.P., "High Aspect-Ratio Unconventional Joined-Wing Aircraft Incorporating Laminar Flow With Tip Sweep Effects", RAeS & CEAS Aerodynamics Research Conference, Paper 14, London, June 2003.

10. NANGIA, R.K., PALMER, M.E. & TILMANN, C.P., "Unconventional High Aspect Ratio Joined-Wing Aircraft Incorporating Laminar Flow", AIAA-3927, June 2003, Orlando, FL, USA.

11. NANGIA, R.K., "Towards Designing Novel High-Altitude Joined-Wing Sensor-Craft (HALE-UAV)", AIAA Paper 2003-2695, AIAA/ICAS Wright Brothers. Centennial, Dayton, OH, USA, July 2003.

12. NANGIA, R.K., PALMER, M.E. & TILMANN, C.P., "Towards Design of a Novel High-Altitude Joined-Wing Sensor-Craft (HALE-UAV)", 19th Bristol Unmanned Air Vehicle Systems Conference, 29-31 March 2004.

13. NANGIA, R.K., PALMER, M.E. & TILMANN, C.P., "Planform Effects on Unconventional High Aspect-Ratio Joined-Wing Aircraft Incorporating Laminar Flow". AIAA-Paper, 2005-0243, accepted for 43rd AIAA Aerospace Sciences Meeting, Reno, January 2005.

"LAMBDA-WING" SENSOR-CRAFT

14. NANGIA, R.K., PALMER, M.E. & TILMANN, C.P. (AFRL), "Design of High Aspect Ratio "Lambda-Wings" Incorporating Laminar Flow ", AIAA-2004-1245, 42nd AIAA Aerospace Sciences Meeting, Reno, January 2004.

15. NANGIA, R.K., PALMER, M.E. & TILMANN, C.P. (AFRL), "Design of High Aspect Ratio Double-crank "Lambda-Wings" Incorporating Laminar Flow ", AIAA Paper, 2004-2141 for 34th AIAA Fluid Dynamics 28th June – 1st July 2004, Portland, Oregon, USA.

SUBSONIC INTAKES, PROPULSION

16. NANGIA, R.K. & PALMER, M.E., "Integration of Over-surface Scarfed Intakes on Aircraft with High Aspect-Ratio Wings (e.g. Sensor-Craft)", Paper 40, RTO-AVT-100, Warsaw, October 2003.

SUPERSONIC STRIKE AIRCRAFT

17. NANGIA, R.K., PALMER, M.E. & IWANSKI, K.P. (AFRL), "Towards Design of Long-range Supersonic Military Aircraft", AIAA –2004-5071, Applied Aero Meeting Providence, R.I., USA.

18. NANGIA, R.K., PALMER, M.E. & IWANSKI, K.P. (AFRL), "Towards Design of Long-range Supersonic "Large" Military Aircraft", RAeS Paper, Paper 16, September 2004, London, UK.

HIGH ASPECT RATIO UNCONVENTIONAL JOINED-WING CONFIGURATIONS INCORPORATING LAMINAR FLOW

Dr. R. K. Nangia

SUMMARY

Unmanned SensorCraft air vehicles have been proposed as the air-breathing component of a future intelligence, surveillance, and reconnaissance (ISR) infrastructure to provide revolutionary capabilities. Such craft must take advantage of high aspect ratio (AR) wings for aerodynamic efficiency, and may also be required to enclose an antenna in a diamond aircraft planform. A large proportion of fuel must be carried, and "loiter" is at high altitudes for a few days in each flight. This implies that a wide C_L–altitude capability is required.

Several types of high AR joined-wing aircraft configurations can be envisaged to meet the possible flight envelope. Previous studies have considered configurations with aft- and forward- swept tips using "conventional" thick super-critical aerofoil sections. Implications of typical flight envelopes on wing design aspects have been mentioned. This report extends the design and analysis to explore incorporation of laminar flow sections for configurations with aft- and forward- swept wing tips.

Using panel codes, results are presented here for configurations with uncambered (symmetric) wing sections and then for configurations with designed camber and twist, trimmed for neutral stability. The designed wings display a considerable reduction in leading edge suction, yet maintain the lift, drag and near-elliptic wing loading characteristics. Potential for laminar flow is shown.

The forward-swept tip configuration appears to give more favourable spanwise loadings and is better in terms of aileron roll control in sideslip.

Further work is proposed in several areas.

This report is Part 2 of a series of six reports relating to high AR, long endurance surveillance aircraft, laminar flow, integrated intakes and long range supersonic military aircraft.

Consulting Engineers
Nangia Aero Research Associates
WestPoint, 78 Queens Road, Clifton
Bristol BS8 1QX, UK

The Investigation which is the subject of this report was initiated by
USAF - EOARD, 223/231 Old Marylebone Road, London, NW1 5TH, UK
and was carried out under the terms of
Contract SPC-02-4051

DISTRIBUTION LIST

1	Mr. W. Donaldson	USAF-EOARD, London NW1 5TH, UK
1	Mr. C. Remillard	Chief, AFRL/VAAA; Bldg 45
		2130 8th Street, WPAFB, Ohio, USA 45433-7542
1	Mr. D. Multhopp	Technical Area Lead, AFRL/VAAA; Bldg 45
		2130 8th Street, WPAFB, Ohio, USA 45433-7542
2	Dr. C. P. Tilmann	Sr. Aerospace Engineer, AFRL/VAAA; Bldg 45
		2130 8th Street, WPAFB, Ohio, USA 45433-7542
1	Mr. William Fields	Tech Area Lead, AFRL/VAAA; Bldg 45
		2130 8th Street, WPAFB, Ohio, USA 45433-7542
1	Dr. K. P. Iwanski	Aerospace Engineer, AFRL/VAAA; Bldg 45
		2130 8th Street, WPAFB, Ohio, USA 45433-7542
1	Mr. Larry Leavitt	Head, Configuration Aerodynamics Branch
		NASA Langley Research Center, Mail Stop 499
		Hampton, VA 23681-2199
1	Dr. James Luckring	Configuration Aerodynamics Branch
		NASA Langley Research Center, Mail Stop 286
		Hampton, VA 23681-2199
1	Mr. John Perdzock	Head, SensorCraft Integrating Concept Office, AFRL/VAC; Bldg 45
		2130 8th Street, WPAFB, Ohio, USA 45433-7542
1	Dr. Maxwell Blair	AFRL/VASD; Bldg 146
		2210 Eighth Street
		Wright-Patterson AFB OH 45433-7531
1	Dr. Keith Numbers	AFRL/VAA, Long Range Strike Integrating Concept Office
1	Mr. D. Adamczak	Sr. Aerospace Engineer, AFRL/VAAA; Bldg 45
		2130 8th Street, WPAFB, Ohio, USA 45433-7542
1	Dr. Michael OL	Research Engineer, AFRL/VAAA Bldg 45
		2130 8th Street, WPAFB, Ohio, USA 45433-7542
2	Dr. R.K. Nangia	Nangia Aero Research Associates
		WestPoint, 78-Queens Road, Clifton
		BRISTOL BS8 1QX, UK.

CONTRACTUAL DECLARATIONS

"The Contractor, Dr. R. K. Nangia,, hereby delcares that, to the best of its knowledge and belief, the technical data delivered herewith under Contract No.SPC-024051 is complete, accurate, and complies with all requirements of the contract.

DATE: **March 2004**   **Name and Title of Authorized Official:**   **Dr R K Nangia**

"I certify that there were no subject inventions to declare as defined in FAR 52.227-13, during the performance of this contract."

DATE: **March 2004**   **Name and Title of Authorized Official:**   **Dr R K Nangia**

CONTENTS

SUMMARY

DISTRIBUTION LIST
RELATED FORMAL PUBLICATIONS

CONTENTS

1. INTRODUCTION, BACKGROUND & WORK PROGRAMME

2. FLIGHT ENVELOPE, REYNOLDS NO. & CONFIGURATION CONSIDERATIONS

3. LAMINAR FLOW AEROFOILS (2-D)

4. SENSORCRAFT CONFIGURATIONS SCOPE, PREDICTION METHODS & DESIGN

5. DESIGN ASPECTS

6. AT1 CONFIGURATION, RESULTS AT Mach 0.6 and 0.15

7. FT1 CONFIGURATION, RESULTS AT Mach 0.6 and 0.15

8. FURTHER WORK

9. CONCLUDING REMARKS

ACKNOWLEDGEMENTS
REFERENCES
LIST OF SYMBOLS & ABBREVIATIONS

FIGURES   1.1-5, 2.1, 3.1-6, 4.1-3, 6.1.1, 6.2.1-7, 6.3.1-3, 6.4.1-3, 6.5.1-3, 6.6.1-4, 6.7.1-4, 7.1.1-7, 7.2.1-3, 7.3.1-3, 7.4.1-3, 7.5.1-6 (62 Total)

1. INTRODUCTION, BACKGROUND & WORK PROGRAMME

1.1. Background, Wider Context

The work discussed in this report relates to high Aspect Ratio (AR) SensorCraft configurations with constant chord wings incorporating Laminar flow. This report is Part 2 of a series of six, Refs.1 to 6, relating to high AR, long endurance surveillance aircraft, laminar flow, integrated intakes and long range supersonic military aircraft. This work follows previous work funded by USAF-EOARD under seeding Contract SPC-01-4087 which was reported in Ref.7.

The Joined Wing concept conceived by Wolkovitch in the 1980's (Refs.8-9) features diamond-shapes in the plan and front views. One of the main advantages claimed was bending moment relief at a very small expense of span efficiency factor, **Figs.1.1-3**. Several aircraft applications were proposed (**Fig.1.4**). Some of the ideas were carried through into experimental research aircraft and Remotely Piloted Vehicles (RPV). These generally had a "mixed reception" but confirmed some of the advantages claimed over "equivalent" conventional aircraft in terms of aerodynamic efficiency (large Aspect Ratio (AR) feasibility) and structural efficiency. There are however some adverse problems; e.g. spanwise flows, lack of fuel volume, junction flows, etc.

With advances in the technologies of flight control, propulsion and flow control, there is emphasis on re-visiting some of the older concepts and devising newer applications. Some have been publicised, **Fig.1.4**, e.g. Lockheed Fuel Tanker, Goldschmied (NASA), SensorCraft, etc. (Refs.10-11). Some shapes feature wings joined at the tips, others joined part way. The tip-wings can be appropriately backward- or forward- swept.

1.2. Introduction to Present work

The AFRL has been formulating a programme to provide revolutionary intelligence, surveillance, and reconnaissance (ISR) capabilities to the Warfighter (Ref.11). This programme blends a wide spectrum of emerging technologies to produce an Unmanned Air Vehicle (UAV), which may be configured and optimised to conduct multiple advanced sensing modes, integrated into a single airframe capable of long endurance. This feature, combined with omni-directional sensing, may enable a virtual presence, allowing vantage point flexibility / optimisation necessary for continuous and detailed theatre air and ground target detection, identification, and tracking. This unique combination of advanced sensors and sustained presence could enable continuous and rapid reaction to the dynamic combat operational requirements confronting current and evolving military operations.

The SensorCraft is envisaged as the air-borne air-breather component of a fully integrated ISR enterprise that cohesively integrates space, air, and ground components of the total ISR apparatus. It is an AFRL shared-vision UAV programme that combines critical vehicle, propulsion, sensor system, emerging flight and information technologies into a highly responsive platform concept to detect mobile, hidden targets. Several emerging sensor technologies are under assessment for platform use, including hyper-spectral imaging, active laser sensing, unattended ground sensors, and foliage penetration radar (Ref.10). **Fig.1.5** illustrates advanced sensor functionalities and modes for the SensorCraft.

Several candidate aircraft and propulsion configurations are being considered to determine the best trade-off between long endurance, altitude, engine efficiency, and power generation. One of the major challenges is the integration of the large antenna apertures, required for the lower frequency transmissions, into the airframe. These lower frequency bands enable the SensorCraft to provide a foliage penetration radar capability, a key sensory mode aimed at defeating extremely difficult camouflaged, concealed, and deceived (CC&D) targets (Ref.11)

Many of the SensorCraft concepts take advantage of high AR wings, as well as enclosing a large antenna in a diamond aircraft planform. Such aircraft carry a large proportion of fuel and are expected to "loiter" at high altitudes for a few days in each flight. This implies a wide C_L - altitude capability, more so than existing operational reconnaissance aircraft e.g. Global Hawk. The "diamond" shapes offer useful survivability "compliance". The aerofoil shapes need to be thick to contain the antenna and provide adequate fuel volume. The cruise Mach number is expected to be "high" subsonic. The low-speed near-field performance is more akin to that of a (very) high aspect ratio wing glider. Take-off and landing phases are also demanding.

1.3. Present Work Programme

Previous work, Ref.13, considered SensorCraft configurations with conventional aerofoil sections. The thick aerofoil sections with relative large LE radii (r) gave an appreciable range of C_L or AoA operation. Predictions showed "attained operation ranges (or bands)" for "attached" flow to be close to 4° in AoA.

We now extend the analysis using laminar aerofoils. In principle, this should enable a significant reduction in profile drag and enhance overall L/D of the vehicle. However the wing planforms may need to be revised.

1.4. Layout of Report

The remainder of this report is contained in **Sections 2 to 9**:

Section 2 discusses briefly the flight envelope, Reynolds number ranges and possible configurations.

Section 3 looks at effects of camber on 2-D aerofoil sections.

Section 4 defines the configurations considered and discusses, briefly, the prediction methods used.

Section 5 outlines further design aspects.

Section 6 discusses results for the backward swept tip, AT1 configuration at Mach 0.6 and 0.15. Symmetric and asymmetric aspects have been studied. Control aspects are included.

Section 7 discusses results for the forward swept tip, FT1 configuration at Mach 0.6 and 0.15. Symmetric and asymmetric aspects have been studied. Control aspects are included.

Section 8 lists some ideas for further work.

Section 9 mentions concluding remarks.

We begin with an outline of the flight envelope, Mach number, Lift Coefficient and Reynolds numbers encountered and possible configuration aspects.

2. FLIGHT ENVELOPE, REYNOLDS NO. & CONFIGURATION CONSIDERATIONS

Previous work conducted at the AFRL indicated that the main sizing driver aspect is the integration of a "rhombic" antenna into very thick aerofoils. The payload / range performance requirements lead to thick aerofoils (t/c normal to the LE, between 15 and 21%), operating at high C_L values, near 1.0.

Fig.2.1 gives an idea of the aircraft flight envelope. Note the Altitude and Weight relationships during a typical mission. The Reynolds number variation is also depicted as well as Mach number and C_L relationships (C_L based on the total front wing area). Take-off is near C_L of 0.95 at Mach 0.2 (Re= 1.414×10^6/ft), whilst landing is at C_L of 0.7 at Mach 0.15 (Re= 1.06×10^6/ft). The Mach 0.6 cruise C_L varies from 1.58 to 0.88 (Re= 0.44×10^6/ft to 0.345×10^6/ft).

It is interesting to reflect that, on conventional aircraft, the cruise C_L values are near 0.5 and take-off / landing C_L values near 0.8 to 1.2.

The thick aerofoil sections with relatively large LE radii (r) give an appreciable range of C_L or AoA operation. Predictions show "attained operation ranges (or bands)" for "attached" flow to be close to 4° in AoA. Previous work has been carried out with such aerofoils (Refs.13 & 14-17).

We now extend the analysis using laminar aerofoils. In principle, this should enable a significant reduction in profile drag and enhance overall L/D of the vehicle. However the wing planforms might well need to be revised.

It is opportune to mention that currently there is significant interest in ensuring existence of laminar flow on swept wing surfaces. Arizona State University research has focussed on addressing the problem of cross-flow instability, using distributed roughness on surfaces. The detailed results are however, not yet available.

3. LAMINAR FLOW AEROFOILS (2-D)

We begin with a brief review of laminar flow aerofoil design work at AFRL, Ref.18. **Fig.3.1** shows low speed results from the XFOIL code. This is a panel code with compressibility corrections, coupled to a boundary layer solver to represent viscous effects. **Fig.3.1(a)** shows a typical laminar flow aerofoil section and **Fig.3.1(b)** shows the resulting low speed C_P distributions (Ref.18). **Fig.3.1(c)** compares inviscid and viscous results near the design point (CL=1.0, α=3.11°). This comparison supports the argument that we can reasonably use inviscid Cp for design purposes. This is not too surprising as laminar boundary layers up to transition are considered fairly "thin". The laminar flow aerofoil section appeared to provide favourable pressure distributions near the design point.

We have established a suitable starting point for further development. Using an inviscid panel code, we have analysed a series of uncambered (symmetric, thickness distribution only from **Fig.3.1(a)**) and designed laminar aerofoil sections. The design operating Mach number range is 0.5 - 0.6. The analysis has also included Mach numbers 0.01, 0.2 and 0.4.

The effects of α (-1° to 8°) on C_P distributions for the laminar uncambered aerofoil section, over a range of Mach numbers, 0.01 to 0.6, are shown in **Fig.3.2**. In these types of C_P plot, upper and lower surface distributions are shown by solid and dashed lines respectively. For uncambered cases, the upper and lower surface distributions coincide at α=0°. The α= -1° and +1° lower surface distributions are obscured by the upper surface α= +1° and -1° distributions respectively. The effects of aerofoil section thickness, 16.0% t/c and 19.5% t/c, are also shown in **Fig.3.2**.

In **Fig.3.3**, the effects of camber and Mach number (0.01 to 0.6) on C_P distribution for the 16.0% thick laminar aerofoil sections are shown. The AoA range is -1° < α < 8°. It is noted that at Mach 0.6, pressure distributions, indicative of laminar flow, are maintained on the cambered section up to α = 6° (C_L = 0.873).

Fig.3.4 shows the effects of camber and Mach number (0.01 to 0.6) on C_P distributions for the 19.5% thick laminar aerofoils. The AoA range is -1° < α < 8°. In this case, at Mach 0.6, pressure distributions, indicative of laminar flow, are maintained to at least α = 8° on the cambered sections.

Fig.3.5 shows the effects of Mach number (0.01 to 0.6) on C_P distributions on laminar cambered aerofoils and compares t/c of 16.0% and 19.5%.

Fig.3.6 summarises laminar aerofoil capabilities through the Mach number range for the uncambered and cambered aerofoil sections. The thicker sections are more "capable" of maintaining laminar flow but may, of course, suffer from pressure and wave drag penalties. The Cp distributions obtained using the panel method are largely similar to those depicted in **Fig.3.1** (XFOIL). The slight differences arising are in the vicinity of the TE. This observation goes some way in justifying the use of an inviscid panel method for preliminary design work. Boundary layer effects can be included in the later stages of the design process as needed.

4. SENSORCRAFT CONFIGURATIONS SCOPE, PREDICTION METHODS & DESIGN

Fig. 4.1 shows the reference configuration. A twin fuselage, twin-engine layout is shown. A single fuselage with one or two power-plants may also be considered. The effects of fuselage, intakes and power-plant have not been included in this study.

Fig. 4.2 shows three concept outlines. Variations include anhedral or dihedral on front or rear wings with either forward or backward swept tips. In concept AT1, the front wing and tip have continuous backward sweep and dihedral. Concepts FT1 and FT2 feature forward-swept, dihedral tips. The difference between FT1 and FT2 is the relative height of the front and rear wing roots. FT1 has a dihedral front wing with anhedral rear wing. FT2 has an anhedral front wing with dihedral rear wing.

The low and high speed demands on the configuration obviously "conflict" and this has led to a challenging work programme leading towards suitable layouts with designed (camber and twist) aerofoil sections. For configuration AT1, Ref.14 (limited audience) emphasised the design work using Panel codes. Refs.15-16 extended the scope, using in addition, an Euler code. Ref.17 introduced comparative work on the AT1 and FT1 configurations with "conventional" aerofoil sections. The work reported here further extends the programme using laminar flow aerofoils on configurations AT1 and FT1.

On novel layouts, often the experience is that the complexities "defy" the use of an automatic "hands-off" design process with any confidence (unique solutions doubted). Therefore, we have chosen a process that allows a significant understanding to be gained with reasonable manual control over the design process (Refs.19-25). Panel and Euler codes (Ref.30) are utilised that enable assessment of the aerodynamic performance over the range of low to high speeds. The camber and twist design, under forces and moments constraints, is via previously validated attained suction design methods (e.g. Refs.19-23, 26-29). The aerodynamic prediction methods are now discussed together with a description of the wing design process.

Aerodynamic Prediction Methods

The aerodynamic prediction methods are described in an order of complexity.

<u>Linear Theory & Attained Thrust Methods</u>

The linear lifting surface theories have been around for 3 or 4 decades. Various formulations in terms of vortex lattice and doublet lattice exist. Methods have been used in subsonic and supersonic linearized flows. Several design approaches for minimizing drag for given lift also exist. Useful Text books are e.g. by Bertin & Smith, "Aerodynamics for Engineers", and McCormick, "Aerodynamics, Aeronautics & Flight mechanics".

A more recent development over last 2 decades has been the incorporation of attained thrust principles in linear theories. The attained thrust method uses empirical correlations of onset flow and aerofoil parameters (along the span of the wing) to establish the proportion of thrust recovered on the wing leading edges. Such methods were pioneered by Carlson et al at NASA Langley. Computer programmes such as WDES are available in USA. The codes also have a camber design facility (using polynomial type modes). We have developed our own codes based on principles similar to those used by Carlson.

<u>Panel Codes</u>

Panel codes (surface singularity methods) are well established and form an important part of the designer's inventory. These have been developed over the last 25 years and have reached a reasonable

level of maturity. Various first and second order codes are available e.g. PMARC, VSAERO, PANAIR and QUADPAN (in USA). Most of these methods produce very similar results for Mach numbers less than about 0.8. Flow compressibility effects are based on the Prandtl-Glauert approximation. The surface of the configuration is overlaid by panels of surface singularities e.g. doublet and sources. A matrix of influence coefficients, relating the effects of each panel on all others is then formed. This matrix is then solved with respect to the boundary conditions and onset flow parameters.

The boundary condition can be set up in different ways. In Neumann or "direct" type formulation, the normal velocity is applied directly, balancing the velocities due to singularities placed on the surface panel network. In the "Dirichlet Potential formulation", the solution assumes zero potential inside a closed body and this implies an "indirect" compliance of zero normal velocity across a surface.

Once the strengths of the flow singularities are known, velocities, pressures, forces and moments can be calculated. In general, the wake geometries are pre-specified. Some methods allow relaxation of wakes in an iterative manner.

Good descriptions of the underlying methods are given in standard texts (e.g. Katz & Plotkin, "Low Speed Aerodynamics").

Euler Codes

Euler codes have become well established over the last 20 years. These are based on the Euler approximation (i.e. ignoring viscosity terms) of the full Navier-Stokes flow equations. The compressibility effects allow shock formation. Many text-books deal with the theoretical and numerical aspects (e.g. finite-difference, finite-volume and finite element). To apply the methods, surface and volume grids are both needed. The grids can be either structured or unstructured (triangles & pyramids). These are therefore more expensive in grid formation and cpu usage (cf. panel codes). We have used the finite element Euler method of Ref.30 as needed for "final" checks on the designed geometries.

Inverse Codes

The inverse approaches can be used with any of the aerodynamic prediction codes. Various methodologies have been pioneered throughout the world e.g. NASA Langley C-DISC. Such codes are usually applied in the final stages to help in fine-tuning and tailoring of flow parameters, e.g. velocities or pressure distributions. We have given an example of the technique in an AIAA publication, Ref.17. As far as the current work programme is concerned, these methods have not needed to be exploited. One would expect their use when fuselages and intakes need to be integrated into the configuration. It is planned to publish a paper on the methodology in due course.

Wing Design Process

The design procedure is illustrated in schematic form in **Fig.4.3**. The over-riding design target is to minimise drag for a design lift coefficient. Some degree of control over pitching moment is also required. The design targets are therefore:
>   Onset flow attachment at the Leading Edge (LE)
>   Elliptical spanwise load distribution
>   Acceptable pitching moment characteristics

The Joined-Wing Sensor-Craft configurations studied here comprise three wings, a swept back front wing, a swept forward rear wing and a tip wing. Both aft and forward swept tips have been considered.

This approach has been specially adapted for configurations with high aspect ratio wings.

1. Set up geometry for the uncambered (symmetric aerofoil) case. All three wing components are uncambered. From this geometry basic aerodynamic trends are established, e.g. $C_{L\alpha}$ and neutral point location and shape of spanwise lift distributions. This also sets the relative loadings balance between the wing components so that center of pressure and neutral point retain the relationship, virtually independent of AoA.

2. Datum Camber aerofoil on all three wings. Establish spanwise distribution of α for attachment at LE and α (twist) effects on local load distributions. This provides the target C_L and spanwise loading. Datum camber, when compared to uncambered (Step 1), can also provide gross camber and AOA effects at each spanwise location. However the experience is that local linearisation provides an improved approach for camber effects as in the following step, taking each wing component in turn (front, aft and tip).

3. Determine differences between datum camber and datum + 10% camber. This permits derivation of spanwise (stripwise) Influence Coefficients (sensitivities) for lift and camber.

4. For the target C_L and spanwise loading, an iterative process allows matching of the camber modes and lift modes to move the attachment lines to the LE for minimum drag. These additional terms effectively describe a new geometry.

5. Evaluate the new geometry. Initially, with Panel code for rapid check on design process. As design condition is approached, more accurate but time intensive solvers can be used (Euler).

6. Repeat steps 3 - 5, if necessary for each wing component.

Notes for the Current Joined-Wing Configurations:

Experience suggests that sensitive areas are basically near forward swept junctions. Further refinements in these areas can be carried out with stripwise influence coefficients.

An additional stage would be to include pitching moment design.

As mentioned earlier, further refinement can be introduced by using an inverse design method such as using 3-D membrane analogy technique. (Ref.26). This can enable "tailoring" and "fine-tuning" of aerofoil shapes for "optimum" C_P distributions as needed, especially when fuselages and intakes are to be integrated.

5. DESIGN ASPECTS

At the outset, there are several aspects that need to be considered, e.g.
   – Type of spanwise loadings and design of wing camber and twist.
   – Trimmed flight at low speeds with different C_L levels. The TE geometry can be varied.
   – High-speed design of thick wings, tolerant to a large C_L variation (fuel usage). Use of TE flaps.
   – Integration of intakes / fuselages.
   – "Reasonable" off-design performance – adequate tolerance to cross-winds during landing / take-off.
   – Roll, Pitch and Yaw Stability levels, Control laws.

Here we take a few of these aspects related to "high-speed" wing design. Intakes / Fuselages remain to be included.

6. AT1 CONFIGURATION, RESULTS AT Mach 0.6 and 0.15

The AT1 configuration has been modelled as three wing components: front and rear wings with an outer backward-swept tip. The front wing has dihedral and is swept back. The rear wing (tail) has anhedral, is swept forward and meets the front wing at 0.7 semispan. At this location, the planar front wing TE is coincident with the planar rear wing LE. The backward swept tip has an extended inboard chord to encompass the outermost chords of the front and rear wings. Basic planform effects have been investigated on a simplified geometry and are discussed in Section 6.1. Designed camber effects at M = 0.6 are assessed on a developed AT1 geometry and are discussed in Sections 6.2 to 6.4. Results for the designed case at M = 0.15 are also discussed.

6.1. Basic Planform Effects, Uncambered Case, Wing & Tail Mutual Interference

The configuration considered, is shown in **Fig.6.1.1**. The dihedral wing (front) has continuous backward sweep and extends to the wing tip. The anhedral tail is forward swept and extends from the root centre-line to 0.7 semi-span. The wing and tail are both uncambered (symmetric aerofoil). AoA effects have been established for this configuration. Chordwise C_P distributions on the wing and tail, in dimensional and non-dimensional geometry context, are shown in **Fig.6.1.1** for AoA of 4°. The distributions help to highlight the tendency for higher LE suctions to occur towards the tip of the front wing, whilst the tail has high LE suctions at the forward-swept centre-section. Spanwise loadings with and without mutual interference are also shown in **Fig.6.1.1**, for AoA 0° to 10°. The wing loadings show an increase in C_{LL} on the outboard region, for the wing and tail combination over the wing only loadings. The tail operates in the down-wash flow-field of the front wing and the reduced C_{LL} on the tail, with the wing present, is clearly evident. The largest downwash effects occurring near the junction.

6.2. Uncambered & Designed Cases at M = 0.6

The general arrangement for the AT1 configuration with laminar flow aerofoil sections is shown in **Fig.6.2.1**. The configuration has been modelled as three wing components: front, rear and the outer tip. Uncambered (dotted line) and designed (solid line) aerofoil shapes are compared in the figure. Note that camber and twist, **Fig.6.2.2**, both vary for the designed configuration. The characteristic twist and camber differences for the forward-swept (rear) and backward-swept (front) wings are evident. The front wing has less twist and camber, compared to the rear wing.

C_L - α and C_m - C_L variations are shown, for the uncambered and designed AT1 configuration, in **Figs.6.2.3** and **6.2.4** respectively. The Moment Reference Centre (MRC), derived from the C_m - C_N relationship with uncambered aerofoil wings, is at x = 0.55, y = 0.0 and z = 0.11, based on a semi-span of 1.0 as shown. The C_L design point bears a relationship to landing and cruise. We have chosen C_L = 0.9 i.e. equivalent flat wing AoA of 5°. Here C_L has been based on the front wing + tip wing area. We have tried to approach an elliptic loading for the designed case, trimmed for neutral stability. In view of the thick sections and anticipated attached flow band-widths, the operational range should extend to C_L of 1.6 prior to any significant flow separations.

The effect of wing setting angle is also shown in **Fig.6.2.4**. By setting either the front wing at +0.5° or the rear wing at -0.5°, a shift of +0.15 C_m can be achieved. There is, of course, a corresponding change in total C_L throughout the AoA range. A suitable combination of front and rear wing twist could attain C_m = 0 without affecting the C_L – AoA relationship. This illustrates a degree of control that can be achieved in the design process.

Fig.6.2.5 compares chordwise C_P distributions for the uncambered and designed cambered configuration at six values of C_L (0.71, 0.9, 1.07, 1.25, 1.42, and 1.6). The chordwise C_P distributions

are supported by spanwise loadings for the designed configuration, at the same C_L values, in **Fig.6.2.6.** This shows the corresponding loadings on the three wing components and their sum. The front wing is more heavily loaded towards the wing junction. At the centre-line, despite the downwash effects, the rear wing carries more loading. This is to be expected at the centre-line junction of a forward-swept wing. For minimum drag of the total configuration, a near elliptic lift loading is required, as shown. For this layout, however, relatively higher loadings appear near the wing tip as AoA increases.

At a given design condition (C_L and α), one could design camber and twist for minimum drag elliptic loading but the tendency at off-design will be to depart from the elliptic loading. This will have implications on pitch trim stability.

The laminar or "flat-top" nature of the upper and lower surface chordwise pressure distributions (c.f. uncambered case) are noted in **Fig.6.2.5**. Laminar flow is maintained up to C_L 1.25. Beyond this, the tip root flow breaks down. Geometry details near the wing junction could do with some local improvements, if required, especially from the point of view of maintaining laminar flow. This will be more opportune at a later design stage when integrating the intakes and fuselages into the configuration.

A useful technique of imposing local improvements is via inverse wing design optimisation. This has been discussed in previous papers and Ref.26.

Laminar flow C_L ranges at M = 0.6, deduced from Cp distributions, are shown in **Fig.6.2.7** for the uncambered and designed wings. The introduction of design camber has raised and broadened the C_L operating range.

6.3. Designed Case at Low Speed (M = 0.15)

C_L - AoA and C_m - C_L variations are compared at M = 0.15 and 0.6 in **Fig.6.3.1** for the designed AT1 configuration. The effects of Mach number on longitudinal stability are noted. At lower speed, the CoP moves forward giving rise to more positive C_m about the MRC. The configuration tends to longitudinal instability at lower speed. The spanwise load distributions, **Fig.6.3.2**, have a similar nature to those at M = 0.6. The front wing is more heavily loaded towards the wing junction and the rear wing experiences typical increased loading at the forward swept, centre-line, junction. **Fig.6.3.3** shows chordwise C_P distributions, at M = 0.15, for the designed (M = 0.6) configuration at six values of C_L (0.64, 0.79, 0.95, 1.10, 1.26, and 1.41). Laminar flow is maintained up to C_L = 1.26 at this reduced Mach number (0.15).

6.4. Longitudinal Control

For maximum effect on Pitching Moment (C_m), flaps on either the front wing, rear wing or both, would need to be positioned as far away as possible (fore and aft) from the aerodynamic centre (moment reference centre). This naturally positions TE flaps near the wing roots as shown in **Fig.6.4.1**. The effect on C_m of deflecting either the front wing TE flap or the rear wing TE flap by 5° TE down or 5° TE up is also shown in **Fig.6.4.2**. It is noted that the change in C_m from C_{mo} for the designed wing with no flap deflection is equal and opposite for TE up or down. The front wing TE flap is approximately twice as effective as that on the rear wing.

The variation, with C_L, of front and rear wing TE Flap angles required to maintain C_L – AoA relationships and reduce C_m to zero is shown in **Fig.6.4.3**.

6.5. Asymmetric Cases (Sideslip Effects)

Spanwise and chordwise loadings are considered at M = 0.6, C_L = 0.90, 1.25 and 1.60, for positive (nose to right) and negative (nose to left) 5° and 0° sideslip. In each case, for chordwise loadings, only

the right side component results are shown. By symmetry, the right wing, ß = +5° distributions, may also be viewed as the left wing, ß = -5° distributions. **Fig.6.5.1** shows spanwise and chordwise loadings at $C_L = 0.9$. At ß = -5° (nose to left) the increased loading on the right front wing and right tip can be seen, relative to the reduced loadings on the left side components. The increased loading results from unsweeping the right wing with negative sideslip. At zero sideslip, the inboard section of the tip indicated loss of laminar flow at $C_L = 1.6$ (see **Fig.6.2.7**, laminar flow limit $C_L = 1.5$). Negative sideslip reduces the laminar flow C_L range of the inboard right tip region, **Fig.6.5.2** ($C_L = 1.25$) and increases the tendency for flow separation, **Fig.6.5.3** ($C_L = 1.6$).

6.6. Aileron Control Effects in Sideslip

The variations of Rolling moment due to sideslip ($C_{l\beta}/°$) with C_L, at M = 0.6 and 0.15 are shown in **Fig.6.6.1**. Simple, constant chord aileron geometry was generated for the AT1 configuration at the TE of the backward swept tip (**Fig.6.6.2**). By deflecting the aileron through small angles, the variation of aileron roll control power ($C_{l\delta A}/°$) with C_L was determined, **Fig.6.6.3**. The amount of aileron deflection required to eliminate roll induced by 5° sideslip is shown in **Fig 6.6.4**. A target condition of M = 0.6, $C_L = 1.0$ and ß = 5° was set. From the above derivatives it was deduced that, for zero rolling moment ($C_l = 0.0$), AT1 would require 2.485° of aileron. The geometry was set up and run. The target C_L was achieved to within 0.5% with residual $C_l = 0.033$. This exercise has shown a degree of control in the design of wing camber and TE flap deflections required for specific flight conditions. Further analysis and comparisons with configuration FT1 appear in Section 7.5.

6.7. On Designing with Constant Aerofoil Sections but Allowing Twist

During the course of the current work a question arose on using a slightly different design philosophy with a view to increasing manufacturing simplicity. The idea was to use a constant (invariant) aerofoil section with reference camber across the front, rear and tip wings and achieve the required design characteristics (elliptic loading) by modification of twist only along the span.

We shall look at longitudinal considerations only.

The constant aerofoil sections (dotted line) are compared with the resultant twisted sections (solid line) in **Fig.6.7.1**. All sections are identical, with reference camber. The twist distribution is shown in **Fig.6.7.2**. A significant twist variation is required on the tip wing to achieve the desired elliptic loading. C_L - AoA and C_m - C_L variations are compared at M = 0.6 in **Fig.6.7.3** for the AT1 configuration designed using camber and twist variation or twist variation only on the reference aerofoil section. Further design work on the latter case is required to improve the stability characteristics. The chordwise C_P distributions are supported by spanwise loadings, **Fig.6.7.4** at $-1^o <$ AoA $< 4^o$. The spanwise loadings show a close approach to the desired elliptic distribution. However, the chordwise distributions show significant departures from the laminar flow type distributions shown in **Fig.6.2.5** for the camber designed case. Taking $C_L = 1.25$ for comparison, the front wing appears to exhibit reasonably well behaved distributions across its span. The rear wing upper surface is also well behaved. However, the lower surface, near the tip wing junction shows deviations from the desired laminar flow type distributions. The tip wing upper surface exhibits laminar flow breakdown as does the lower surface at the tip. Further design work would be required on the tip wing and at the tip / wing junction.

7. FT1 CONFIGURATION, RESULTS AT Mach 0.6 and 0.15

The FT1 configuration has been modelled as three wing components: front, rear and outer forward-swept tip. Aerodynamic characteristics for both uncambered (symmetric aerofoil) and designed aerofoil sections are considered at M = 0.6. Results for the designed case at M = 0.15 are also discussed.

7.1. Uncambered and Designed Cases at M = 0.6

Fig.7.1.1 shows the general arrangement of the FT1 configuration (front and rear wings with outer forward-swept tip). Uncambered and designed aerofoil shapes are illustrated. Note that camber and twist, **Fig.7.1.2**, both vary for the designed configuration. The characteristic twist and camber differences for the forward-swept and backward-swept wings are evident. The front wing has less twist and camber compared to the rear wing. C_L - AoA and C_m - C_L variations are shown for the uncambered and designed FT1 configuration in **Figs.7.1.3** and **7.1.4** respectively. The moment reference centre (MRC) is at x = 0.55, y = 0.0 and z = 0.11, based on semi-span of 1.0 as shown. As previously discussed, the C_L design point chosen is 0.9 i.e. equivalent flat wing AoA of 5°. **Fig.7.1.5** compares chordwise C_P distributions for the uncambered and designed cambered configurations at six different values of C_L (0.71, 0.90, 1.06, 1.24, 1.42, and 1.59). The chordwise C_P distributions are supported by spanwise loadings for the designed wing in **Fig.7.1.6**. This shows the corresponding loadings on the three components and their sum at the same C_L values. The AoA varies from —1° to 4°. The front wing is more heavily loaded towards the wing-juncture. At the centre-line, in spite of the downwash effects, the rear wing carries more loading and this is to be expected on a forward-swept wing. For minimum drag of the total configuration, a near elliptic lift loading is required, as shown. For this layout, however, relatively lower loadings appear near the wing tip as AoA increases. At a given design condition (C_L and α), one could design camber and twist for minimum drag elliptic loading, but the tendency at off-design will be to depart from the elliptic loading. This will have implications on pitch trim stability. From **Fig.7.1.5**, note the laminar or "flat-top" nature of the upper and lower surface chordwise pressure distributions (c.f. uncambered case). As may be expected, the inboard region of the FT1 uncambered tip shows a greater tendency towards separation than the AT1 tip at equivalent conditions. This has required larger twist and camber values to achieve the elliptical loading requirement. However, laminar flow is maintained over a much wider C_L range for the FT1 configuration, **Fig.7.1.7**, than for the AT1 case (**Fig.6.2.7**).

7.2. Designed Case at Low Speed (M = 0.15)

C_L - AoA and C_m - C_L variations are compared at M = 0.15 and 0.6 in **Fig.7.2.1** for the designed FT1 configuration. The effects of Mach number on longitudinal stability are noted. At lower speed, the CoP moves forward, giving rise to more positive C_m about the MRC. The configuration tends to longitudinal instability at lower speed. The spanwise load distributions, **Fig.7.2.2**, have a similar nature to those at M = 0.6. The front wing is more heavily loaded towards the wing junction and the rear wing experiences typical increased loading at the forward swept, center-line, junction. **Fig.7.2.3** shows chordwise C_P distributions at M = 0.15 for the designed (M = 0.6) configuration at six values of C_L (0.63, 0.79, 0.94, 1.10, 1.25, and 1.41).

7.3. Longitudinal Control

As described in Section 6.4, for effective control power, the TE flaps need to be positioned as far away as possible (fore and aft) from the aerodynamic centre (moment reference centre). This naturally positions TE flaps near the wing roots as shown in **Fig.7.3.1**. The effect on C_m of deflecting either the front wing TE flap or the rear wing TE flap 5° TE down or 5° TE up is shown in **Fig.7.3.2**.It is noted that the change in C_m from C_{mo} for the designed wing with no flap deflection is equal and opposite for TE up or down. The front wing TE flap is approximately twice as effective as that on the rear wing.

The variation, with C_L, of front and rear wing TE Flap angles required to maintain C_L – AoA relationships and reduce C_m to zero is shown in **Fig.7.3.3**.

7.4. Asymmetric Cases (Sideslip Effects)

Spanwise and chordwise loadings are considered at M = 0.6, C_L = 0.89, 1.25 and 1.59, for positive (nose to right) and negative (nose to left) 5° and 0° sideslip. In each case, for chordwise loadings, only the right side components are shown. By symmetry, the right wing, ß = +5° distributions, may also be viewed as the left wing, ß = -5° distributions. **Fig.7.4.1** shows spanwise and chordwise loadings at C_L = 0.89. At ß = -5° (nose to left) the increased loading on the right front wing and right tip can be seen, relative to the reduced loadings on the left side components. The changes in spanwise loading with sideslip on the front and rear wings result from the effects described in Section 6.4 (Configuration AT1). At zero sideslip, the inboard section of the FT1 tip indicated loss of laminar flow at C_L = 1.25 but this is more localised than on the AT1 configuration (see **Fig.7.1.7**). Negative sideslip reduces the laminar flow C_L range of the right tip region but less significantly than on the AT1 tip, **Figs.7.4.2** and **7.4.3** (C_L = 1.25 and 1.59) compared with **Figs.6.4.2** and **6.4.3** (C_L = 1.25 and 1.60).

7.5. Aileron Control Effects in Sideslip

The variations of Rolling moment due to sideslip ($C_{lß}$/°) with C_L, at M = 0.6 and 0.15 are shown in **Fig.7.5.1**. Simple, constant chord aileron geometry was generated for the FT1 configuration at the TE of the forward swept tip (**Fig.7.5.2**). By deflecting the aileron through small angles, the variation of aileron roll control power ($C_{l\delta A}$/°) with C_L was determined, **Fig.7.5.3**. The amount of aileron deflection required to eliminate roll induced by 5° sideslip is shown in **Fig 7.5.4**. As in the case of configuration AT1, a target condition of M = 0.6, C_L = 1.0 and ß = 5° was set. From the above derivatives it was deduced that, for zero rolling moment (C_l =.0), FT1 would require 0.339°. AT1 had required 2.485° of aileron for zero rolling moment. The geometry was set up and run and the target C_L was achieved to within 0.5% with residual C_l = 0.005.

Rolling moment due to sideslip and Aileron deflection requirements are compared for AT1 and FT1 in **Fig 7.5.5**. The spanwise loadings for AT1 and FT1 at the test condition (zero roll at 5° sideslip, C_L = 1.0, Mach 0.6) are compared in **Fig 7.5.6**. These comparison figures clearly show the advantages of the forward swept tip over the conventional backward swept tip. The greater aileron control power exhibited by the FT1 configuration has many implications. Less aileron deflection requirement to counter a given "upset" results in less local drag and hence less induced yaw. This leads to a smaller correcting rudder deflection requirement and therefore less rudder drag.

This exercise has shown a degree of control in the design of wing camber and TE flap deflections required for specific flight conditions.

8. FURTHER WORK

So far, a type of SensorCraft with a joined-wing layout has been considered for high-speed design at Mach 0.6. Several interesting features have emerged from the application of direct design methods. Further work is envisaged in a number of areas:

- Continued assessment of cross-flow instability research (e.g. Arizona State University) and how it can help the existence of laminar flow on swept surfaces.
- Lower speeds, field performance considerations.
- Parametric geometric studies with appropriate method development.
- Further confirmation with Euler.
- Different design C_L studies as required. The forward-swept root (rear wing) needs attention.
- Different aerofoils incorporation, from the point of view of validation with CFD and transonic codes.
- Pitching moment, static margins control with LE / TE Flap within geometry restrictions, segmentation.
- Fuselage & Intake incorporation, additional effects on forces and moments.
- Inclusion of viscous effects, spanwise pressure gradients and flow control.
- Drag prediction.
- Off-design performance including lateral and directional characteristics. Include aero-elastics.
- Experimental work (various aspects).

9. CONCLUDING REMARKS

A type of SensorCraft with a joined-wing layout has been considered for design at Mach 0.6. Several interesting features have emerged. The emphasis in this report has been on incorporating laminar flow capability.

At the design conditions, the designed case displays considerable reductions in LE suctions when compared with the uncambered (symmetric aerofoil) wings case. Considerable potential exists for laminar flow. Further, near-elliptic spanwise loadings have been maintained. Attention needs to be given to the forward-swept root area of the rear wing (high AoA). The wing junction area will require some tailoring to ensure laminarity at high AoA.

Thicker sections are able to maintain laminar flow over a wider AoA range than thinner sections. However, we have to work under configuration and aerodynamic limits imposed by features such as antennae and fuel tanks.

The configuration FT1 appears to give more favourable spanwise loadings and is better in terms of aileron roll control in sideslip.

Typical results presented demonstrate the flexibility and potential of the techniques for direct and inverse design. The Panel codes go a long way to defining the preliminary designs before the need for high order CFD methods arises.

It is apparent that we are only at a starting post and a sizeable, interesting work programme remains! Capability for study of several geometric variables of configurations is offered in a timely sense. Data for detail design of wind tunnel models and possibly a flight demonstrator can be enabled. An understanding of control laws arises. The potential and limitations of the aircraft in meeting a given design envelope can be assessed.

Several areas for continued work have emerged.

REFERENCES

1. NANGIA, R.K., "Pilot Document Introducing all Aspects of Work Accomplished under USAF-EOARD Contract SPC-024051", RKN/AERO/REPORT/2004-10 – Part 1, Issue 1, 2004.

2. NANGIA, R.K., "High Aspect Ratio Unconventional Joined-Wing Configurations Incorporating Laminar Flow", RKN/AERO/REPORT/2004-10 – Part 2, Issue 1, 2004. *This Report.*

3. NANGIA, R.K., "Planform Effects on High Aspect Ratio Unconventional Joined-Wing Configurations Incorporating Laminar Flow", RKN/AERO/REPORT/2004-10 – Part 3, Issue 1, 2004.

4. NANGIA, R.K., "High Aspect Ratio Lambda-Wing Configurations Incorporating Laminar Flow", RKN/AERO/REPORT/2004-10 – Part 4, Issue 1, 2004.

5. NANGIA, R.K., "Integration of Over-Surface Scarfed Intakes on Aircraft with High Aspect Ratio Wings (e.g. Sensor-Craft)", RKN/AERO/REPORT/2004-10 – Part 5, Issue 1, 2004.

6. NANGIA, R.K., "Towards Design of Long-Range Supersonic Military Aircraft", RKN/AERO/REPORT/2004-10 – Part 6, Issue 1, 2004.

7. NANGIA, R.K., "Configuration & Aerodynamic Design Studies of Joined-Wing High Aspect Ratio Sensor-Craft Concept", RKN/Aero/Report/2002-10, June 2002, (USAF-EOARD Contract SPC-01-4087).

8. WOLKOVITCH, J., "The Joined Wing: An Overview", J. of Aircraft, Vol 23, pp. 161-178, March 1986.

9. WOLKOVITCH, J., "A Second Look at the Joined Wing", Proc. of NVVL Symposium "Unconventional Aircraft Concepts", Delft Uni. Press, 1987.

10. JOHNSON, F. P., "Sensor Craft : Tomorrow's Eyes and Ears of the Warfighter," AIAA-2001-4370, Aug. 2001. *See* www.afrlhorizons.com */Briefs/Mar01/SN0001.html*

11. Aerospace America, Dec. 01, pp 50.

12. TYLER, C., SCHWABACHER & CARTER, D., "Comparison of Computational and Experimental Studies for a Joined-Wing Aircraft", AIAA 2002-0702, January 2002.

13. NANGIA, R.K., "Configuration & Aerodynamic Design Studies of Joined-Wing High Aspect Ratio Sensor Craft Concept", RKN/Aero/Report/2002-10, June 2002, (USAF-EOARD Contract SPC-01-4087).

14. NANGIA, R.K., PALMER, M.E. & TILMANN, C.P., "Towards Design of Unconventional High Aspect Ratio Joined-Wing Type Aircraft Configurations", RAeS Conference — "A 2020 Vision", April 2002, London UK.

15. NANGIA, R.K., PALMER, M.E. & TILMANN, C.P., "Towards Design and Optimisation of Unconventional High Aspect Ratio Joined-Wing Type Aircraft Configurations", CEAS Conference, June 2002, Cambridge UK.

16. NANGIA, R.K., PALMER, M.E. & TILMANN, C.P., "On Design of Unconventional High Aspect Ratio Joined-Wing Type Aircraft Configurations", ICAS 2002-25R2,Toronto, Canada.

17. NANGIA, R.K., PALMER, M.E. & TILMANN, C.P., "Unconventional High Aspect Ratio Joined-Wing Aircraft with Aft- & Forward- Swept Wing-Tips", AIAA-2003-0605, Jan. 2003, Reno, USA.

18. BIBER, K. & TILMANN, C.P., "Laminar Aerofoils….", Paper presented at AIAA Aerospace Sciences Meeting, Reno, Jan 2003.

19. NANGIA, R.K., "The Design of "Manoeuvrable" Wings using Panel Methods, Attained Thrust & Euler Codes", ICAS-92.

20. NANGIA, R.K. & GREENWELL, D.I., "Wing Design of Oblique Wing Combat Aircraft", ICAS 2000-1.6.1, 2000.

21. NANGIA, R. K. & GALPIN, S.A., "Towards Design of High-Lift Krueger Flap Systems with Mach & Reynolds No. Effects for Conventional & Laminar Flow Wings", CEAS European Forum, Bath, UK, 1995.

22. NANGIA, R. K. & GALPIN, S.A., "Prediction of LE & TE Devices Aerodynamics in High-Lift Configurations with Mach & Reynolds No. Effects", ICAS-1996-2.7.6..

23. NANGIA, "Design of Conventional & Unconventional Wings for UAV's", RTA-AVT Symposium, "UV for Aerial & Naval Military Operations", Ankara, Turkey, Oct. 2000.

24. NANGIA, R.K., PALMER, M.E. & DOE, R.H., "A Study of Supersonic Aircraft with Thin Wings of Low Sweep", AIAA-2002-0709, January 2002.

25. NANGIA, R.K. & MILLER, A.S. "Vortex Flow Dilemmas & Control on Wing Planforms for High Speeds", RTO AVT Symposium, Loen, Norway, May 01.

26. NANGIA, R.K., "Developing an Inverse Design Method using 3-D Membrane Analogy", Future Paper.

27. KUCHEMANN, D. "The Aerodynamic Design of Aircraft", Pergamon.

28. JUPP, J., Wing aerodynamics and the Science of Compromise", RAeS Lanchester Lecture, 2001.

29. JONES, R.T., "Wing Theory", Princeton.

30. GUPTA, K.K. & MEEK, J.L., "Finite Element Multidisciplinary Analysis", AIAA, 2000.

31. NANGIA, R.K., PALMER, M.E. & TILMANN, C.P., "Unconventional High Aspect Ratio Joined-Wing Aircraft Incorporating Laminar Flow", AIAA-3927, June 2003, Orlando, FL, USA

32. NANGIA, R.K., "Towards Designing Novel High Altitude Joined-Wing Sensor-Craft (HALE-UAV) ", AIAA-2695, July 2003, Dayton, OH, USA.

LIST OF SYMBOLS & ABBREVIATIONS

Only the general symbols are defined here. Other symbols are of local significance within the Section they arise in.

AoA	Angle of Attack (α), usually referred to the body axis
AR	Aspect Ratio
A	Axial Force along wing-plane x-axis (for definition of CA)
b	= 2 s, Wing span
BL	Boundary Layer
c	Local Wing Chord
c_{aero}	= c, Aerodynamic Wing Chord
c_{av}	= c = cref, Average Wing Chord
C_A	= A/(q S), Axial Force Coefficient, measured in Wing plane
C_{AL}	= Local Axial Force Coefficient
C_D	= Drag Force /(q S), Drag Coefficient
C_{D0}	Drag Coefficient at zero lift (see text)
C_{Di}	Lift Induced Drag
CG	Centre of Gravity
C_l	= l/(q S b), Rolling Moment (Body Axis)
C_L	= CL = L/(q S), Lift Coefficient
C_{LL}	= Local Lift Coefficient
C_{Lmax}	Maximum Lift Coefficient
C_m	= m/(q S c), Pitching Moment (Body Axis)
C_{mo}	C_m at zero lift
C_n	= n/(q S b), Yawwing Moment (Body Axis)
C_N	= N/(q S), Normal Force Coefficient
CoP	Centre of Pressure
Cp	Coefficient of Pressure
c_r, c_t	Wing Root chord, Wing Tip chord
k	= π A C_{Di}/C_L^2, Lift Induced Drag Factor
l	Rolling moment (Body Axis)
LE	Leading Edge
LEF	Leading Edge Flap
m	Pitching moment (Body Axis)
M	Mach Number
MRC	Moment Reference Centre
n	Yawing moment (Body Axis)
N	Normal Force
q	= 0.5 ρ V^2, Dynamic Pressure
r	Aerofoil radius
rn	Aerofoil radius normal to c
R	Reynolds Number, based on cav (unless otherwise stated)
s	Wing semi-span
S	Wing Area, taken here as (front-wing + tip-wing) area
t	Aerofoil thickness
TE	Trailing Edge
TEF	Trailing Edge Flap
V	Airstream Velocity
x,y,z	Orthogonal Wing Co-ordinates, x along body axis
x_{ac}	Location of Aerodynamic Centre along x-axis
x_{cp}	Location of Centre of pressure along x-axis
α	Angle of Attack (AoA), usually referred to the body axis
λ	Wing Taper Ratio
Λ	LE Sweep Angle
ρ	Air Density
η	= y/s, Non-dimensional spanwise Distance

FIG.1. 1   AVA – RPV & EFFECT OF SPAN RATIO ON SPAN EFFICIENCY

FIG.1. 2   BENDING MOMENTS

FIG.1.3   JOINED-WING CRAFT (WOLKOVITCH)

FIG.1. 4   SEVERAL RECENT JOINED-WING
APPLICATIONS

FIG.1.5 SENSOR-CRAFT'S ADVANCED SENSOR MULTI-MODALITY & DIVERSE FUNCTIONALITY
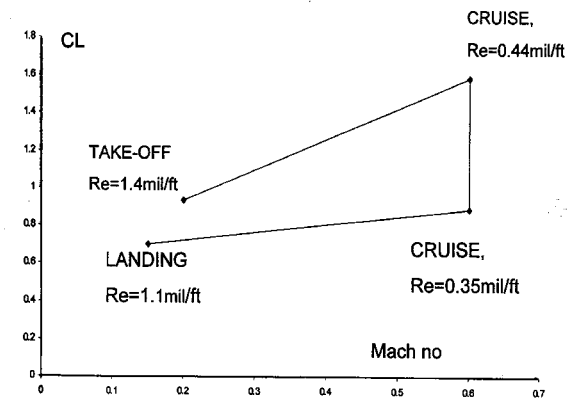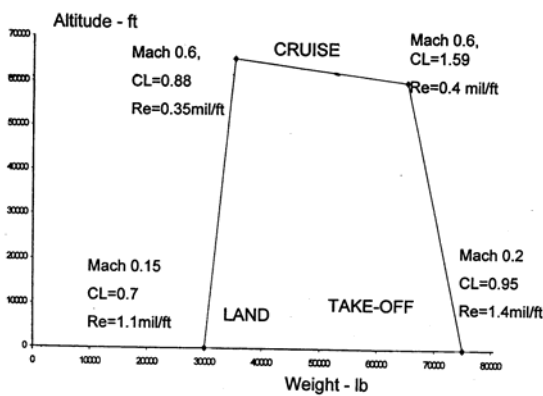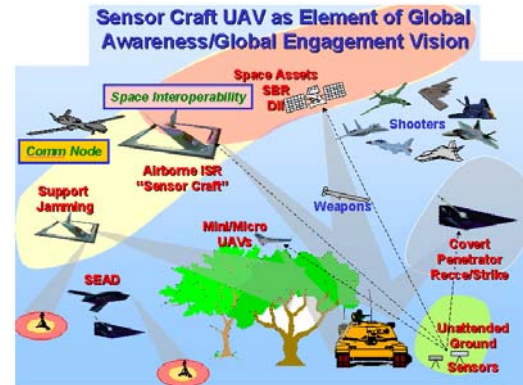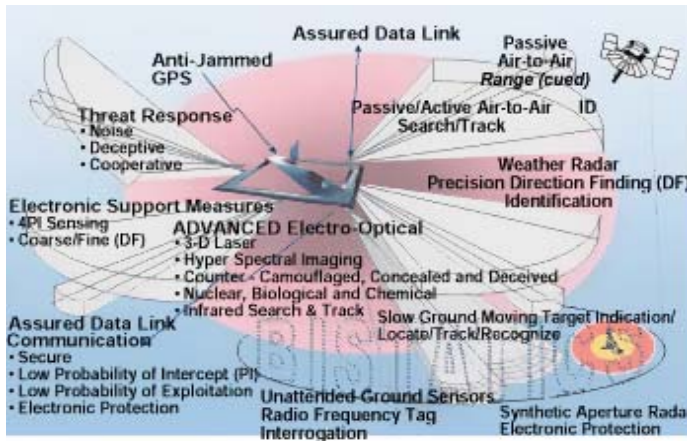
FIG. 2.1 FLIGHT ENVELOPE, ALTITUDE - WEIGHT & CL - MACH RELATIONSHIPS

(a)

(b)

(c)

FIG. 3.1 TY{ICAL LAMINAR AEROFOIL, 16%t/c PROFILE & RESULTS FROM XFOIL

a) $C_L = 1$: ———, viscous solution and - - - -, inviscid solution
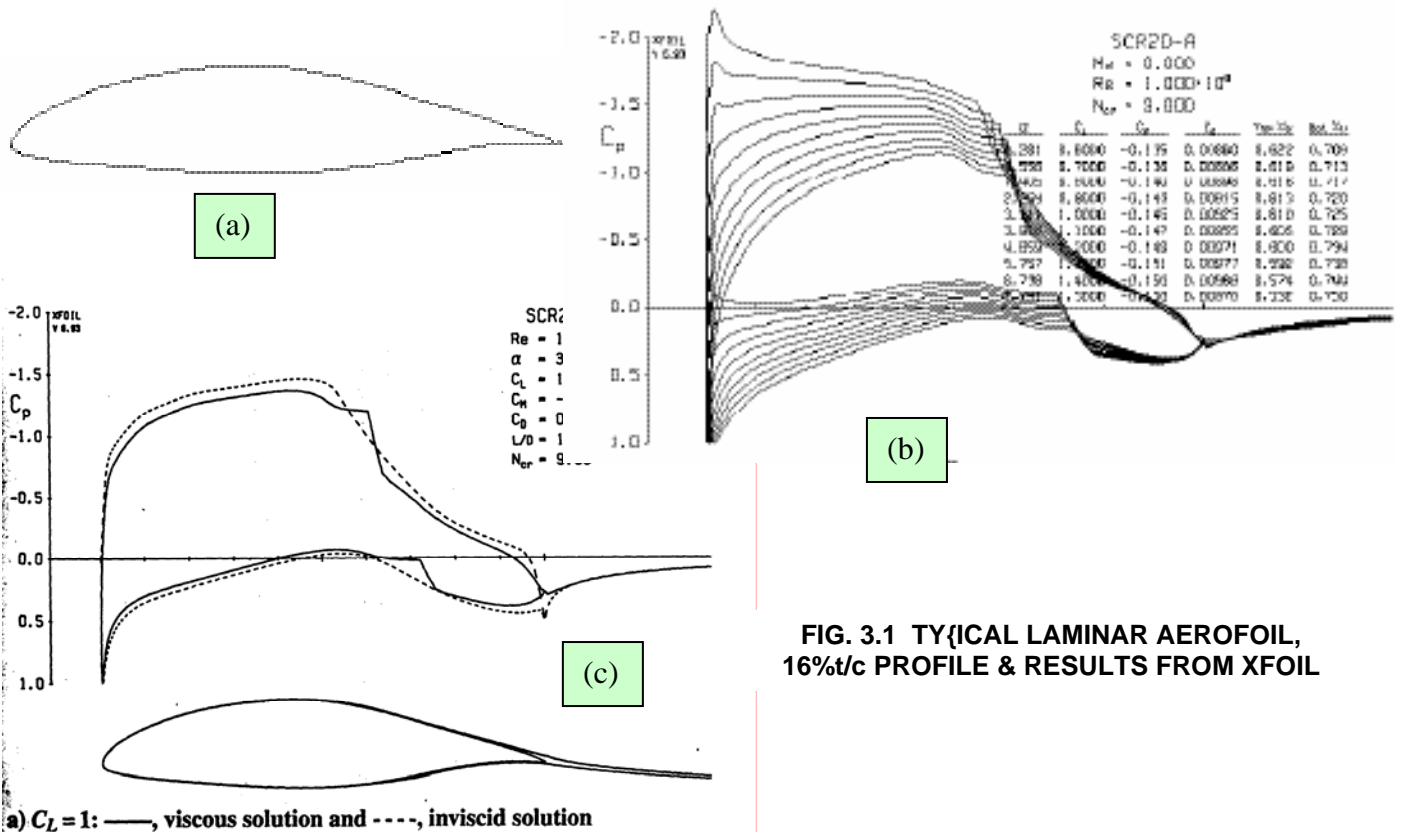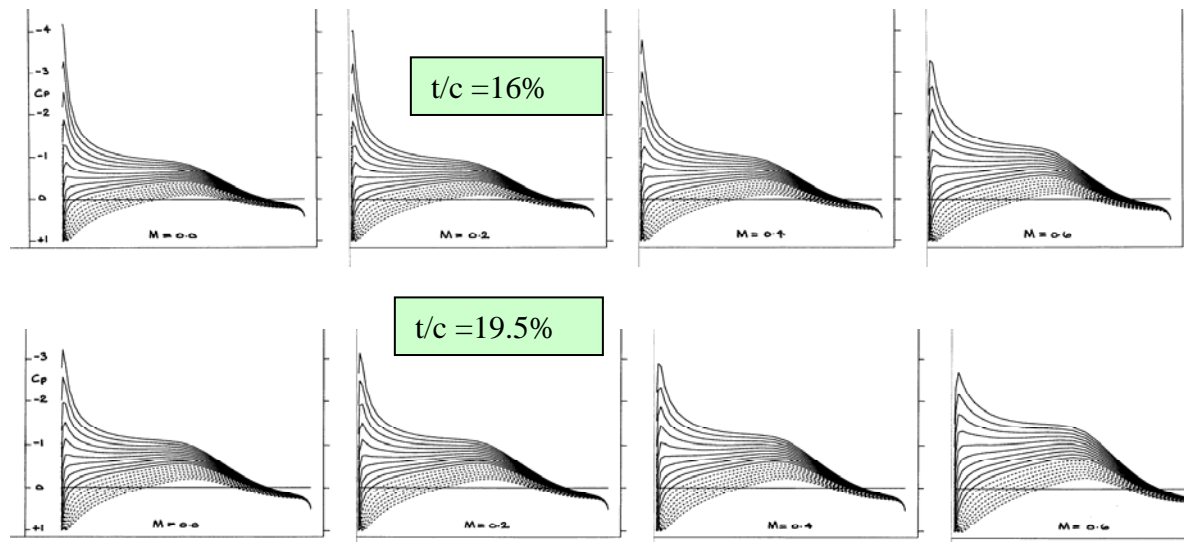
t/c =16%

t/c =19.5%

FIG. 3.2 Cp DISTRIBUTIONS ON LAMINAR UNCAMBERED AEROFOILS,
AoA between -1° and 8° [1°],Mach 0.01, 0.2, 0.4, 0.6

t/c 16% Uncambered
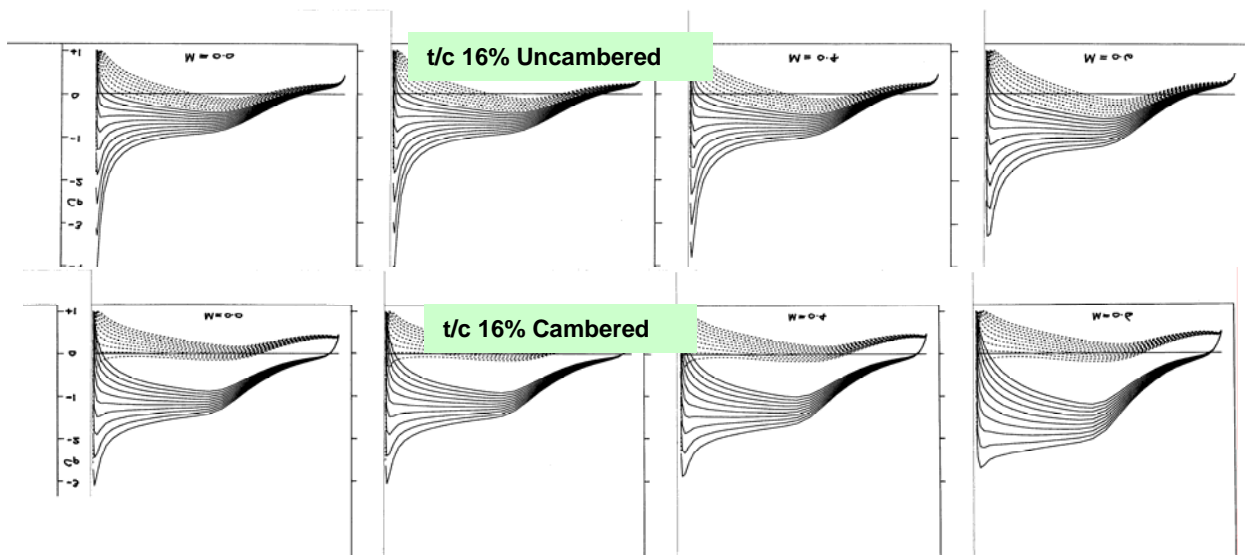
t/c 16% Cambered

FIG. 3.3. 2-D CALCULATIONS, INVISCID, t/c = 16%,
AoA between -1° and 8° [1°], MACH no VARIES from 0.01 to 0.6

t/c 19.5% Uncambered
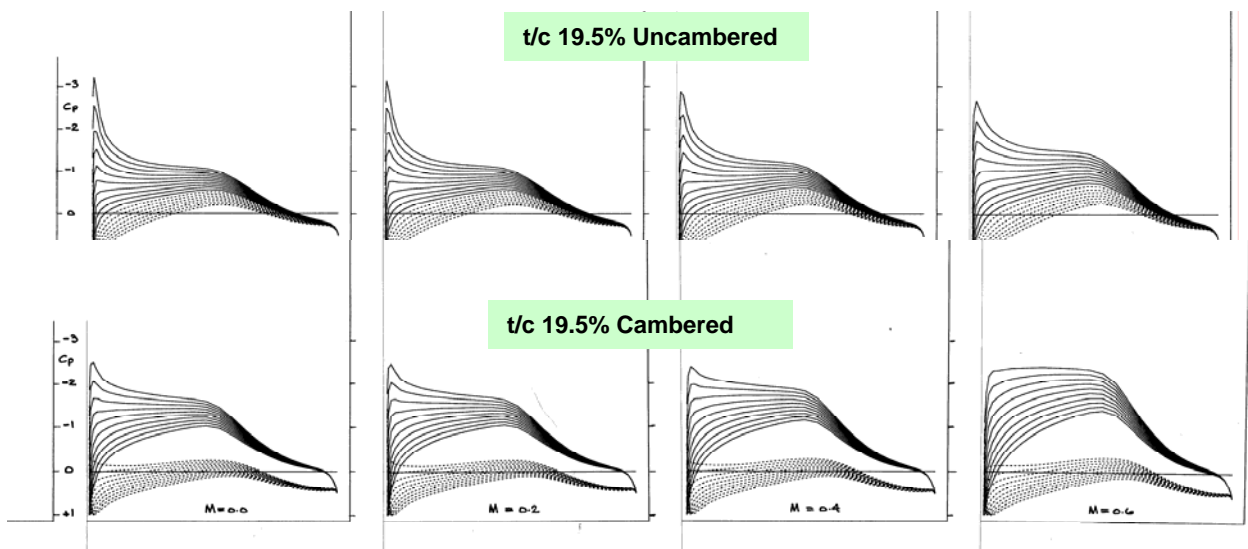
t/c 19.5% Cambered

FIG. 3.4 2-D CALCULATIONS, INVISCID, t/c = 19.5%,
AoA between -1° and 8° [1°], MACH no VARIES from 0.01 to 0.6

t/c =16%

t/c =19.5%
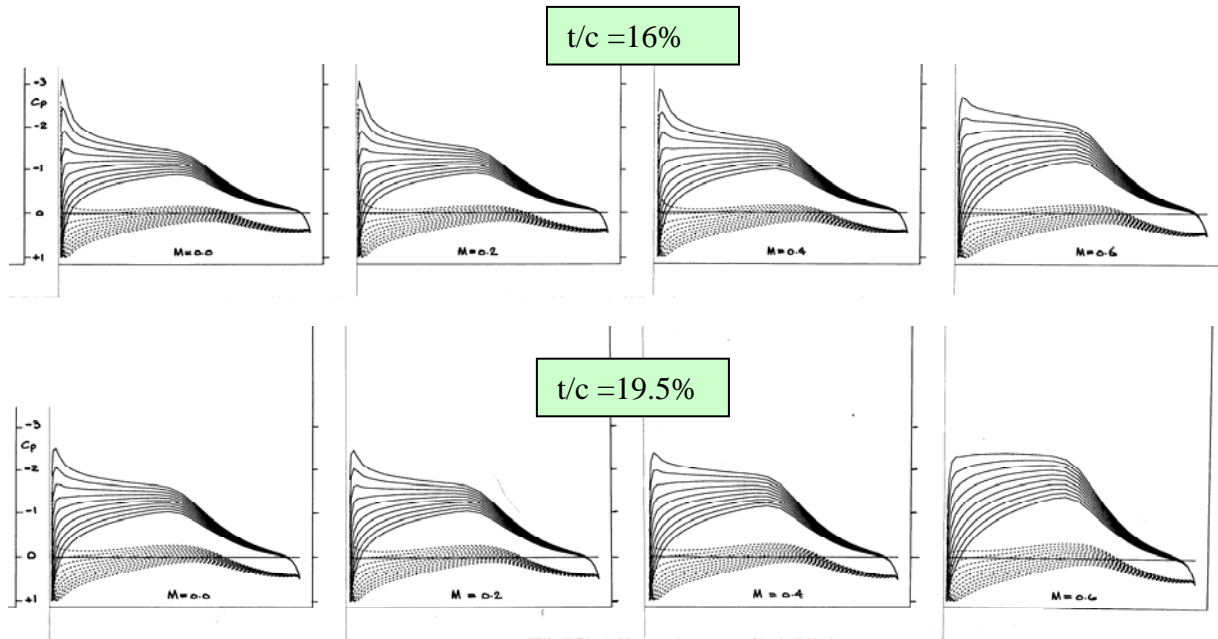
**FIG. 3.5 Cp DISTRIBUTIONS ON LAMINAR CAMBERED AEROFOILS , t/c = 16% & 19.5%,
AoA between -1° and 8° [1°], Mach 0.01, 0.2, 0.4, 0.6**
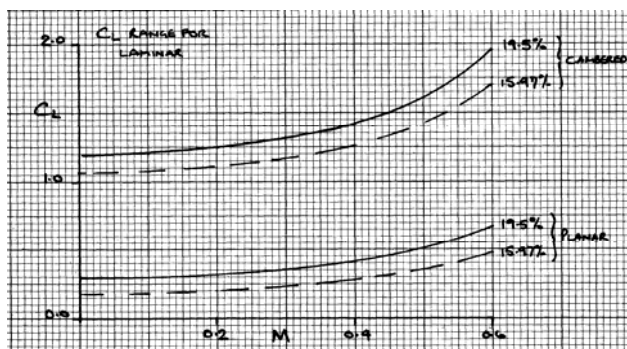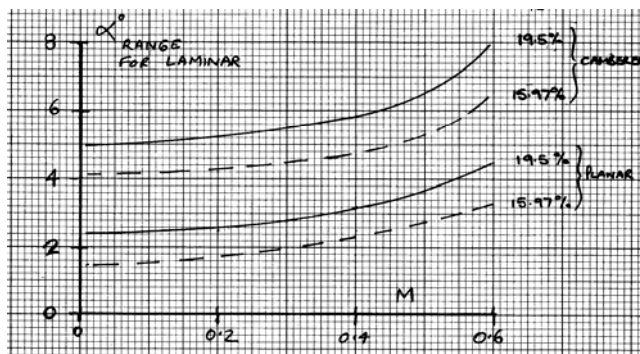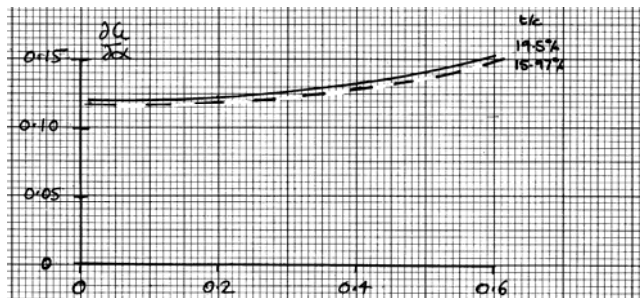
**FIG. 3.6 LAMINAR AEROFOIL
CAPABILITIES THROUGH MACH RANGE,
UNCAMBERED & CAMBERED**

Reference Configuration

AR wet = 5.5

Span = 200 ft

Sweep = 35 deg

X - Band Antenna

FIG. 4.1 REFERENCE HIGH AR SENSOR-CRAFT

(3D)

note

note

Identical frontal View

AT1

FT1

FT2
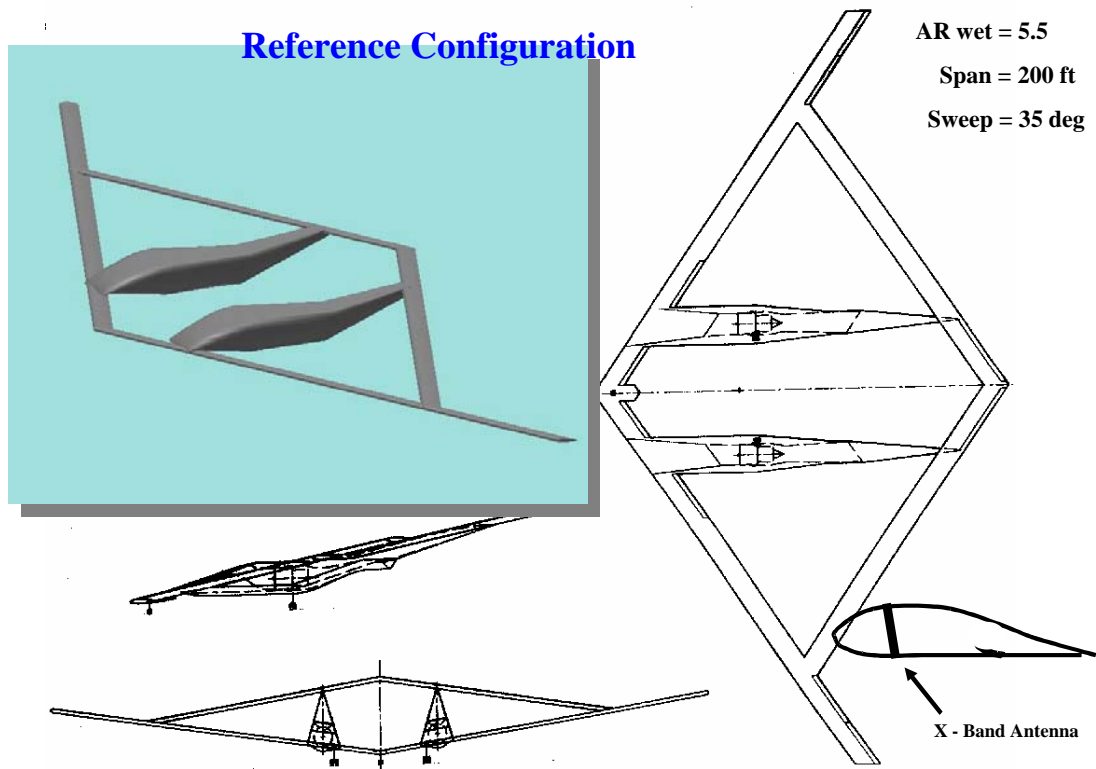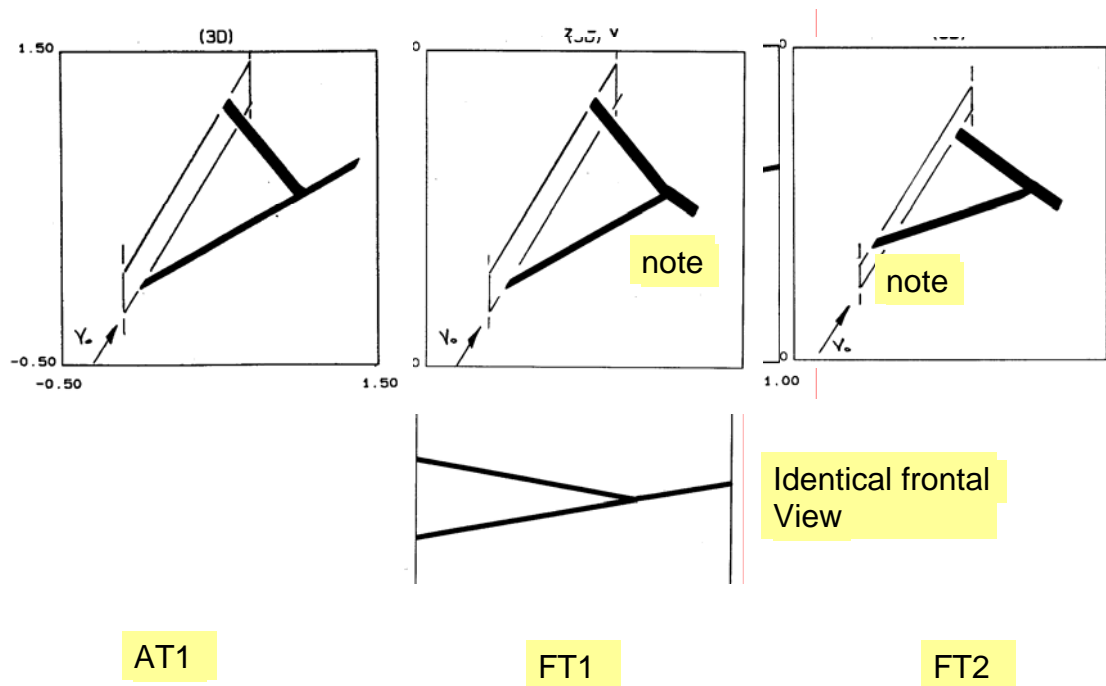
FIG. 4.2 THREE DIFFERENT SWEPT–TIP POSSIBILITIES, AT1, FT1,& FT2
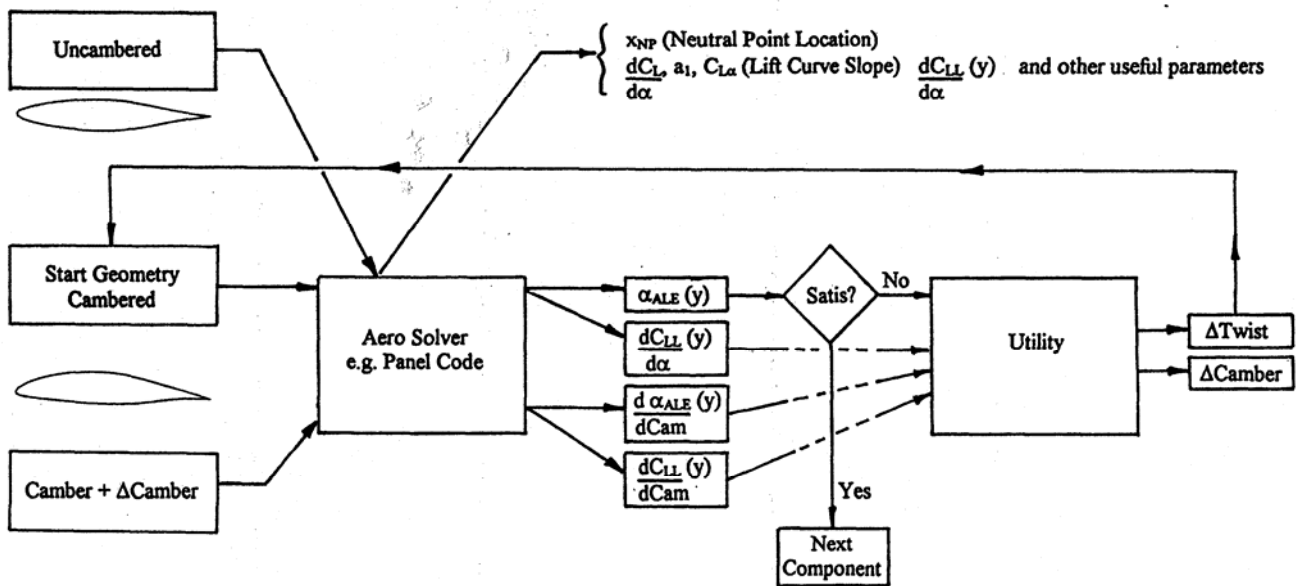
FIG. 4.3 DESIGN PROCEDURE
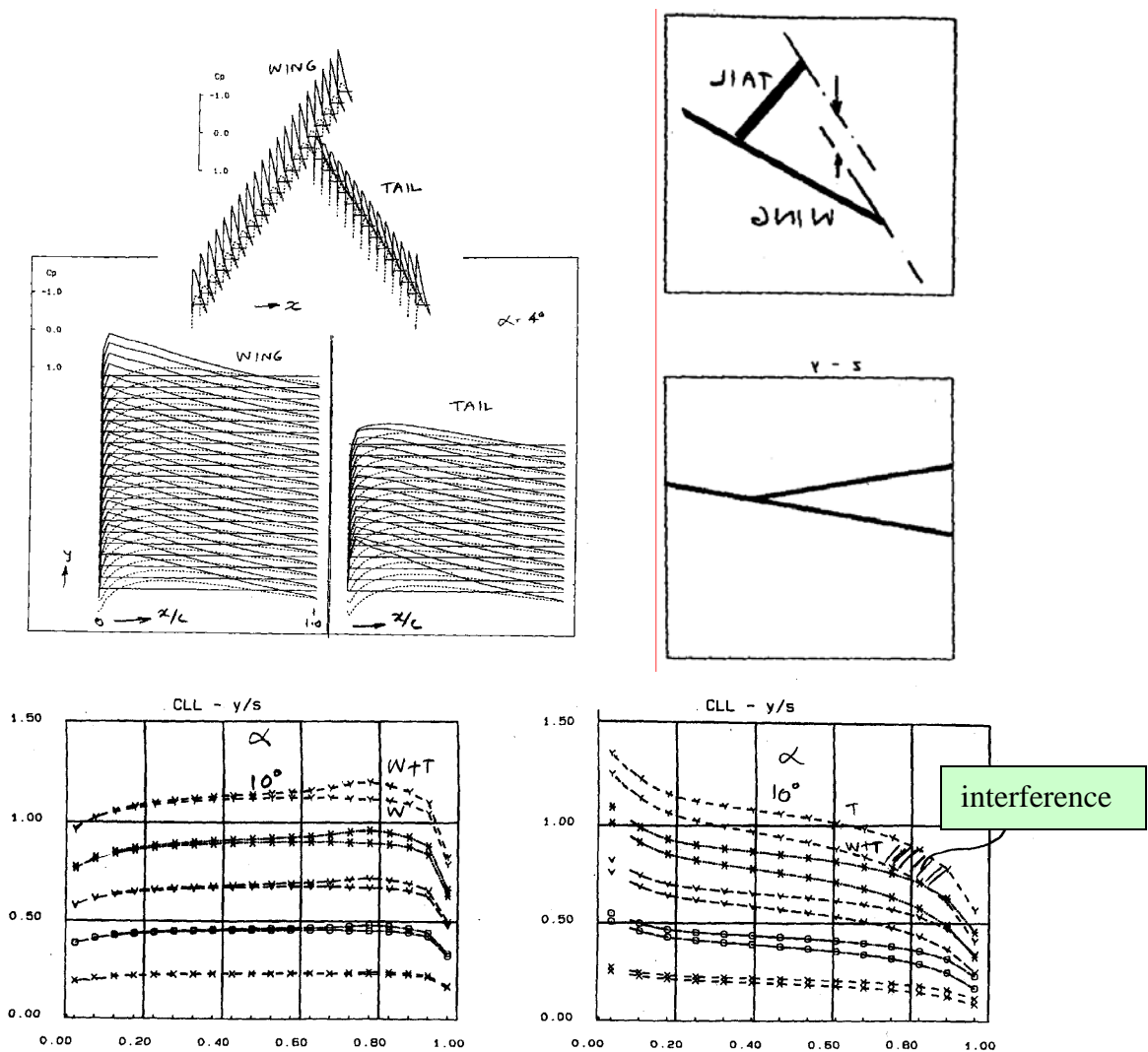
FIG. 6.1.1 CONCEPT AT1, SPANWISE LOADINGS WITH & WITHOUT MUTUAL INTERFERENCE

25

UNCAMBERED AEROFOIL CONFIGURATION

CAMBERED , DESIGNED AEROFOIL CONFIGURATION
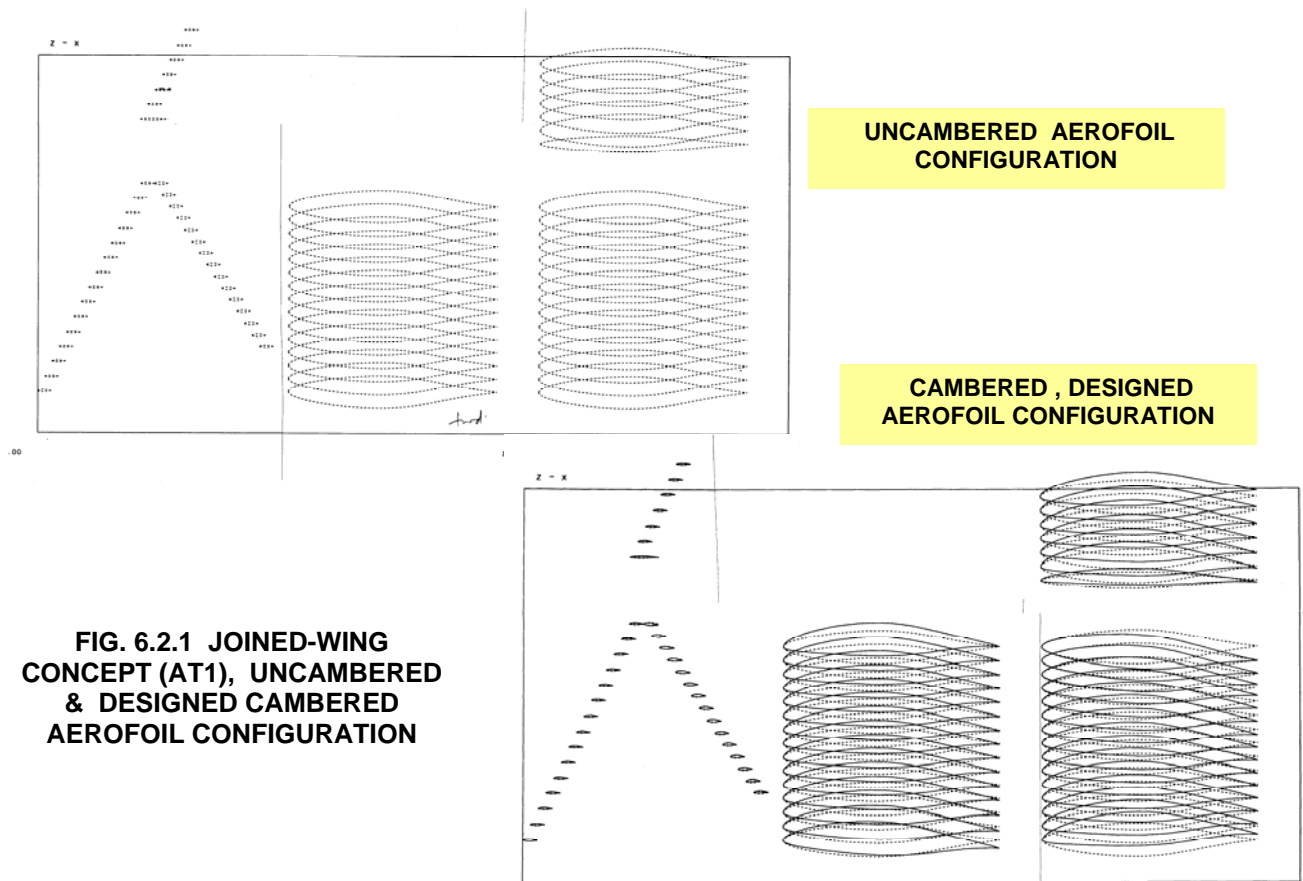
FIG. 6.2.1 JOINED-WING CONCEPT (AT1), UNCAMBERED & DESIGNED CAMBERED AEROFOIL CONFIGURATION
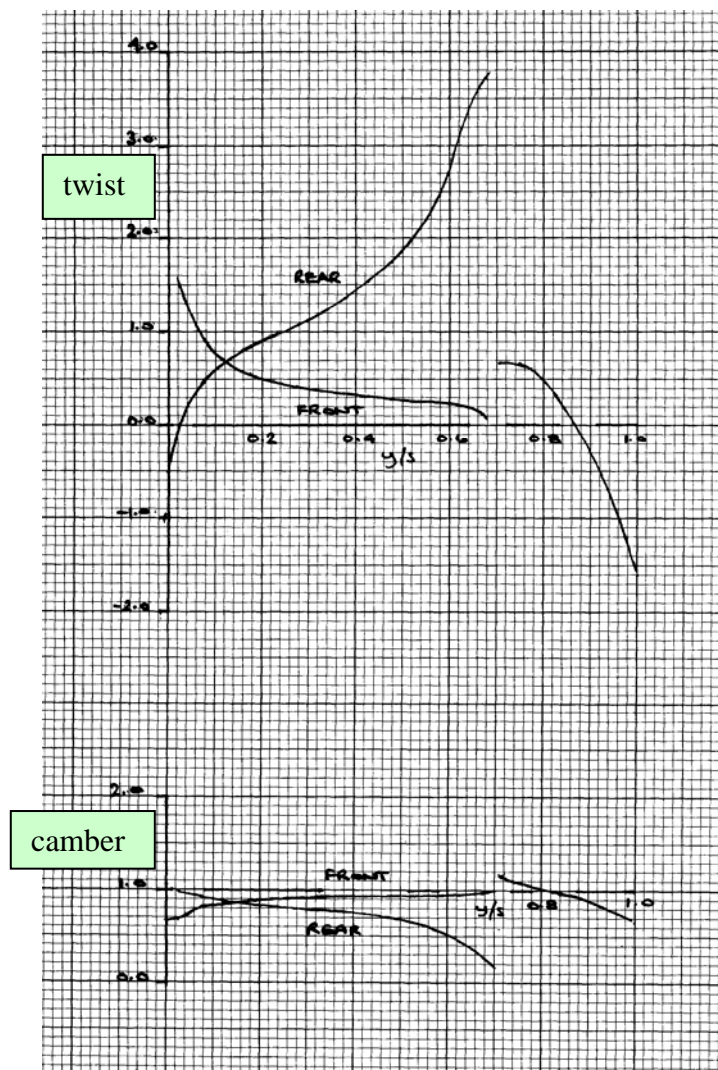
twist

camber

FIG. 6.2.2 CONFIG. AT1, DESIGNED TWIST & CAMBER DISTRIBUTIONS
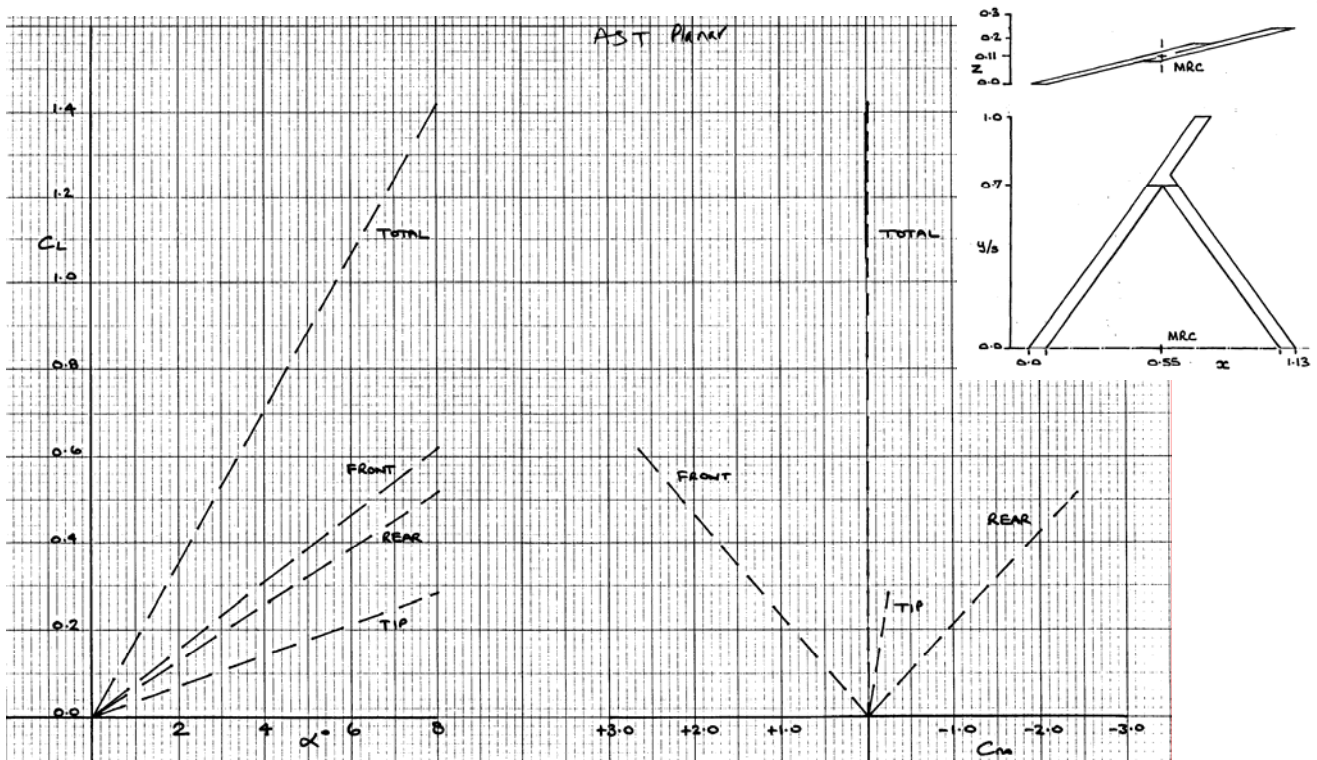
FIG. 6.2.3 CONFIG. AT1 UNCAMBERED, CL, Cm COMPONENT CONTRIBUTIONS, Mach 0.6
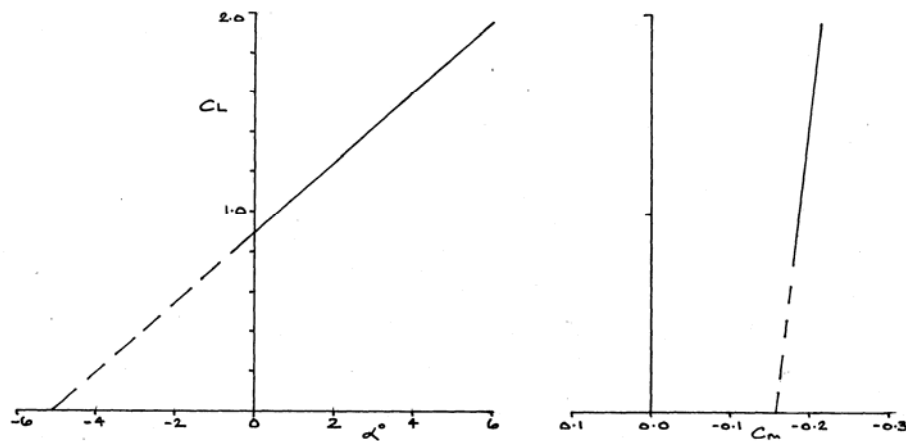
CL & Cm Reference
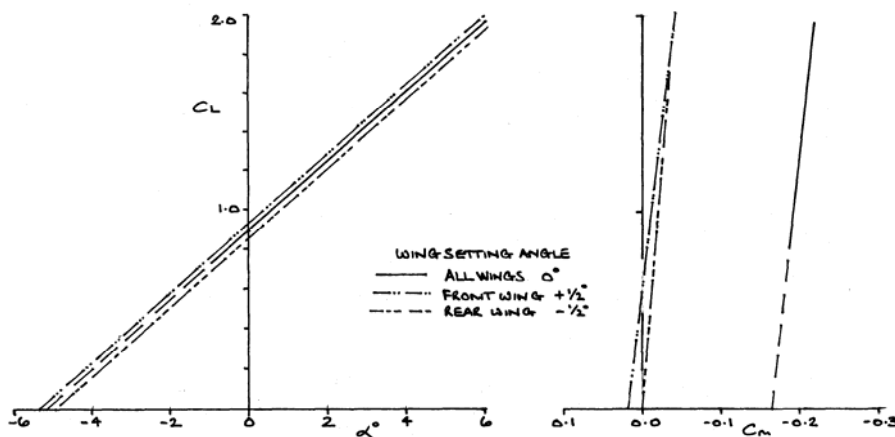
Control due to 0.5° setting angle changes

FIG. 6.2.4 CONFIG. AT1 DESIGNED, CL, Cm, CONTROL DUE TO 0.5° SETTING ANGLE CHANGES

CL=0.71

CL=0.9

uncambered

CL=1.07

cambered

CL=1.25

CL=1.42

CL=1.6
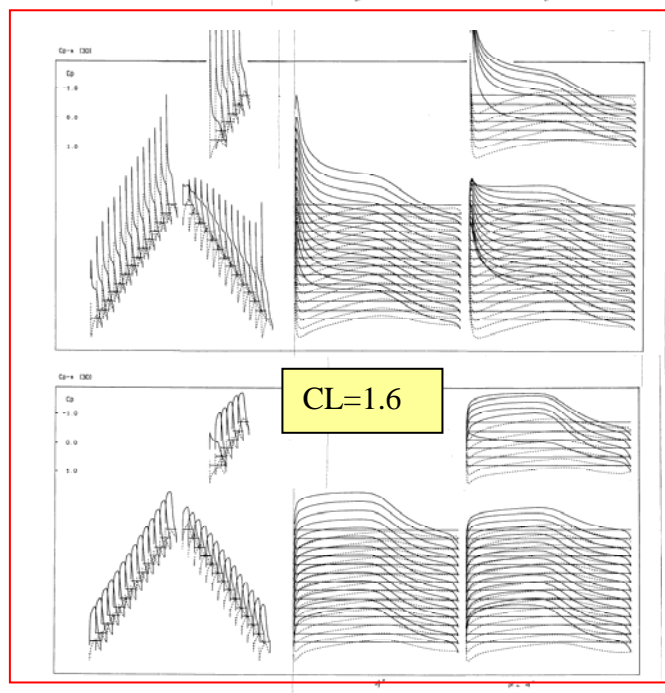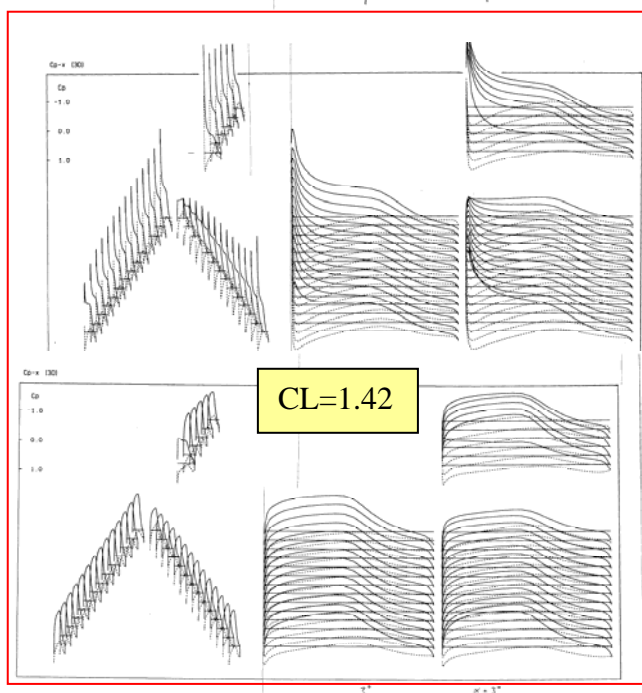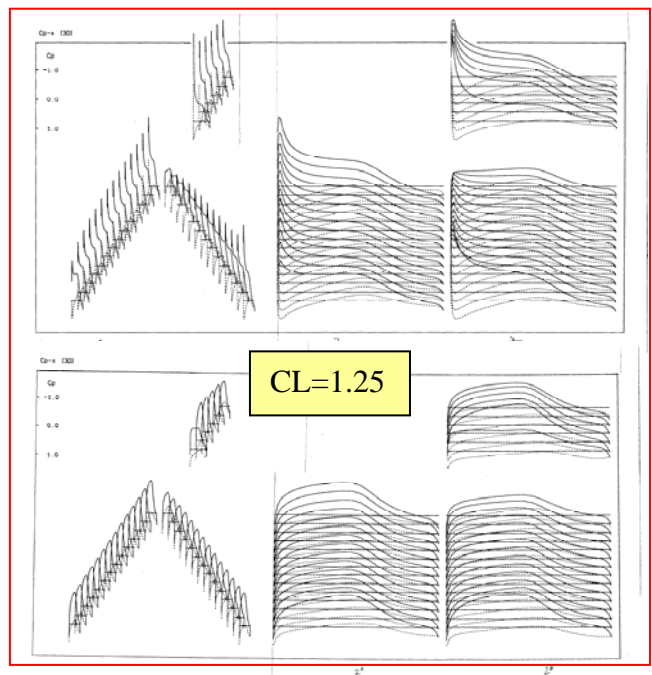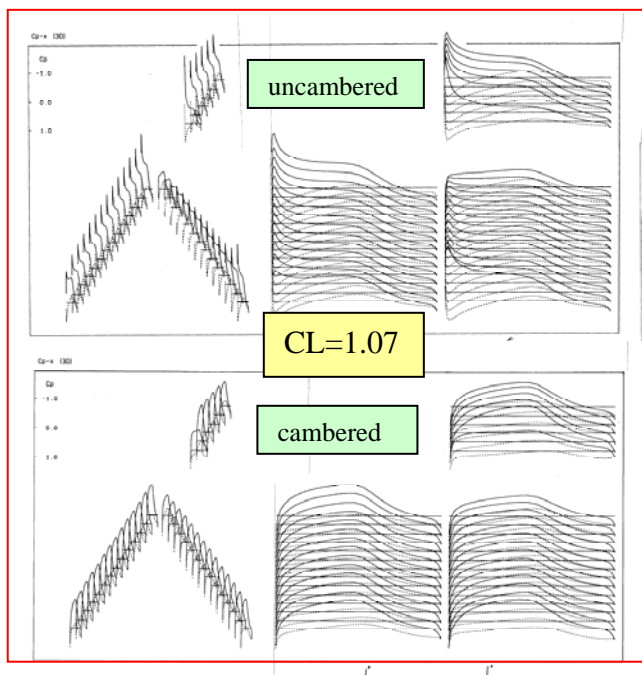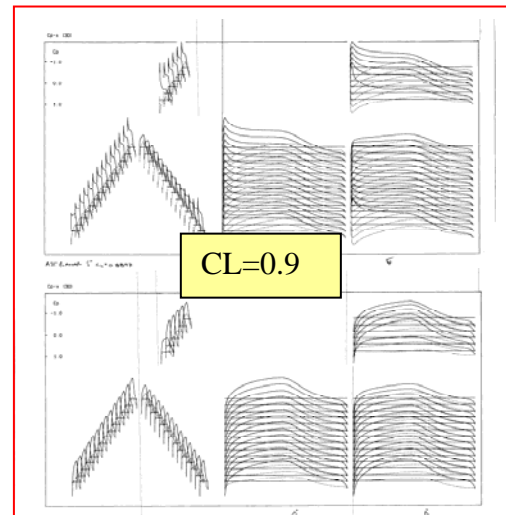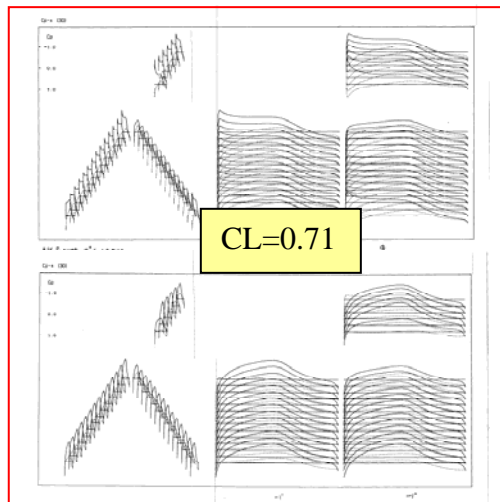
**FIG. 6.2.5   CONFIG. AT1, COMPARING UNCAMBERED & DESIGNED CAMBERED
AEROFOIL CONFIGURATION, Cp DISTRIBUTIONS AT EQUIVALENT CL, Mach 0.6**
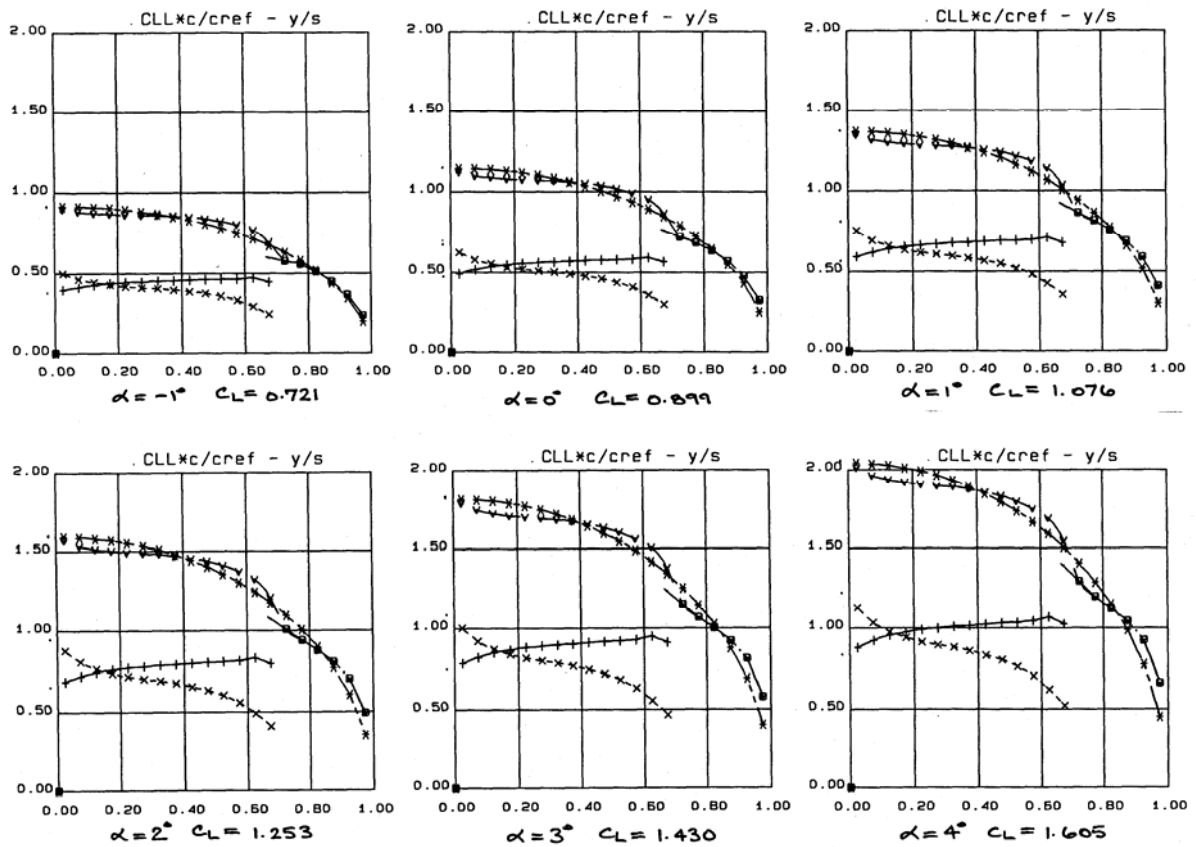
**FIG. 6.2.6   CONFIG. AT1, SPANWISE LOADINGS THROUGH AoA RANGE
DESIGNED CAMBERED AEROFOIL CONFIGURATION, Mach 0.6
(Total compared with elliptic)**
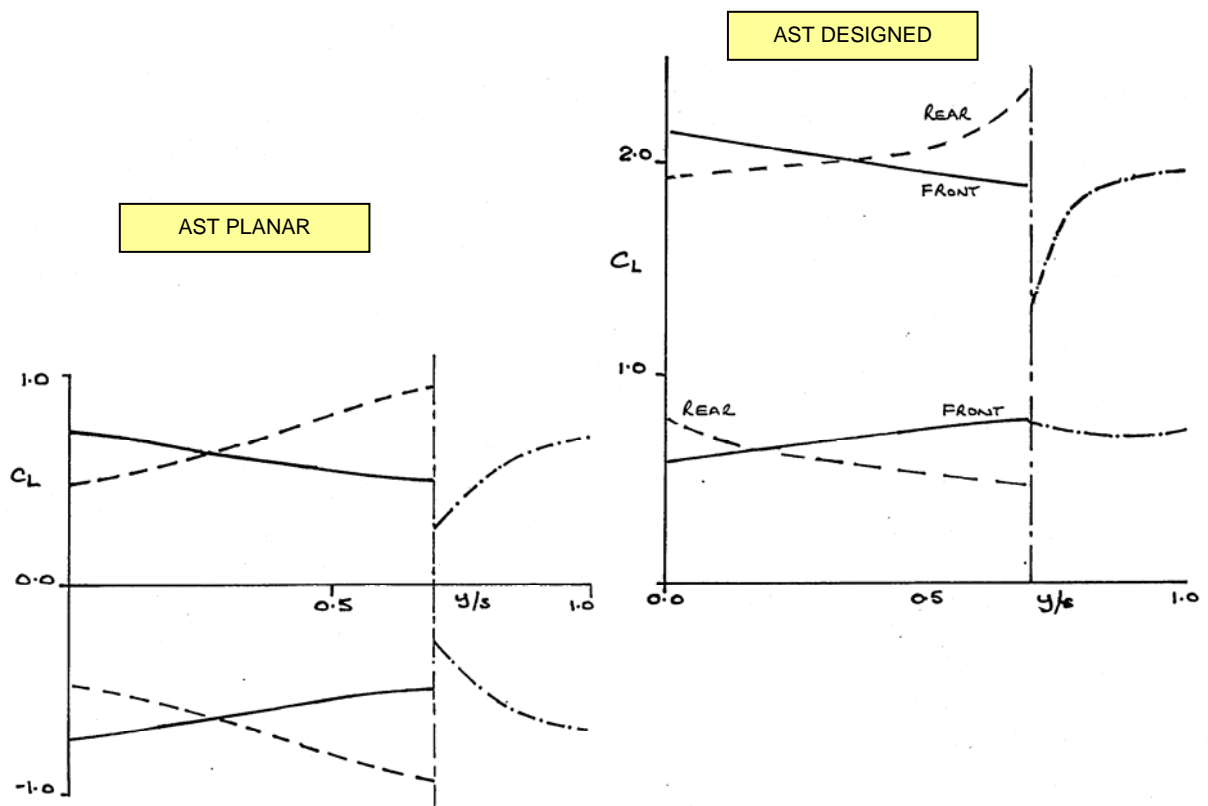
**FIG. 6.2.7   CONFIG. AT1, SPANWISE DUISTRIBUTION OF CL RANGES FOR
LAMINAR FLOW , PLANAR & DESIGNED WINGS, Mach 0.6**

29
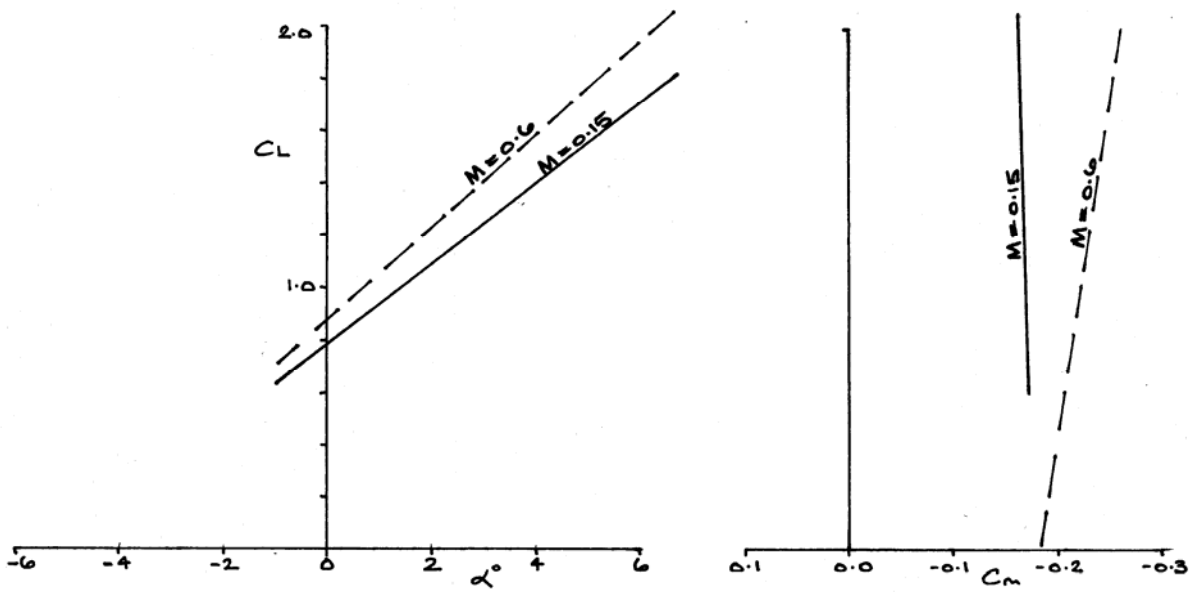
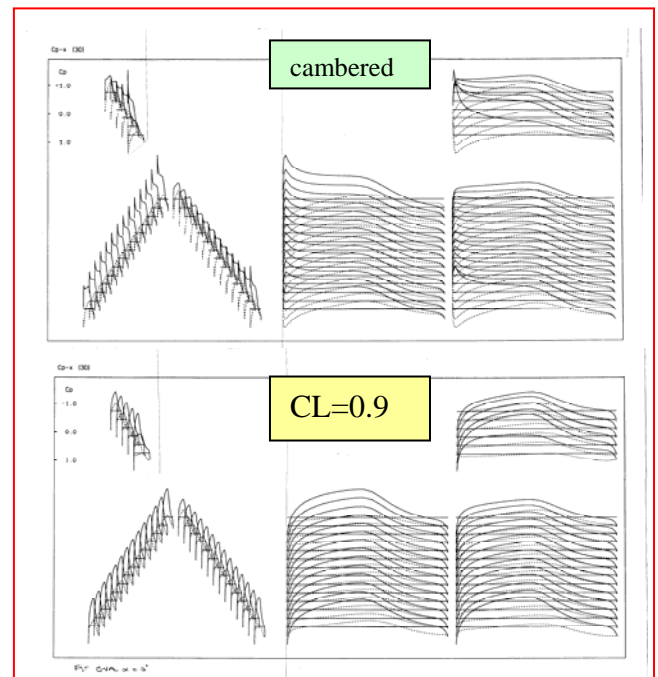FIG. 6.3.1 CONFIG. AT1, DESIGNED, CL, Cm and α VARIATIONS, Mach 0.15 & 0.6
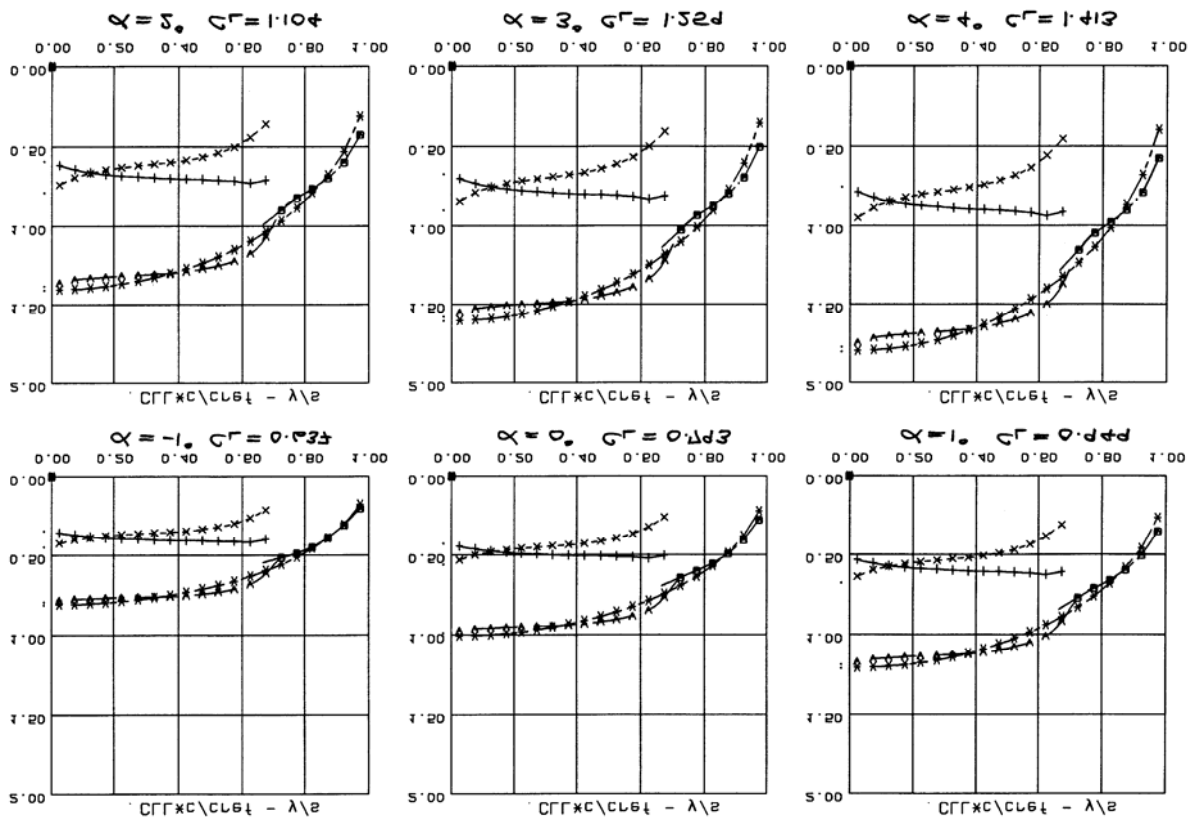
FIG. 6.3.2   CONFIG. AT1, SPANWISE LOADINGS THROUGH AoA RANGE, DESIGNED
CAMBERED AEROFOIL CONFIGURATION, Mach 0.15
(Total compared with elliptic)

30
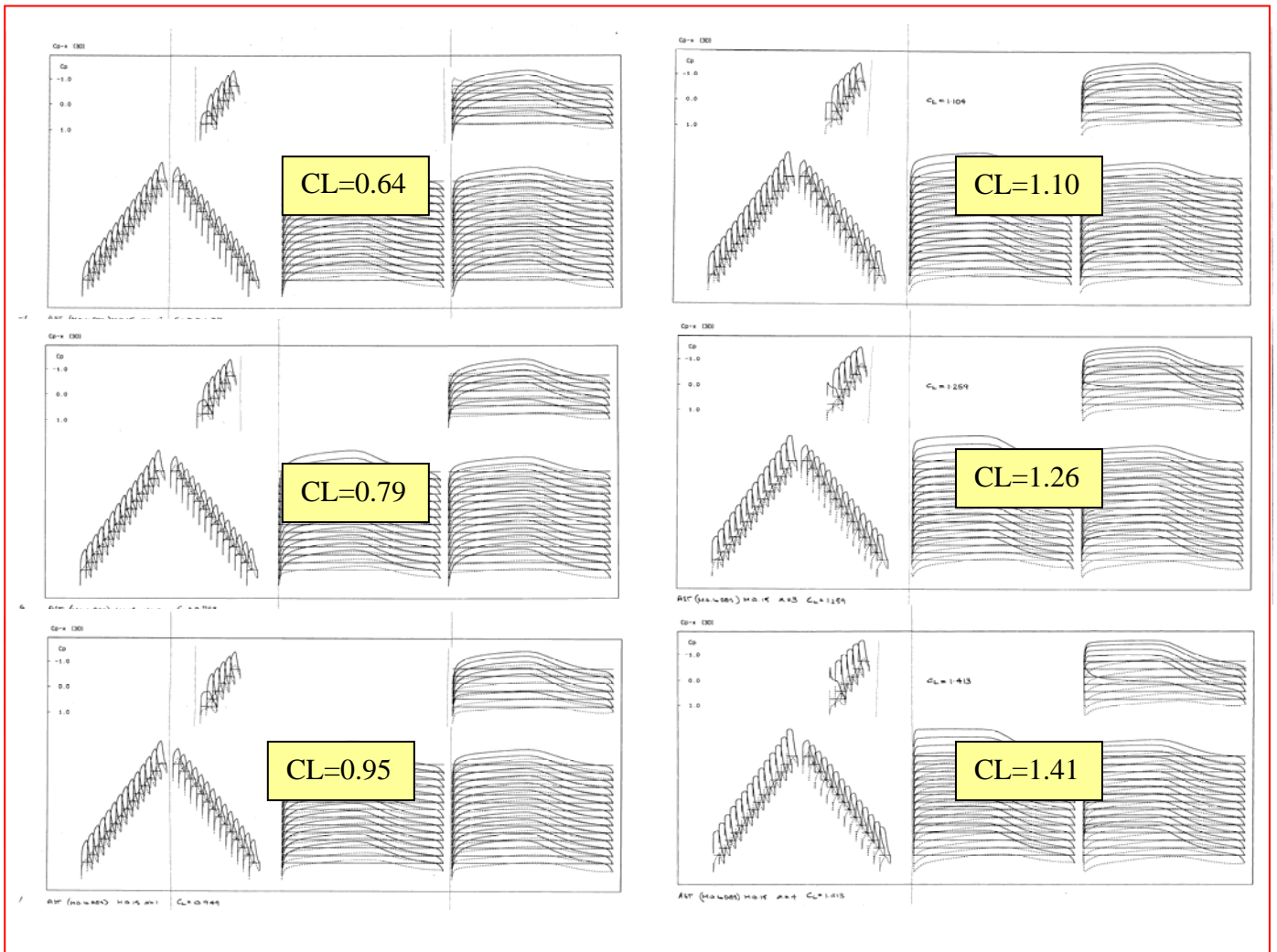
FIG. 6.3.3   CONFIG. AT1, DESIGNED, Cp DISTRIBUTIONS THROUGH AoA RANGE, Mach 0.15
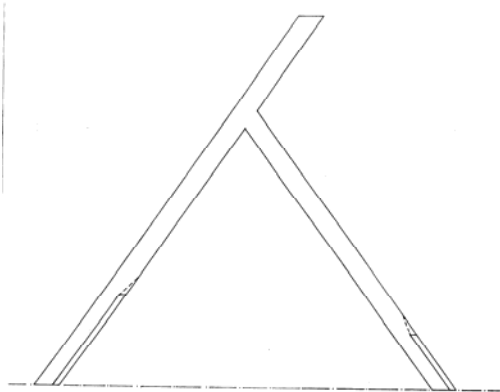
FIG. 6.4.1   CONFIG. AT1, DESIGNED, TEF LOCATION AND EFFECT ON C_m OF +/-5° TEF DEFLECTION, Mach 0.6
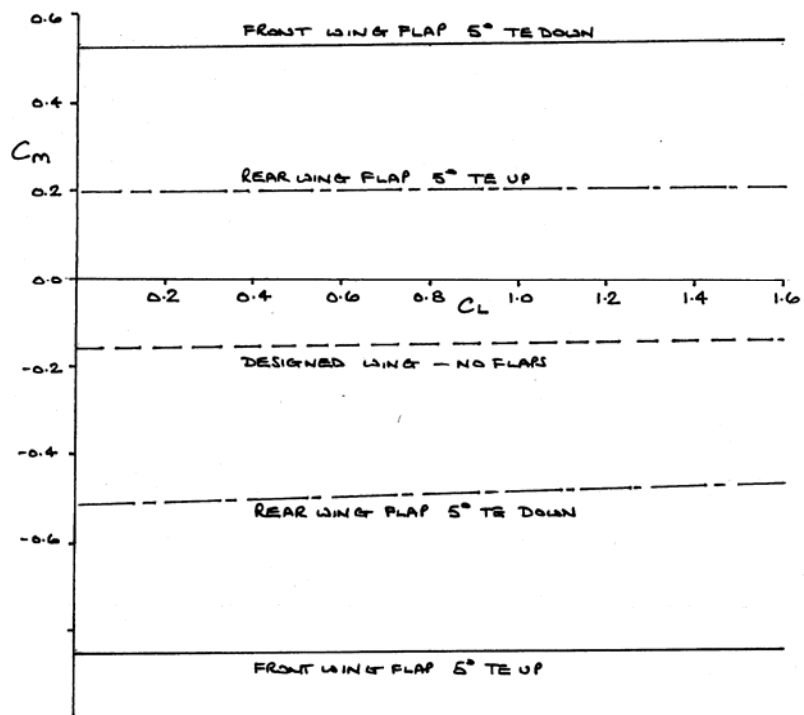
FIG. 6.4.2   CONFIG. AT1, TEF POWER, Mach 0.6
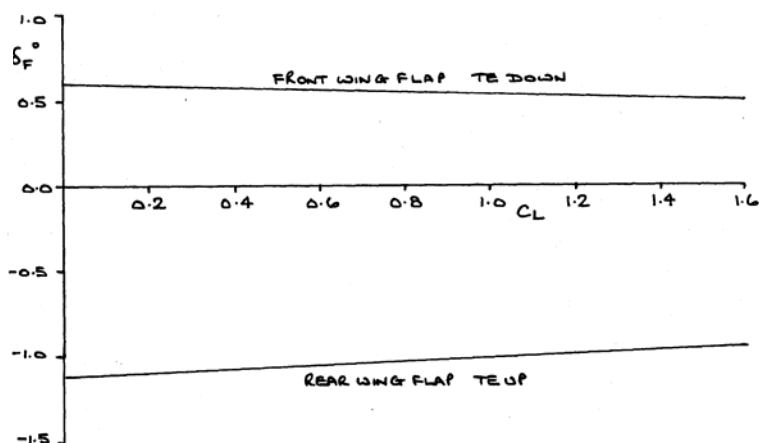
FIG. 6.4.3   CONFIG. AT1, DESIGNED, TEF DEFLECTION REQUIRED TO MAINTAIN C_L – AoA, C_m = 0.0, Mach 0.6
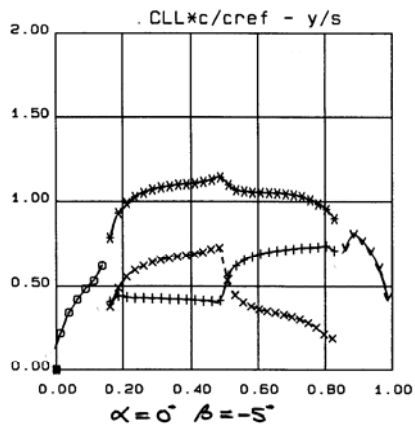
| Beta = -5° | Beta = 0° | Beta = 5° |
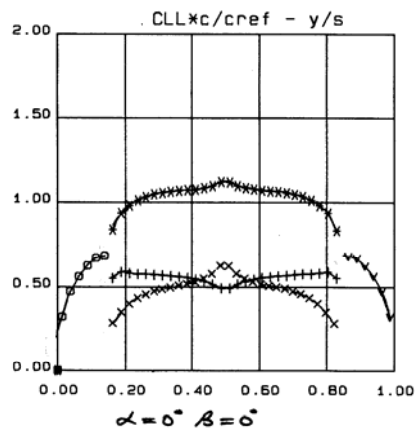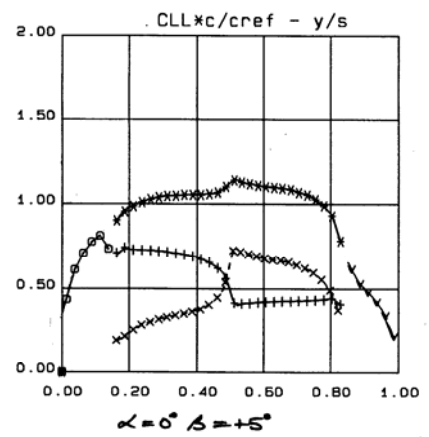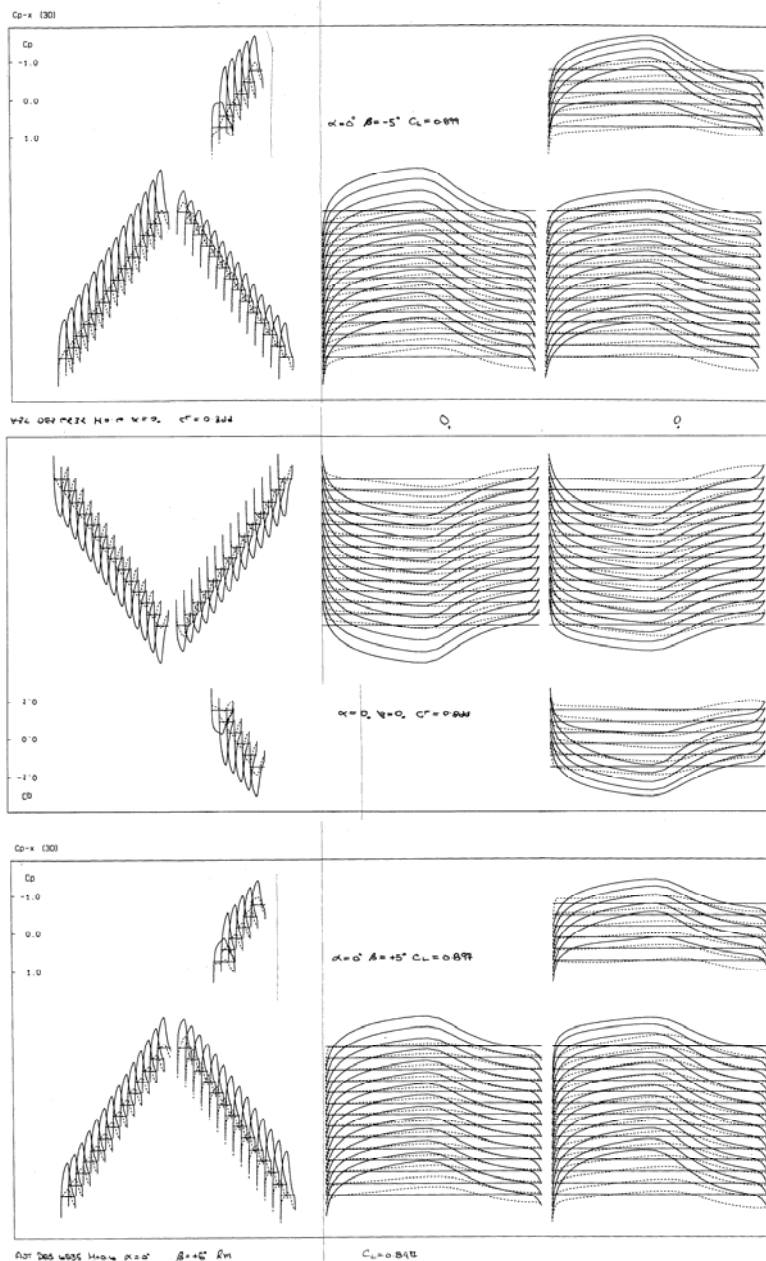
Beta = -5°

Beta = 0°

Beta = 5°

FIG. 6.5.1 ASYMMETRIC CASE, EFFECT OF SIDESLIP, SPANWISE LOADINGS
& Cp DISTRIBUTIONS, AoA 0°, CL = 0.9, Mach 0.6
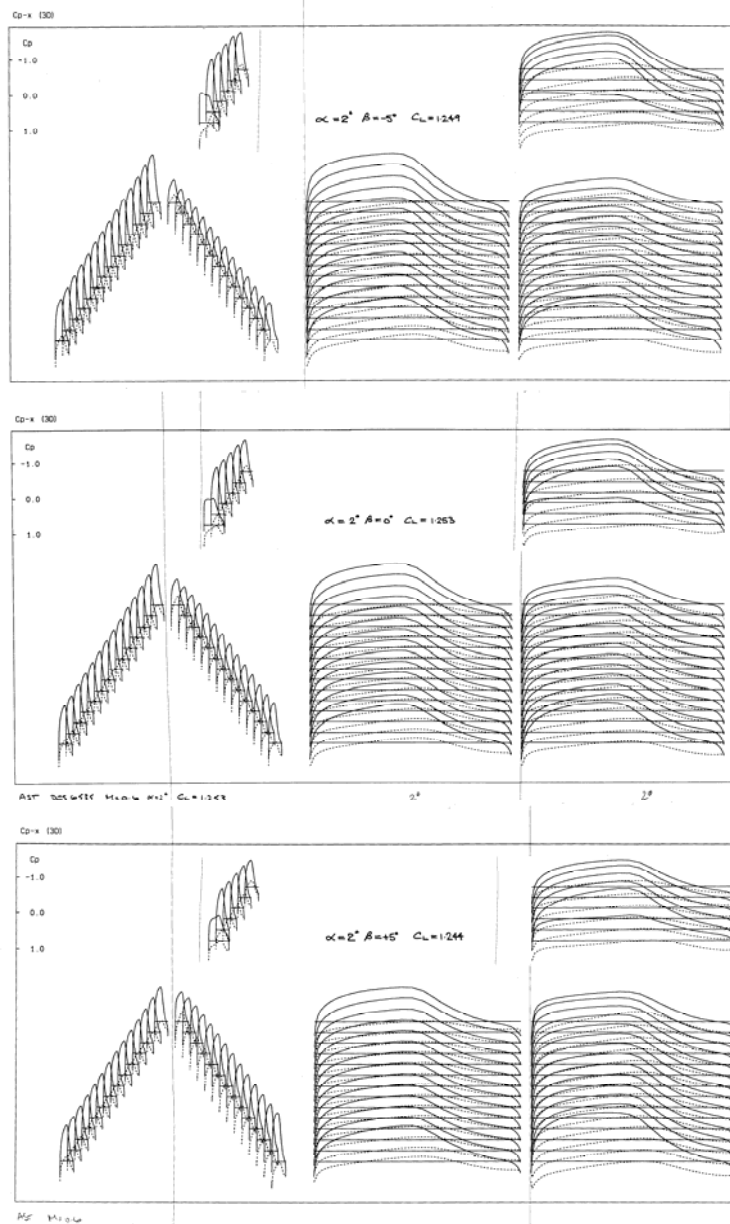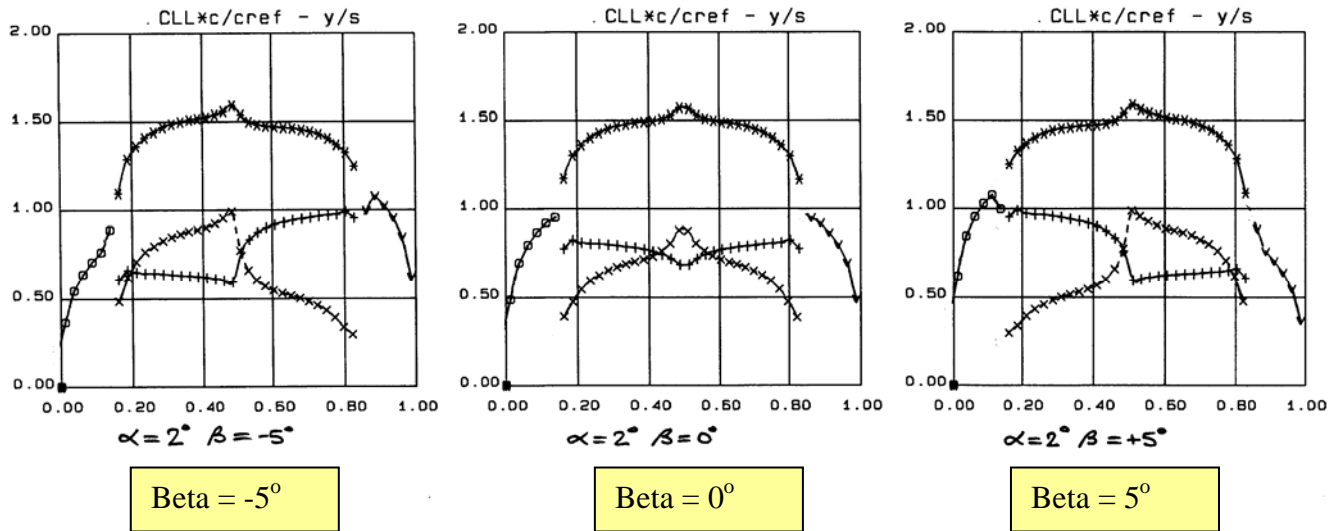
FIG. 6.5.2 ASYMMETRIC CASE, EFFECT OF SIDESLIP, SPANWISE LOADINGS
& Cp DISTRIBUTIONS, AoA $2°$, CL = 1.25, Mach 0.6

34
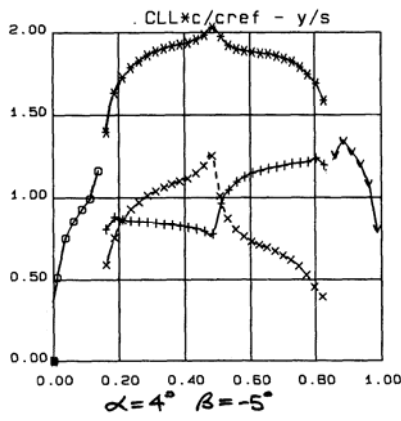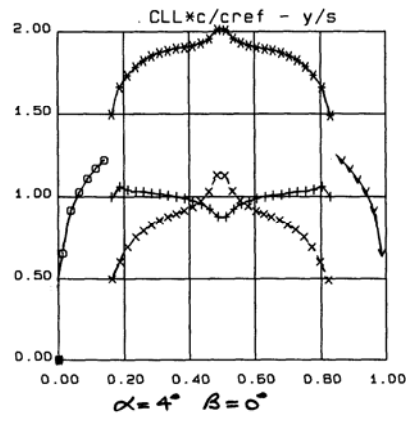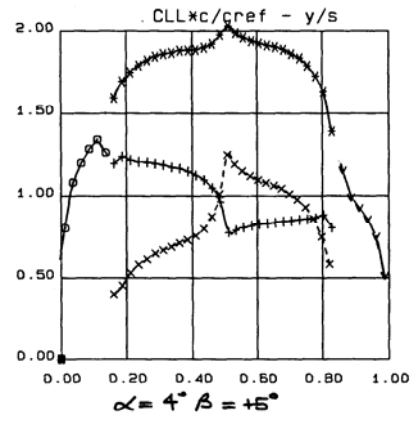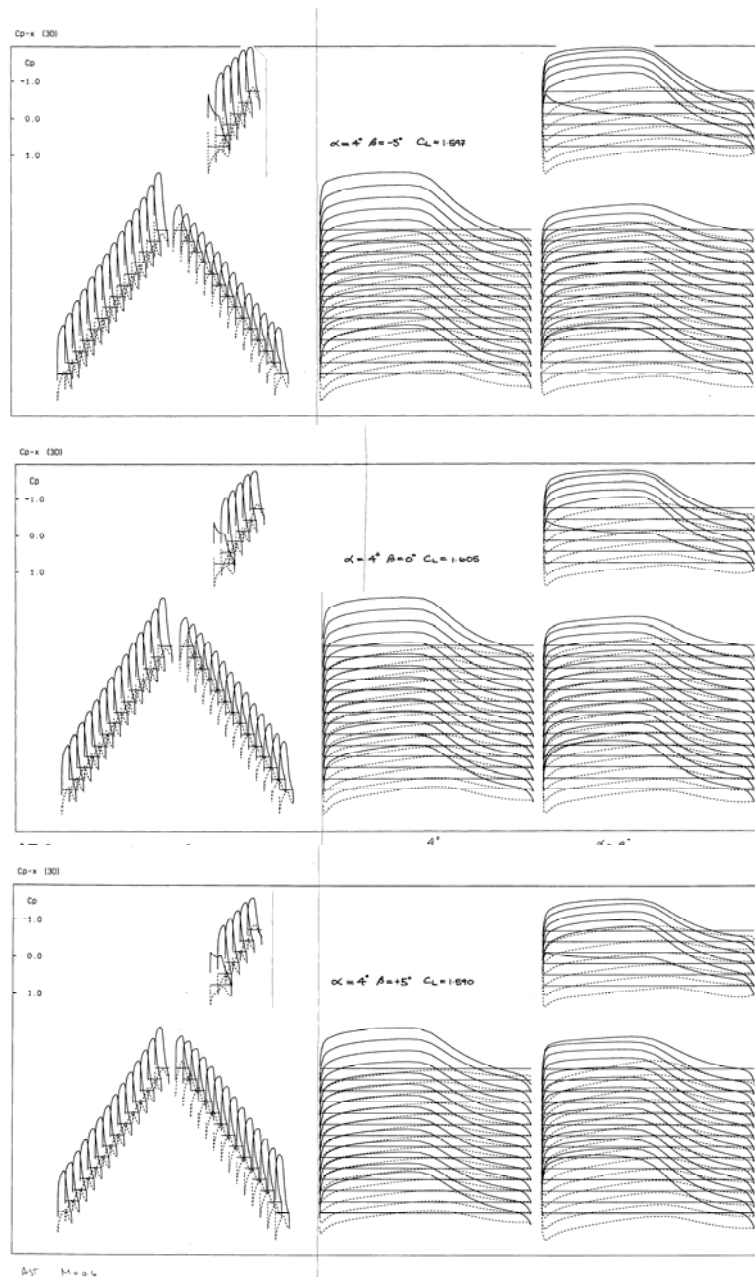
Beta = -5°   Beta = 0°   Beta = 5°

Beta = -5°

Beta = 0°

Beta = 5°

FIG. 6.5.3 ASYMMETRIC CASE, EFFECT OF SIDESLIP, SPANWISE LOADINGS & Cp DISTRIBUTIONS, AoA 4°, CL = 1.6, Mach 0.6
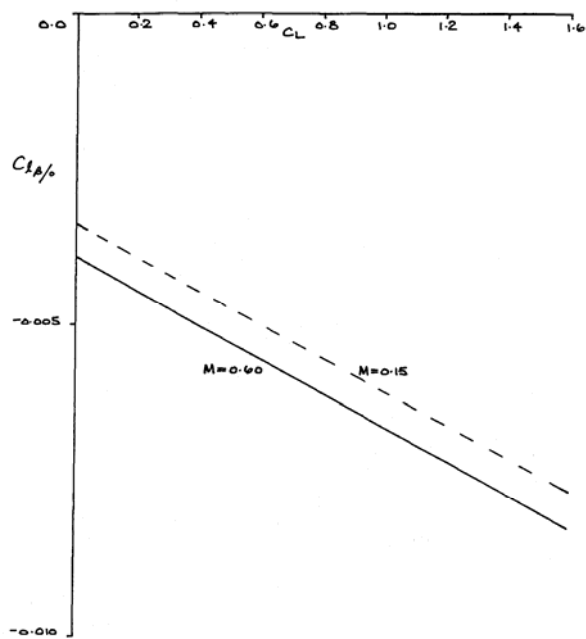
FIG. 6.6.1 CONFIG. AT1, VARIATION OF ROLLING MOMENT DUE TO SIDESLIP WITH CL, Mach 0.6 & 0.15
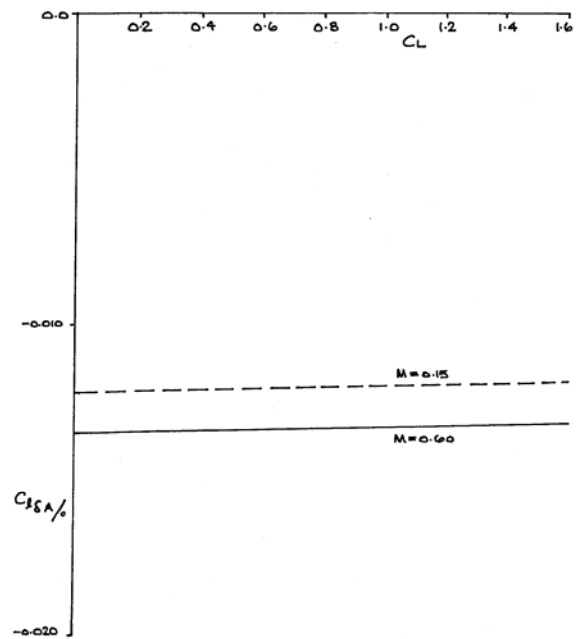
FIG. 6.6.3 CONFIG. AT1, ROLL CONTROL POWER VARIATION WITH CL, Mach 0.6 & 0.15
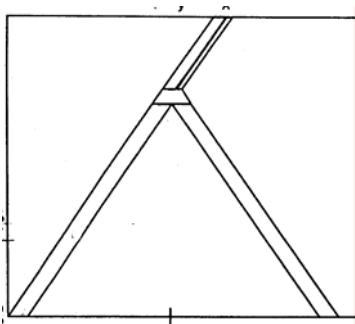
FIG. 6.6.2 CONFIG. AT1, LOCATION & EXTENT OF AILERON
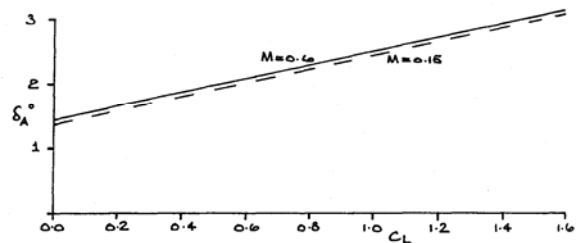
FIG. 6.6.4 CONFIG. AT1, VARIATION OF AILERON REQUIREMENT (for ZERO ROLL at 5 deg SIDESLIP) WITH CL, Mach 0.6 & 0.15
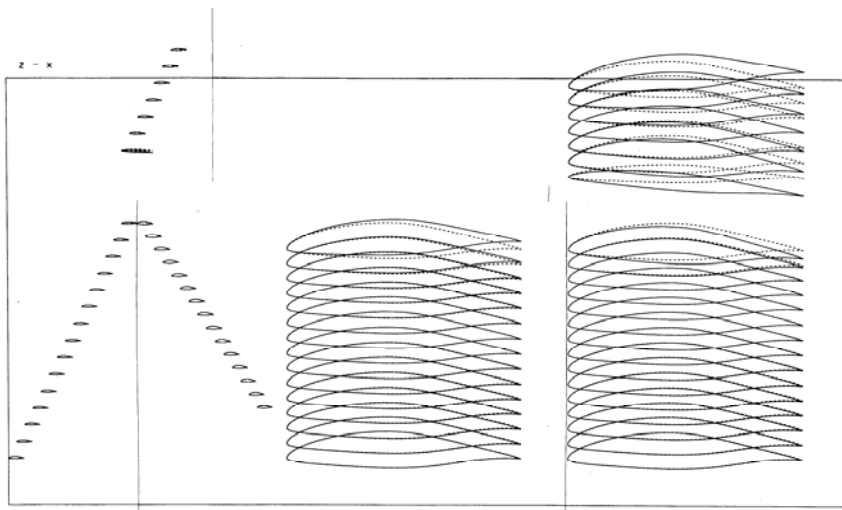
FIG. 6.7.1 CONFIG. AT1 USING TWIST ONLY ON REFERENCE CAMBER

FIG. 6.7.2 CONFIG. AT1 TWIST DISTRIBUTION REQUIRED, REFERENCE CAMBER
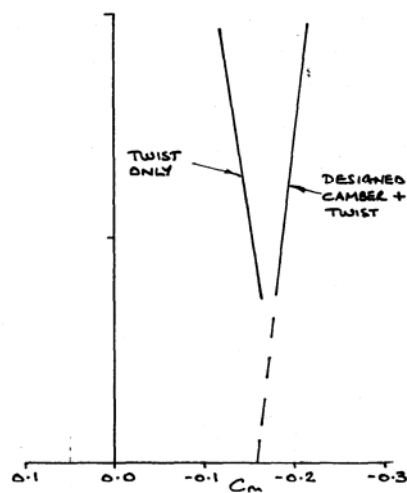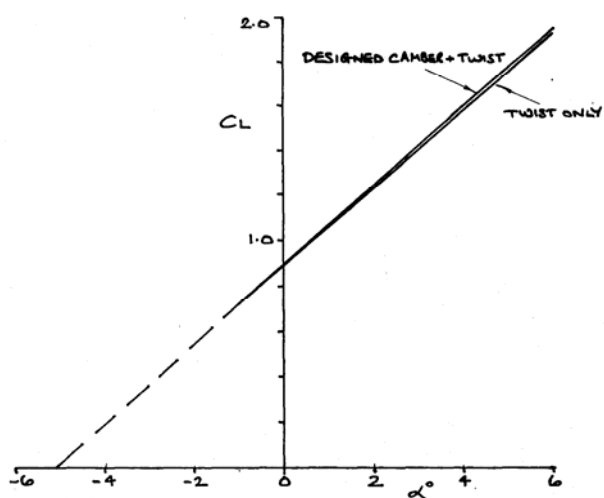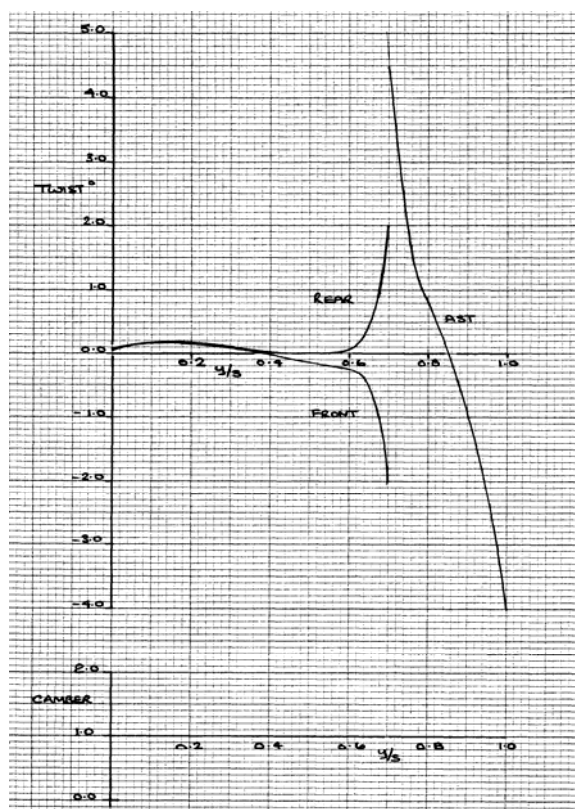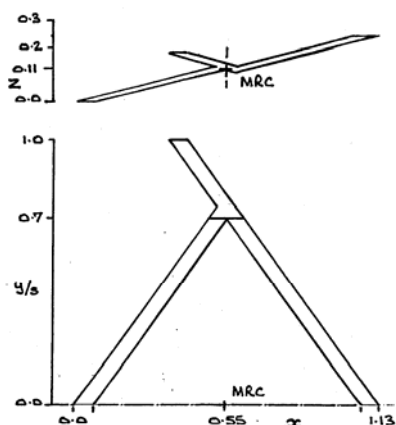
FIG. 6.7.3 CONFIG. AT1 DESIGNED AND TWIST ONLY DESIGN, CL, Cm and α VARIATIONS, Mach 0.6
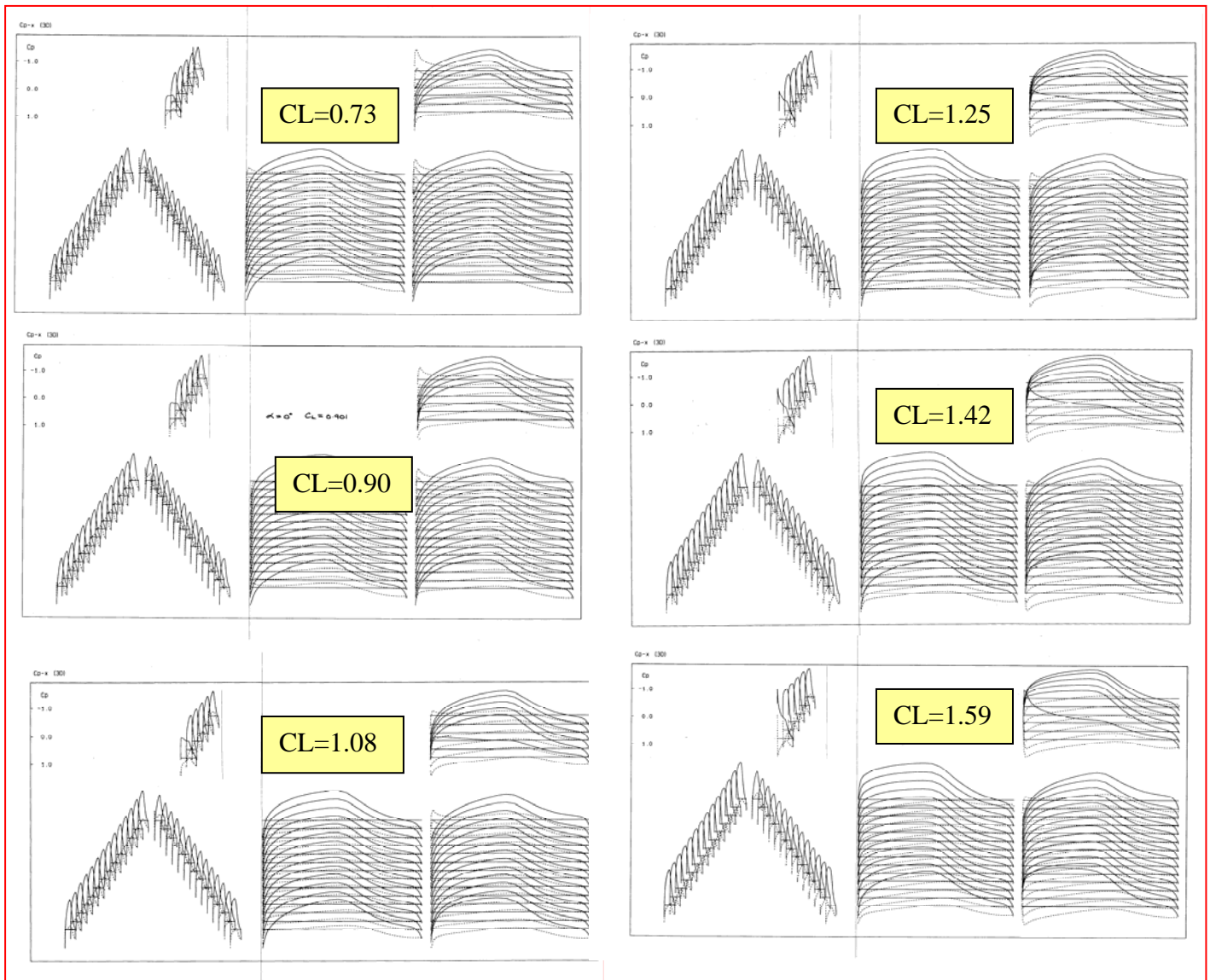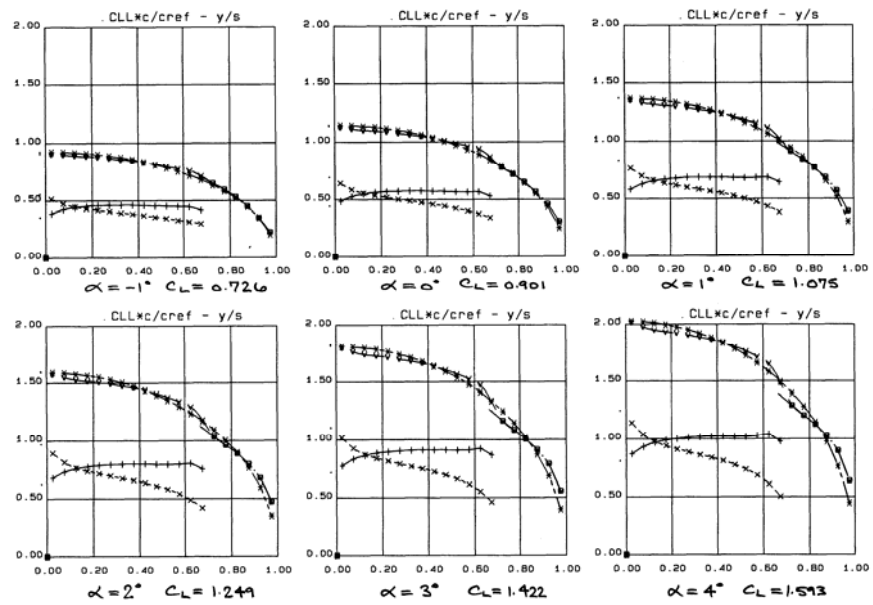
**FIG. 6.7.4 CONFIG. AT1 REFERENCE CAMBER AND TWIST ONLY DESIGN,
SPANWISE LOADINGS & CP DISTRIBUTIONS, Mach 0.6**

38
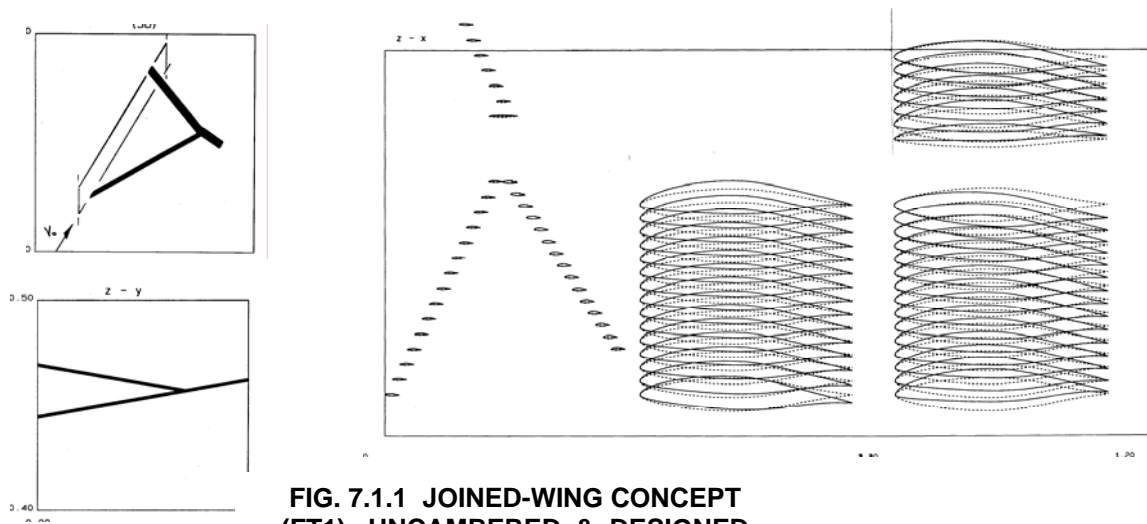
FIG. 7.1.1 JOINED-WING CONCEPT (FT1), UNCAMBERED & DESIGNED CAMBERED AEROFOIL CONFIGURATION
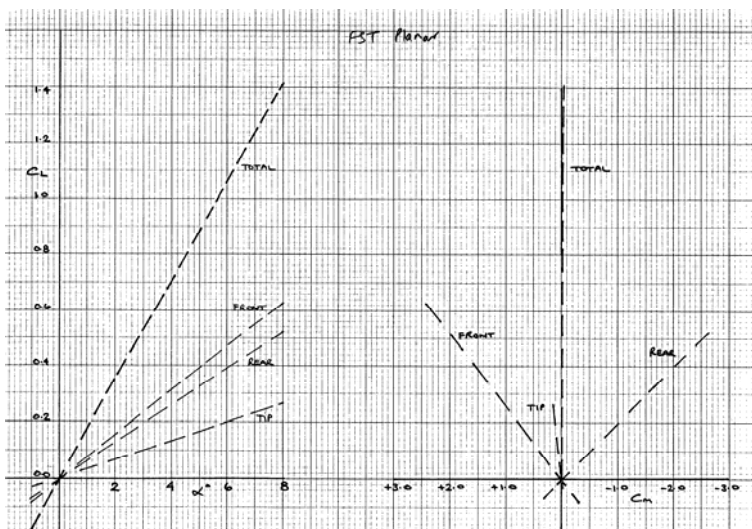
FIG. 7.1.3 CONFIG. FT1, UNCAMBERED, CL, Cm COMPONENT CONTRIBUTIONS, Mach 0.6
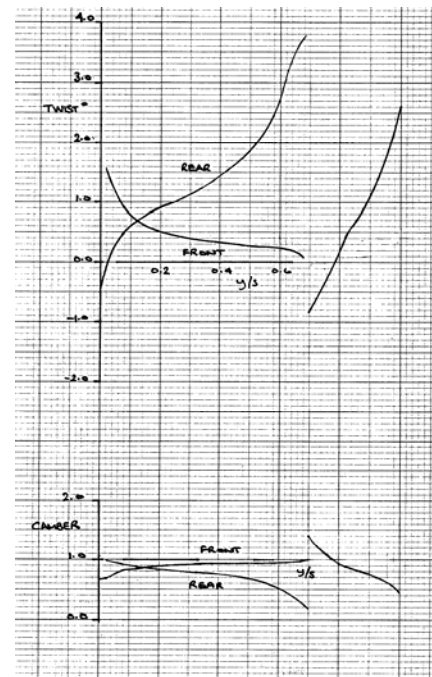
FIG. 7.1.2 CONFIG. FT1, DESIGNED TWIST & CAMBER DISTRIBUTIONS
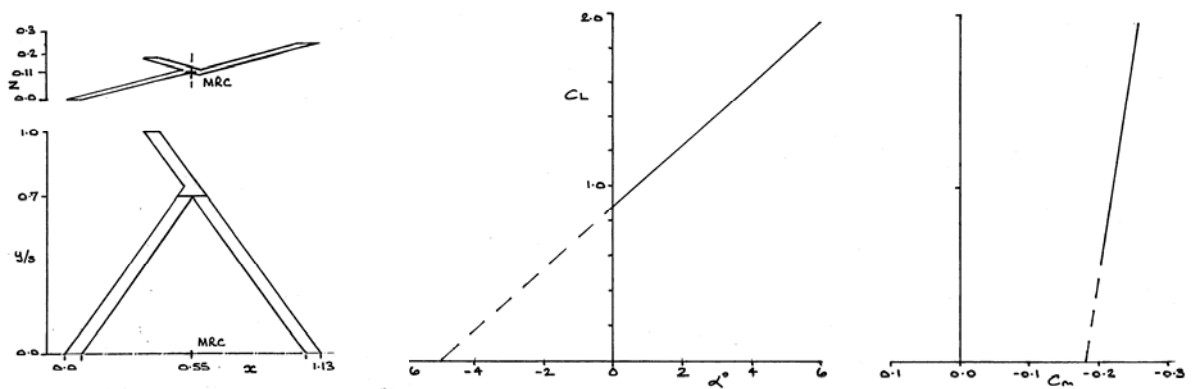
FIG. 7.1.4 FT1 DESIGNED, CL, Cm and α VARIATIONS, Mach 0.6

uncambered

cambered

CL=0.71

CL=0.9

CL=1.06

CL=1.24

CL=1.42

CL=1.59
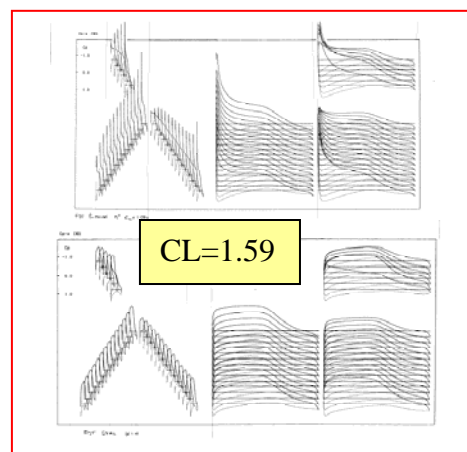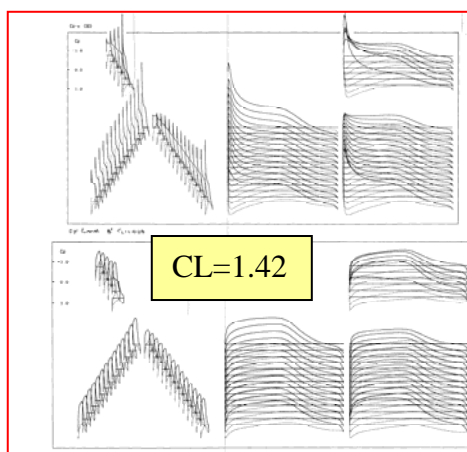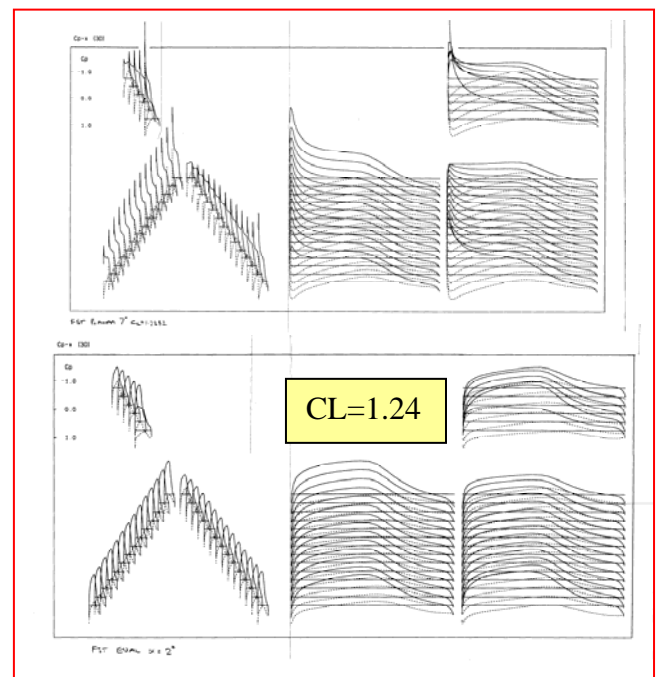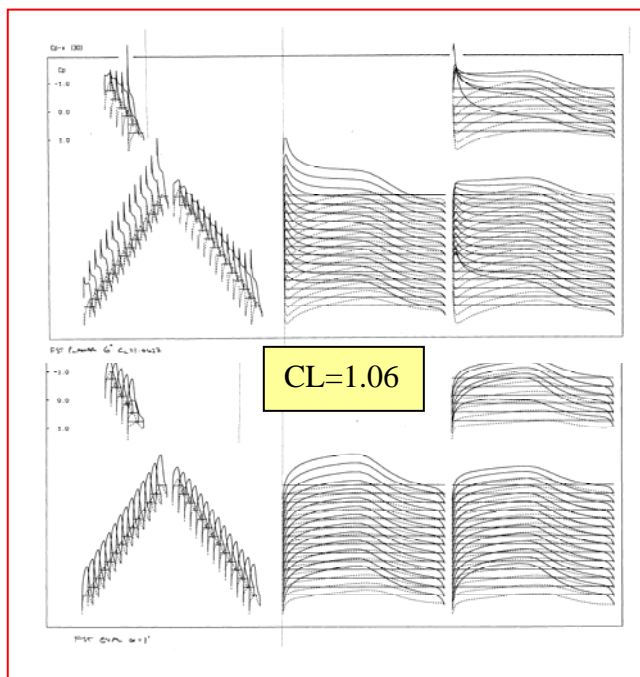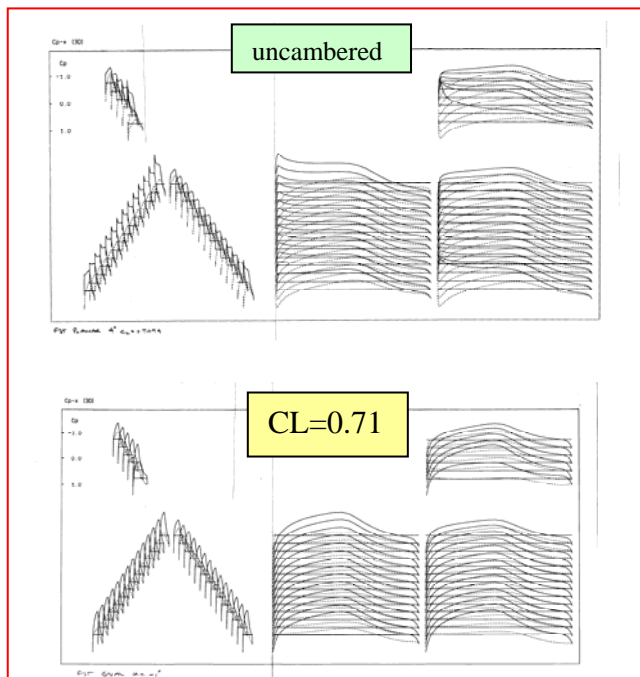
**FIG. 7.1.5 CONFIG. FT1, COMPARING UNCAMBERED & DESIGNED CAMBERED AEROFOIL
CONFIGURATION, Cp DISTRIBUTIONS AT EQUIVALENT CL, Mach 0.6**
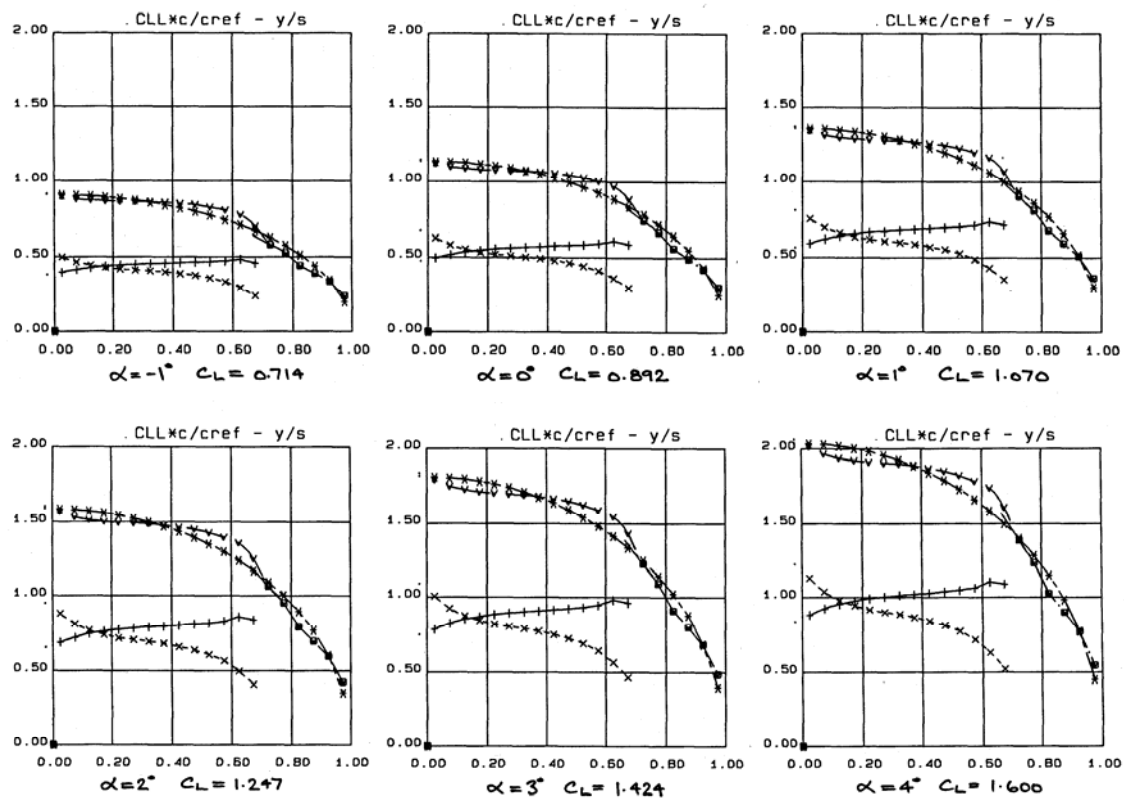
FIG. 7.1.6   CONFIG.FT1, SPANWISE LOADINGS THROUGH AoA RANGE
DESIGNED CAMBERED AEROFOIL CONFIGURATION
(Total compared with elliptic)
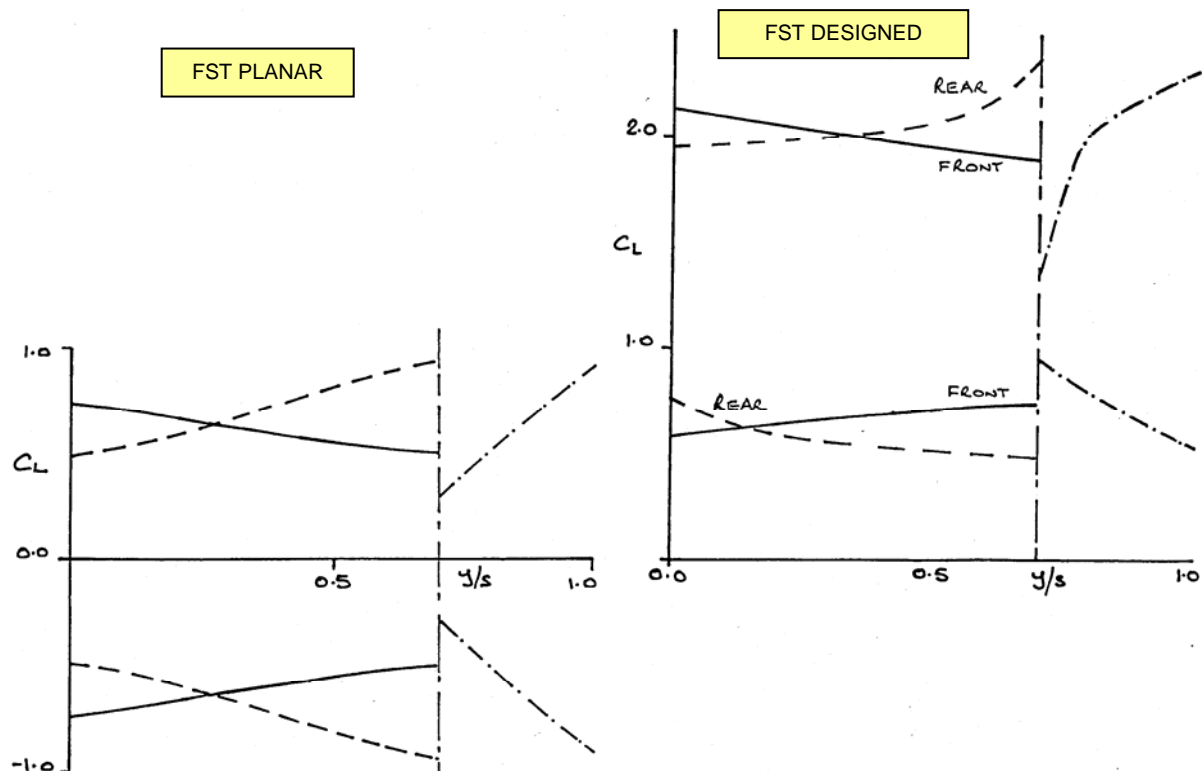
FIG. 7.1.7   CONFIG. FT1, LAMINAR FLOW DESIGN RANGES
ALONG SPAN, PLANAR & DESIGNED WINGS, Mach 0.6

41
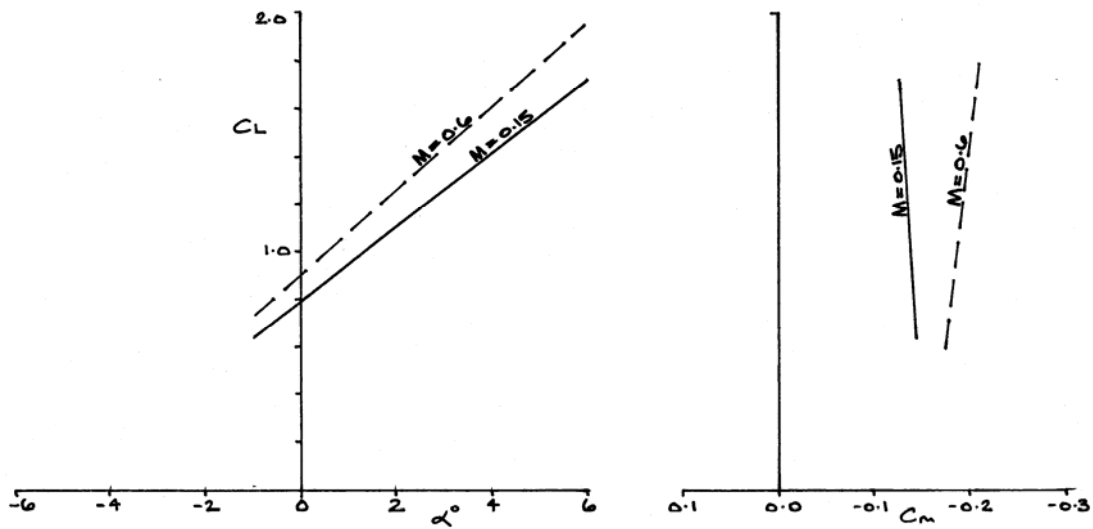
FIG. 7.2.1 CONFIG. FT1, DESIGNED, CL, Cm and α VARIATIONS, Mach 0.15 & 0.6
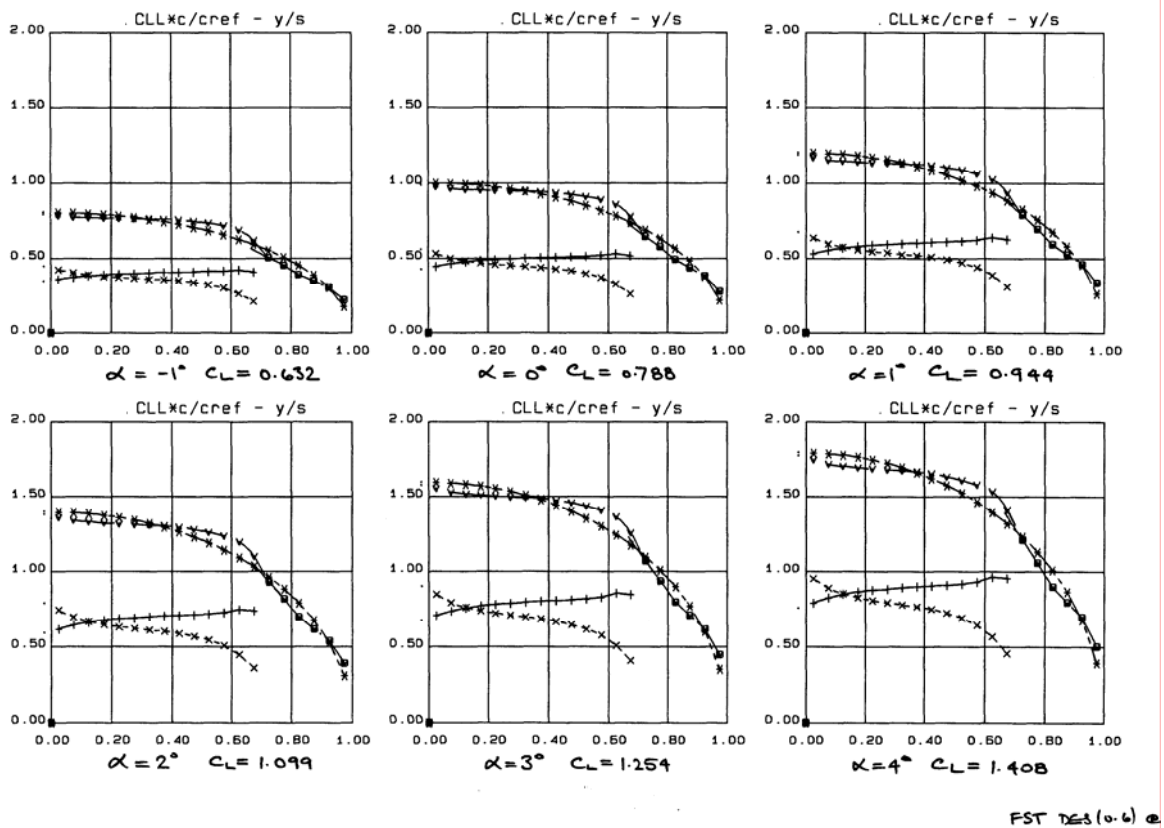
FIG. 7.2.2   CONFIG. FT1, SPANWISE LOADINGS THROUGH AoA RANGE
DESIGNED CAMBERED AEROFOIL CONFIGURATION, Mach 0.15
(Total compared with elliptic)
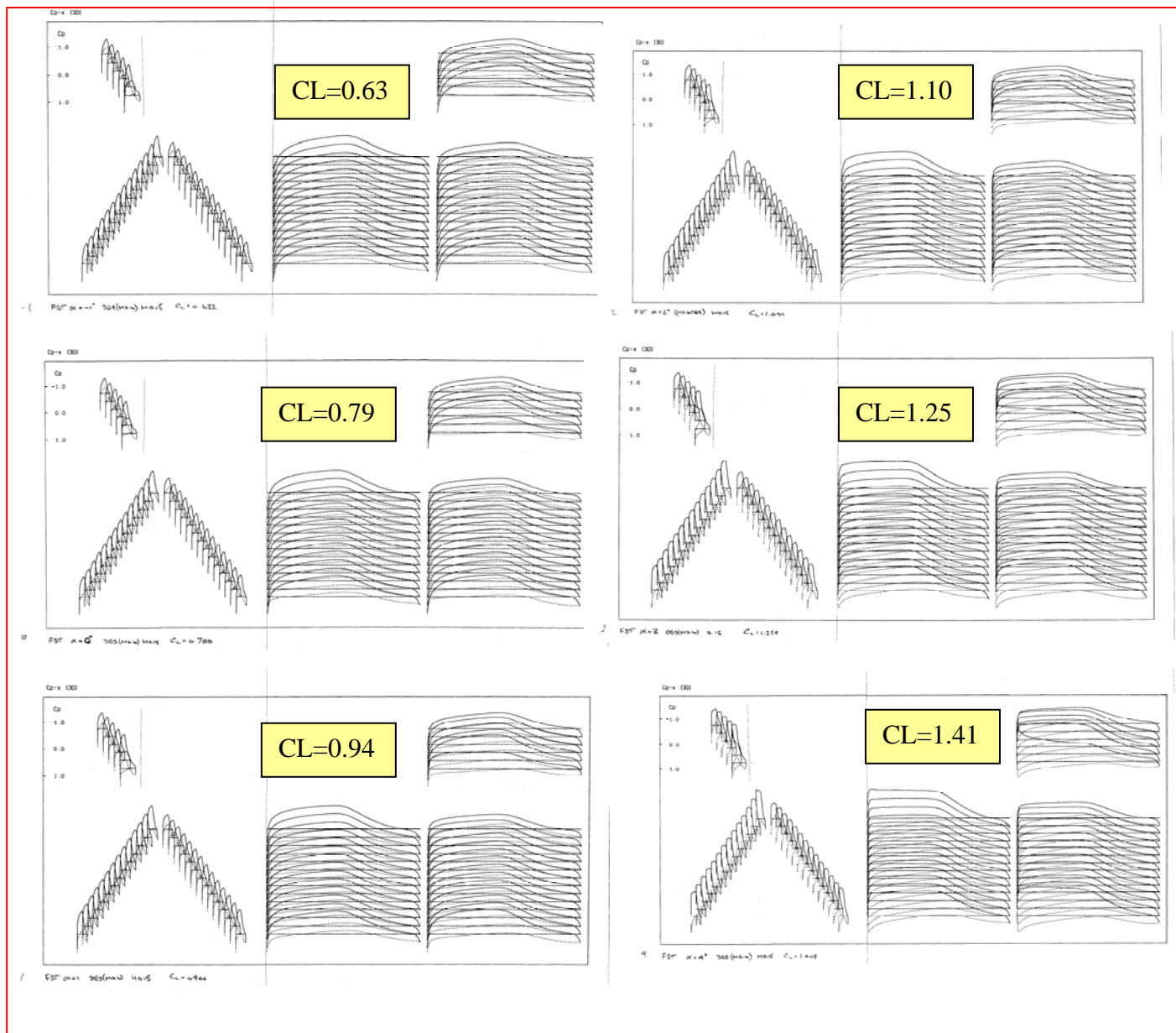
FIG. 7.2.3   CONFIG. FT1, DESIGNED, Cp DISTRIBUTIONS THROUGH AoA RANGE, Mach 0.15

43
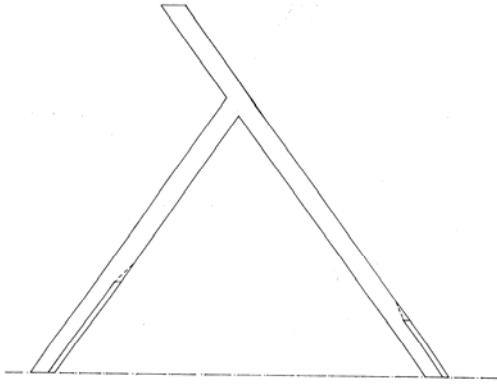
FIG. 7.3.1   CONFIG. FT1, DESIGNED, TEF LOCATION AND EFFECT ON C_m OF +/-5° TEF DEFLECTION, Mach 0.6
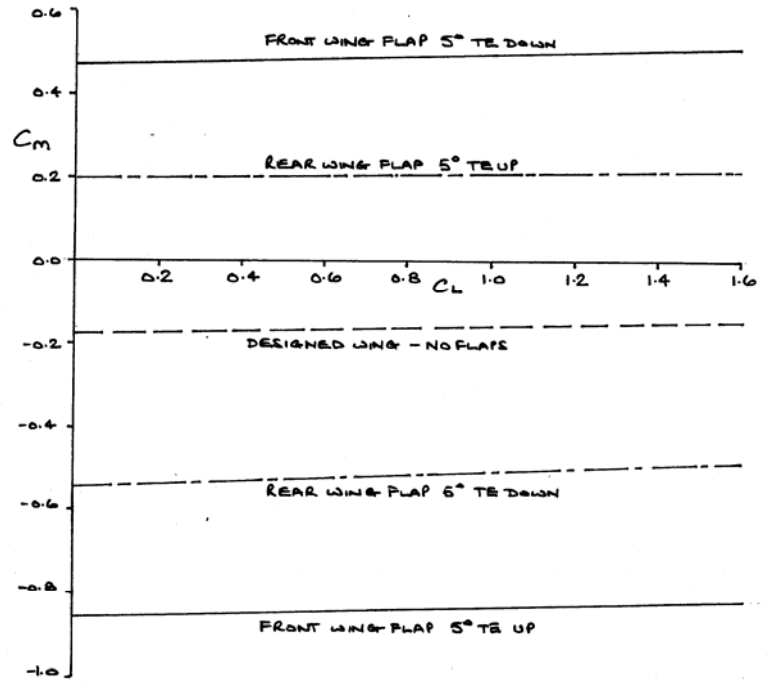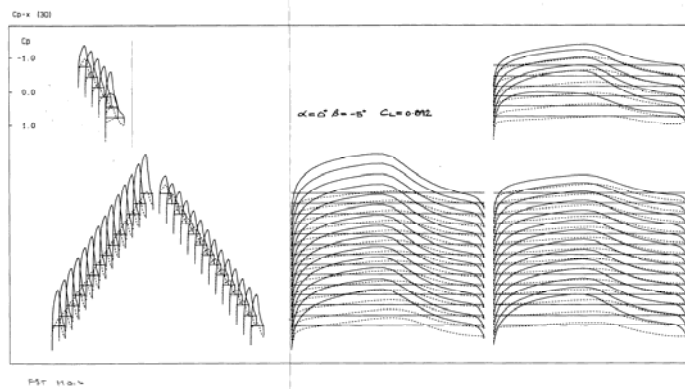

FIG. 7.3.2 CONFIG. FT1, TEF POWER, Mach 0.6
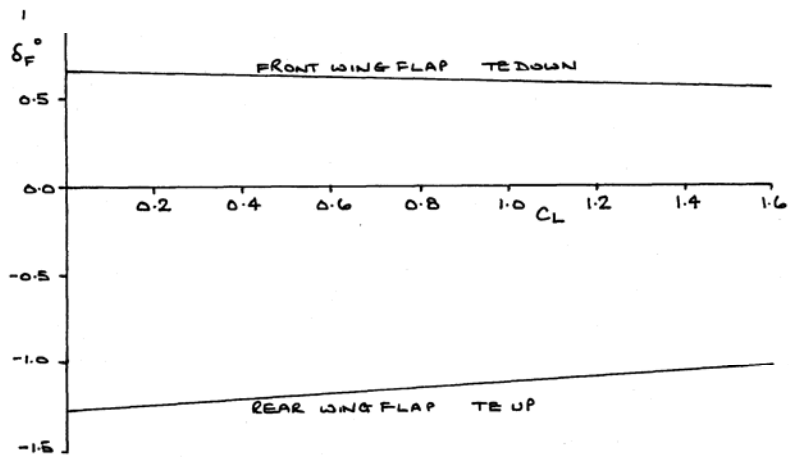
FIG. 7.3.3   CONFIG. FT1, DESIGNED, TEF DEFLECTION REQUIRED TO MAINTAIN C_L – AoA, C_m = 0.0, Mach 0.6
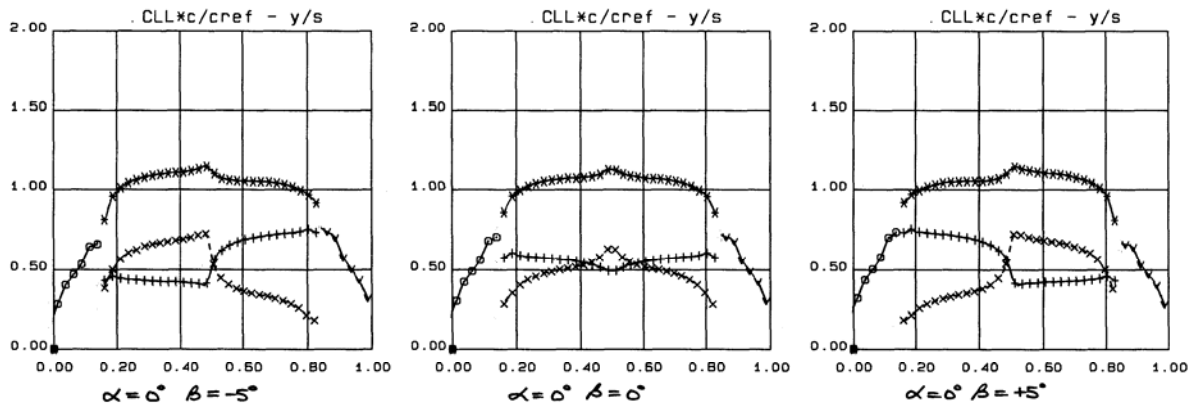
44

Beta = -5°	Beta = 0°	Beta = 5°

Beta = -5°

Beta = 0°

Beta = 5°

FIG. 7.4.1 ASYMMETRIC CASE, EFFECT OF SIDESLIP, SPANWISE LOADINGS & Cp DISTRIBUTIONS, AoA 0°, CL = 0.89

45
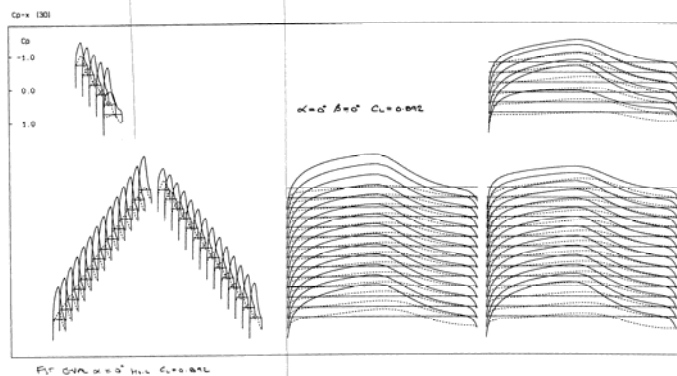
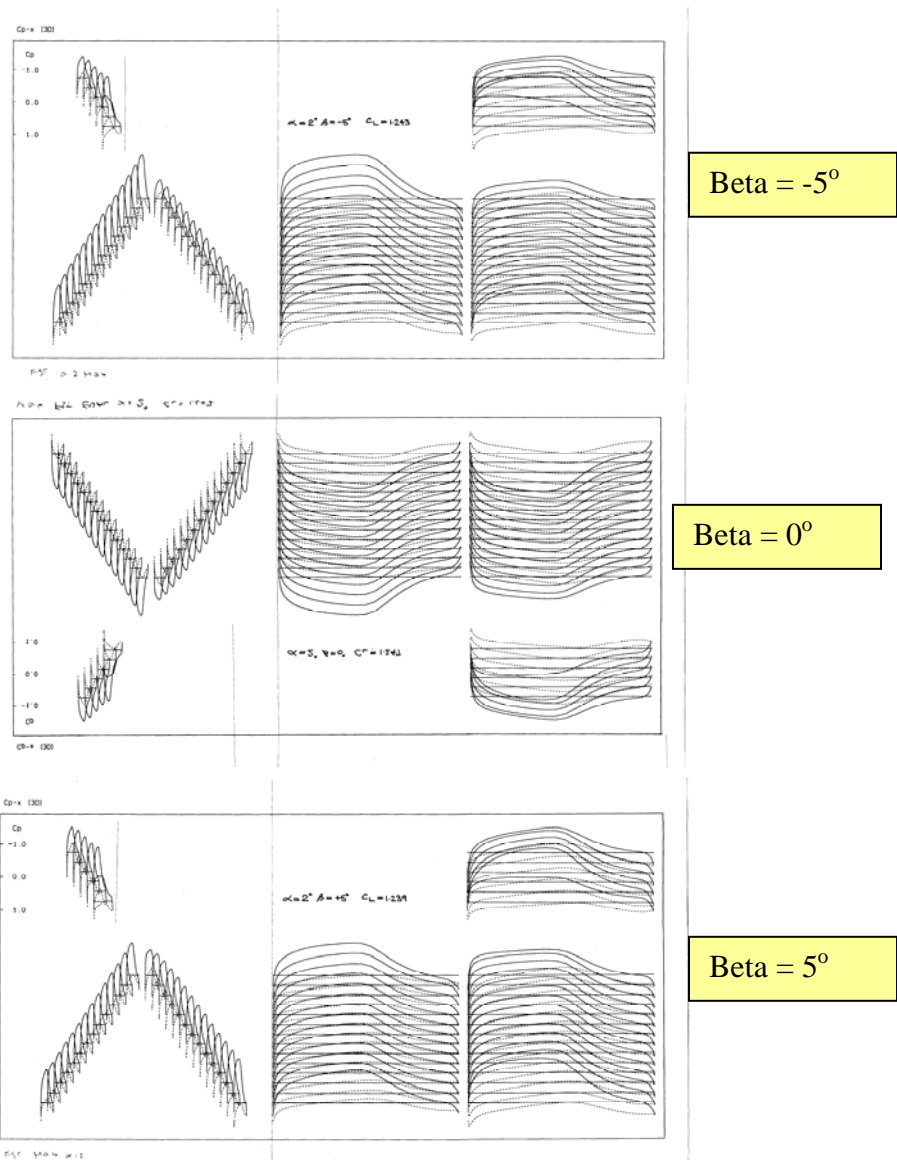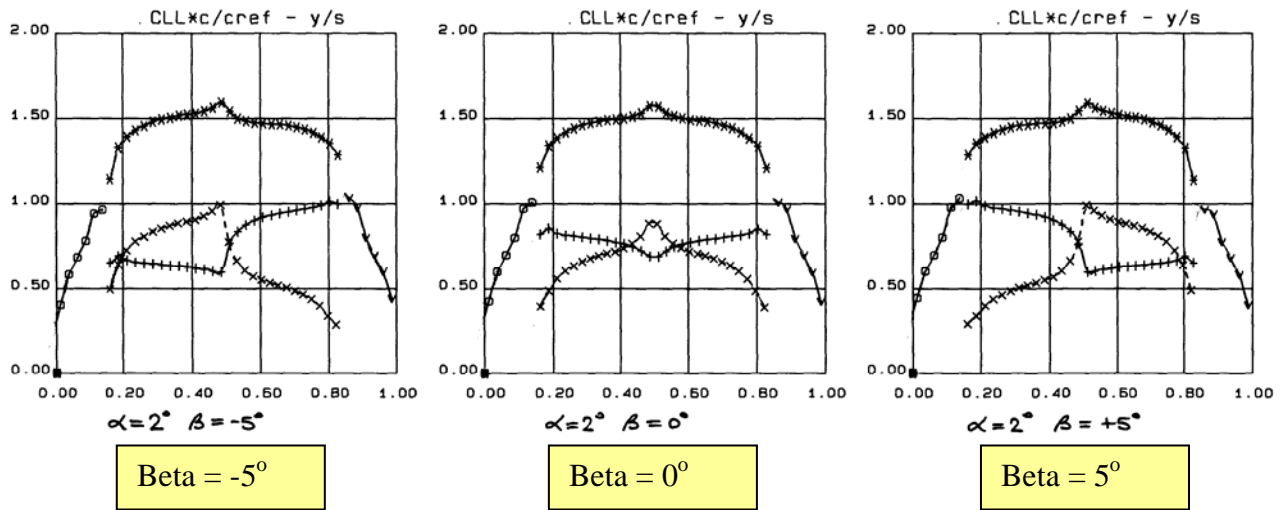Beta = -5°   Beta = 0°   Beta = 5°

Beta = -5°

Beta = 0°
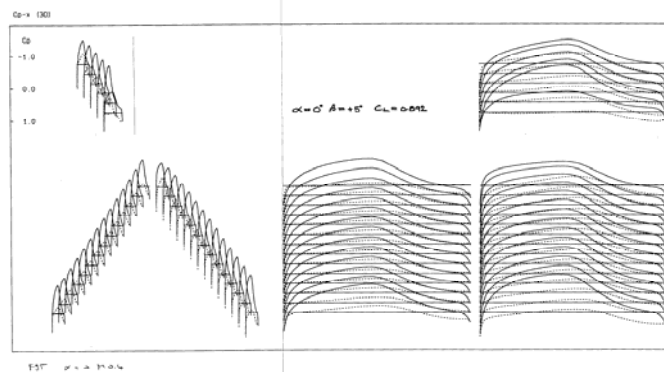
Beta = 5°

**FIG. 7.4.2 ASYMMETRIC CASE, EFFECT OF SIDESLIP, SPANWISE LOADINGS
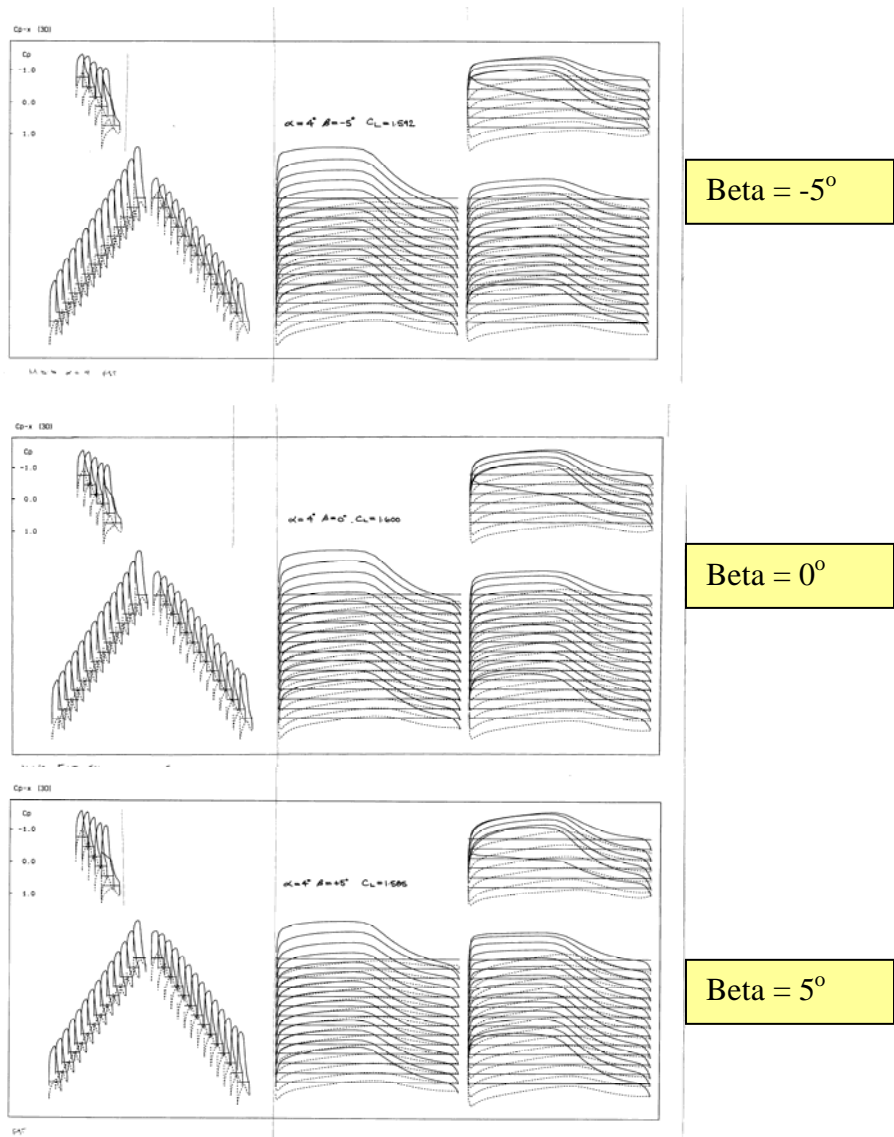& Cp DISTRIBUTIONS, AoA 2°, CL =1.25**

46

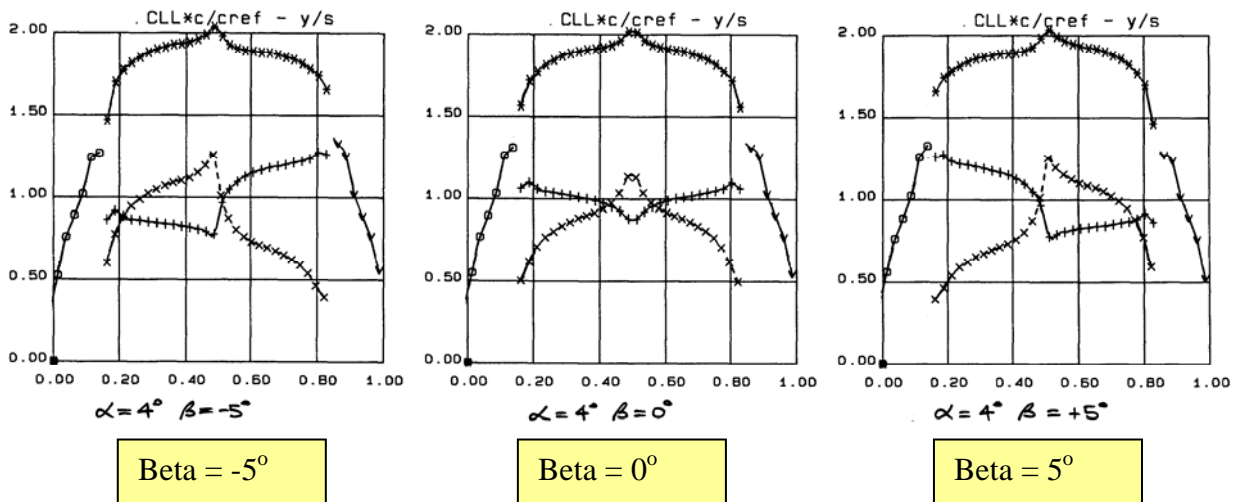FIG. 7.4.3 ASYMMETRIC CASE, EFFECT OF SIDESLIP, SPANWISE LOADINGS
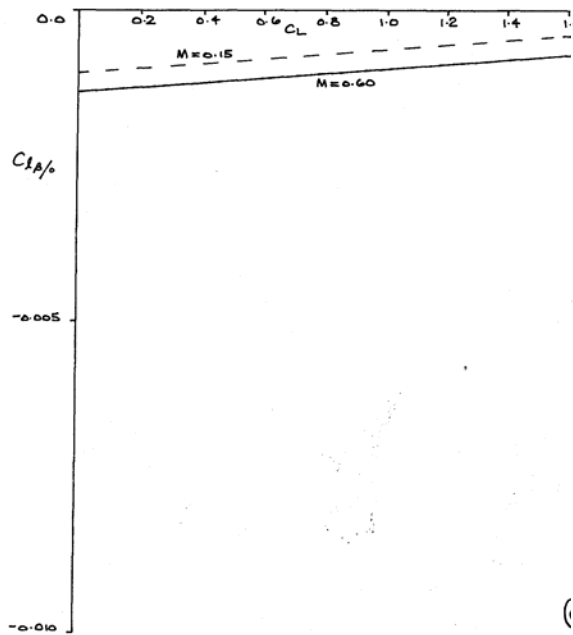& Cp DISTRIBUTIONS, AoA 4°, CL =1.59

47

FIG. 7.5.1 CONFIG. FT1, VARIATION OF ROLLING MOMENT DUE TO SIDESLIP WITH CL, Mach 0.6 & 0.15
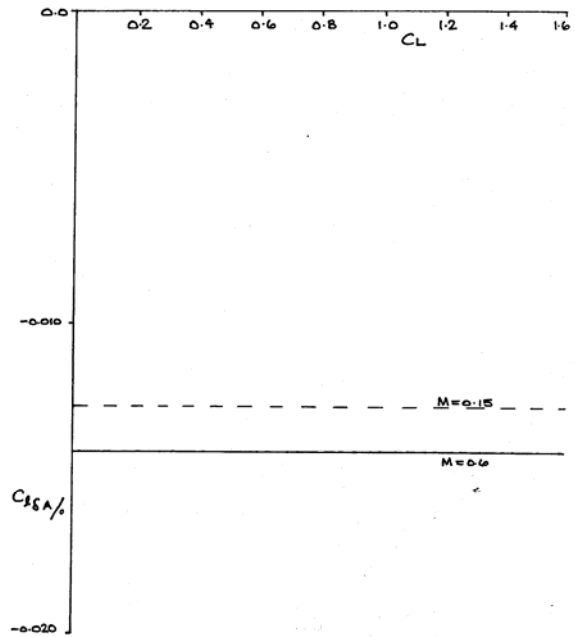

FIG. 7.5.3 CONFIG. FT1, ROLL CONTROL POWER VARIATION WITH CL, Mach 0.6 & 0.15
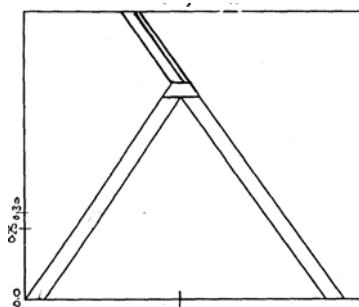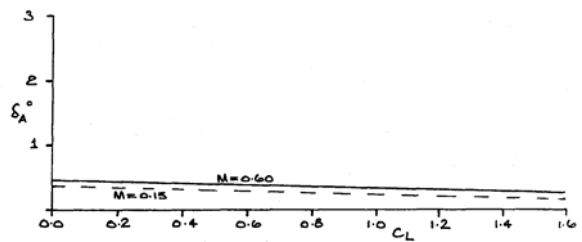

FIG. 7.5.2 CONFIG. FT1, LOCATION & EXTENT OF AILERON

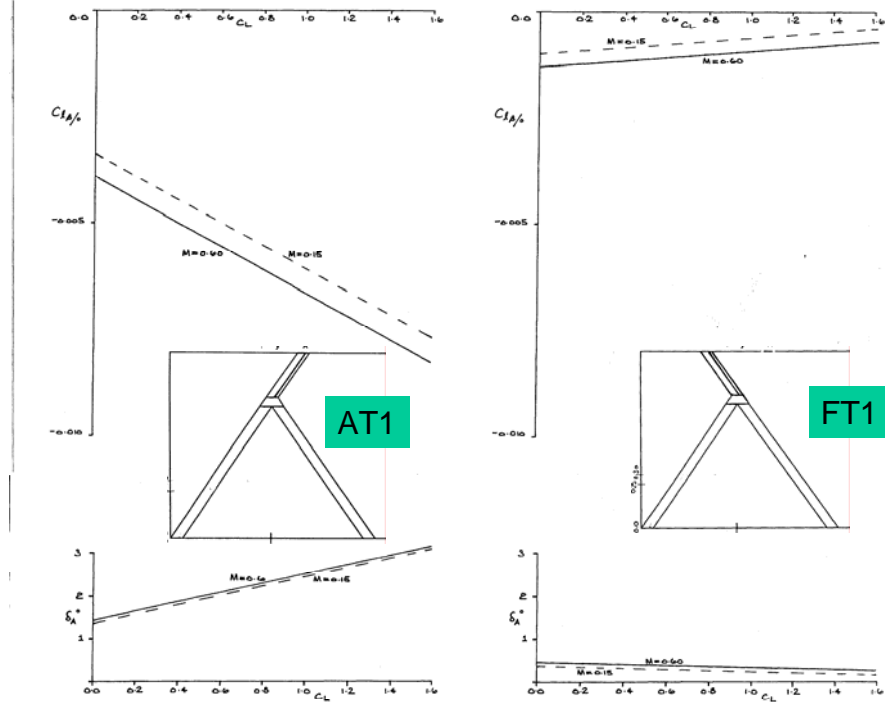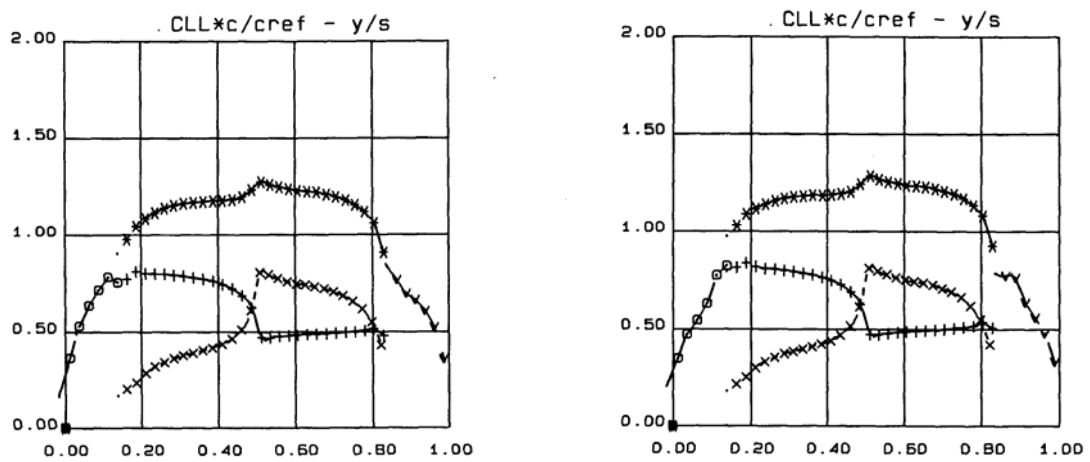**FIG. 7.5.4 CONFIG. FT1, VARIATION OF AILERON REQUIREMENT (for ZERO ROLL at 5 deg SIDESLIP) WITH CL, Mach 0.6 & 0.15**

Comparison of Aileron Deflection Required to cope with 5 deg sideslip, CONFIGS. AT1 & FT1

FIG. 7.5.5

AST, CL = 1.00, Aileron=2.485°

FST, CL = 1.00, Aileron=0.329°

FIG. 7.5.6 CONFIGS.AT1 & FT1, SPANWISE LOADINGS AT CL =1.0, ß = 5°

PLANFORM EFFECTS ON HIGH ASPECT RATIO UNCONVENTIONAL JOINED- & LAMBDA-WING CONFIGURATIONS INCORPORATING LAMINAR FLOW

Dr. R. K. Nangia

SUMMARY

Unmanned Sensor-Craft air vehicles have been proposed as the air-breathing component of a future intelligence, surveillance, and reconnaissance (ISR) infrastructure to provide revolutionary capabilities. Such craft must take advantage of high aspect ratio (AR) wings for aerodynamic efficiency, and may also be required to enclose an antenna in a diamond aircraft planform. A large proportion of fuel must be carried and "loiter" is at high altitudes for a few days in each flight. This implies that a wide C_L–altitude capability is required.

Several types of high AR joined-wing aircraft configurations can be envisaged to meet the possible flight envelope. Previous studies have considered configurations with aft- and forward- swept tips using "conventional" thick super-critical aerofoil sections. Implications of typical flight envelopes on wing design aspects have been mentioned. The work was extended to include laminar flow sections on the Joined-wing configurations with aft- and forward- swept wing tips. Structural considerations led to planforms with extended root chords or lambda shaped front wings being assessed. This report discusses these planform effects and also includes results from wings with Single and Double Lambda planforms.

Using panel codes, results are presented for configurations with uncambered (symmetric) wing sections and then for configurations with designed camber and twist, trimmed for neutral stability. The designed wings display a considerable reduction in leading edge suction, yet maintain the lift, drag and near-elliptic wing loading characteristics. Potential for laminar flow is shown.

The forward-swept tip configurations appear to give more favourable spanwise loadings and are better in terms of aileron roll control in sideslip. We have attempted to correlate drag against various geometric parameters over a wide range of planforms. The Joined-wing cases show a drag advantage over the Single and Double Lambda wings which requires further investigation and analysis.

Further work is proposed in several areas.

This report is Part 3 of a series of six relating to high AR, long endurance surveillance aircraft, laminar flow, integrated intakes and long range supersonic military aircraft.

**Consulting Engineers
Nangia Aero Research Associates
WestPoint, 78 Queens Road, Clifton
Bristol BS8 1QX, UK**

The Investigation which is the subject of this report was initiated by USAF - EOARD, 223/231 Old Marylebone Road, London, NW1 5TH, UK and was carried out under the terms of Contract SPC-024051

DISTRIBUTION LIST

1	Mr. W. Donaldson	USAF-EOARD, London NW1 5TH, UK
1	Mr. C. Remillard	Chief, AFRL/VAAA; Bldg 45 2130 8th Street, WPAFB, Ohio, USA 45433-7542
1	Mr. D. Multhopp	Technical Area Lead, AFRL/VAAA; Bldg 45 2130 8th Street, WPAFB, Ohio, USA 45433-7542
2	Dr. C. P. Tilmann	Sr. Aerospace Engineer, AFRL/VAAA; Bldg 45 2130 8th Street, WPAFB, Ohio, USA 45433-7542
1	Mr. William Fields	Tech Area Lead, AFRL/VAAA; Bldg 45 2130 8th Street, WPAFB, Ohio, USA 45433-7542
1	Dr. K. P. Iwanski	Aerospace Engineer, AFRL/VAAA; Bldg 45 2130 8th Street, WPAFB, Ohio, USA 45433-7542
1	Mr. Larry Leavitt	Head, Configuration Aerodynamics Branch NASA Langley Research Center, Mail Stop 499 Hampton, VA 23681-2199
1	Dr. James Luckring	Configuration Aerodynamics Branch NASA Langley Research Center, Mail Stop 286 Hampton, VA 23681-2199
1	Mr. John Perdzock	Head, SensorCraft Integrating Concept Office, AFRL/VAC; Bldg 45 2130 8th Street, WPAFB, Ohio, USA 45433-7542
1	Dr. Maxwell Blair	AFRL/VASD; Bldg 146 2210 Eighth Street Wright-Patterson AFB OH 45433-7531
1	Dr. Keith Numbers	AFRL/VAA, Long Range Strike Integrating Concept Office
1	Mr. D. Adamczak	Sr. Aerospace Engineer, AFRL/VAAA; Bldg 45 2130 8th Street, WPAFB, Ohio, USA 45433-7542
1	Dr. Michael OL	Research Engineer, AFRL/VAAA Bldg 45 2130 8th Street, WPAFB, Ohio, USA 45433-7542
2	Dr. R.K. Nangia	Nangia Aero Research Associates WestPoint, 78-Queens Road, Clifton BRISTOL BS8 1QX, UK.

CONTRACTUAL DECLARATIONS

"The Contractor, Dr. R. K. Nangia,, hereby delcares that, to the best of its knowledge and belief, the technical data delivered herewith under Contract No.SPC-024051 is complete, accurate, and complies with all requirements of the contract.

DATE: **March 2004**   **Name and Title of Authorized Official:**   **Dr R K Nangia**

"I certify that there were no subject inventions to declare as defined in FAR 52.227-13, during the performance of this contract."

DATE: **March 2004**   **Name and Title of Authorized Official:**   **Dr R K Nangia**

CONTENTS

SUMMARY

DISTRIBUTION LIST

CONTRACTUAL DECLARATIONS

CONTENTS

1. INTRODUCTION, BACKGROUND & WORK PROGRAMME

1.1. Background

The work discussed in this report relates specifically to planform effects on high Aspect Ratio (AR) joined wing configurations. This report is Part 3 of a series of six, Refs.1 to 6, relating to high AR, long endurance surveillance aircraft, laminar flow, integrated intakes and long range supersonic military aircraft. This work follows previous work funded by USAF-EOARD under seeding Contract SPC-01-4087 which was reported in Ref.7.

The Joined Wing concept conceived by Wolkovitch in the 1980's (Refs.8-9) features diamond-shapes in the plan and front views. One of the main advantages claimed was bending moment relief at a very small expense of span efficiency factor, **Figs.1.1-3**. Several aircraft applications were proposed (**Fig.1.4**). Some of the ideas were carried through into experimental research aircraft and Remotely Piloted Vehicles (RPV). These generally had a "mixed reception" but confirmed some of the advantages claimed over "equivalent" conventional aircraft in terms of aerodynamic efficiency (large Aspect Ratio (AR) feasibility) and structural efficiency. There are however some adverse problems; e.g. spanwise flows, lack of fuel volume, junction flows, etc.

With advances in the technologies of flight control, propulsion and flow control, there is emphasis on re-visiting some of the older concepts and devising newer applications. Some have been publicised, **Fig.1.4**, e.g. Lockheed Fuel Tanker, Goldschmied (NASA), Sensor-Craft, etc. (Refs.10-13). Some shapes feature wings joined at the tips, others joined part way. The tip-wings can be appropriately backward- (AST) or forward- swept (FST).

1.2. Introduction to Present work and Methods

The AFRL has been formulating a programme to provide revolutionary intelligence, surveillance, and reconnaissance (ISR) capabilities to the Warfighter (Refs.10-12). This programme blends a wide spectrum of emerging technologies to produce an Unmanned Air Vehicle (UAV), which may be configured and optimised to conduct multiple advanced sensing modes, integrated into a single airframe capable of long endurance. This feature, combined with omni-directional sensing, may enable a virtual presence, allowing vantage point flexibility / optimisation necessary for continuous and detailed theatre air and ground target detection, identification, and tracking. This unique combination of advanced sensors and sustained presence could enable continuous and rapid reaction to the dynamic combat operational requirements confronting current and evolving military operations.

The Sensor-Craft is envisaged as the air-borne air-breather component of a fully integrated ISR enterprise that cohesively integrates space, air, and ground components of the total ISR apparatus. It is an AFRL shared-vision UAV programme that combines critical vehicle, propulsion, sensor system, emerging flight and information technologies into a highly responsive platform concept to detect mobile, hidden targets. Several emerging sensor technologies are under assessment for platform use, including hyper-spectral imaging, active laser sensing, unattended ground sensors, and foliage penetration radar (Ref.10). **Fig.1.5** illustrates advanced sensor functionalities and modes for the Sensor-Craft.

Several candidate aircraft and propulsion configurations are being considered to determine the best trade-off between long endurance, altitude, engine efficiency, and power generation. One of the major challenges is the integration of the large antenna apertures, required for the

lower frequency transmissions, into the airframe. These lower frequency bands enable the Sensor-Craft to provide a foliage penetration radar capability, a key sensory mode aimed at defeating extremely difficult camouflaged, concealed, and deceived (CC&D) targets (Ref.11)

Many of the Sensor-Craft concepts take advantage of high AR wings, as well as enclosing a large antenna in a diamond aircraft planform. Such aircraft carry a large proportion of fuel and are expected to "loiter" at high altitudes for a few days in each flight. This implies a wide C_L - altitude capability, more so than existing operational reconnaissance aircraft e.g. Global Hawk. The "diamond" shapes offer useful survivability "compliance". The aerofoil shapes need to be thick to contain the antenna and provide adequate fuel volume. The cruise Mach number is expected to be "high" subsonic. The low-speed near-field performance is more akin to that of a (very) high aspect ratio wing glider. Take-off and landing phases are also demanding.

1.3. Content and Layout of this Report

Previous work, Ref.7, considered Sensor-Craft configurations with conventional aerofoil sections. The thick aerofoil sections with relative large LE radii (r) gave an appreciable range of C_L or AoA operation. Predictions showed "attained operation ranges (or bands)" for "attached" flow to be close to 4° in AoA.

The analysis was extended using laminar aerofoils whilst maintaining the Sensor-Craft planform, constant chord joined-wing (Ref.2). The use of laminar aerofoil sections should, in principle, enable a significant reduction in profile drag and enhance overall L/D of the vehicle.

The work programme was developed to include planform variations. Chord lengths on the inboard sections of both front and rear wings were increased, extended root chord joined-wing. Further planform development led to the lambda joined-wing. These planform variations form the basis of this report.

The remainder of this report is contained in **Sections 2 to 9**:

>**Section 2** discusses briefly the flight envelope, Reynolds number ranges and possible configurations.

>**Section 3** summarises the characteristics of Laminar Flow aerofoils discussed in detail in Part 2

>**Section 4** summaries results for the constant chord joined-wing configuration, Part 2.

>**Section 5** discusses results for the extended root chord joined-wing configuration.

>**Section 6** discusses results for the lambda joined wing.

>**Section 7** discusses planform comparisons

>**Section 8** lists some ideas for further work.

>**Section 9** mentions concluding remarks.

We begin with an outline of the flight envelope, Mach number, Lift Coefficient and Reynolds numbers encountered and possible configuration aspects.

2. FLIGHT ENVELOPE, REYNOLDS NO., CONFIGURATION CONSIDERATIONS & PREDICTION METHODS

There are several aspects that need to be considered in the design and development of aircraft configurations, e.g.
- Type of spanwise loadings and design of wing camber and twist.
- Trimmed flight at low speeds with different C_L levels. The TE geometry can be varied.
- High-speed design of thick wings, tolerant to a large C_L variation (fuel usage). Use of TE flaps.
- Integration of intakes / fuselages.
- "Reasonable" off-design performance – adequate tolerance to cross-winds during landing / take-off.
- Roll, Pitch and Yaw Stability levels, Control laws.

The low speed and high speed demands on the configurations obviously "conflict" and this has led to a challenging work programme leading towards suitable layouts with designed (camber and twist) aerofoil sections.

Previous work conducted at the AFRL indicated that the main sizing driver aspect is the integration of a "rhombic" antenna into very thick aerofoils. The payload / range performance requirements lead to thick aerofoils (t/c normal to the LE, between 15 and 21%), operating at high C_L values, near 1.0.

Fig.2.1 gives an idea of the aircraft flight envelope. Note the Altitude and Weight relationships during a typical mission. The Reynolds number variation is also depicted as well as Mach number and C_L relationships (C_L based on the total front wing area). Take-off is near C_L of 0.95 at Mach 0.2 (Re = 1.414×10^6/ft), whilst landing is at C_L of 0.7 at Mach 0.15 (Re = 1.06×10^6/ft). The Mach 0.6 cruise C_L varies from 1.58 to 0.88 (Re = 0.44×10^6/ft to 0.345×10^6/ft).

It is interesting to reflect that, on conventional aircraft, the cruise C_L values are near 0.5 and take-off / landing C_L values near 0.8 to 1.2.

Initial work on a reference Sensor-Craft configuration, **Fig.2.2**, was carried out with conventional, thick aerofoil sections with relatively large LE radii (r). These gave appreciable ranges of C_L or AoA operation. Predictions showed "attained operation ranges (or bands)" for "attached" flow to be close to 4° in AoA, Refs.14 - 18. The current design work and comparison of planform shapes has been carried out with Laminar flow type aerofoils. In principle, this should enable a significant reduction in profile drag and enhance overall L/D of the vehicle. The integration of laminar flow aerofoils into the constant-chord Sensor-Craft planform configuration has been reported in Ref.19. Some experimental validation appears in Ref.20.

It is opportune to mention that, currently, there is significant interest in ensuring the existence of laminar flow on swept wing surfaces. Arizona State University research has focussed on addressing the problem of cross-flow instability, using Distributed Roughness Elements (DRE) on surfaces. Detailed results are however, not yet available but **Fig.2.3** summarises some of the work.

The reference Sensor-Craft planform, with laminar flow aerofoils, is discussed in Ref.2 and summarised in Section 4. Alternative joined wing planforms, with laminar flow sections, are

discussed in Sections 5 and 6 of this report. The scope of the planforms considered is shown in **Fig.2.4**. In summary this covers the reference high AR case, extended root chord case and the lambda joined wing concept. Results for the Lambda wing configurations reported in Ref.4 have been included in the planform comparisons in Section.7. The effects of fuselage, intakes and powerplant have not been included in the studies.

On novel layouts, often the experience is that the complexities "defy" the use of an automatic "hands-off" design process with any confidence (unique solutions doubted). Therefore, we have chosen a process that allows a significant understanding to be gained with reasonable manual control over the design process (Refs.21 - 31).

Prediction Methods

The design process used here is described in Part 2 of this report (i.e. Ref.2). Camber and twist design, under forces and moments constraints, is via previously validated attained suction design methods (e.g. Refs.21-26). The process allows a significant understanding to be gained with reasonable manual control over the design process. Panel and Euler codes (Ref.32) are utilised that enable assessment of the aerodynamic performance over the range of low to high speeds.

An inverse design method using 3-D membrane analogy (Ref.28) can "tailor" and "fine-tune" aerofoil shapes for "optimum" Cp distributions as needed in future.

3. LAMINAR FLOW AEROFOILS (2-D)

Some initial work on the Sensor-Craft concept, Ref.7, was carried out using conventional aerofoil shapes. The design work on Sensor-Craft planforms discussed in this report has utilised laminar flow aerofoil sections.

The C_p distributions obtained from the XFOIL solver for typical laminar flow aerofoil sections are presented and discussed in Ref.2. These provided a suitable starting point for further development and the validtion of a panel method. The validation involved analysis of uncambered (symmetric) and designed laminar aerofoil sections with design operating Mach number range of 0.5 - 0.6. The analysis also included Mach numbers 0.01, 0.2 and 0.4. The effects of incidence (α) and aerofoil section thickness (16.0% t/c and 19.5% t/c) were also assessed and it was shown that the thicker sections are more "capable" of maintaining laminar flow.

The C_p distributions obtained using the inviscid panel method were largely similar to those produced by the XFOIL method with boundary layer effects. There were slight differences in the vicinity of the TE. This observation goes some way in justifying the use of an inviscid panel method for preliminary design work. Boundary layer effects can be included in the later stages of the design process as needed.

4. CONSTANT CHORD JOINED-WING (CC), Mach 0.6 and Low speed

The reference configuration, **Fig. 2.2**, shows a twin fuselage, twin engine layout. The front wing is swept back at 35° and the rear wing is swept forward at 35°. A single fuselage with one or two powerplants may also be considered. The effects of fuselage, intakes and powerplant have not been included in this study. Several configuration variations are possible. These included anhedral or dihedral on front or rear wings with either aft (AST) or forward (FST) swept tips. The high AR and large span of the Sensor-Craft eliminated the possibility of anhedral front wings. This left two basic planforms. In concept AT1, the front wing and tip have continuous backward sweep and dihedral with anhedral rear wing. Concept FT1 has a dihedral front wing, anhedral rear wing and features forward-swept, dihedral tips. The rear wings (tail) are swept forward and meet the front wings at 0.7 semispan. At this location, the planar front wing TE is coincident with the planar rear wing LE. In general the front, rear and tip wings have identical, constant chords across their spans. Effectively, the tip has an extended inboard chord to encompass the outermost chords of the front and rear wings.

For the purposes of planform comparisons, in this report, configuration AT1 is designated CCAST and configuration FT1 is designated CCFST.

A full analysis of the Sensor-Craft, reference configuration is given in Ref.2. Salient points are now highlighted.

4.1. Basic Planform Effects, Uncambered Case, Wing & Tail Mutual Interference

Initially AoA effects were established. The C_P distributions highlight the tendency for higher LE suctions to occur towards the tip of the front wing, whilst the tail has high LE suctions at the forward-swept centre-section. The wing loadings show an increase in C_{LL} on the outboard region, for the wing and tail combination over the wing only case. The tail operates in the down-wash flow-field of the front wing and the reduced C_{LL} on the tail, with the wing present, is clearly evident. The largest downwash effects occur near the junction.

4.2. Uncambered & Designed AST & FST Cases

The design process attempts to approach an elliptic spanwise loading distribution, trimmed for neutral stability. In view of the relatively thick sections and anticipated attached flow band-widths, the operational range should extend to C_L of 1.6 prior to any significant flow separations.

Trends are established for a uniform, known camber distribution on each wing (front, rear and tip). The design process establishes camber factors and twist distributions required for elliptic loading at the design point. Characteristic twist and camber differences between the forward-swept (rear) and backward-swept (front) wings are evident. The front wing has less twist and camber, compared to the rear wing, irrespective of AST or FST.

The effect of wing setting angle, post design, has also been assessed. By setting either the front wing at $+0.5°$ or the rear wing at $-0.5°$, a shift of $+0.15$ C_m can be achieved. There is, of course, a corresponding change in total C_L throughout the AoA range. A suitable combination of front and rear wing twist could attain $C_m = 0$ without affecting the C_L – AoA relationship. This illustrates a degree of control that can be achieved in the design process.

The C_P distributions on the uncambered (symmetric) and designed camber wings together with the spanwise loadings showed that the front wing is more heavily loaded towards the wing junction (y/s = 0.7). At the centre-line (y/s = 0.0), despite the downwash effects, the rear wing carries more loading. This is to be expected at the centre-line junction of a forward-swept wing. For the uncambered AST case, relatively higher loadings appear on the outboard region of the tip as AoA increases. As may be expected, the inboard region of the CCFST uncambered tip shows a greater tendency towards separation than the CCAST tip at equivalent conditions. This has required larger twist and camber values to achieve the elliptical loading requirement.

At a given design condition (C_L and α), one could design camber and twist for minimum drag elliptic loading but the tendency at off-design will be to depart from the elliptic loading. This will have implications on pitch trim stability.

The laminar or "flat-top" nature of the upper and lower surface chordwise pressure distributions are noted. Laminar flow is maintained up to C_L 1.25. Beyond this, the tip root flow breaks down. Geometry details near the wing junction could do with some local improvements, if required, especially from the point of view of maintaining laminar flow. This will be more opportune at a later design stage when integrating the intakes and fuselages into the configuration.

A useful technique of imposing local improvements is via inverse wing design optimisation. This has been discussed in previous papers and Ref.28.

Laminar flow C_L ranges at M = 0.6, deduced from C_P distributions, are discussed in Section 7 and shown in **Fig.7.7** for the uncambered and designed wings. The introduction of design camber has raised and broadened the C_L operating ranges in general. Laminar flow on CCFST is maintained over a much wider C_L range than for CCAST.

The low speed (M = 0.15) characteristics of the M = 0.6 CCAST and CCFST designed cases were also established. At lower speed, the CoP moves forward giving rise to more positive C_m about the MRC. The configurations tend to longitudinal instability at lower speed. The spanwise load distributions have a similar nature to those at M = 0.6. The front wing is more heavily loaded towards the wing junction and the rear wing experiences typical increased loading at the forward swept, centre-line, junction. The laminar flow C_L ranges are limited by the performance of the inboard regions of both the AST and FST. Assuming that this region will be subject to further rigorous design and adaptation, the FST exhibits advantages over the AST in terms of achievable Laminar flow C_L range at reduced Mach number (0.15).

Further design analysis of both CCAST and CCFST configurations is reported in detail in Ref.2. The additional areas investigated include:-
      Longitudinal control using flaps on either the front wing, rear wing or both
      Sideslip effects, $\beta = 5°$ (laminar flow C_L range less adversely affected on FST)
      Aileron control in sideslip (FST has greater roll control hence less drag penalty)
      Constant aerofoil section design, twist only (increased manufacturing simplicity)

5. EXTENDED ROOT CHORD JOINED-WING (EX), Mach 0.6 and Low speed

This configuration differs from the Sensor-Craft in that it has chord extensions on both the front and rear wings on the inboard sections ($0 < y/s < 0.15$). The configuration has been modelled as three wing components: front wing, rear wing or tail and an outer tip, swept either aft (EXAST) or forwards (EXFST). In general, the wing chords are 0.0664 based on a maximum semi-span of 1.0. The front wing has dihedral and is swept back (35°). The inboard planform is extended rearwards, root chords increased by 50% to 0.0996, tapering back to 0.0664 at $y/s = 0.2$. The rear wing (tail) has anhedral and is swept forward (-35°). The inboard planform is extended forwards, root chords increased by 50% to 0.0996, tapering back to 0.0664 at $y/s = 0.2$. Outboard of $y/s = 0.2$, the uncambered (symmetric) configurations are identical to the Sensor-Craft discussed in Section 4, with the tail meeting the front wing at $y/s = 0.7$ and the front wing TE coincident with the rear wing LE. The tips, AST and FST, have extended inboard chords to encompass the outermost chords of the front and rear wings.

Basic planform, wing and tail interference effects on a constant chord, joined wing configuration, are discussed in Section 4 and Ref.2. Results for the uncambered EXAST case are discussed in Section 5.1. Designed camber effects at $M = 0.6$ are assessed on a developed AST geometry and are compared with results for the planar, uncambered case in Section 5.2. Low speed ($M = 0.15$) effects on the $M = 0.6$ designed configuration are also assessed. Further modifications to the designed camber case are outlined in Section 5.3. The uncambered EXFST case is discussed in Section 5.4. Designed camber effects at $M = 0.6$ for the FST planform are discussed in Section 5.5 together with an assessment at $M = 0.15$.

At this stage, Fuselage representation has not been included. Moments have been taken about the MRC derived for the planar wing configurations. It is noted that, for this type of configuration, fuselages are likely to contribute a positive pitching moment.

5.1. Uncambered, Zero Twist Case, Aft Swept Tip

The configuration considered, is shown in **Fig.5.1.1**. For consistency with previous work on joined wing configurations, aerodynamic coefficients are based on the front wing area, including root extensions. In Section 7, comparisons for all Sensor-Craft planforms considered (joined wing, Ref.2 and Lambda wing, Ref.4) are based on total wing area. The dihedral wing (front) has continuous LE Aft sweep and extends to the wing tip. The anhedral tail is forward swept and extends from the root centre-line to $y/s = 0.7$. **Fig.5.1.2** shows the distribution of the uncambered, laminar flow aerofoil sections. The extended root chords on the front and rear wings are evident.

Total and component C_L - α and C_m - C_L variations are shown in **Fig.5.1.3**. The Moment Reference Centre (MRC) location is shown in **Fig.5.1.1**. The effect of increased chord on the inboard region of the front wing is evident. The rear wing operates in the downwash flow-field of the front wing and is therefore less heavily loaded. The spanwise loadings shown in **Fig.5.1.4**, $4° < \alpha < 9°$ confirm this trend. The largest downwash effects occur near the junction. Chordwise Cp distributions on the wing and tail, in dimensional and non-dimensional geometry context, are shown in **Fig.5.1.5** for $4° < \alpha < 9°$. The distributions help to highlight the tendency for higher LE suctions to occur towards the tip of the front wing, whilst the tail has high LE suctions at the forward-swept centre-section. The root chord extensions, wing and tail, have reduced the suctions locally.

5.2. Designed Case, Aft Swept Tip

The effects of applying a reference camber to the laminar flow sections have been assessed on the constant chord joined wing configuration, Section 4.2 and Ref.2. The same reference camber has been used on this configuration. **Fig.5.2.1** shows the twist and camber multiplying factors applied to the reference sections to obtain the designed geometry shown in **Fig.5.2.2**. The front wing has constant camber and almost zero twist for $0.2 < y/s < 0.7$. The camber reduces steadily inboard of $y/s = 0.2$ whilst the twist increases to 2.5^o. The tail exhibits reducing camber and increasing twist, from the centreline to $y/s = 0.7$. The tip is twisted LE up at its inboard station and LE down at $y/s = 1.0$ (outwash). The camber reduces inboard to tip.

Total loads, C_L - α and C_m - C_L, variations are shown in **Fig.5.2.3**. The Moment Reference Centre (MRC) location is shown in **Fig.5.1.1**. The spanwise loadings for $-1° < \alpha < 4°$, **Fig.5.2.4**, indicate that the front wing (aft swept) is more heavily loaded than the rear wing (forward swept) near the outboard junction. It is noted that the rear wing operates in the downwash flow-field of the front wing reducing the loading. The largest downwash effects occur near the junction. The chordwise C_p distributions on the wing and tail, in dimensional and non-dimensional geometry context are shown in **Fig.5.2.5**. The root chord extensions, wing and tail, have helped to reduce the suctions locally. The design camber and twist have reduced the regions of high suction, tip of the front and root of the rear wing. The C_L ranges over which Laminar flow is maintained are shown in **Fig.5.2.6**.

Low speed (M = 0.15) characteristics of the designed configuration have been assessed. Total loads are compared in **Fig.5.2.7**. It is noted that at lower M, $C_{L\alpha}$ is reduced and the configuration tends to longitudinal instability.

5.3. Design Modifications, Aft Swept Tip

To further improve the spanwise load distributions and demonstrate a degree of pitching moment control, a modified twist distribution has been applied, initially to the rear wing only, **Fig.5.3.1**. The positive twist (LE up) on the inboard stations has been reduced such that the root station is near -2°. The resulting geometry is compared with the uncambered case in **Fig.5.3.2**. Total loads and spanwise distributions are shown in **Figs.5.3.3** and **5.3.4** respectively. The magnitude of C_m has been reduced but the configuration is now unstable (C_m positive, rear wing lift contribution decreased). The reduced loading on the inboard region of the rear wing is evident in the spanwise distributions and is just discernable in the chordwise C_P distributions, **Fig.5.3.5**. The twist distribution on the front wing was then modified, **Fig.5.3.6**. The positive twist on the inboard stations has been reduced but the centreline station remains at $+2.5^o$. The resulting geometry is compared with the uncambered case in **Fig.5.3.7**. Total loads and spanwise distributions are shown in **Figs.5.3.8** and **5.3.9** respectively. The reduced loading on the inboard regions of both wings is evident in the spanwise distributions. The effects of reduced twist on the inboard and tip regions of the front wing are just discernable in the chordwise C_P distributions, **Fig.5.3.10**. The near elliptical spanwise load distributions and near zero C_m at the design point, illustrates a degree of control that can be achieved in the design process.

5.4. Uncambered, Zero Twist Case, Forward Swept Tip

The planform, configuration layout and panelling are shown in **Fig.5.4.1**. **Fig.5.4.2** shows the aerofoil (symmetrical) distribution on front, rear and tip wings. AoA effects have been

established for this uncambered configuration. The total loads with component breakdown are shown in **Fig.5.4.3.** Spanwise loadings are shown in **Fig.5.4.4**, for AoA 4° to 9°. The wing loadings show an increase in C_{LL} on the outboard region. The tail operates in the downwash flow-field of the front wing. The largest downwash effects occurring near the junction. Chordwise C_p distributions on the wing and tail, in dimensional and non-dimensional geometry context, are shown in **Fig.5.4.5** for AoA of 4°. The distributions help to highlight the tendency for higher LE suctions to occur towards the tip of the front wing, whilst the tail has high LE suctions at the forward-swept centre-section.

5.5. Designed Case, Forward Swept Tip

The twist and camber multiplying factors required for the design case are shown in **Fig.5.5.1**. The resulting designed sections are compared with the uncambered case in **Fig.5.5.2**. The front wing has constant camber and almost zero twist for 0.2 < y/s < 0.7. The camber reduces steadily inboard of y/s = 0.2 whilst the twist increases to 2.5°. The tail exhibits reducing camber and increasing twist, from the centreline to y/s = 0.7. The tip is twisted LE down at its inboard station and LE up at y/s = 1.0 (inwash). This is the opposite requirement to the AST (outwash). The camber reduces inboard to tip and the FST requires less camber at the tip than the AST.

Total loads, C_L - α and C_m - C_L, variations are shown in **Fig.5.5.3**. These suggest that the FST is slightly more unstable than the AST for this initial design. Spanwise loadings for -1° < α < 4°, **Fig.5.5.4**, indicate that the front wing (aft swept) is more heavily loaded than the rear wing (forward swept) near the outboard junction. The effects are the same as those experienced for the AST case. The chordwise C_p distributions on the wing and tail, in dimensional and non-dimensional geometry context, **Fig.5.5.5**, confirm the trends. The distributions show that the high LE suctions occurring towards the tip of the uncambered, aft swept front wing have been reduced. The extended root chords and the design camber and twist have reduced the suctions at the forward-swept centre-section of the rear wing.

The C_L ranges over which Laminar flow is maintained on the EXFST case, uncambered and designed, are shown in **Fig.5.5.6**. For the front and rear wings the ranges are similar to those achieved on the EXAST. It might be suggested that the relatively poor performance of the root of the FST adversely affects the performance of the front wing tip. It is acknowledged that further work on the design of the FST root is required to improve its performance and enhance its affect on adjacent surfaces. The considerable advantages, in terms of extended laminar flow C_L ranges, for the FST over the AST need exploiting.

Low speed (M = 0.15) characteristics of the designed configuration have been assessed. Total loads are compared in **Fig.5.5.7** for both the FST and AST and M = 0.6 and 0.15. It is noted that at lower M, $C_{L\alpha}$ is reduced and the configurations tends to longitudinal instability. The instability is more marked on the FST case.

6. LAMBDA JOINED-WING CONFIGURATION, M = 0.6 and Low speed

The configuration has been modelled as three wing components: front and rear wings with an outer tip, swept either aft (LJAST) or forwards (LJFST). The front wing, lambda planform, has dihedral and is swept back at 35°. The inboard region, $0.0 < y/s < 0.25$, has a forward swept TE. The mid-section, $0.25 < y/s < 0.7$, has a constant chord of 0.15. The rear wing (tail) has anhedral, a constant chord of 0.1075, is swept forward (-35°) and meets the front wing at 0.7 semispan. At this location, for planar aerofoil sections, the front wing TE is coincident with the rear wing LE. The tip has an extended inboard chord to encompass the outermost chords of the front and rear wings. The outboard section, $0.75 < y/s < 1.0$, has a chord of 0.1875 on both AST and FST.

6.1. Uncambered, Zero Twist Case, Aft Swept Tip

The planform considered is shown in **Fig.6.1.1** together with details of alternative reference areas. For consistency with previous work on joined wing configurations, the majority of the present work uses the shaded areas (front wing and tip) as the reference area. **Fig.6.1.2** shows the panelling and configuration layout. AoA effects have been established for this configuration with planar (symmetric, uncambered) aerofoil sections, **Fig.6.1.3**.

The total loads with component breakdown are shown in **Fig.6.1.4**. Spanwise loadings are shown in **Fig.6.1.5**, for AoA 4° to 9°. The effect of the triangular planform of the front wing inboard region is evident. Also the constant chord rear wing is lightly and consistently loaded across its span. As for all these joined wing configurations, the tail (rear wing) operates in the down-wash flow-field of the front wing. The largest downwash effects occurring near the junction. Chordwise C_P distributions on the wing and tail, in dimensional and non-dimensional geometry context, are shown in **Fig.6.1.6** for $4° < \alpha < 9°$. For this, the uncambered aerofoil section case, the inboard (lambda) region of the front wing exhibits typical laminar flow C_P –x profiles up to about $C_L = 0.7$. At this condition, the rear wing (forward swept) also performs well. However, the outboard region of the front wing and the AST show typical peaky C_P distributions indicating possible onset of flow separation.

Laminar flow limits, in terms of C_L, were established for the uncambered LJAST configuration. These are presented and discussed in Section 6.3.

6.2. Reference Camber, Zero Twist Case, Aft Swept Tip

Trends are established for a uniform, known camber distribution on each wing (front, rear and tip). The design process establishes camber factors and twist distributions required for elliptic loading at the design point. This process was outlined for the EX and CC cases, Section 4.2 and Ref.2. Characteristic twist and camber differences between the forward-swept (rear) and backward-swept (front) wings are evident. The front wing has less twist and camber, compared to the rear wing, irrespective of AST or FST.

6.3. Designed Case, Aft Swept Tip

The twist and camber distributions required for the design case are shown in **Fig.6.3.1**. The resulting geometry is compared with the uncambered sections in **Fig.6.3.2**. The front wing has constant camber and almost zero twist for $0.35 < y/s < 0.7$. The camber reduces steadily inboard of y/s = 0.35 whilst the twist increases to 2.5°. The tail exhibits a very smooth camber distribution across the semispan, almost constant for $0.0 < y/s < 0.35$ and then

reducing towards the tip. The twist distribution is almost sinusoidal from root to tip (y/s = 0.7) rising to about 4° at the tip. The AST is twisted, very slightly, LE down at its inboard station and, surprisingly, LE up at y/s = 1.0. This is in the opposite sense to the usual outwash required on aft swept wings. The camber is almost constant across the tip span.

Total loads, C_L - α and C_m - C_L, variations are shown in **Fig.6.3.3**. The Moment Reference Centre (MRC) location is shown in **Fig.6.1.2**. The spanwise loadings for -1° < α < 4°, **Fig.6.3.4**, indicate that the front wing (aft swept and larger chord) is, in general, more heavily loaded than the rear wing (forward swept). The rear wing operates in the downwash flow-field of the front wing reducing the loading. The largest downwash effects occur near the junction. The chordwise Cp distributions on the wing and tail, in dimensional and non-dimensional geometry context are shown in **Fig.6.3.5**. On the front lambda wing, the peak suctions, although high near the tip (aft sweep), tend to be highest near y/s = 0.25 (TE kink). The design camber and twist has eliminated the peaky C_P distributions evident on the outboard stations of the front uncambered wing. The increased root chord region on the front wing has helped to reduce the suctions locally, requiring only modest twist and reduced camber to maintain the laminar flow characteristics evident at equivalent C_L for the uncambered case.

The C_L ranges over which Laminar flow is maintained are shown in **Fig.6.3.6**. Compared to the uncambered configuration, the design case exhibits broadened and higher C_L ranges for laminar flow.

Low speed (M = 0.15) characteristics of the designed configuration have been assessed. Total loads are compared in **Fig.6.3.7**. It is noted that at lower M, $C_{L\alpha}$ is reduced and the configuration tends to longitudinal instability.

6.4. Uncambered, Zero Twist Case, Forward Swept Tip

The planform considered is shown in **Fig.6.4.1** together with details of alternative reference areas. For consistency with previous work on joined wing configurations, the majority of the present work uses the shaded areas (front wing and tip) as the reference area. **Fig.6.4.2** shows the panelling and configuration layout. Wing and Tail mutual interference and AoA effects have been established for this configuration with planar, uncambered, aerofoil sections, **Fig.6.4.3**. The location of the MRC is also shown in **Fig.6.4.2**. Predictably, the MRC for the FST case is slightly forward of that for the AST case.

The total loads with component breakdown are shown in **Fig.6.4.4**. Spanwise loadings are shown in **Fig.6.4.5**, for AoA 4° to 9°. Similar wing to tail interference effects and forward and backward sweep effects are evident for this configuration (FST) as for the AST case. Chordwise C_P distributions on the wing and tail, in dimensional and non-dimensional geometry context, are shown in **Fig.6.4.6** for 4° < α < 9°. For this, the uncambered aerofoil section case, the inboard (lambda) region of the front wing exhibits typical laminar flow C_P – x profiles up to about C_L = 0.7. At this condition, the rear wing (forward swept) also performs well. However, the outboard region of the front wing shows typical peaky C_P distributions indicating possible onset of flow separation. The uncambered FST exhibits typical laminar flow C_P –x profiles up to about C_L = 0.5 apart from, as expected, the inboard tip-wing junction.

Laminar flow limits, in terms of C_L, were established for the uncambered LJFST configuration. These are presented and discussed in Section 6.5.

6.5. Designed Case, Forward Swept Tip

The twist and camber distributions required for the design case are shown in **Fig.6.5.1**. The resulting geometry is compared with the uncambered sections in **Fig.6.5.2**. As expected, the twist and camber requirements for the wing and tail components are similar to those required for the AST case, **Fig.6.3.1**. The FST is twisted LE down at its inboard station and LE up at $y/s = 1.0$. As expected, sweep effects allow the tip of the FST to accommodate higher positive twist than at its root. The camber varies significantly across the tip span.

Total loads, C_L - α and C_m - C_L, variations are shown in **Fig.6.5.3** and compared with those of the AST configuration. The Moment Reference Centre (MRC) location is shown in **Fig.6.4.2**. The trends in **Fig.6.5.3** suggest that the FST case has a slightly lower $C_{L\alpha}$ than the AST case and that it is slightly more unstable for this initial design. The spanwise loadings for $-1° <$ $\alpha < 4°$ are shown in **Fig.6.5.4**. Again, as for the AST case, these indicate that the wing is more heavily loaded than the tail (downwash and sweep effects). The chordwise C_p distributions on the wing and tail, in dimensional and non-dimensional geometry context are shown in **Fig.6.5.5**. On the front lambda wing, the peak suctions, although high near the tip (aft sweep), tend to be highest near $y/s = 0.25$ (TE kink). The design camber and twist has eliminated the peaky C_P distributions evident on the outboard stations of the front uncambered wing. The increased root chord region on the front wing has helped to reduce the suctions locally, requiring only modest twist and reduced camber to maintain the laminar flow characteristics evident at equivalent C_L for the uncambered case. The FST has accommodated extreme variations in camber and twist across its span whilst maintaining the almost inherent laminar flow characteristics.

The C_L ranges over which Laminar flow is maintained are shown in **Fig.6.5.6**. Compared to the uncambered configuration, the design case exhibits broadened and higher C_L ranges for laminar flow. The inboard region of the FST requires further design work to improve its capability. However, it has already point pointed out that, for structural reasons, this area may be required to accommodate a streamwise body and that further design will be required.

Low speed ($M = 0.15$) characteristics of the designed configuration have been assessed. Total loads are compared in **Fig.6.5.7** for the FST and AST configurations at $M = 0.6$ and 0.15. It is noted that at lower M, $C_{L\alpha}$ is reduced and the configurations tend to longitudinal instability in both cases.

6.6. Further Design Modifications, Forward Swept Tip

The design method indicated twist and camber requirements on the FST component that had large discontinuities at the inboard station ($y/s = 0.7$). These would be almost impossible to manufacture in a full-scale aircraft. Further constraints were applied to the twist and camber modes such that the inboard station of the FST became more amenable to the outboard stations of the front and rear wings, **Fig.6.6.1**. The resulting aerofoil sections are compared with the uncambered case in **Fig.6.6.2**.The more acceptable aerofoil shape of the FST root is clearly shown, c.f. **Fig.6.5.2**. The total loads (C_L & C_m) are compared with the initial LJFST design and also the LJAST design in **Fig.6.6.3**. There are only very slight changes from the initial FST design. The spanwise load distributions, **Fig.6.6.4**, indicate a more elliptic loading near the FST root at the design condition ($C_L = 0.6$). However, the chordwise C_P distributions, **Fig.6.6.5,** suggest a greater tendency to deviate from laminar flow.

This exercise has shown that the design methods can be used to optimise chosen configurations. The methods quickly highlight poorly designed areas and unfavourable performance as well as regions where the desired effects have been attained.

7. PLANFORM COMPARISONS, Mach 0.6 and Low Mach Number

The three basic planform layouts are shown in **Fig.7.1**. The first case, Sensor-Craft (CC), has constant chord wings. The second case (EX) has extended root chords (+50%) on the front and rear wings to help alleviate possible structural loading difficulties. Typical extent and location of twin fuselages on the CC and EX planforms are shown. Single, centreline fuselages are also being considered. A third planform (LJ) has a lambda planform main wing and a joined tail. This planform has been proposed with an integral, centreline fuselage as shown. Fuselage effects have not been assessed at this stage of the work. The planforms considered are defined by the solid outlines in **Fig.7.1**. All three planforms have been assessed with both aft swept (AST) and forward swept (FST) outer tips.

The variation of lift curve slope ($C_{L\alpha}$), derived using panel methods, with Aspect Ratio (AR) is given in **Fig.7.2** for the joined wing configurations at M = 0.6 and low Mach number (0.15). Both $C_{L\alpha}$ and AR are based on total planform area.

The theoretical variation of $C_{L\alpha}$ / AR with AR / cos(Λ) was derived using the equation:
$$C_{L\alpha} = a_o AR / [(a_o/\pi) + ((AR/\cos(\Lambda))^2 + (a_o/\pi)^2 - (AR.M_o)^2)^{½}]$$
for incompressible flow, Ref.33.
Considering compressibility effects $C_{L\alpha \text{ (compressible)}} = C_{L\alpha \text{ (incompressible)}} / \beta$, where $\beta = (1-M^2)^{½}$. Hence $a_o = 2\pi/\beta$.

The effects of Mach number and sweep are evident in **Fig.7.3**. Using values of $C_{L\alpha}$ derived from panel methods at M = 0.6, the $C_{L\alpha}$ / AR trends, for planforms CC, EX and LJ, are also shown in **Fig.7.3**. These values lie close to the theoretical line. Total loads, based on total wing planform area ($C_L - \alpha$, $C_m - C_L$), are compared in **Fig.7.4** for the designed CC, EX and LJ cases with both AST and FST. It is noted that there is little, discernable, difference in $C_{L\alpha}$ for the CC and EX (AR = 17.46 and 15.85, respectively) cases. As AR falls to 8.15 (LJAST and LJFST), the decrease in $C_{L\alpha}$ is noticeable. These cases have not been designed trimmed. However, it has been shown that C_m can be reduced to zero using small angular deflections of front and rear wings without significantly affecting the spanwise, elliptic loading. In general, the FST cases are more unstable than the AST cases.

The theoretical relationship, $C_{Di}/C_L^2 = \beta(\pi AR)^{-1}$, where $\beta = (1-M^2)^{0.5}$, was used to establish the trend shown in **Fig.7.5**. In this case, $\beta = 1$ since M = 0. Values of lift induced drag, C_{Di}/C_L^2, were derived for each configuration, with uncambered (symmetric) wings at low Mach number (0.15) and low CL ($0° < \alpha < 1°$). The usual caution regarding drag estimation from Panel methods should be exercised and the geometry is not yet optimised for drag analysis. C_{Di}/C_L^2 variations with AR for the uncambered configurations at low M lie very close to the theoretical line, **Fig.7.5**. A degree of confidence is established. The variation of C_{Di}/C_L^2 with C_L for the designed configurations at M = 0.6 is shown in **Fig.7.6**. Levels for the uncambered wings at M = 0.6 are also indicated. The trends for C_{Di}/C_L^2 against AR are shown in **Fig.7.7**. AR has a marked effect on the value of C_{Di}/C_L^2. There is an apparent drag advantage for AST over FST configurations for all planforms. However, it should be noted that the planforms may optimise at different design C_L and that the designed FST cases carry significantly more twist than the equivalent AST cases.

At the design point, laminar flow is maintained at all stations across the wings and tips. As C_L increases the laminar flow distributions on the upper surface will begin to break down at a particular location somewhere on the configuration. The precise location will depend upon planform and section distribution. Similarly as C_L decreases the laminar flow distributions on the lower surfaces will begin to break down. The C_L ranges over which laminar flow is maintained are shown in **Fig.7.8**, for the three joined wing planforms, each with either AST or FST. Results for planar (uncambered) and designed camber aerofoils are given.

The variation of L/D with C_L is an important parameter used in aircraft performance studies. The accurate estimation of total drag remains a difficult target. In detailed design studies it is of interest to reduce drag into its various components, e.g. lift induced (vortex), trim, profile (form), skin friction, wave, etc. In these current studies, we have taken induced drag, C_{Di}, as a total of its parts (lift induced and trim resulting from design camber and twist).

Using a wide, but typical, range of C_{Do} values (0.0050 to 0.0200) and modest, "best design" levels of C_{Di}/C_L^2, variations of L/D with C_L were derived for each planform, with both AST and FST, as shown in **Figs.7.9, 10** and **11** (CC, EX and LJ respectively). In general, for a given planform and C_{Do} level, the AST shows an L/D advantage over the FST by virtue of its lower C_{Di}/C_L^2, **Fig.7.7**. Similarly, L/D reduces as AR reduces (higher C_{Di}/C_L^2). It is noted that C_{Do} levels as low as 0.0050 imply that a degree of laminar flow control is necessary. However, we have seen from **Figs. 5.2.6** (EXAST) and **5.5.6** (EXFST) and **6.3.6** (LJAST) and **6.5.6** (LJFST), that the FST is naturally more amenable to laminar flow. This typifies the designer's dilemma when selecting AST or FST:- the trade-off between higher C_{Di}/C_L^2 and more extensive laminar flow C_L range or reduced drag but with reduced laminar flow C_L range. As C_{Do} increases, L/D naturally decreases and occurs at higher C_L.

Work on single and double Lambda wing planforms is presented in Part 4 of this report. These planforms have LE sweep of 30°. Some direct comparisons with the results for the joined-wing configurations are now discussed. The Joined-wing and Lambda-wing planforms are compared in **Fig.7.12**. $C_{L\alpha}$ variation with AR for all planforms considered is shown in **Fig.7.13**. The trends with AR and Mach number are remarkably consistent. The slight advantage implied for the double lambda cases requires further analysis. Panelling and trailing wake effects need to be taken into account. $C_{L\alpha}$ / AR trends, for the Lambda wings, are shown in **Fig.7.14**. Again these values lie close to the theoretical line. The Total loads (C_L − α, C_m - C_L) based on total planform area, for all cases considered (Joined-wing and Lambda-wing) are shown in **Fig.7.15**. As already discussed, fuselage effects have not yet been considered on the Joined-wing configurations and these will have an effect on pitching moment. Adequate pitching moment control using additional twist on front and rear wings has already been shown, Section 5.3. In the case of the Lambda wing configurations, it is implied that a central fuselage, yet to be defined, will be integral with the wing centre section. The design process has demonstrated adequate pitch control on these configurations. However, in the final design, the centre section may require increased volume to encompass intakes, power-plant, payload, etc. This may entail both spanwise and chordwise redistribution of thickness and hence further local re-design.

Low speed, induced drag factors for all planforms are compared in **Fig.7.16** (C_{Di}/C_L^2 – AR). The Lambda-wing configurations lie close to the trends established by theory and the Joined-wing cases. The single lambdas lie on the FST joined wing trend whilst the double lambdas lie midway between AST and FST joined wing cases. Induced drag factor trends with C_L and AR for the designed Lambda-wing cases are shown in **Figs.7.17** and **7.18**. These figures should be compared with **Figs.7.6** and **7.7** for the Joined-wing cases. Possible advantages, in

terms of lower induced drag, for Joined-wing configurations can be seen. However, it is emphasised that the geometries considered have not been optimised for drag analysis. Also, the designed cases may optimise at different C_L values. The drag analysis presented here has established useful trends for configuration planform selection. Further detailed drag analysis can then be carried out selected candidate configurations.

The designed Joined-wing configurations offer laminar flow C_L ranges of about 0.4 to 1.0, provided the inboard regions of the tips can be suitably tailored. The Lambda wings have been designed for $C_m = 0$ and their laminar flow ranges extend to $C_L = 0.5$ or 0.8 depending upon the design case.

L/D – C_L trends for the Single and Double Lambda-wings are shown in **Figs.7.19** and **7.20** respectively. These have been established using a consistent range of C_{Do} values and may therefore be compared directly with **Figs.7.9** to **7.11** for the various Joined-wing configurations. The effect of higher induced drag on the Lambda wings is apparent in the lower L/D values predicted.

In general, for all cases considered, peak L/D ($C_{Do} = 0.0075$) increases with AR. The derived values are some 10% higher for the Joined-wing configurations over the Lambda wings. Caution needs to be exercised in view of drag estimation. Peak L/D occurs at higher C_L for higher AR ($C_L = 0.4$ for AR = 8 and $C_L = 0.55$ for AR = 18). Peak L/D is higher for the Double Lambda wings.

Using the Breguet range equation we can derive graphs of the type shown in **Fig.7.21**. This takes into consideration the following weights and their ratios, Operating Empty Weight (OEW), Payload (WP), Fuel Load (WF) and Take-Off Weight (TOW) or Maximum Take-Off Weight (MTOW). By definition, TOW = OEW + WP + WF. Performance parameters considered include Flight speed (V), Specific fuel consumption (sfc), Range (R) and L/D. Endurance can be found from R / V.

MTOW is usually a structural limitation of the aircraft. For passenger aircraft and military strike aircraft it is a compromise between fuel required for a given payload and range combination. In the case of surveillance aircraft, WP and OEW are fixed and WF is limited only by the capacity of the fuel tanks. For maximum range and endurance, surveillance aircraft naturally operate with TOW = MTOW.

In Sensor-Craft type configurations the Payload is small, 3% - 5% of TOW. OEW/TOW is in the region of 0.42, confirming that more than 50% of TOW is fuel. We consider Mach = 0.6 operation at 60,000 ft and a typical sfc of 0.52 which might be achievable with advanced engines. The variation of Endurance with OEW/TOW and (WP+OEW)/TOW is shown in **Fig.7.21** for various values of L/D. To achieve 50hrs endurance with (WP+OEW)/TOW = 0.45, L/D of 38 to 40 will be required. This can only be achieved with flow control, reducing CD_o whilst maintaining laminar flow. There is obviously scope for further performance work, along the lines indicated, for comparative purposes and exchange rates.

8. FURTHER WORK

So far, a type of Sensor-Craft with a joined-wing layout has been considered for high-speed design at Mach 0.6. Planform effects on Joined-wing configurations have been assessed and compared, briefly, with results from Lambda-wing layouts. Several interesting features have

emerged from the application of direct design methods. Further work is envisaged in a number of areas:

- Continued assessment of cross-flow instability research (e.g. Arizona State University) and how it can help existence of laminar flow on swept surfaces.
- Lower speeds and field performance considerations.
- Parametric geometric studies with appropriate method development.
- Further confirmation with Euler.
- Additional planforms of varying AR.
- Different design C_L studies as required. On joined-wings, the forward-swept root (rear wing) needs attention.
- Different aerofoils incorporation, from the point of view of validation with CFD and transonic codes.
- Pitching moment, static margins control with LE / TE Flap within geometry restrictions, segmentation.
- Fuselage & Intake incorporation, additional effects on forces and moments.
- Inclusion of viscous effects, spanwise pressure gradients and flow control.
- Drag prediction.
- Off-design performance including lateral and directional characteristics. Include aero-elastics.
- Experimental work (various aspects).

9. CONCLUDING REMARKS

A type of Sensor-Craft with a joined-wing layout has been considered for design at Mach 0.6. The emphasis in this report has been on assessing the planform effects on Joined-wing, Sensor-Craft, configurations. These have also been compared, briefly, with results from Lambda-wing layouts. Several interesting features have emerged.

At the design conditions, the design cases display considerable reductions in LE suctions when compared with those with uncambered (symmetric) wings. Considerable potential exists for laminar flow. Further, near-elliptic spanwise loadings have been maintained in all cases. Attention needs to be given to the forward-swept root area of the rear wing (high AoA) on the joined-wing configurations. The wing junction area will require some tailoring to ensure laminarity at high AoA.

Thicker sections are able to maintain laminar flow over a wider AoA range than thinner sections. However, we have to work under configuration and aerodynamic limits imposed by features such as antennae and fuel tanks.

The FST configurations appear to give more favourable spanwise loadings and in earlier work have been shown to be better in terms of aileron roll control in sideslip.

A broad and general drag analysis has been carried out on the three joined-wing configurations (CC, EX and LJ, with both AST and FST) and the four Lambda wing configurations. Good correlations for the variation of C_{Di} with AR have been achieved. This provides a degree of confidence for further project orientated work. In general, drag reduces as AR increases and, for those planforms considered, the FST carries a slight drag penalty over AST.

The designed Joined-wing configurations offer laminar flow C_L ranges of about 0.4 to 1.0, provided the inboard regions of the tips can be suitably tailored. The Lambda wings have been designed for $C_m = 0$ and their laminar flow ranges extend to $C_L = 0.5$ or 0.8 depending upon the design case.

For a constant C_{Do} value (0.0075 say) Peak L/D increases with AR. It occurs at higher C_L at higher AR. At constant AR, Peak L/D is approximately 10% higher for the Joined-wing configurations over the Lambda wings. Configuration CCAST, with $C_{Do} = 0.0075$, gives L/D = 36 at $C_L = 0.55$.

Using suitable inputs to the Breguet range equation, endurance trends have been established. To achieve 50hrs endurance, L/D of 38 to 40 will be required. This can only be achieved with flow control, reducing CD_o whilst maintaining laminar flow.

Typical results presented demonstrate the flexibility and potential of the techniques for direct and inverse design. The Panel codes go a long way to defining the preliminary designs before the need for high order CFD methods arises.

We have considered various planforms, covering an extensive AR range. The choice of planform has been constrained by the type of antennae to be housed within the configuration and survivability considerations. Several important parameters have been highlighted as the main drivers in the final choice of planform. There is obviously scope for further performance work, along the lines indicated, for comparative purposes and exchange rates. It is apparent that we are only at a starting post and a sizeable, interesting work programme remains!

The capability of studying several geometric variables of the configurations is offered in a timely sense. Data for detail design of wind tunnel models and possibly flight demonstrators can be enabled. An understanding of control laws has been developed. The potential and limitations of the aircraft in meeting a given design envelope can be assessed.

Several areas for continued work have emerged.

ACKNOWLEDGEMENTS

REFERENCES

1. NANGIA, R.K., "Pilot Document Introducing all Aspects of Work Accomplished under USAF-EOARD Contract SPC-024051", RKN/AERO/REPORT/2004-10 – Part 1, Issue 1, 2004.

2. NANGIA, R.K., "High Aspect Ratio Unconventional Joined-Wing Configurations Incorporating Laminar Flow", RKN/AERO/REPORT/2004-10 – Part 2, Issue 1, 2004.

3. NANGIA, R.K., "Planform Effects on High Aspect Ratio Unconventional Joined-Wing Configurations Incorporating Laminar Flow", RKN/AERO/REPORT/2004-10 – Part 3, Issue 1, 2004.*This Report*.

4. NANGIA, R.K., "High Aspect Ratio Lambda-Wing Configurations Incorporating Laminar Flow", RKN/AERO/REPORT/2004-10 – Part 4, Issue 1, 2004.

5. NANGIA, R.K., "Integration of Over-Surface Scarfed Intakes on Aircraft with High Aspect Ratio Wings (e.g. Sensor-Craft)", RKN/AERO/REPORT/2004-10 – Part 5, Issue 1, 2004.

6. NANGIA, R.K., "Towards Design of Long-Range Supersonic Military Aircraft", RKN/AERO/REPORT/2004-10 – Part 6, Issue 1, 2004.

7. NANGIA, R.K., "Configuration & Aerodynamic Design Studies of Joined-Wing High Aspect Ratio Sensor-Craft Concept", RKN/Aero/Report/2002-10, June 2002, (USAF-EOARD Contract SPC-01-4087).

8. WOLKOVITCH, J., "The Joined Wing: An Overview", J. of Aircraft, Vol 23, pp. 161-178, March 1986.

9. WOLKOVITCH, J., "A Second Look at the Joined Wing", Proc. of NVVL Symposium "Unconventional Aircraft Concepts", Delft Uni. Press, 1987.

10. JOHNSON, F. P., "Sensor Craft : Tomorrow's Eyes and Ears of the Warfighter," AIAA-2001-4370, Aug. 2001. *See www.afrlhorizons.com /Briefs/Mar01/SN0001.html*

11. Aerospace America, Dec. 01, pp 50.

12. TILMANN, C.P., FLICK, P.M., MARTIN, C.A. & LOVE, M.H., "High Altitude Long Endurance Technologies for SensorCraft". RTO-AVT-99, Paper 25, Brussels, 2003.

13. TYLER, C., SCHWABACHER & CARTER, D., "Comparison of Computational and Experimental Studies for a Joined-Wing Aircraft", AIAA 2002-0702, January 2002.

14. NANGIA, R.K., "Configuration & Aerodynamic Design Studies of Joined-Wing High Aspect Ratio Sensor Craft Concept", RKN/Aero/Report/2002-10, June 2002, (USAF-EOARD Contract SPC-01-4087).

15. NANGIA, R.K., PALMER, M.E. & TILMANN, C.P., "Towards Design of Unconventional High Aspect Ratio Joined-Wing Type Aircraft Configurations", RAeS Conference — "A 2020 Vision", April 2002, London UK.

16. NANGIA, R.K., PALMER, M.E. & TILMANN, C.P., "Towards Design and Optimisation of Unconventional High Aspect Ratio Joined-Wing Type Aircraft Configurations", CEAS Conference, June 2002, Cambridge UK.

17. NANGIA, R.K., PALMER, M.E. & TILMANN, C.P., "On Design of Unconventional High Aspect Ratio Joined-Wing Type Aircraft Configurations", ICAS 2002-25R2,Toronto, Canada.

18. NANGIA, R.K., PALMER, M.E. & TILMANN, C.P., "Unconventional High Aspect Ratio Joined-Wing Aircraft with Aft- & Forward- Swept Wing-Tips", AIAA-2003-0605, Jan. 2003, Reno, USA.

19. NANGIA, R.K., PALMER, M.E. & TILMANN, C.P., "Unconventional High Aspect Ratio Joined-Wing Aircraft Incorporating Laminar Flow", AIAA-3927, June 2003, Orlando, FL, USA

20. BIBER, K. & TILMANN, C.P., "Laminar Aerofoils….", Paper presented at AIAA Aerospace Sciences Meeting, Reno, Jan 2003.

21. NANGIA, R.K., "The Design of "Manoeuvrable" Wings using Panel Methods, Attained Thrust & Euler Codes", ICAS-92.

22. NANGIA, R.K. & GREENWELL, D.I., "Wing Design of Oblique Wing Combat Aircraft", ICAS 2000-1.6.1, 2000.

23. NANGIA, R. K. & GALPIN, S.A., "Towards Design of High-Lift Krueger Flap Systems with Mach & Reynolds No. Effects for Conventional & Laminar Flow Wings", CEAS European Forum, Bath, UK, 1995.

24. NANGIA, R. K. & GALPIN, S.A., "Prediction of LE & TE Devices Aerodynamics in High-Lift Configurations with Mach & Reynolds No. Effects", ICAS-1996-2.7.6..

25. NANGIA, "Design of Conventional & Unconventional Wings for UAV's", RTA-AVT Symposium, "UV for Aerial & Naval Military Operations", Ankara, Turkey, Oct. 2000.

26. NANGIA, R.K., PALMER, M.E. & DOE, R.H., "A Study of Supersonic Aircraft with Thin Wings of Low Sweep", AIAA-2002-0709, January 2002.

27. NANGIA, R.K. & MILLER, A.S. "Vortex Flow Dilemmas & Control on Wing Planforms for High Speeds", RTO AVT Symposium, Loen, Norway, May 01.

28. NANGIA, R.K., "Developing an Inverse Design Method using 3-D Membrane Analogy", Future Paper.

29. KUCHEMANN, D. "The Aerodynamic Design of Aircraft", Pergamon.

30. JUPP, J., Wing aerodynamics and the Science of Compromise", RAeS Lanchester Lecture, 2001.

31. JONES, R.T., "Wing Theory", Princeton.

32. GUPTA, K.K. & MEEK, J.L., "Finite Element Multidisciplinary Analysis", AIAA, 2000.

33. McCORMICK, B.W. "Aerodynamics Aeronautics and Flight Mechanics", Wiley.

LIST OF SYMBOLS & ABBREVIATIONS

Only the general symbols are defined here. Other symbols are of local significance within the Section they arise in.

AoA	Angle of Attack (α), usually referred to the body axis
AR	Aspect Ratio
A	Axial Force along wing-plane x-axis (for definition of CA)
b	= 2 s, Wing span
BL	Boundary Layer
c	Local Wing Chord
c_{aero}	= c, Aerodynamic Wing Chord
c_{av}	= c = cref, Average Wing Chord
C_A	= A/(q S), Axial Force Coefficient, measured in Wing plane
C_{AL}	= Local Axial Force Coefficient
C_D	= Drag Force /(q S), Drag Coefficient
C_{D0}	Drag Coefficient at zero lift (see text)
C_{Di}	Lift Induced Drag
CG	Centre of Gravity
C_l	= l/(q S b), Rolling Moment (Body Axis)
C_L	= CL = L/(q S), Lift Coefficient
C_{LL}	= Local Lift Coefficient
C_{Lmax}	Maximum Lift Coefficient
C_m	= m/(q S c), Pitching Moment (Body Axis)
C_{mo}	Cm at zero lift
C_n	= n/(q S b), Yawwing Moment (Body Axis)
C_N	= N/(q S), Normal Force Coefficient
CoP	Centre of Pressure
C_P	Coefficient of Pressure
c_r, c_t	Wing Root chord, Wing Tip chord
k	= π A C_{Di}/C_L^2, Lift Induced Drag Factor
l	Rolling moment (Body Axis)
LE	Leading Edge
m	Pitching moment (Body Axis)
M	Mach Number
MRC	Moment Reference Centre
n	Yawing moment (Body Axis)
N	Normal Force
q	= 0.5 ρ V^2, Dynamic Pressure
r	Aerofoil radius
rn	Aerofoil radius normal to c
R	Reynolds Number, based on cav (unless otherwise stated)
s	Wing semi-span
S	Wing Area, taken here as (front-wing + tip-wing) area
t	Aerofoil thickness
TE	Trailing Edge
V	Airstream Velocity
x,y,z	Orthogonal Wing Co-ordinates, x along body axis
x_{ac}	Location of Aerodynamic Centre along x-axis
x_{cp}	Location of Centre of pressure along x-axis
α	Angle of Attack (AoA), usually referred to the body axis
λ	Wing Taper Ratio
Λ	LE Sweep Angle
ρ	Air Density
η	= y/s, Non-dimensional spanwise Distance

FIG.1. 1   AVA – RPV & EFFECT OF SPAN RATIO ON SPAN EFFICIENCY

FIG.1. 2   BENDING MOMENTS

FIG.1.3   JOINED-WING CRAFT (WOLKOVITCH)

FIG.1. 4   SEVERAL RECENT JOINED-WING
APPLICATIONS

Fig. 1.5 SENSOR CRAFT VISION

FIG. 2.1 REFERENCE SENSOR-CRAFT FLIGHT ENVELOPE, ALTITUDE - WEIGHT & CL - MACH RELATIONSHIPS
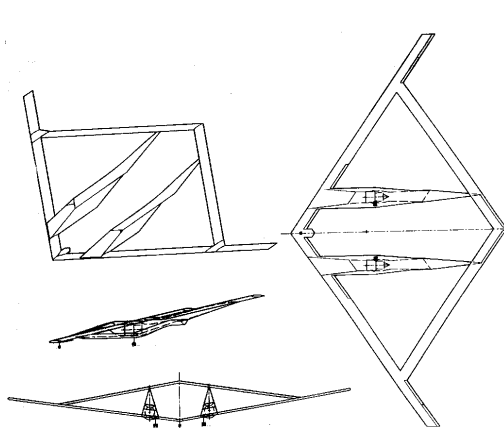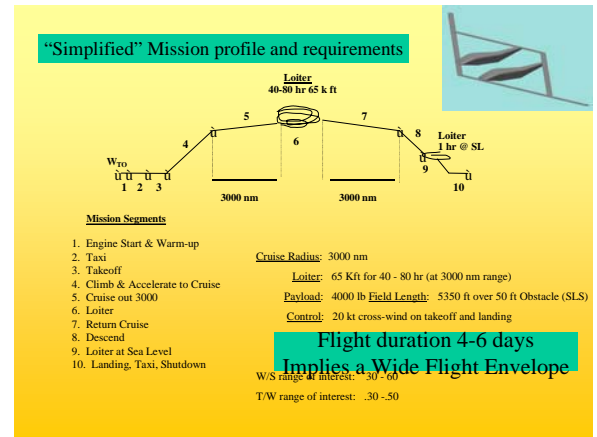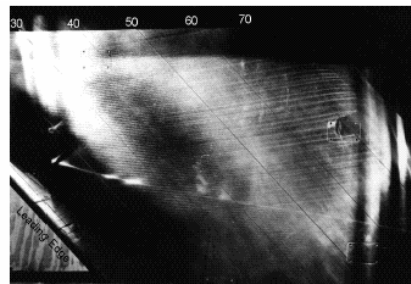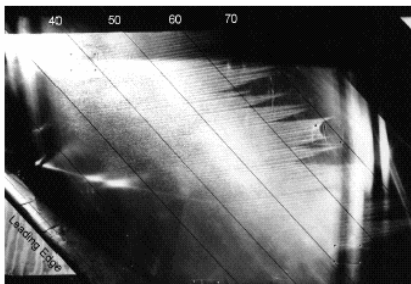
FIG. 2.2 REFERENCE HIGH AR SENSOR-CRAFT

Figure 1. Natural transition at 65% chord.

Figure 2. Distributed roughness of 8-mm spacing at leading edge. Transition delayed beyond 80% chord.

Figures 1 and 2. Crossflow-vortex visualization via naphthalene applied to the wing surface. 45°-swept NLF(2)-0415 airfoil in ASU low-speed experiment. Flow from left to right.

FIG. 2.3 LAMINAR FLOW INSTABILITY, DISTRIBUTED ROUGHNESS ELEMENTS
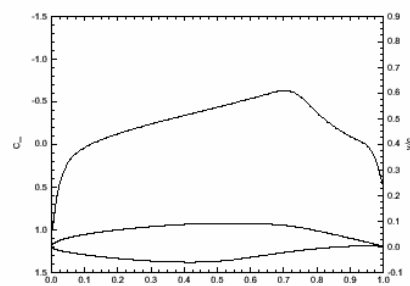
Figure 3. Upper surface C_p distribution for 45°-swept NLF(2)-0415 airfoil in ASU low-speed experiment.

25
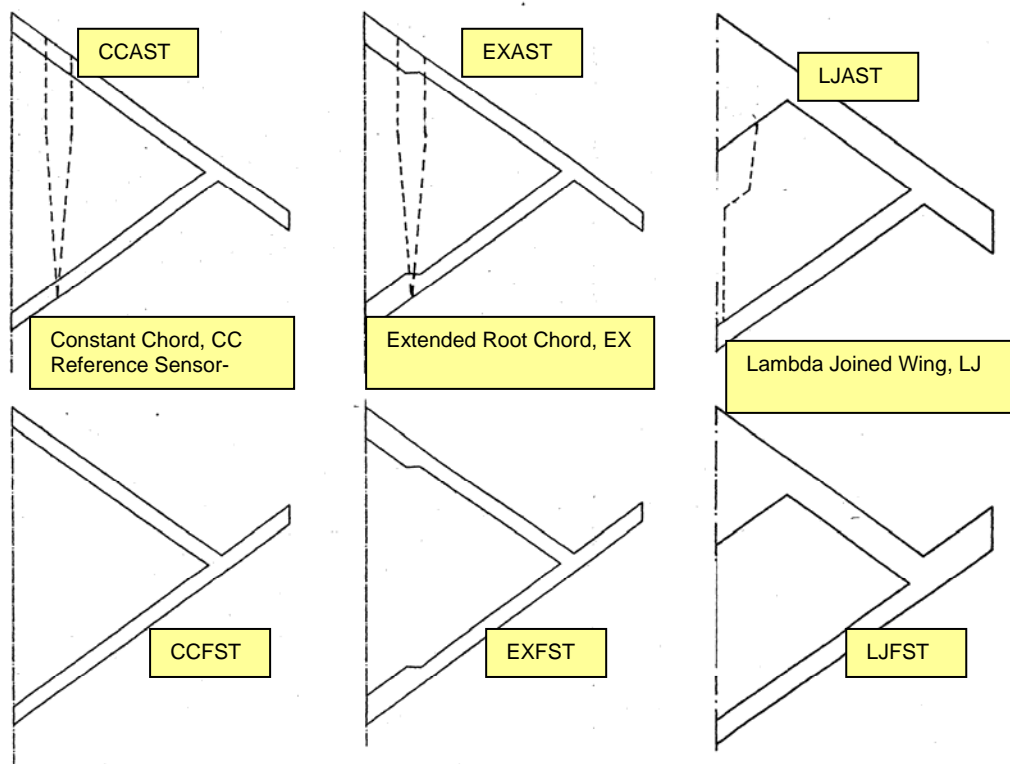
**FIG. 2.4 SENSOR-CRAFT CONCEPT PLANFORMS:
HIGH AR, EXTENDED ROOT CHORD & LAMBDA JOINED WING
AFT & FORWARD SWEPT TIPS**
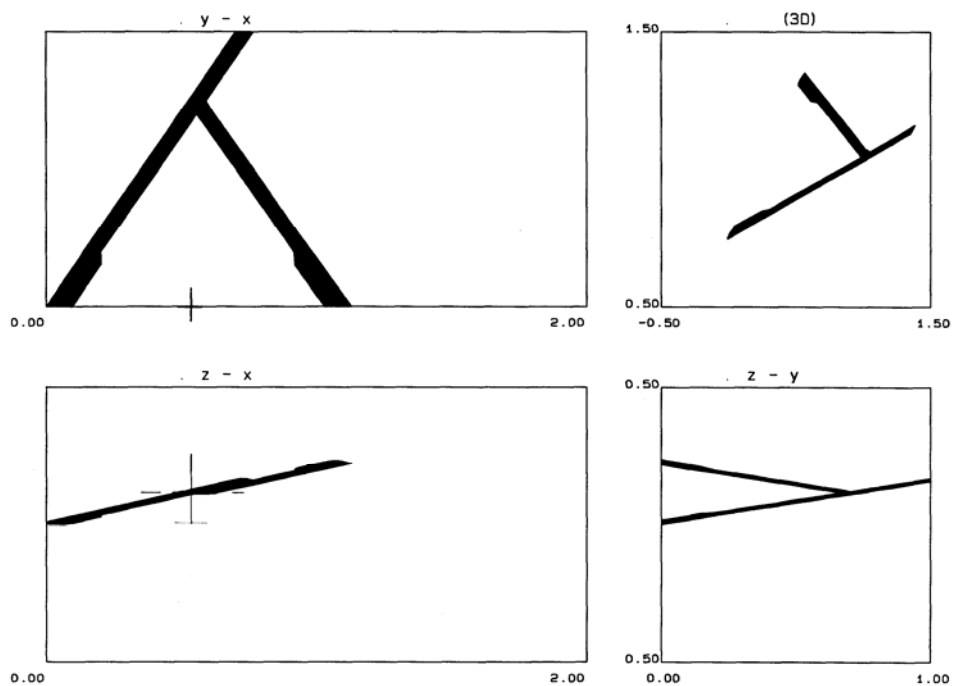
**FIG. 5.1.1 HIGH AR SENSOR-CRAFT CONFIGURATION WITH
EXTENDED ROOT CHORDS, AFT SWEPT TIP (EXAST)**

26
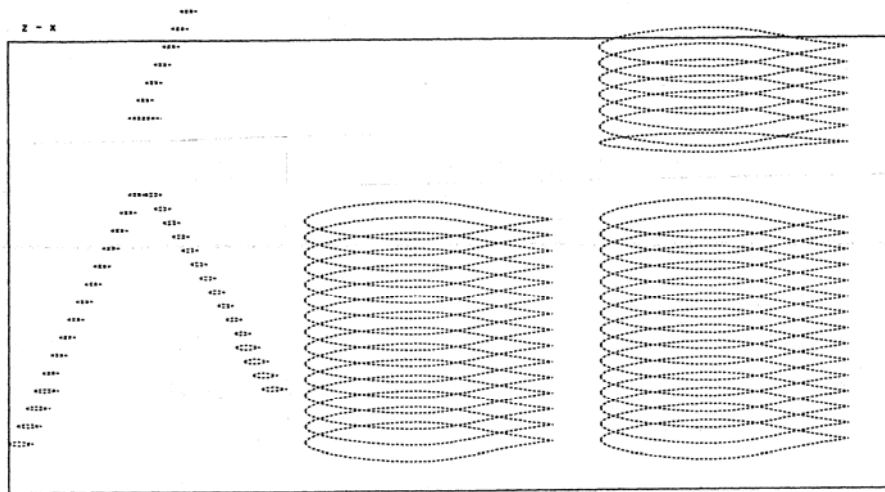
FIG. 5.1.2 CONFIGURATION EXAST, SYMMETRICAL AEROFOILS ON BOTH WINGS
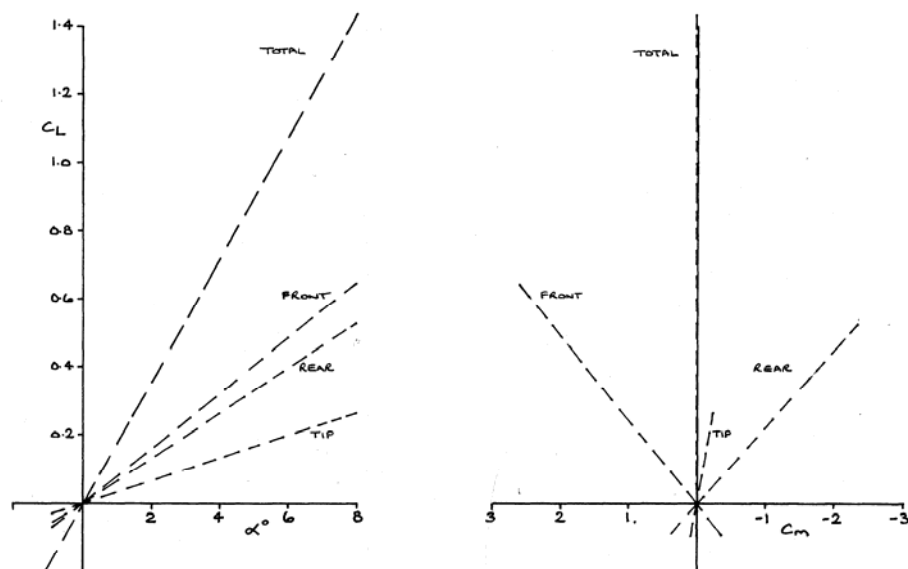
FIG. 5.1.3 CONFIGURATION EXAST UNCAMBERED, CL, Cm COMPONENT CONTRIBUTIONS, Mach 0.6
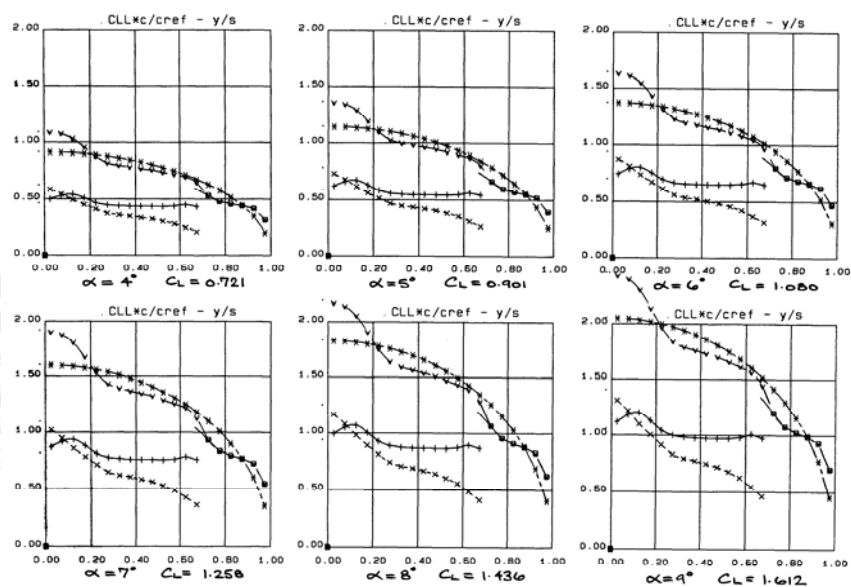
FIG. 5.1.4 CONFIGURATION EXAST UNCAMBERED, SPANWISE LOADINGS THROUGH AoA RANGE, Mach 0.6
(Total compared with elliptic)

27

AoA 4° CL=0.721

AOA 5° CL=0.901

AOA 6° CL=1.080

AOA 7° CL=1.250

AOA 8° CL=1.436

AOA 9° CL=1.612
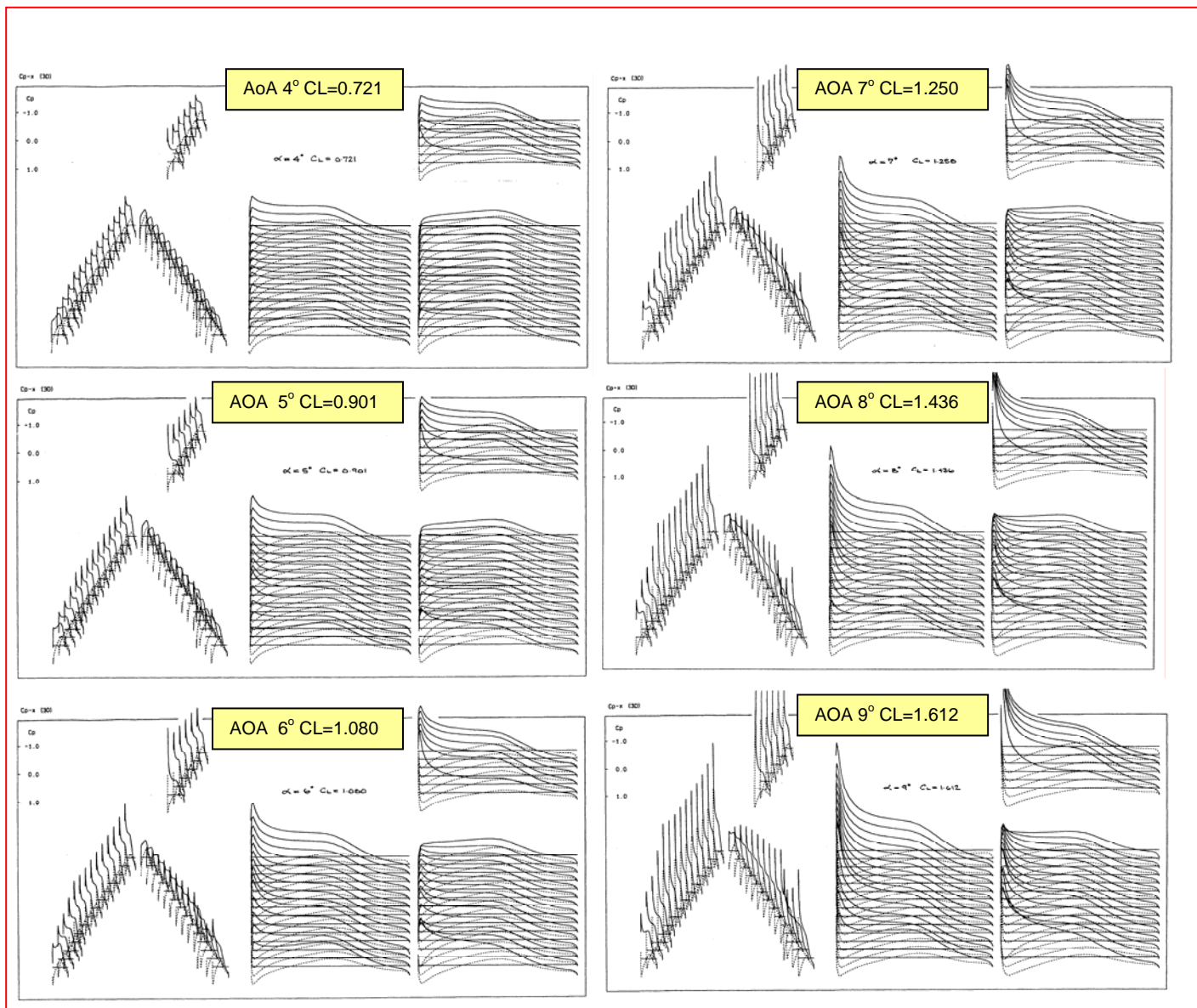
FIG. 5.1.5   CONFIGURATION EXAST UNCAMBERED, Cp DISTRIBUTIONS THROUGH AoA RANGE, Mach 0.6
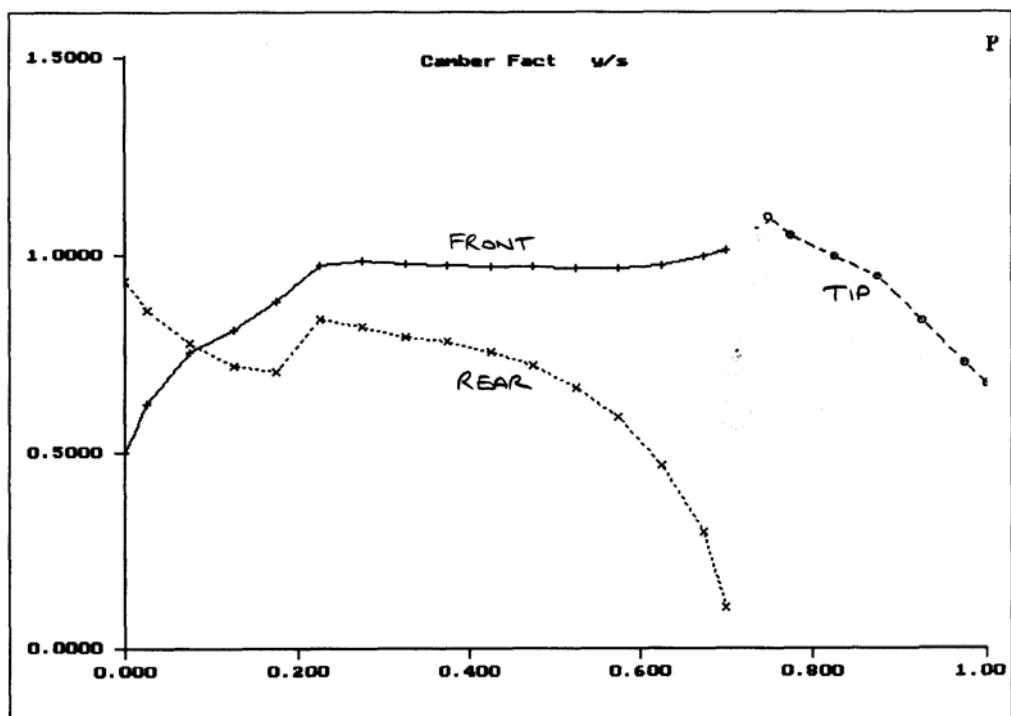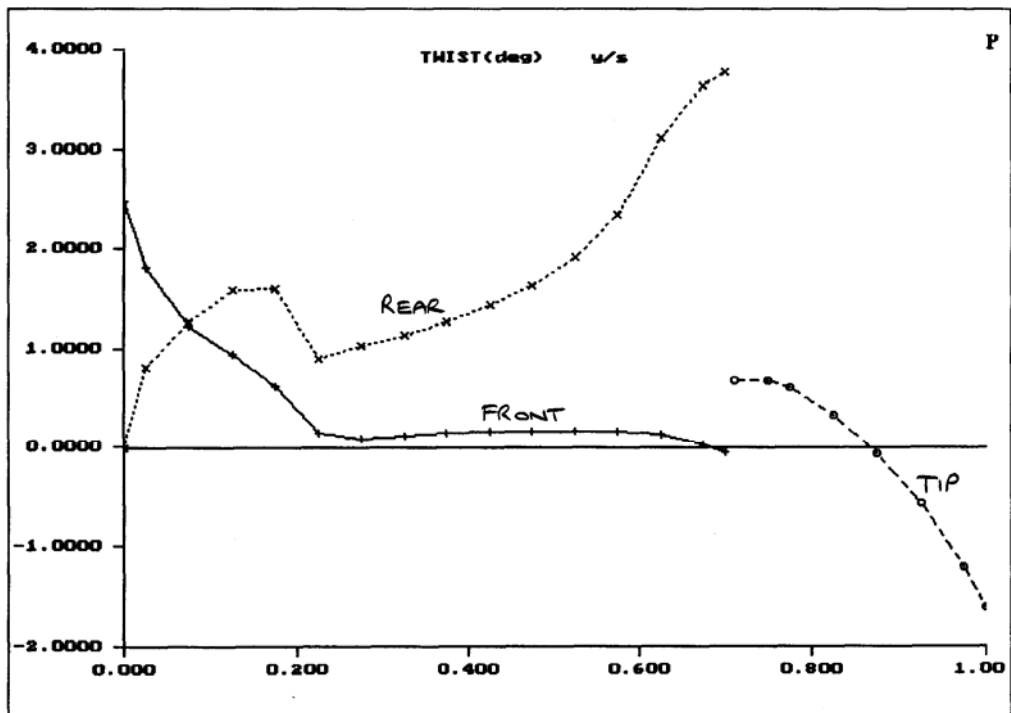
**FIG. 5.2.1 CONFIGURATION EXAST,
DESIGNED TWIST & CAMBER DISTRIBUTIONS**
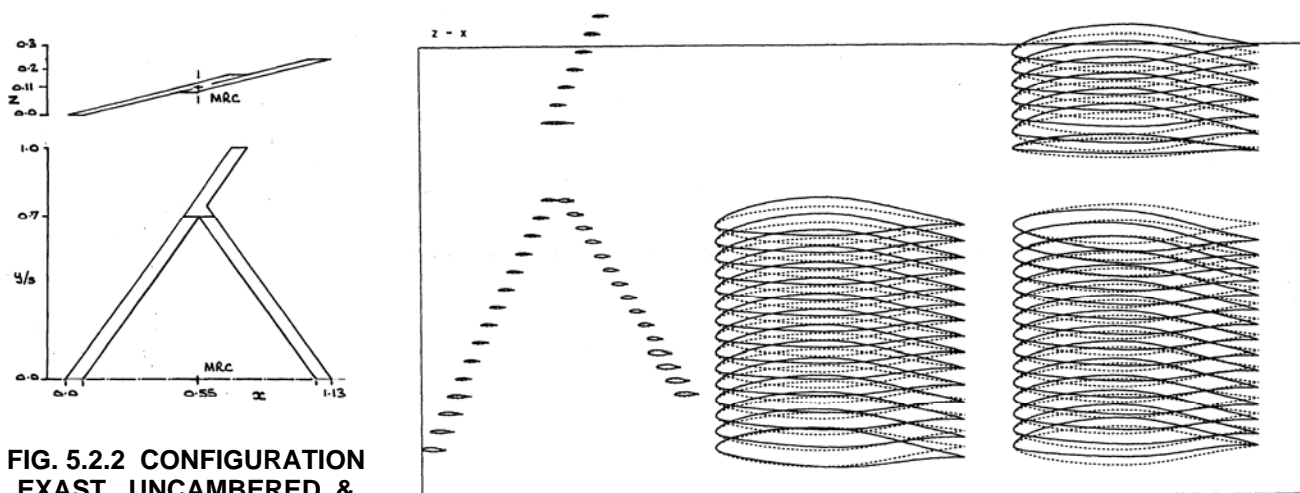
FIG. 5.2.2 CONFIGURATION EXAST, UNCAMBERED & DESIGNED CAMBER
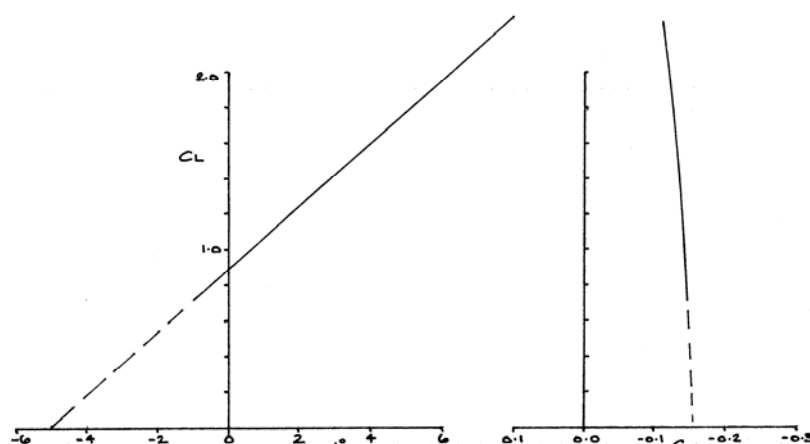
FIG. 5.2.3 CONFIGURATION EXAST DESIGNED, CL, Cm and α VARIATIONS , Mach 0.6
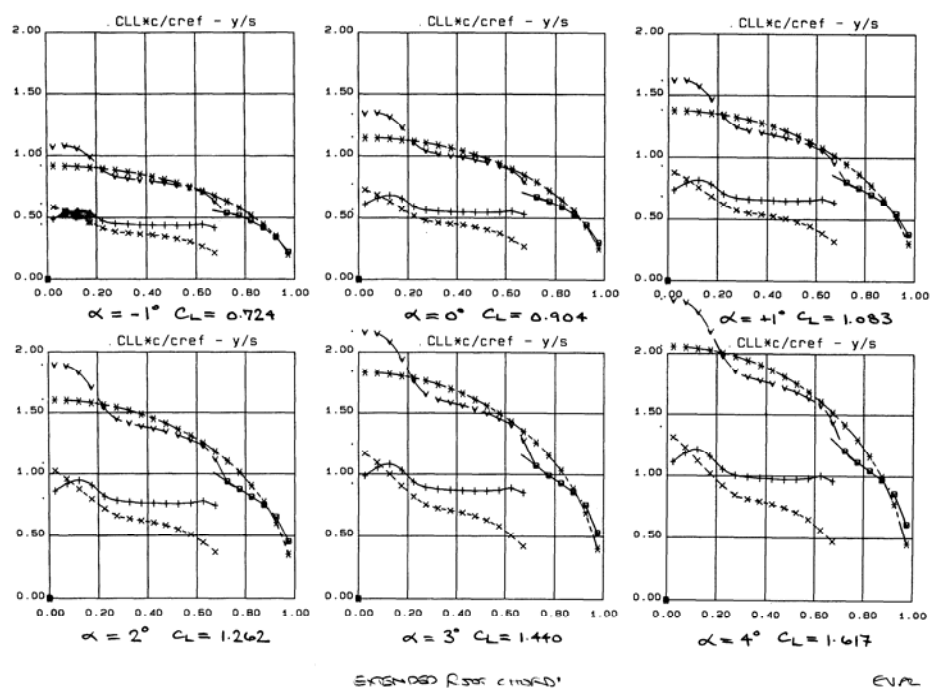
FIG. 5.2.4 CONFIGURATION EXAST, SPANWISE LOADINGS THROUGH AoA RANGE, DESIGNED CAMBERED AEROFOIL CONFIGURATION, Mach 0.6 (Total compared with elliptic)

30

AoA −1° CL=0.724

AoA 2° CL=1.262

AoA 0° CL=0.904

AoA 3° CL=1.440
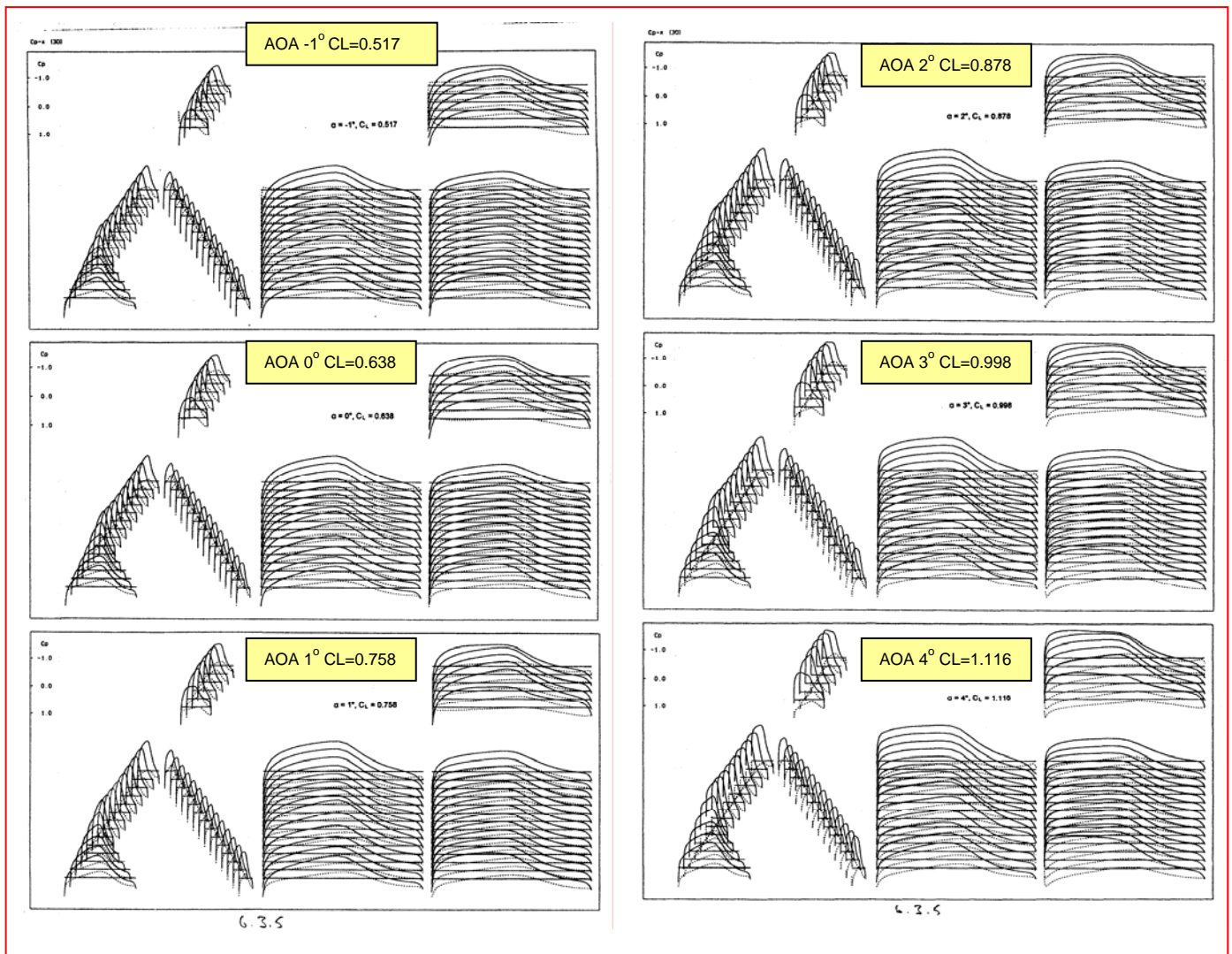
AoA 1° CL=1.083

AoA 4° CL=1.617
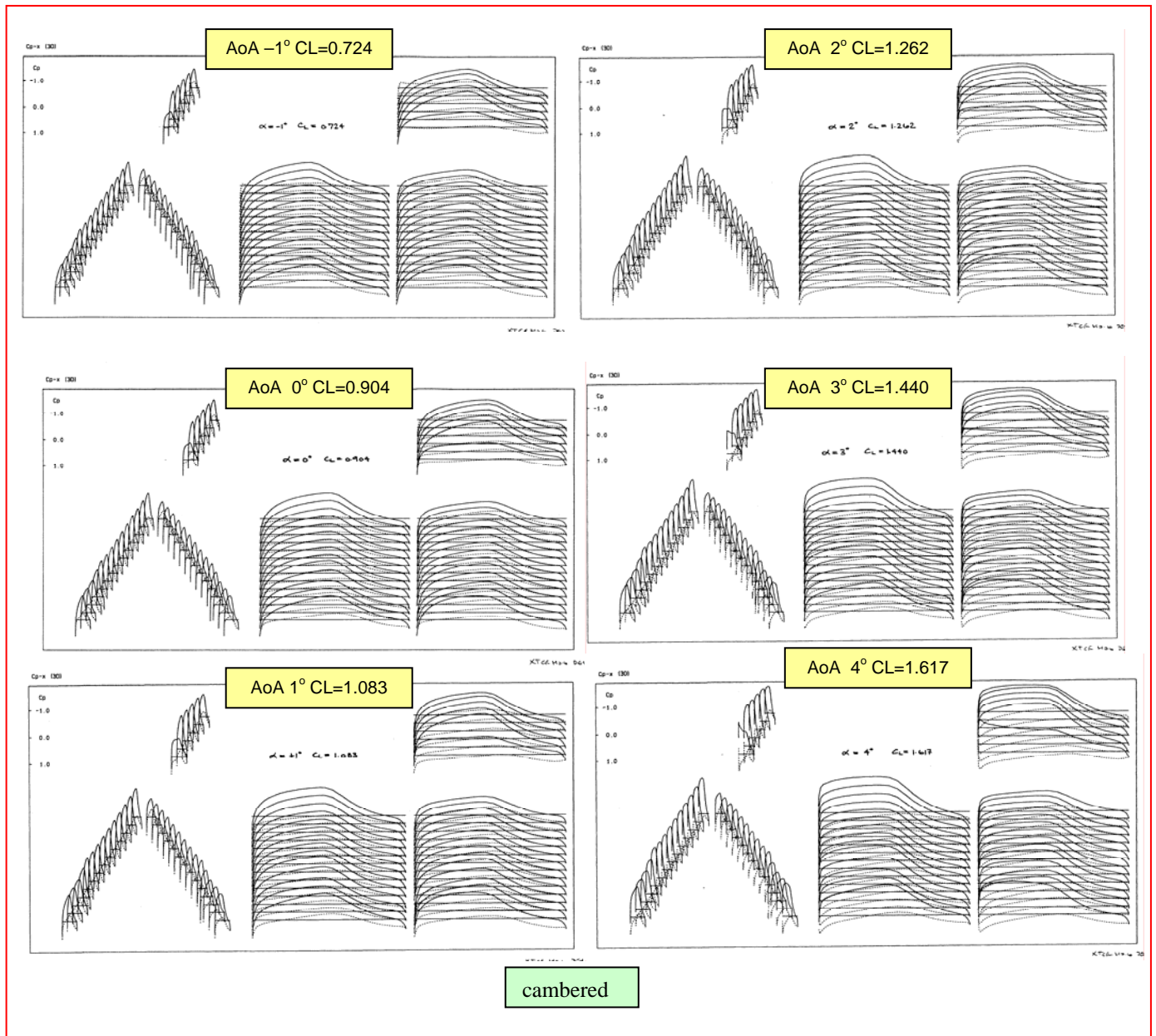
cambered

**FIG. 5.2.5   CONFIGURATION EXAST DESIGNED CAMBER, Cp DISTRIBUTIONS THROUGH
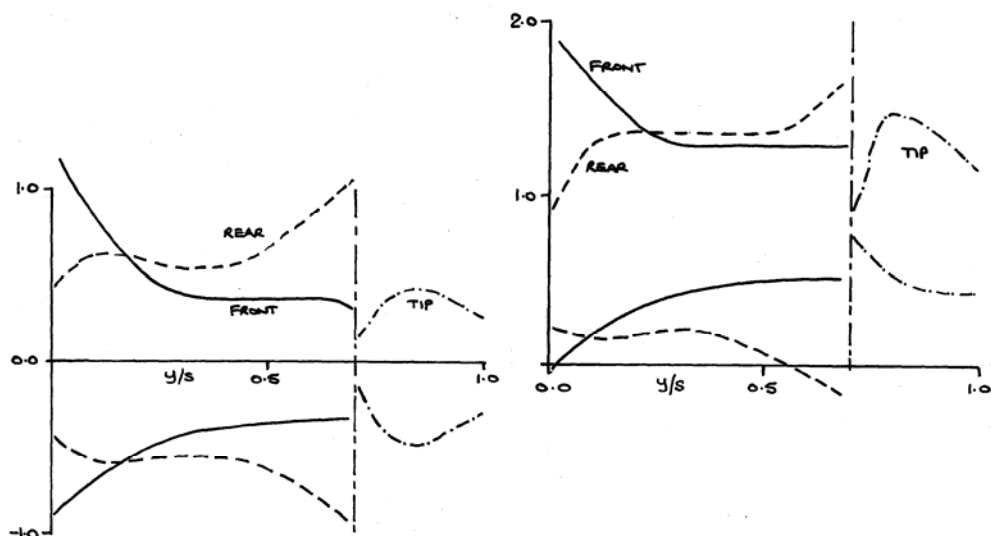AoA RANGE, Mach 0.6**
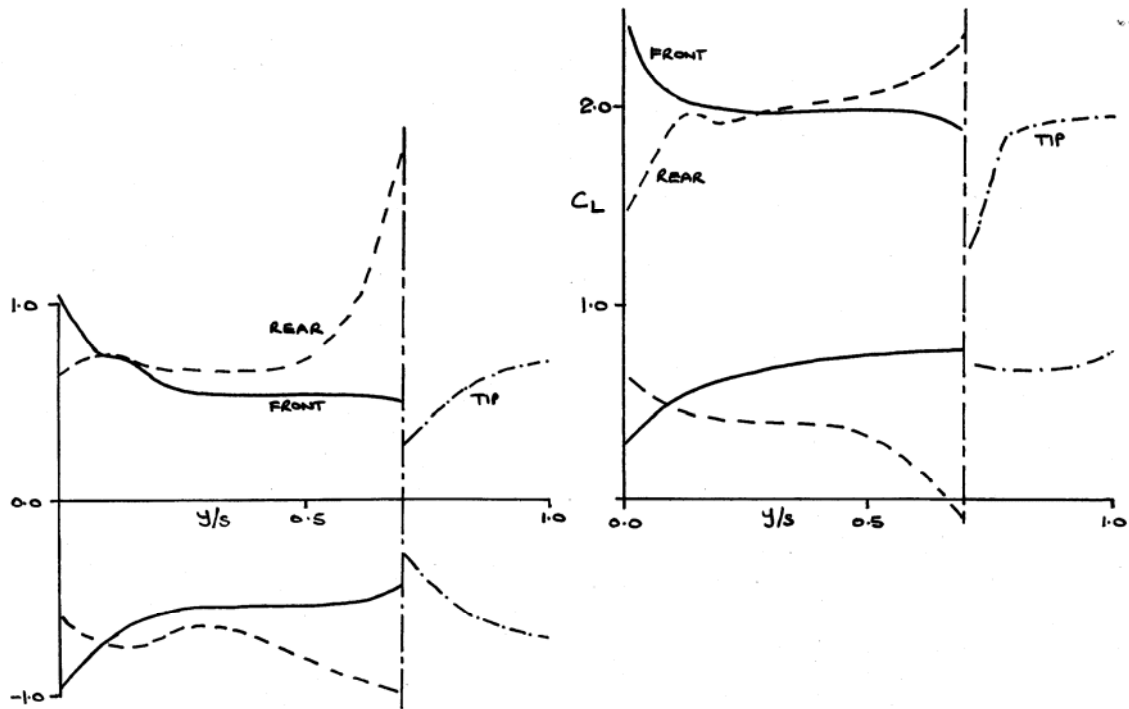
**FIG. 5.2.6 CONFIGURATION EXAST, LAMINAR FLOW RANGES,
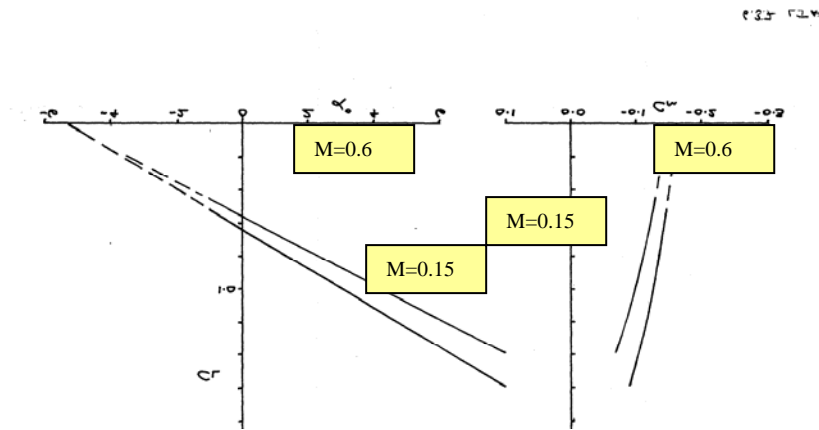UNCAMBERED AND DESIGN CAMBER**
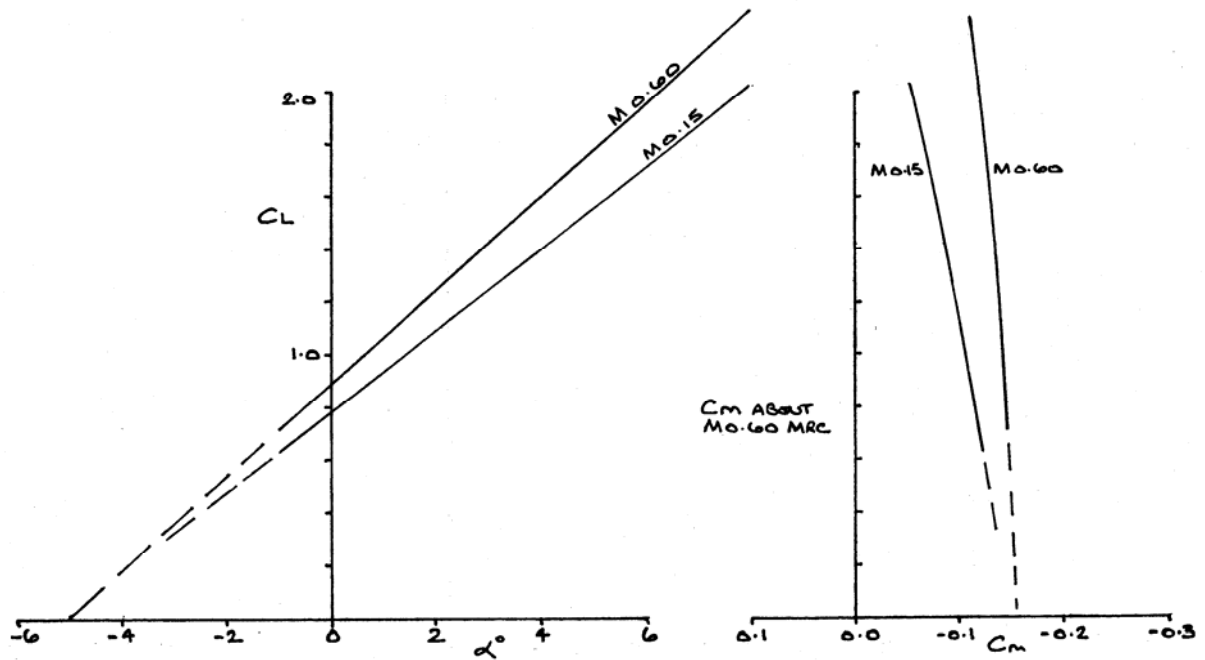
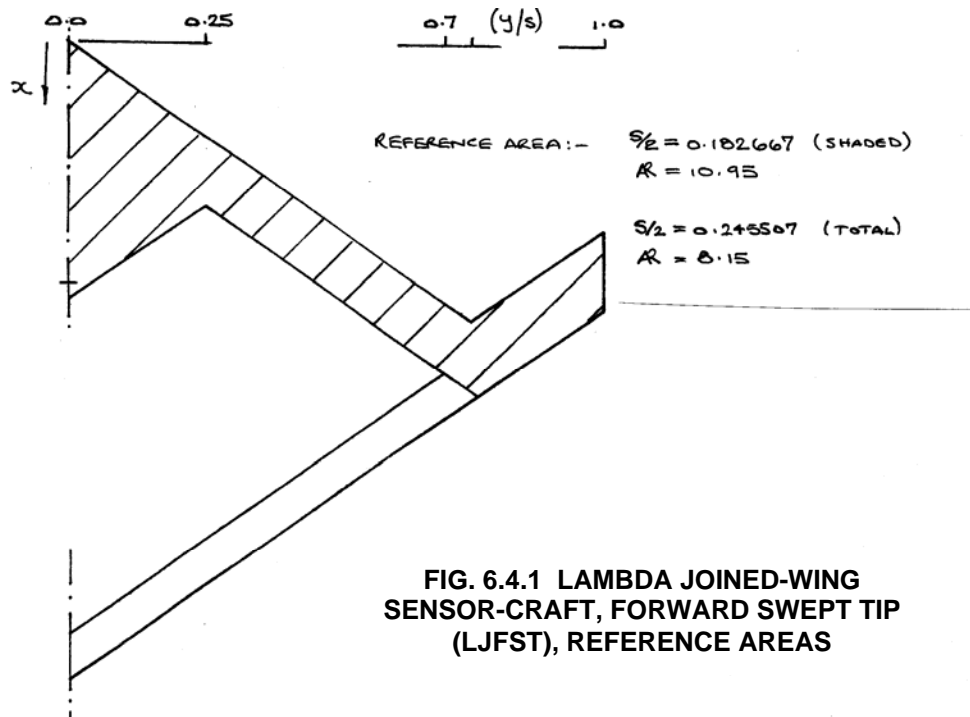**FIG. 5.2.7 CONFIGURATION EXAST DESIGNED, CL, Cm and α VARIATIONS ,
Mach 0.6 & 0.15**
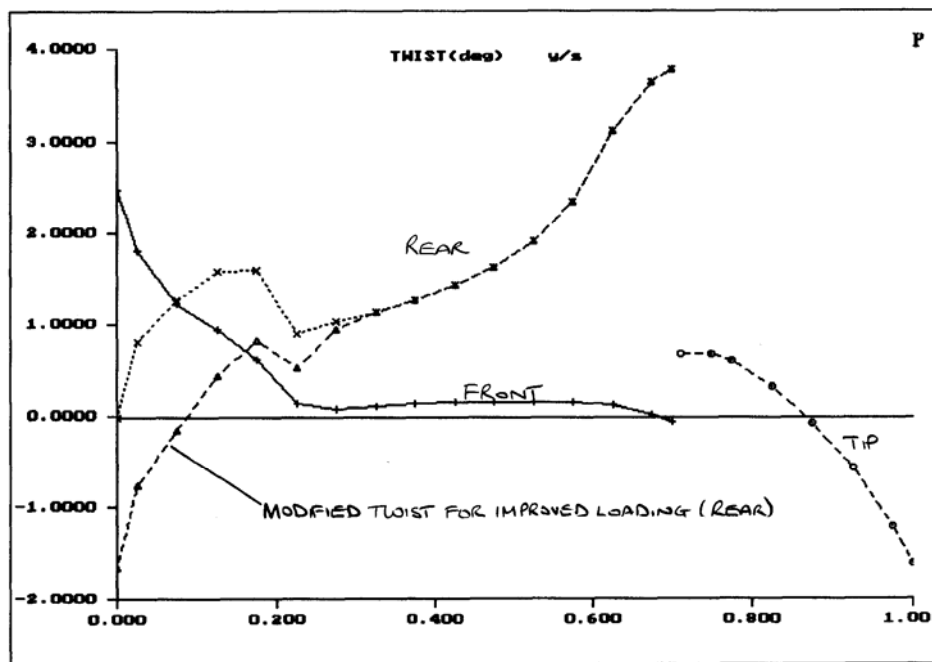
FIG. 5.3.1 CONFIGURATION EXAST MODIFIED REAR WING TWIST DISTRIBUTIONS

FIG. 5.3.2 CONFIGURATION EXAST, UNCAMBERED & DESIGNED CAMBER, REAR WING TWIST MODIFIED
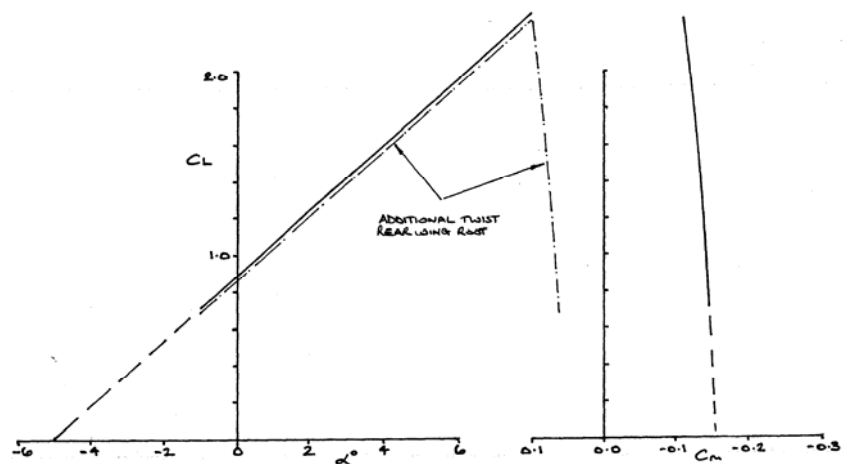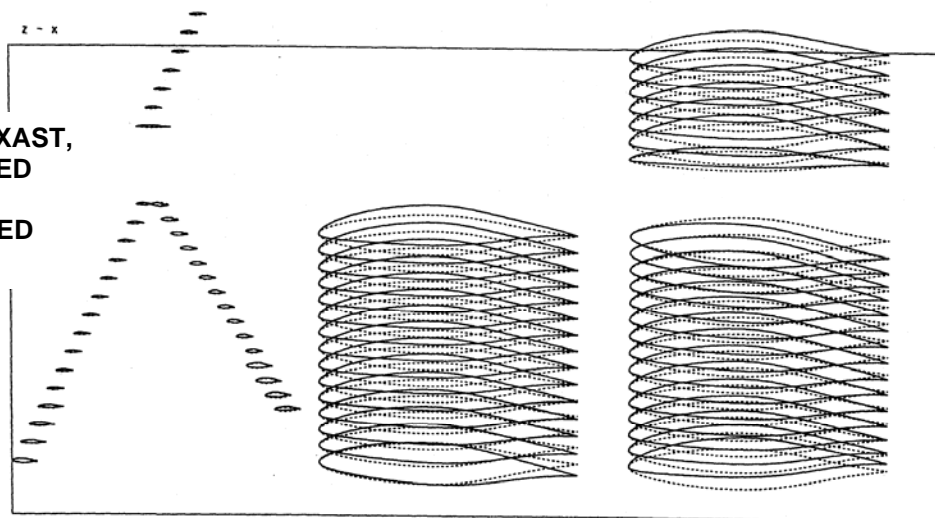
FIG. 5.3.3 CONFIGURATION EXAST MODIFIED REAR WING TWIST, CL, Cm and α VARIATIONS , Mach 0.6
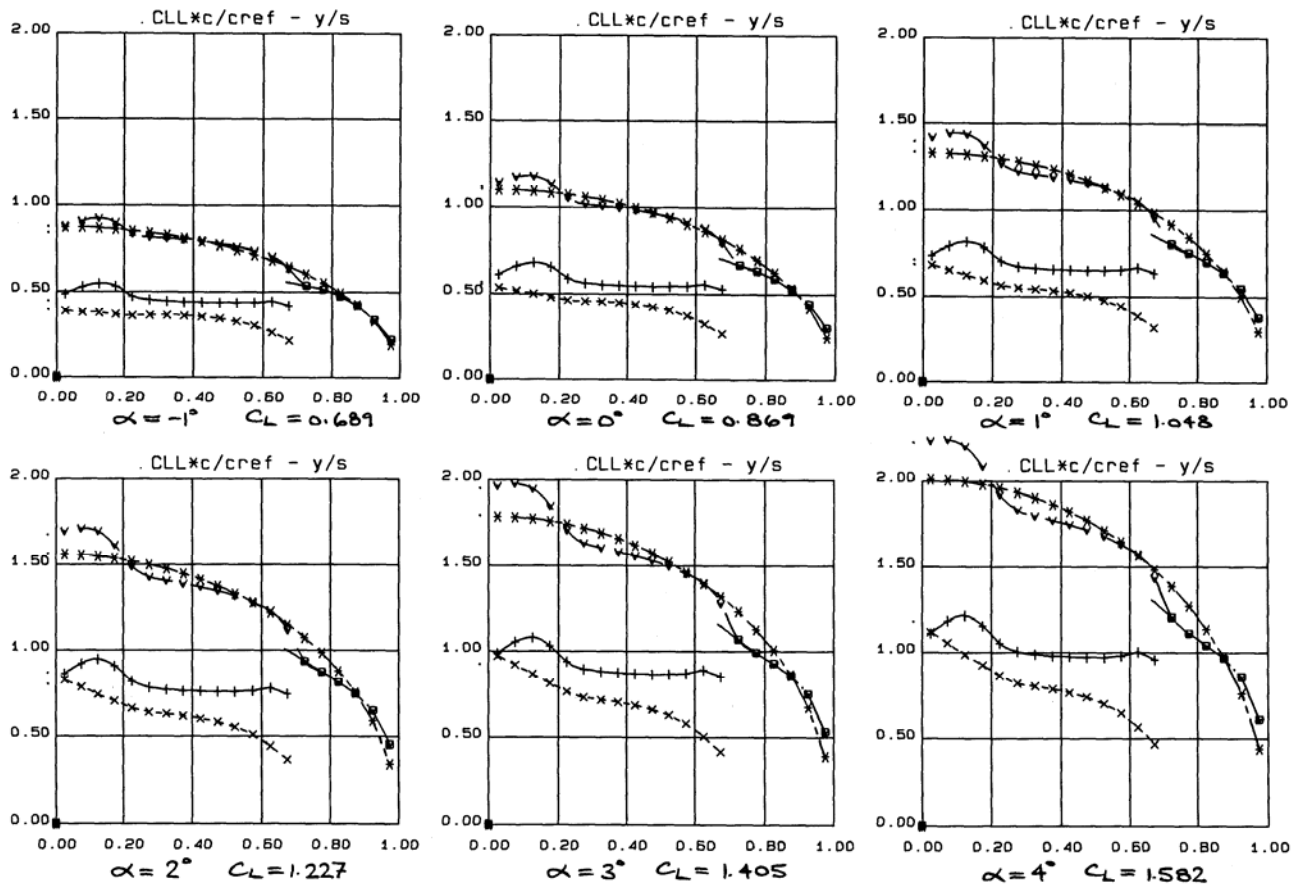
**FIG. 5.3.4 CONFIGURATION EXAST MODIFIED REAR WING TWIST,
SPANWISE LOADINGS THROUGH AoA RANGE, Mach 0.6
(Total compared with elliptic)**

34

AOA -1° CL=0.689

AOA 2° CL=1.227

AOA 0° CL=0.869

AOA 3° CL=1.405

AOA 1° CL=1.048

AOA 4° CL=1.582
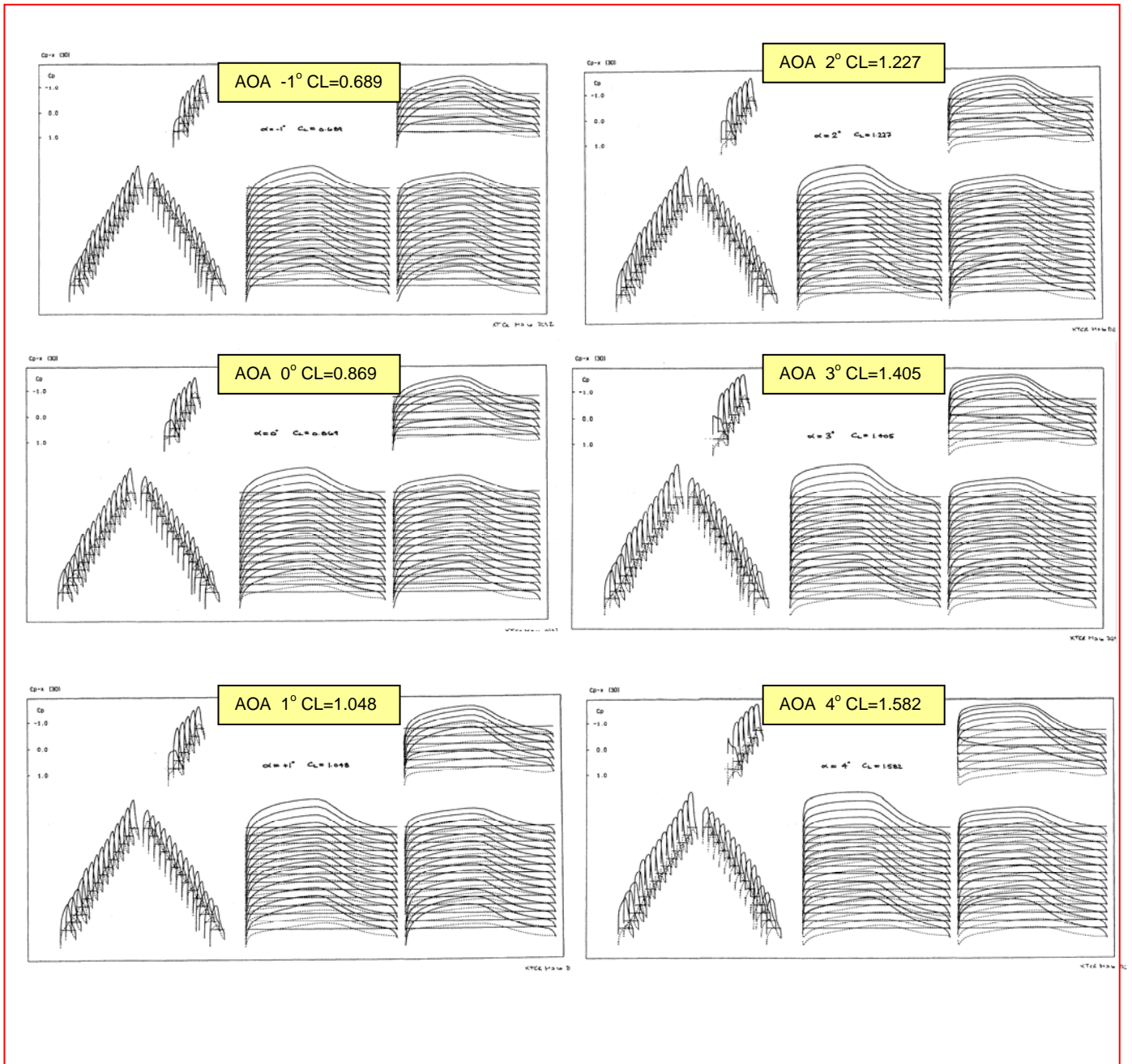
**FIG. 5.3.5 CONFIGURATION EXAST MODIFIED REAR WING TWIST, Cp
DISTRIBUTIONS THROUGH AoA RANGE, Mach 0.6**

35
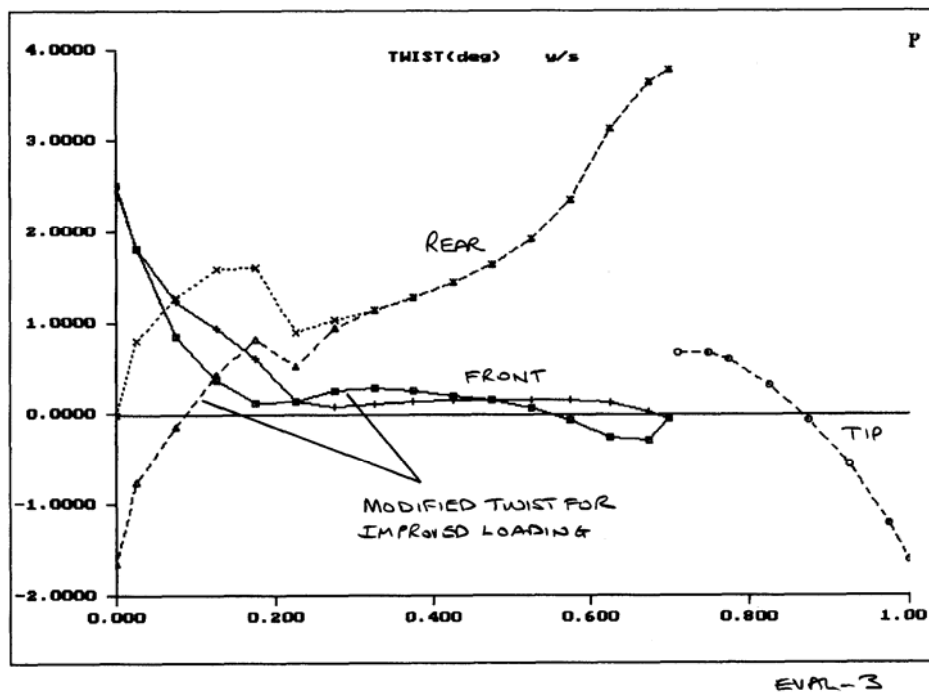
FIG. 5.3.6 CONFIGURATION EXAST MODIFIED FRONT & REAR WING TWIST DISTRIBUTIONS
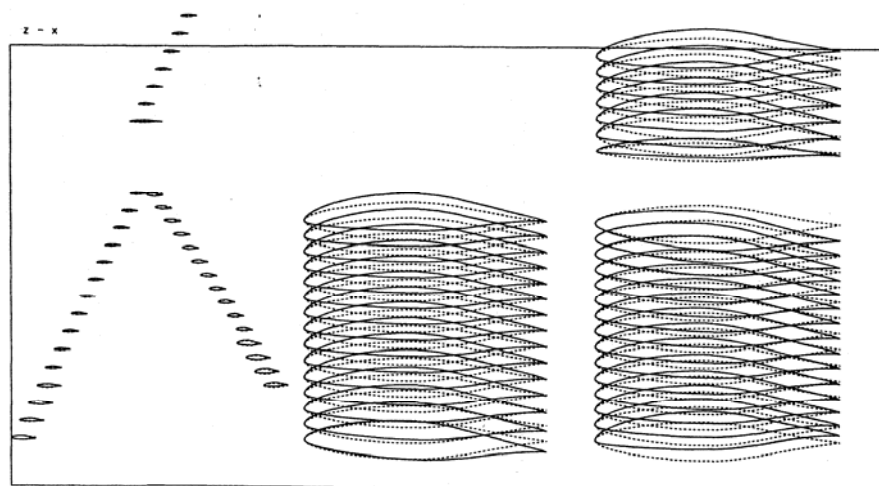
**FIG. 5.3.7 CONFIGURATION EXAST,
UNCAMBERED & DESIGNED CAMBER,
FRONT & REAR WING TWIST MODIFIED**
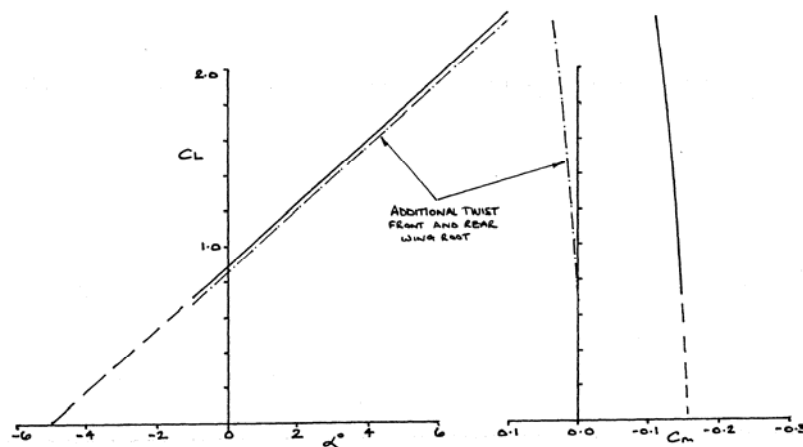
**FIG. 5.3.8 CONFIGURATION EXAST MODIFIED FRONT & REAR WING TWIST,
CL, Cm and α VARIATIONS , Mach 0.6 & 0.15**
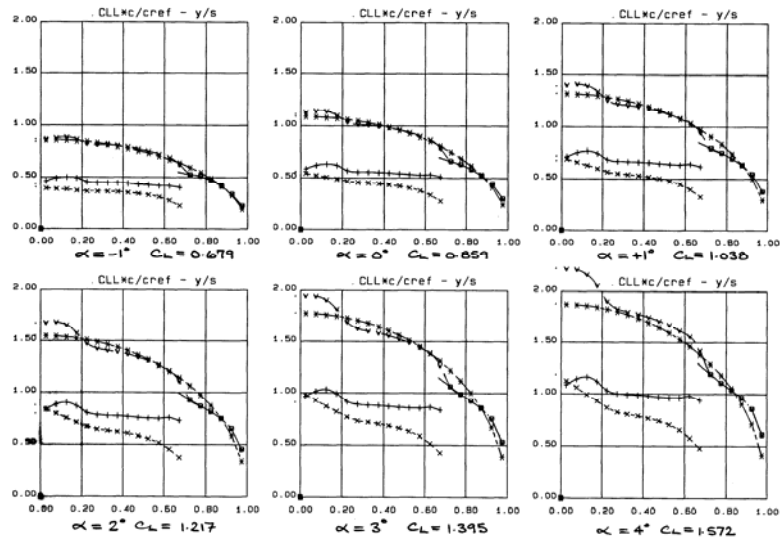
FIG. 5.3.9 CONFIGURATION EXAST MODIFIED FRONT & REAR WING TWIST, SPANWISE LOADINGS THROUGH AoA RANGE, Mach 0.6 (Total compared with elliptic)
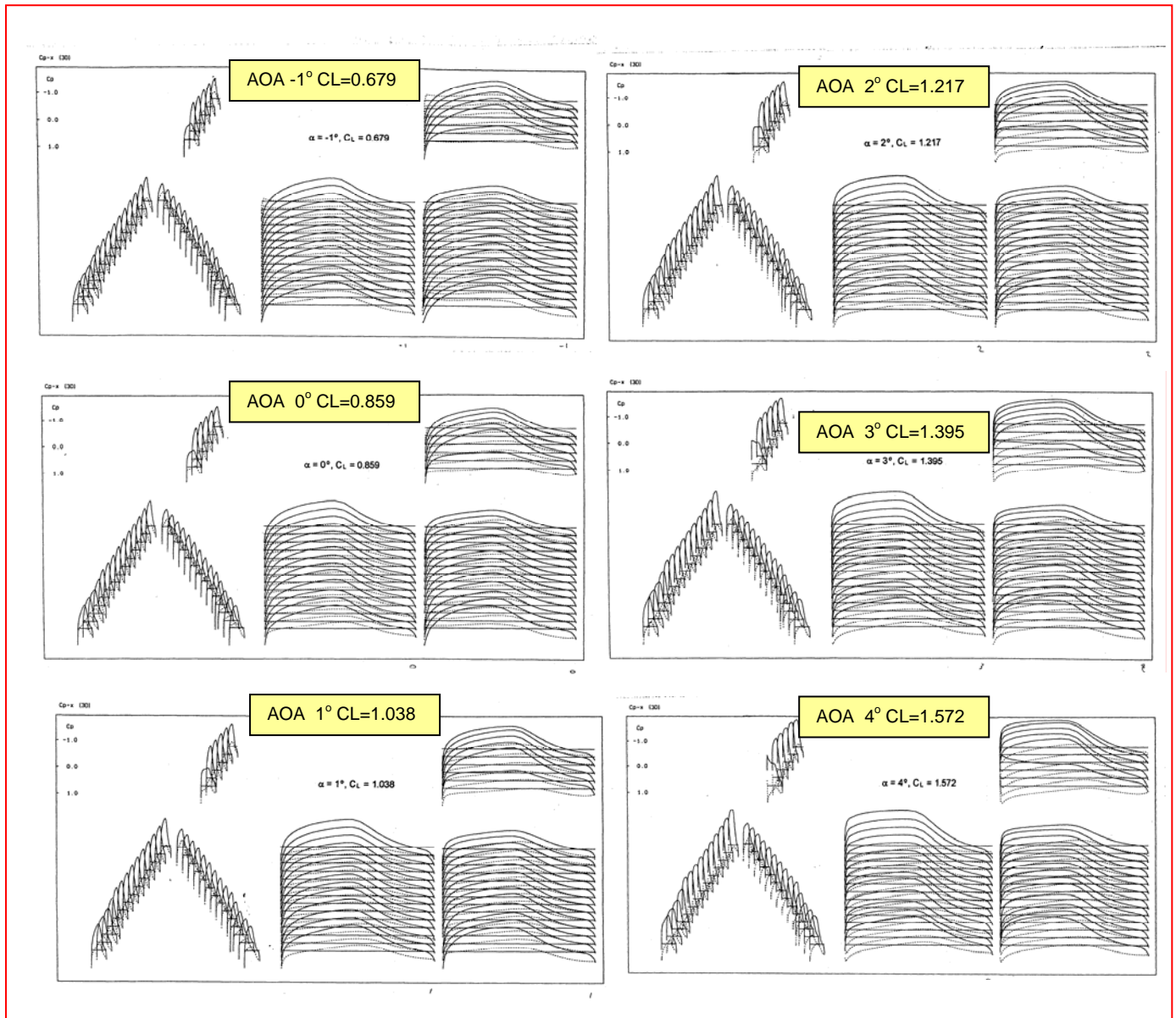
FIG. 5.3.10 CONFIGURATION EXAST MODIFIED FRONT & REAR WING TWIST, Cp DISTRIBUTIONS THROUGH AoA RANGE, Mach 0.6
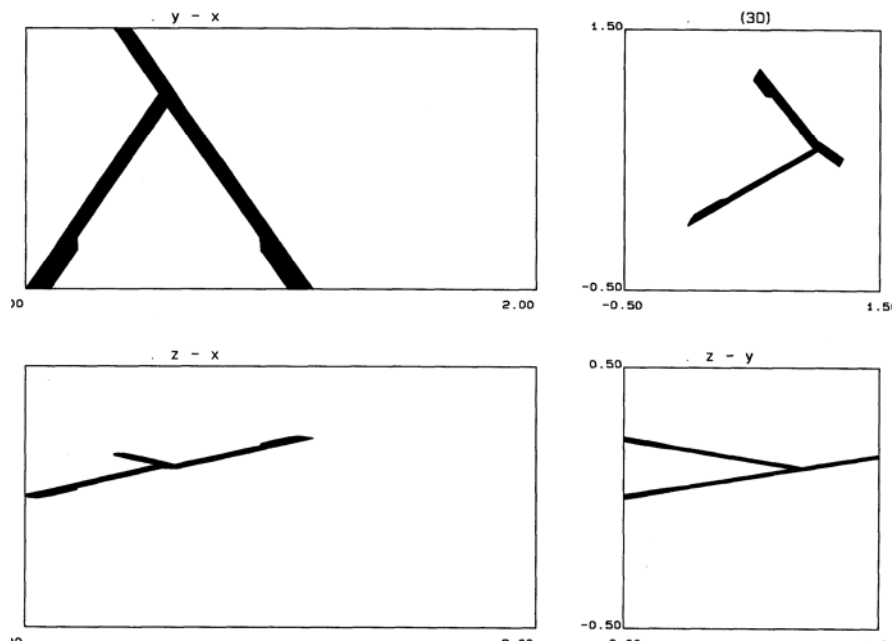
FIG. 5.4.1 HIGH AR SENSOR-CRAFT CONFIGURATION WITH EXTENDED ROOT CHORDS, FORWARD SWEPT TIP (EXFST)
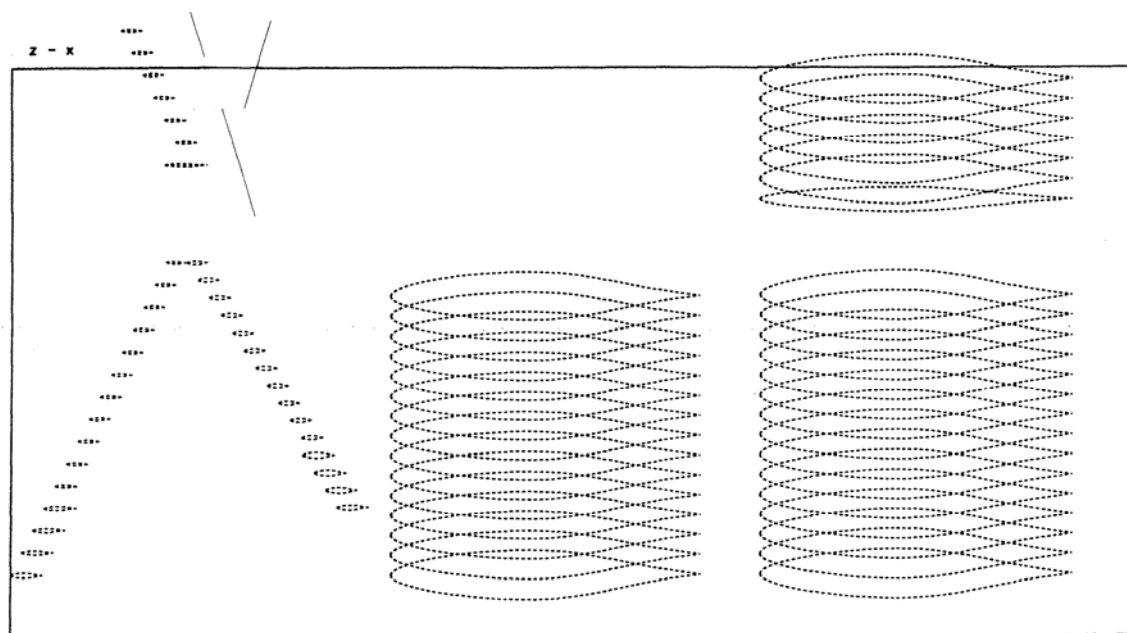
FIG. 5.4.2 CONFIGURATION EXFST, SYMMETRICAL AEROFOILS ON BOTH WINGS
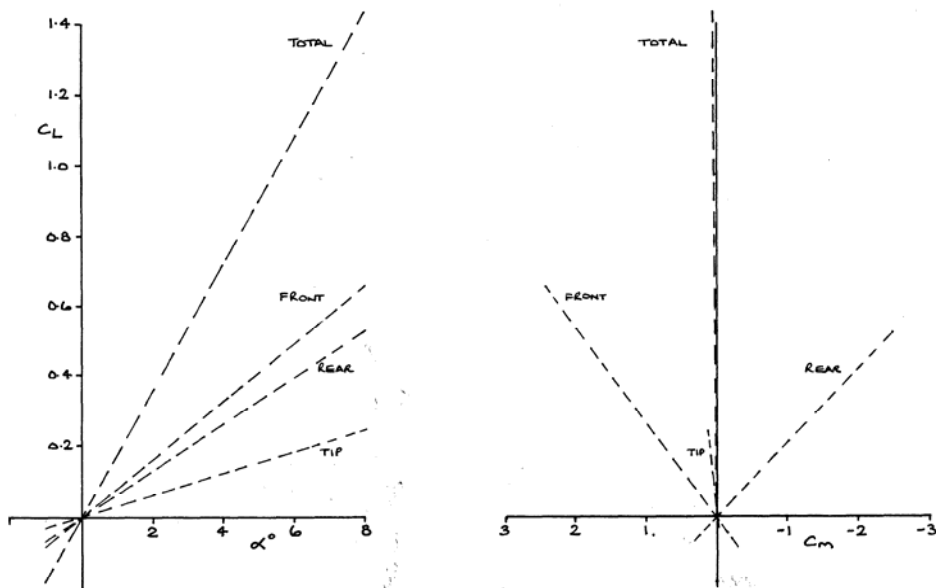
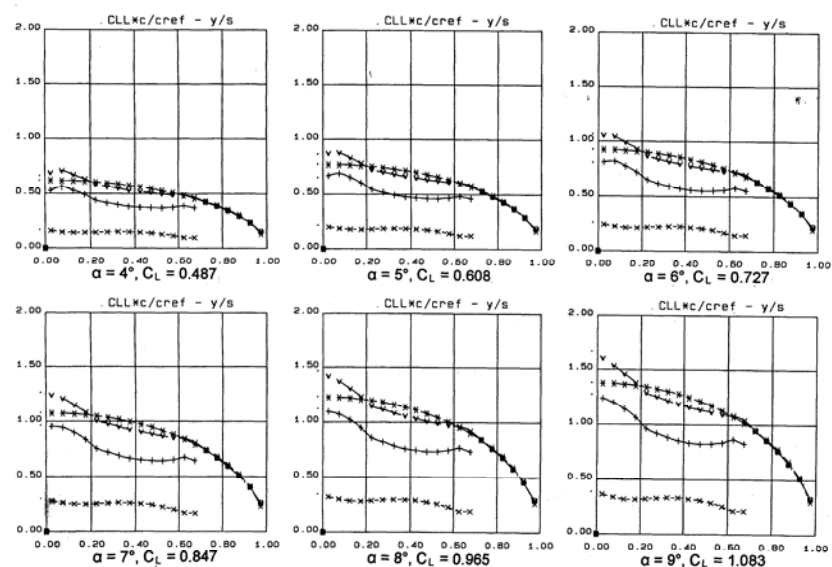**FIG. 5.4.3 CONFIGURATION EXFST UNCAMBERED, CL, Cm COMPONENT CONTRIBUTIONS, Mach 0.6**
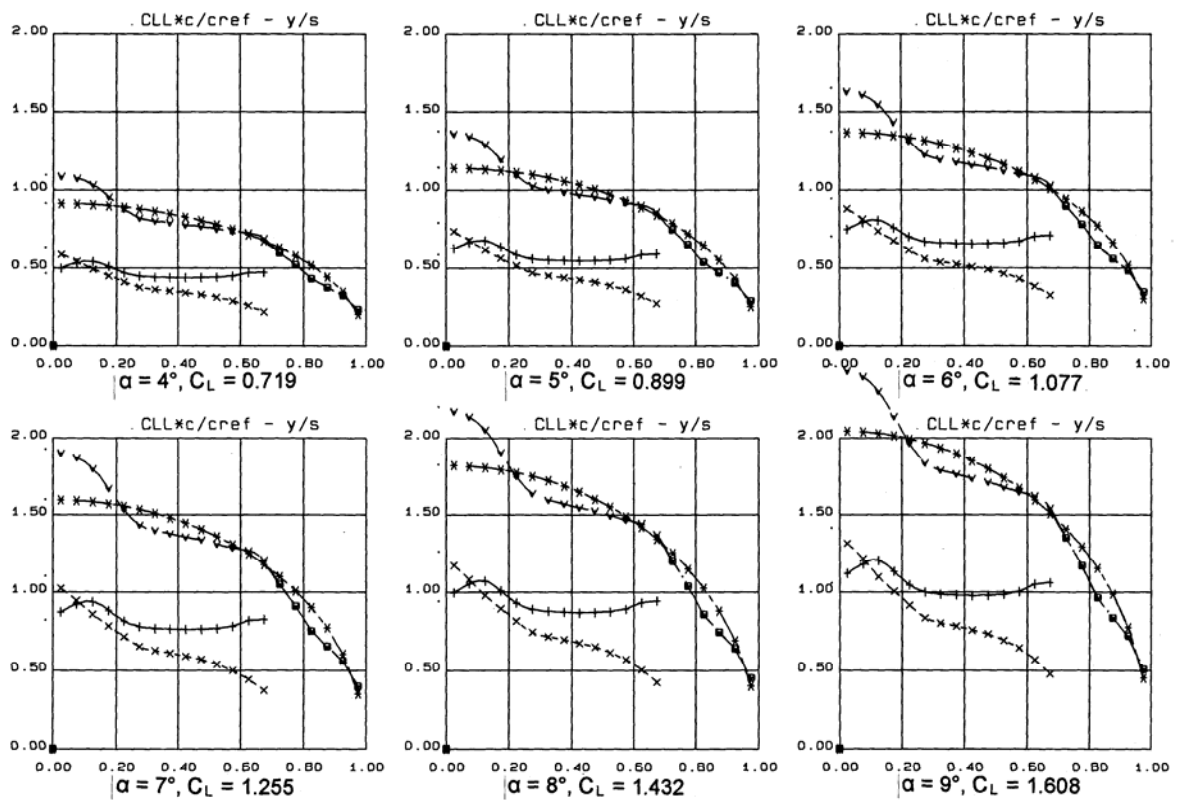
FIG. 5.4.4   CONFIGURATION EXFST UNCAMBERED, SPANWISE LOADINGS THROUGH AoA RANGE, Mach 0.6 (Total compared with elliptic)

39

AOA 4° CL=0.719

AOA 7° CL=1.255

AOA 5° CL=0.899

AOA 8° CL=1.432

AOA 6° CL=1.077

AOA 9° CL=1.609
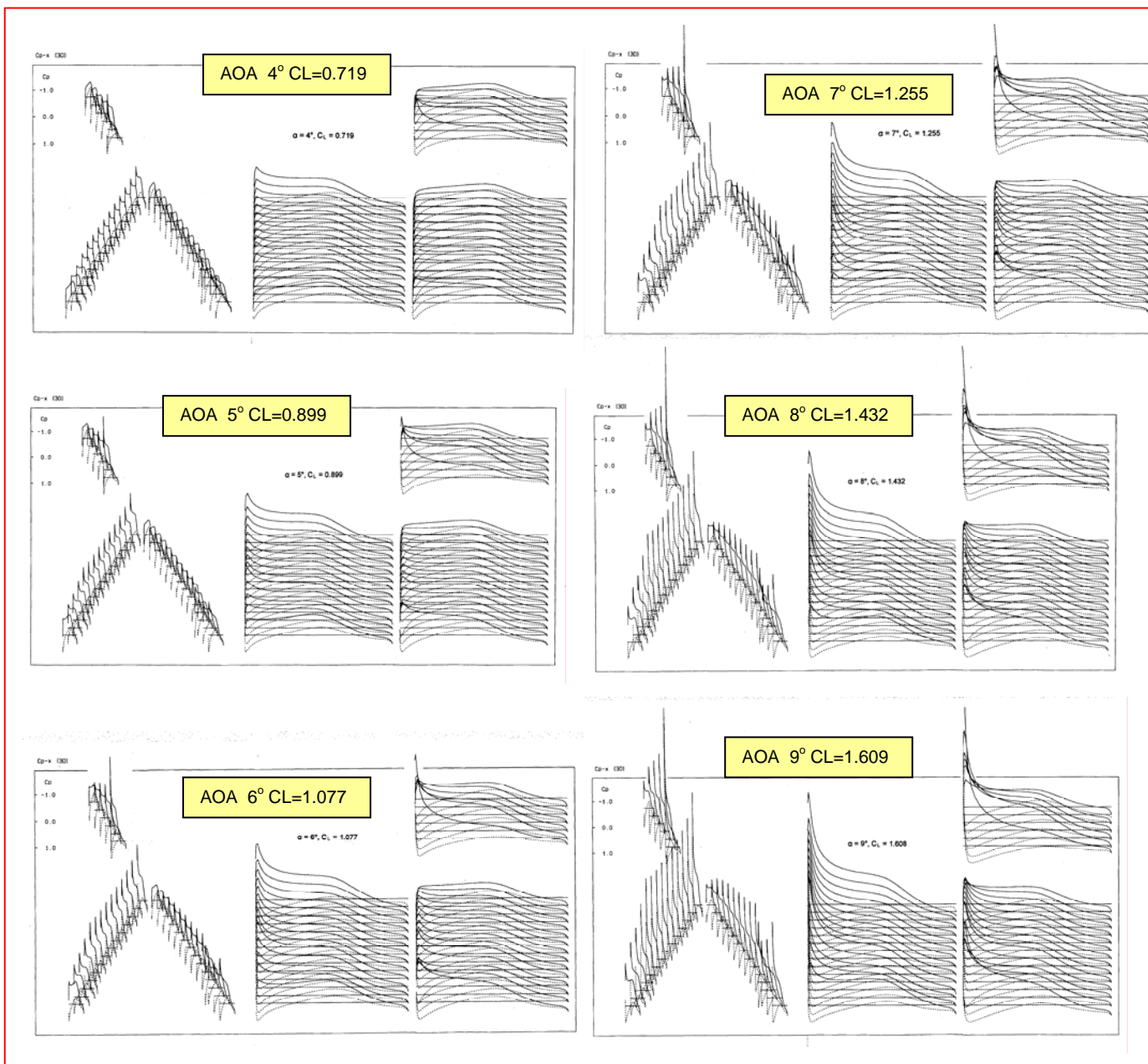
FIG. 5.4.5   CONFIGURATION EXFST UNCAMBERED, Cp DISTRIBUTIONS THROUGH AoA RANGE, Mach 0.6
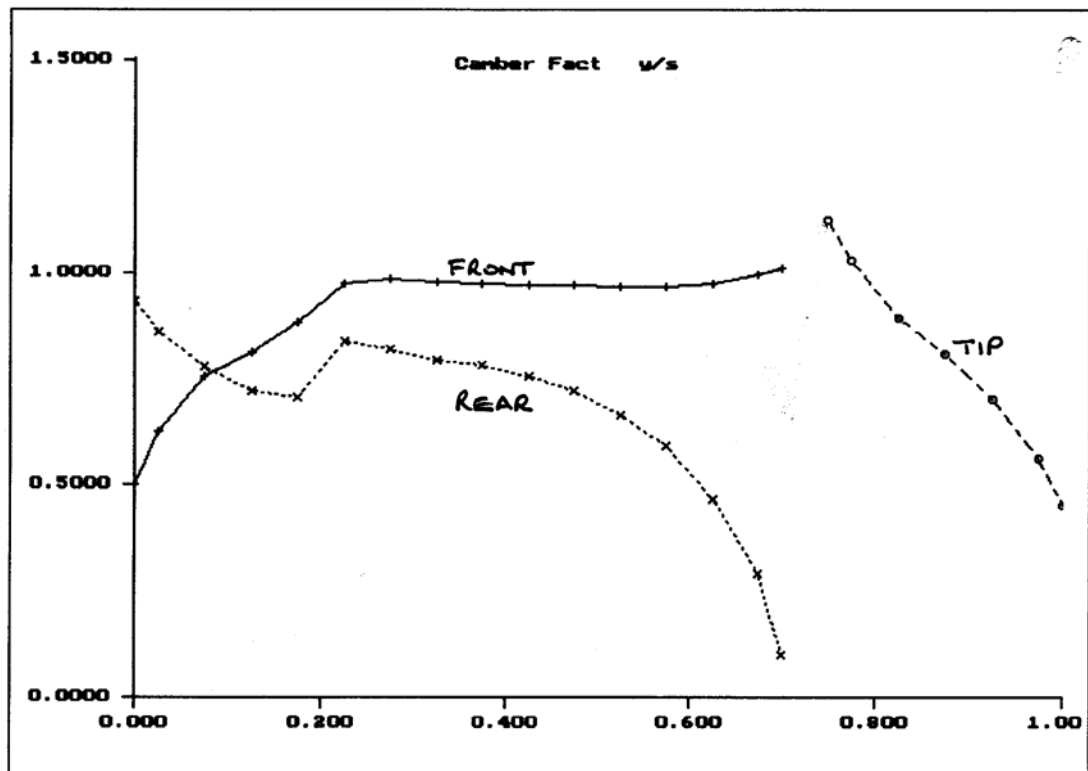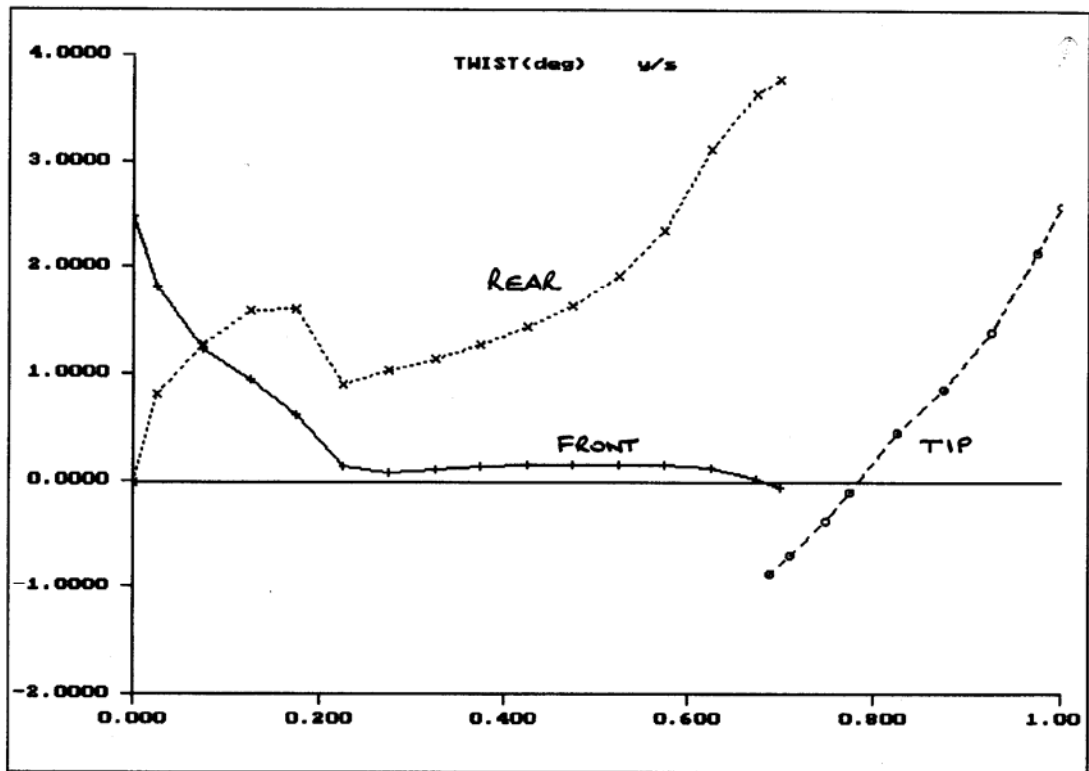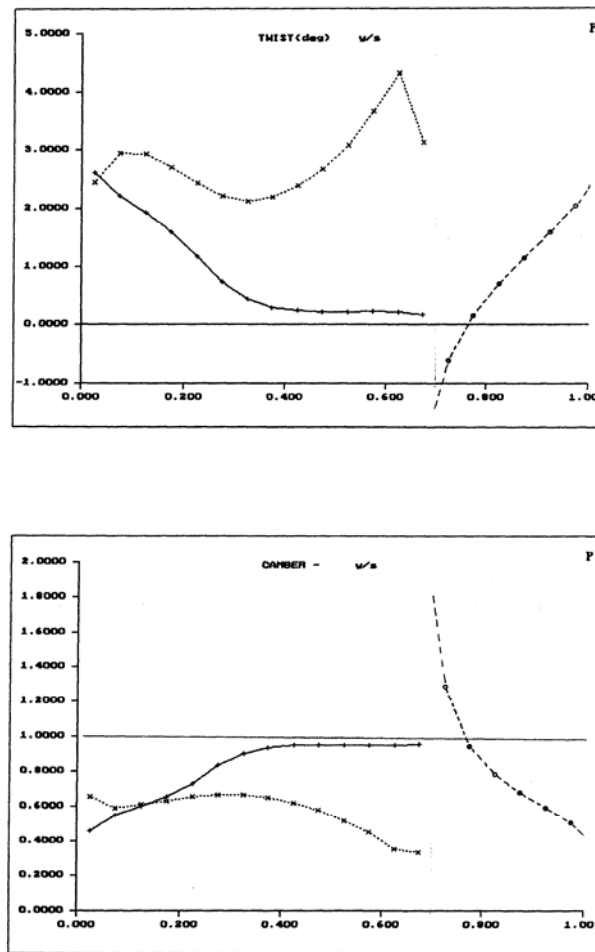
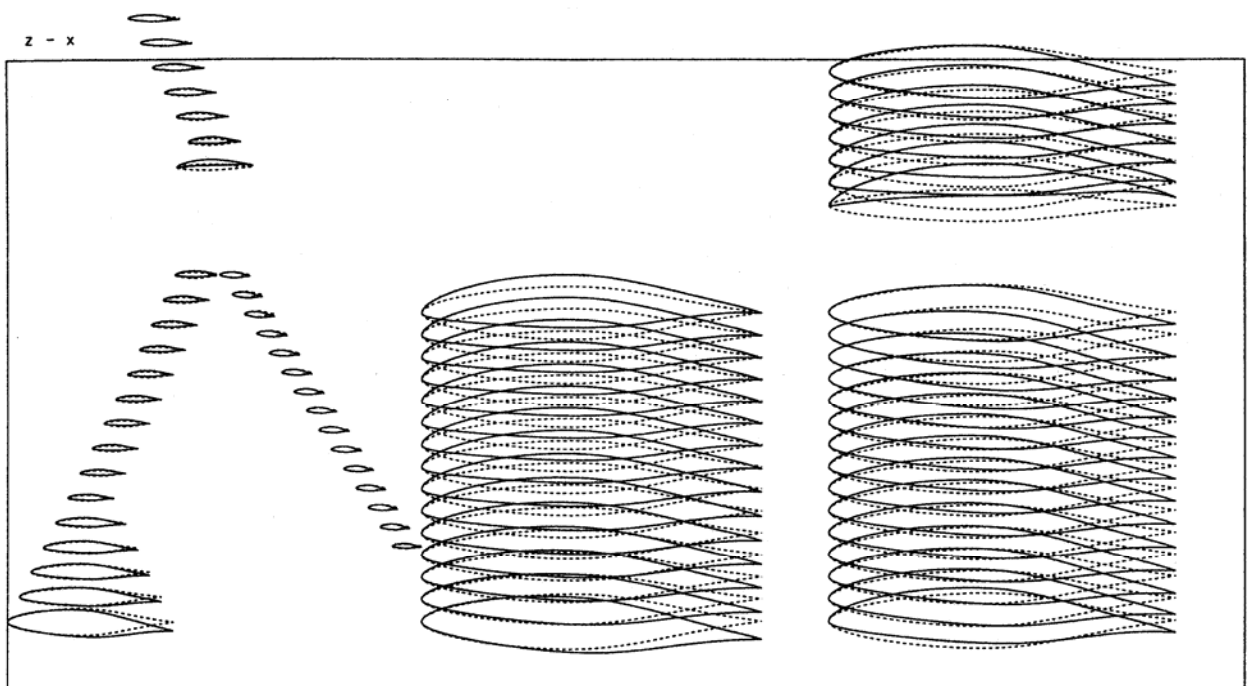**FIG. 5.5.1 CONFIGURATION EXFST, DESIGNED TWIST & CAMBER DISTRIBUTIONS**

41
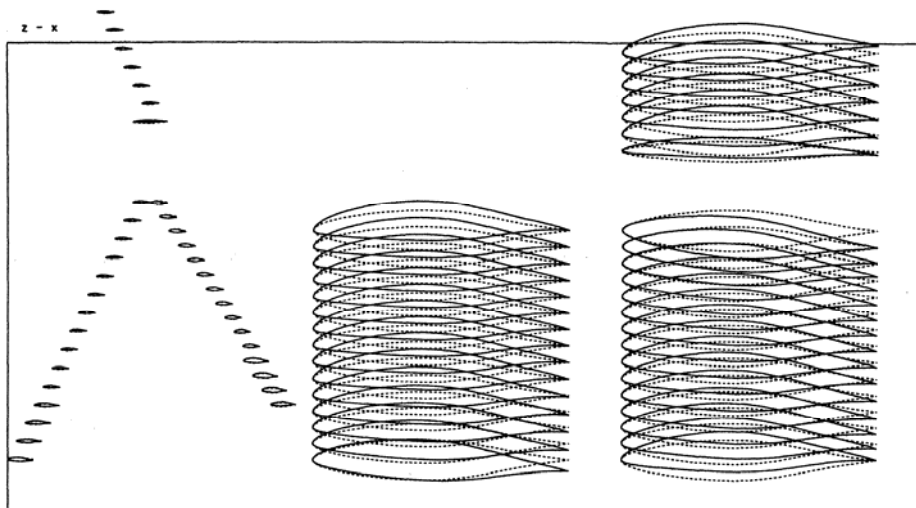
**FIG. 5.5.2 CONFIGURATION EXFST, UNCAMBERED & DESIGNED CAMBER**
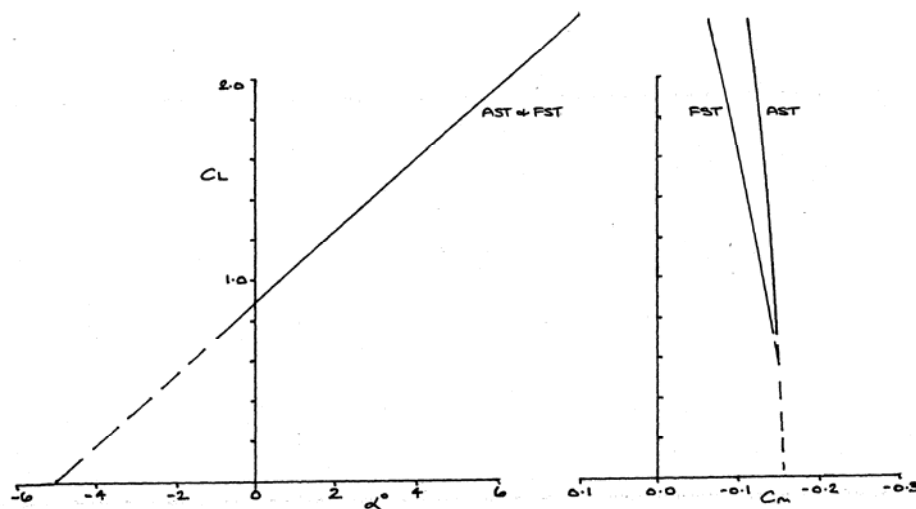
**FIG. 5.5.3 CONFIGURATION EXFST DESIGNED, CL, Cm and α VARIATIONS , Mach 0.6**
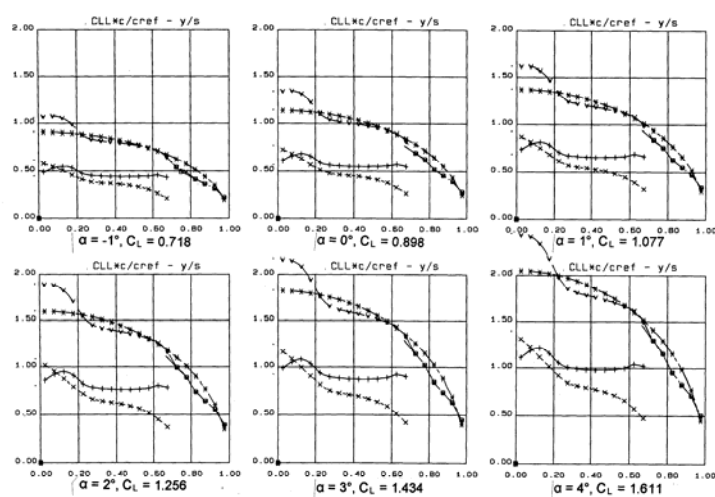
FIG. 5.5.4   CONFIGURATION EXFST, SPANWISE LOADINGS THROUGH AoA RANGE,
DESIGNED CAMBERED AEROFOIL CONFIGURATION, Mach 0.6
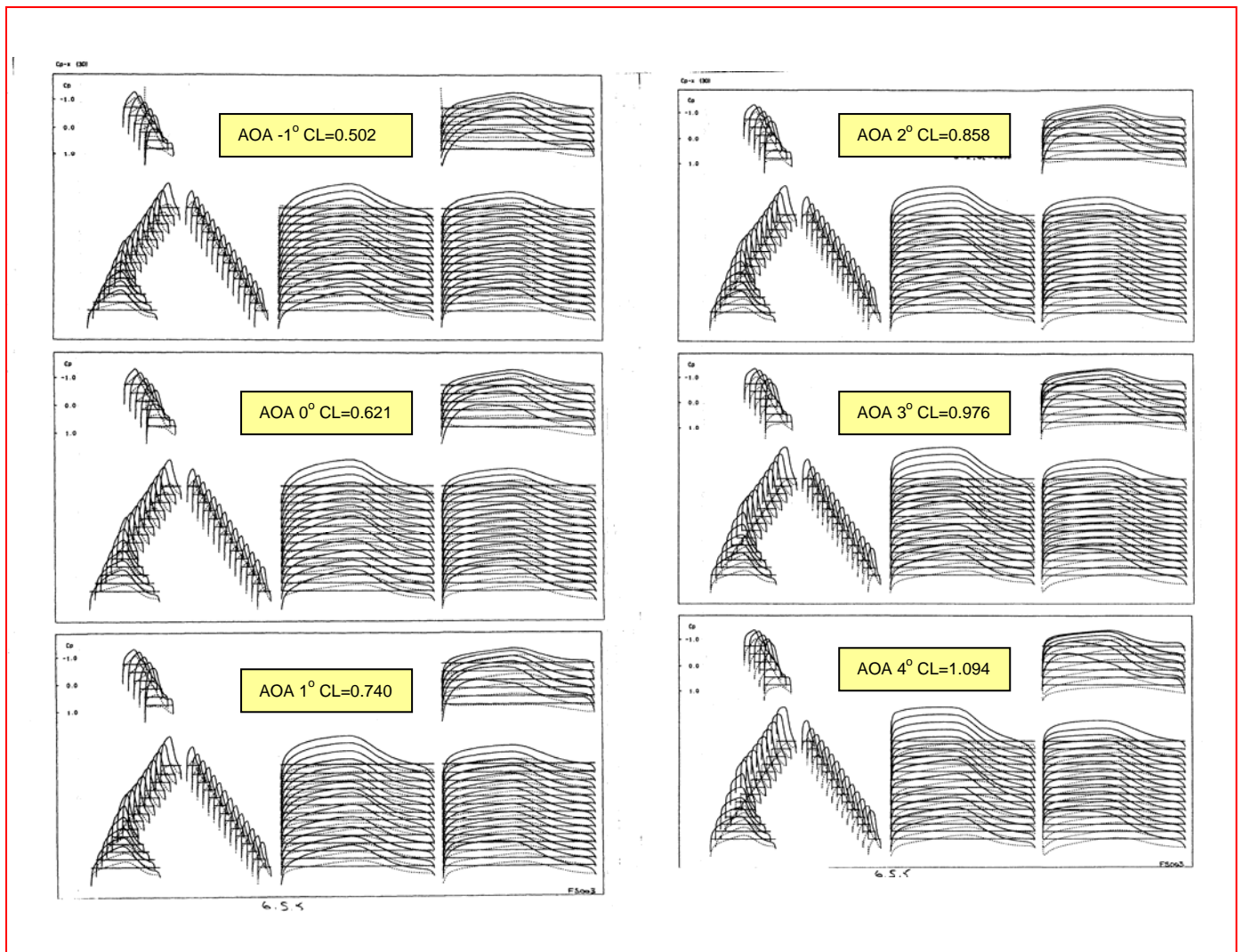**(Total compared with elliptic)**

42
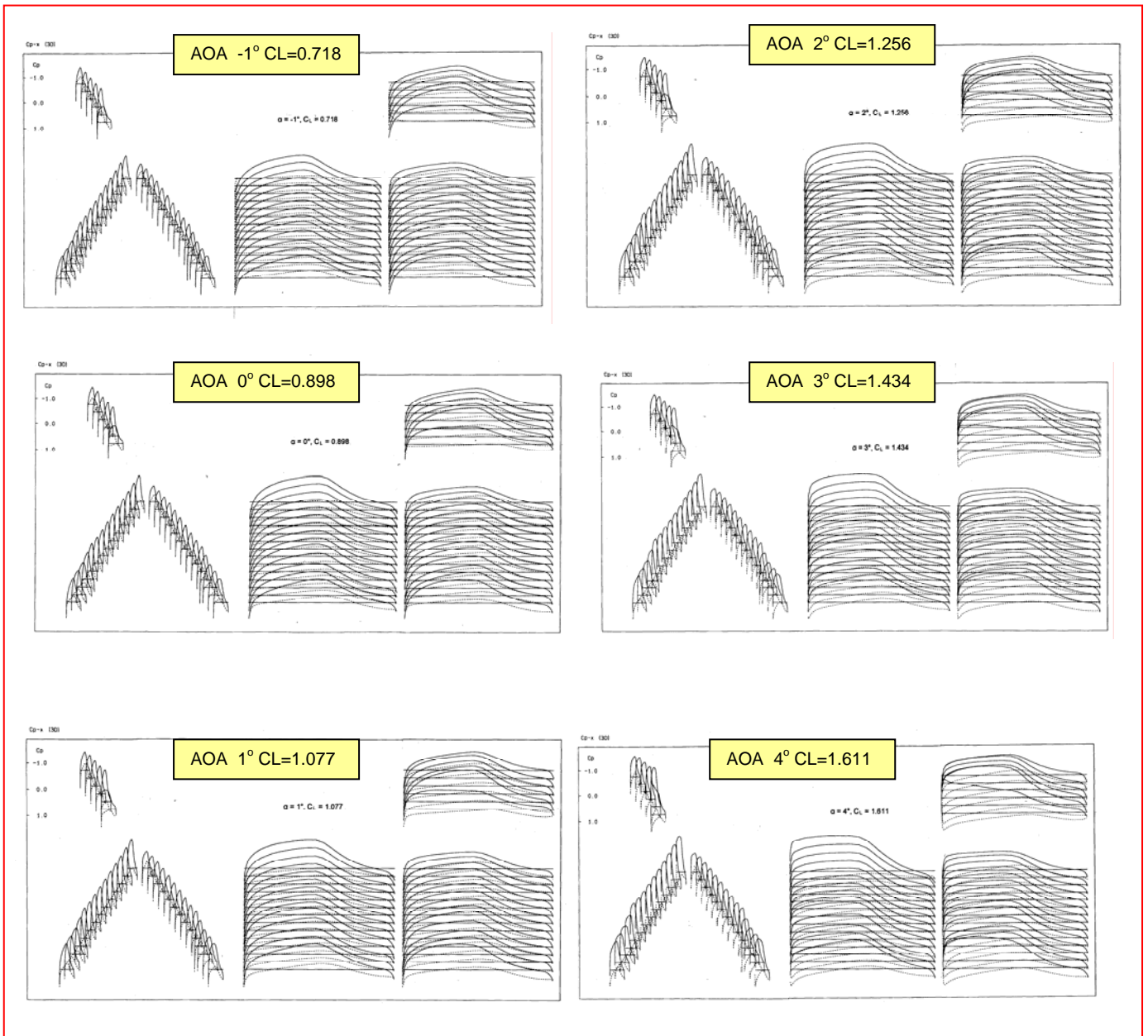
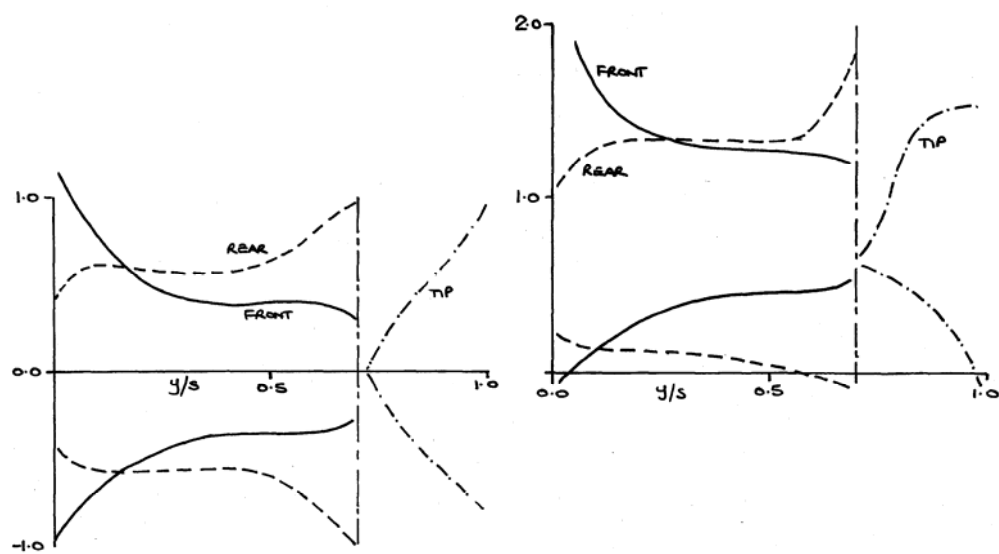**FIG. 5.5.5   CONFIGURATION EXFST DESIGNED CAMBER, Cp DISTRIBUTIONS THROUGH AoA RANGE, Mach 0.6**
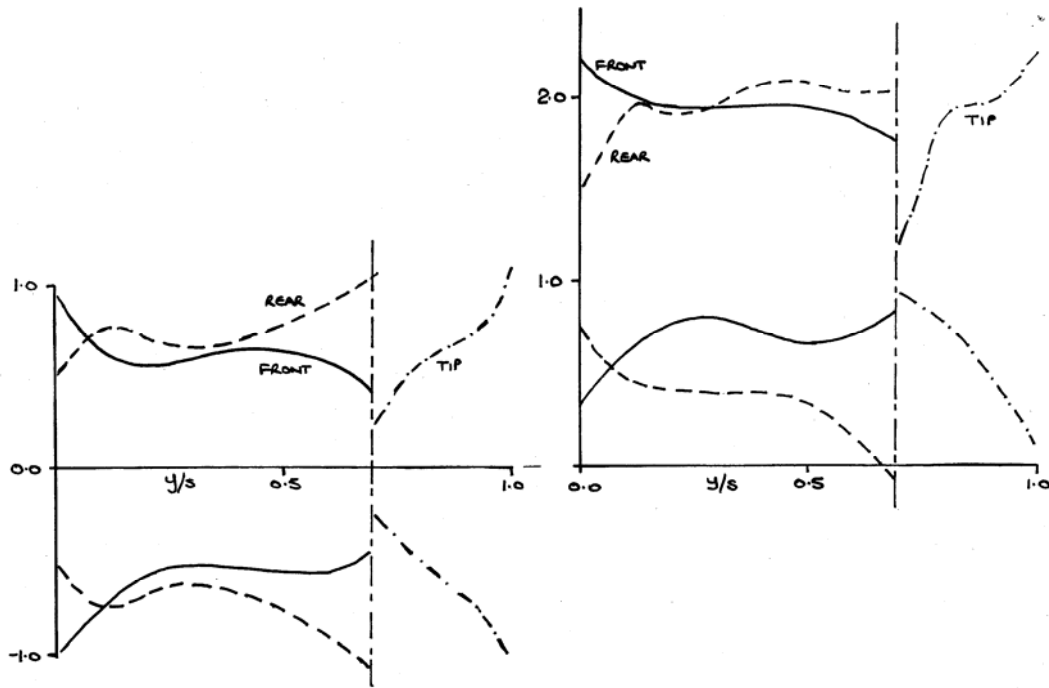
**FIG. 5.5.6 CONFIGURATION EXFST, LAMINAR FLOW RANGES,
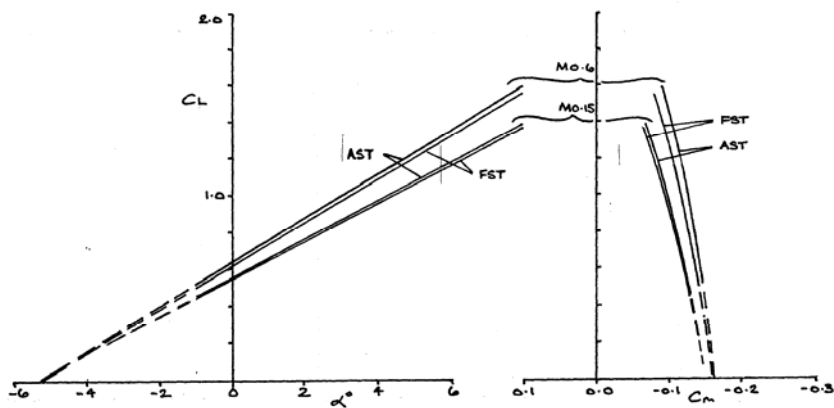UNCAMBERED AND DESIGN CAMBER**
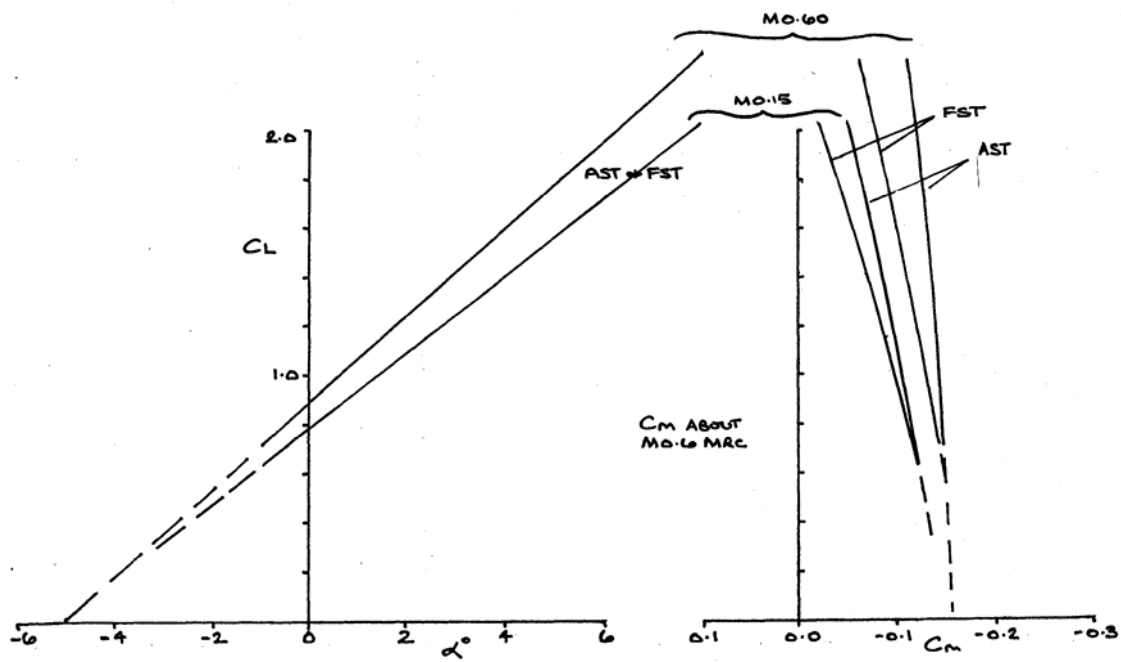
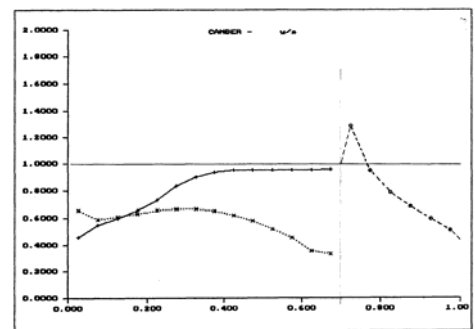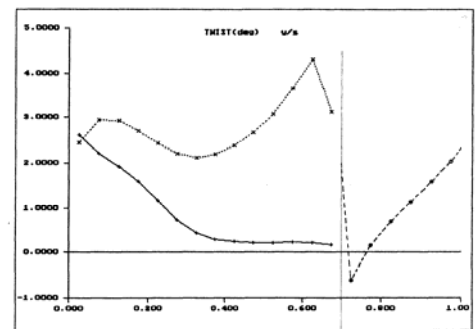**FIG. 5.5.7 CONFIGURATION EXFST DESIGNED, CL, Cm and α VARIATIONS , Mach 0.6 & 0.15**

- Operates over a large range in C_L & Re
- Crossflow instabilities destroy laminar boundary
- Joined-wing juncture flow
- Joined-wing structural modes not completely understoo
- Propulsion integration (?)

Boeing

FIG. 6.1.1 LAMBDA JOINED-WING SENSOR-CRAFT, AFT SWEPT TIP (LJAST)

0.0   0.25   0.7 (y/s)   1.0

x

REFERENCE AREA:— $S/2 = 0.182758$ (SHADED)
                     $AR = 10.94$

                     $S/2 = 0.245507$ (TOTAL)
                     $AR = 8.15$
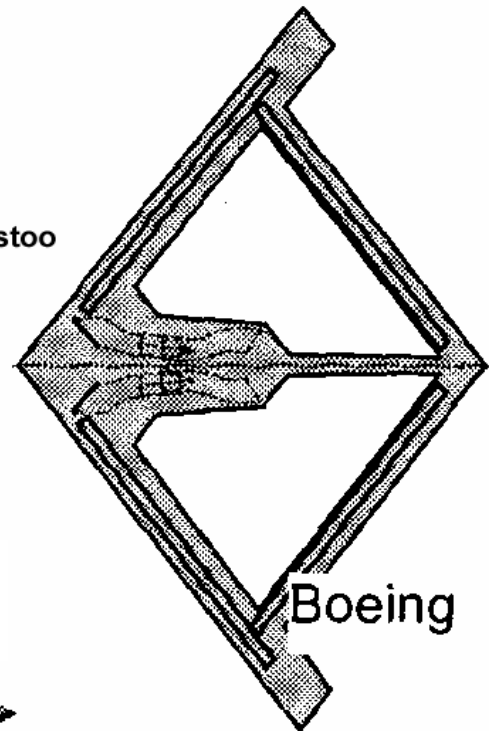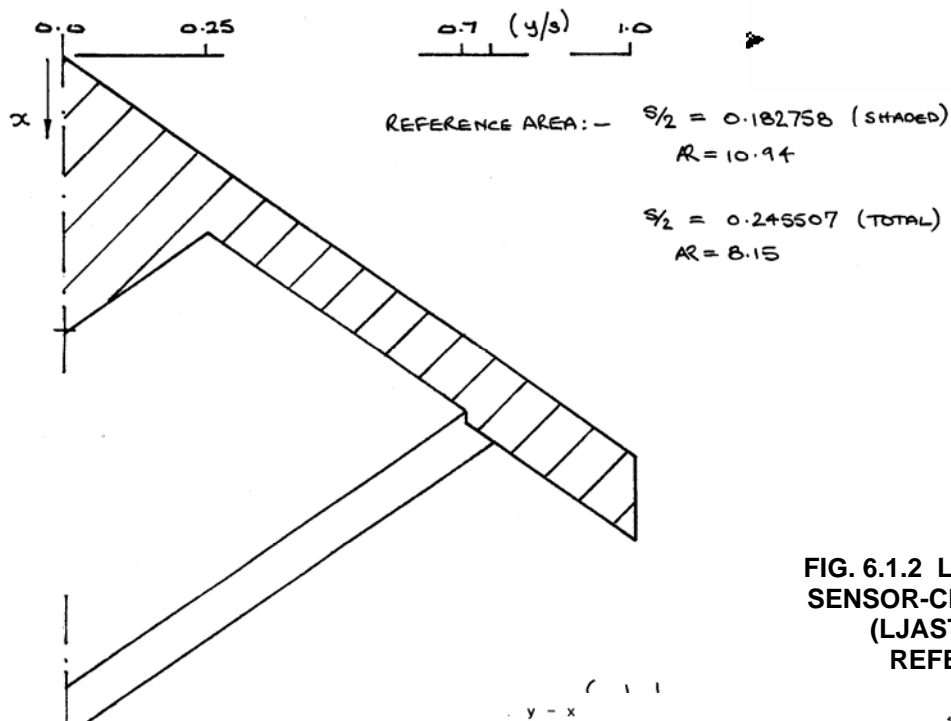
FIG. 6.1.2 LAMBDA JOINED-WING SENSOR-CRAFT, AFT SWEPT TIP (LJAST), MODELLING & REFERENCE AREAS

y – x

0.0   2.00

(3D)
1.50

−0.50
−0.50   1.50

z – x

MRC

z – y
0.50

−0.50

45
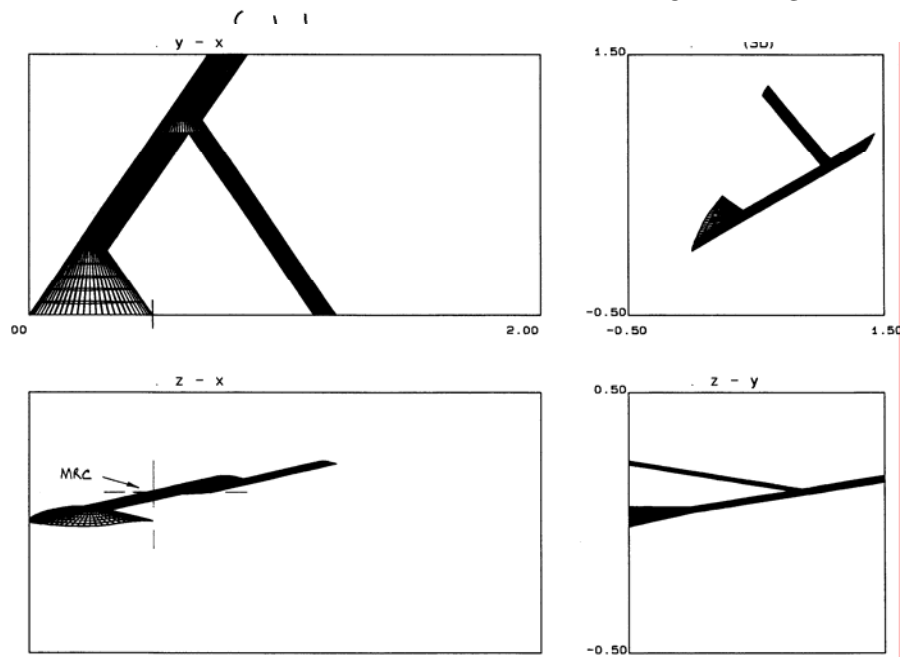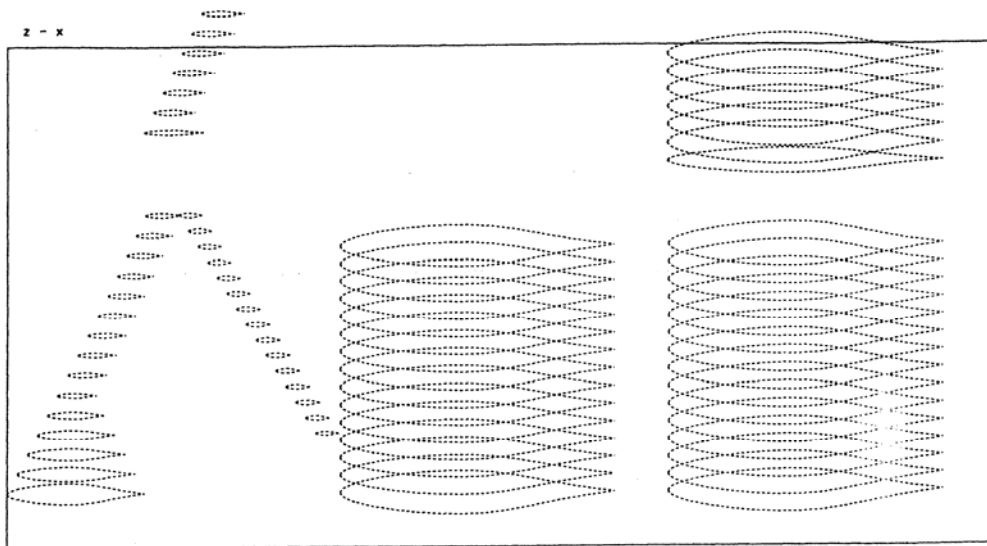
FIG. 6.1.3 CONFIGURATION LJAST, SYMMETRICAL AEROFOILS ON BOTH WINGS
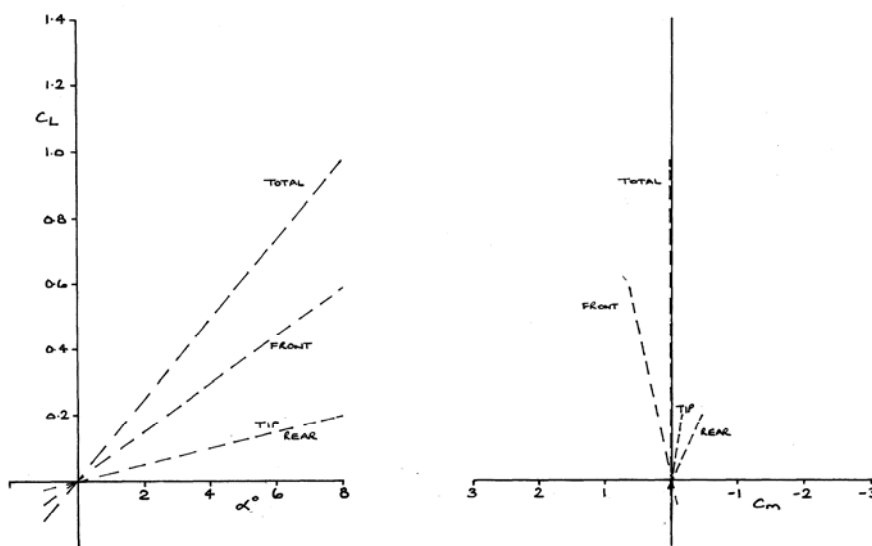
FIG. 6.1.4 CONFIGURATION LJAST UNCAMBERED, CL, Cm COMPONENT CONTRIBUTIONS, Mach 0.6
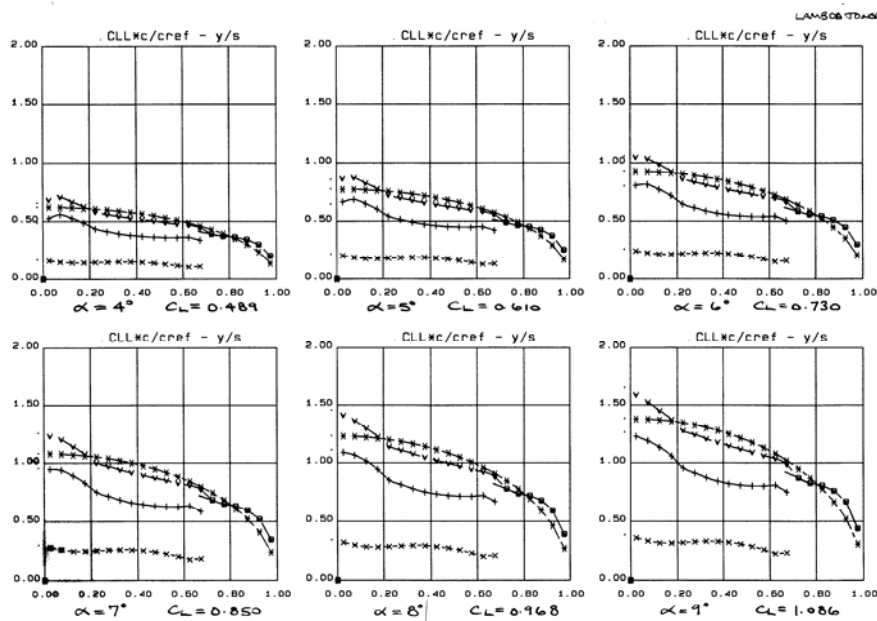
FIG. 6.1.5   CONFIGURATION LJAST UNCAMBERED, SPANWISE LOADINGS THROUGH AoA RANGE, Mach 0.6 (Total compared with elliptic)

46
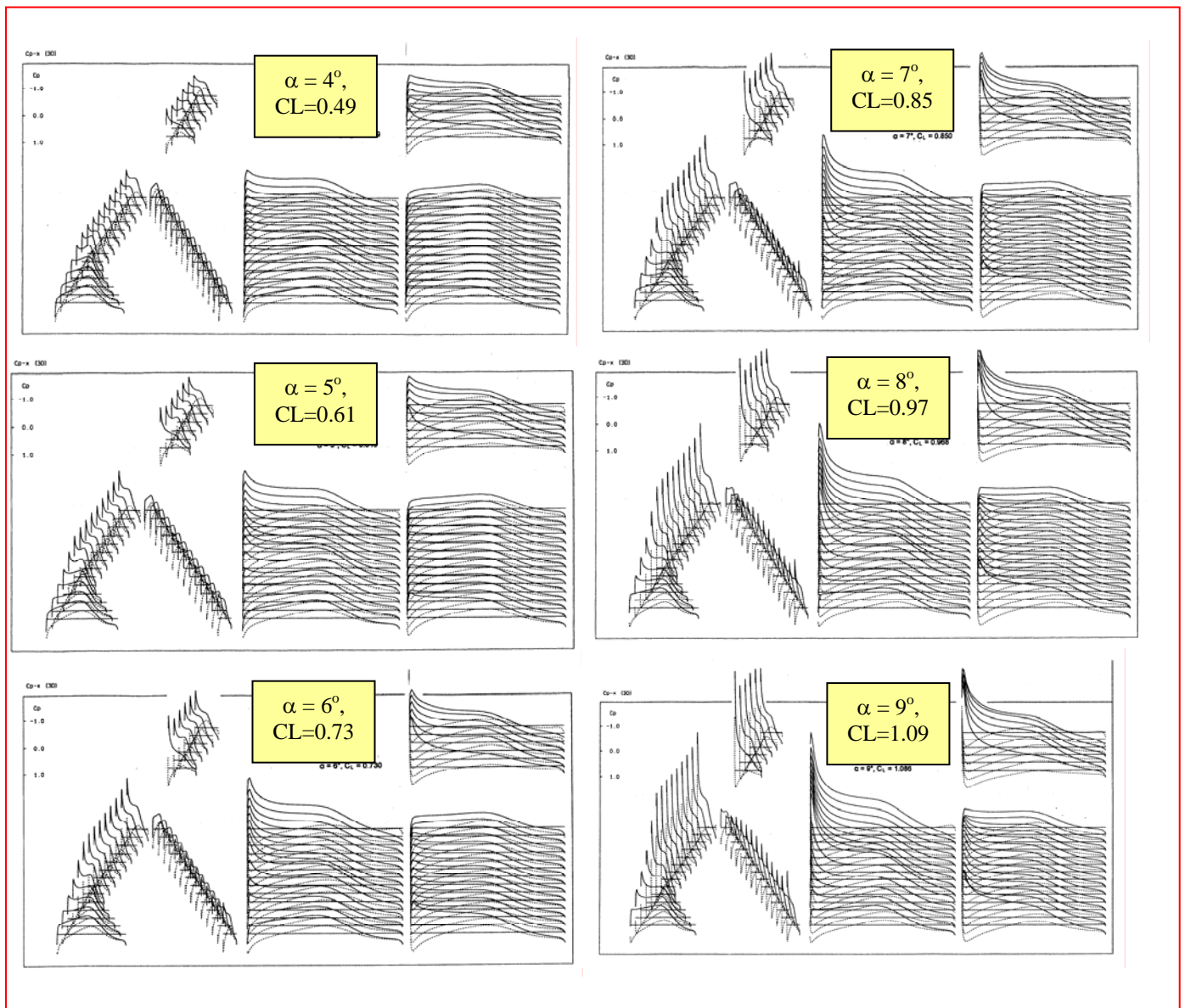
FIG. 6.1.6 CONFIGURATION LJAST UNCAMBERED, Cp DISTRIBUTIONS THROUGH AoA RANGE, Mach 0.6
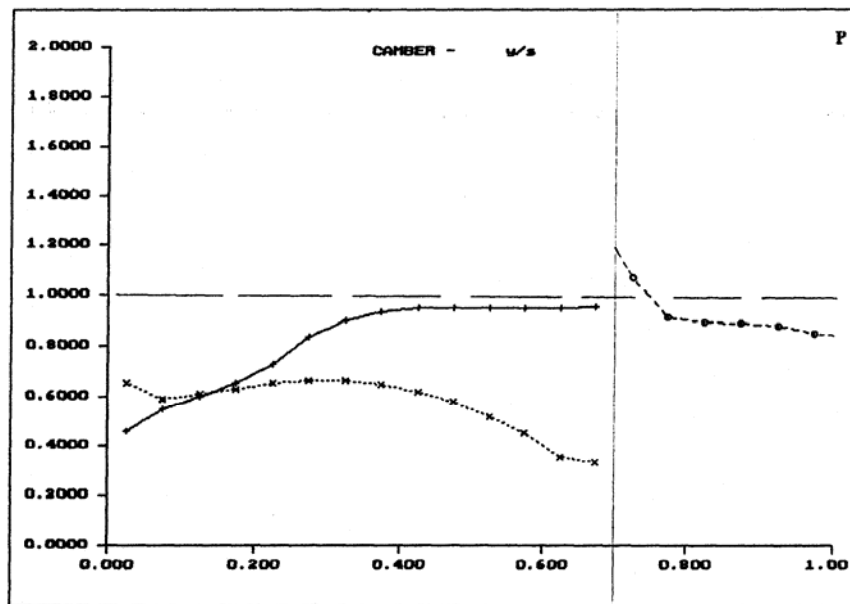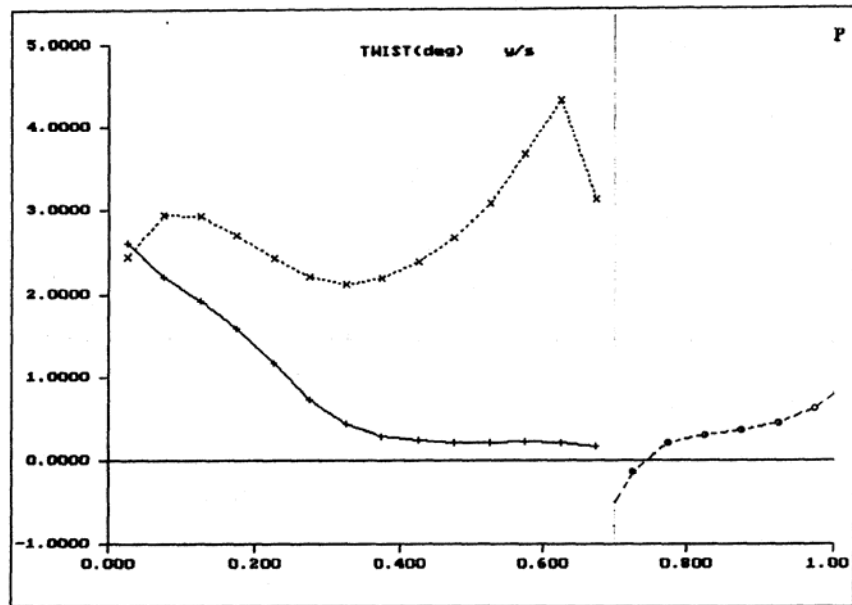
FIG. 6.3.1 CONFIGURATION LJAST, DESIGNED TWIST & CAMBER DISTRIBUTIONS

48
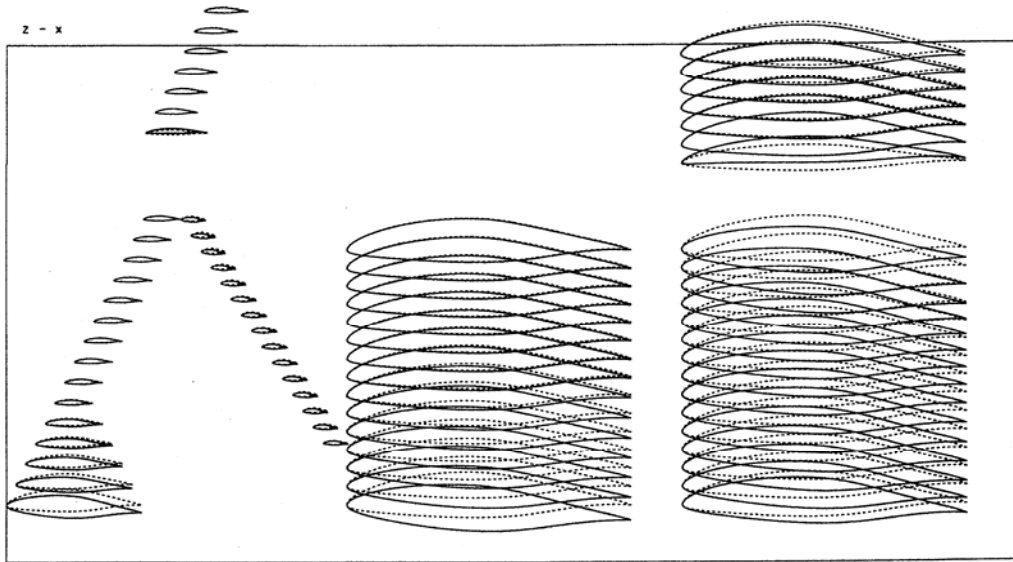
**FIG. 6.3.2 CONFIGURATION LJAST, UNCAMBERED & DESIGNED CAMBER**
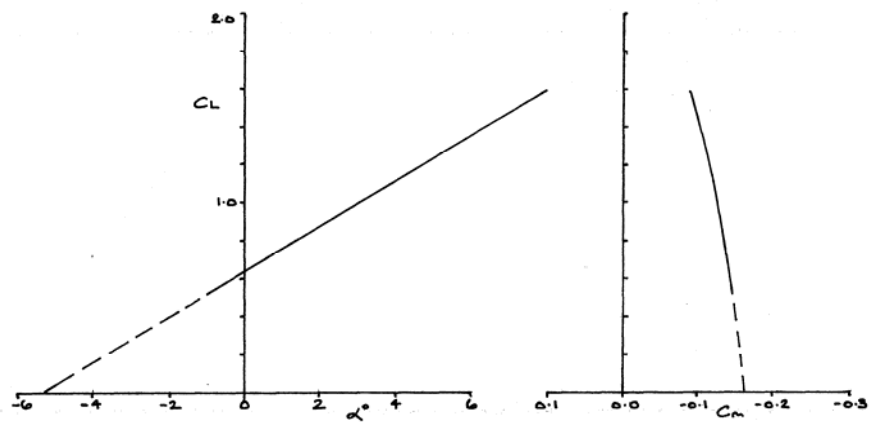
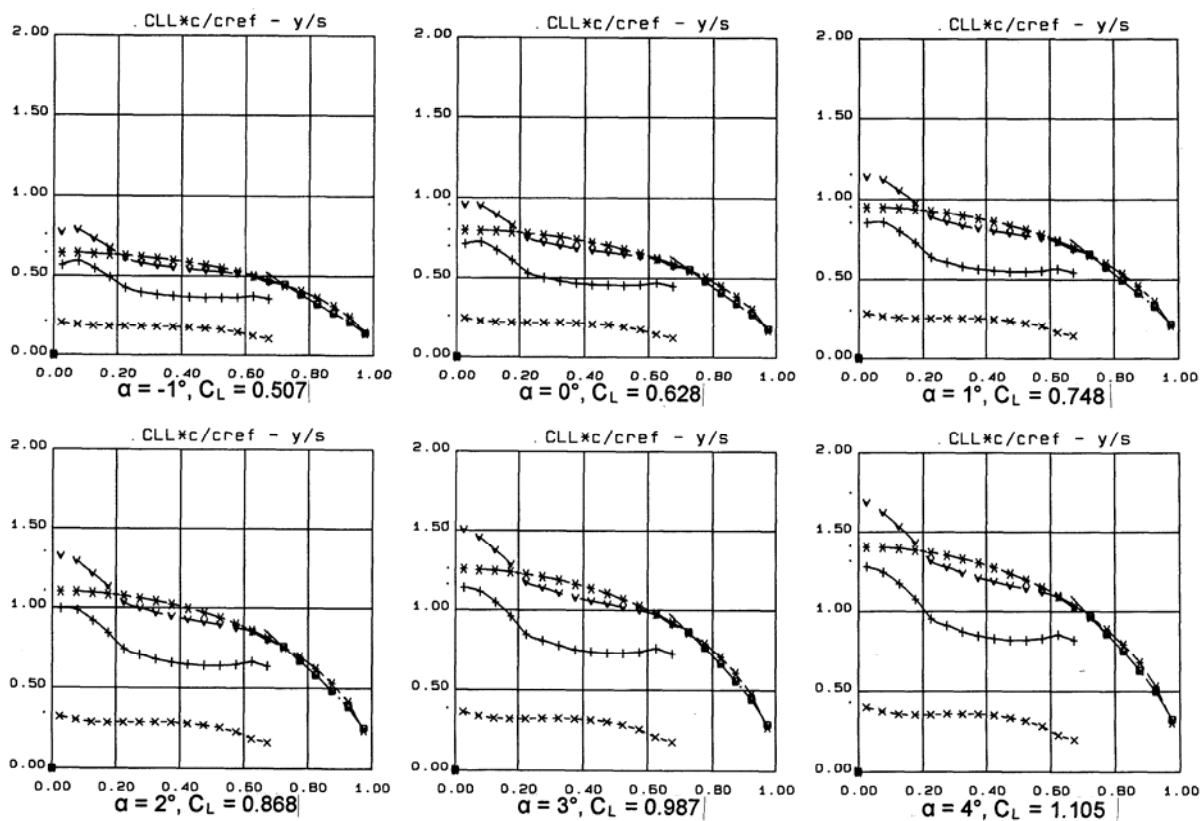**FIG. 6.3.3 CONFIGURATION LJAST DESIGNED, CL, Cm and α VARIATIONS , Mach 0.6**
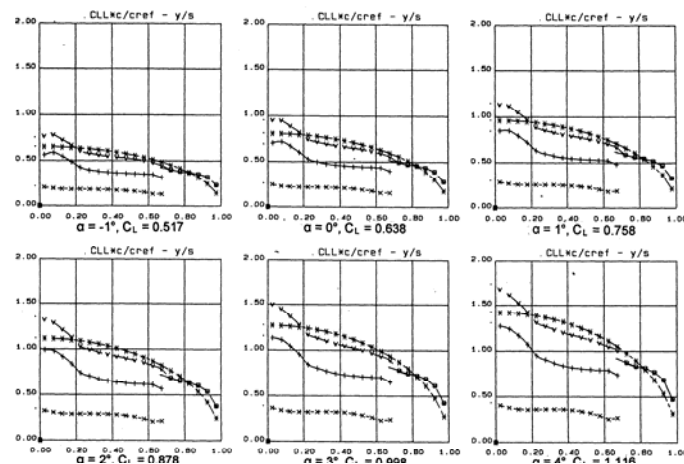
FIG. 6.3.4   CONFIGURATION LJAST DESIGN CAMBER, SPANWISE LOADINGS THROUGH AoA RANGE,
Mach 0.6
**(Total compared with elliptic)**

49

AOA -1° CL=0.517

AOA 2° CL=0.878

AOA 0° CL=0.638

AOA 3° CL=0.998

AOA 1° CL=0.758

AOA 4° CL=1.116

FIG. 6.3.5 CONFIGURATION LJAST DESIGN CAMBER, Cp DISTRIBUTIONS THROUGH AoA RANGE, Mach 0.6

FIG. 6.3.6 CONFIGURATION LJAST, LAMINAR FLOW RANGES, UNCAMBERED AND DESIGN CAMBER

50

FIG. 6.3.7 CONFIGURATION LJAST DESIGNED, CL, Cm and α VARIATIONS , Mach 0.6 & 0.15

REFERENCE AREA:— $S/2 = 0.182667$ (SHADED)
$AR = 10.95$

$S/2 = 0.245507$ (TOTAL)
$AR = 8.15$

FIG. 6.4.1 LAMBDA JOINED-WING
SENSOR-CRAFT, FORWARD SWEPT TIP
(LJFST), REFERENCE AREAS
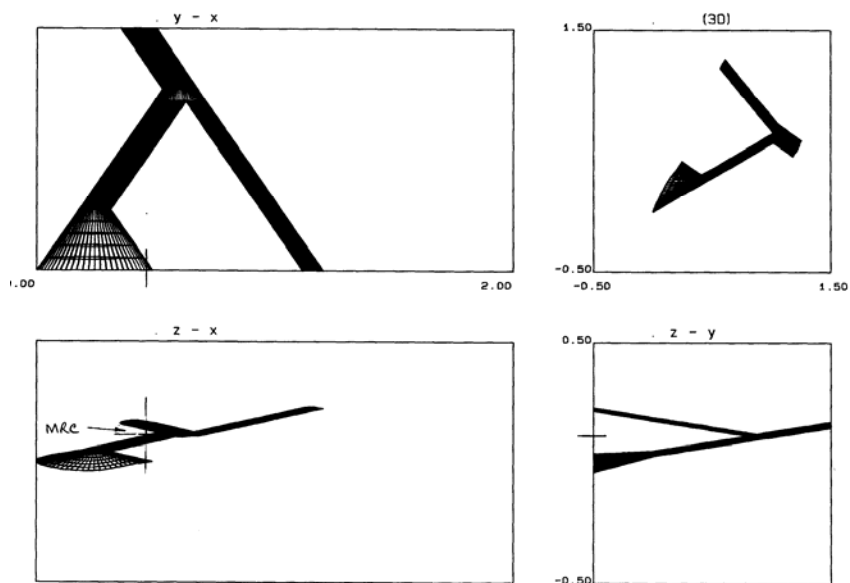
FIG. 6.4.2 LAMBDA JOINED-WING SENSOR-CRAFT,
FORWARD SWEPT TIP (LJFST)
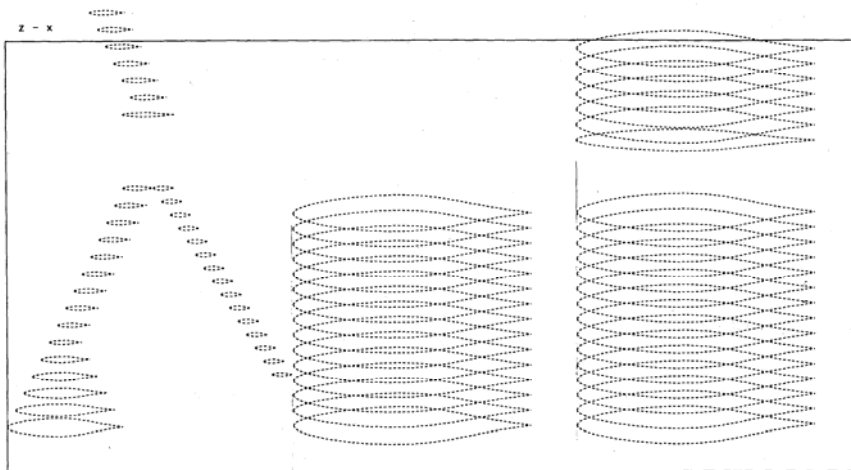
FIG. 6.4.3 CONFIGURATION LJFST, SYMMETRICAL AEROFOILS ON BOTH WINGS
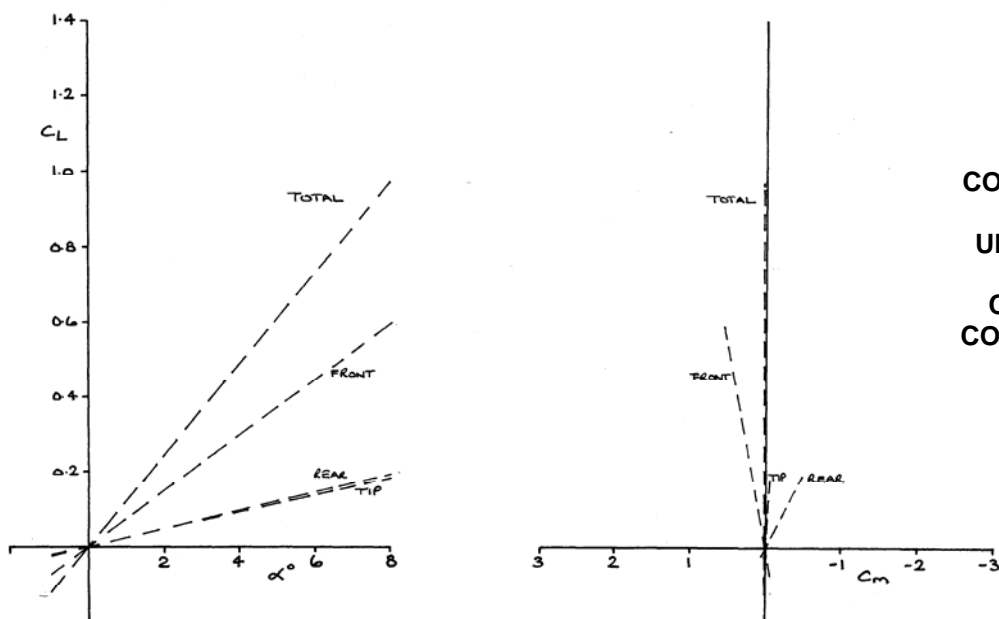
FIG. 6.4.4 CONFIGURATION LJFST UNCAMBERED, CL, Cm COMPONENT CONTRIBUTIONS, Mach 0.6

FIG. 6.4.5   CONFIGURATION LJFST UNCAMBERED, SPANWISE LOADINGS THROUGH AoA RANGE, Mach 0.6
(Total compared with elliptic)

52
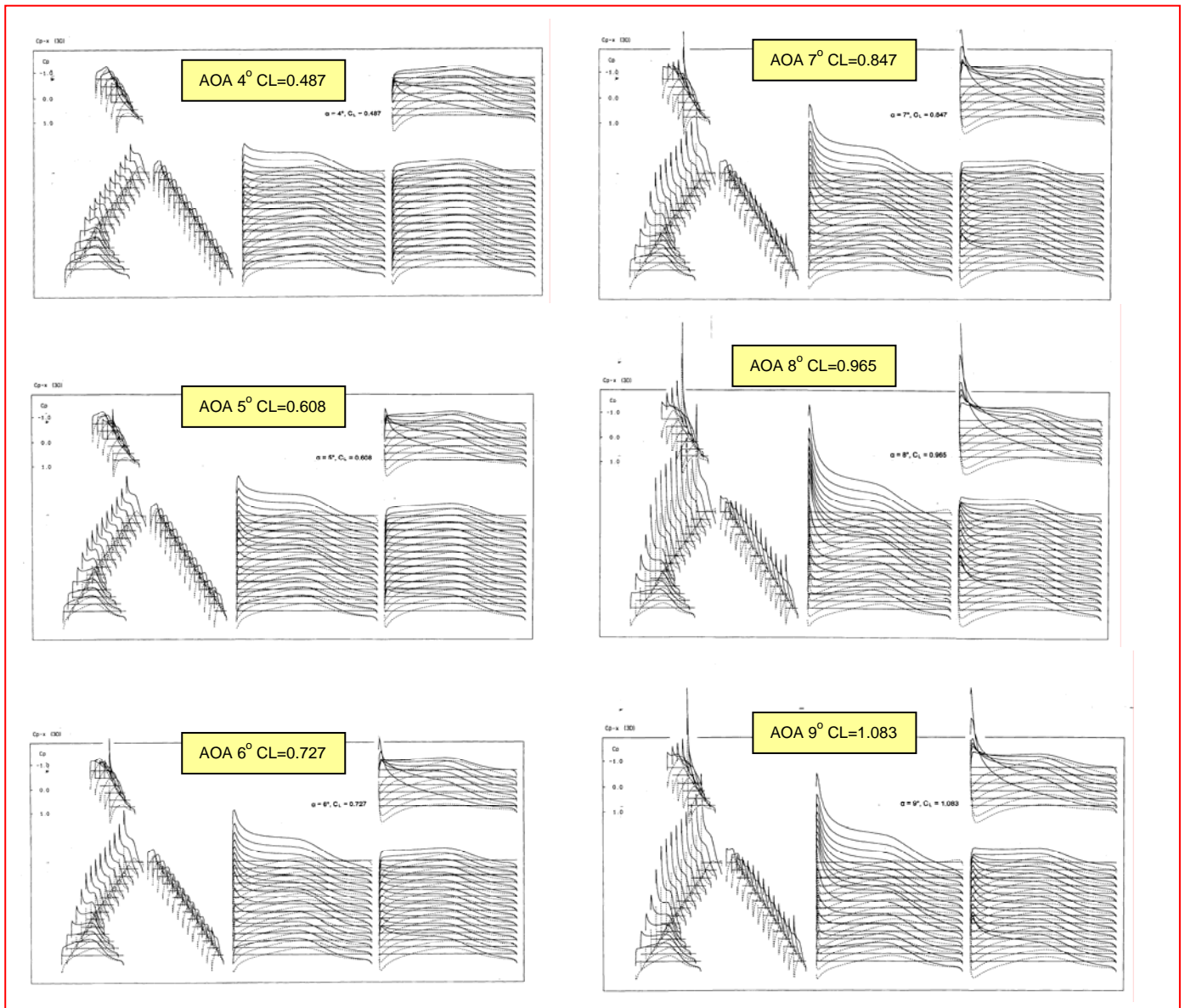
FIG. 6.4.6 CONFIGURATION LJFST UNCAMBERED, Cp DISTRIBUTIONS THROUGH AoA RANGE, Mach 0.6

53

FIG. 6.5.1 CONFIGURATION LJFST, DESIGNED TWIST & CAMBER DISTRIBUTIONS

FIG. 6.5.2 CONFIGURATION LJFST, UNCAMBERED & DESIGNED CAMBER
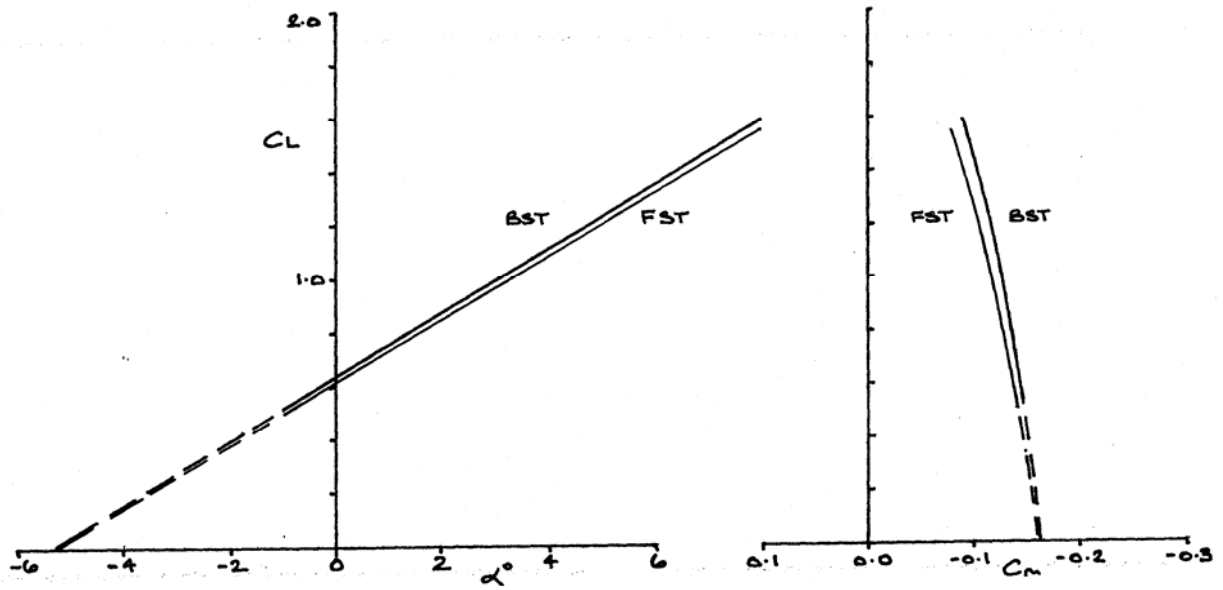
FIG. 6.5.3 CONFIGURATION LJFST & LJAST DESIGNED, CL, Cm and α VARIATIONS , Mach 0.6
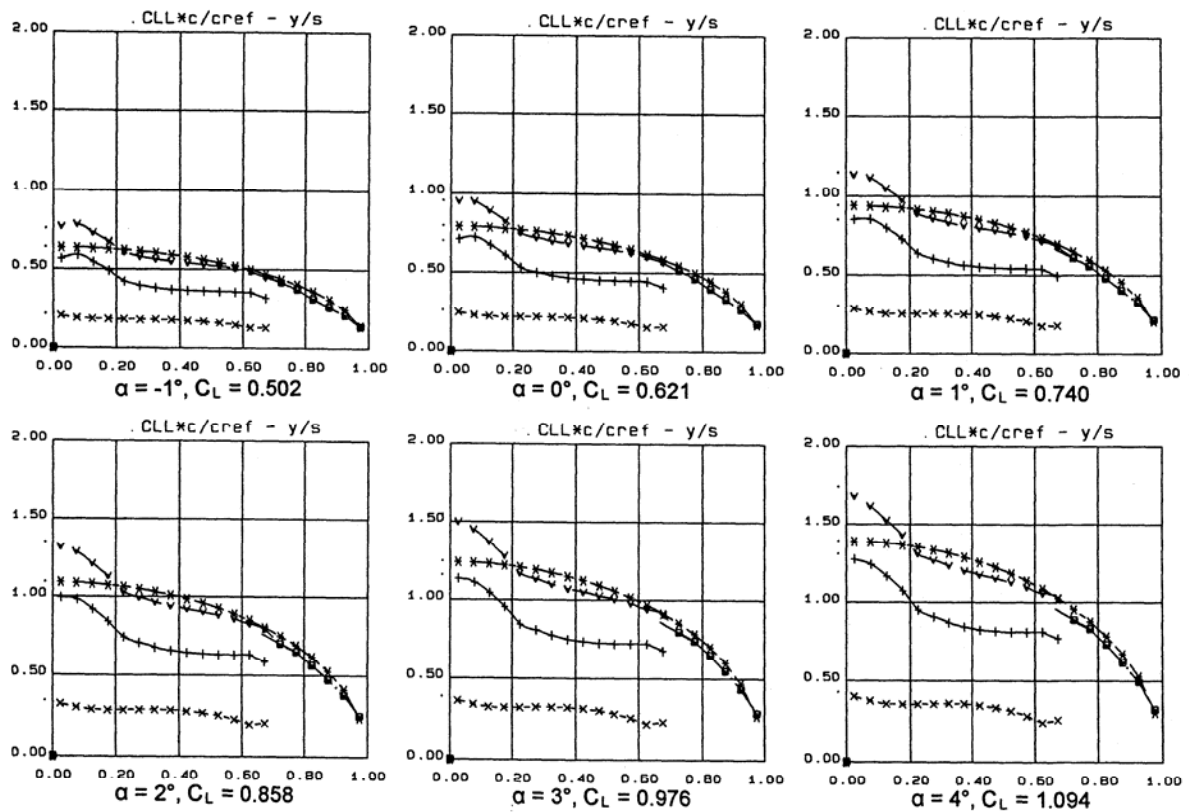
FIG. 6.5.4   CONFIGURATION LJFST DESIGN CAMBER, SPANWISE LOADINGS THROUGH AoA RANGE, Mach 0.6
(Total compared with elliptic)

55

FIG. 6.5.5 CONFIGURATION LJFST DESIGN CAMBER, Cp DISTRIBUTIONS THROUGH AoA RANGE, Mach 0.6

FIG. 6.5.6 CONFIGURATION LJFST, LAMINAR FLOW RANGES, UNCAMBERED AND DESIGN CAMBER

56

**FIG. 6.5.7 CONFIGURATION LJFST & LJAST DESIGNED,
CL, Cm and α VARIATIONS , Mach 0.6 & 0.15**

**FIG. 6.6.1 CONFIGURATION LJFST, MODIFIED DESIGN TWIST &
CAMBER DISTRIBUTIONS**
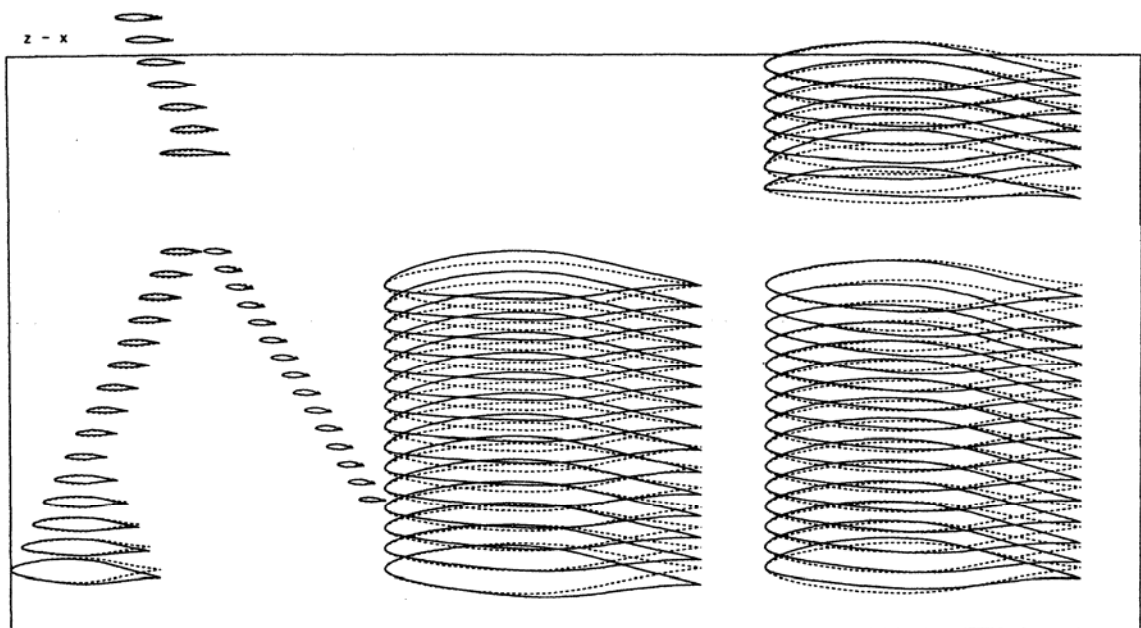
FIG. 6.6.2 CONFIGURATION LJFST, UNCAMBERED & MODIFIED DESIGN CAMBER
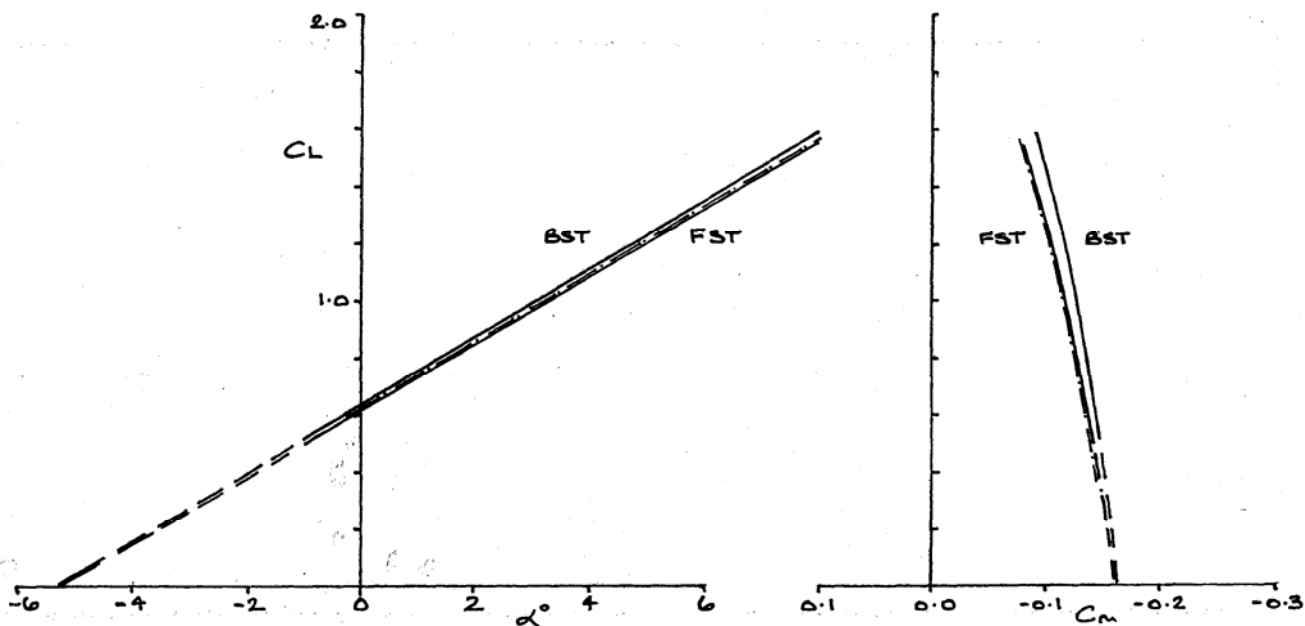
**FIG. 6.6.3 CONFIGURATION LJFST & LJAST DESIGNED & LJST MODIFIED,
CL, Cm and α VARIATIONS , Mach 0.6**

**FIG. 6.6.4 CONFIGURATION LJFST MODIFIED DESIGN CAMBER, SPANWISE LOADINGS
THROUGH AoA RANGE, Mach 0.6
(Total compared with elliptic)**
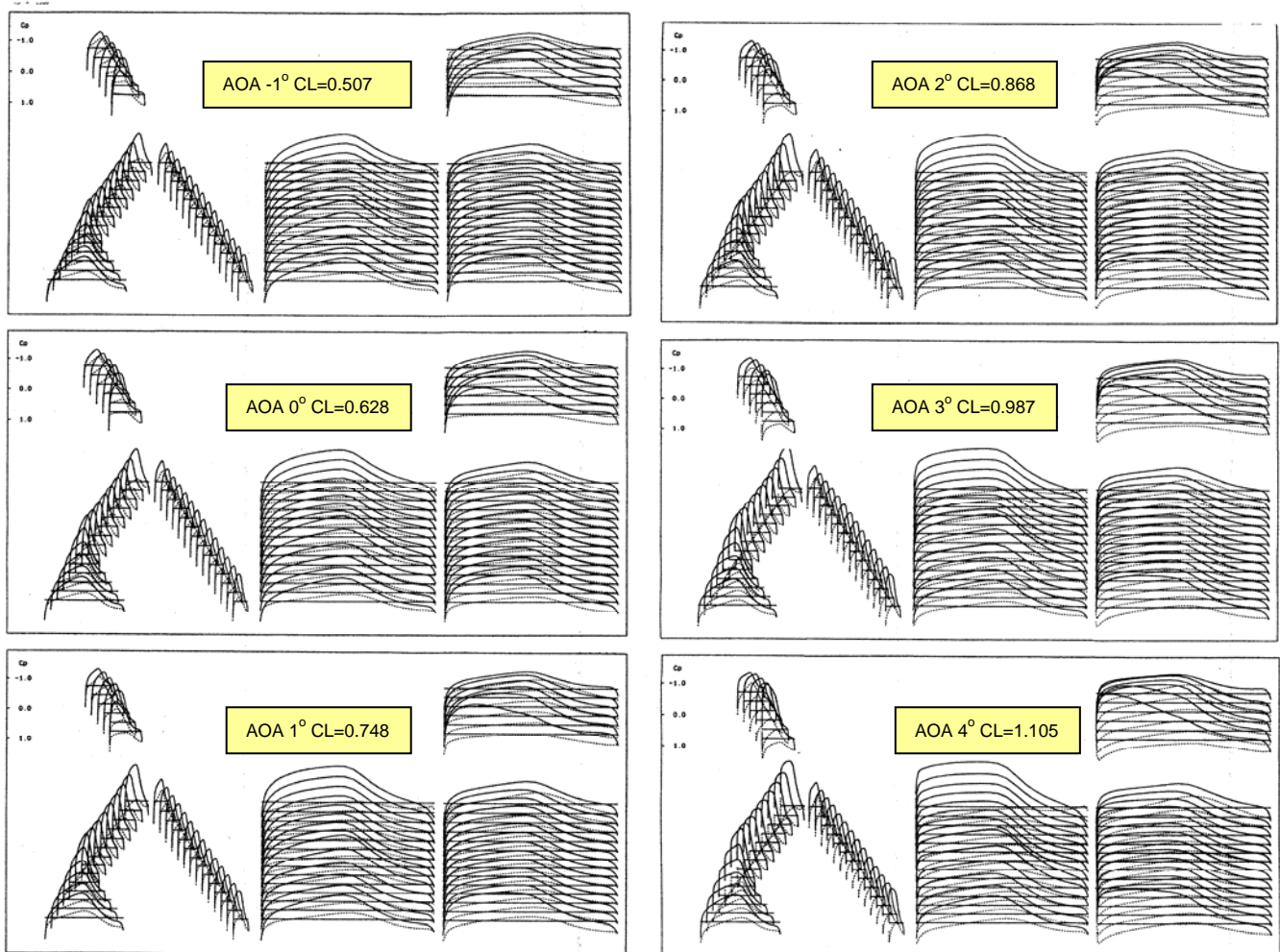
FIG. 6.6.5 CONFIGURATION LJFST MODIFIED DESIGN CAMBER, Cp DISTRIBUTIONS THROUGH AoA RANGE, Mach 0.6

The panels are labeled:
- AOA -1° CL=0.507
- AOA 2° CL=0.868
- AOA 0° CL=0.628
- AOA 3° CL=0.987
- AOA 1° CL=0.748
- AOA 4° CL=1.105

CCAST

Constant Chord, CC Reference Sensor-

Extended Root Chord, EX

Lambda Joined Wing, LJ
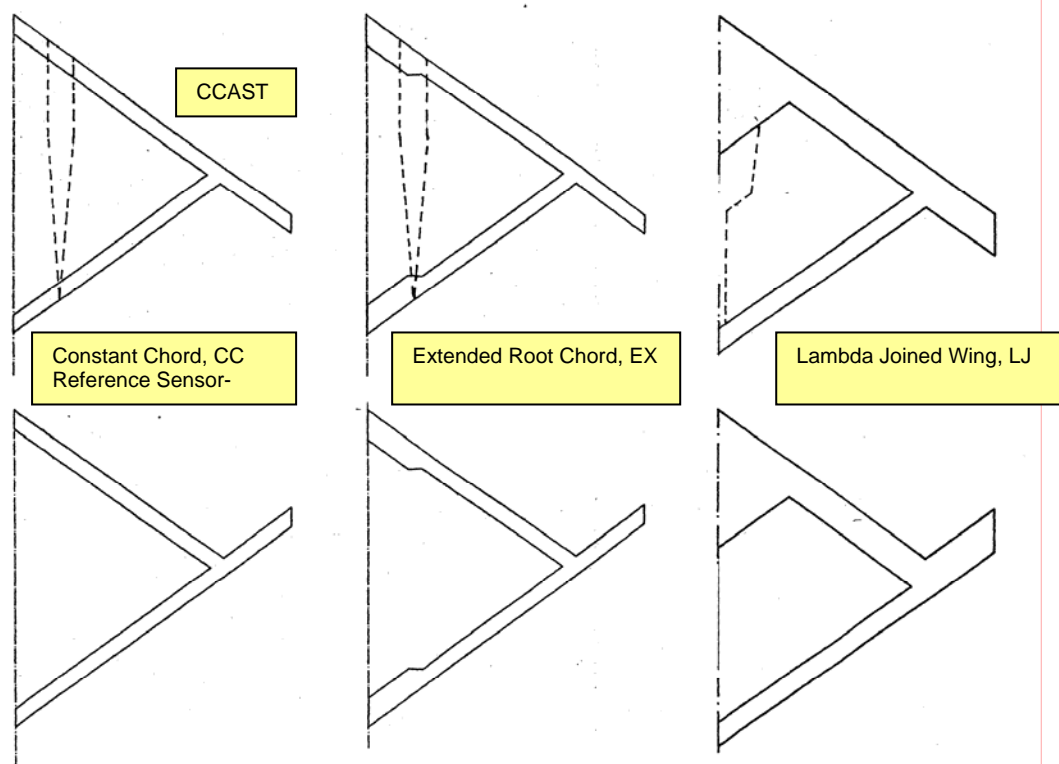
FIG. 7.1 SENSOR-CRAFT CONCEPT PLANFORMS: HIGH AR, EXTENDED ROOT CHORD & LAMBDA JOINED WING AFT & FORWARD SWEPT TIPS WITH POSSIBLE FUSELAGE LOCATIONS
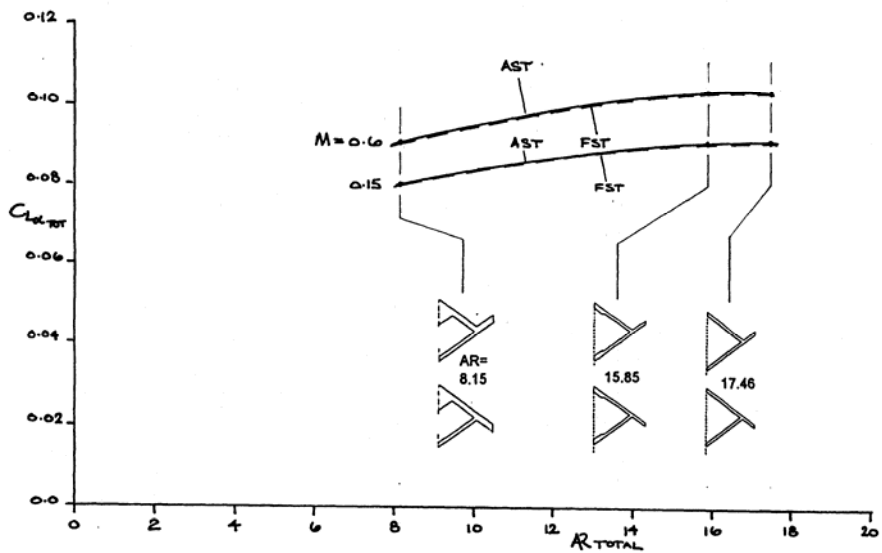
FIG. 7.2 CLα VARIATION WITH AR, JOINED WING CASES, M = 0.6 & 0.15
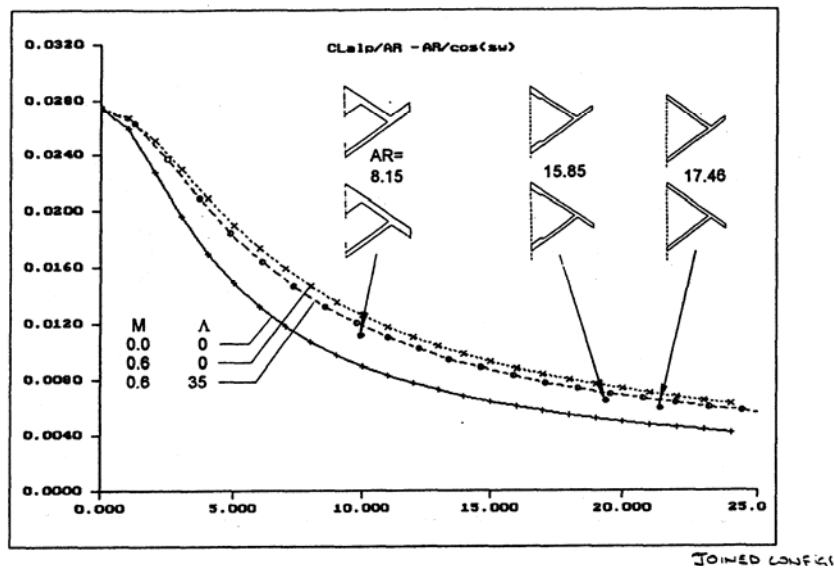
**FIG. 7.3 CLα/AR VARIATION WITH AR,/cos(Λ), THEORETICAL EFFECT OF M & Λ,
JOINED WING CASES M = 0.6**
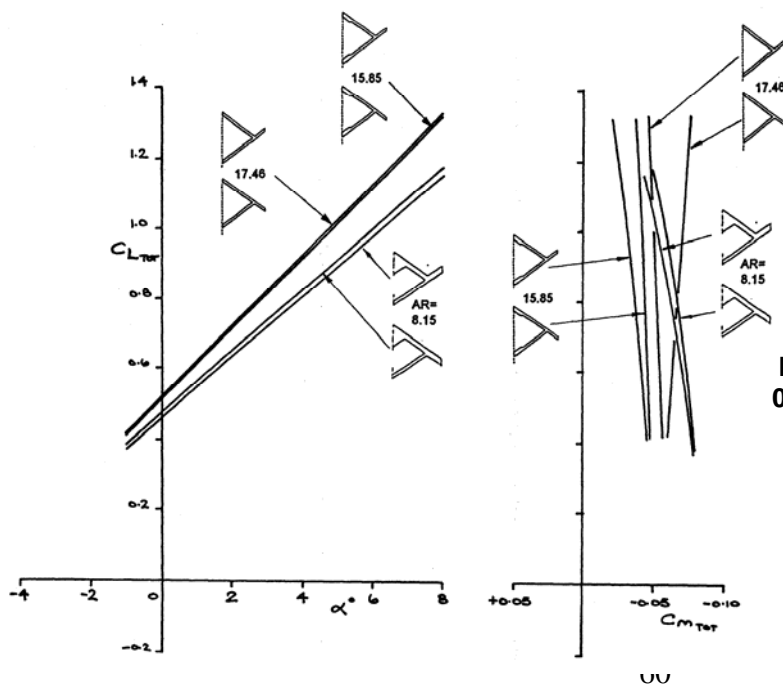
FIG. 7.4 TOTAL LOADS (C_L - α, C_m – C_L), M = 0.6 COMPARISON FOR JOINED WING CASES
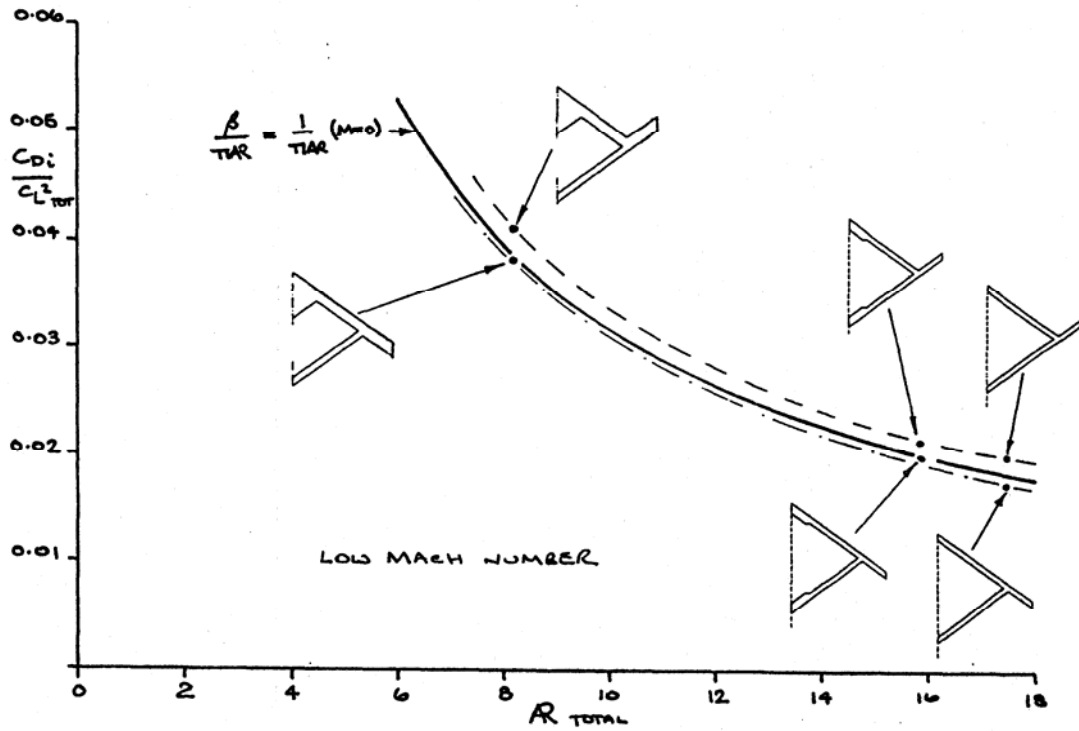
FIG. 7.5 INDUCED DRAG FACTOR VARIATION WITH AR, UNCAMBERED WINGS, LOW M COMPARISON FOR JOINED WING CASES
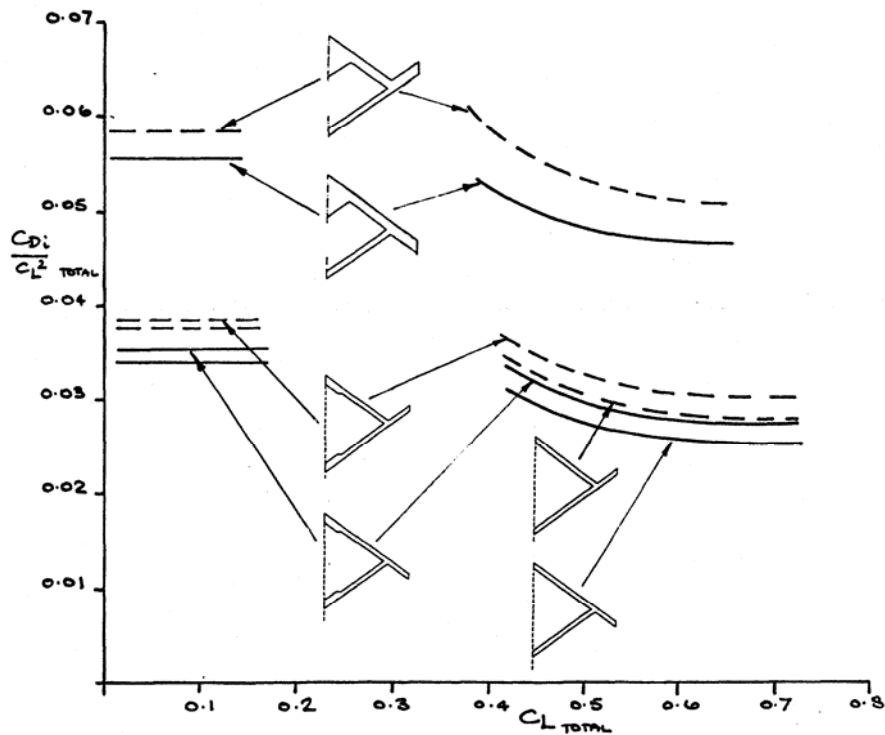
FIG. 7.6 INDUCED DRAG FACTOR VARIATION WITH CL, DESIGNED WINGS, M = 0.6 COMPARISON FOR JOINED WING CASES

61
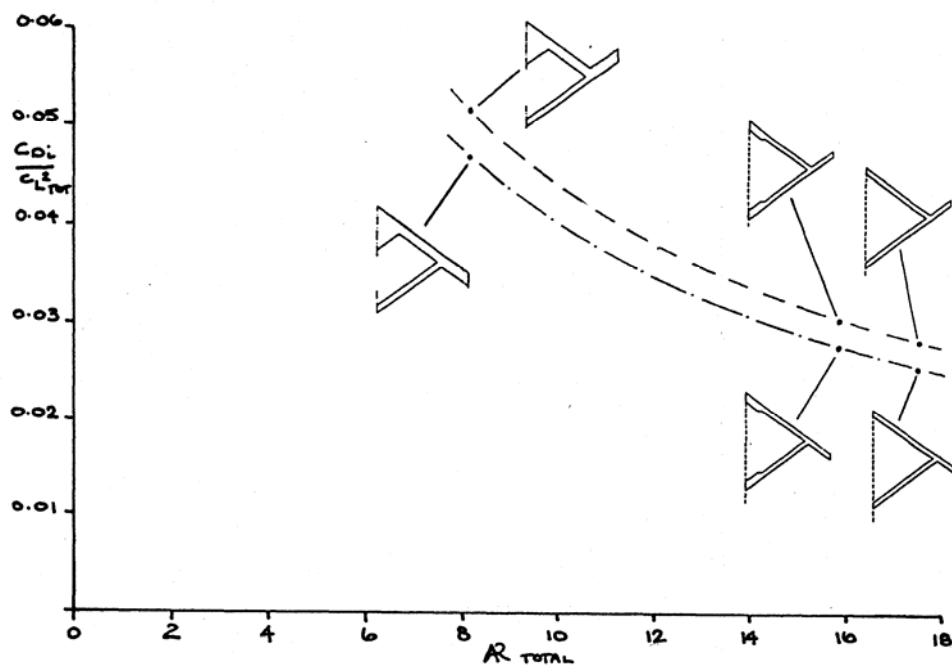
FIG. 7.7 INDUCED DRAG FACTOR VARIATION WITH AR, DESIGNED WINGS, M = 0.6 COMPARISON FOR JOINED WING CASES
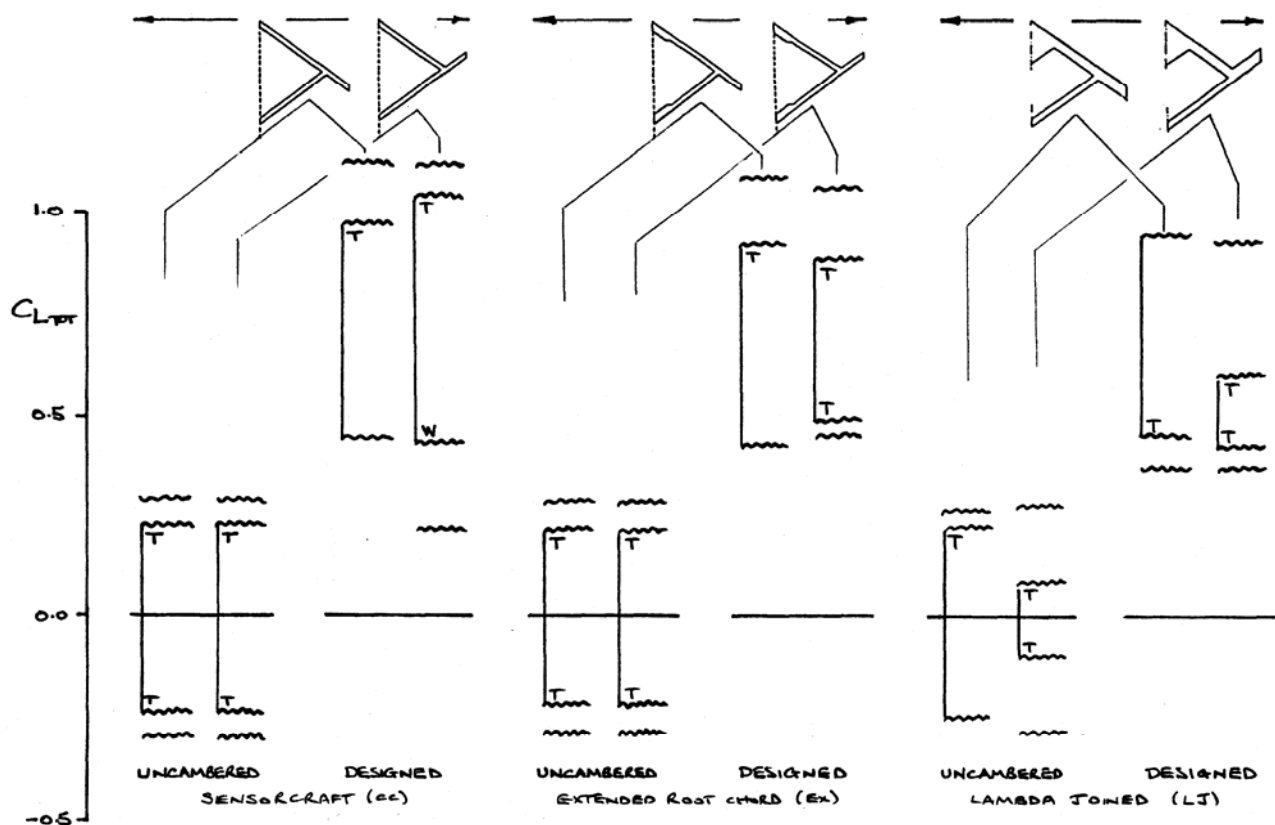
FIG. 7.8 UNCAMBERED & DESIGNED JOINED WING CONFIGURATIONS, C_L RANGES FOR LAMINAR FLOW, M = 0.6
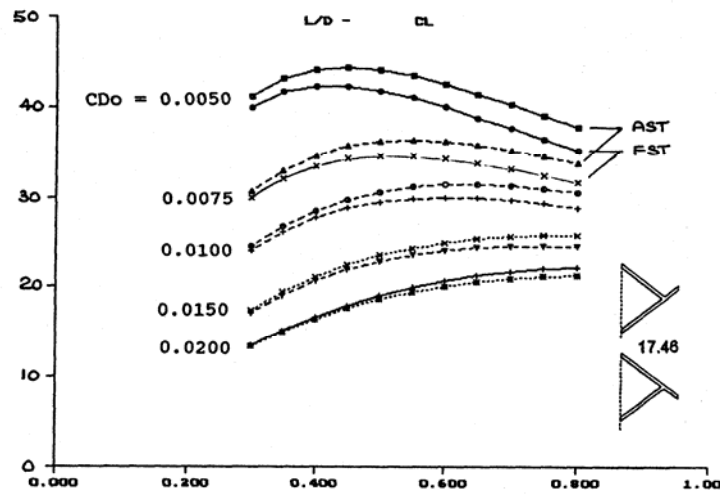
FIG. 7.9 L/D VARIATION WITH C_L, DESIGNED CCAST & CCFST CONFIGURATIONS, M = 0.6, C_{Do} VARIES
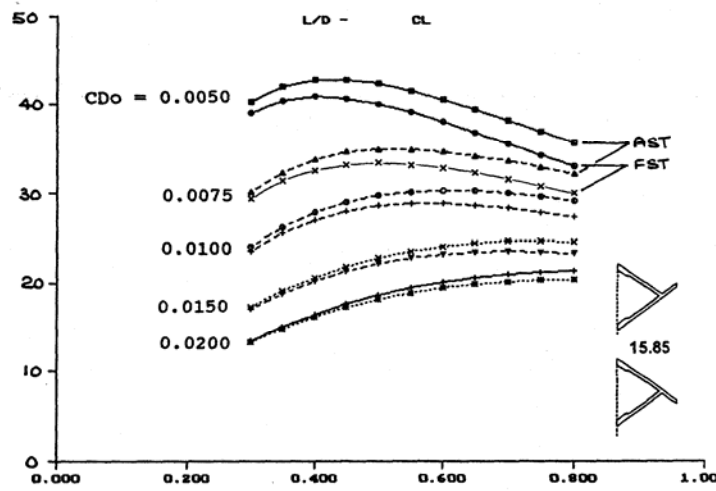
FIG. 7.10 L/D VARIATION WITH C_L, DESIGNED EXAST & EXFST CONFIGURATIONS, M = 0.6, C_{Do} VARIES
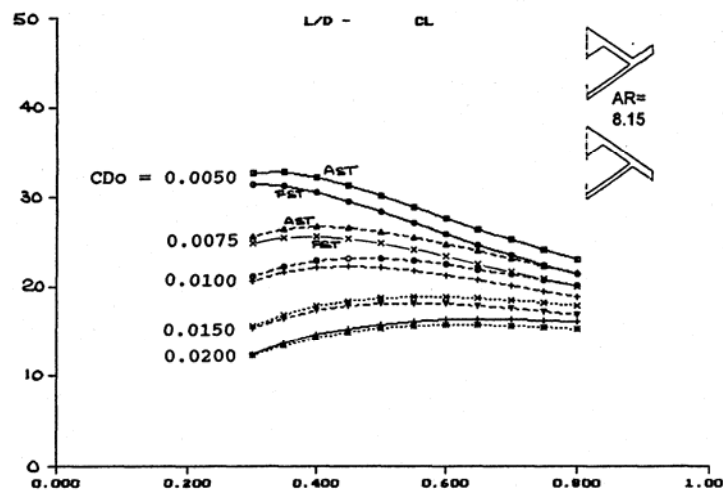
FIG. 7.11 L/D VARIATION WITH C_L, DESIGNED LJAST & LJFST CONFIGURATIONS, M = 0.6, C_{Do} VARIES
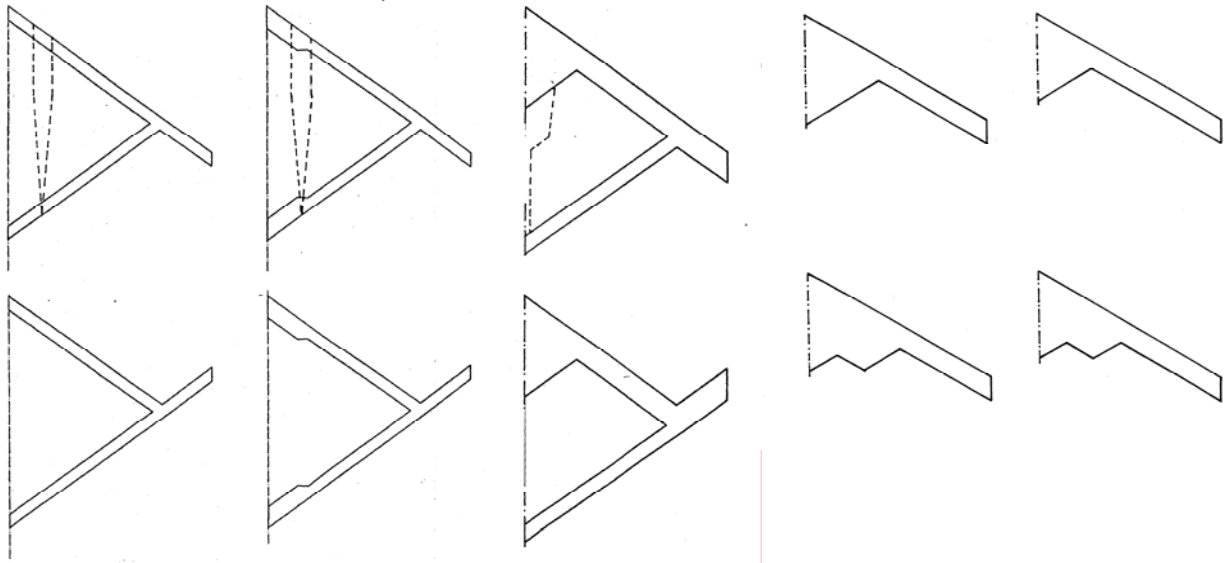
**FIG. 7.12 SENSOR-CRAFT CONCEPT PLANFORMS:
HIGH AR JOINED-WING AND LAMBDA-WING**
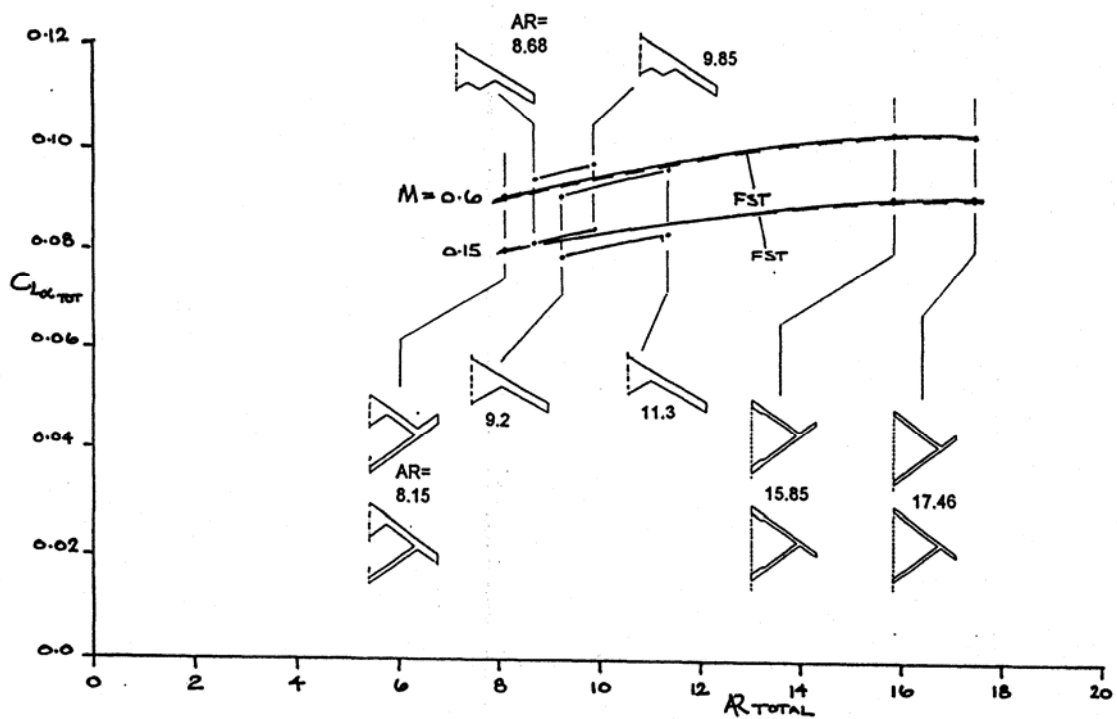
FIG. 7.13 CLα VARIATION WITH AR, JOINED WING & LAMBDA-WING CASES, M = 0.6 & 0.15
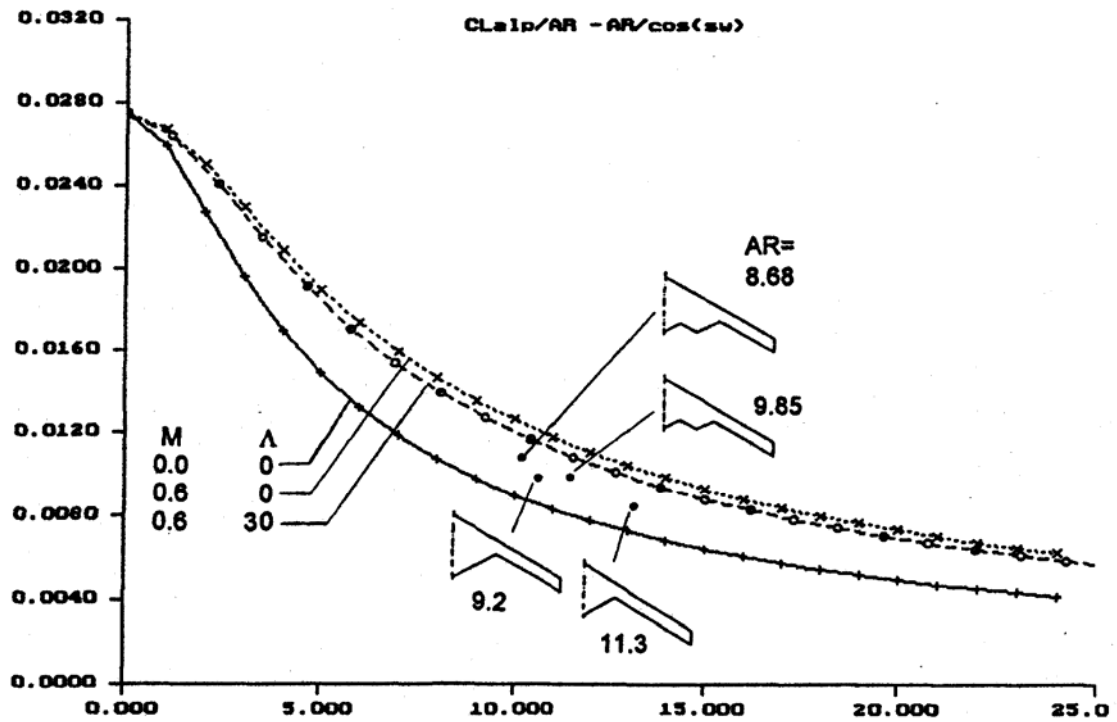
FIG. 7.14 CLα/AR VARIATION WITH AR,/cos(Λ), THEORETICAL EFFECT OF M & Λ, LAMBDA-WING CASES M = 0.6
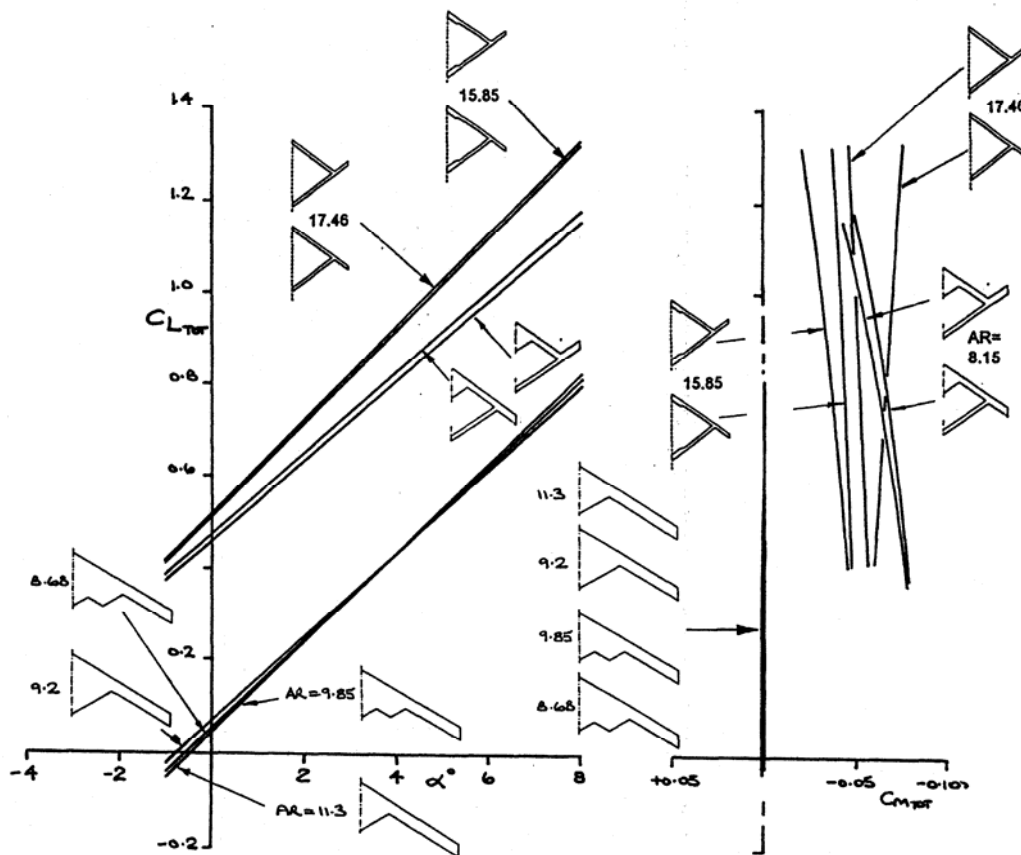
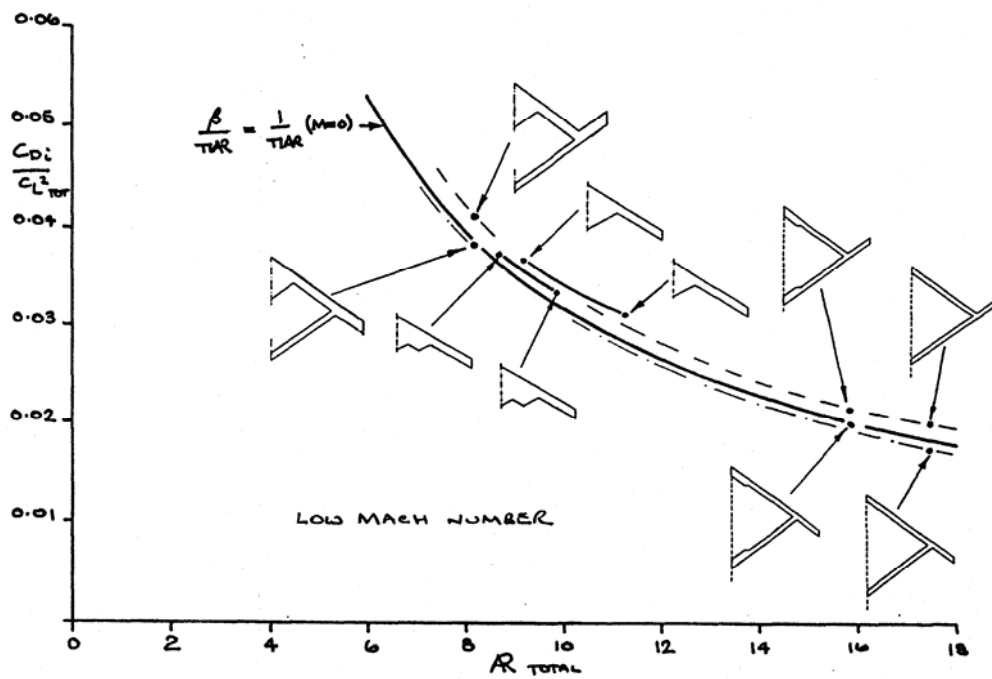**FIG. 7.15 TOTAL LOADS (C$_L$ - α, C$_m$ – C$_L$), M = 0.6 COMPARISON FOR JOINED WING AND LAMBDA-WING CASES**

FIG. 7.16 INDUCED DRAG FACTOR VARIATION WITH AR, UNCAMBERED WINGS, LOW M COMPARISON FOR JOINED-WING AND LAMBDA-WING CASES
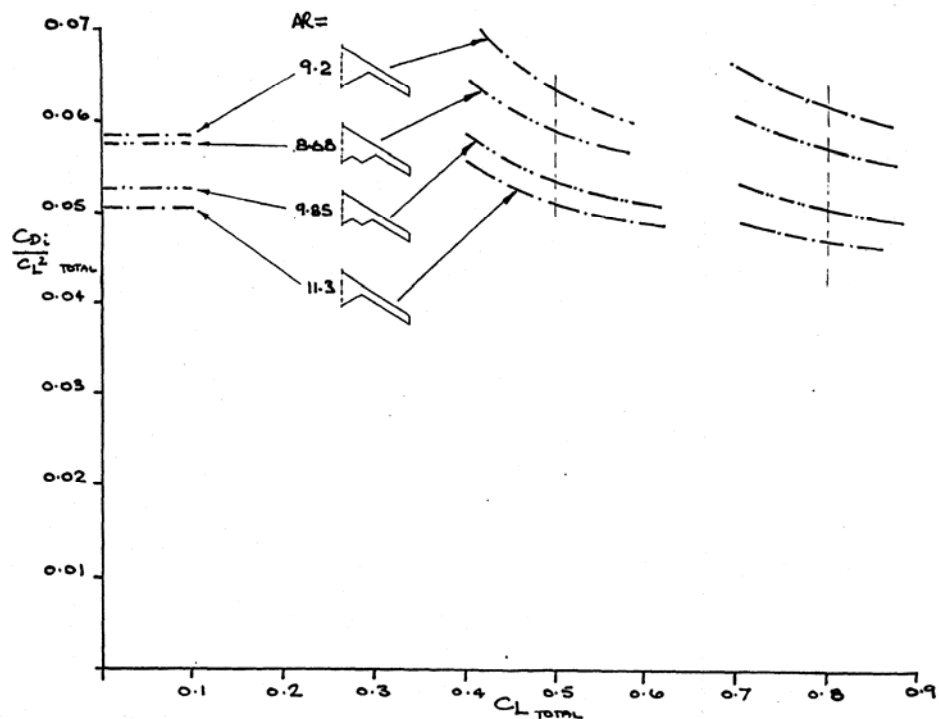

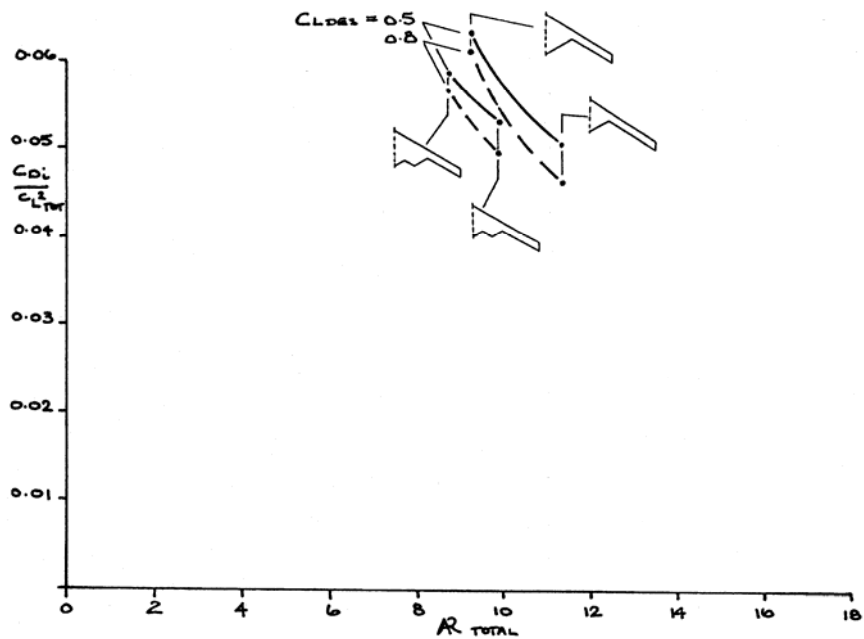**FIG. 7.17 INDUCED DRAG FACTOR VARIATION WITH CL, DESIGNED LAMBDA-WING CASES, M = 0.6,**

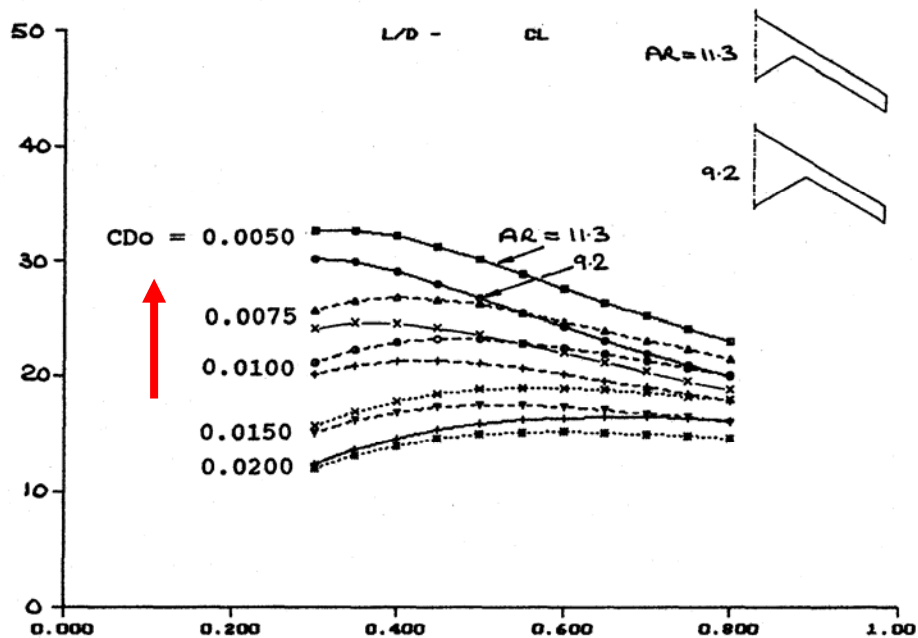**FIG. 7.18 INDUCED DRAG FACTOR VARIATION WITH AR,
DESIGNED LAMBDA-WINGS, M = 0.6**

Flow Control needed

**FIG. 7.19 L/D VARIATION WITH C_L, DESIGNED SINGLE LAMBDA-WINGS,
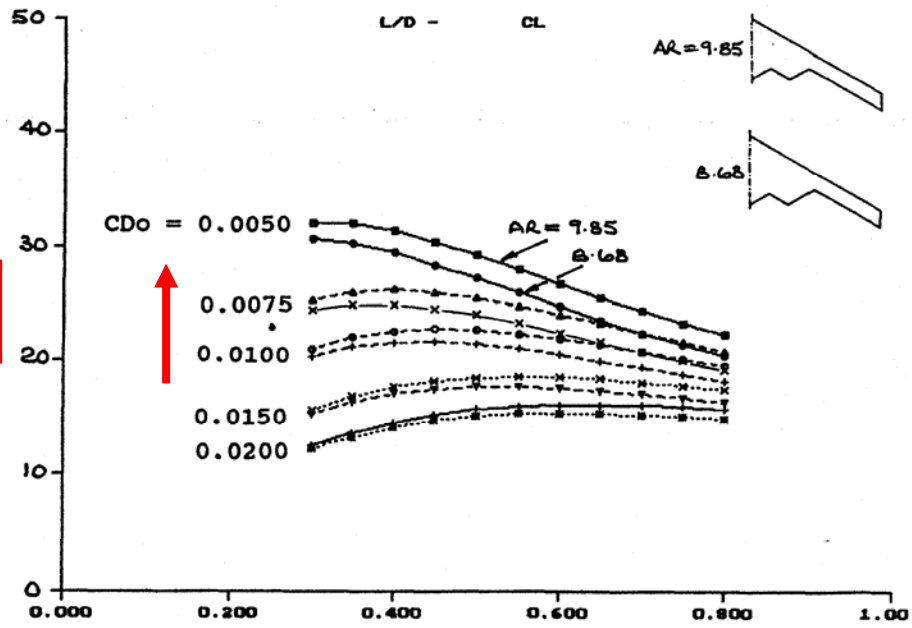M = 0.6, C_{Do} VARIES**

FIG. 7.20 L/D VARIATION WITH C_L, DESIGNED DOUBLE LAMBDA-WINGS, M = 0.6, C_{Do} VARIES
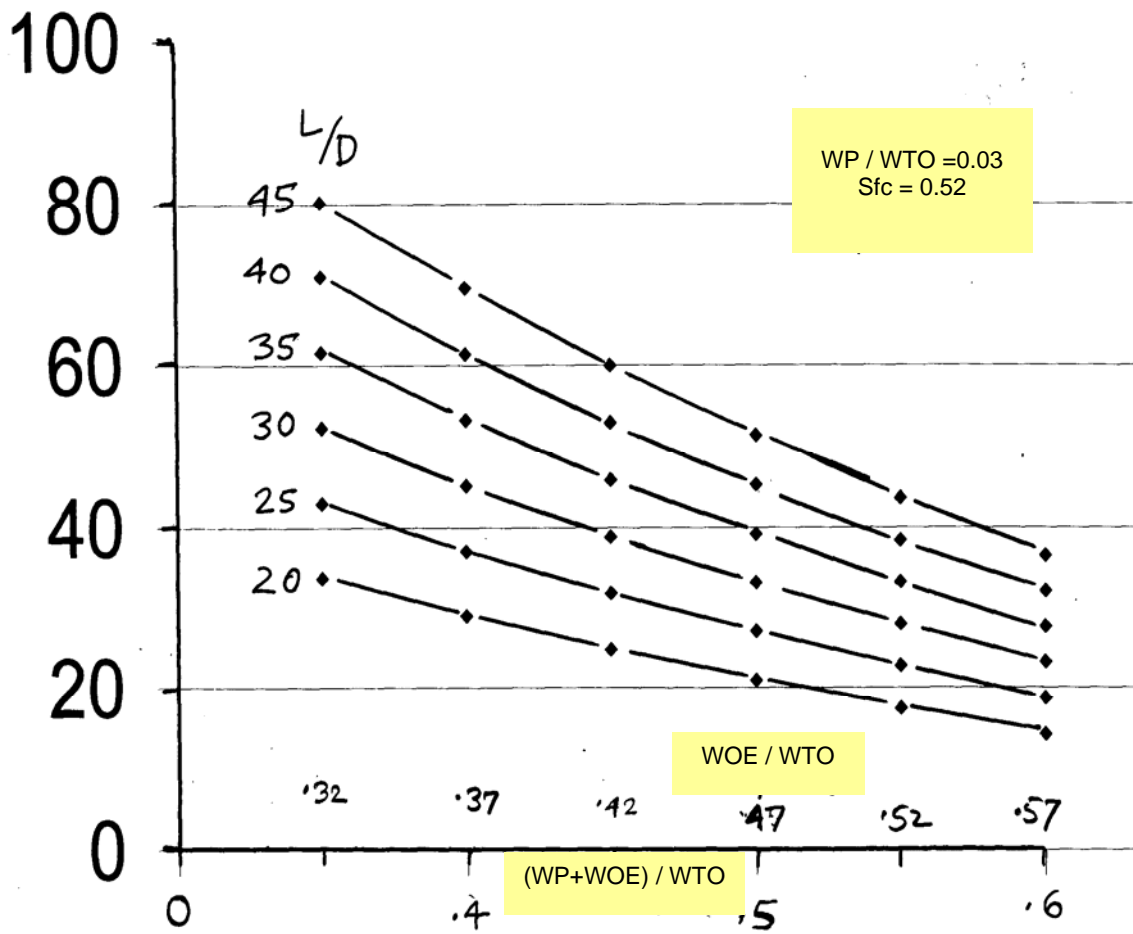

FIG. 7.21 ENDURANCE (HOURS) VARIATION WITH WEIGHT RATIOS, CONSTANT L/D VALUES, M = 0.6

HIGH ASPECT RATIO LAMBDA-WING CONFIGURATIONS INCORPORATING LAMINAR FLOW

Dr. R. K. Nangia

SUMMARY

Unmanned Sensor-Craft air vehicles have been proposed as the air-breathing component of a future intelligence, surveillance, and reconnaissance (ISR) infrastructure to provide revolutionary capabilities. Such craft must take advantage of high aspect ratio (AR) wings for aerodynamic efficiency, and may also be required to enclose a large, possibly diamond shaped antenna within the aircraft planform. A large proportion of fuel must be carried, and "loiter" is at high altitudes for a few days in each flight. This implies that a wide C_L–altitude capability is required.

A "Lambda" wing planform with single or double TE cranks has been considered for design at Mach 0.6 for a Sensor-Craft configuration. The study has looked at the effects of AR and the chordwise section design. Planar sections and sections with reference camber were assessed initially. Two laminar flow design conditions were defined, C_L 0.5 and 0.8 at Mach 0.6 with zero pitching moment and the appropriate camber and twist distributions determined. In addition, selected configurations were evaluated at Mach 0.15. Validation against an Euler code was also carried out.

Consideration of the theoretical methods has required that the wing tip TE sweeps be modified. This will have some effect on stability evaluation but this is considered relatively "fine" detail in view of other configuration aspects yet to be included such as fuselage, intakes and engine nozzles.

The designed cases show considerable reductions in LE suctions when compared with the uncambered, symmetric wing case. The Double Crank configuration gives more favourable spanwise loadings. We have attempted to correlate drag against various geometric parameters. The Double Crank case shows a drag advantage over the Single Crank which requires further investigation and analysis. Typical results presented demonstrate the flexibility and potential of the design techniques. The capability of studying several geometric configuration variables can be achieved rapidly. Data for detail design of wind tunnel models and possibly a flight demonstrator can be enabled. An understanding of control laws arises. The potential and limitations of the aircraft in meeting a given design envelope can be assessed. It is apparent that we are only at a starting post and a sizeable, interesting work programme remains! Several areas for continued work have emerged.

This report is Part 4 of a series of six relating to high AR, long endurance surveillance aircraft, laminar flow, integrated intakes and long range supersonic military aircraft.

**Consulting Engineers
Nangia Aero Research Associates
WestPoint, 78 Queens Road, Clifton
Bristol BS8 1QX, UK**

The Investigation which is the subject of this report was initiated by
USAF - EOARD, 223/231 Old Marylebone Road, London, NW1 5TH, UK
and was carried out under the terms of Contract SPC-024051

1	Mr. W. Donaldson	USAF-EOARD, London NW1 5TH, UK
1	Mr. C. Remillard	Chief, AFRL/VAAA; Bldg 45 2130 8th Street, WPAFB, Ohio, USA 45433-7542
1	Mr. D. Multhopp	Technical Area Lead, AFRL/VAAA; Bldg 45 2130 8th Street, WPAFB, Ohio, USA 45433-7542
2	Dr. C. P. Tilmann	Sr. Aerospace Engineer, AFRL/VAAA; Bldg 45 2130 8th Street, WPAFB, Ohio, USA 45433-7542
1	Mr. William Fields	Tech Area Lead, AFRL/VAAA; Bldg 45 2130 8th Street, WPAFB, Ohio, USA 45433-7542
1	Dr. K. P. Iwanski	Aerospace Engineer, AFRL/VAAA; Bldg 45 2130 8th Street, WPAFB, Ohio, USA 45433-7542
1	Mr. Larry Leavitt	Head, Configuration Aerodynamics Branch NASA Langley Research Center, Mail Stop 499 Hampton, VA 23681-2199
1	Dr. James Luckring	Configuration Aerodynamics Branch NASA Langley Research Center, Mail Stop 286 Hampton, VA 23681-2199
1	Mr. John Perdzock	Head, SensorCraft Integrating Concept Office, AFRL/VAC; Bldg 45 2130 8th Street, WPAFB, Ohio, USA 45433-7542
1	Dr. Maxwell Blair	AFRL/VASD; Bldg 146 2210 Eighth Street Wright-Patterson AFB OH 45433-7531
1	Dr. Keith Numbers	AFRL/VAA, Long Range Strike Integrating Concept Office
1	Mr. D. Adamczak	Sr. Aerospace Engineer, AFRL/VAAA; Bldg 45 2130 8th Street, WPAFB, Ohio, USA 45433-7542
1	Dr. Michael OL	Research Engineer, AFRL/VAAA Bldg 45 2130 8th Street, WPAFB, Ohio, USA 45433-7542
2	Dr. R.K. Nangia	Nangia Aero Research Associates WestPoint, 78-Queens Road, Clifton BRISTOL BS8 1QX, UK.

CONTRACTUAL DECLARATIONS

"The Contractor, Dr. R. K. Nangia,, hereby delcares that, to the best of its knowledge and belief, the technical data delivered herewith under Contract No.SPC-024051 is complete, accurate, and complies with all requirements of the contract.

DATE: **March 2004**   **Name and Title of Authorized Official:**   **Dr R K Nangia**

"I certify that there were no subject inventions to declare as defined in FAR 52.227-13, during the performance of this contract."

DATE: **March 2004**   **Name and Title of Authorized Official:**   **Dr R K Nangia**

CONTENTS

1. INTRODUCTION, BACKGROUND & WORK PROGRAMME

1.1. Background, Wider Context

The work discussed in this report relates specifically to high Aspect Ratio (AR) Lambda-Wing configurations incorporating Laminar flow. This report is Part 4 of a series of six, Refs.1 to 6, relating to high AR, long endurance surveillance aircraft, laminar flow, integrated intakes and long range supersonic military aircraft. This work follows previous work funded by USAF-EOARD under seeding Contract SPC-01-4087 which was reported in Ref.7.

The AFRL has been formulating a programme to provide revolutionary intelligence, surveillance and reconnaissance (ISR) capabilities to the warfighter (Refs.8-10). This programme blends a wide spectrum of emerging technologies into design proposals for an Unmanned Air Vehicle (UAV). The UAV is a single airframe, with long endurance capability, which may be configured and optimised to conduct multiple advanced sensing modes. These features, combined with omni-directional sensing, enable a virtual presence in a specific area. This allows vantage point flexibility / optimisation necessary for continuous and detailed air and ground target detection, identification, and tracking within the specified theatre. This unique combination of advanced sensors and sustained presence could enable continuous and rapid reaction to the dynamic combat operational requirements confronting current and evolving military operations.

The "Sensor-Craft" is envisaged as the air-borne, air-breathing component of a fully integrated ISR enterprise that cohesively integrates space, air, and ground components. It is an AFRL shared-vision UAV programme that combines critical vehicle, propulsion, sensor system, emerging flight and information technologies into a highly responsive platform concept to detect mobile, hidden targets. Several emerging sensor technologies are under assessment for platform use, including hyper-spectral imaging, active laser sensing, unattended ground sensors, and foliage penetration radar (Refs.8-10).

Several candidate aircraft and propulsion configurations are being considered to determine the best trade-off between long endurance, altitude, engine efficiency, and power generation. One of the major challenges is the integration of the large antenna apertures required for lower frequency operations into the airframe. These lower frequency bands of operation enable the Sensor-Craft to provide foliage penetration radar capabilities, a key sensory mode aimed at defeating extremely difficult camouflaged, concealed, and deceived (CC&D) targets (Ref.9)

Many of the Sensor-Craft concepts take advantage of high AR wings, as well as enclosing a large antenna in a "diamond" shaped aircraft planform. Such aircraft carry a large proportion of fuel and are expected to "loiter" at high altitudes for a few days in each flight. This implies a wide C_L - altitude capability, more so than existing operational reconnaissance aircraft e.g. Global Hawk. The "diamond" shapes offer useful survivability "compliance". The aerofoil shapes need to be thick for antenna and fuel tanks. The cruise Mach number is expected to be "high" subsonic. The low-speed near-field performance is more akin to that of a (very) high aspect ratio (AR) wing glider. Take-off and landing phases are demanding.

Previous work, Refs.11-14, has considered joined-wing Sensor-Craft configurations with conventional and laminar flow aerofoil sections. Two planforms were considered, one with a backward swept outer tip (AT1), the other with a forward swept outer tip (FT1). The Joined-wing concept was initially proposed by Wolkovitch in the 1980's (Ref.11). The layout is ideal for enclosing a diamond shaped aerial and the concept offers some design advantages, e.g. bending moment relief and high AR are achievable. The use of laminar flow sections

increased the C_L range for laminar flow from 1.00 to 1.09 for AT1 and from 1.00 to 1.14 for FT1. Laminar flow should provide a significant reduction in profile drag and enhance overall L/D of the vehicle.

1.2. Introduction to Present Work

There are many alternative planforms and configuration layouts that need to be considered as candidates for the airborne, air-breathing component of the ISR programme. Previous work has focussed on a joined-wing "Sensor-Craft" configuration. Alternative aerial layouts and further survivability considerations have allowed the possibility of a more conventional flying wing planform, reminiscent of the B-2. **Fig.1.2.1** illustrates several proposed and existing flying wing configurations. The work reported in this document includes consideration of the "Lambda" type planforms.

1.3. Present Work Programme

This report covers work on Lambda type planforms for use in the Sensor-Craft programme. Various planforms have been considered (single or double Lambda) covering a range of Aspect Ratio. An initial analysis of each configuration with planar (uncambered, symmetric) aerofoil sections was carried out. Constant reference camber, laminar flow aerofoil sections were then introduced and assessed. A design camber, with spanwise variation, was then developed for each planform for zero pitching moment and as near elliptic loading as possible. 12% aerofoil thickness has been used throughout. The wings have been designed for high speed cruise, M = 0.6 and also evaluated at low speed, M = 0.15. Several other aspects have yet to be considered, e.g. side-slip, stability, controls, etc.

1.4. Layout of Report

The remainder of this report is contained in **Sections 2 to 9**:

> **Section 2** discusses briefly the flight envelope, Reynolds number ranges and possible configurations.
>
> **Section 3** looks at effects of camber on 2-D aerofoil sections.
>
> **Section 4** defines the configurations considered and discusses, briefly, the prediction methods used.
>
> **Section 5** outlines further design aspects.
>
> **Section 6** discusses results for the Single Crank Lambda (SC) wing at Mach 0.6 and 0.15. Aspect Ratio effects are included. Selected Euler results are presented.
>
> **Section 7** discusses results for the Double Crank Lambda (DC) wing at Mach 0.6 and 0.15. Aspect Ratio effects are included. Selected Euler results are presented.
>
> **Section 8** lists some ideas for further work.
>
> **Section 9** mentions concluding remarks.

We begin with an outline of the flight envelope, Mach number, Lift Coefficient and Reynolds numbers encountered and possible configuration aspects.

2. FLIGHT ENVELOPE, REYNOLDS NO. & CONFIGURATION CONSIDERATIONS

Previous work conducted at the AFRL indicated that the main sizing driver aspect is the integration of a "rhombic" antenna in very thick aerofoils. The payload / range performance demands lead to thick aerofoils (t/c normal to the LE, between 15 to 21%) operating at high C_L values, near 1.0.

Fig.2.1 gives an idea of the aircraft flight envelope. The relationships between C_L and W/S are based on wing Aspect Ratio (AR) of 10, cruise Mach number of 0.6, an initial cruise weight of 100 000 lb and wing span of either 150 ft or 180 ft. Estimates for cruise altitudes of 60 000 ft, 65 000 ft and 70 000 ft are shown. The Altitude – Weight flight envelope has been derived for the larger, 180 ft span wing. This has a reference area of 3240 ft^2. Note the Altitude and Weight relationships during a typical mission. The Reynolds number variation is also depicted. From these figures, the C_L – Mach number envelope can be derived. For the 180 ft span wing, Take-off is near C_L of 0.63 at Mach 0.2 (Re = 1.42 x 10^6/ft), whilst landing is at C_L of 0.45 at Mach 0.15 (Re = 1.07 x 10^6/ft). The Mach 0.6 cruise C_L varies from 1.03 to 0.59 (Re = 0.38 x 10^6/ft to 0.34 x 10^6/ft). For the smaller, 150 ft span wing, the C_L values required are much higher, almost 1.5 at start of cruise. Reynolds number values per foot remain unchanged.

It is interesting to reflect that on conventional aircraft the cruise C_L values are near 0.5 and take-off / landing C_L values near 0.8 to 1.2.

Fig.2.2 summarises some early Linear Theory results. A series of planforms, with LE sweep of +30 ^{o}, were analysed. The planform geometry is non-dimensionalised by semi-span, s = 1.0. The trapezoidal wing has constant chord, c = 0.125 (based on s) and AR = 16. By increasing the length of the root chord and sweeping the inboard TE at -30 ^{o} a series of planforms, with a single TE crank (SC Series) was produced. As the spanwise location of the TE crank increased, y/s = 0.0 to 0.4, planform area increased and AR decreased from 16.0 to 9.2. A second series of planforms with Double TE cranks was also derived (DC Series). These had an inboard TE crank at y/s = 0.15 with outboard TE cranks at y/s = 0.45 and 0.50 (AR = 9.85 and 8.68 respectively). **Fig.2.2** shows the variation of lift curve slope ($C_{L\alpha}$) with AR at M = 0.6 for the two series. The likely, improved performance of the DC series can be seen.

The thick aerofoil sections with relative large LE radii (r) give an appreciable range of C_L or AoA operation. Predictions show "attained operation ranges (or bands)" for "attached" flow to be close to 4° in AoA. Previous work has been done with such aerofoils (Refs.11-13).

We now extend the analysis using laminar aerofoils. In principle, this should enable a significant reduction in profile drag and enhance overall L/D of the vehicle. However the wing planforms might well need to be revised.

3. LAMINAR FLOW AEROFOILS (2-D)

Fig.3.1 shows typical laminar flow aerofoil and C_P distributions from the XFOIL solver, based on work at AFRL (Ref.14). This is a suitable starting point for further developments. Using a panel code, we have analysed a series of uncambered (symmetric) and designed laminar sections for operation in the Mach 0.5-0.6 range.

Fig.3.2 shows C_P distributions on laminar uncambered aerofoils of t/c 16.0% and 19.5%. The AoA varies from -1° to 8° and the Mach number settings are: 0.01, 0.2, 0.4 and 0.6. Note that C_P distributions obtained are largely similar to those depicted in **Fig.3.1**, the slight difference arising are in the vicinity of the TE. This inference goes some way in justifying the use of an inviscid panel code for preliminary design. The addition of boundary layer effects can be carried out in the later stages of design as needed.

Figs.3.3 and **3.4** show the effect of camber on the C_P distributions of laminar aerofoils of t/c 16.0% and 19.5% respectively. The AoA varies from -1° to 8° and the Mach number settings are: 0.01, 0.2, 0.4 & 0.6. The effects of thickness (t/c = 16.0% and 19.5%) on C_P distributions on laminar cambered aerofoils are shown in **Fig.3.5**. The AoA varies from -1° to 8° and the Mach number settings are: 0.01, 0.2, 0.4 & 0.6. From these distributions we may establish the limit of laminar flow in terms of AoA. At Mach 0.6, further thickness effects have been established. **Fig.3.6** shows C_P distributions on laminar aerofoils, uncambered and cambered, with t/c = 12%, 14%, 16% and 19.5% at M = 0.6. As thickness increases, the laminar properties remain intact at higher AoA.

Fig.3.7 summarises laminar aerofoil capabilities, uncambered and cambered, through the Mach number range. The thicker aerofoils are more "capable". Also shown in **Fig.3.7** is the variation of maximum C_L achieved with laminar flow against t/c for planar and cambered aerofoil sections at M = 0.6. Additional data for t/c = 12% and 14% have been added. For the Lambda sensor-craft wing planforms proposed, t/c values as low as 12% may be required. The effects of camber, through the t/c range considered, are also shown for M = 0.6. From this study, it is evident that at t/c = 12%, for 3-D configurations, laminar flow at C_L beyond 1.0 will be very difficult to achieve.

Recent work of Saric et al at Arizona State University is summarised in **Fig.3.8**. The idea is to control the boundary layer development using distributed surface roughness. The figure shows surface flow visualisation on a wing of 45° sweep. Natural transition from laminar flow occurs at about 65% chord. Using distributed roughness at the LE, it is claimed that laminar flow can be encouraged to exist beyond 80% chord. On full scale aircraft, it is proposed that Distributed Roughness Elements (DREs) will simulate the required surface roughness. If crossflow induced transition can be delayed until 60% chord rather than occurring at the LE (fully turbulent), it is claimed that the Take-off weight of a designed aircraft could be reduced by 25%, **Fig.3.9**. A significant number of questions remain concerning the effectiveness of DRE. These are highlighted in **Fig.3.10**.

Features of flow over Lambda wings and the effects on load distributions are shown in **Fig.3.11**. The Lambda wing is highly loaded at the spanwise location of the TE kink.

4. LAMBDA SENSOR-CRAFT CONFIGURATIONS SCOPE, PREDICTION METHODS & DESIGN

In the original, joined wing, sensor-craft concept (Ref.11), it was intended to house the diamond shaped (planform) aerial within the wing structure, either as part of the wing spar or wing surface coating. In the Lambda sensor-craft layout, the diamond shaped aerial may be accommodated within the centre portion of the wing, again, either as part of the wing structure or skin laminate.

The reference planform is shown in **Fig.4.1**. The LE sweep is 30°. The outer portion of the wing has constant chord (0.125 for b = 2.0), giving a TE sweep of 30° also. The inner portion of the TE is swept forward 30°. With the TE crank at y/s = 0.3, the Aspect Ratio (AR) of the wing is 11.3. Moving the TE crank outboard, with the tip y/s maintained at 1.0, increases the planform area and reduces the AR. With the TE crank at y/s 0.4, AR = 9.2. Planforms with a single TE crank have been designated SC Series.

A typical, single engine-intake with single nozzle, configuration is sketched in **Fig.4.2**. Twin intake, twin engined configurations with multiple nozzles may also be considered. In the current analysis, the wing design process has extended from the centreline to the tip. It is noted that the wing root region may be significantly modified to accommodate fuselage, intakes, engines and nozzles. Also, thick, streamwise tips have been modelled. It is possible that, in the final design, the tip region would be swept forward 30° and taper to zero thickness at the resulting outer TE.

An elliptic type wing load distribution is desirable for minimum drag. For continuous, smoothly tapering wings, an elliptic loading can be readily achieved with a suitable distribution of cambered, twisted aerofoil sections. For wings with straight LE and straight, cranked TE, elliptic loadings cannot be taken for granted.

In an attempt to make the planform more amenable to elliptic type load distributions the Double Crank Lambda Wing (DC Series) concept was introduced, **Fig.4.3**. The two planforms shown have AR = 9.85 and 8.68 with inboard TE cranks at y/s = 0.15 and outboard TE cranks at y/s = 0.45 and 0.50 respectively. A typical, single engine-intake with single nozzle, configuration for this type of planform is sketched in **Fig.4.4**. Again, twin intake, twin engined configurations with multiple nozzles may be considered.

Preliminary analysis showed that at M = 0.6, Lift curve slope ($C_{L\alpha}$) values would lie in the range 0.084 to 0.089, for AR between 8.68 and 11.3. The double crank lambda wing planform achieved higher $C_{L\alpha}$ values. The main difficulties for these planforms, essentially high AR flying wings, are trimming at high and low speeds whilst maintaining laminar flow. On novel layouts, often the experience is that the complexities "defy" an automatic "hands-off" design process being used with confidence (unique solutions doubted). Therefore, we have chosen a process that allows a significant understanding to be gained with reasonable manual control over the design process (Refs.15 - 25).

The low speed and high speed demands on the configuration obviously "conflict" and this has led to a challenging work programme towards suitable layouts. Panel and Euler codes are being utilised that enable assessment of the aerodynamic performance over the range of low to high speeds. The camber and twist design, under forces and moments constraints, is via previously validated methods, similar to the NASA Langley R C (attained thrust methods of Carlson).

The aerodynamic prediction methods are now discussed together with a description of the wing design process.

Aerodynamic Prediction Methods

The aerodynamic prediction methods are described in an order of complexity.

Linear Theory & Attained Thrust Methods

The linear lifting surface theories have been around for 3 or 4 decades. Various formulations in terms of vortex lattice and doublet lattice exist. Methods have been used in subsonic and supersonic linearized flows. Several design approaches for minimizing drag for given lift also exist. Useful Text books are e.g. by Bertin & Smith, "Aerodynamics for Engineers", and McCormick, "Aerodynamics, Aeronautics & Flight mechanics".

A more recent development over last 2 decades has been the incorporation of attained thrust principles in linear theories. The attained thrust method uses empirical correlations of onset flow and aerofoil parameters (along the span of the wing) to establish the proportion of thrust recovered on the wing leading edges. Such methods were pioneered by Carlson et al at NASA Langley. Computer programmes such as WDES are available in USA. The codes also have a camber design facility (using polynomial type modes). We have developed our own codes based on principles similar to those used by Carlson.

Panel Codes

Panel codes (surface singularity methods) are well established and form an important part of the designer's inventory. These have been developed over the last 25 years and have reached a reasonable level of maturity. Various first and second order codes are available e.g. PMARC, VSAERO, PANAIR and QUADPAN (in USA). Most of these methods produce very similar results for Mach numbers less than about 0.8. Flow compressibility effects are based on the Prandtl-Glauert approximation. The surface of the configuration is overlaid by panels of surface singularities e.g. doublet and sources. A matrix of influence coefficients, relating the effects of each panel on all others is then formed. This matrix is then solved with respect to the boundary conditions and onset flow parameters.

The boundary condition can be set up in different ways. In Neumann or "direct" type formulation, the normal velocity is applied directly, balancing the velocities due to singularities placed on the surface panel network. In the "Dirichlet Potential formulation", the solution assumes zero potential inside a closed body and this implies an "indirect" compliance of zero normal velocity across a surface.

Once the strengths of the flow singularities are known, velocities, pressures, forces and moments can be calculated. In general, the wake geometries are pre-specified. Some methods allow relaxation of wakes in an iterative manner.

Good descriptions of the underlying methods are given in standard texts (e.g. Katz & Plotkin, "Low Speed Aerodynamics").

Euler Codes

Euler codes have become well established over the last 20 years. These are based on the Euler approximation (i.e. ignoring viscosity terms) of the full Navier-Stokes flow equations. The compressibility effects allow shock formation. Many text-books deal with the theoretical and numerical aspects (e.g. finite-difference, finite-volume and finite element). To apply the methods, surface and volume grids are both needed. The grids can be either structured or unstructured (triangles & pyramids). These are therefore more expensive in grid formation and cpu usage (cf. panel codes). We have used the finite element Euler method of Ref.26 as needed for "final" checks on the designed geometries.

Inverse Codes

The inverse approaches can be used with any of the aerodynamic prediction codes. Various methodologies have been pioneered throughout the world e.g. NASA Langley C-DISC. Such codes are usually applied in the final stages to help in fine-tuning and tailoring of flow parameters, e.g. velocities or pressure distributions. We have given an example of the technique in an AIAA publication, Ref.12. As far as the current work programme is concerned, these methods have not needed to be exploited. One would expect their use when fuselages and intakes need to be integrated into the configuration. It is planned to publish a paper on the methodology in due course.

Wing Design Process

The design procedure is illustrated in schematic form in **Fig.4.5**. The over-riding principle is to achieve a "tolerant" design and at the same time to minimise drag for a reasonable design lift coefficient range. For these, essentially flying wing planforms, control over pitching moment is required. The design targets are therefore:

> Onset flow attachment at the Leading Edge (LE) near the design C_L
> Elliptical spanwise load distribution
> Acceptable pitching moment characteristics

1. Set up geometry for the uncambered (symmetric aerofoil) case. This has the required aerofoil thickness distribution that will be used for all three design stages, uncambered, reference camber and designed camber. From the uncambered geometry, basic aerodynamic trends are established, e.g. $C_{L\alpha}$, neutral point location and shape of spanwise lift distributions. The thickness distribution of the uncambered case will be used in Steps 2 and 4.

2. Set up geometry for the Datum Camber aerofoil case. Establish spanwise distribution of α for attachment at LE and α (twist) effects on local load distributions. This provides the target C_L and spanwise loading.

3. A camber surface is generated via a Camber Design process with specified C_L and C_m targets. Several approaches are feasible, modal, direct or inverse. As mentioned, we use an in-house approach based on the well-known NASA Langley R C pioneering work of Carlson and attained thrust.

4. The thickness distribution used in Steps 1 and 2 is added to the designed camber surface to give the required design geometry.

5. Evaluate the new geometry

6. Repeat steps 3 - 5, if necessary.

As mentioned earlier, further refinement can be introduced by using an inverse design method such as using 3-D membrane analogy technique. (Ref.27). This can enable "tailoring" and "fine-tuning" of aerofoil shapes for "optimum" C_P distributions as needed, especially when fuselages and intakes are to be integrated.

5. DESIGN ASPECTS

At the outset, there are several aspects that need to be considered, e.g.

- Type of spanwise loadings and design of wing camber and twist.
- Trimmed flight at low speeds with different C_L levels. The TE geometry can be varied.
- High-speed design of thick wings, tolerant to a large C_L variation (fuel usage). Use of TE flaps.
- Integration of intakes / fuselages.
- "Reasonable" off-design such as cross-winds, landing / take-off.
- Roll, Pitch and Yaw Stability levels, Control laws.

Here we take a few of these aspects related to "high-speed" wing design. As noted earlier, Fuselages, Intakes and Nozzles remain to be included. The high speed design cases for both the Single and Double Lambda layouts have also been evaluated at low speeds (M = 0.15).

6. SINGLE CRANK LAMBDA (SC) WING, Mach 0.6 and Low Speed

The reference planform is discussed in Section 4. We consider two planform variations. With the TE crank at $y/s = 0.4$, the AR of the wing is 9.2. Moving the TE crank inboard to $y/s = 0.3$, maintaining $s = 1.0$, decreases the planform area and increases the AR to 11.3. Root (centreline) chords are 0.587 and 0.471 respectively. High speed design and evaluation has been carried out on both the AR 9.2 and 11.3 planforms for design C_L of 0.5 and 0.8. Low speed (Mach 0.15) evaluation of the designed AR 11.3 cases are also included.

6.1. AR 9.2 Wing

The planform distribution of the planar (symmetric, uncambered) aerofoil sections is shown in **Fig.6.1.1**. Also shown in this figure are the C_L – AoA variation and the spanwise loadings at $M = 0.6$. The chordwise location of the Moment Reference Centre is established at $x = 0.307$ ($s = 1.0$). C_P – x and C_P – x/c distributions are given for AoA = 0°, 1° and 2°. Laminar flow is maintained up to and including AoA = 1° ($C_L = 0.094$).

In **Fig.6.1.2**, the reference cambered aerofoil sections are compared with the planar sections. The wing has a zero incidence (AoA = 0°) $C_L = 0.45$ and a constant $C_m = -0.15$. The spanwise loadings are less elliptical than those for the planar wing. C_P – x and C_P – x/c distributions are given for AoA = 3°, 4° and 5°. Laminar flow is maintained up to and including AoA = 4° ($C_L = 0.812$).

The design approach, outlined in Section 4, was used to design the AR9.2 SC wing for two C_L values (0.5 and 0.8) at Mach 0.6. Camber and twist modes were applied to achieve zero pitching moment and as near elliptic loading as possible.

CL Design 0.5 Mach 0.6

Using Linear Theory design methods, a camber (and twist) distribution was established that would maintain laminar flow up to $C_L = 0.5$ (C_{Ldes}) with $C_m = 0.0$ throughout the C_L range. The resulting aerofoil distiribution is compared with the planar aerofoil distribution in **Fig.6.1.3**. The wing has a zero incidence (AoA = 0°) $C_L = 0.07$ and a constant $C_m = 0.0$ as required. C_P – x and C_P – x/c distributions are given for AoA = 3°, 4° and 5°. Laminar flow is maintained up to and including AoA = 4° ($C_L = 0.432$). At AoA = 5° ($C_L = 0.522$), laminar flow is not maintained over the outboard part of the wing. The limiting C_L for laminar flow is therefore estimated to be 0.5.

CL Design 0.8 Mach 0.6

The design process was repeated for a design C_L (extent of laminar flow) of 0.8. The resulting aerofoil distribution is compared with the planar aerofoil distribution in **Fig.6.1.4**. The wing has a zero incidence (AoA = 0°) $C_L = 0.13$ and a constant $C_m = 0.0$ as required. C_P – x and C_P – x/c distributions are given for AoA = 6°, 7° and 8°. Laminar flow is maintained up to and including AoA = 7° ($C_L = 0.764$). At AoA = 8° ($C_L = 0.852$) there is little evidence of laminar flow.

The results for the planar aerofoil section wing, reference camber aerofoil wing and the two design cases are summarised in **Fig.6.1.5**. The 2-D aerofoil section is capable of maintaining laminar flow up to almost $C_L = 1.3$. Using the reference camber aerofoil on this AR = 9.2

wing, laminar flow can be maintained up to $C_L = 0.8$ but at the expense of a severe nose down pitching moment ($C_m = -0.15$). Designing for zero pitching moment and laminar flow up to $C_L = 0.5$, results in a moderately cambered / twist wing design. Extending the design to $C_L = 0.8$ results in a more heavily cambered and twisted wing.

6.2. AR 11.3 Wing

The planform distribution of the planar aerofoil sections is shown in **Fig.6.2.1** together with the C_L – AoA variation and the spanwise loadings at M = 0.6. The chordwise location of the Moment Reference Centre is established at x = 0.302 (s = 1.0). C_P – x and C_P – x/c distributions are given for an extensive AoA range, 0° to 10° at 1° intervals. Laminar flow is maintained up to and including AoA = 1° ($C_L = 0.097$).

In **Fig.6.2.2**, the reference cambered aerofoil sections are compared with the planar sections. The wing has a zero incidence (AoA = 0°) $C_L = 0.48$ and a constant $C_m = -0.14$. The spanwise loadings are less elliptical than those for the planar wing. C_P – x and C_P – x/c distributions are given for AoA = 3°, 4° and 5°. Laminar flow is maintained up to and including AoA = 4° ($C_L = 0.864$).

Using the design process outlined in Secton 6.1 two wings were designed, $C_{Ldes} = 0.5$ and 0.8 with $C_m = 0.0$ throughout the C_L range.

CL Design 0.5 Mach 0.6

The design process outlined in Section 6.1 was repeated for this wing. The resulting aerofoil distribution for $C_{Ldes} = 0.5$ is compared with the planar aerofoil distribution in **Fig.6.2.3**. The wing has a zero incidence (AoA = 0°) $C_L = 0.04$ and a constant $C_m = 0.0$ as required. C_P – x and C_P – x/c distributions are given for AoA = 3°, 4° and 5°. Laminar flow is maintained up to and including AoA = 4° ($C_L = 0.428$). At AoA = 5° ($C_L = 0.524$), laminar flow is not maintained over the outboard part of the wing. The limiting C_L for laminar flow is therefore estimated to be 0.5.

CL Design 0.5 at Mach 0.6 evaluated at Mach 0.15

The designed configuration (M = 0.6, $C_{Ldes} = 0.5$) was also evaluated at M = 0.15. The characteristics are shown in **Fig.6.2.4**. There is ony a small change in the C_m - C_L relationship as Mach number falls from 0.6 to 0.15. Laminar flow is maintained up to about $C_L = 0.37$.

CL Design 0.8 Mach 0.6

The aerofoil distribution for $C_{Ldes} = 0.8$ is compared with the planar aerofoil distribution in **Fig.6.2.5**. The wing has a zero incidence (AoA = 0°) $C_L = 0.07$ and a constant $C_m = 0.0$ as required. C_P – x and C_P – x/c distributions are given for AoA = 6°, 7° and 8°. Laminar flow is maintained up to and including AoA = 7° ($C_L = 0.762$). At AoA = 8° ($C_L = 0.858$) there is little evidence of laminar flow.

CL Design 0.8 at Mach 0.6 evaluated at Mach 0.15

The designed configuration (M = 0.6, $C_{Ldes} = 0.8$) was also evaluated at M = 0.15. The characteristics are shown in **Fig.6.2.6**. Again, there is only a small change in the C_m - C_L

relationship as Mach number falls from 0.6 to 0.15. In this case, laminar flow is maintained up to about $C_L = 0.57$.

<u>Wing Tip Refinement to Extend the C_{Ldes} Range (CL Design 0.8 at Mach 0.6)</u>

As noted above, the configuration performance, in terms of laminar flow C_L, is limited by the outboard region of the wing. The configuration performance may be extended overall if local performance is improved. By moving the chordwise location of the aerofoil maximum thickness rearwards and adjusting local twist accordingly it is intended to extend the laminar flow range without adversely affecting pitching moment.

Aerofoil maximum thickness, chordwise location ($x_{t/cmax}$), is defined in **Fig.6.2.7**. For the reference aerofoil, $x_{t/cmax} = 0.43$ remains constant across the span as shown. On the refined tip geometry, $x_{t/cmax}$ gradually moves rearwards from x/c = 0.43 at y/s = 0.925 to x/c = 0.55 at y/s = 1.0. These minor geometry changes had the desired effects. The C_L, AoA and C_m relationships remain unchanged but locally at the tip, laminar flow breakdown is delayed by about 0.1 C_L until approximately $C_L = 0.86$. However, additional camber will be required on the outboard LE to fully establish laminar flow characteristics.

The results for the planar aerofoil section wing, reference camber aerofoil wing and the two design cases are summarised in **Fig.6.2.8**. The 2-D aerofoil section is capable of maintaining laminar flow up to almost $C_L = 1.3$. Using the reference camber aerofoil on this AR = 11.3 wing, laminar flow can be maintained up to $C_L = 0.86$ but at the expense of a severe nose down pitching moment ($C_m = -0.14$). Designing for zero pitching moment and laminar flow up to $C_L = 0.5$, results in a moderately cambered / twist wing design. Extending the design to $C_L = 0.8$ results in a more heavily cambered and twisted wing.

6.3. Summary Comparisons, AR 9.2 and 11.3 Wings

At the design point, laminar flow is maintained at all stations across the wing. As C_L increases laminar flow will begin to break down at a particular location across the semi-span, depending upon planform and section distribution. C_L values at which laminar flow is first seen to breakdown for the two SC wings (AR = 9.2 and 11.3) are summarised in **Figs.6.3.1** and **2**. CoP and $c_{1/4}$ locations are also indicated on the planforms. **Fig.6.3.1** shows limiting C_L for laminar flow for the planar and reference camber wings. 2-D results are shown as potential targets. Using the reference camber aerofoil sections a laminar flow C_L limit of about 0.8 can be achieved irrespective of AR. However, in both cases, there is a severe nose down pitching moment. This can be designed out but at the expense of laminar flow C_L range, **Fig.6.3.2**. The higher AR wing requires less camber and twist to achieve C_{Ldes}.

6.4. Selected Euler Validations, Mach 0.6

Results from Euler code (Ref.26) on the AR 11.3 configurations designed for laminar flow up to $C_L = 0.5$ and 0.8 are compared with panel code results in **Figs.6.4.1** and **6.4.2** respectively. Results for the planar aerofoils at equivalent C_L are also shown. There is good agreement between the two methods. On the planar wings, the Euler code gives reduced LE suctions. For the designed cases, the Euler results indicate that more LE camber might be required.

7. DOUBLE CRANK LAMBDA (DC) WING, Mach 0.6 and Low Speed

The planforms are discussed in detail in Section 4. Here we consider two planforms with double cranked TE. The planforms have AR = 9.85 and 8.68 with inboard TE cranks at y/s = 0.15 and outboard TE cranks at y/s = 0.45 and 0.50 respectively. Root (centreline) chords are 0.529 and 0.471 respectively. High speed design and evaluation has been carried out on both the AR 8.68 and 9.85 planforms. Two C_L design targets were set in each case (0.5 & 0.8). Low speed (Mach 0.15) evaluation of the designed AR 9.85 cases are also included.

7.1. AR 8.68 Wing

The planform distribution of the planar aerofoil sections is shown in **Fig.7.1.1** together with the C_L – AoA variation and the spanwise loadings at M = 0.6. The chordwise location of the Moment Reference Centre is established at x = 0.310 (s = 1.0). C_P – x and C_P – x/c distributions are given for AoA = 0°, 1° and 2°. Laminar flow is maintained up to and including AoA = 1° (C_L = 0.094).

In **Fig.7.1.2**, the reference cambered aerofoil sections are compared with the planar sections. The wing has a zero incidence (AoA = 0°) C_L = 0.47 and a constant C_m = -0.15. The spanwise loadings are less elliptical than those for the planar wing but are possibly better than those for the Single cranked wing. C_P – x and C_P – x/c distributions are given for AoA = 2°, 3° and 4°. Laminar flow is maintained up to and including AoA = 3° (C_L = 0.755) and has possibly only just broken down at AoA = 4° (C_L = 0.848).

Using the design process outlined in Secton 6.1 two wings were designed, C_{Ldes} = 0.5 and 0.8 with C_m = 0.0 throughout the C_L range.

CL Design 0.5 Mach 0.6

The resulting aerofoil distiribution for C_{Ldes} = 0.5 is compared with the planar aerofoil distribution in **Fig.7.1.3**. The wing has a zero incidence (AoA = 0°) C_L = 0.05 and a constant C_m = 0.0 as required. C_P – x and C_P – x/c distributions are given for AoA = 3°, 4° and 5°. Laminar flow is maintained up to and including AoA = 4° (C_L = 0.432). At AoA = 5° (C_L = 0.525), laminar flow is not maintained over the outboard part of the wing. The limiting C_L for laminar flow is therefore estimated to be 0.5.

CL Design 0.8, Mach 0.6

The C_{Ldes} = 0.8 aerofoil distiribution is compared with the planar aerofoil distribution in **Fig.7.1.4**. The wing has a zero incidence (AoA = 0°) C_L = 0.12 and a constant C_m = 0.0 as required. C_P – x and C_P – x/c distributions are given for AoA = 6°, 7° and 8°. Laminar flow is maintained up to and including AoA = 7° (C_L = 0.774). At AoA = 8° (C_L = 0.867) laminar flow is not maintained over the outboard part of the wing.

The results for the planar aerofoil section wing, reference camber aerofoil wing and the two design cases are summarised in **Fig.7.1.5**. The 2-D aerofoil section is capable of maintaining laminar flow up to almost C_L = 1.3. Using the reference camber aerofoil on this AR = 8.68 wing, laminar flow can be maintained up to C_L = 0.75 but at the expense of a severe nose down pitching moment (C_m = -0.147). Designing for zero pitching moment and laminar flow

up to $C_L = 0.5$, results in a moderately cambered / twist wing design. Extending the design to $C_L = 0.8$ results in a more heavily cambered and twisted wing.

7.2. AR 9.85 Wing

The planform distribution of the planar aerofoil sections is shown in **Fig.7.2.1** together with the C_L – AoA variation and the spanwise loadings at M = 0.6. The chordwise location of the Moment Reference Centre is established at x = 0.297 (s = 1.0). C_P – x and C_P – x/c distributions are given for AoA = 0°, 1° and 2°. Laminar flow is maintained up to and including AoA = 1° ($C_L = 0.098$).

In **Fig.7.2.2**, the reference cambered aerofoil sections are compared with the planar sections. The wing has a zero incidence (AoA = 0°) $C_L = 0.49$ and a constant $C_m = -0.14$. The spanwise loadings are less elliptical than those for the planar wing but are possibly better than those for the Single cranked wing. C_P – x and C_P – x/c distributions are given for AoA = 2°, 3° and 4°. Laminar flow is maintained up to and including AoA = 3° ($C_L = 0.781$)and has possibly only just broken down at AoA = 4° ($C_L = 0.877$).

Using the design process outlined in Secton 6.1 two wings were designed, $C_{Ldes} = 0.5$ and 0.8 with $C_m = 0.0$ throughout the C_L range.

CL Design 0.5, Mach 0.6

The resulting aerofoil distiribution for $C_{Ldes} = 0.5$ is compared with the planar aerofoil distribution in **Fig.7.2.3**. The wing has a zero incidence (AoA = 0°) $C_L = 0.05$ and a constant $C_m = 0.0$ as required. C_P – x and C_P – x/c distributions are given for AoA = 3°, 4° and 5°. Laminar flow is maintained up to and including AoA = 4° ($C_L = 0.441$). At AoA = 5° ($C_L = 0.538$), laminar flow is not maintained over the outboard part of the wing. The limiting C_L for laminar flow is therefore estimated to be 0.5.

CL Design 0.5 at Mach 0.6 evaluated at Mach 0.15

The designed configuration (M = 0.6, $C_{Ldes} = 0.5$) was also evaluated at M = 0.15. The characteristics are shown in **Fig.7.2.4**. There is ony a small change in the C_m - C_L relationship as Mach number falls from 0.6 to 0.15. Laminar flow is maintained up to about $C_L = 0.38$.

CL Design 0.8, Mach 0.6

The $C_{Ldes} = 0.8$ aerofoil distiribution is compared with the planar aerofoil distribution in **Fig.7.2.5**. The wing has a zero incidence (AoA = 0°) $C_L = 0.10$ and a constant $C_m = 0.0$ as required. C_P – x and C_P – x/c distributions are given for AoA = 6°, 7° and 8°. Laminar flow is maintained up to and including AoA = 7° ($C_L = 0.788$). At AoA = 8° ($C_L = 0.884$) laminar flow is not maintained over the outboard part of the wing.

CL Design 0.8 at Mach 0.6 evaluated at Mach 0.15

The designed configuration (M = 0.6, $C_{Ldes} = 0.8$) was also evaluated at M = 0.15. The characteristics are shown in **Fig.7.2.6**. Changes in the C_m - C_L relationship as Mach number falls from 0.6 to 0.15 are becoming noticeable but are still relatively small. Laminar flow is maintained up to $C_L = 0.6$, possibly up to $C_L = 0.65$.

The results for the planar aerofoil section wing, reference camber aerofoil wing and the two design cases are summarised in **Fig.7.2.7**. The 2-D aerofoil section is capable of maintaining laminar flow up to almost $C_L = 1.3$. Using the reference camber aerofoil on this AR = 9.85 wing, laminar flow can be maintained up to $C_L = 0.77$ but at the expense of a severe nose down pitching moment ($C_m = -0.141$). Designing for zero pitching moment and laminar flow up to $C_L = 0.5$, results in a moderately cambered / twist wing design. Extending the design to $C_L = 0.8$ results in a more heavily cambered and twisted wing.

7.3. Summary Comparisons, AR 8.68 and 9.85 Wings

At the design point, laminar flow is maintained at all stations across the wing. As C_L increases laminar flow will begin to break down at a particular location across the semi-span, depending upon planform and section distribution. C_L values at which laminar flow is first seen to breakdown for the two DC wings (AR =8.68 and 9.85) are summarised in **Figs.7.3.1** and **2**. CoP and $c_{1/4}$ locations are also indicated on the planforms. **Fig.7.3.1** shows limiting C_L for laminar flow for the planar and reference camber wings. 2-D results are shown as potential targets. Using the reference camber aerofoil sections a laminar flow C_L limit of about 0.8 can be achieved irrespective of AR. However, in both cases, there is a severe nose down pitching moment. This can be designed out but at the expense of laminar flow C_L range, **Fig.7.3.2**. The higher AR wing requires less camber and twist to achieve C_{Ldes}.

7.4. Selected Euler Validations, Mach 0.6

Results from Euler code (Ref.26) on the AR 9.85 configurations designed for laminar flow up to $C_L = 0.5$and 0.8 are compared with panel code results in **Figs.7.4.1** and **7.4.2** respectively. Results for the planar aerofoils at equivalent C_L are also shown. There is good agreement between the two methods. On the planar wings, the Euler code gives reduced LE suctions. For the designed cases, the Euler results indicate that more LE camber might be required. The presentation of the Euler results highlights a localised area (outboard TE crank) that requires further design work for the $C_L = 0.5$ design case, **Figs.7.4.1**.

8. PLANFORM COMPARISONS, Mach 0.6 and Low Speed

The reference planform, **Fig.4.1** has LE sweep of 30°. The outer portion of the wing has constant chord (0.125 for b = 2.0), giving a TE sweep of 30° also. The inner portion of the TE is swept forward 30°. With the TE crank at y/s = 0.3, the Aspect Ratio (AR) of the wing is 11.3. Moving the TE crank outboard (tip y/s = 1.0) increases the planform area and reduces the AR. With the TE crank at y/s = 0.4, AR = 9.2. Planforms with a single TE crank have been designated SC Series. To make the planform more amenable to elliptic type load distributions the Double Crank Lambda Wing (DC Series) concept was introduced. Two DC planforms were assessed. One with TE cranks at y/s = 0.15 and 0.45 giving AR = 9.85. The second with TE cranks at y/s = 0.15 and 0.50 giving AR = 8.68. The four planforms are shown in **Fig.8.1**.

The variation of lift curve slope ($C_{L\alpha}$) with Aspect Ratio (AR) is given in **Fig.8.2** for the Lambda wing configurations at M = 0.6 and low Mach number (0.15).

The theoretical variation of $C_{L\alpha}$ / AR with AR / cos(Λ) was derived using the equation:
$$C_{L\alpha} = a_o AR / [(a_o/\pi) + ((AR/\cos(\Lambda))^2 + (a_o/\pi)^2 - (AR.M_o)^2)^{1/2}]$$
for incompressible flow.
Considering compressibility effects $C_{L\alpha \text{ (compressible)}} = C_{L\alpha \text{ (incompressible)}} / \beta$, where $\beta = (1-M^2)^{1/2}$. Hence $a_o = 2\pi/\beta$.

The effects of Mach number and sweep are evident in **Fig.8.3**. Using values of $C_{L\alpha}$ derived from panel methods at M = 0.6, the $C_{L\alpha}$/ AR trends, for the Lambda wing planforms, are also shown in **Fig.8.3**. These values lie close to the theoretical line. Total loads ($C_L - \alpha$, $C_m - C_L$), are compared in **Fig.8.4** for the designed Single Lambda (AR = 11.3 and 9.2) and Double Lambda (AR = 8.68 and 9.85) wings.

Values of the lift induced drag, C_{Di}/C_L^2, were derived for each configuration, with uncambered (symmetric aerofoil) wings at low Mach number (0.15) and low CL ($0^o < \alpha < 1^o$). The variation with AR is shown in **Fig.8.5**. The trends lie very close to the theoretical line given by $\beta.(\pi AR)^{-1}$ where $\beta = (1-M^2)^{0.5}$. In this case, $\beta = 1$ since M = 0. The variation of C_{Di}/C_L^2 with C_L for the designed configurations at M = 0.6 is shown in **Fig.8.6**. Levels for the uncambered wings at M = 0.6 are also indicated. It is noted that AR has a marked effect on the value of C_{Di}/C_L^2. The trends for C_{Di}/C_L^2 against AR are shown in **Fig.8.7**.

At the design point, laminar flow is maintained at all stations across the wing. As C_L increases the laminar flow distributions on the upper surface will begin to break down at a particular location somewhere on the configuration. The precise location will depend upon planform and section distribution. In establishing the laminar flow ranges we have initially looked at the 2-D aerofoil perfromance, both uncambered (symmetrical) and with a datum camber profile. In the 2-D case, the datum camber extends the laminar flow C_L limit from about 0.2 to almost 1.4 as shown in **Fig.8.8**. Applying these aerofoil shapes (uncambered and datum camber) to the four Lambda wing planforms reduces the effective laminar flow C_L range as shown in **Fig.8.8**. The lower symbol indicates that laminar flow is maintained at all points on the wing, the higher symbol indicates that laminar flow has broken down at some point on the configuration. With datum camber, laminar flow is maintained up to about $C_L = 0.75$ for all four planforms. It is noted that the datum camber introduces large nose down pitching moments on each configuration. The Centre of Pressure (CoP) and quarter chord

($c_{1/4}$), MRC, locations are also indicated on the planforms. In the designed cases, the laminar flow ranges are further reduced (up to $C_L = 0.5$) as a result of the twist and camber required for zero C_m, **Fig.8.9**. The higher AR wings require less camber and twist to achieve C_{Ldes}.

The variation of L/D with C_L is an important parameter used in aircraft performance studies. The accurate estimation of total drag remains a difficult target. In detailed design studies it is of interest to reduce drag into its various components, e.g. lift induced (vortex), trim, profile (form), skin friction, wave, etc. In these current studies, we have taken induced drag, C_{Di}, as a total of its parts (lift induced and trim resulting from design camber and twist).

We have used a wide, but typical, range of C_{Do} values (0.0050 to 0.0200) and modest, "best design" levels of C_{Di}/C_L^2 for each configuration. To achieve C_{Do} values as low as 0.0050 or 0.0075 a degree of surface flow control will be required (maintaining laminar flow). The variation of L/D with C_L, using different C_{Do} levels is shown in **Fig.8.10** for Single Lambda and **Fig.8.11** for the Double Lambda wings. In general, peak L/D increases with AR and is higher for the Double Lambda wings. However, for $C_{Do} = 0.0075$, peak L/D occurs in the range $0.38 < C_L < 0.40$. As C_{Do} increases, L/D naturally decreases and occurs at higher C_L.

Using the Breguet range equation we can derive graphs of the type shown in **Fig.8.12**. This takes into consideration the following weights and their ratios, Operating Empty Weight (OEW), Payload (WP), Fuel Load (WF) and Take-Off Weight (TOW) or Maximum Take-Off Weight (MTOW). By definition, TOW = OEW + WP + WF. Performance parameters considered include Flight speed (V), Specific fuel consumption (sfc), Range (R) and L/D. Endurance can be found from R / V.

MTOW is usually a structural limitation of the aircraft. For passenger aircraft and military strike aircraft it is a compromise between fuel required for a given payload and range combination. In the case of surveillance aircraft, WP and OEW are fixed and WF is limited only by the capacity of the fuel tanks. For maximum range and endurance, surveillance aircraft naturally operate with TOW = MTOW.

In Sensor-Craft type configurations the Payload is small, 3% - 5% of TOW. OEW/TOW is in the region of 0.42, confirming that more than 50% of TOW is fuel. We consider Mach = 0.6 operation at 60,000 ft and a typical sfc of 0.52 which might be achievable with advanced engines. The variation of Endurance with OEW/TOW and (WP+OEW)/TOW is shown in **Fig.8.12** for various values of L/D. To achieve 50hrs endurance with (WP+OEW)/TOW = 0.45, L/D of 38 to 40 will be required. This can only be achieved with flow control, reducing CD_o whilst maintaining laminar flow. There is obviously scope for further performance work, along the lines indicated, for comparative purposes and exchange rates.

9. FURTHER WORK

So far, two types of Lambda planforms Sensor-Craft have been considered for high-speed design at Mach 0.6. Several interesting features have emerged from the application of direct and inverse design methods. Further work is envisaged in a number of areas:

- Continued assessment of cross-flow instability research (e.g. Arizona State University) and how it can help the existence of laminar flow on swept surfaces.
- Lower speeds, field performance considerations.
- Parametric geometric studies, planform development with appropriate method development.
- Further confirmation with Euler.
- Different design C_L studies as required.
- Different aerofoils incorporation, from the point of view of validation with CFD and transonic codes.
- Pitching moment, static margins control with LE / TE Flap within geometry restrictions, segmentation.
- Fuselage & Intake incorporation, additional effects on forces and moments.
- Inclusion of viscous effects, spanwise pressure gradients and flow control.
- Drag prediction.
- Off-design performance including lateral and directional characteristics. Include aero-elastics.
- Experimental work (various aspects).

10. CONCLUDING REMARKS

A "Lambda" wing planform with single or double TE cranks and varying AR has been considered for design at Mach 0.6 for a Sensor-Craft configuration. Initial analysis was conducted using planar (uncambered), 12% thick, aerofoil sections. Configurations using a constant (across the span) Laminar Flow aerofoil section (12% thick) with reference camber were assessed. The wings were then designed (camber modification) for zero pitching moment with as near elliptic loading as feasible at two design C_L (0.5 & 0.8) at Mach 0.6. Selected configurations were also evaluated at Mach 0.15. Validation against an Euler code was also carried out.

Consideration of the theoretical methods has required that the wing tip TE sweeps be modified from the actual flight design. The planforms as defined in the current work have been designed for neutral stability at Mach 0.6. It is noted, however, that the tip sweep modifications would have some effect on the stability evaluation. This is considered fine detail in view of other configuration aspects yet to be included such as fuselage, intakes and engine nozzles.

At the design conditions, the designed camber case displays considerable reductions in LE suctions when compared with the uncambered (symmetric aerofoil) wings. The double crank configuration appears to give more favourable spanwise loadings. We have attempted to correlate drag against various geometric parameters. The Double Crank case shows a drag advantage over the Single Crank which requires further investigation and analysis. Typical results presented demonstrate the flexibility and potential of the techniques for direct and inverse design.

The capability for the study of several geometric configuration variables is offered in a timely sense. Data for detail design of wind tunnel models and possibly a flight demonstrator can be enabled. An understanding of control laws arises. The potential and limitations of the aircraft in meeting a given design envelope can be assessed.

It is apparent that we are only at a starting post and a sizeable, interesting work programme remains! Several areas for continued work have emerged.

REFERENCES

1. NANGIA, R.K., "Pilot Document Introducing all Aspects of Work Accomplished under USAF-EOARD Contract SPC-024051", RKN/AERO/REPORT/2004-10 – Part 1, Issue 1, 2004.

2. NANGIA, R.K., "High Aspect Ratio Unconventional Joined-Wing Configurations Incorporating Laminar Flow", RKN/AERO/REPORT/2004-10 – Part 2, Issue 1, 2004.

3. NANGIA, R.K., "Planform Effects on High Aspect Ratio Unconventional Joined-Wing Configurations Incorporating Laminar Flow", RKN/AERO/REPORT/2004-10 – Part 3, Issue 1, 2004.

4. NANGIA, R.K., "High Aspect Ratio Lambda-Wing Configurations Incorporating Laminar Flow", RKN/AERO/REPORT/2004-10 – Part 4, Issue 1, 2004. *This Report*.

5. NANGIA, R.K., "Integration of Over-Surface Scarfed Intakes on Aircraft with High Aspect Ratio Wings (e.g. Sensor-Craft)", RKN/AERO/REPORT/2004-10 – Part 5, Issue 1, 2004.

6. NANGIA, R.K., "Towards Design of Long-Range Supersonic Military Aircraft", RKN/AERO/REPORT/2004-10 – Part 6, Issue 1, 2004.

7. NANGIA, R.K., "Configuration & Aerodynamic Design Studies of Joined-Wing High Aspect Ratio Sensor-Craft Concept", RKN/Aero/Report/2002-10, June 2002, (USAF-EOARD Contract SPC-01-4087).

8. JOHNSON, F. P., "Sensor Craft : Tomorrow's Eyes and Ears of the Warfighter", AIAA-2001-4370, Aug. 2001. *See www.afrlhorizons.com /Briefs/Mar01/SN0001.html*

9. Aerospace America, Dec. 01, pp 50.

10. TILMANN, C.P., FLICK, P.M., MARTIN, C.A. & LOVE, M.H., "High Altitude Long Endurance Technologies for SensorCraft". RTO-AVT-99, Paper 25, Brussels, 2003.

11. NANGIA, R.K., "High Aspect Ratio Unconventional Joined-Wing Configurations Incorporating Laminar Flow", RKN/AERO/REPORT/2003-10, Issue 1, May 2003

12. NANGIA, R.K., PALMER, M.E. & TILMANN, C.P., "Unconventional High Aspect Ratio Joined-Wing Aircraft with Aft- & Forward- Swept Wing-Tips", AIAA-2003-0605, Jan. 2003, Reno, USA.

13. NANGIA, R.K., PALMER, M.E. & TILMANN, C.P., "Unconventional High Aspect Ratio Joined-Wing Aircraft Incorporating Laminar Flow", AIAA-2003-3927, June 2003, Orlando, USA.

14. BIBER, K. & TILMANN, C.P., "Laminar Aerofoils…", Paper presented at Reno, January 2003.

15. NANGIA, R.K., "The Design of "Manoeuvrable" Wings using Panel Methods, Attained Thrust & Euler Codes", ICAS-92.

16. NANGIA, R.K. & GREENWELL, D.I., "Wing Design of Oblique Wing Combat Aircraft", ICAS 2000-1.6.1, 2000.

17. NANGIA, R.K., "Configuration & Aerodynamic Design Studies of Joined-Wing High Aspect Ratio Sensor Craft Concept", RKN/Aero/Report/2002-10, June 2002, (USAF-EOARD Contract SPC-01-4087).

18. NANGIA, R. K. & GALPIN, S.A., "Towards Design of High-Lift Krueger Flap Systems with Mach & Reynolds No. Effects for Conventional & Laminar Flow Wings", CEAS European Forum, Bath, UK, 1995.

19. NANGIA, R. K. & GALPIN, S.A., "Prediction of LE & TE Devices Aerodynamics in High-Lift Configurations with Mach & Reynolds No. Effects", ICAS-1996-2.7.6..

20. NANGIA, "Design of Conventional & Unconventional Wings for UAV's", RTA-AVT Symposium, "UV for Aerial & Naval Military Operations", Ankara, Turkey, Oct. 2000.

21. NANGIA, R.K., PALMER, M.E. & DOE, R.H., "A Study of Supersonic Aircraft with Thin Wings of Low Sweep", AIAA-2002-0709, January 2002.

22. NANGIA, R.K. & MILLER, A.S. "Vortex Flow Dilemmas & Control on Wing Planforms for High Speeds", RTO AVT Symposium, Loen, Norway, May 01.

23. KUCHEMANN, D. "The Aerodynamic Design of Aircraft", Pergamon.

24. JUPP, J., Wing aerodynamics and the Science of Compromise", RAeS Lanchester Lecture, 2001.

25. JONES, R.T., "Wing Theory", Princeton.

26. GUPTA, K.K. & MEEK, J.L., "Finite Element Multidisciplinary Analysis", AIAA, 2000.

27. NANGIA, R.K., "Developing an Inverse Design Method using 3-D Membrane Analogy", Future Paper.

LIST OF SYMBOLS & ABBREVIATIONS

Only the general symbols are defined here. Other symbols are of local significance within the Section they arise in.

AoA   Angle of Attack (α), usually referred to the body axis

AR   Aspect Ratio

A   Axial Force along wing-plane x-axis (for definition of CA)

b	= 2 s, Wing span
BL	Boundary Layer
c	Local Wing Chord
c_{aero}	= c, Aerodynamic Wing Chord
c_{av}	= c = cref, Average Wing Chord
C_A	= A/(q S), Axial Force Coefficient, measured in Wing plane
C_{AL}	= Local Axial Force Coefficient
C_D	= Drag Force /(q S), Drag Coefficient
C_{D0}	Drag Coefficient at zero lift (see text)
C_{Di}	Lift Induced Drag
CG	Centre of Gravity
C_l	= l/(q S b), Rolling Moment (Body Axis)
C_L	= CL = L/(q S), Lift Coefficient
C_{LL}	= Local Lift Coefficient
C_{Lmax}	Maximum Lift Coefficient
C_m	= m/(q S c), Pitching Moment (Body Axis)
C_{mo}	Cm at zero lift
C_n	= n/(q S b), Yawwing Moment (Body Axis)
C_N	= N/(q S), Normal Force Coefficient
CoP	Centre of Pressure
C_P	Coefficient of Pressure
c_r	Wing Root chord
c_t	Wing Tip chord
k	= π A C_{Di}/C_L^2, Lift Induced Drag Factor
l	Rolling moment (Body Axis)
LE	Leading Edge
m	Pitching moment (Body Axis)
M	Mach Number
MRC	Moment Reference Centre
n	Yawing moment (Body Axis)
N	Normal Force
q	= 0.5 ρ V^2, Dynamic Pressure
r	Aerofoil radius
rn	Aerofoil radius normal to c
R	Reynolds Number, based on cav (unless otherwise stated)
s	Wing semi-span
S	Wing Area, taken here as (front-wing + tip-wing) area
t	Aerofoil thickness
TE	Trailing Edge
V	Airstream Velocity
x,y,z	Orthogonal Wing Co-ordinates, x along body axis
x_{ac}	Location of Aerodynamic Centre along x-axis
x_{cp}	Location of Centre of pressure along x-axis
α	Angle of Attack (AoA), usually referred to the body axis
λ	Wing Taper Ratio
Λ	LE Sweep Angle
ρ	Air Density
η	= y/s, Non-dimensional spanwise Distance

Military Flying
Wings

FIG.1.2.1   PROPOSED AND EXISTING
FLYING WING CONFIGURATIONS
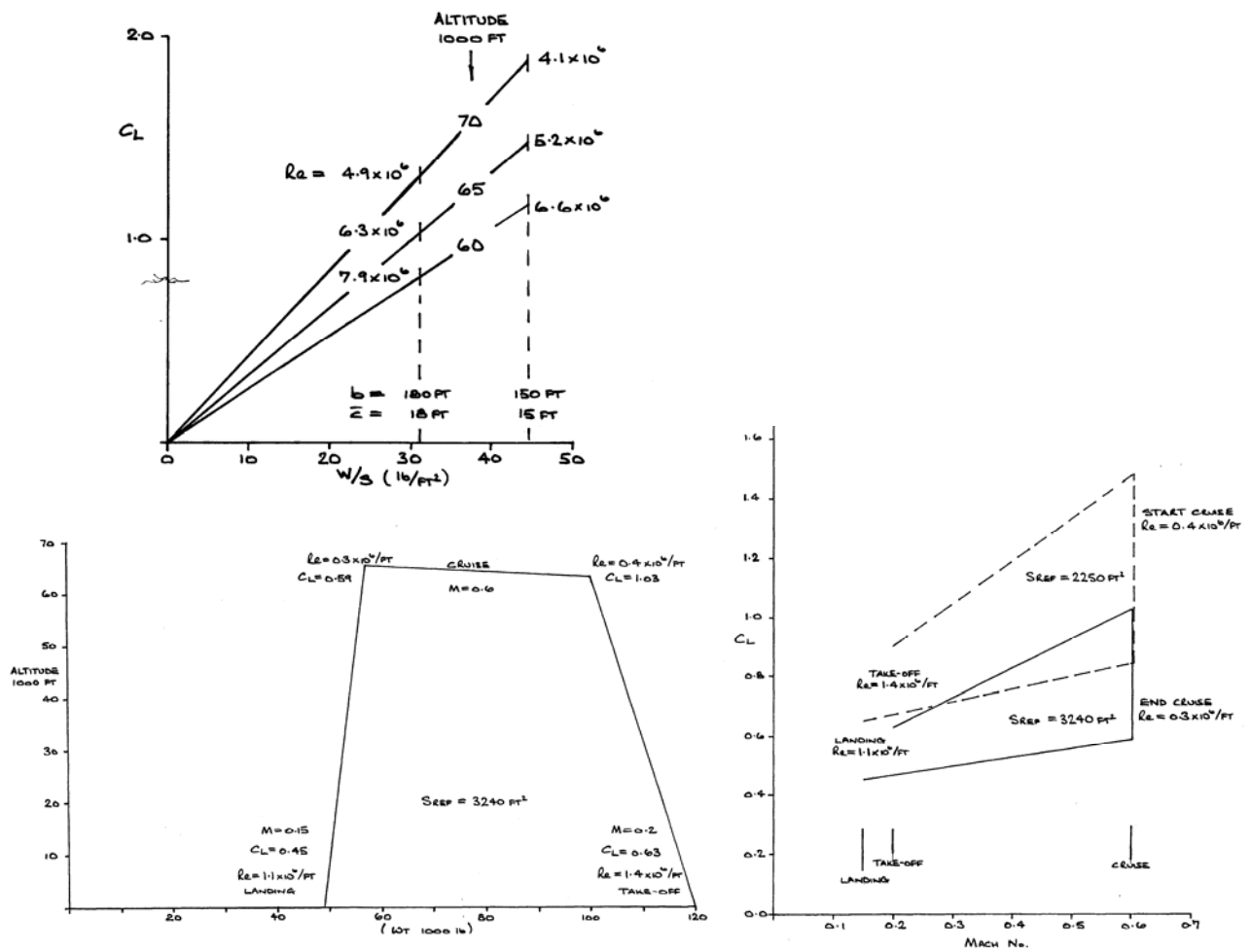
FIG. 2.1 FLIGHT ENVELOPE, ALTITUDE - WEIGHT & CL - MACH RELATIONSHIPS
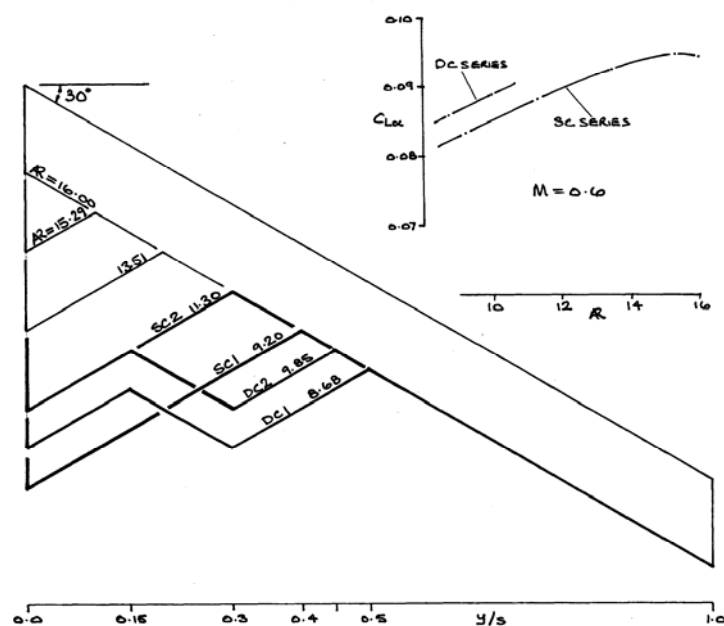
**FIG. 2.2 TRAPEZOIDAL & LAMBDA (SINGLE & DOUBLE TE CRANK) WINGS,
LINEAR THEORY RESULTS, Mach 0.6**

FIG. 3.1 TYPICAL LAMINAR AEROFOIL PROFILE & RESULTS FROM XFOIL

t/c =16%

t/c =19.5%
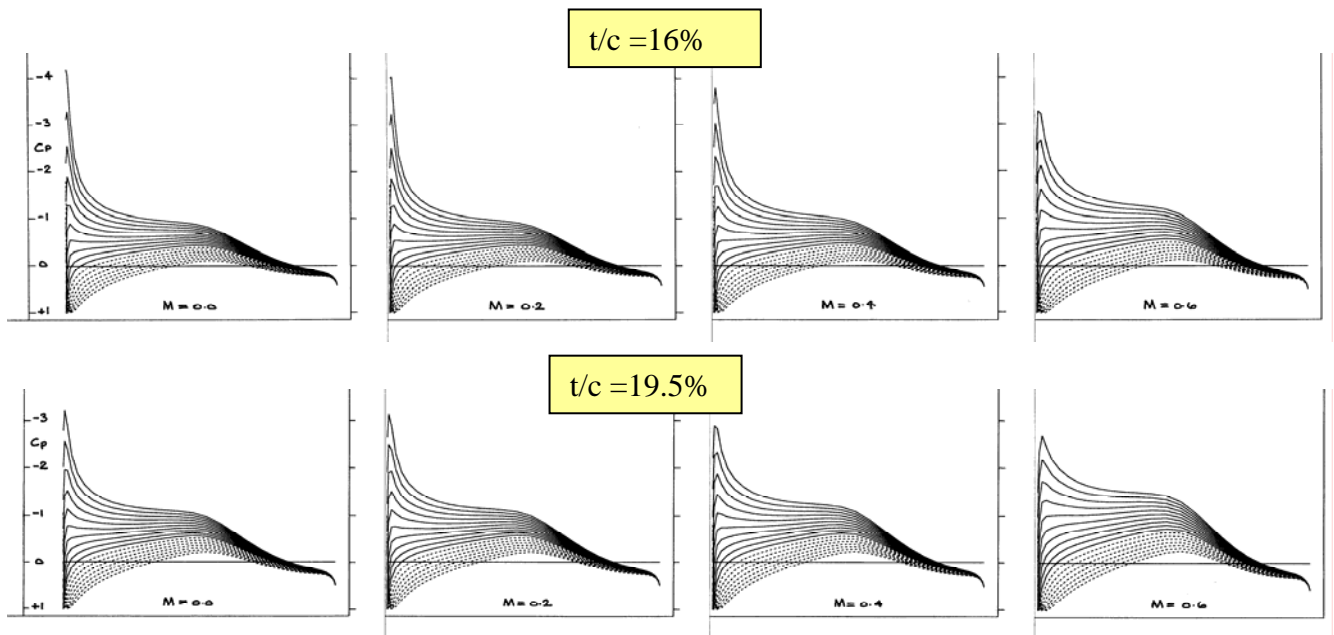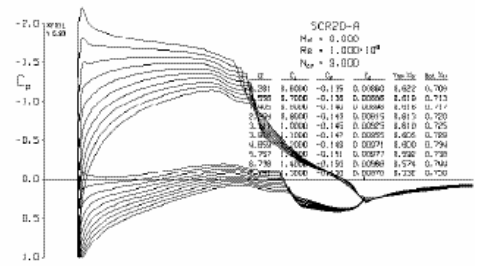
FIG. 3.2 Cp DISTRIBUTIONS ON LAMINAR UNCAMBERED AEROFOILS , 2-D CALCULATIONS, EFFECT OF t/c, AoA between –1° & 8°, Mach 0.01, 0.2, 0.4, 0.6

t/c 16% Uncambered

t/c 16% Cambered
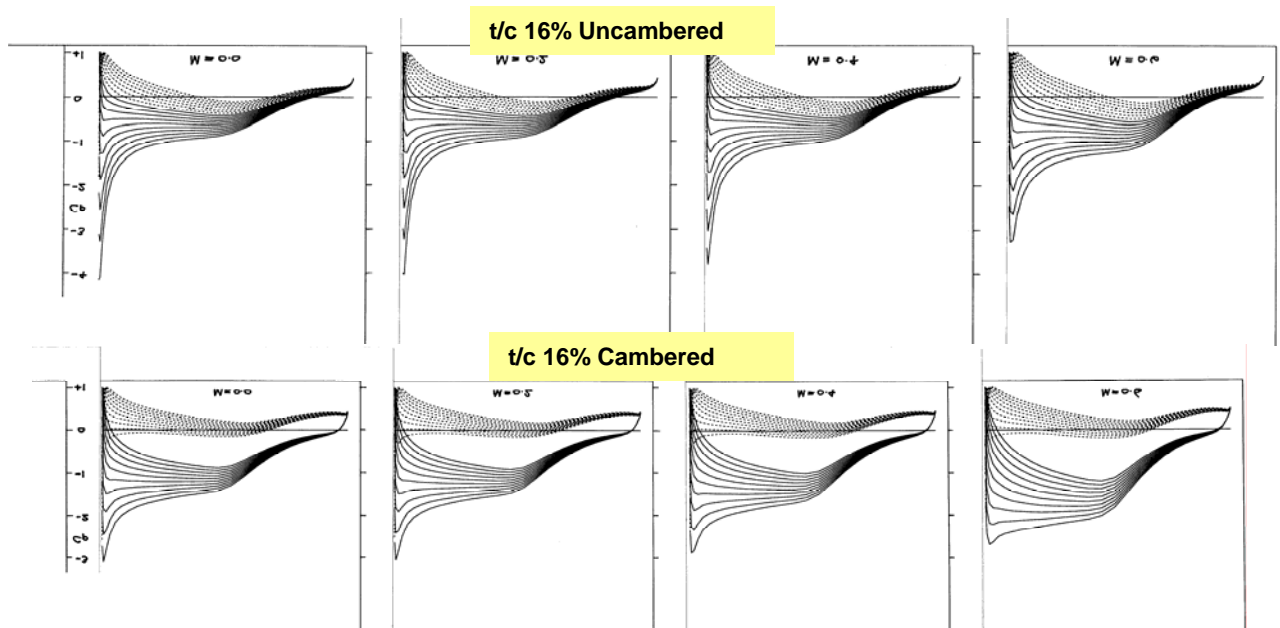
FIG. 3.3. Cp DISTRIBUTIONS ON 16% t/c LAMINAR AEROFOILS, 2-D CALCULATIONS, EFFECT OF CAMBER, AoA BETWEEN –1° & 8°, INVISCID, MACH = 0.01, 0.2, 0.4 & 0.6
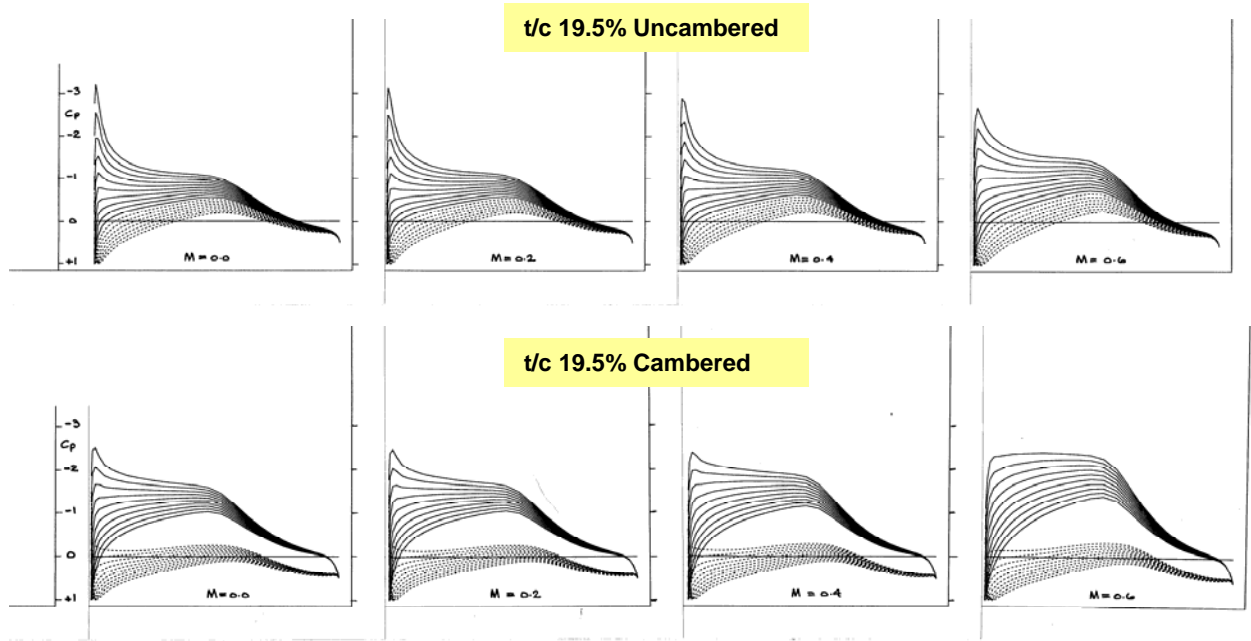
FIG. 3.4   Cp DISTRIBUTIONS ON 19.5% t/c LAMINAR AEROFOILS, 2-D CALCULATIONS, AoA BETWEEN −1° & 8° , MACH 0.01, 0.2, 0.4 & 0.6
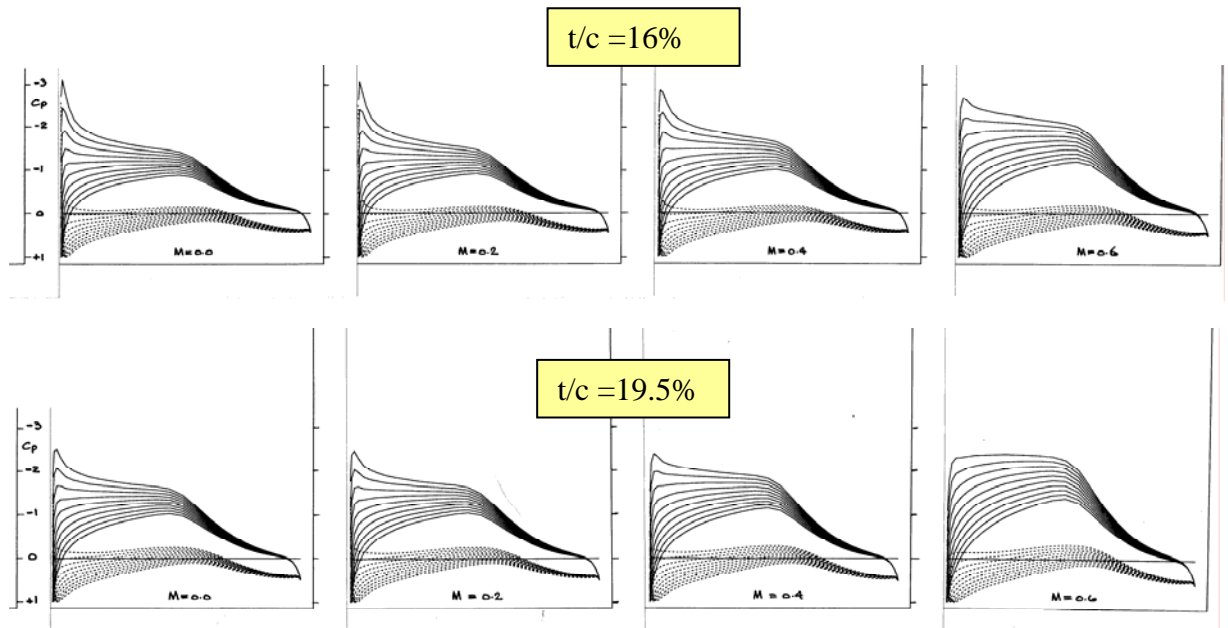
t/c =16%

t/c =19.5%

FIG. 3.5 Cp DISTRIBUTIONS ON LAMINAR CAMBERED AEROFOILS , 2-D CALCULATIONS, EFFECT OF THICKNESS, AoA BETWEEN −1° & 8°, Mach 0.01, 0.2, 0.4, 0.6

Uncambered - t/c =12% - cambered

Uncambered - t/c =14% - cambered

Uncambered - t/c =16% - cambered

Uncambered - t/c =19.5% - cambered
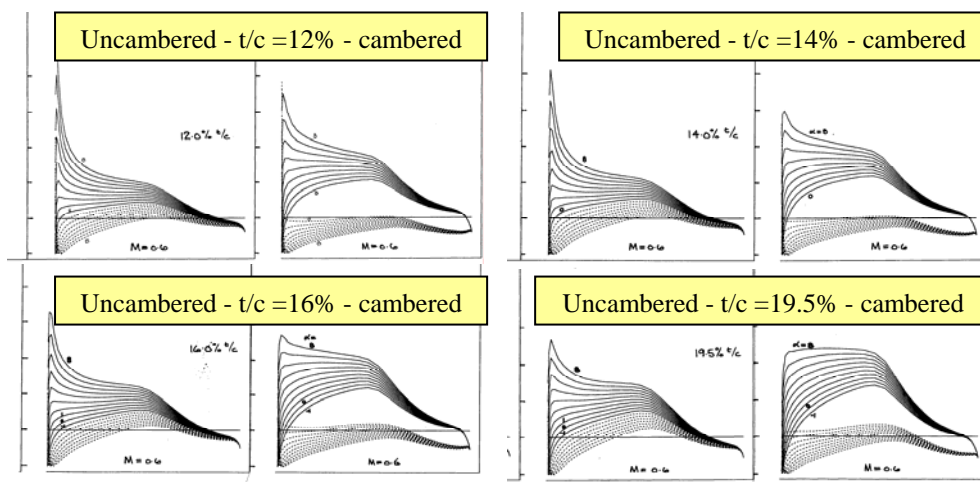
FIG. 3.6 Cp DISTRIBUTIONS ON LAMINAR AEROFOILS, 2-D CALCULATIONS, EFFECT OF THICKNESS & CAMBER, AoA BETWEEN −1° & 8°, Mach 0.6

27
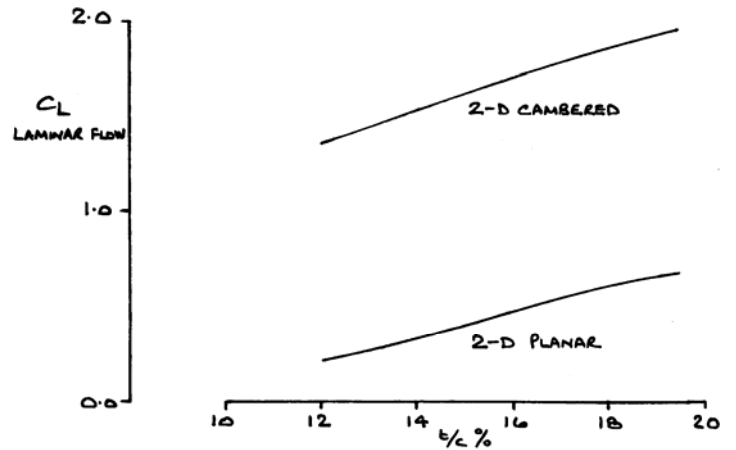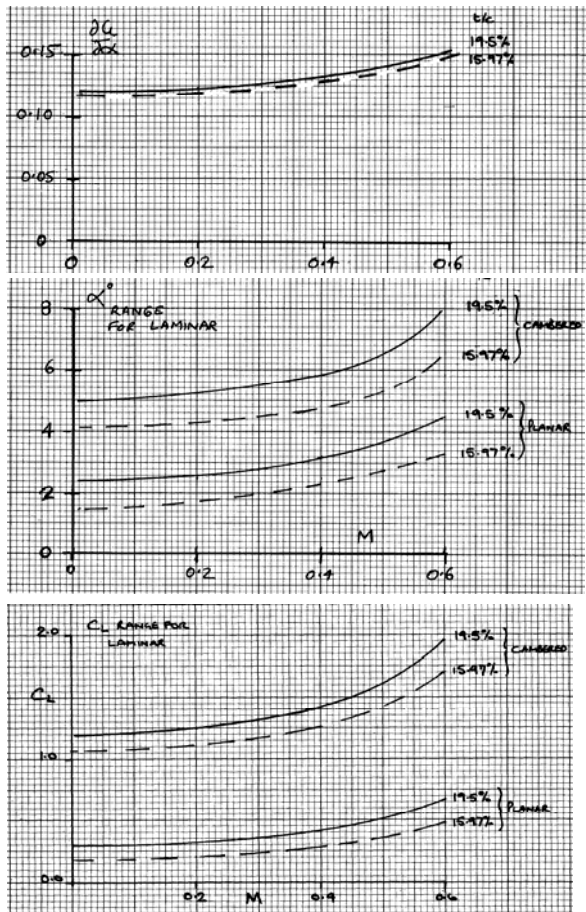
FIG. 3.7 LAMINAR AEROFOIL CAPABILITIES
THROUGH MACH & AoA (CL) RANGES,
UNCAMBERED & CAMBERED
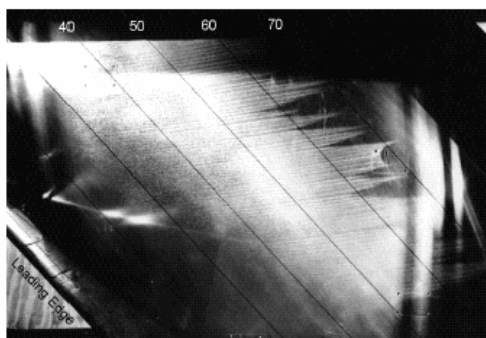
Figure 1. Natural transition at 65% chord.   Figure 2. Distributed roughness of 8-mm spacing at leading edge.
Transition delayed beyond 80% chord.
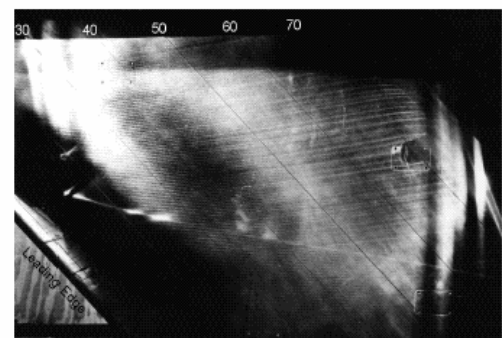
Figures 1 and 2. Crossflow-vortex visualization via naphthalene applied to the wing surface.
45°-swept NLF(2)-0415 airfoil in ASU low-speed experiment. Flow from left to right.
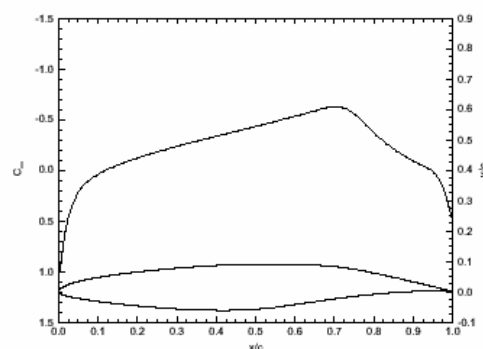
. Upper surface C_p distribution for 45°-swept NLF(2)-0415 airfoil in ASU low-speed experiment.

Fig.3.8 LAMINARISING USING SURFACE ROUGHNESS, 45° SWEEP, Ref. SARIC et al

Fig.3.9 TREATMENT OF CROSS FLOW INDUCED TRANSITION USING DISTRIBUTED ROUGHNESS ELEMENTS, Ref. SARIC et al

Laminar Flow on Swept Wings
Distributed Roughness Elements

PAYOFF:

SOLUTION: Distributed Roughness Elements (DREs) of the proper spacing (wavelength) and size can create "favorable" disturbances that overwhelm the amplified-wavelength disturbances that otherwise lead to transition.

25% Reduction in TOGW

Laminar Flow Coverage
- All Turbulent
- 60% Laminar (Average Upper & Lower)
- 100% Laminar Top & Bottom

Total Streamwise Velocity Contours
$Re_c = 2.4 \times 10^6$ $x/c = 0.40$
48 μm Roughness at $x/c = 0.023$, 12 mm Spacing
Computations Include Curvature

Experiment

Nonlinear Parabolized Stability Equations

PROBLEM: Crossflow Induced Transition
Favorable pressure gradient stabilizes traveling (TS) waves in boundary layer, but does not affect stationary (crossflow) waves. In the past, suction has been required for crossflow stabilization.

ASU ARIZONA STATE UNIVERSITY

Benefit to Sensorcraft: Laminar Flow Results in Large TOGW Reductions

33rd AIAA Fluid Dynamics Conference and Exhibit, Orlando, 25 June 2003

Fig.3.10 INTRODUCTION OF DISTRIBUTED ROUGHNESS TECNOLOGY

Research Needs
Many DRE Questions Remain

- **Will it work at high M, C_L, Re ?**
- **How to design distribution… for the mission**
- **How robust is it?**
  - **Variations in M, C_L, Re**
  - **Aeroelastic bending & twisting**
  - **Dirty environments**
  - **Manufacturing tolerances**
- **Must it be active or adaptive?**
  - **Spacing, placement, bump height, dimple depth…**
  - **If so, how do we change the distribution?**
- **How do we demonstrate it?**
  - **Tunnel, flight test, flight experiment, combination?**
  - **Under what conditions?**
- **How do we design it in to a system?**
  - **Tools need to be developed**

33rd AIAA Fluid Dynamics Conference and Exhibit, Orlando, 25 June 2003

Fig.3.11 LOAD DISTRIBUTION ON LAMBDA WINGS

λ-Wing Loading Distribution

u / a_∞
0.0 0.2 0.4 0.6 0.8 1.0 1.2 1.4

- **High endurance and payload is high risk**
  - Nonlinear aero
  - Flexible structure
- **Reduce risk with nonlinear analysis**
- **Research needs**
  - Physics
  - Numerical methods

Figure courtesy of Northrop Grumman

Lift

Elliptic

C_L

Highly Loaded at Break

y/b'

33rd AIAA Fluid Dynamics Conference and Exhibit, Orlando, 25 June 2003

29

Single Lambda

AR = 11.3

AR = 9.2

**FIG. 4.1 LAMBDA WINGS, SC SERIES,
Sweep 30°, Aspect Ratio Varied by altering
TE "Crank"**
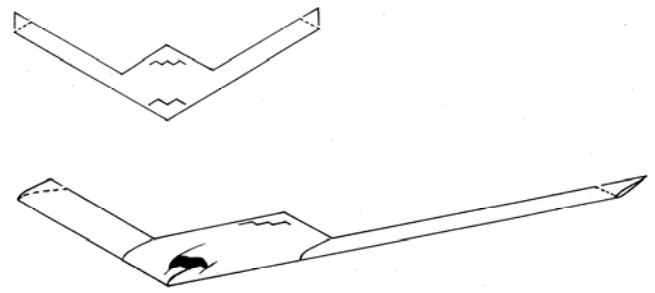
**FIG. 4.2 LAMBDA WINGS, SC SERIES,
Sweep 30°, Wing Root Intake & Possible Tip
Modifications**

y – x

Double Lambda
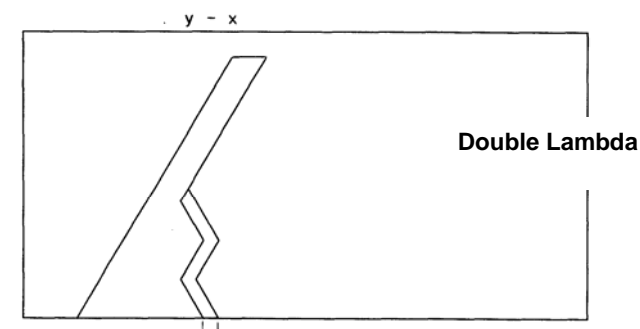
**FIG. 4.3 LAMBDA WINGS, DC SERIES,
Sweep 30°, Aspect Ratio Varied by altering
TE "Crank"**
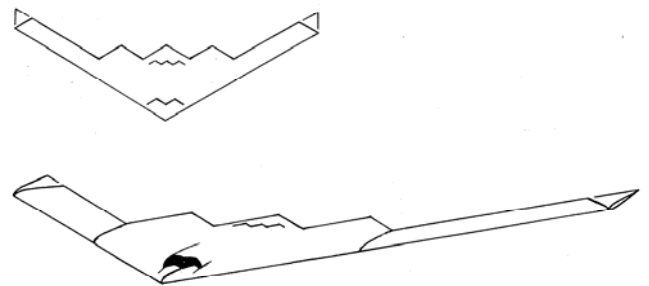
**FIG. 4.4 LAMBDA WINGS, DC SERIES,
Sweep 30°, Wing Root Intake & Possible Tip
Modifications**

Define C_{Ldes}, C_{mdes}

Camber Design

Design Camber Surface

$+$

Aerofoil Thickness

$=$

Design Geometry

Uncambered

Aero Solver e.g. Panel Code

x_{NP} (Neutral Point Location)

$\dfrac{dC_L}{d\alpha}$, a_1, $C_{L\alpha}$ (Lift Curve Slope)

$\dfrac{dC_{LL}}{d\alpha}$ (y) and other useful parameters

C_{Ldes}, C_{mdes}

Satis?

No

Yes

FIG. 4.5   DESIGN PROCEDURE

Aerofoils

CL, AoA & Cm Variations

Spanwise Loadings

AoA = 0°. CL = 0.0

AoA = 2°. CL = 0.198

AoA = 1°. CL = 0.094
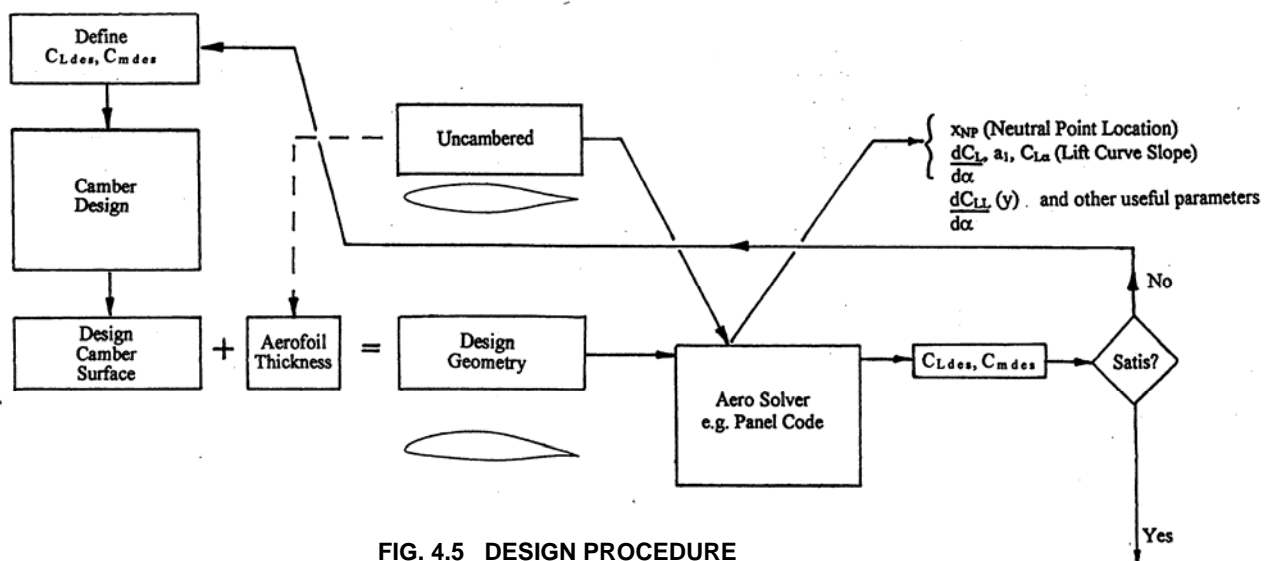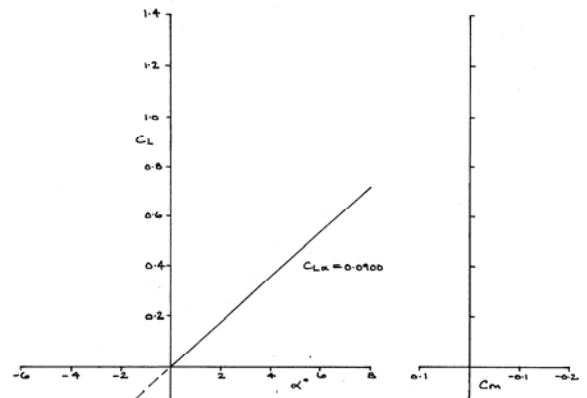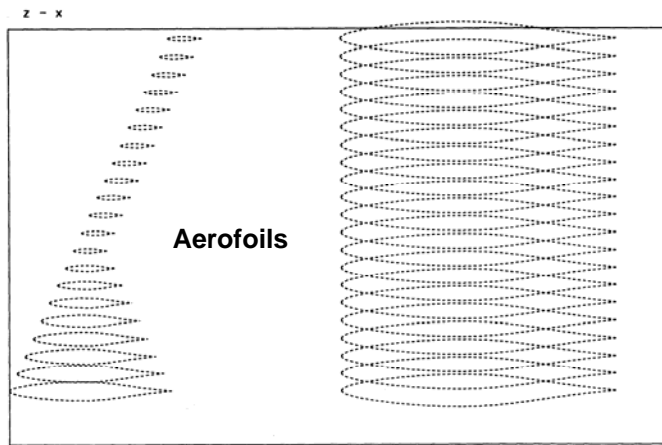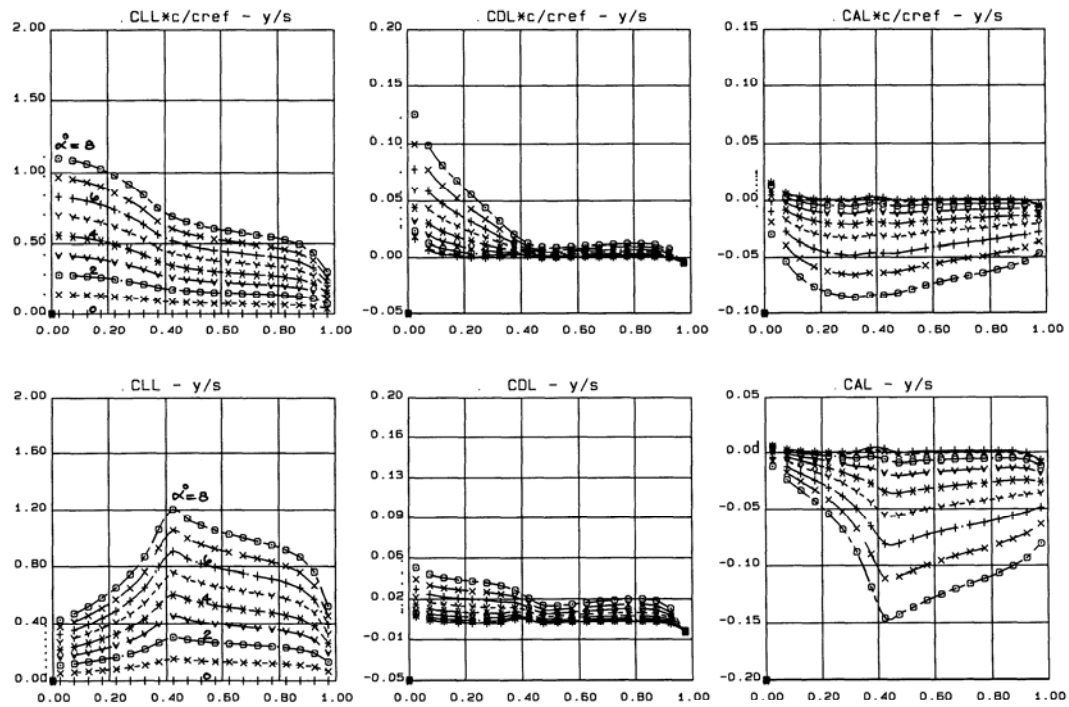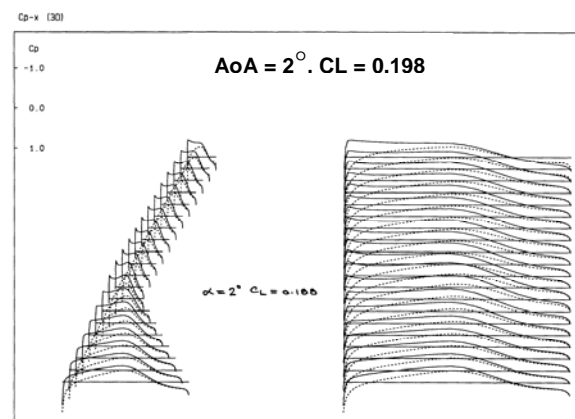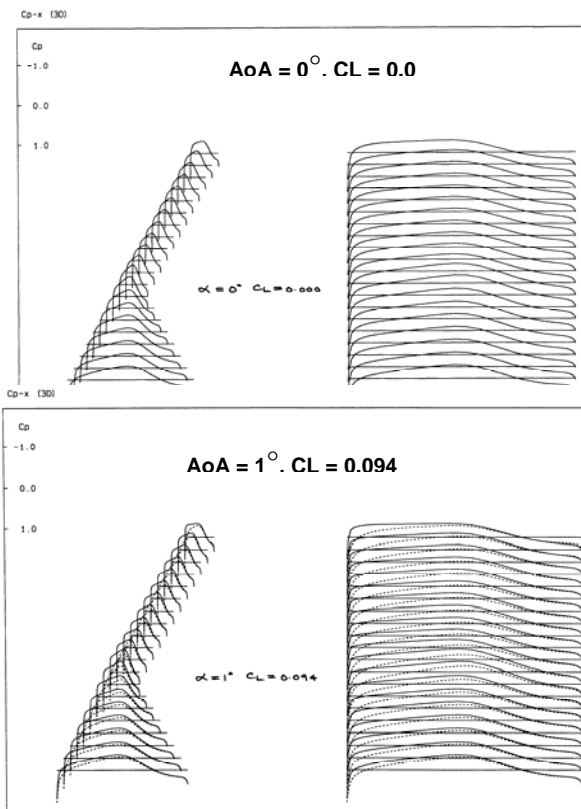
Cp Distributions

FIG. 6.1.1 SC AR 9.2 UNCAMBERED WING CHARACTERISTICS, Mach 0.6

Aerofoils

$C_{L\alpha} = 0.0893$

CL, AoA & Cm Variations

CLL*c/cref - y/s

CDL*c/cref - y/s

CAL*c/cref - y/s

CLL - y/s

CDL - y/s

CAL - y/s

Spanwise Loadings

AoA = 3°. CL = 0.722

AoA = 4°. CL = 0.812

AoA = 5°. CL = 0.901

Cp Distributions

32
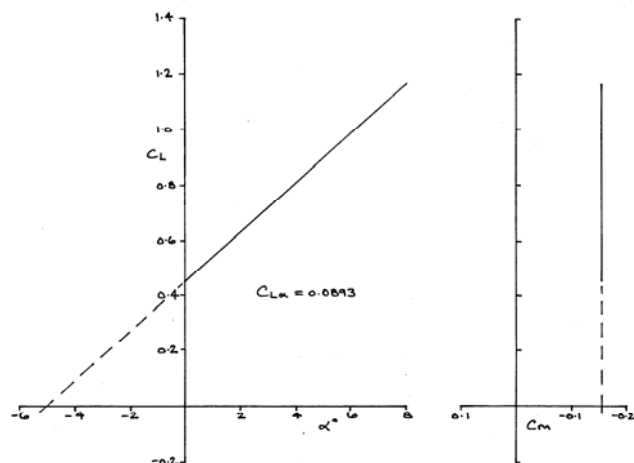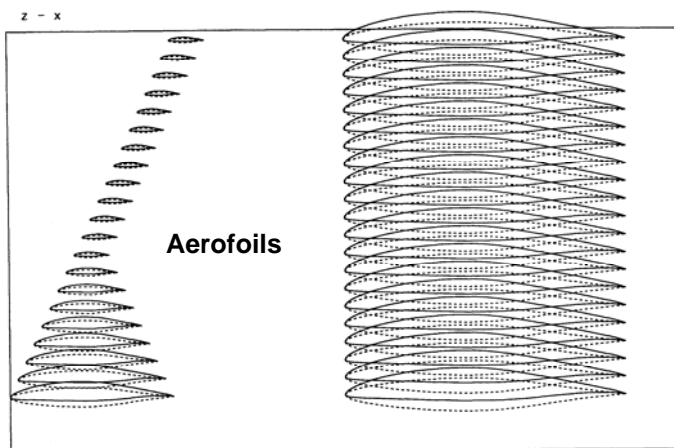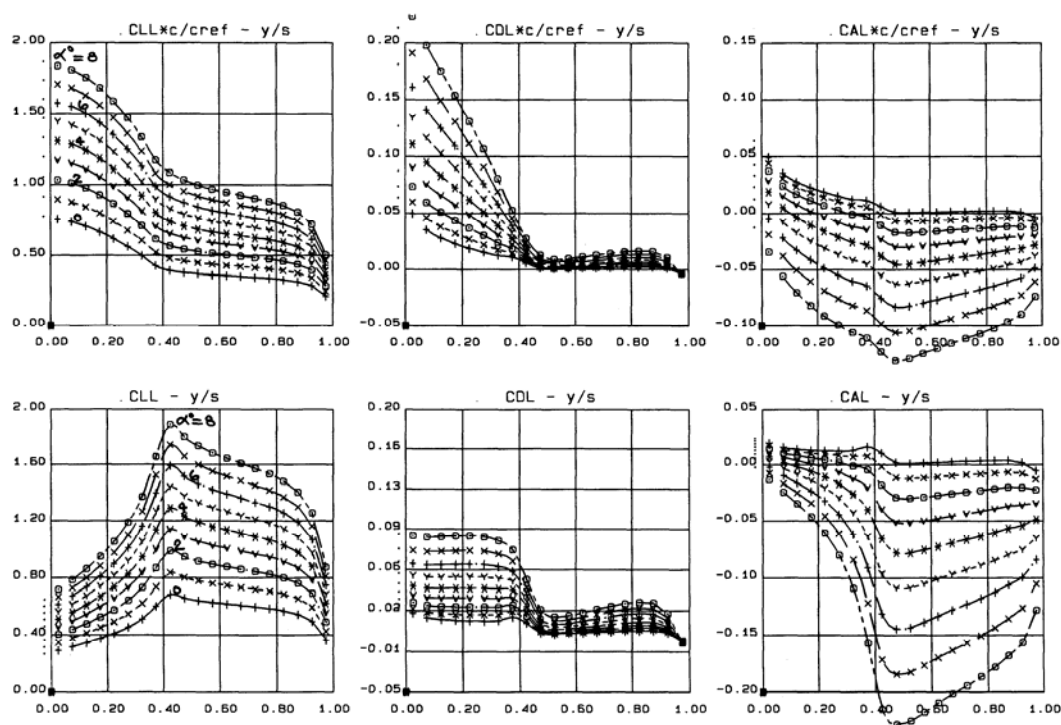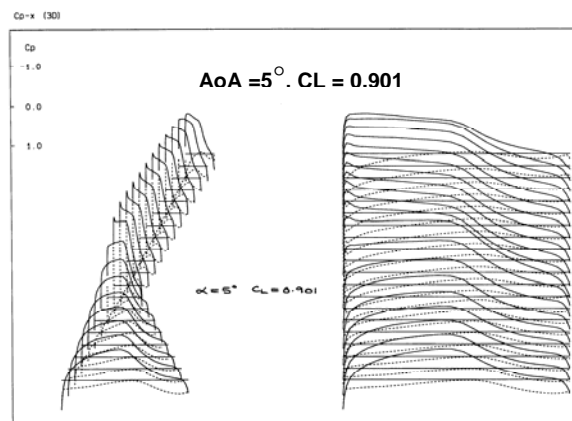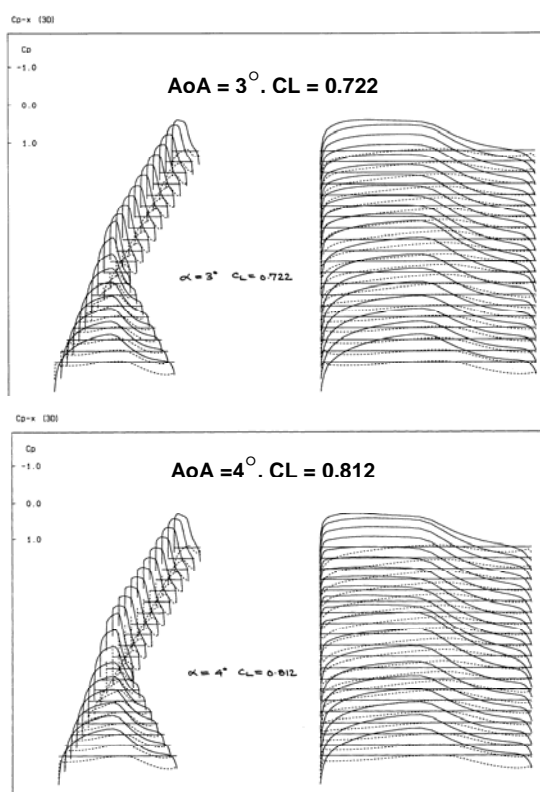
FIG. 6.1.2 SC AR 9.2 REFERENCE CAMBER WING (No Twist) CHARACTERISTICS, Mach 0.6

Aerofoils

CL, AoA & Cm Variations

Spanwise Loadings

AoA =3°. CL = 0.341

AoA = 5°. CL = 0.522

AoA = 4°. CL = 0.432
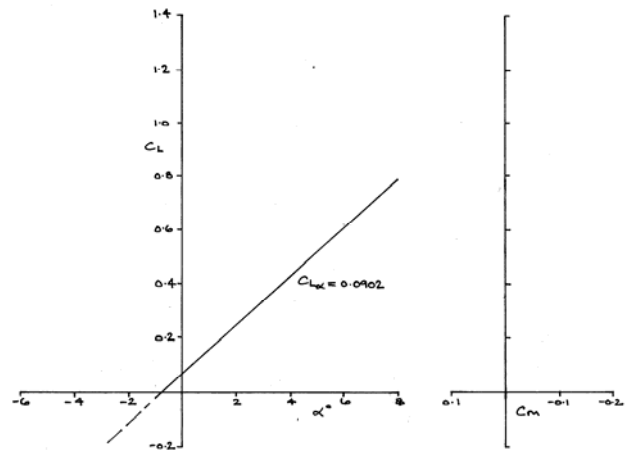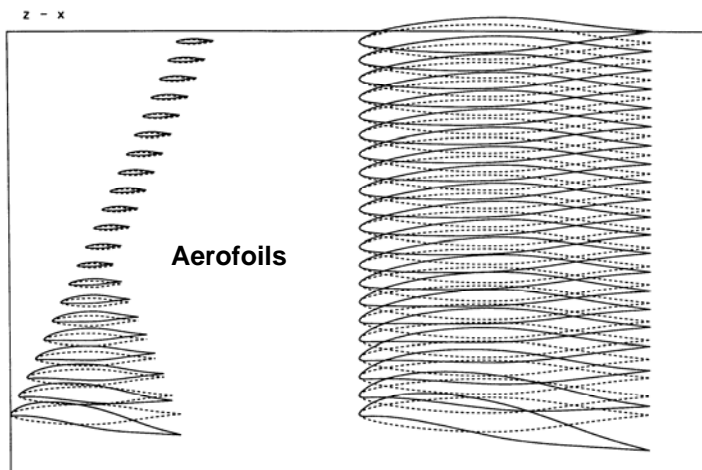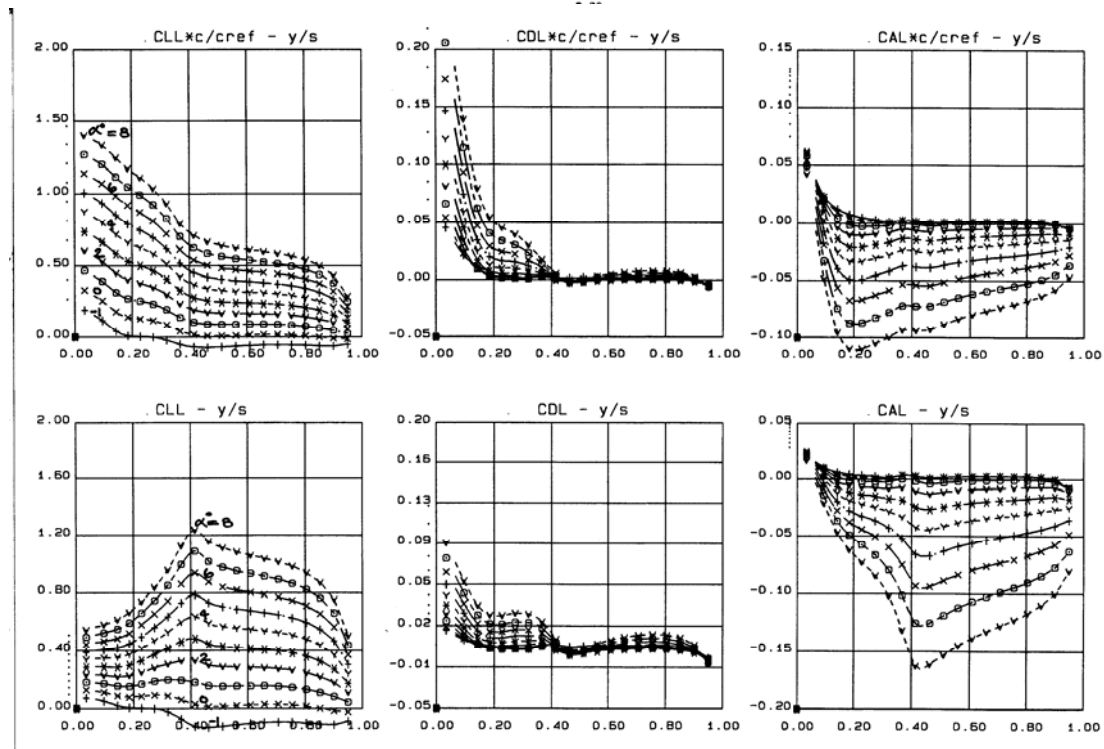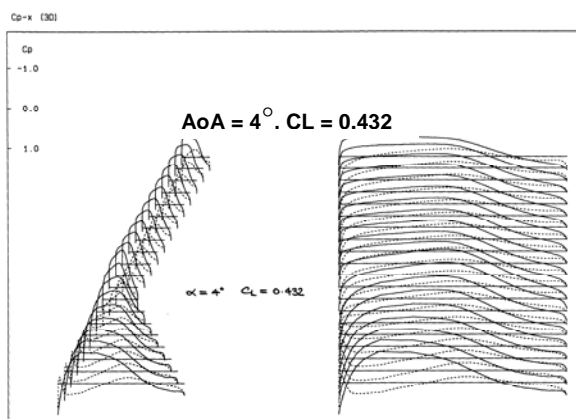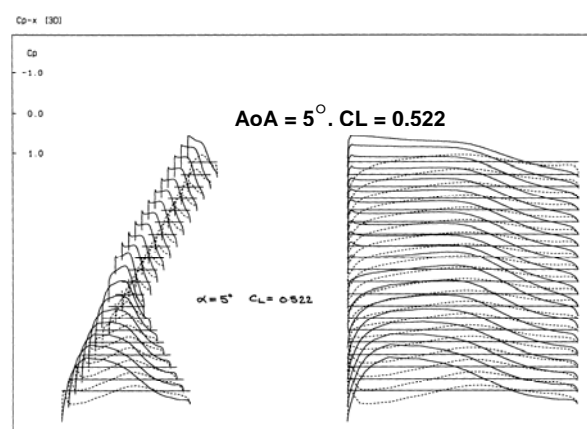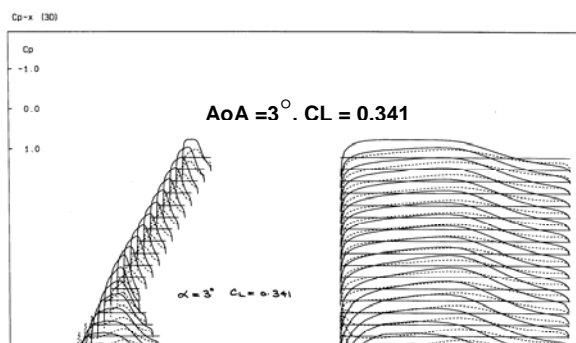
Cp Distributions

**FIG. 6.1.3 SC AR 9.2 DESIGNED FOR
LAMINAR FLOW UP TO CL 0.5
CHARACTERISTICS, Mach 0.6**

33

Aerofoils

CL, AoA & Cm Variations

$CL_\alpha = 0.090$

Spanwise Loadings

.CLL*c/cref – y/s

.CDL*c/cref – y/s

.CAL*c/cref – y/s

CLL – y/s

CDL – y/s

.CAL – y/s

Cp–x (3D)

AoA=6°. CL=0.675

$\alpha = 6° \quad C_L = 0.675$

Cp–x (3D)

AoA=8°, CL=0.862

$\alpha = 8° \quad C_L = 0.862$

Cp–x (3D)

AoA=7°. CL=0.764

$\alpha = 7° \quad C_L = 0.764$
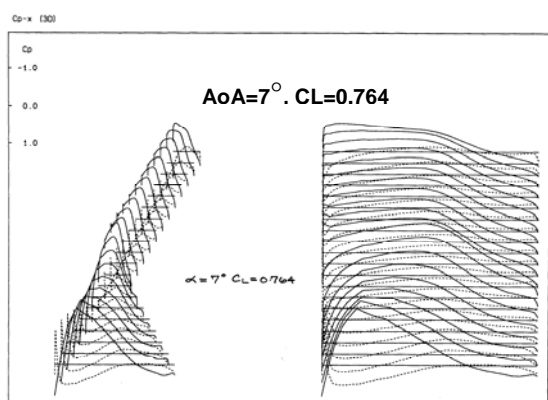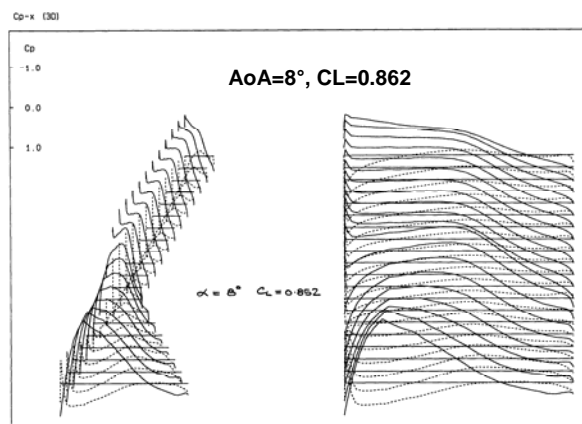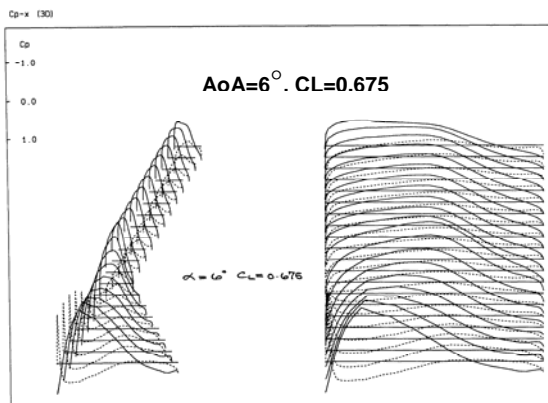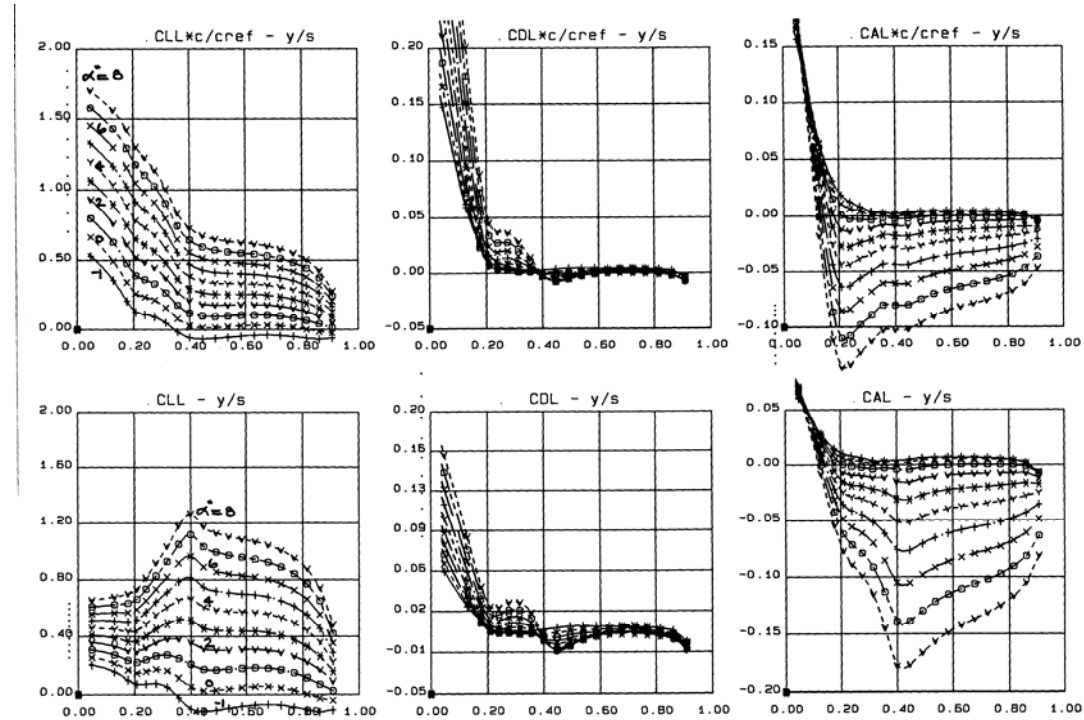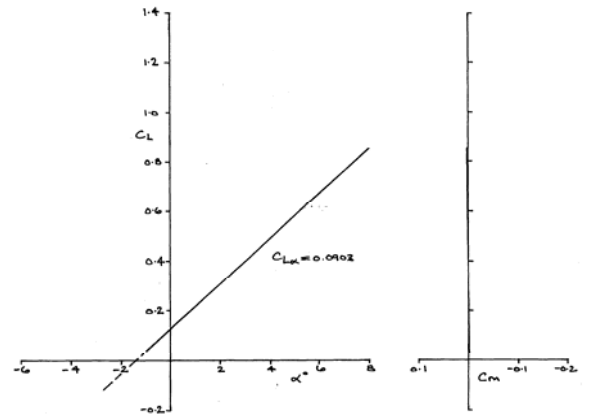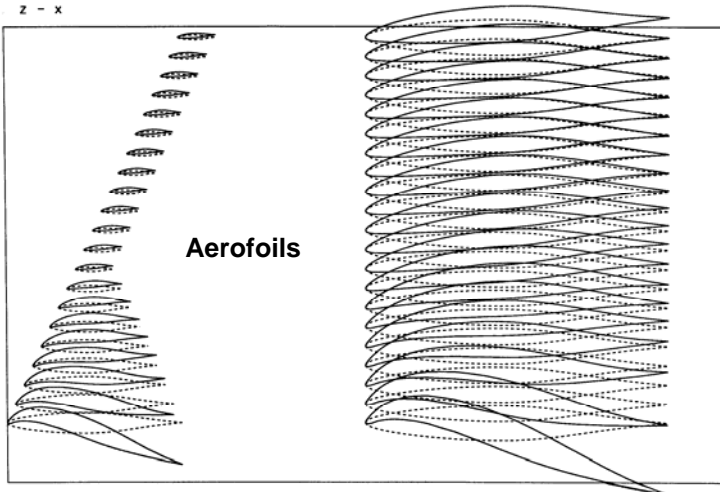
Cp Distributions

**FIG. 6.1.4 SC AR 9.2 DESIGNED FOR
LAMINAR FLOW UP TO CL 0.8
CHARACTERISTICS, Mach 0.6**

34
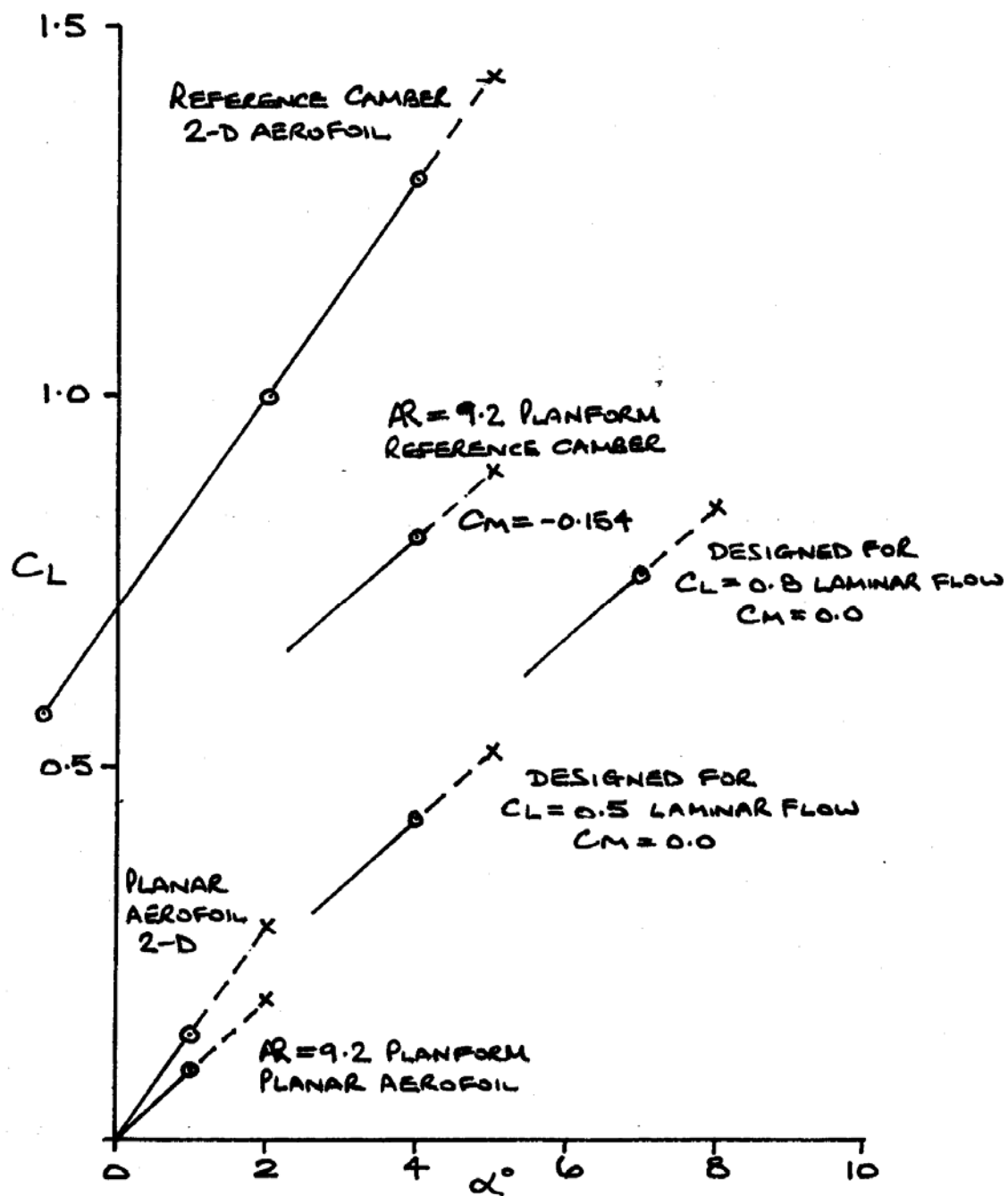
**FIG. 6.1.5 SC AR 9.2, SUMMARY OF DESIGNS
FOR LAMINAR FLOW CL RANGES, Mach 0.6**
Laminar up to CL = 0.5 & 0.8

Aerofoils

CL, AoA & Cm Variations

Spanwise Loadings

Cp Distributions

AoA=0°. CL=0.0

AoA=2°. CL=0.194

AoA=1°. CL=0.097

AoA=3°. CL=0.291
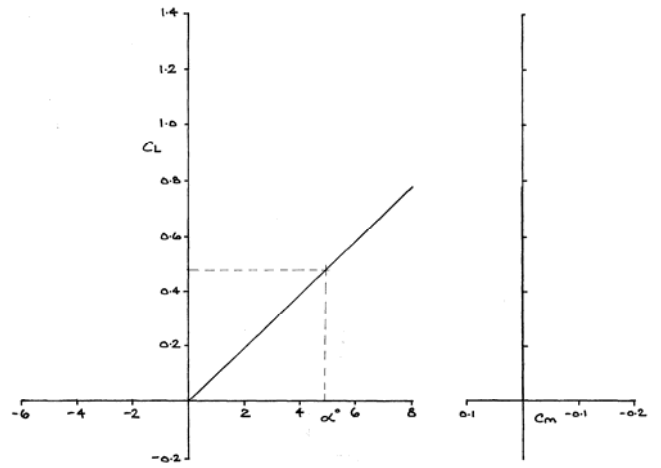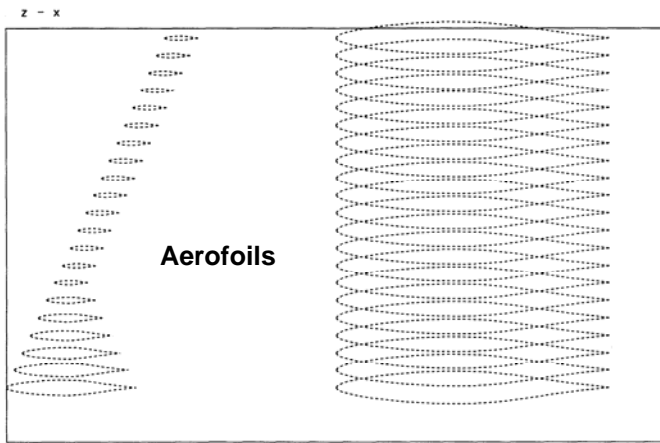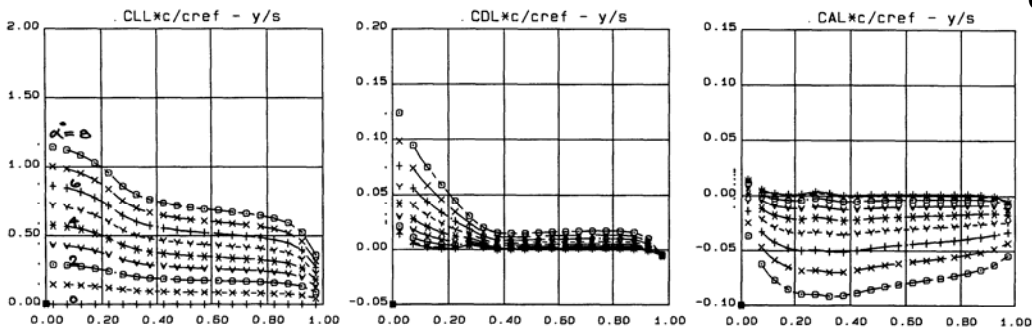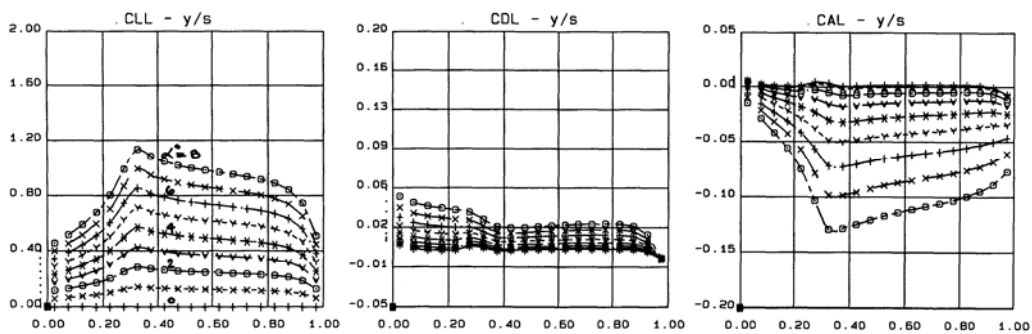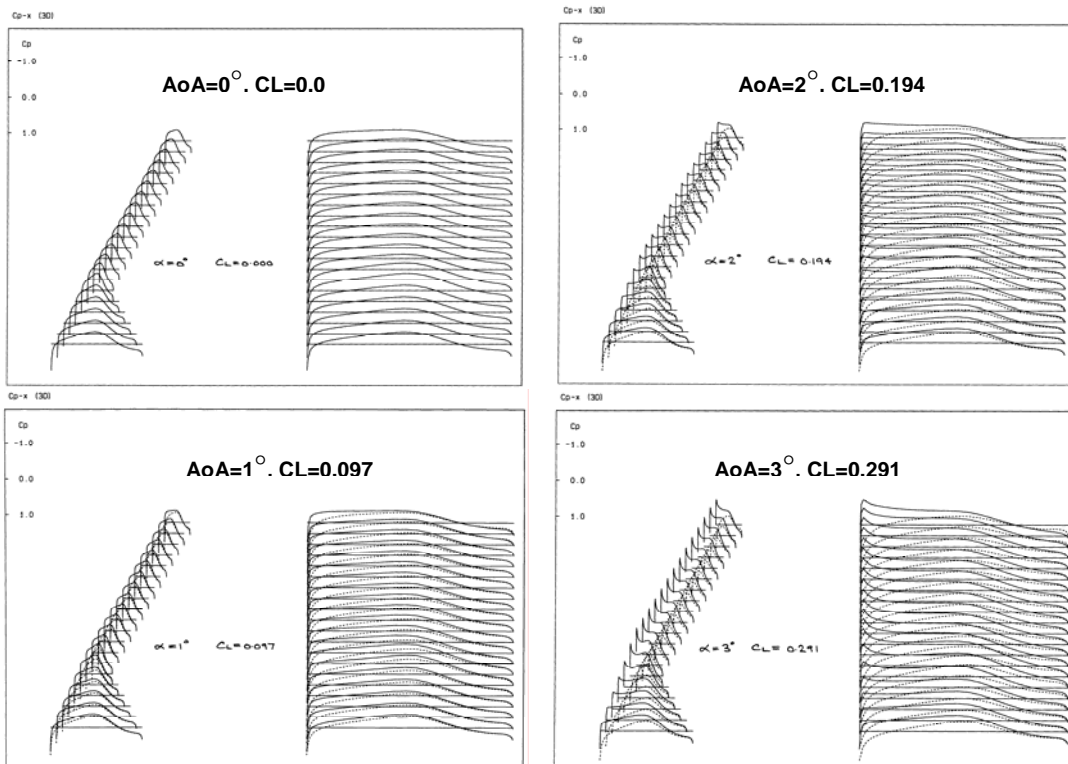
FIG. 6.2.1 SC AR 11.3 UNCAMBERED WING CHARACTERISTICS, Mach 0.6

AoA=4°. CL=0.388

AoA=8°. CL=0.770

AoA=5°. CL=0.484

AoA=9°. CL=0.863

AoA=6°. CL=0.580

AoA=10°. CL=0.956

AoA=7°. CL=0.675

FIG. 6.2.1 Cont'd

Aerofoils

Spanwise Loadings

AoA = 3°, CL = 0.768

AoA = 5°, CL = 0.959

AoA = 4°, CL = 0.864
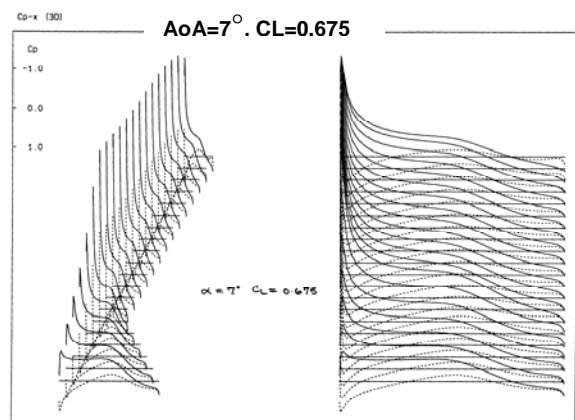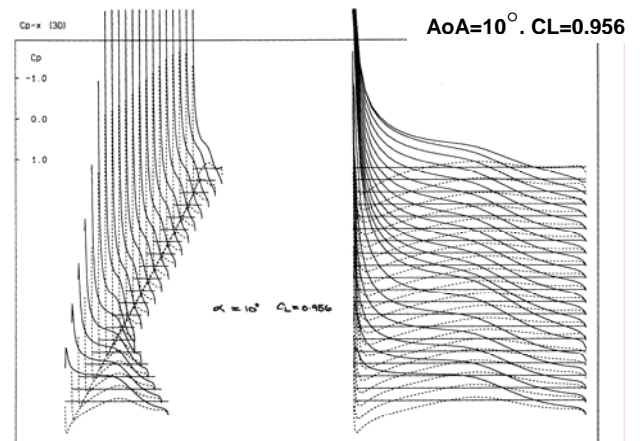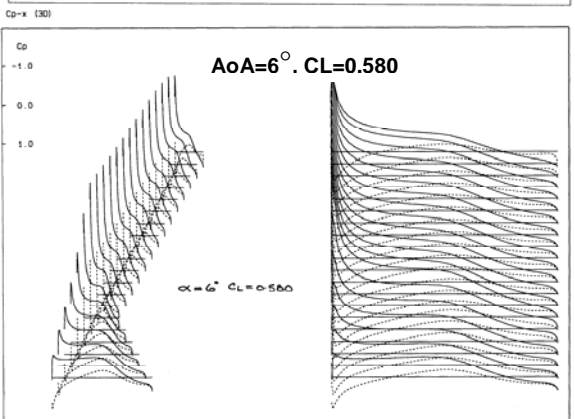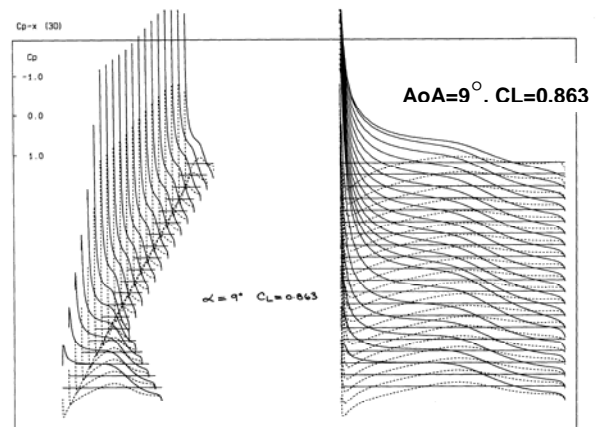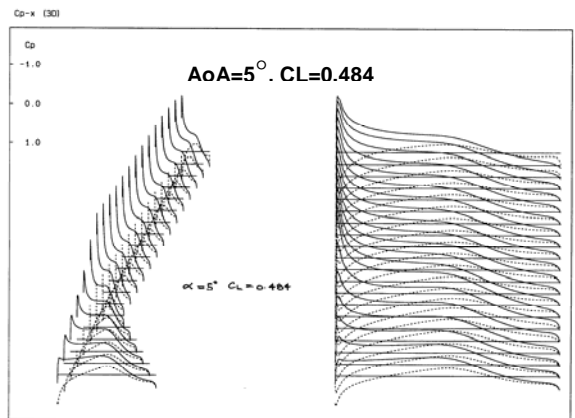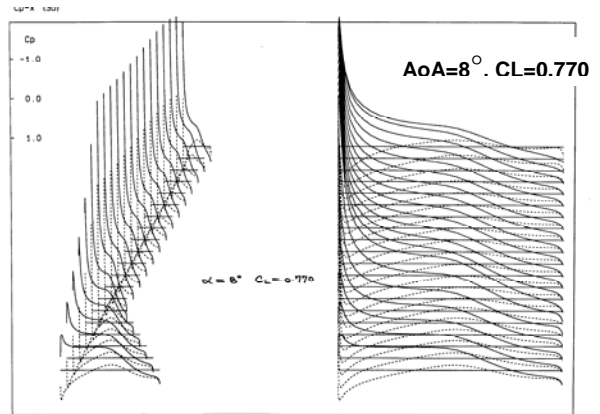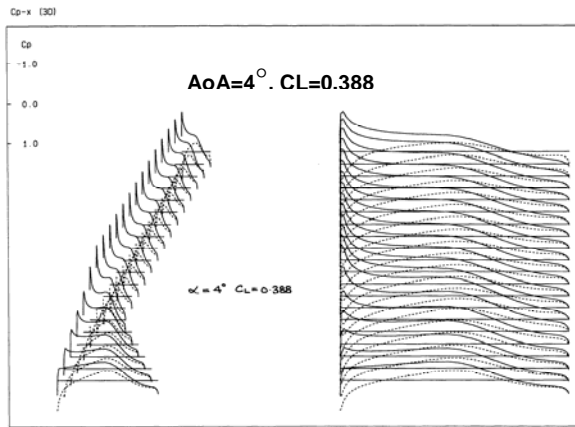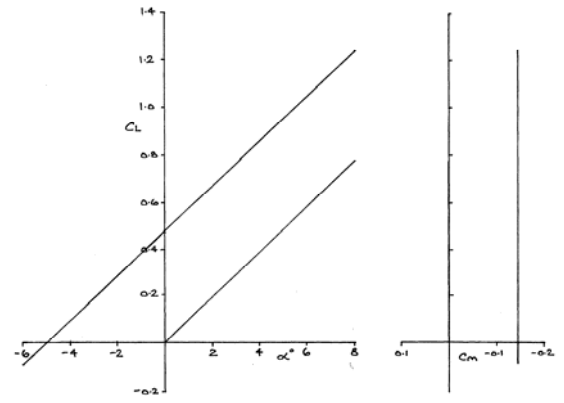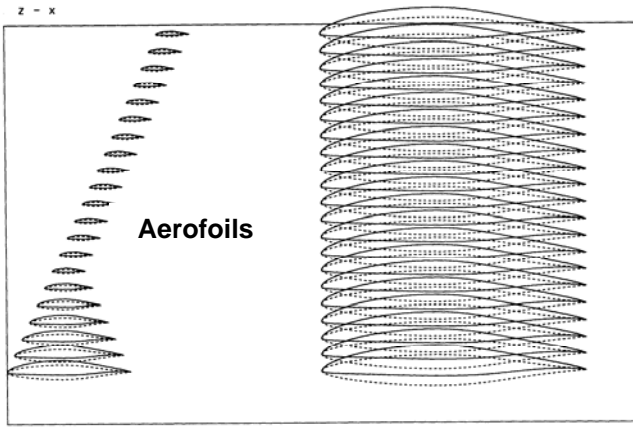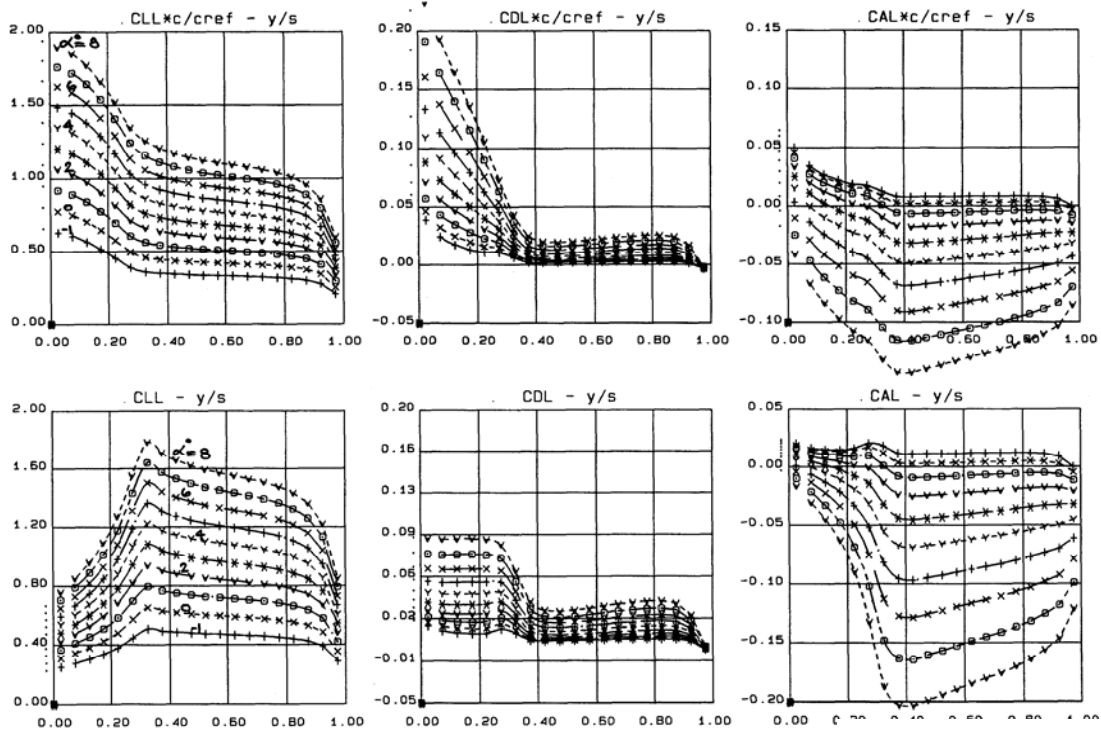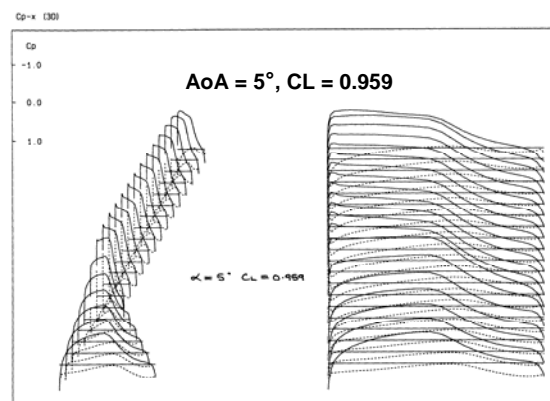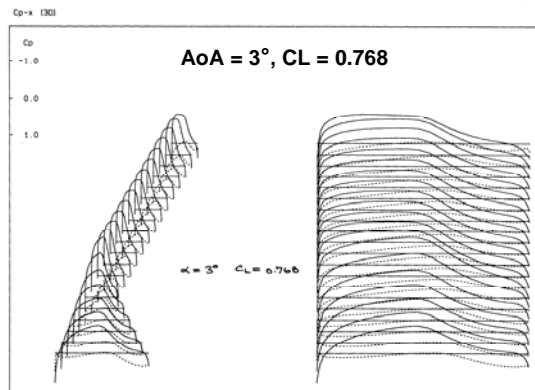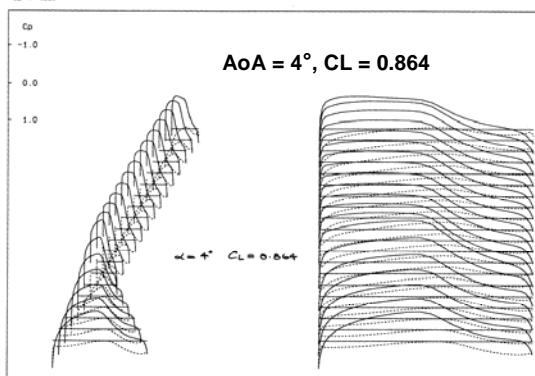
Cp Distributions

**FIG. 6.2.2 SC AR 11.3 REFERENCE CAMBER
WING (No Twist) CHARACTERISTICS, Mach 0.6**

38

Aerofoils

CL, AoA & Cm Variations

$CL_\alpha = 0.0962$

Spanwise Loadings

AoA = 3°, CL = 0.331

AoA = 4°, CL = 0.428

Cp Distributions

AoA = 5°, CL = 0.524
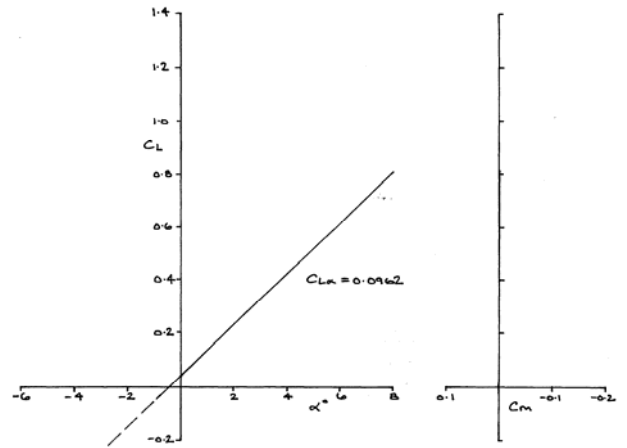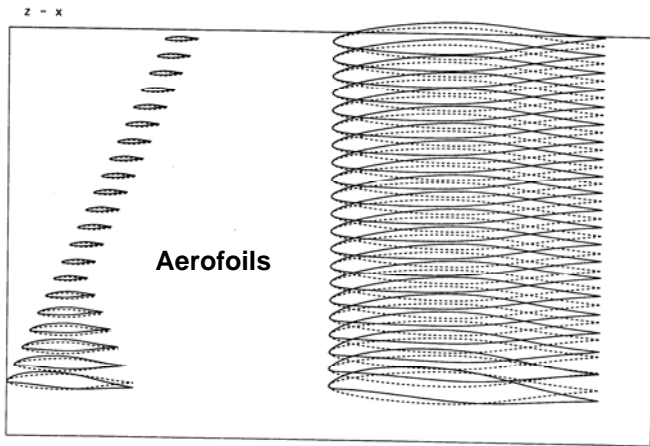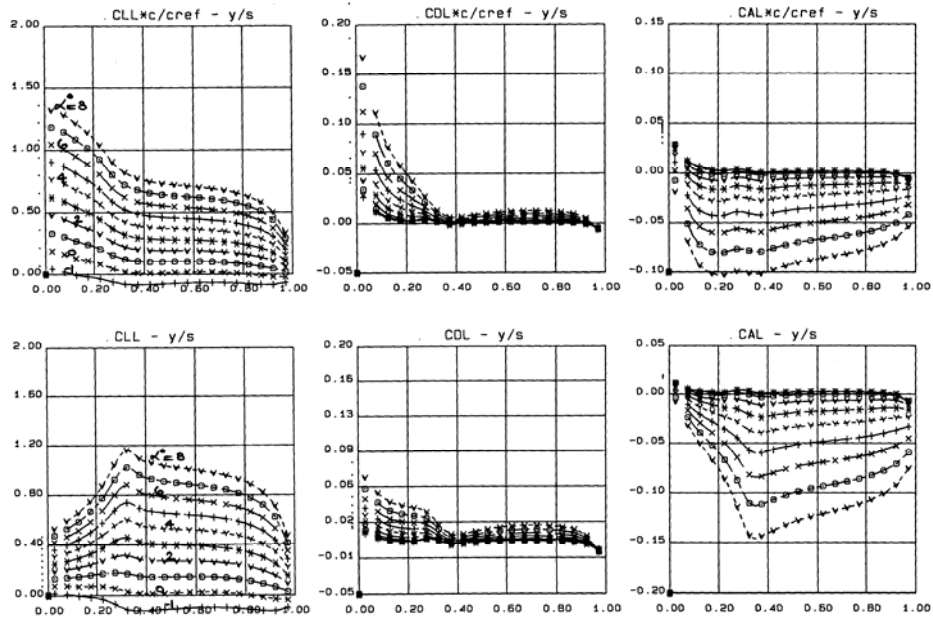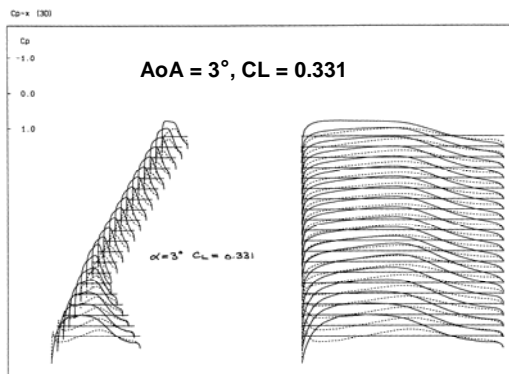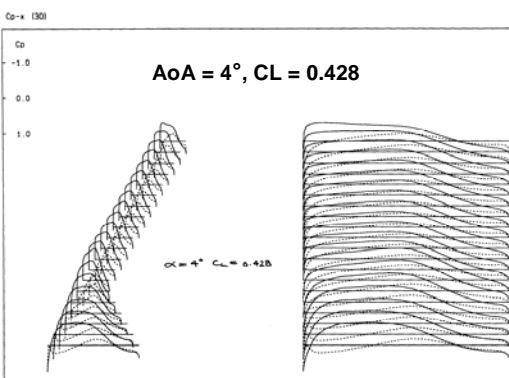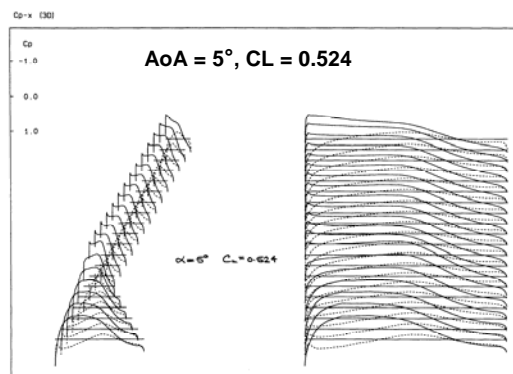
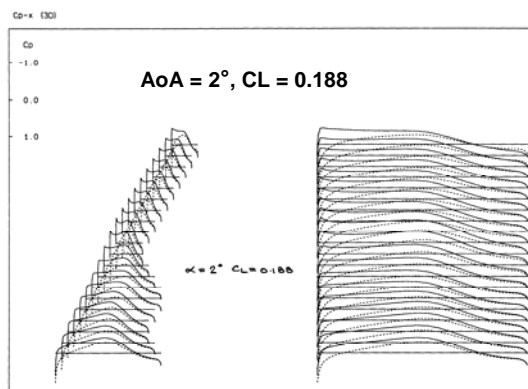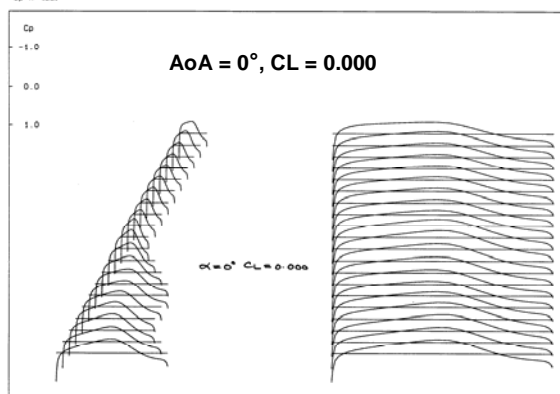**FIG. 6.2.3 SC AR 11.3 DESIGNED FOR LAMINAR FLOW UP TO CL 0.5 CHARACTERISTICS, Mach 0.6**

39

CL, AoA & Cm Variations

Spanwise Loadings

Cp Distributions

AoA = 3°, CL = 0.280

AoA = 5°, CL = 0.450

AoA = 4°, CL = 0.367

AoA = 6°, CL = 0.533
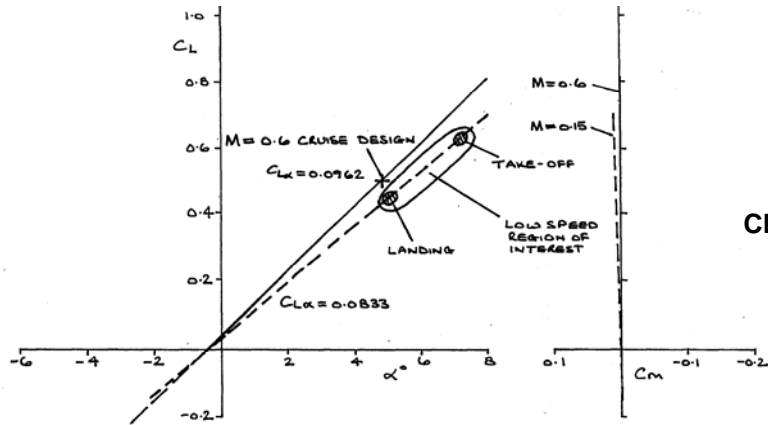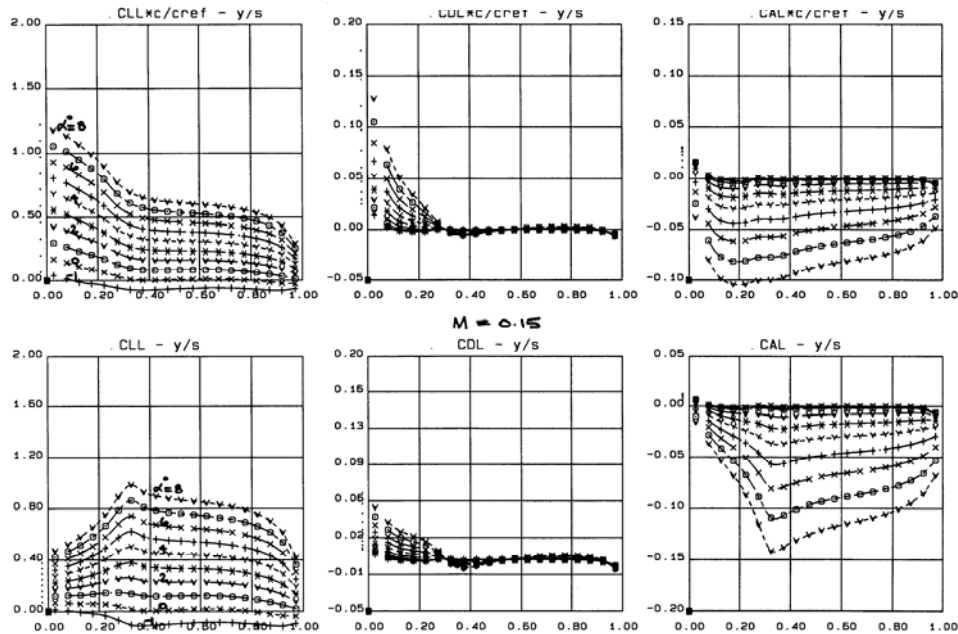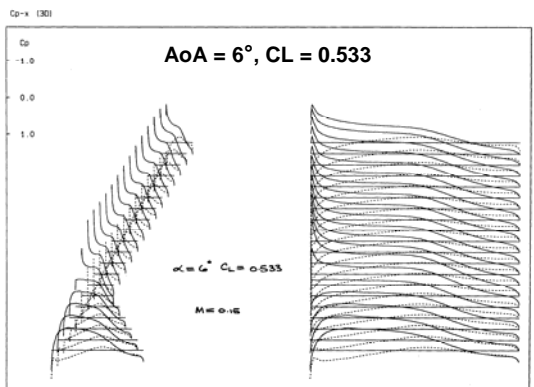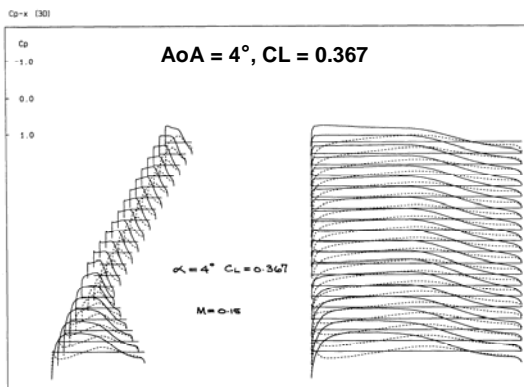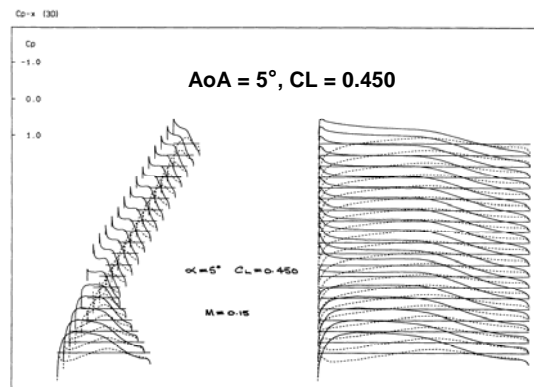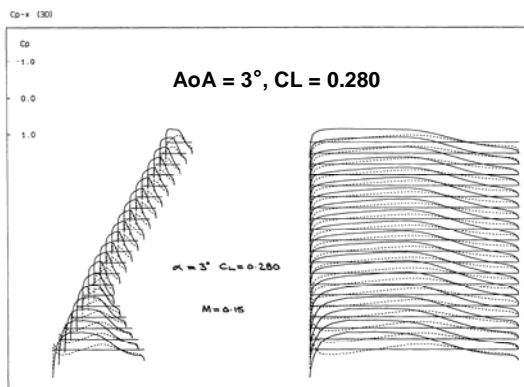
FIG. 6.2.4 SC AR 11.3 DESIGNED (LAMINAR FLOW TO CL 0.5, Mach 0.6) CHARACTERISTICS, Mach 0.15

Aerofoils

$C_{Lm} = 0.0965$

Spanwise Loadings

Cp Distributions

AoA = 6°. CL = 0.666

$\alpha = 6°$ $C_L = 0.666$

AoA = 7°, CL = 0.762

$\alpha = 7°$ $C_L = 0.762$

AoA = 8°, CL = 0.858

$\alpha = 8°$ $C_L = 0.858$
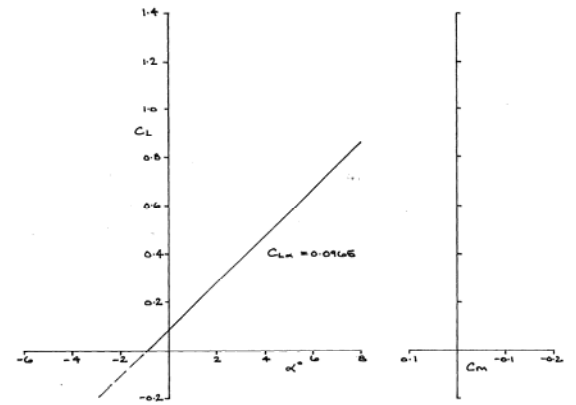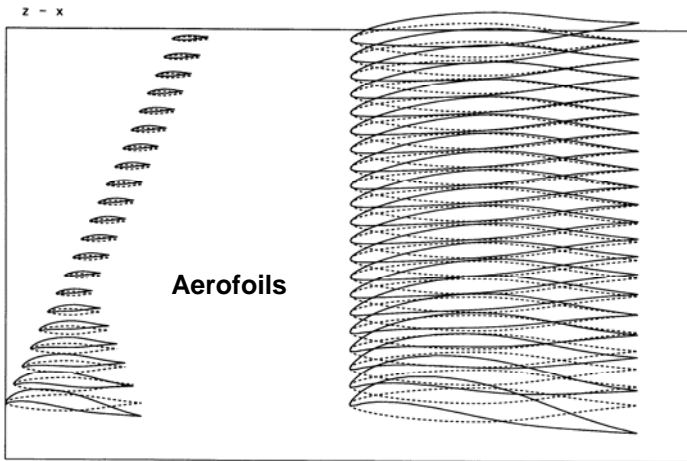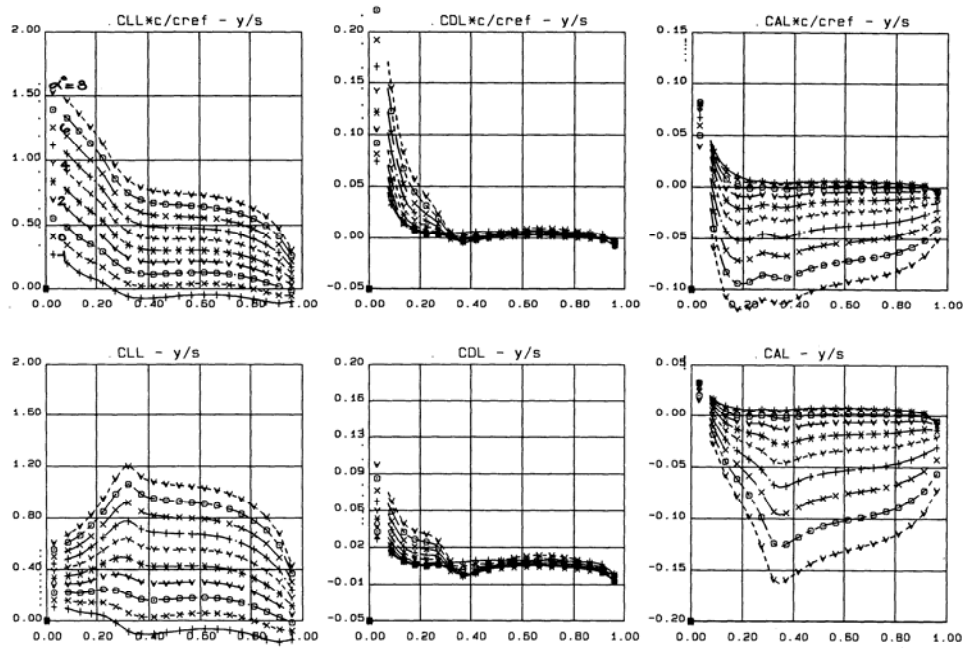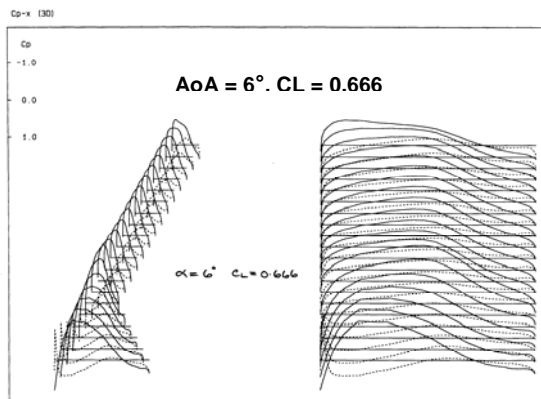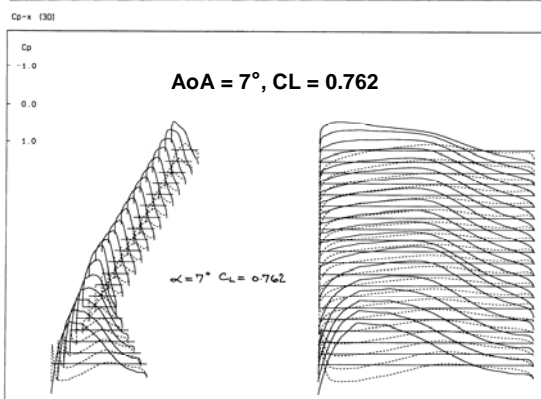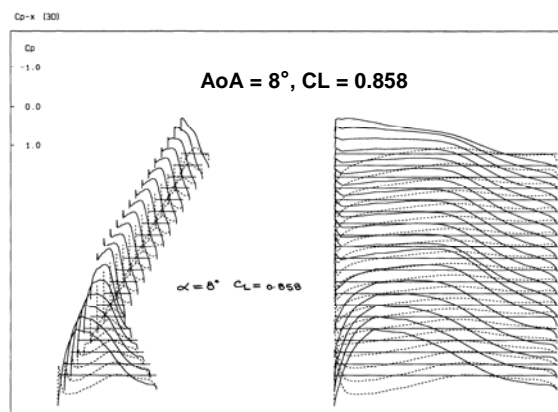
FIG. 6.2.5 SC AR 11.3 DESIGNED FOR LAMINAR FLOW UP TO CL 0.8 CHARACTERISTICS, Mach 0.6

41

CL, AoA & Cm Variations

Spanwise Loadings

M = 0.15

Cp Distributions

AoA = 4°, CL = 0.403

AoA = 6°, CL = 0.570

AoA = 5°, CL = 0.487

AoA = 7°, CL = 0.652
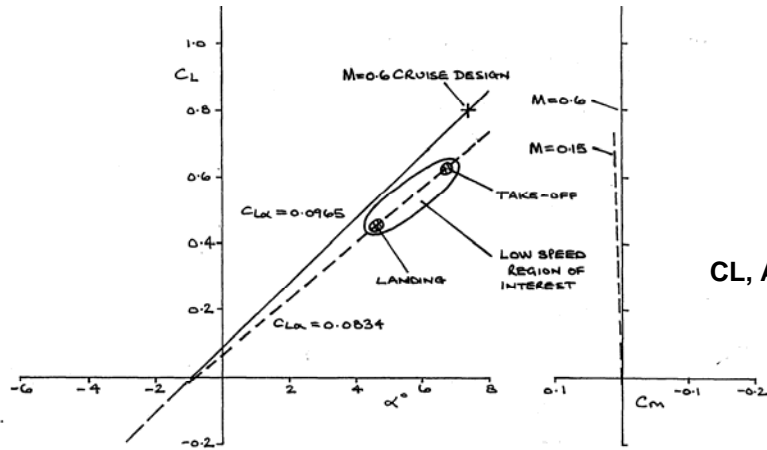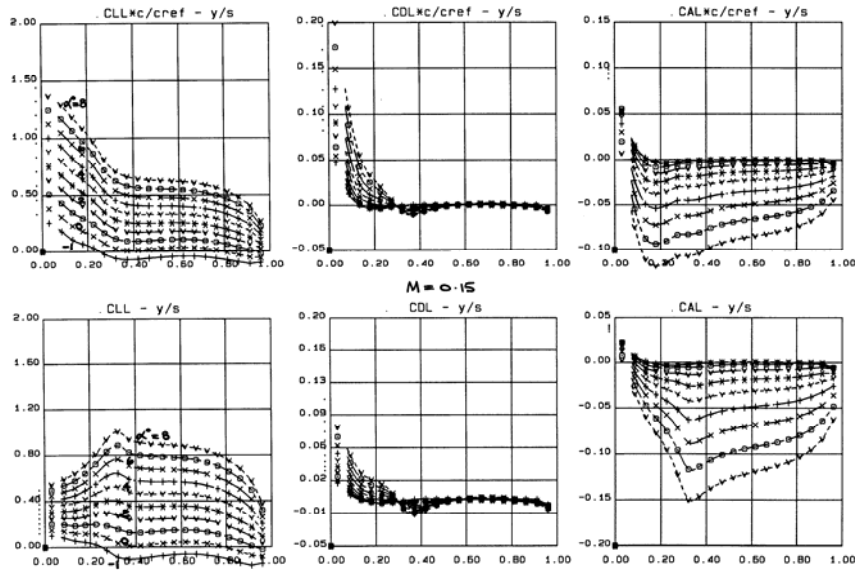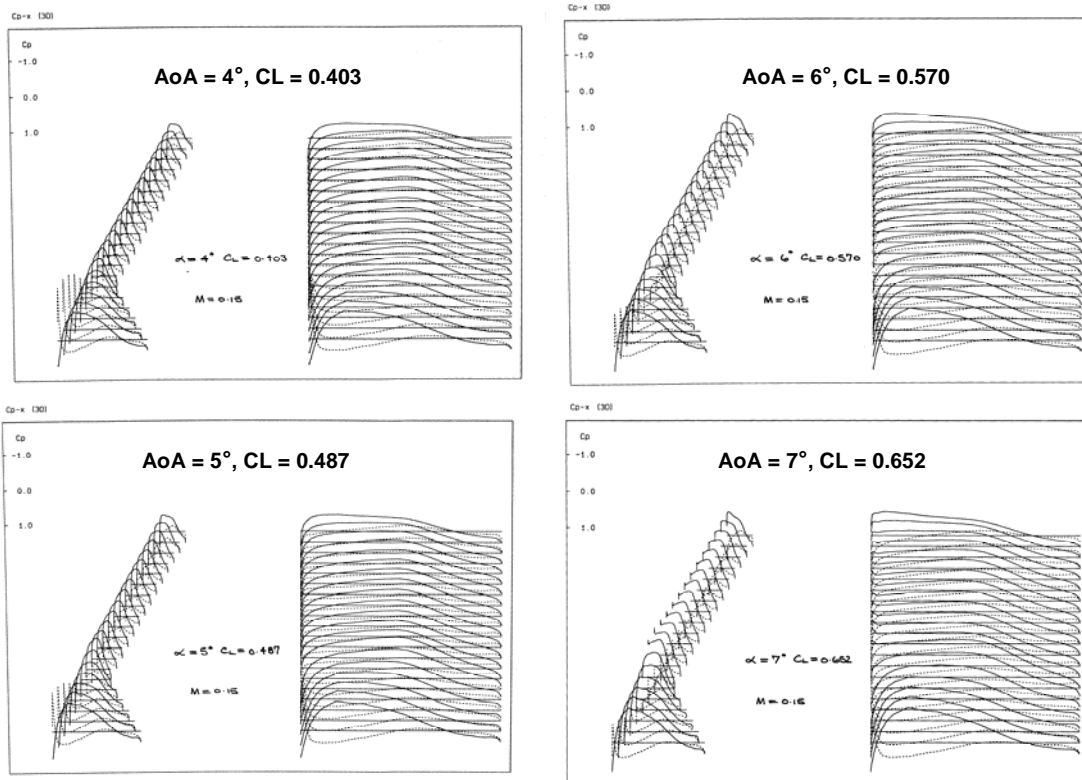
FIG. 6.2.6 SC AR 11.3 DESIGNED (LAMINAR FLOW TO CL 0.8, Mach 0.6) CHARACTERISTICS, Mach 0.15

42

Aerofoils

Max t/c Location

AoA = 6°, CL = 0.664

AoA = 8°, CL = 0.855

AoA = 7°, CL = 0.759
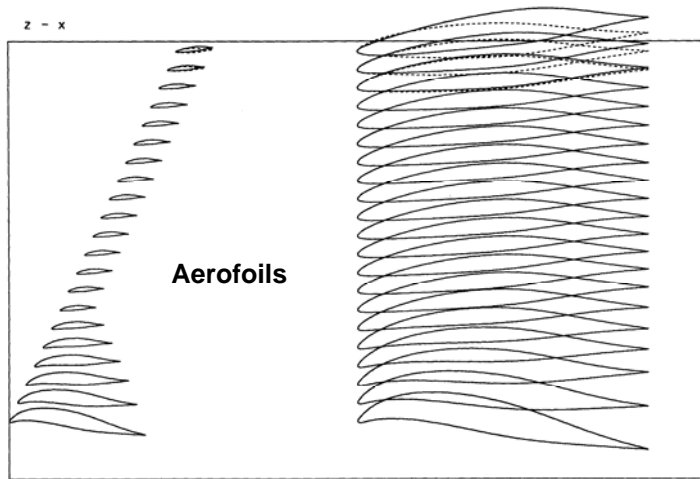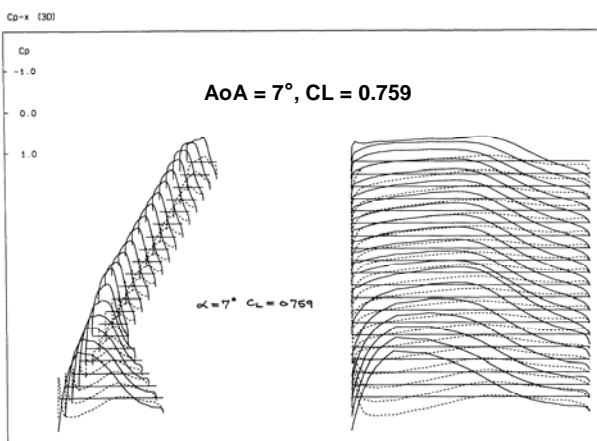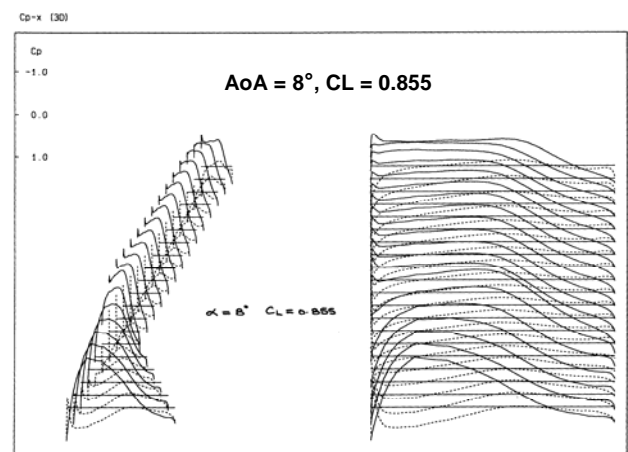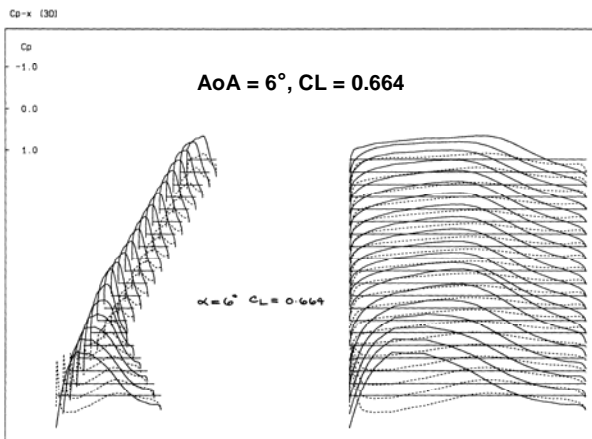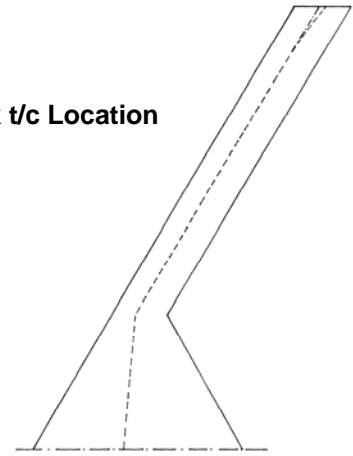
Cp Distributions

FIG. 6.2.7 SC AR 11.3 DESIGNED FOR LAMINAR FLOW UP TO CL 0.8 WITH TIP REFINEMENT CHARACTERISTICS, Mach 0.6
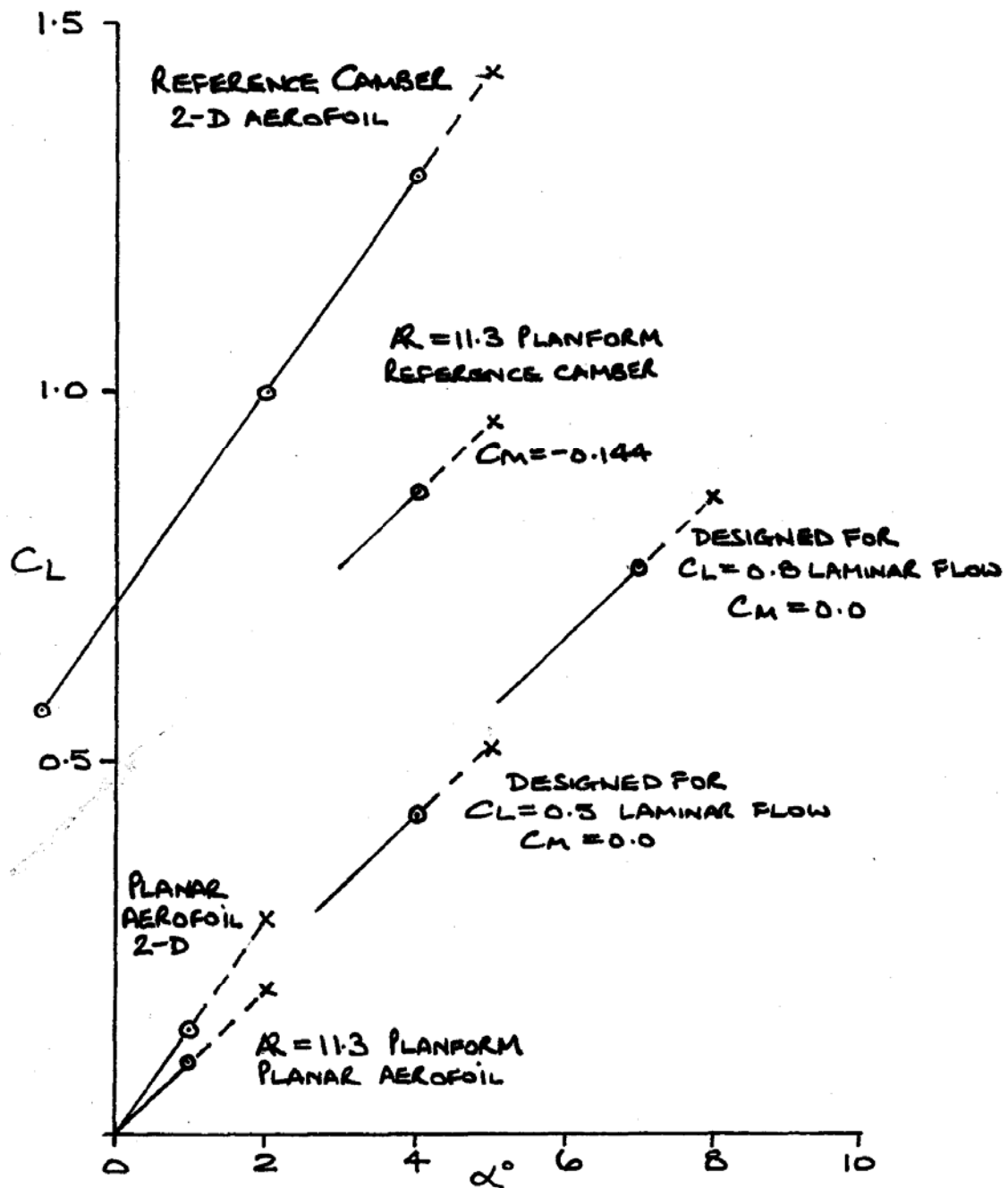
**FIG. 6.2.8 SC AR 11.3, SUMMARY OF DESIGNS FOR LAMINAR FLOW CL
RANGES, Mach 0.6
Laminar up to CL = 0.5 & 0.8**

44
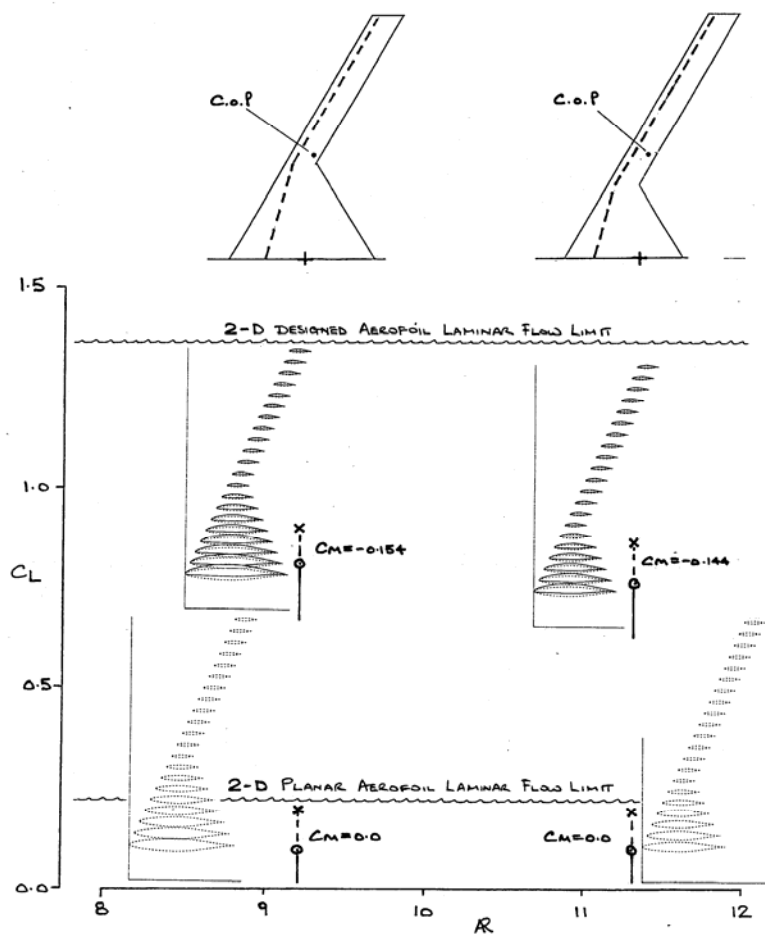
FIG.6.3.1 SC WINGS SUMMARY
PLANAR & REFERENCE CAMBER,
Mach 0.6
No Cm control
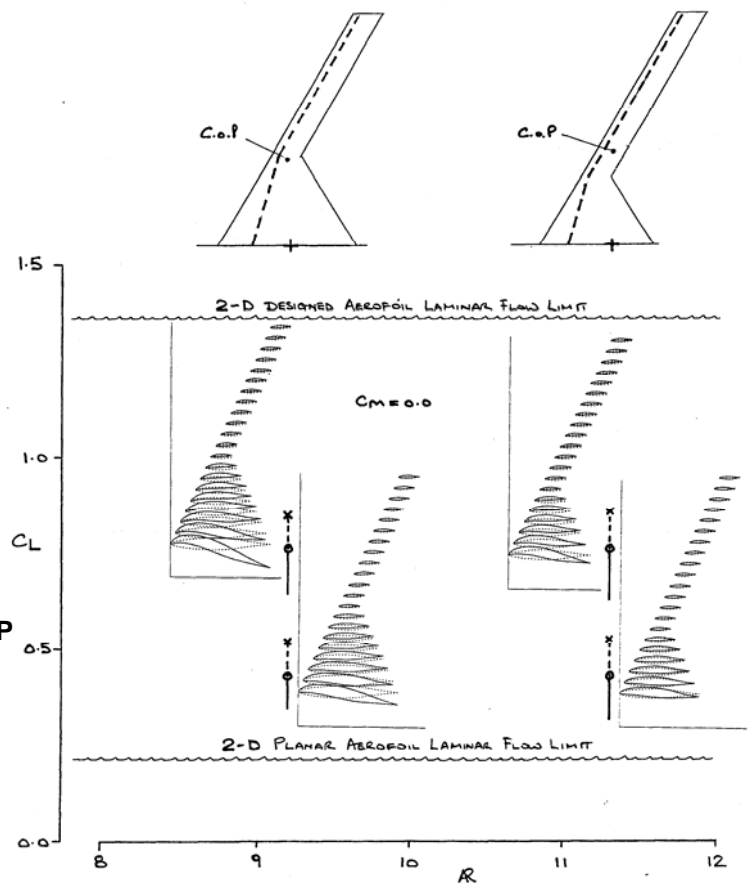
FIG.6.3.2 SC WINGS SUMMARY
DESIGNED FOR LAMINAR FLOW UP
TO CL 0.5 & 0.8, Mach 0.6
Cm controlled
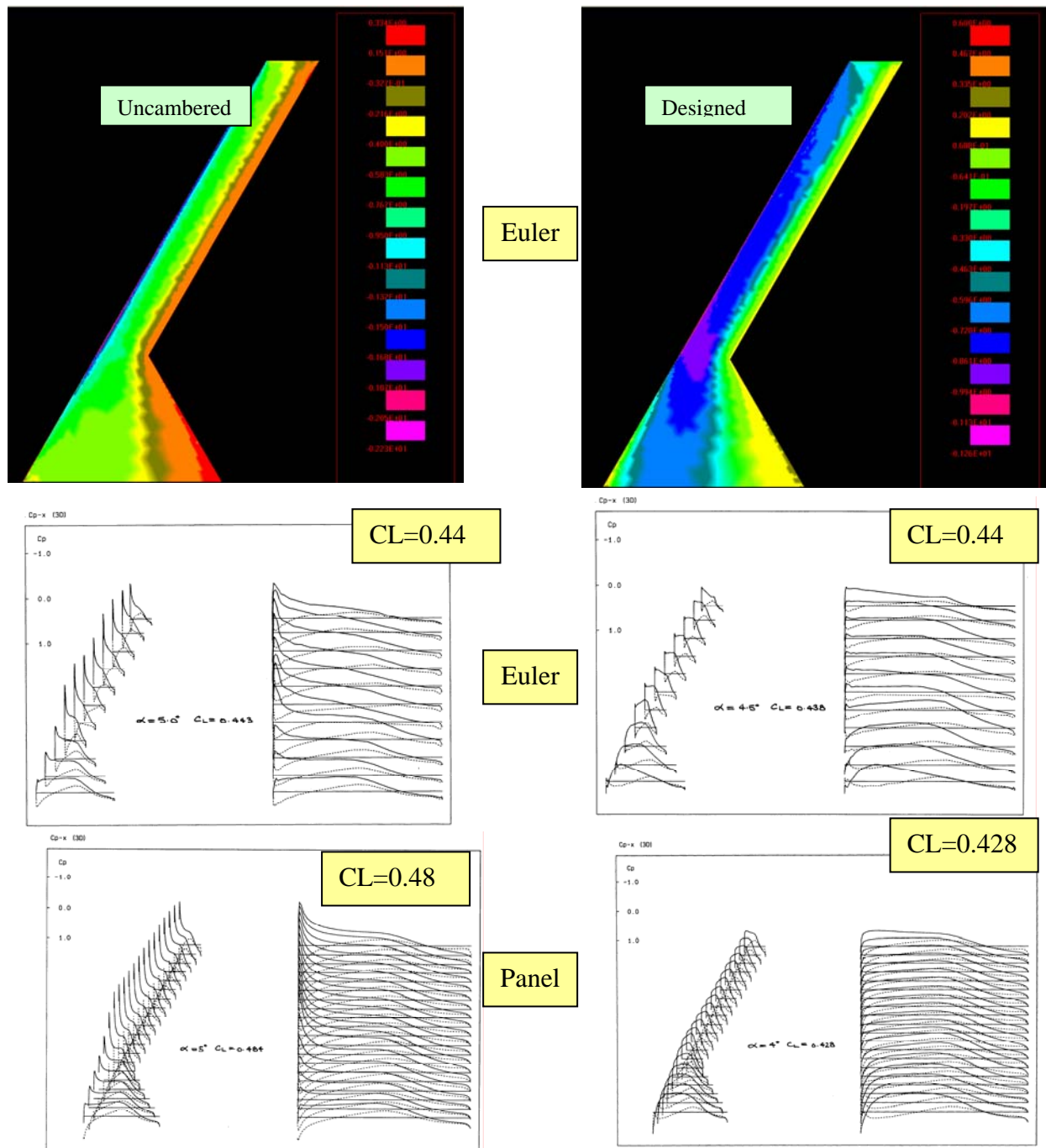
FIG. 6.4.1 SC AR 11.3 COMPARING UNCAMBERED & DESIGNED (C_L 0.5) CAMBERED AEROFOIL CONFIGURATION, Cp ISOBARS & DISTRIBUTIONS AT NEARLY EQUIVALENT CL, Euler & Panel, Mach 0.6

Uncambered

Designed

Euler

CL=0.66

CL=0.75

Euler

CL=0.77

CL=0.76
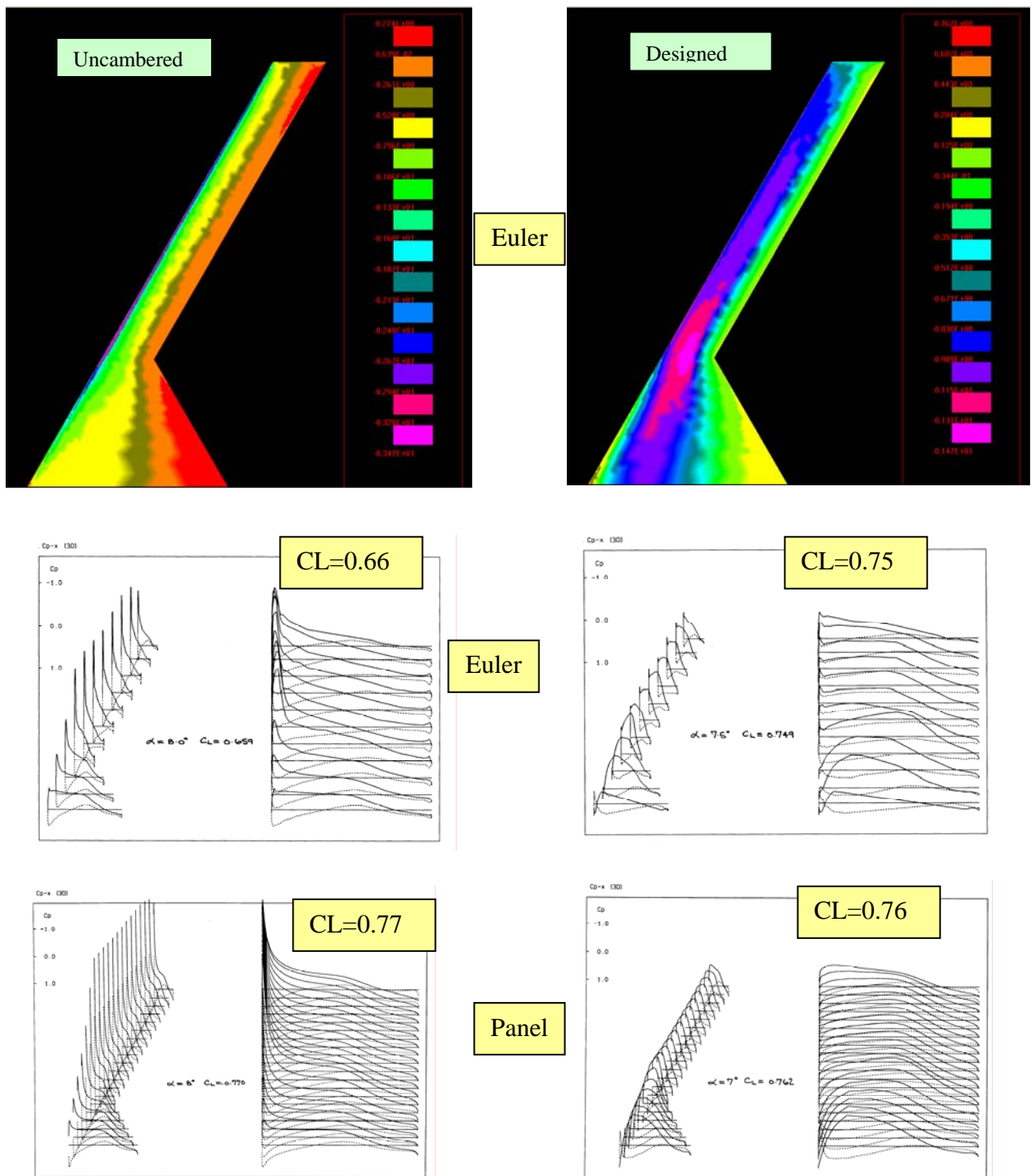
Panel

FIG. 6.4.2 SC AR 11.3 COMPARING UNCAMBERED & DESIGNED (C_L 0.8) CAMBERED AEROFOIL CONFIGURATION, Cp ISOBARS & DISTRIBUTIONS AT NEARLY EQUIVALENT CL, EULER & Panel, Mach 0.6

Aerofoils

CL, AoA & Cm Variations

$CL\alpha = 0.0932$

CLL*c/cref - y/s

CDL*c/cref - y/s

CAL*c/cref - y/s

$\alpha^\circ = 8$

CLL - y/s

CDL - y/s

CAL - y/s

Spanwise Loadings

AoA = 0°, CL = 0.000

$\alpha = 0^\circ$ CL = 0.000

AoA = 2°, CL = 0.188

$\alpha = 2^\circ$ CL = 0.188

AoA = 1°, CL = 0.094

$\alpha = 1^\circ$ CL = 0.094
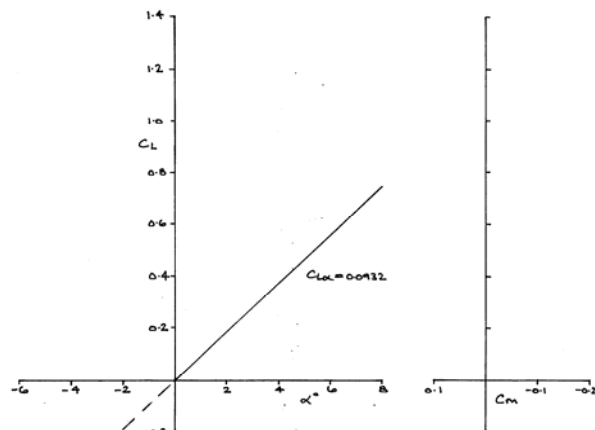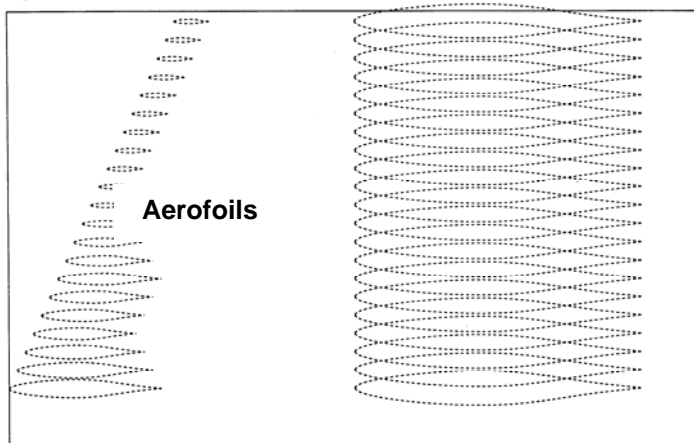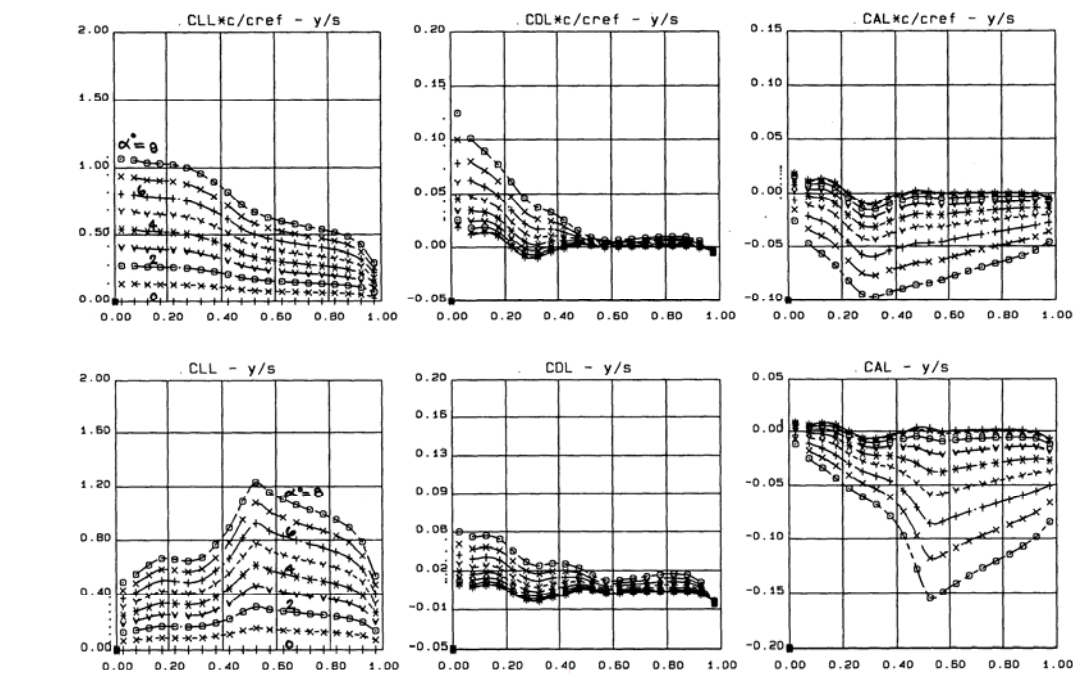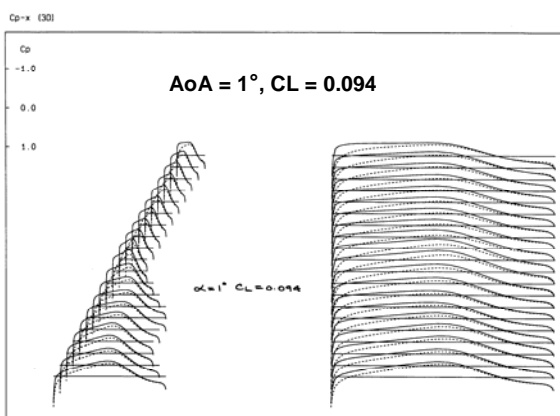
Cp Distributions

**FIG. 7.1.1 DC AR 8.68 UNCAMBERED WING
CHARACTERISTICS, Mach 0.6**

48

Aerofoils

CL, AoA & Cm Variations

$C_{L\alpha} = 0.0927$

Spanwise Loadings

AoA = 2°, CL = 0.661

AoA = 4°, CL = 0.848

AoA = 3°, CL = 0.755
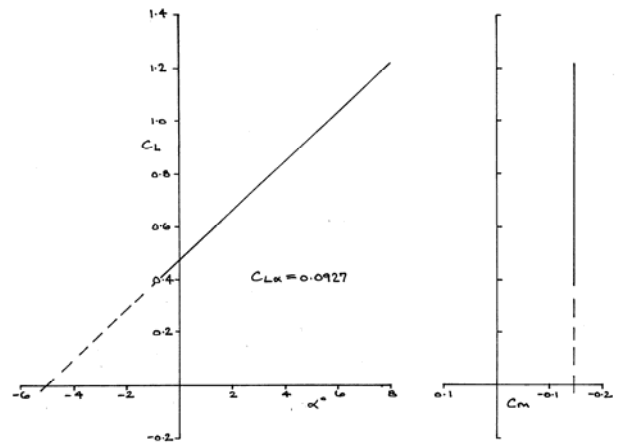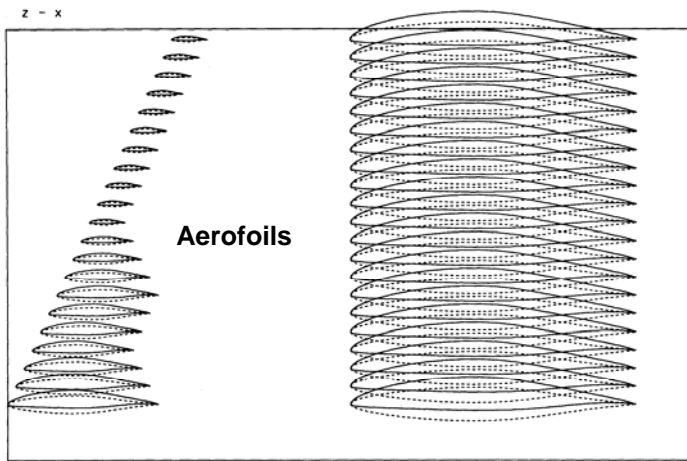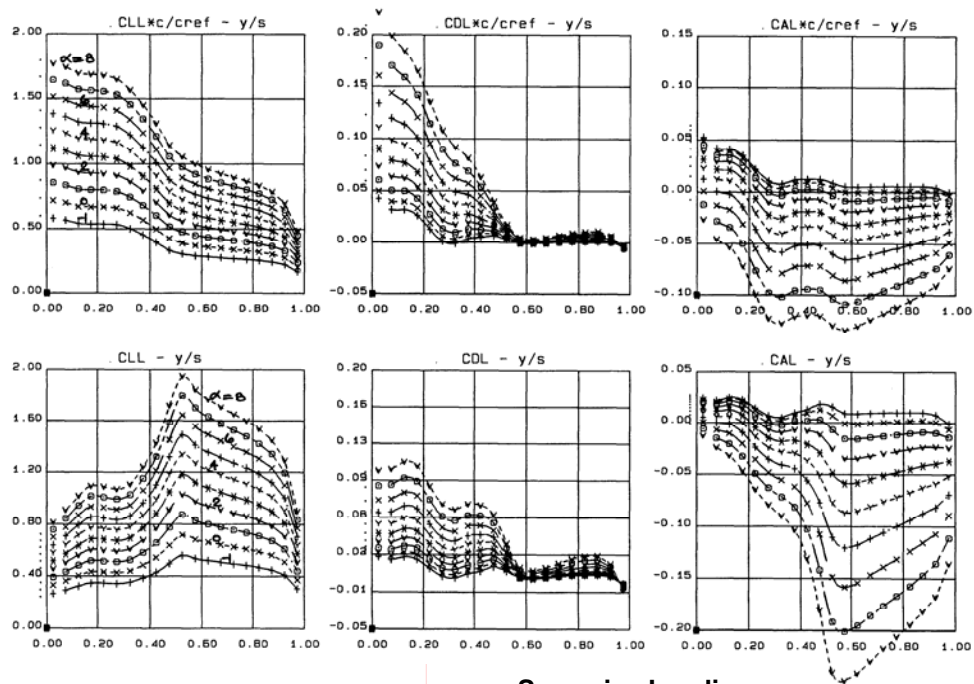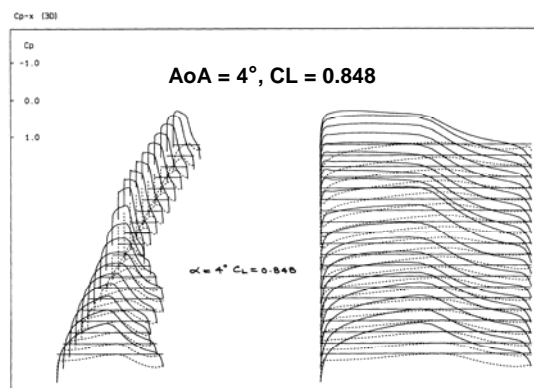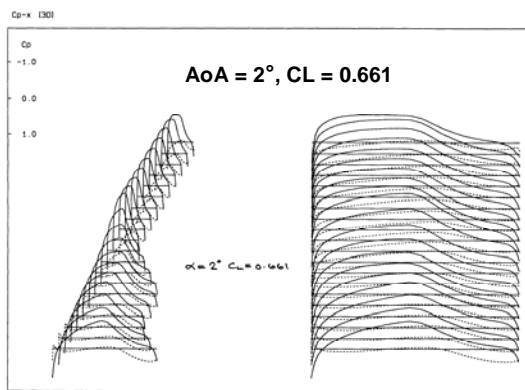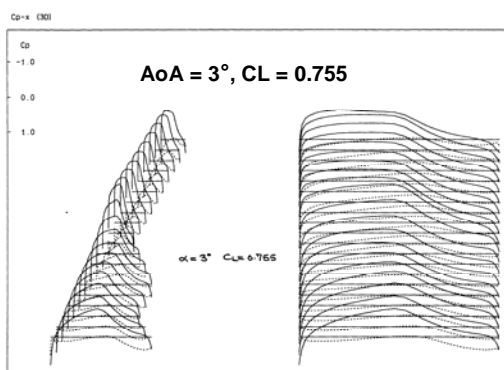
Cp Distributions

FIG. 7.1.2 DC AR 8.68 REFERENCE CAMBER WING (No Twist) CHARACTERISTICS, Mach 0.6

Aerofoils

CL, AoA & Cm Variations

Spanwise Loadings

AoA = 3°, CL = 0.338

AoA = 5°, CL = 0.525

AoA = 4°, CL = 0.432
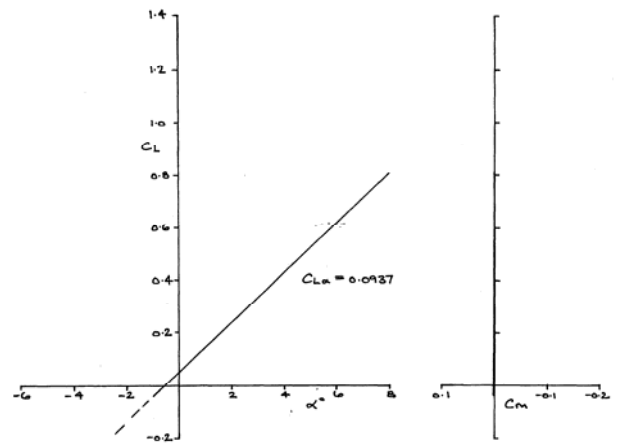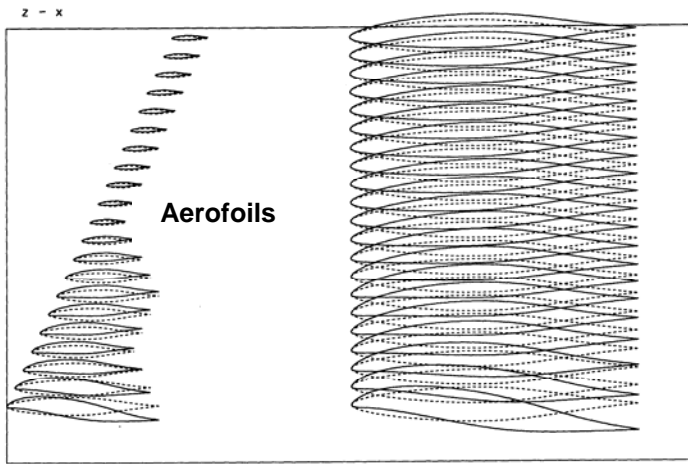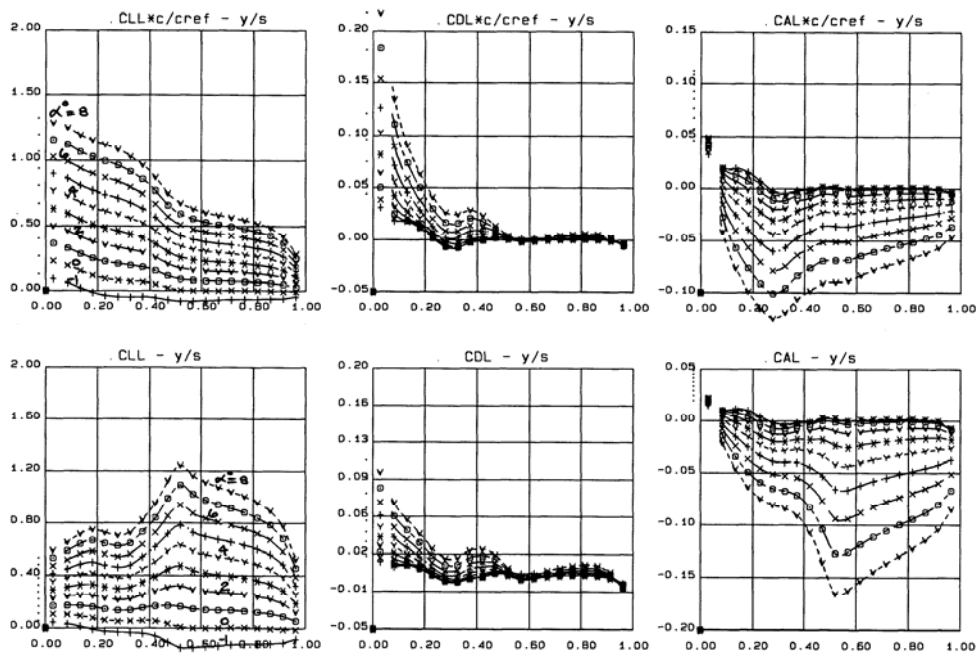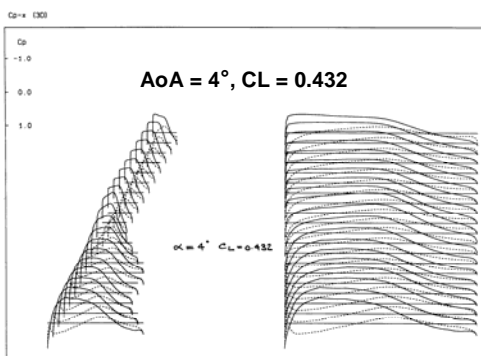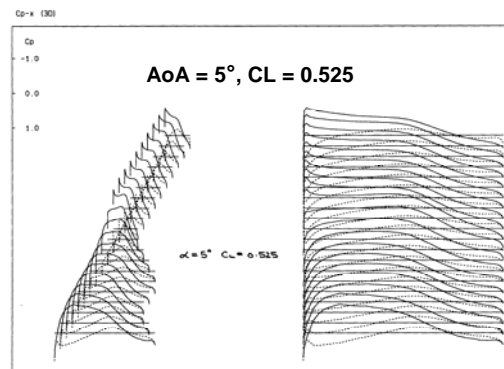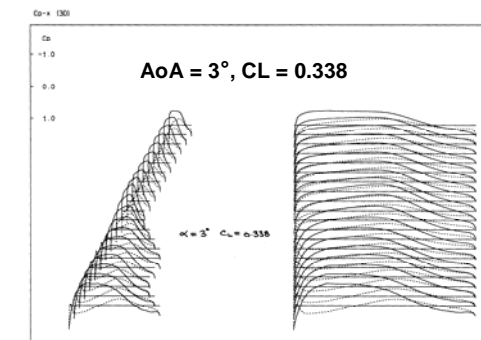
Cp Distributions

FIG. 7.1.3 DC AR 8.68 DESIGNED FOR LAMINAR FLOW UP TO CL 0.5 CHARACTERISTICS, Mach 0.6

50

Aerofoils

CL, AoA & Cm Variations

$C_{L\alpha} = 0.0940$

Spanwise Loadings

AoA = 6°, CL = 0.681

$\alpha = 6°$ $C_L = 0.681$

AoA = 8°, CL = 0.867

$\alpha = 8°$ $C_L = 0.867$

AoA = 7°, CL = 0.774

$\alpha = 7°$ $C_L = 0.774$
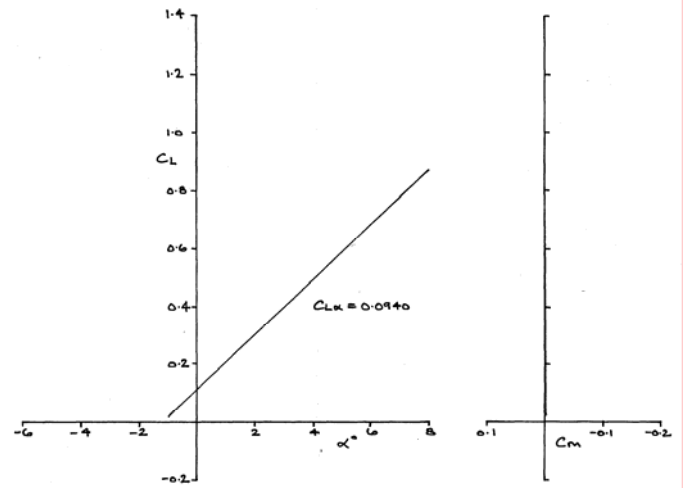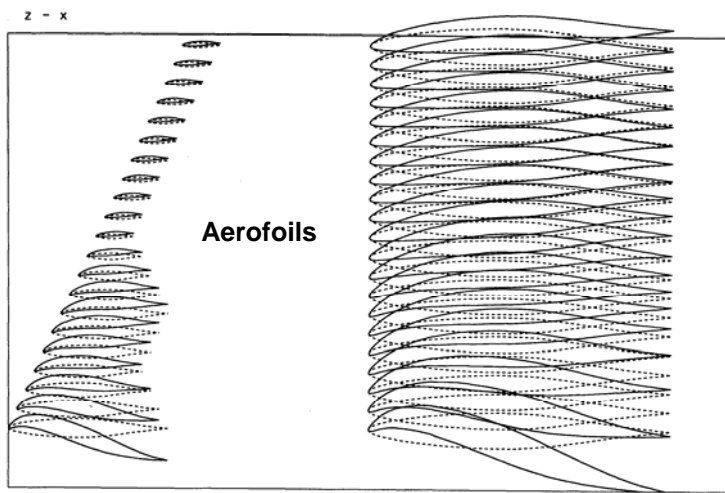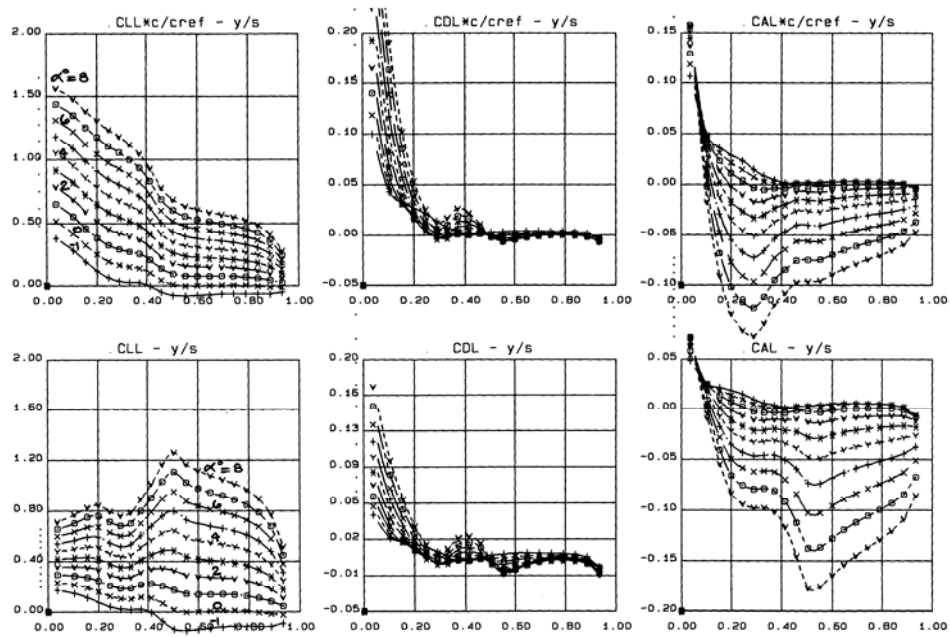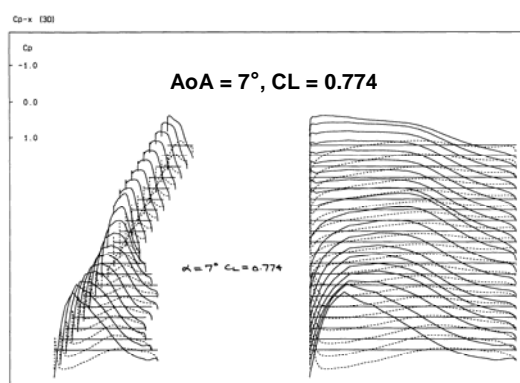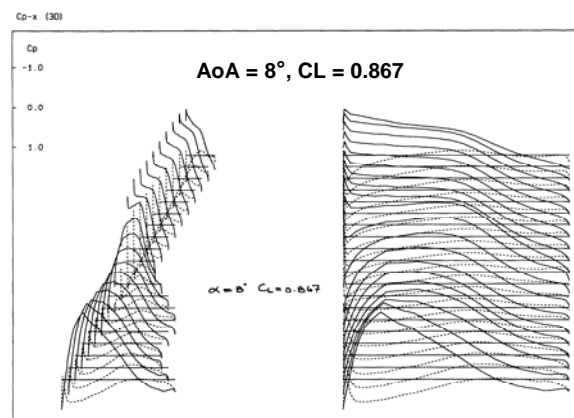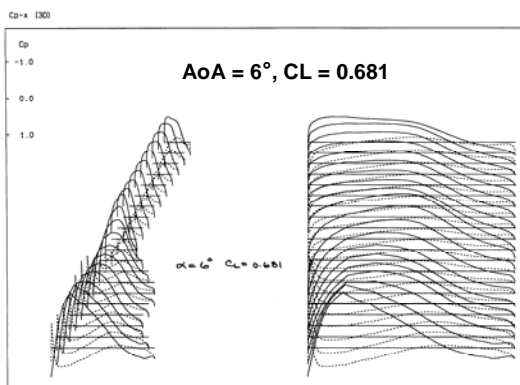
Cp Distributions

**FIG. 7.1.4 DC AR 8.68 DESIGNED FOR
LAMINAR FLOW UP TO CL 0.8
CHARACTERISTICS, Mach 0.6**

51

Graph axes: vertical axis labeled C_L with markings 1·5, 1·0, 0·5; horizontal axis labeled $\alpha°$ with markings 0, 2, 4, 6, 8, 10.

Labels on graph:
REFERENCE CAMBER 2-D AEROFOIL

AR = 8.68 PLANFORM REFERENCE CAMBER

$C_M = -0.147$

DESIGNED FOR $C_L = 0.8$ LAMINAR FLOW $C_M = 0.0$

DESIGNED FOR $C_L = 0.5$ LAMINAR FLOW $C_M = 0.0$
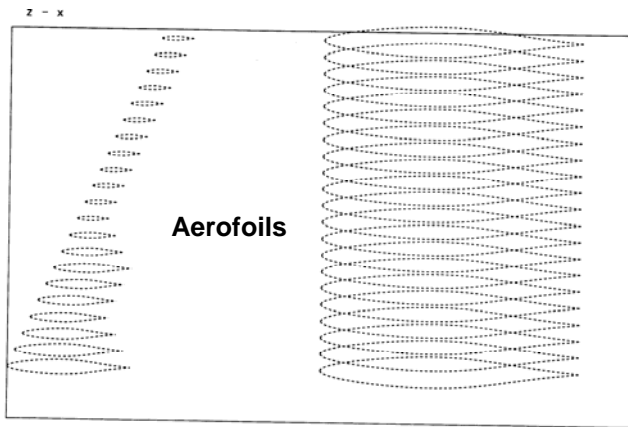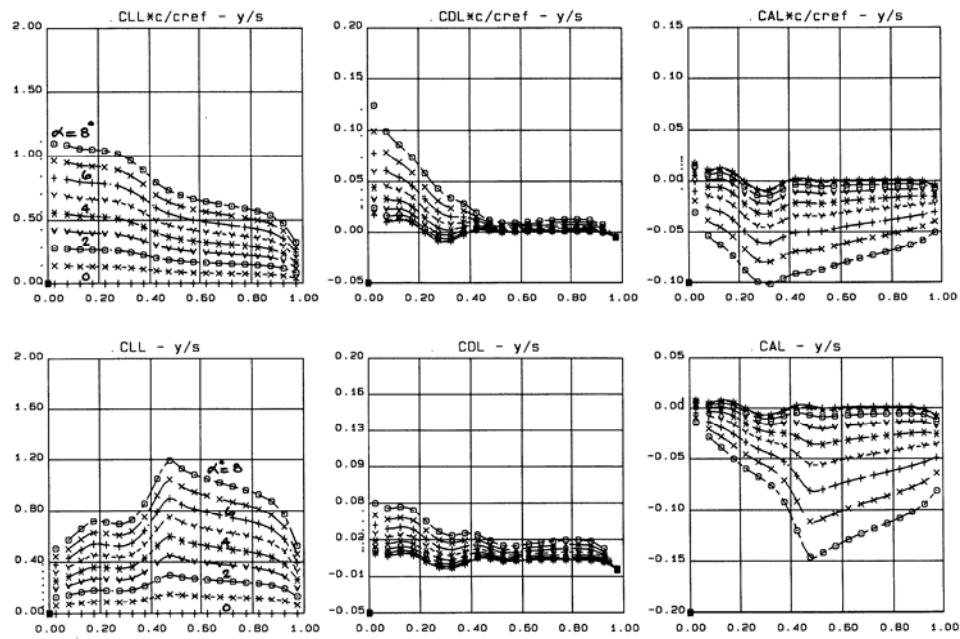
PLANAR AEROFOIL 2-D
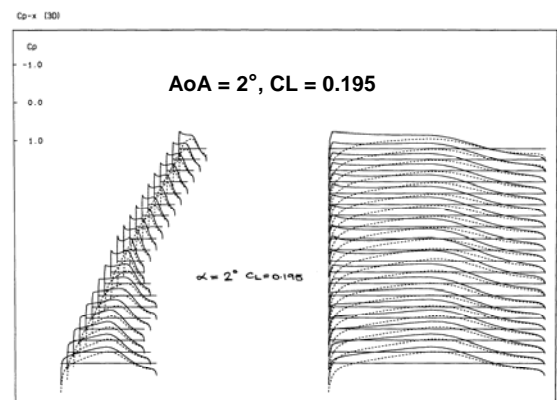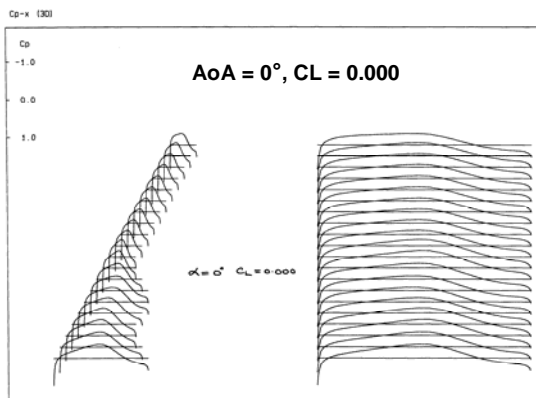
AR = 8.68 PLANFORM PLANAR AEROFOIL
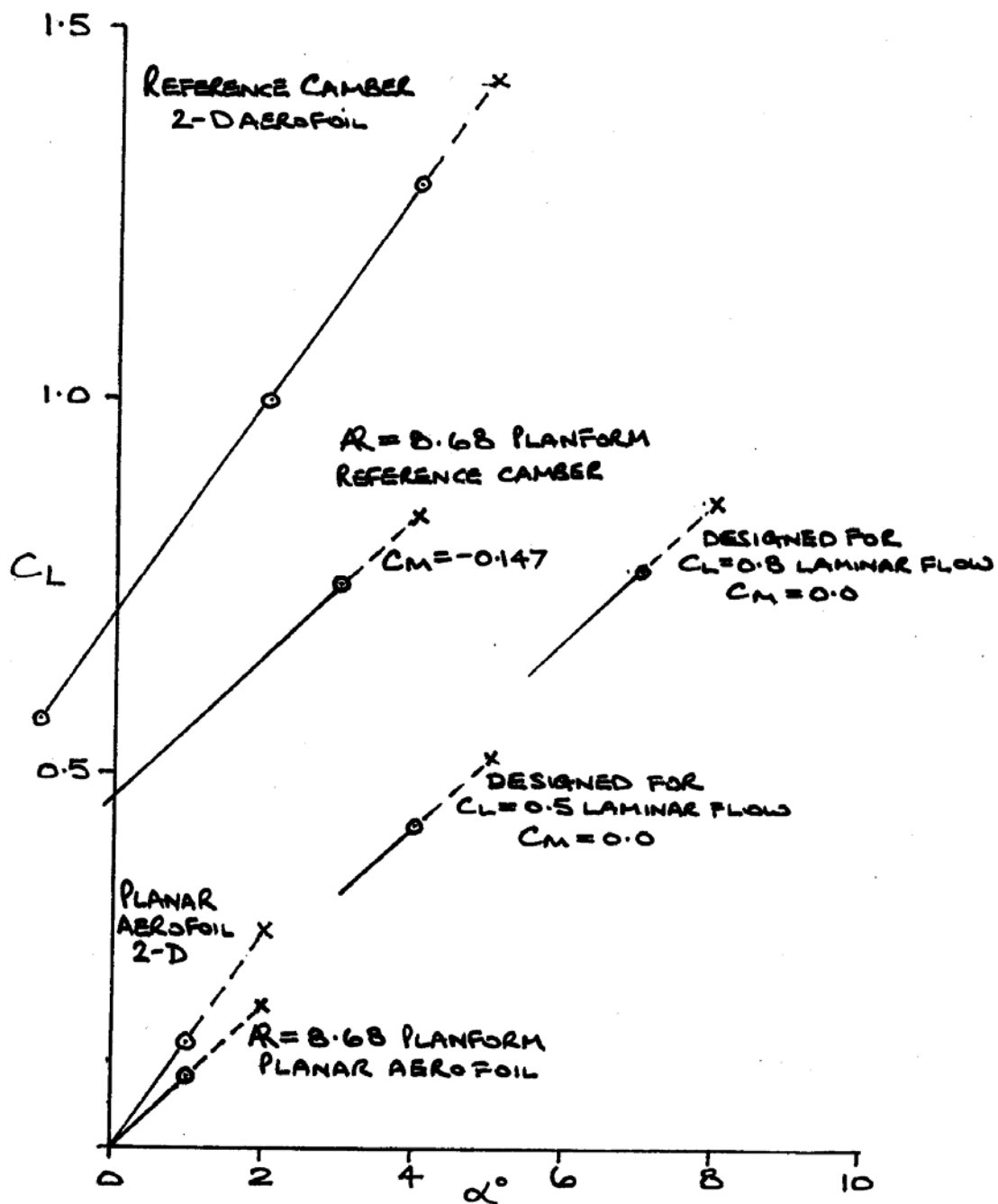
**FIG.7.1.5 DC AR 8.68, SUMMARY OF
DESIGNS FOR LAMINAR FLOW CL
RANGES, Mach 0.6
Laminar up to CL = 0.5 & 0.8**

52

Aerofoils

CL, AoA & Cm Variations

Spanwise Loadings

AoA = 0°, CL = 0.000

AoA = 2°, CL = 0.195

AoA = 1°, CL = 0.098
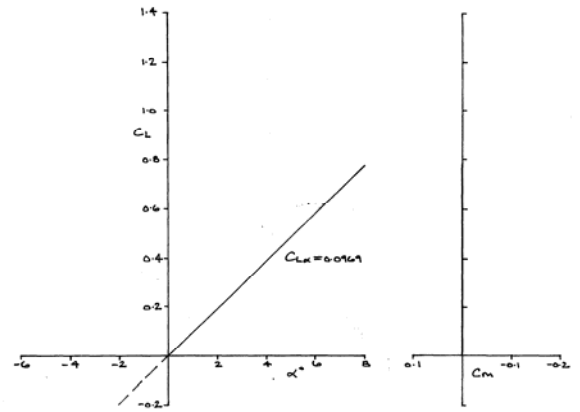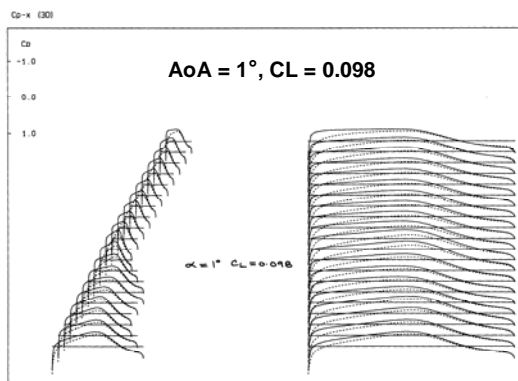
Cp Distributions

FIG. 7.2.1 DC AR 9.85 UNCAMBERED WING CHARACTERISTICS, Mach 0.6

53

Aerofoils

CL, AoA & Cm Variations

$C_{L\alpha} = 0.0959$

Spanwise Loadings

AoA = 2°, CL = 0.684

AoA = 4°, CL = 0.877

AoA = 3°, CL = 0.781
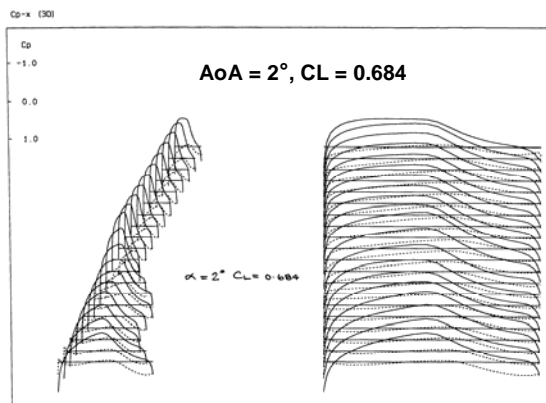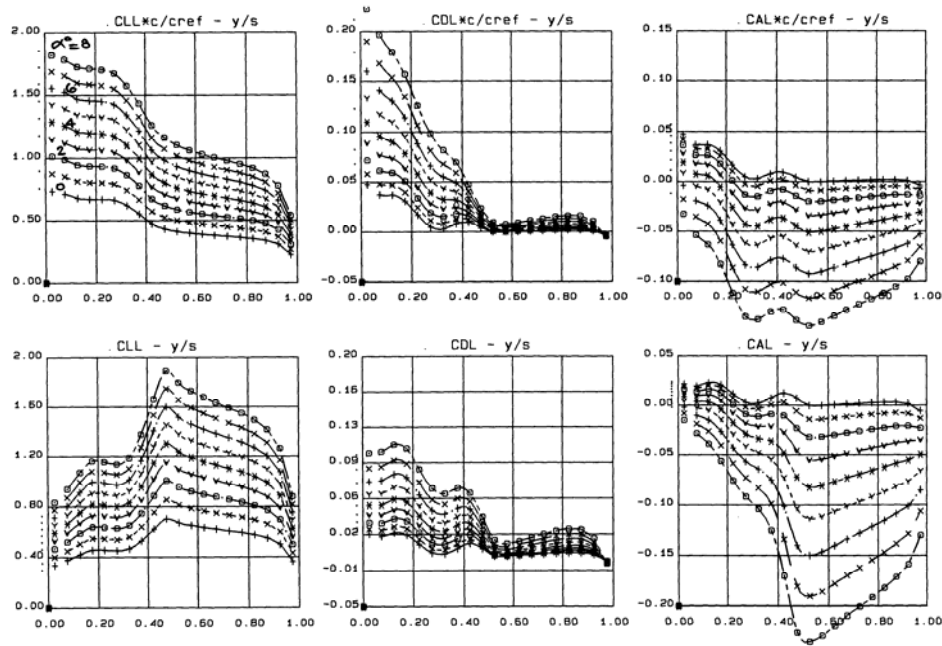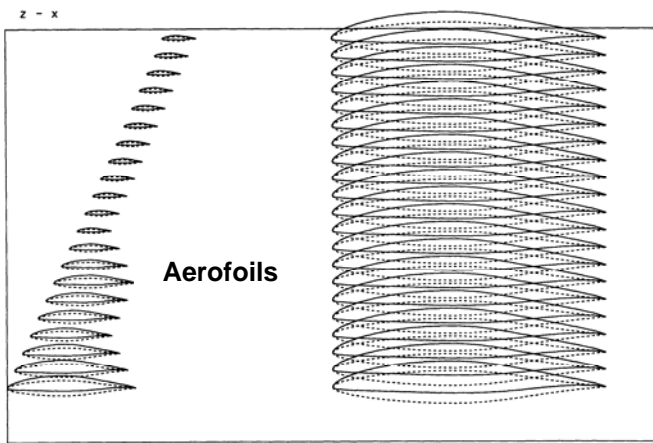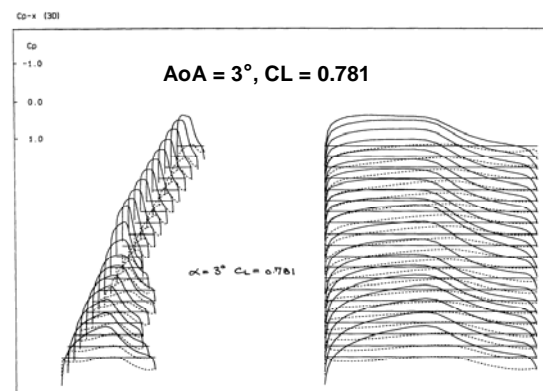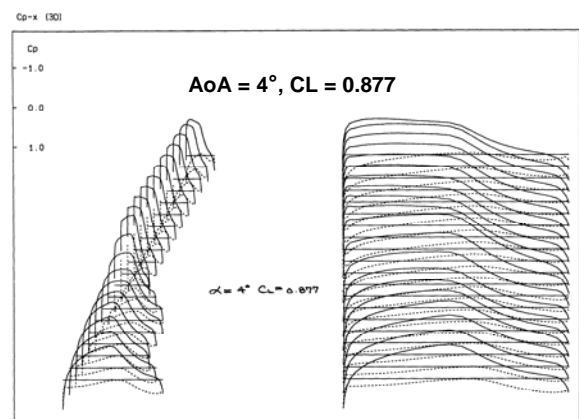
Cp Distributions

**FIG.7.2.2 DC AR 9.85 REFERENCE CAMBER
WING (No Twist) CHARACTERISTICS, Mach 0.6**

Aerofoils

CL, AoA & Cm Variations

Spanwise Loadings

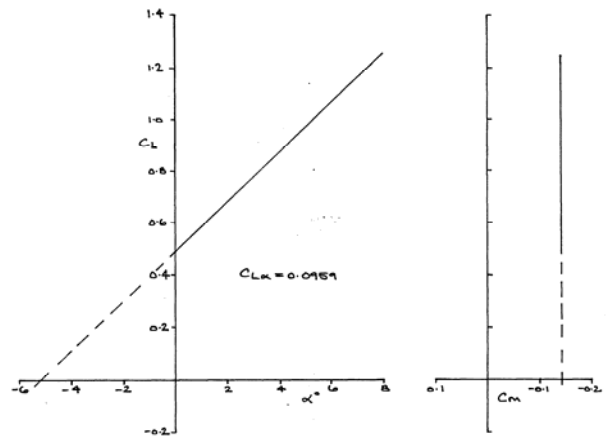**AoA = 3°, CL = 0.343**

AoA = 4°, CL = 0.441

AoA = 5°, CL = 0.538
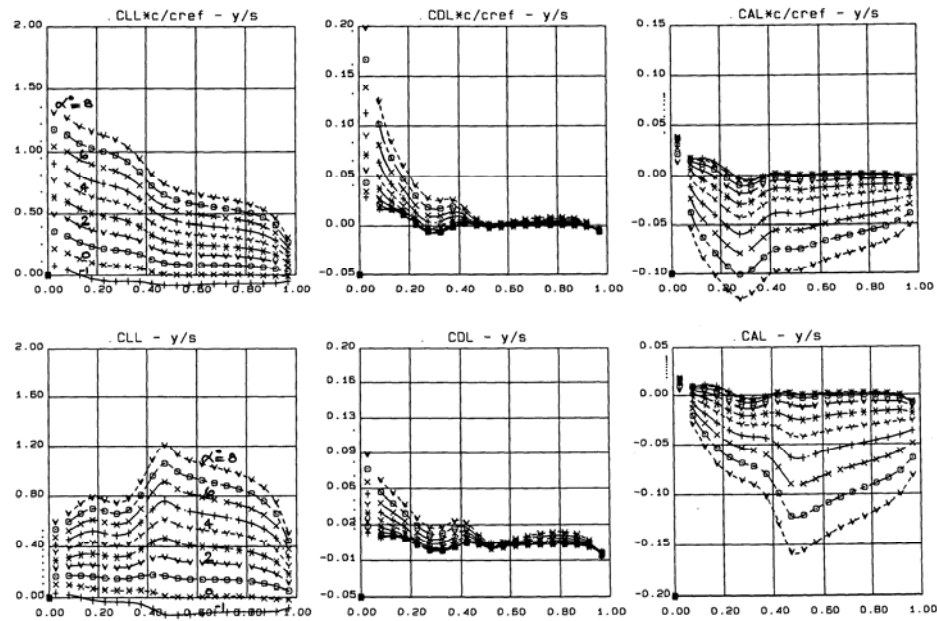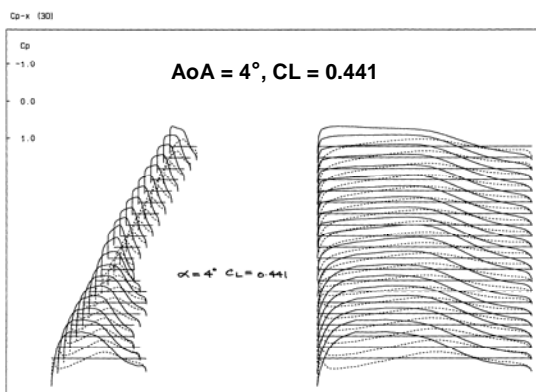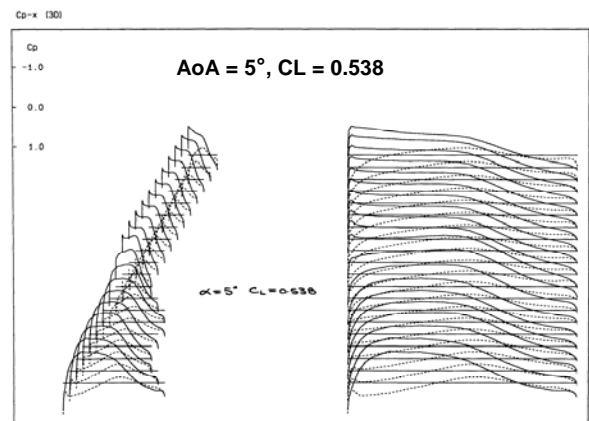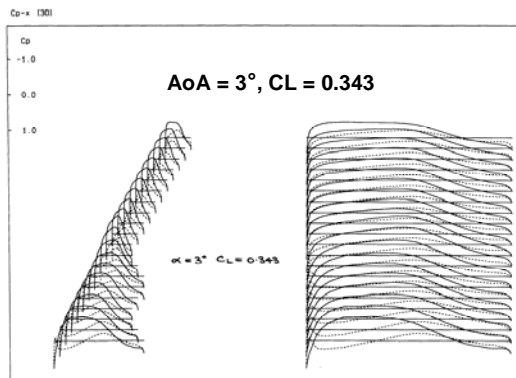
Cp Distributions

FIG. 7.2.3 DC AR 9.85 DESIGNED FOR LAMINAR FLOW UP TO CL 0.5 CHARACTERISTICS, Mach 0.6

CL, AoA & Cm Variations

Spanwise Loadings

AoA = 2°, CL = 0.209

AoA = 4°, CL = 0.377

AoA = 3°, CL = 0.293

AoA = 5°, CL = 0.461
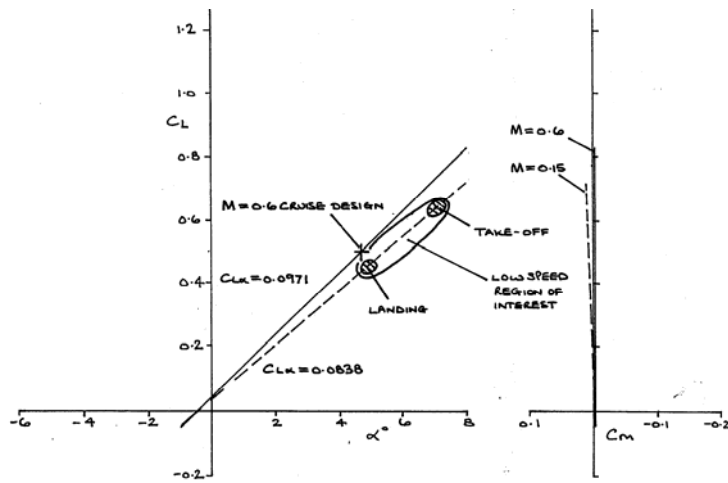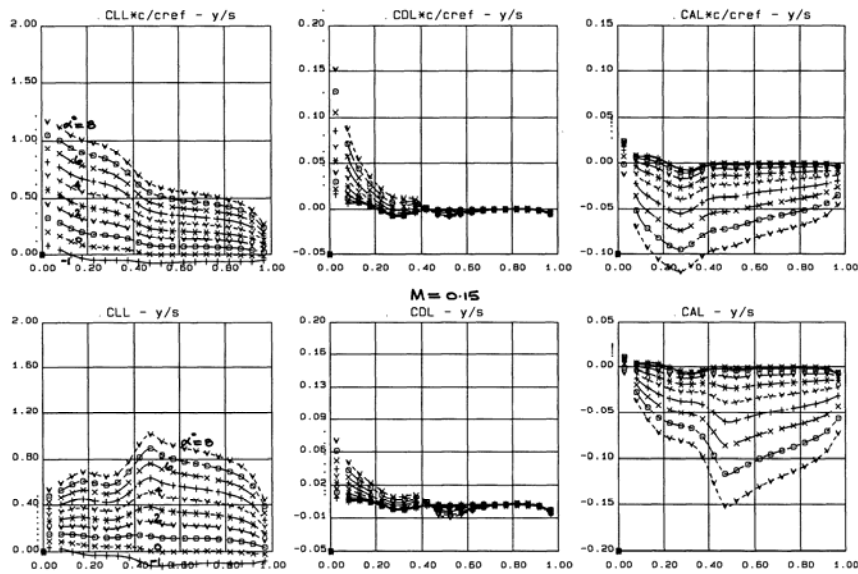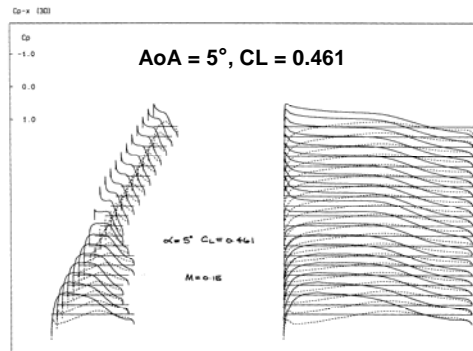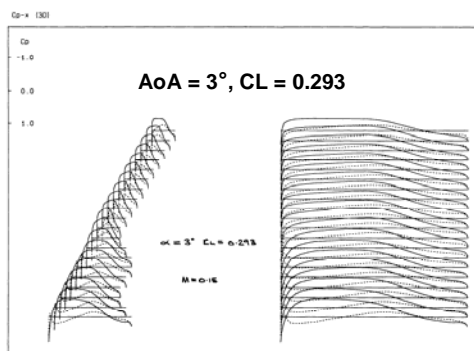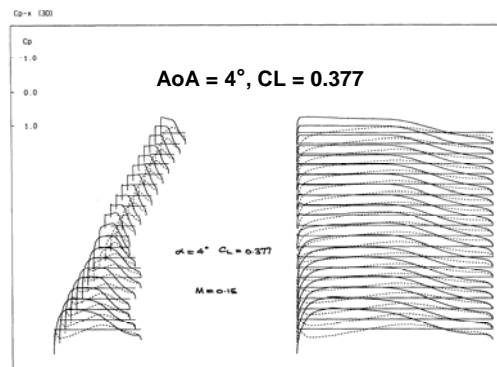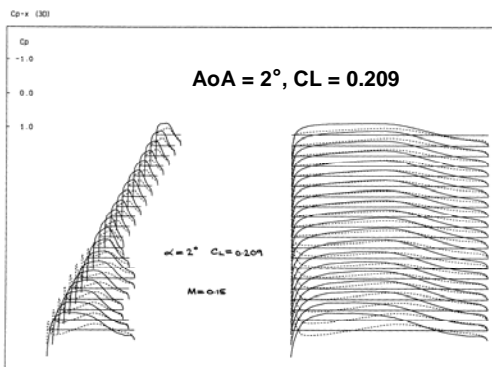
**FIG. 7.2.4 DC AR 9.85 DESIGNED (LAMINAR FLOW TO CL 0.5, Mach 0.6)
CHARACTERISTICS, Mach 0.15**

Aerofoils

CL, AoA & Cm Variations

$C_{L\alpha} = 0.0976$

Spanwise Loadings

AoA = 6°, CL = 0.692

AoA = 7°, CL = 0.788

AoA = 8°, CL = 0.884
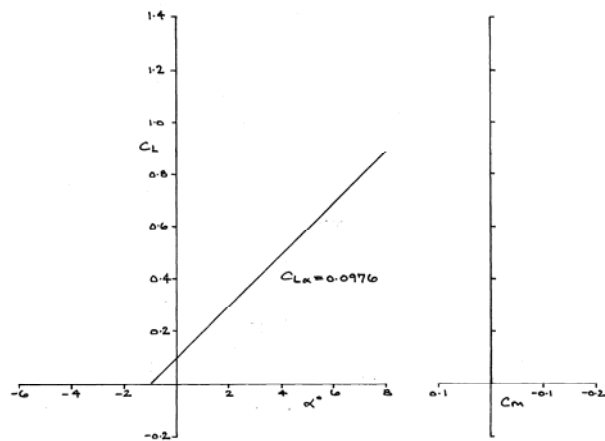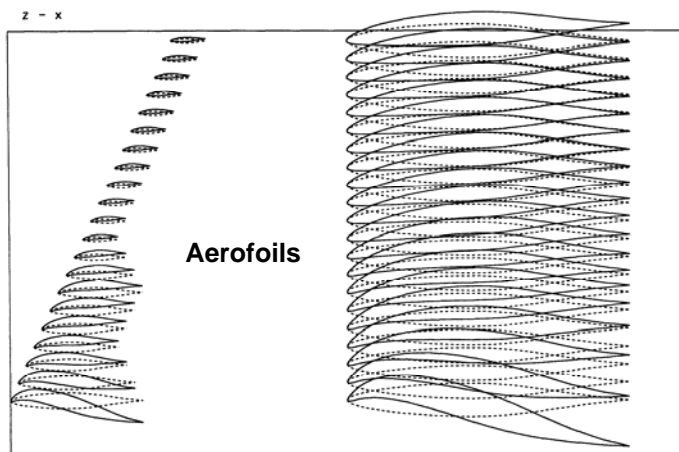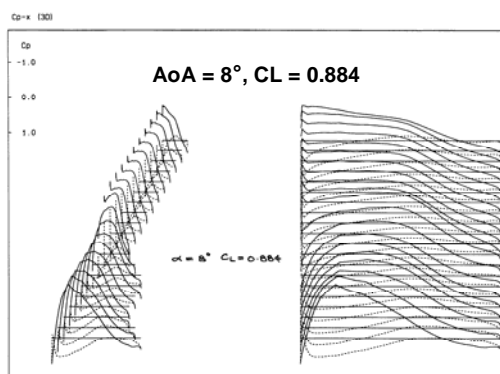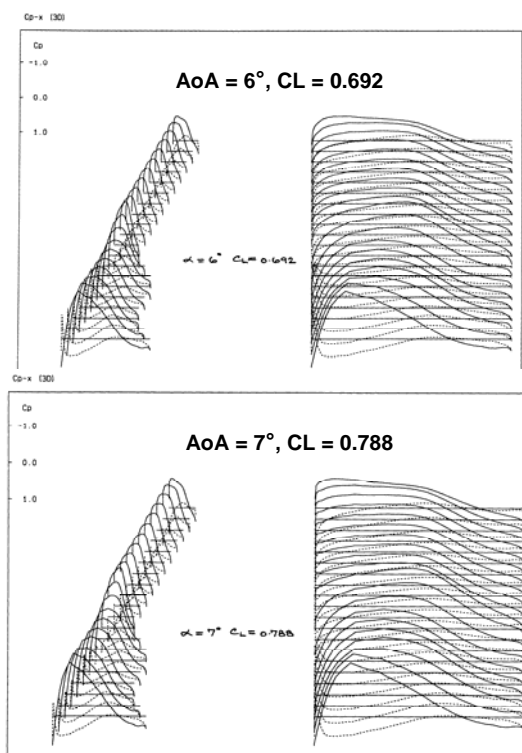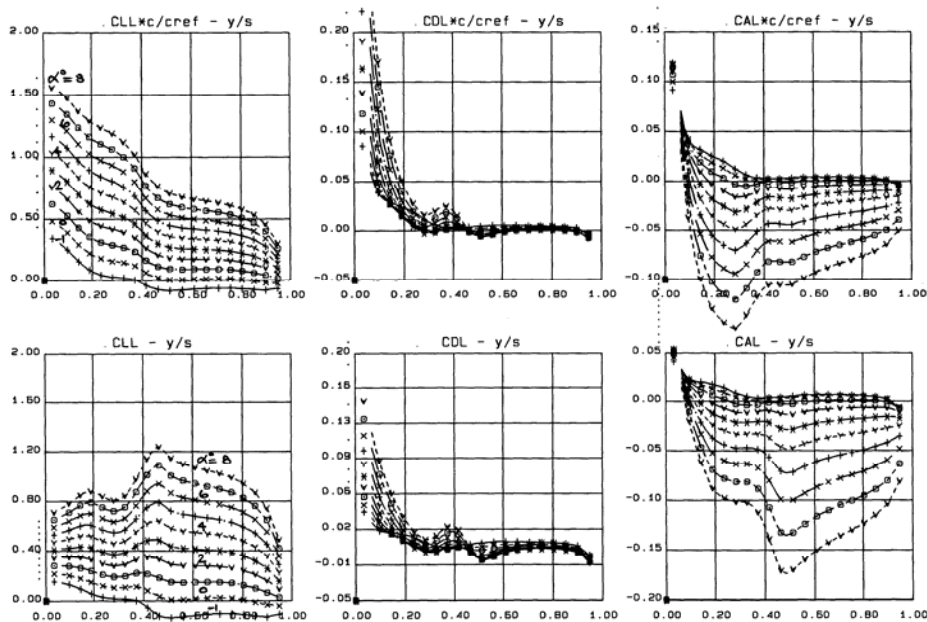
Cp Distributions

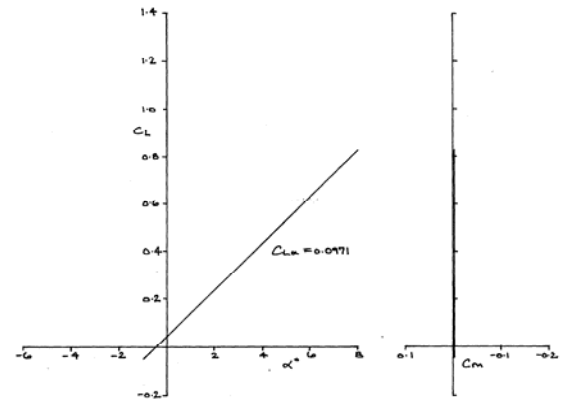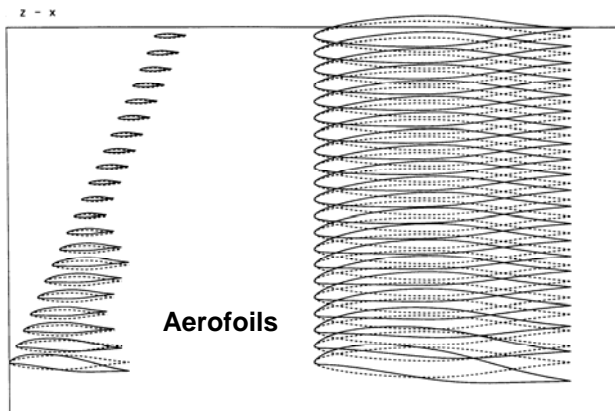**FIG. 7.2.5 DC AR 9.85 DESIGNED FOR LAMINAR FLOW UP TO CL 0.8 CHARACTERISTICS, Mach 0.6**

CL, AoA & Cm Variations

Spanwise Loadings

Cp Distributions

AoA = 4°, CL = 0.424

AoA = 6°, CL = 0.591

AoA = 5°, CL = 0.507

AoA = 7°, CL = 0.674
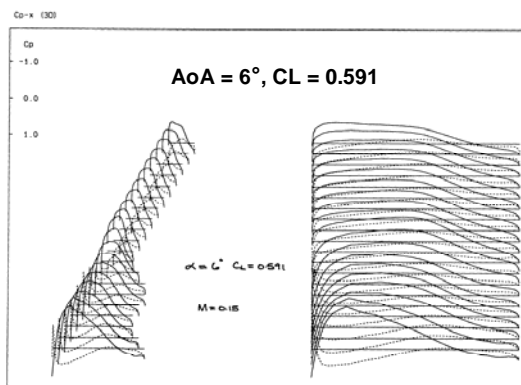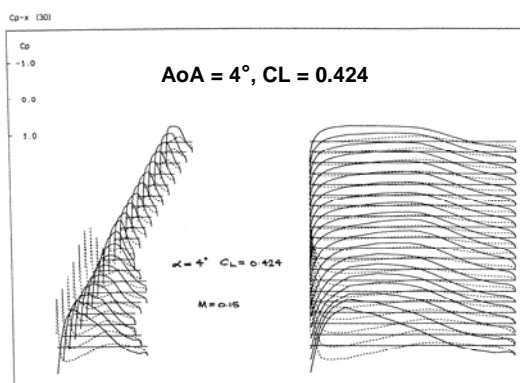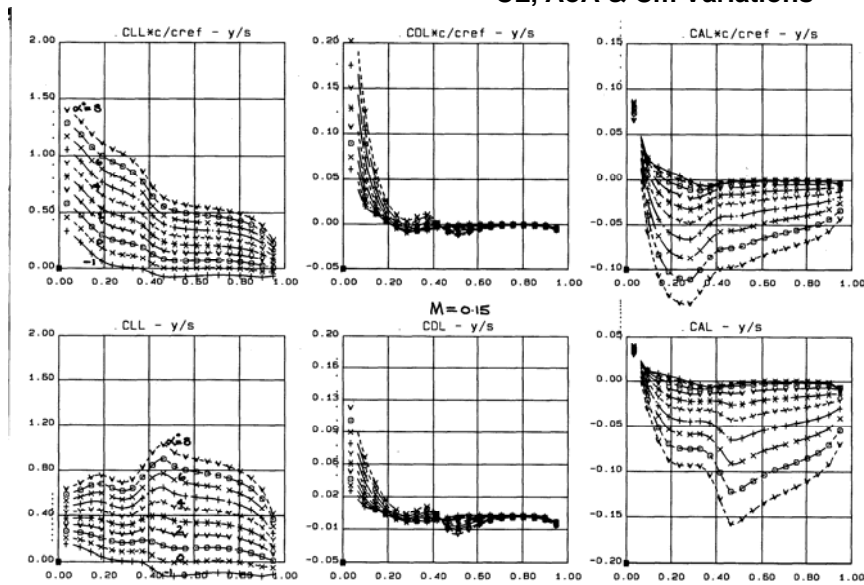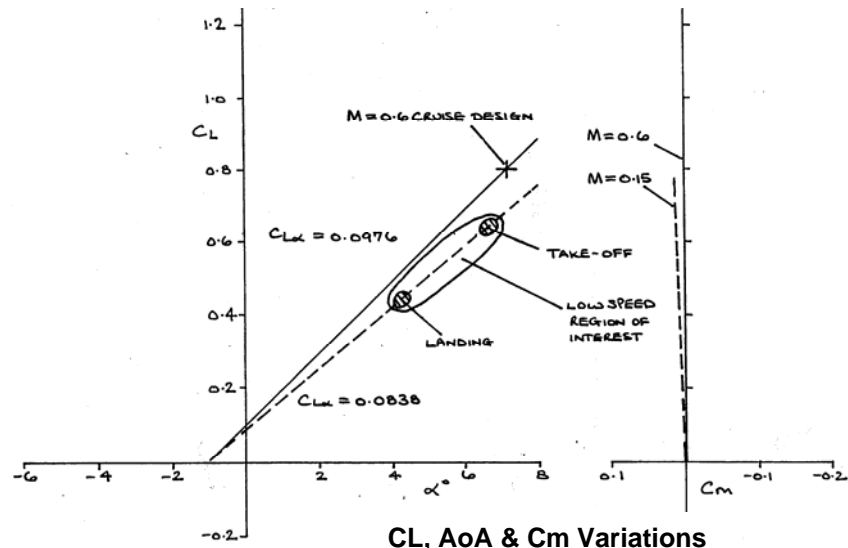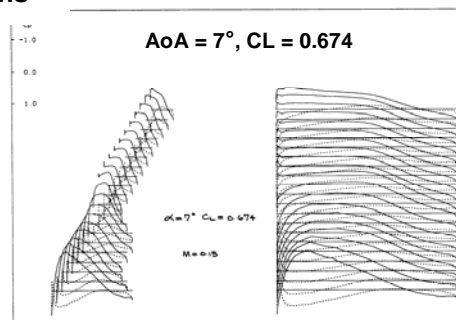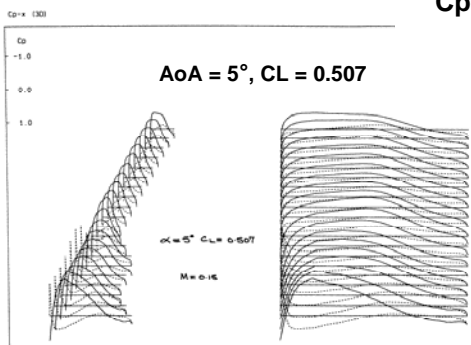
FIG. 7.2.6 DC AR 9.85 DESIGNED (LAMINAR FLOW TO CL 0.8, Mach 0.6)
CHARACTERISTICS, Mach 0.15
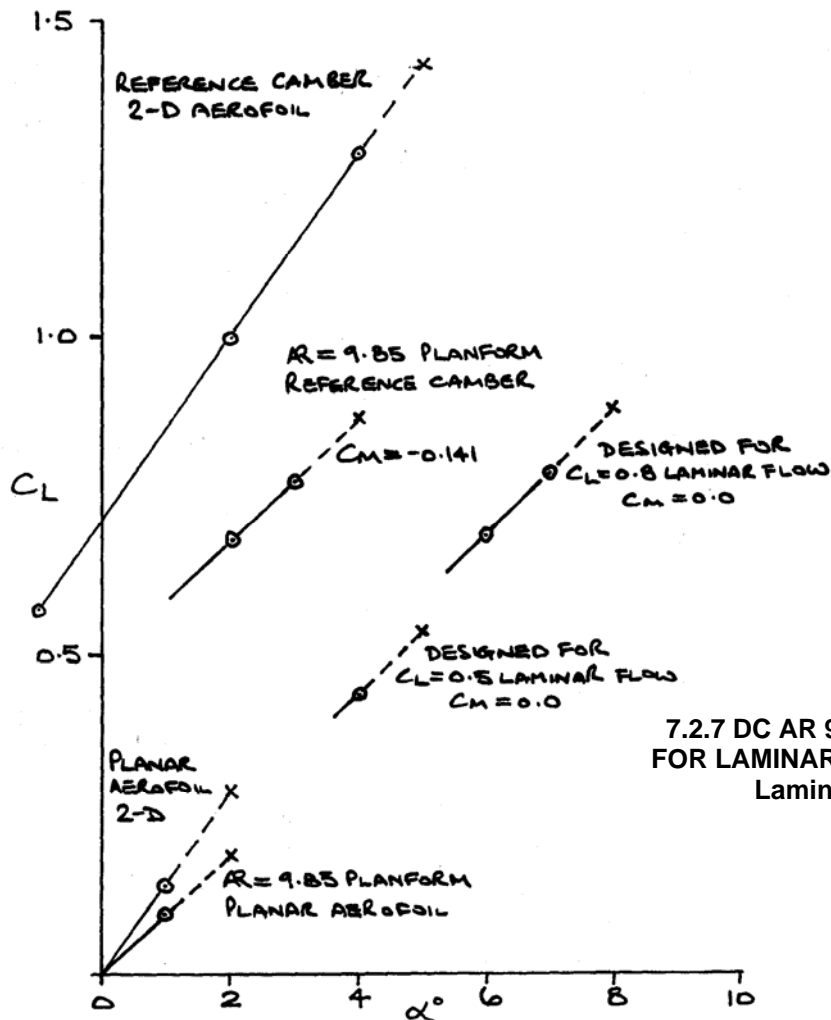
7.2.7 DC AR 9.85, SUMMARY OF DESIGNS
FOR LAMINAR FLOW CL RANGES, Mach 0.6
Laminar up to CL = 0.5 & 0.8
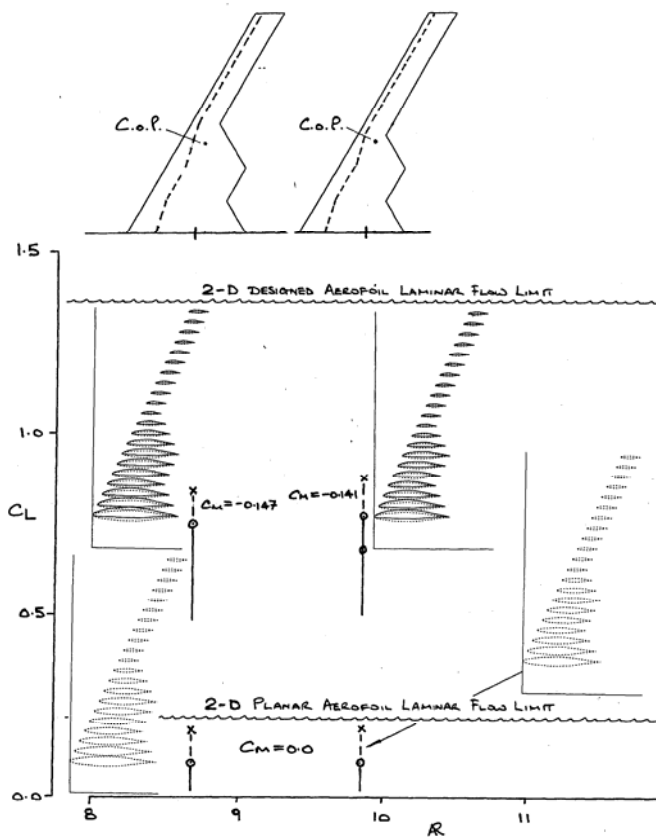
FIG. 7.3.1 DC WINGS SUMMARY
PLANAR & REFERENCE CAMBER,
Mach 0.6, No Cm control
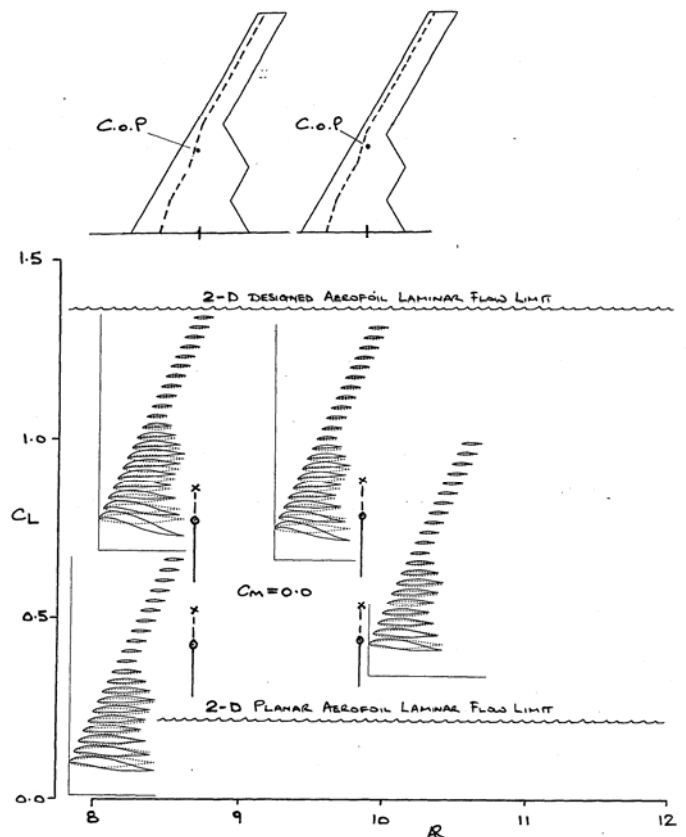
FIG. 7.3.2 DC WINGS SUMMARY
DESIGNED FOR LAMINAR FLOW UP TO
CL 0.5 & 0.8, Mach 0.6, Cm controlled

59
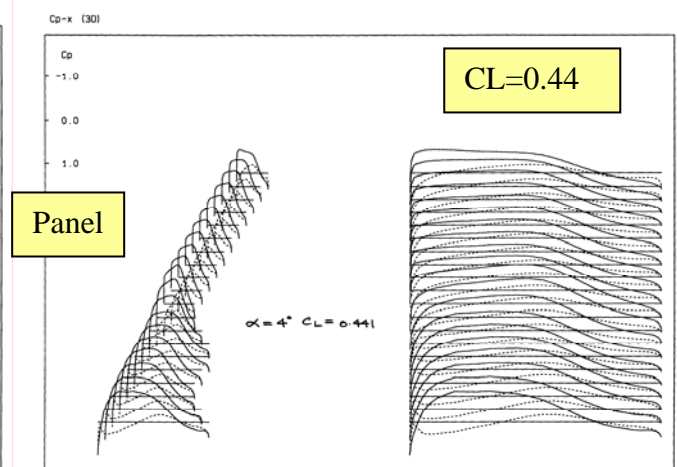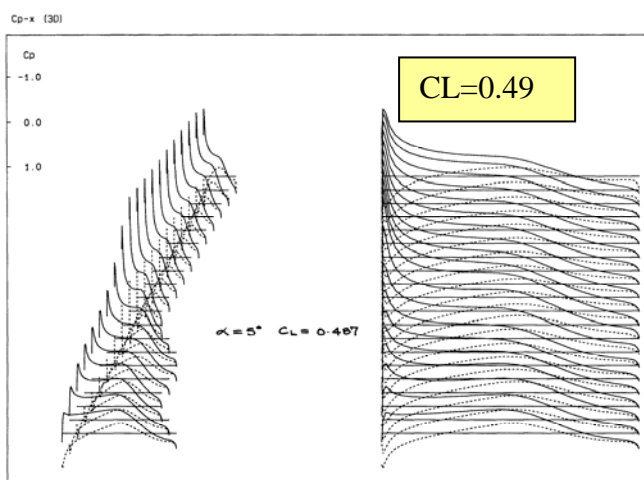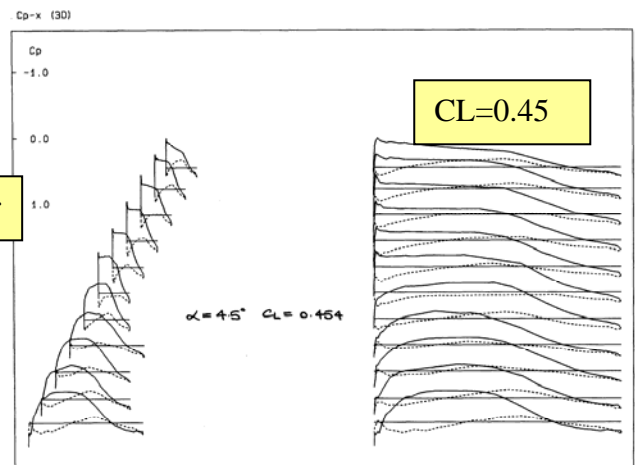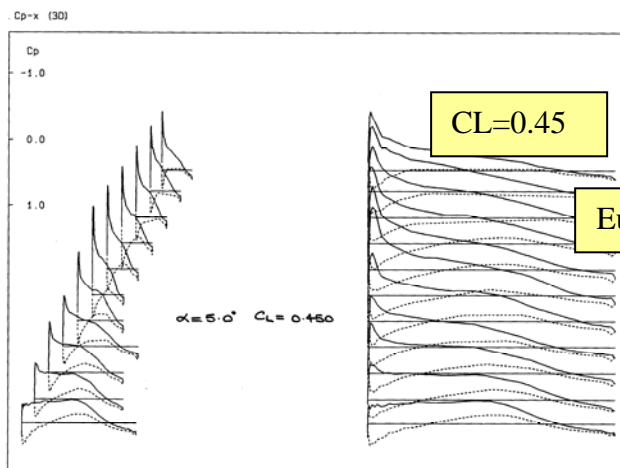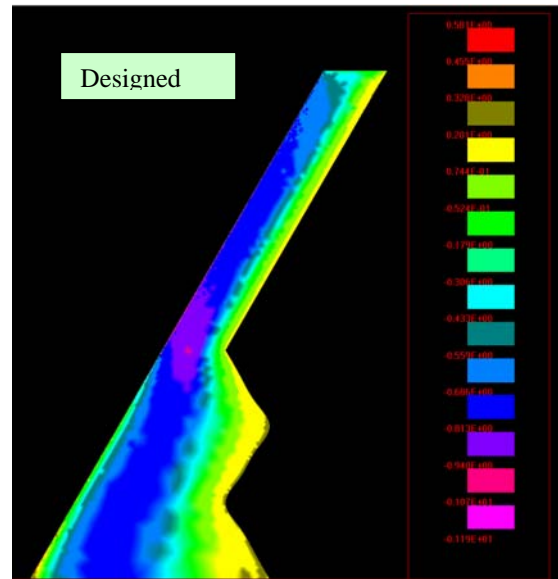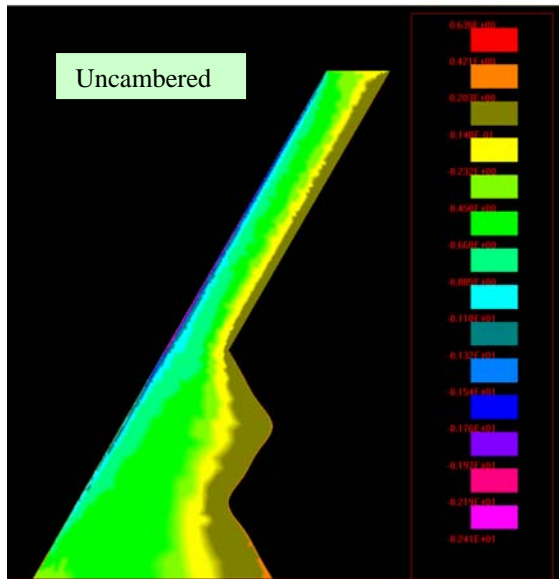
FIG. 7.4.1 COMPARING UNCAMBERED & DESIGNED (C_L 0.5) CAMBERED AEROFOIL CONFIGURATION, Cp ISOBARS & DISTRIBUTIONS AT NEARLY EQUIVALENT CL, EULER & Panel, Mach 0.6
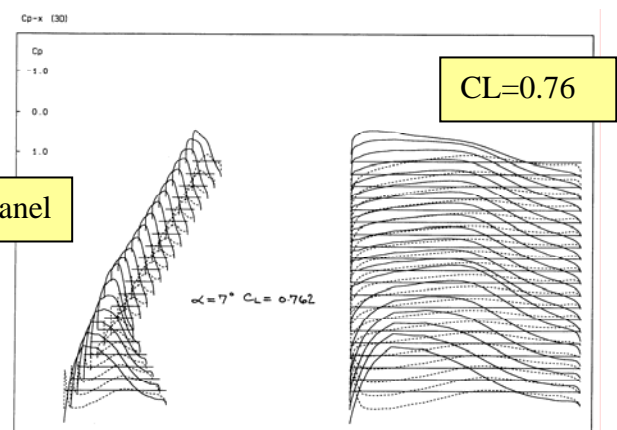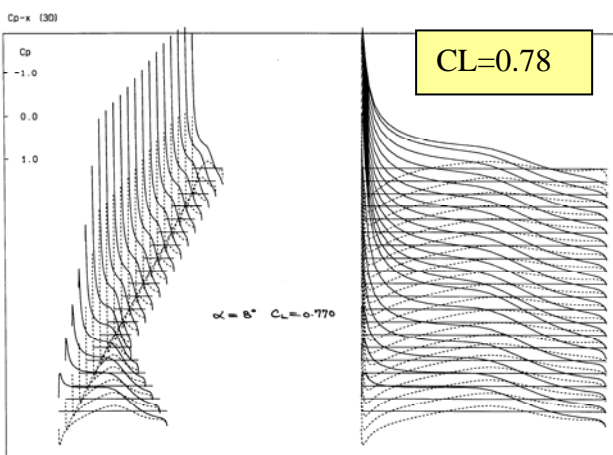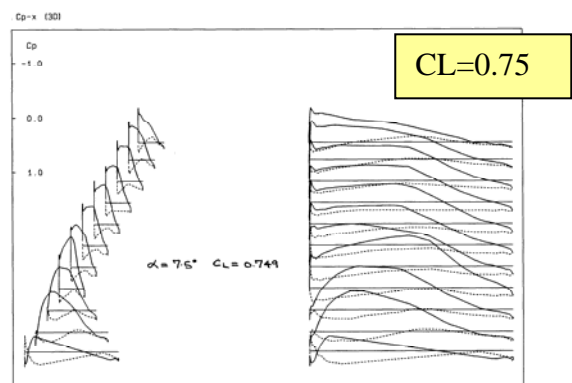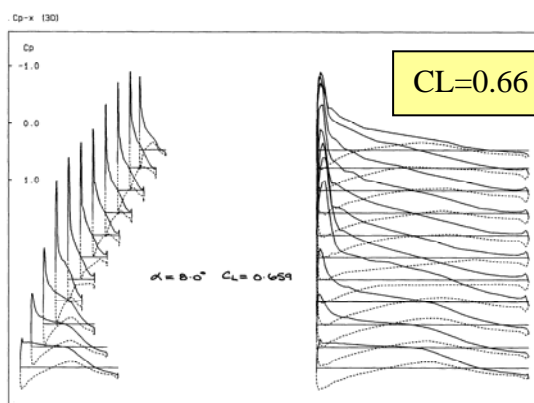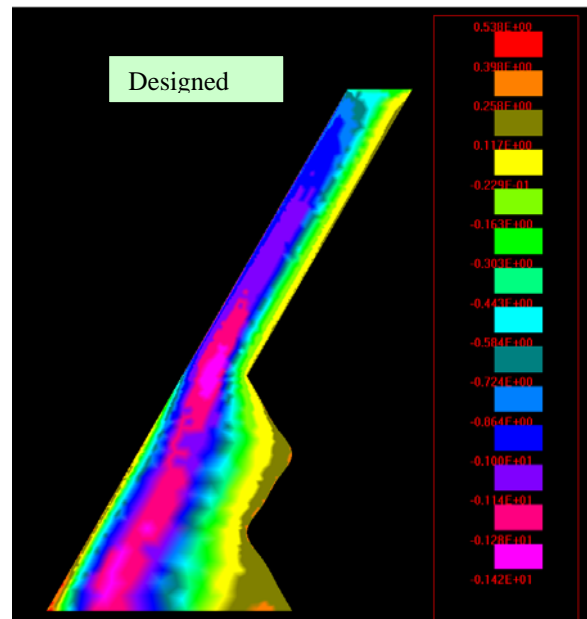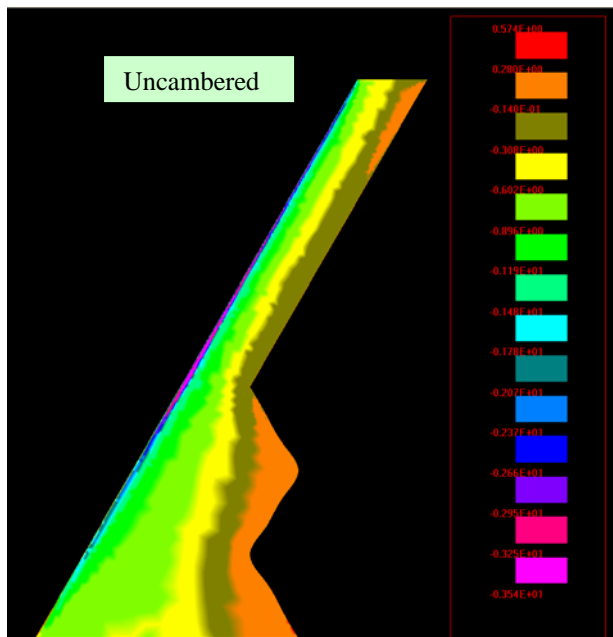
FIG. 7.4.2 COMPARING UNCAMBERED & DESIGNED (C_L 0.8) CAMBERED AEROFOIL CONFIGURATION, Cp ISOBARS & DISTRIBUTIONS AT NEARLY EQUIVALENT CL, EULER & Panel, Mach 0.6
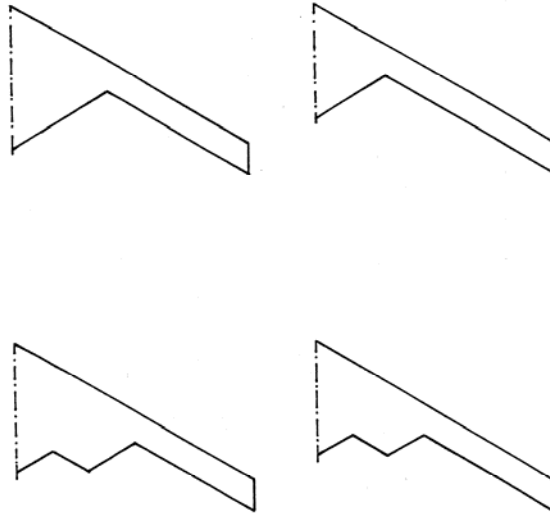
FIG. 8.1 SINGLE & DOUBLE LAMBDA WING PLANFORMS
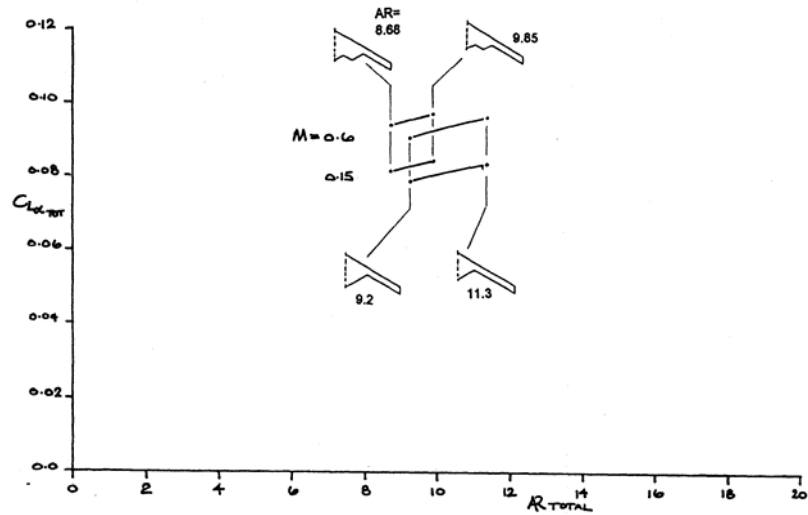
FIG. 8.2 CLα VARIATION WITH AR, LAMBDA WING CASES, M = 0.6 & 0.15
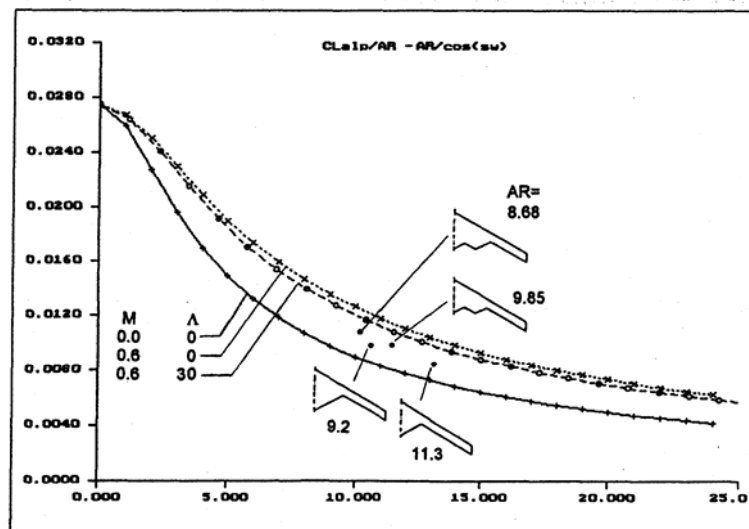
**FIG. 8.3 CLα/AR VARIATION WITH AR/cos(Λ), THEORETICAL EFFECT OF M & Λ,
LAMBDA WING CASES M = 0.6**
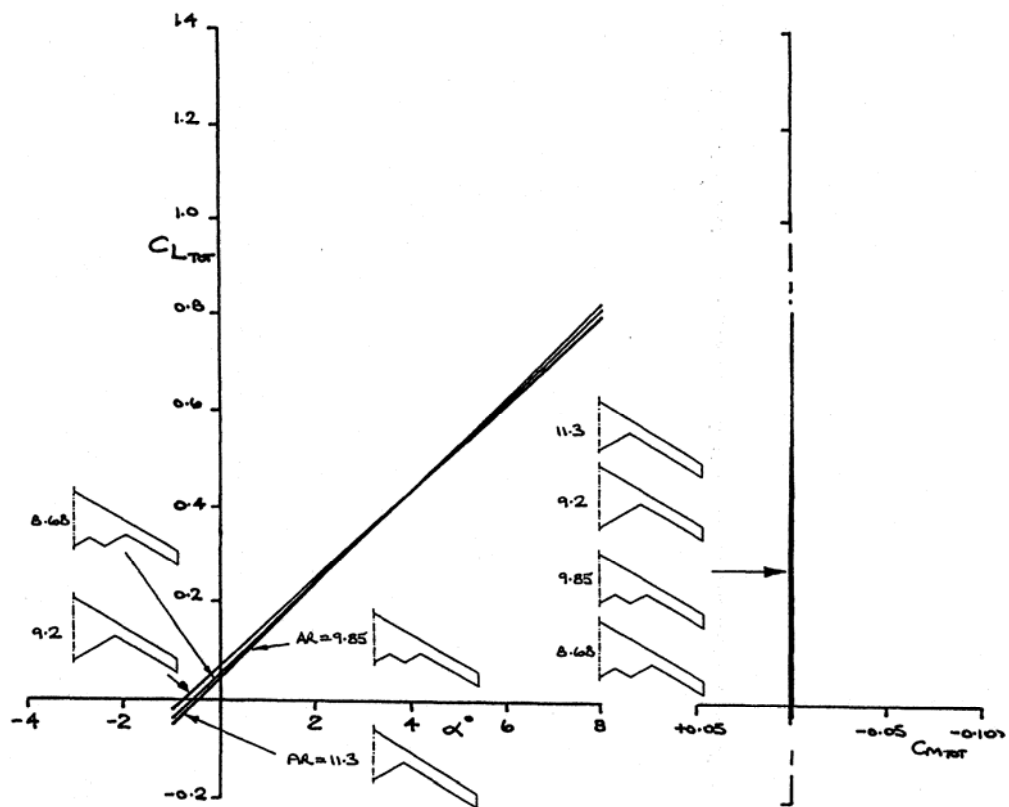
FIG. 8.4 TOTAL LOADS (C_L - α, C_m – C_L), M = 0.6 COMPARISON FOR LAMBDA-WING CASES
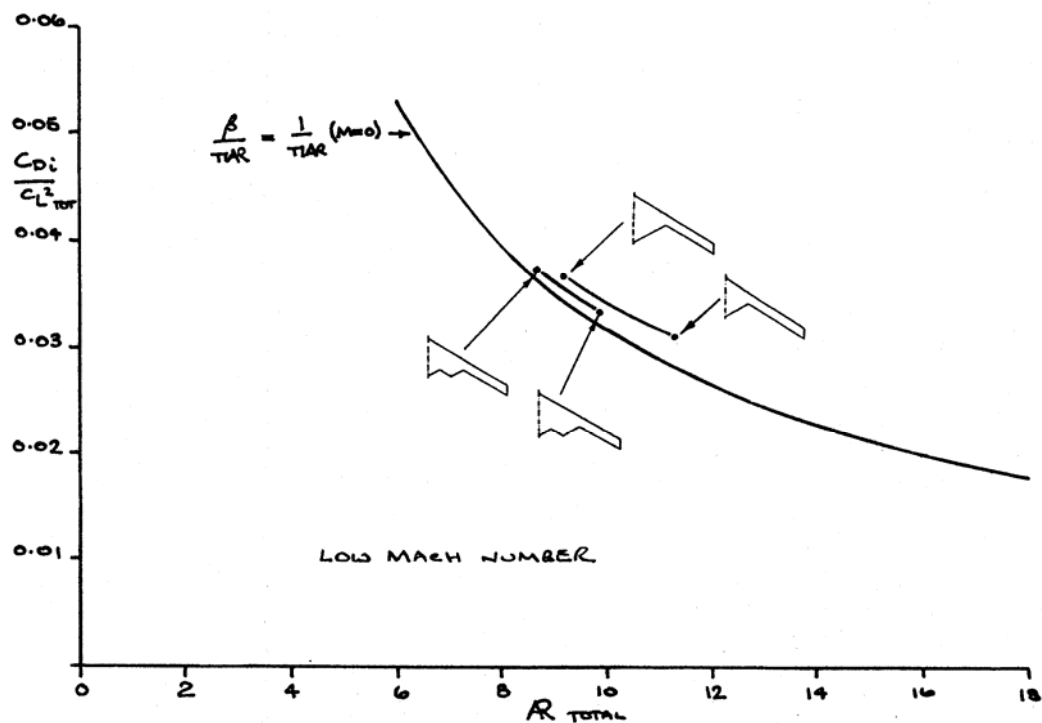
FIG. 8.5 INDUCED DRAG FACTOR VARIATION WITH AR, UNCAMBERED WINGS, LOW M COMPARISON FOR LAMBDA WING CASES

63
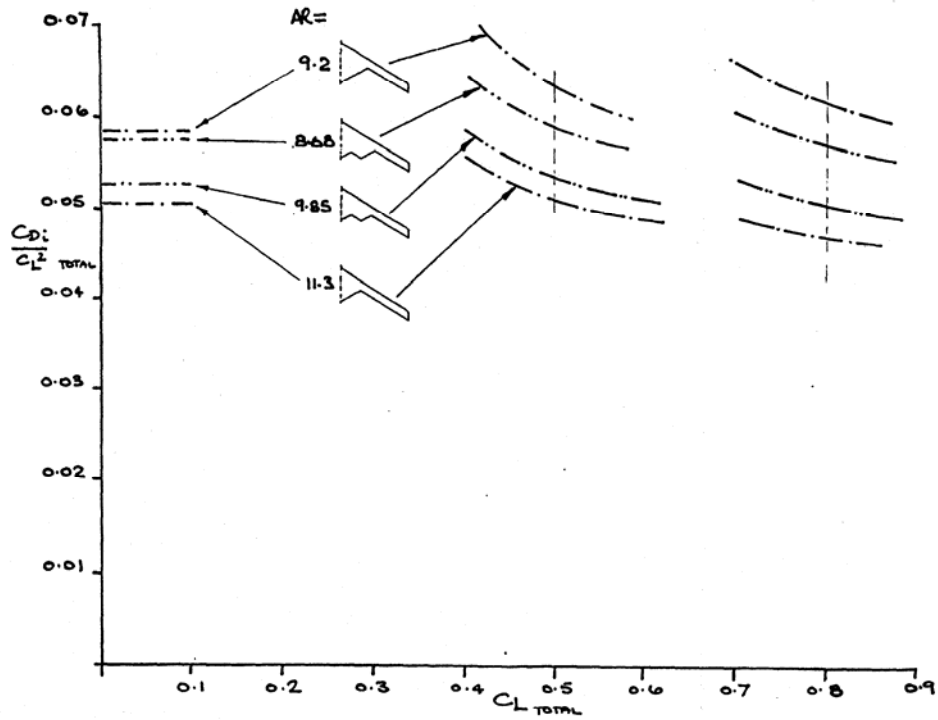
FIG. 8.6 INDUCED DRAG FACTOR VARIATION WITH CL, DESIGNED WINGS, $C_m = 0$, M = 0.6 COMPARISON FOR LAMBDA WING CASES
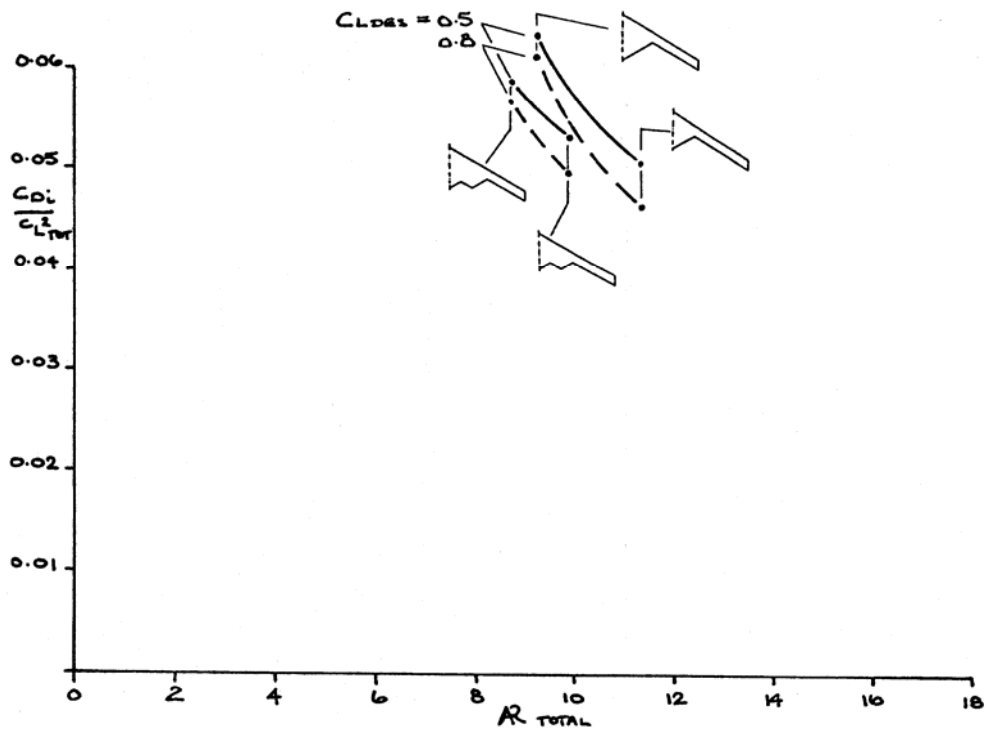
FIG. 8.7 INDUCED DRAG FACTOR VARIATION WITH AR, DESIGNED WINGS, $C_m = 0$, M = 0.6 COMPARISON FOR LAMBDA WING CASES
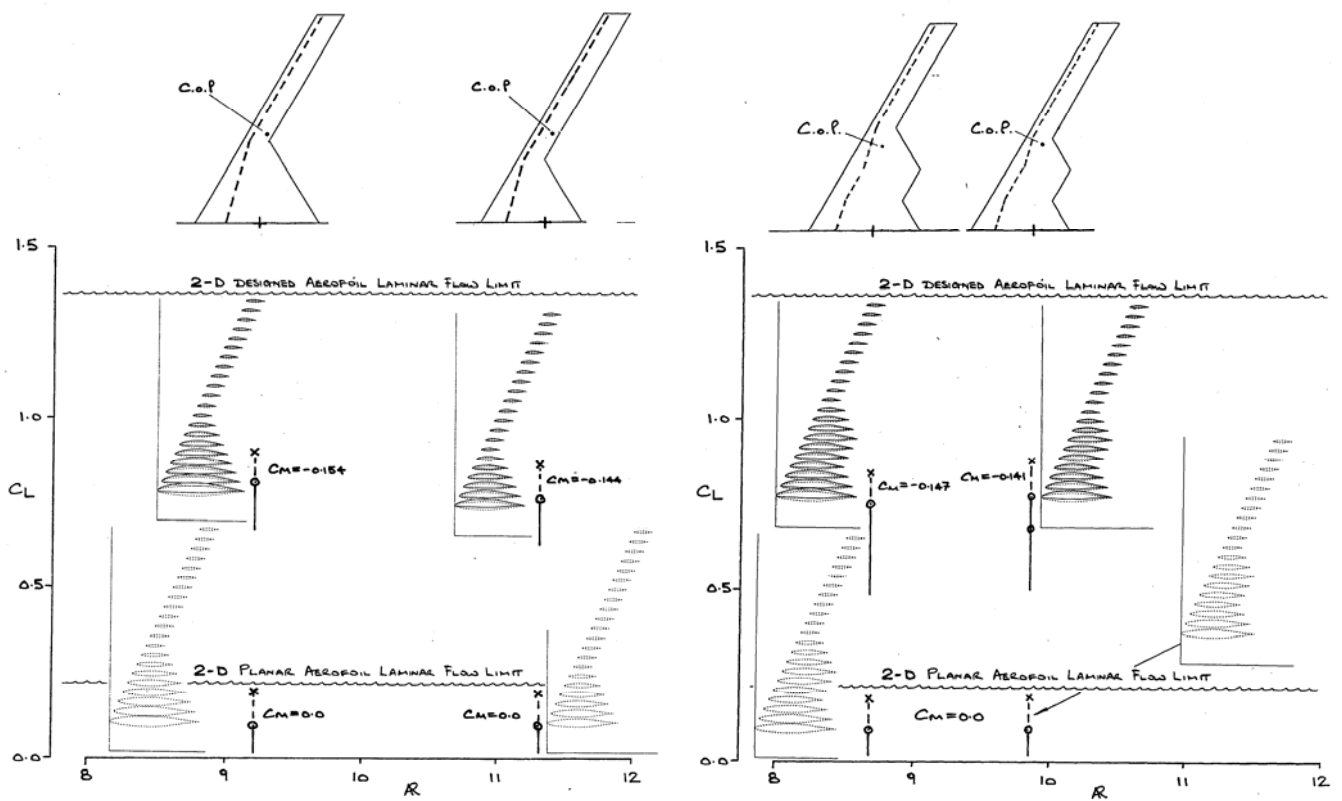
FIG. 8.8 UNCAMBERED LAMBDA WINGS, EXTENT OF LAMINAR FLOW, M = 0.6
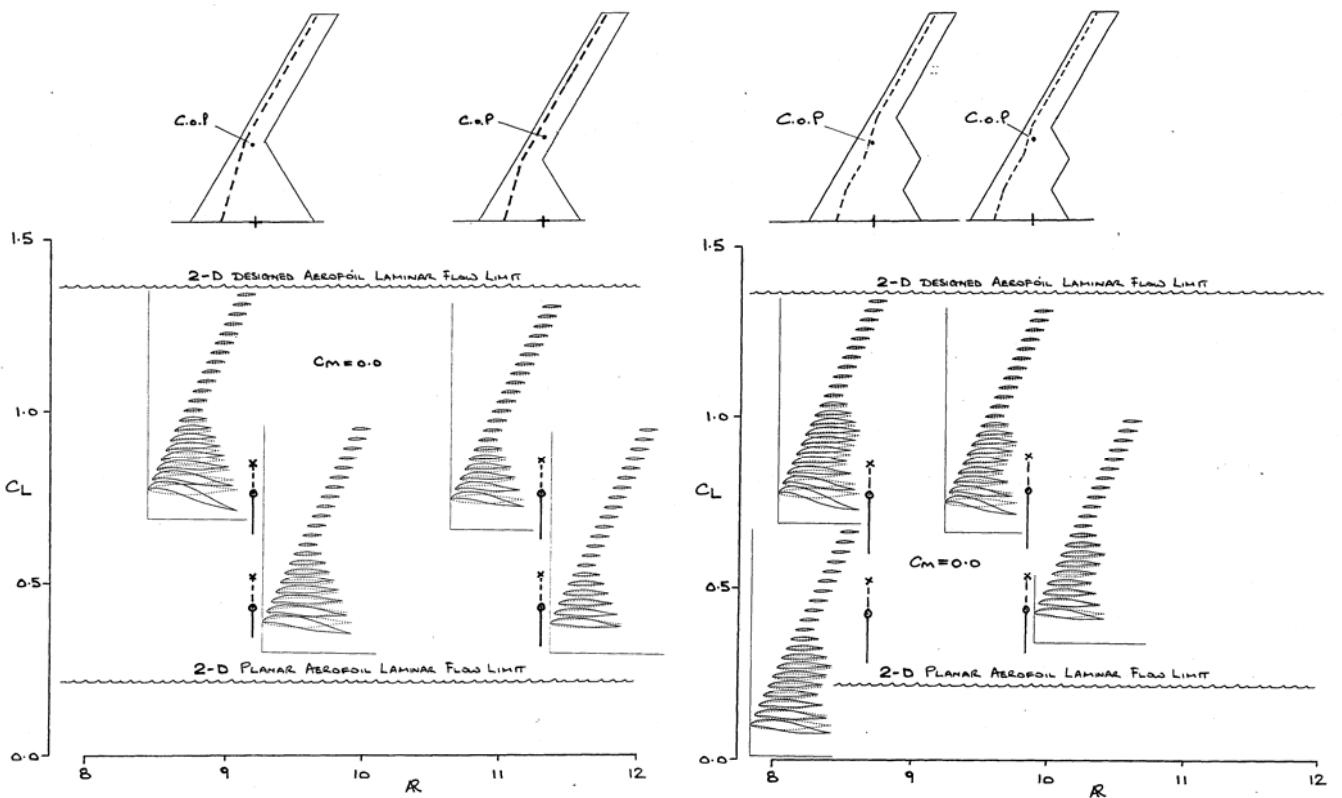
FIG. 8.9 DESIGNED LAMBDA WINGS, EXTENT OF LAMINAR FLOW, M = 0.6

65
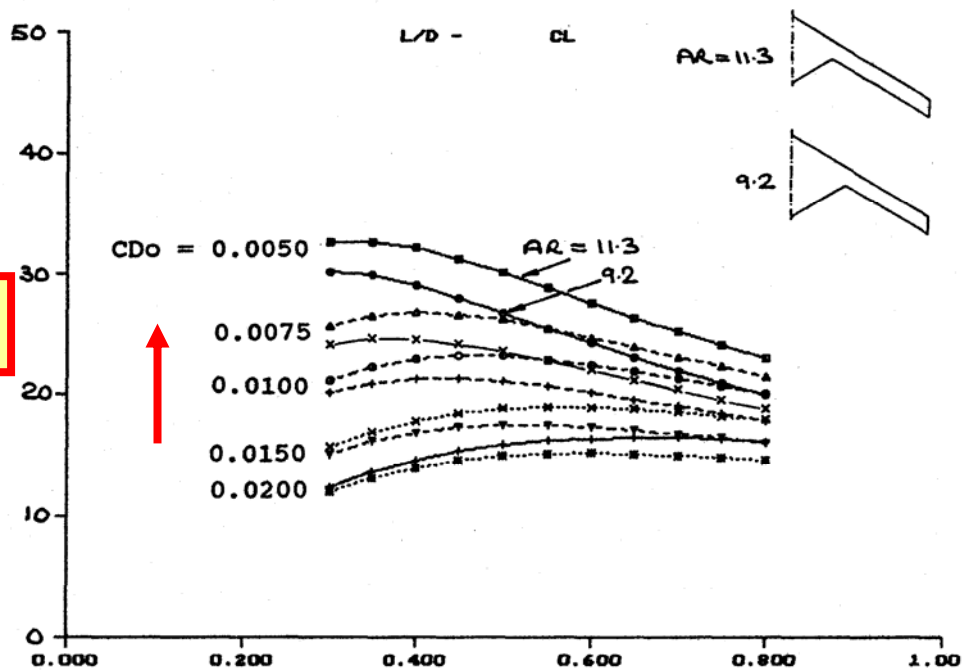
FIG. 8.10 L/D VARIATION WITH C_L, DESIGNED SINGLE LAMBDA-WINGS, M = 0.6, C_{Do} VARIES
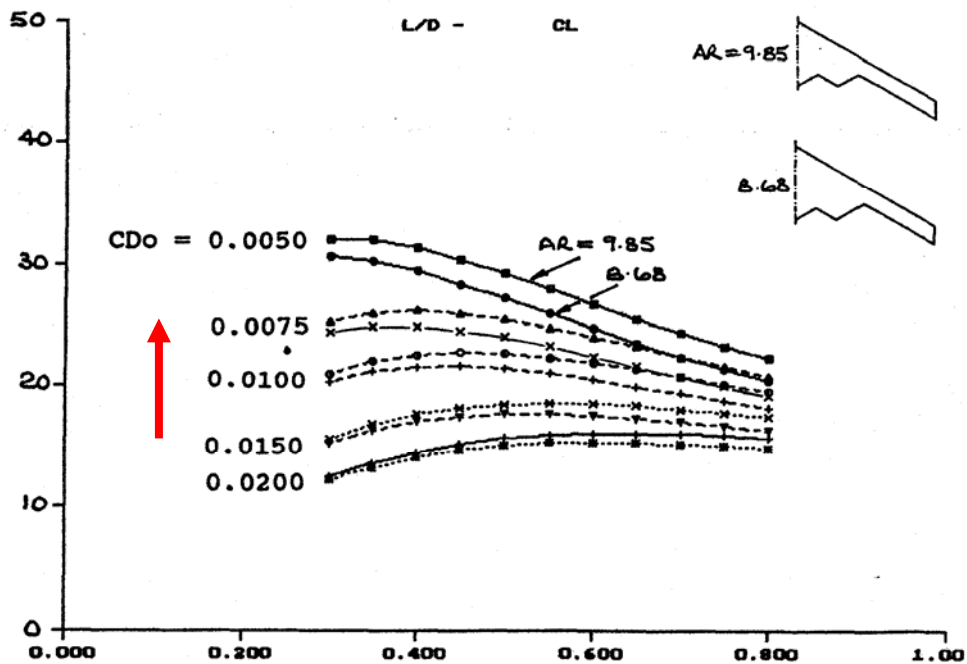
FIG. 8.11 L/D VARIATION WITH C_L, DESIGNED DOUBLE LAMBDA-WINGS, M = 0.6, C_{Do} VARIES
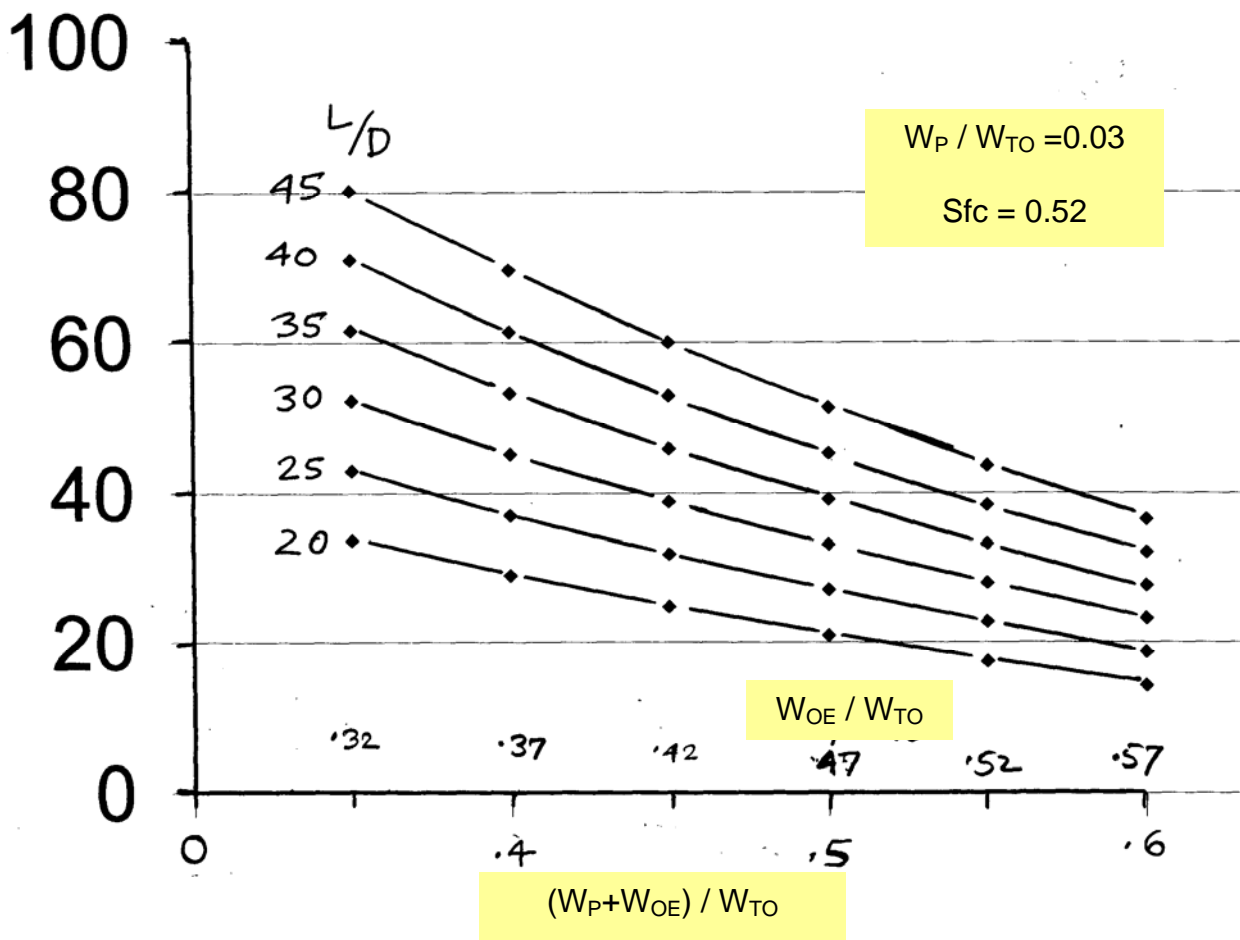
FIG. 8.12 ENDURANCE (HOURS) VARIATION WITH WEIGHT RATIOS, CONSTANT L/D VALUES, M = 0.6

TOWARDS DESIGN OF LONG-RANGE SUPERSONIC MILITARY AIRCRAFT

Dr. R. K. Nangia

SUMMARY

A component of future defence infra-structure to deal with world conflicts brings into consideration supersonic strike aircraft. These need to be capable of high speed cruise over long ranges. After deriving a series of basic relationships based on current supersonic trends, this report compares "cranked delta" layouts that may provide viable options. "Large" and "small" strike aircraft configurations are considered, 400,000 lb MTOW class with 50,000 lb payload and 250,000 lb MTOW class with 20,000 lb payload respectively. A feature of the approach is that we can see various parametric influences maximising the design range and payload capabilities. Further improvements in L/D may be gained using appropriate flow control. This type of analysis highlights the various technologies that need to be "pushed". Avenues for further work are indicated.

This report is Part 6 of a series of six relating to high AR, long endurance surveillance aircraft, laminar flow, integrated intakes and long range supersonic military aircraft.

Consulting Engineers
Nangia Aero Research Associates
WestPoint, 78 Queens Road, Clifton
Bristol BS8 1QX, UK

The Investigation which is the subject of this report was initiated by
USAF - EOARD, 223/231 Old Marylebone Road, London, NW1 5TH, UK
and was carried out under the terms of Contract SPC-024051

DISTRIBUTION LIST

1	Mr. W. Donaldson	USAF-EOARD, London NW1 5TH, UK
1	Mr. C. Remillard	Chief, AFRL/VAAA; Bldg 45
		2130 8th Street, WPAFB, Ohio, USA 45433-7542
1	Mr. D. Multhopp	Technical Area Lead, AFRL/VAAA; Bldg 45
		2130 8th Street, WPAFB, Ohio, USA 45433-7542
2	Dr. C. P. Tilmann	Sr. Aerospace Engineer, AFRL/VAAA; Bldg 45
		2130 8th Street, WPAFB, Ohio, USA 45433-7542
1	Mr. William Fields	Tech Area Lead, AFRL/VAAA; Bldg 45
		2130 8th Street, WPAFB, Ohio, USA 45433-7542
1	Dr. K. P. Iwanski	Aerospace Engineer, AFRL/VAAA; Bldg 45
		2130 8th Street, WPAFB, Ohio, USA 45433-7542
1	Mr. Larry Leavitt	Head, Configuration Aerodynamics Branch
		NASA Langley Research Center, Mail Stop 499
		Hampton, VA 23681-2199
1	Dr. James Luckring	Configuration Aerodynamics Branch
		NASA Langley Research Center, Mail Stop 286
		Hampton, VA 23681-2199
1	Mr. John Perdzock	Head, SensorCraft Integrating Concept Office, AFRL/VAC; Bldg 45
		2130 8th Street, WPAFB, Ohio, USA 45433-7542
1	Dr. Maxwell Blair	AFRL/VASD; Bldg 146
		2210 Eighth Street
		Wright-Patterson AFB OH 45433-7531
1	Dr. Keith Numbers	AFRL/VAA, Long Range Strike Integrating Concept Office
1	Mr. D. Adamczak	Sr. Aerospace Engineer, AFRL/VAAA; Bldg 45
		2130 8th Street, WPAFB, Ohio, USA 45433-7542
1	Dr. Michael OL	Research Engineer, AFRL/VAAA Bldg 45
		2130 8th Street, WPAFB, Ohio, USA 45433-7542
1	Mr. R.M. Wood	NASA Langley Research Center, Mail Stop 499
		Hampton, VA 23681-2199
2	Dr. R.K. Nangia	Nangia Aero Research Associates
		WestPoint, 78-Queens Road, Clifton
		BRISTOL BS8 1QX, UK.

CONTRACTUAL DECLARATIONS

"The Contractor, Dr. R. K. Nangia,, hereby delcares that, to the best of its knowledge and belief, the technical data delivered herewith under Contract No.SPC-024051 is complete, accurate, and complies with all requirements of the contract.

DATE: **March 2004**   **Name and Title of Authorized Official:**   **Dr R K Nangia**

"I certify that there were no subject inventions to declare as defined in FAR 52.227-13, during the performance of this contract."

DATE: **March 2004**   **Name and Title of Authorized Official:**   **Dr R K Nangia**

CONTENTS

SUMMARY

DISTRIBUTION LIST

CONTRACTURAL DECLARATIONS

CONTENTS

1. INTRODUCTION & BACKGROUND

The work discussed in this report relates specifically to long range supersonic military aircraft. This report is Part 6 of a series of six, Refs.1 to 6, relating to high AR, long endurance surveillance aircraft, laminar flow, integrated intakes and long range supersonic military aircraft. This work follows previous work funded by USAF-EOARD under seeding Contract SPC-01-4087 which was reported in Ref.7.

Currently there is interest in Long-range Supersonic strike Aircraft as a component of a future defence infra-structure to deal with the World conflicts. The need for such aircraft (manned or unmanned) has been identified in several studies undertaken at the AFRL and DARPA, e.g. Refs.8-10. The key attributes are Inter-continental range, responsiveness, survivability and flexibility in terms of multi-targets, **Fig.1.1**.

Several candidate aircraft and propulsion configurations conventional and unconventional, are being considered to determine the best trade-off between long endurance, altitude, engine efficiency, and power generation. Additionally, recent R & D on flow control, **Fig.1.2**, needs to be included in future studies (Refs.11-12). **Fig.1.3** illustrates the status and the projected goals for future supersonic aircraft (based on DARPA initiatives) in terms efficiency (L/D). In general, larger aircraft achieve a higher L/D because of higher Reynolds number, but the square-cube law may negate the overall performance benefits.

Based on such interest it appears reasonable to study long-range military supersonic aircraft now, for operation in 10-15 years time frame.

The approach followed here is to start from known information on Supersonic cruise vehicles, derive a basis for the main parameters for supersonics and then adapt them towards military applications, bearing in mind the characteristic differences, the main one being that one does not have to allow for passenger related details. This implies a more slender and perhaps lighter OEW structure for the military vehicle. However survivability obviously plays a greater role in dictating the design attributes.

2. SUPERSONIC AIRCRAFT OBSERVATIONS, TRENDS, CRANKED DELTAS & OTHER PLANFORMS

Assessing historical aircraft, **Fig2.1** shows a host of "long-range" supersonic configurations (civil and military) including the most recent studies of the US HSCT. Some of the aircraft designs were taken beyond project stage and continue to be successful.

A classification based upon slenderness parameter (semi-span/length, s/l) versus Mach number is shown in **Fig.2.2** for subsonic, supersonic and hypersonic aircraft throughout the speed regime (Ref.13). Note that slenderness parameter reduces as cruise Mach number increases.

Fig.2.3 considers design issues and challenges for supersonic aircraft, see Ref.13. Using variable geometry, an aircraft can obviously "transcend" across the classes. This discussion is supported by the following figures.

Typical SST weight breakdown on Concorde and the derivatives is shown in **Fig.2.4**. Using current technology (fly-by-wire, improved materials and structures, more efficient engines, etc.), the overall weight of a "derived Concorde" could be reduced and the range increased. The payload fraction would increase from 5 - 6% to near 8%. Further, a scaling to 250-seater, 760 Klb aircraft is shown.

An example of fuel usage and weight breakdown for a SST over a range of 5,500nm is shown in **Fig.2.5** (Ref.14). It is interesting to note that a quarter of the fuel (26%) is burnt in climb-out / acceleration in reaching a Mach 2 cruise speed at 55,000 ft.

Fig.2.6 (based on Ref.14) emphasizes the drag breakdown for a SST. Extreme care needs to be exercised in interpretation of C_{Do}. The correction required from model tests to flight is large and its impact on aircraft fuel burnt is of the same order as the payload. Further detail is in Ref.14. Reduction of C_{Do} is literally the challenge for supersonic flight. Skin friction drag of the wing contributes to 35% of C_{Do} , while the fuselage skin friction contributes 15% of C_{Do}. For the future, this emphasises the need for laminar flow control, passive or active.

Fig.2.7 shows a possible military mission. We would obviously like to quantify the configuration related parameters e.g. C_L, best altitude etc. within practical and feasible limits of current, state of the art, and future technology. The military mission shows in-flight delivery/release of the "payload" but we have to cater for the fail-safe or aborted mission when the payload may not be released.

3. PERFORMANCE, RANGE, WEIGHT, PAYLOAD, FUEL CONSIDERATIONS

Enabling Basic Work, Starting from 28,000 lb Payload Aircraft

We shall take the Concorde Technology and see if its efficiency Rp or L/D can be improved in steps of 10% to 50%. In this way, we can get a feel for relationships and derive a "modern" 20000 - 28000 lb payload aircraft possibly of longer range.

We use the Breguet Range Equation (e.g. Ref.15) for Design range R:

R = Rp * log(W1/W2)

   Rp = (L/D*V/sfc) is the Range parameter

   W1 Initial Mass, W2 Final Mass = W1 – WF, WF relates to Fuel

   R is ESAR (Equivalent Still Air range) = Typically 568+1.06*Design Range (based on Jenkinson. Can be adapted for supersonic cruise)

   WF / MTOW = 1 - W2/W1

   MTOW = Wpay + Woe + WF

   MTOW = WF/(1-(Woe - WF)/MTOW)

Fig.3.1 shows the sfc trends with Mach no (Lowrie, Ref.16).

In this way, we can get a feel for the relationships needed to derive a "modern" 28000 lb payload aircraft or lead towards 50,000 lb payload aircraft of different range.

Derived trends for weight and range are shown in **Fig.3.2**. Parameters plotted against Design Range are: Wp/MTOW, MTOW and work Efficiency Wp*Range/Wfuel. With increasing range, Payload proportion drops and MTOW increases (sharply). There is always an efficiency penalty for supersonic flight c.f. subsonic aircraft of the same payload and range capability. The penalty decreases as range reduces.

Some further benefits will arise because a military aircraft fuselage is relatively "slender" or is integrated as a wing+body. Further work is needed with lower TSFC assumptions, based on improving technologies.

Such graphs have given an idea of the benchmarks and demonstrate the likely improvements with future technologies. We now need to see if suitable aerodynamic performance can be derived.

4. PREDICTION METHODS & CONFIGURATION PLANFORMS

On "novel" designs, the experience is that the complexities often "defy" the confident use of an automatic "hands-off" design process, which may offer more than one solution. Therefore, we have chosen a staged process, allowing a significant understanding with reasonable manual control over the design process.

Linear theory, Panel and Euler codes are available to enable assessment of the aerodynamic performance over the range of low to high speeds. The camber and twist design, under forces and moments constraints, is via previously validated attained suction design methods (e.g. Refs.17-20, 23-25). The Euler method has been utilised in checking the validity of the linear theory codes.

4.1. Prediction Methods

The aerodynamic prediction methods are described in an order of complexity.

Linear Theory & Attained Thrust Methods

The linear lifting surface theories have been around for 3 or 4 decades. Various formulations in terms of vortex lattice and doublet lattice exist. Methods have been used in subsonic and supersonic linearized flows. Several design approaches for minimizing drag for given lift also exist. Useful Text books are e.g. by Bertin & Smith, "Aerodynamics for Engineers", and McCormick, "Aerodynamics, Aeronautics & Flight mechanics".

A more recent development over last 2 decades has been the incorporation of attained thrust principles in linear theories. The attained thrust method uses empirical correlations of onset flow and aerofoil parameters (along the span of the wing) to establish the proportion of thrust recovered on the wing leading edges. Such methods were pioneered by Carlson et al at NASA Langley. Computer programmes such as WDES are available in USA. The codes also have a camber design facility (using polynomial type modes). We have developed our own codes based on principles similar to those used by Carlson.

Euler Codes

Euler codes have become well established over the last 20 years. These are based on the Euler approximation (i.e. ignoring viscosity terms) of the full Navier-Stokes flow equations. The compressibility effects allow shock formation. Many text-books deal with the theoretical and numerical aspects (e.g. finite-difference, finite-volume and finite element). To apply the methods, surface and volume grids are both needed. The grids can be either structured or unstructured (triangles & pyramids). These are therefore more expensive in grid formation and cpu usage (cf. panel codes). We have used the finite element Euler method of Ref.26 as needed for "final" checks on the designed geometries.

Further refinement can be introduced by using an inverse design method such as using 3-D membrane analogy technique. (Ref.27). This can enable "tailoring" and "fine-tuning" of aerofoil shapes for "optimum" C_P distributions as needed, especially when fuselages and intakes are to be integrated. It enables a "known" loading (target) to be "supplanted" (within reason and small tolerances) onto a general planform wing. Aerofoil geometry, camber and twist are calculated simultaneously by iteration. Suitable targets can be arranged e.g. we can impose a loading created on rectangular unswept wing as the "target" for a delta-wing.

4.2. Military Aircraft Planforms For Supersonic Aircraft

A couple of possibly suitable planforms SR301 and SR401 are shown in relation to other supersonic aircraft planforms in **Fig.4.1**. With a view to achieving adequate subsonic performance criteria, the nominal W/S loadings of these relatively "slender" wings have been intentionally kept somewhat lower c.f, other planforms.

In this Report we examine the "cranked delta wing" planforms SR401 and SR301. Configuration SR401 has a notional MTOW of 250,000 lb (W/S 67) and a payload of 20,000 lb, Ref.13, and is discussed in Section 5. Planform SR301 is aimed at an aircraft with a notional MTOW of about 400,000 lb (W/S 54) and a payload of 49,000 lb, Section 6.

5. SR401 (Smaller Strike Aircraft)

We discuss first the SR401 planform aimed at an aircraft with a notional MTOW of 250,000 lb, W/S = 67 and a payload of 20,000 lb. The designed wing (neutral stability) for Mach 2 and its predicted aerodynamic characteristics (forces, moments and spanwise loadings) are shown in **Fig.5.1**.

For the wing at this design point, **Fig.5.2** shows the characteristics through the Mach number range using linear theory results. Verification of selected (key) points is with Euler. It is recognised that the performance parameter most difficult to predict in the early design stages is supersonic L/D. Estimates suggest that it is of the order 8.5 at Mach 2, close to the projected trends of **Fig.1.3**. It is however, interesting to understand the parametric effects of L/D. We will therefore take a range of values (8.0 to 9.0) at Mach 2.0.

Fig.5.3 shows the preliminary estimates of MTOW against Range using the Breguet Range formulae. We vary combinations of L/D (8.0, 8.5 & 9.0) and sfc (1.2 & 1.25). Also shown are WOE, Wfuel (total & consumed) and Wp. In deriving the graphs, the empty weight fraction WOE/MTOW has been allowed to vary as a function of MTOW (Ref.8) but biased towards MTOW weight of 250,000 lb aircraft. With MTOW increasing, the empty weight factor reduces slightly. The payload is kept at 20,000 lb.

The estimated MTOW and WOE trends are summarised in **Fig.5.4**. We note that an aircraft of 250,000 lbs will have a range of about 4500 nm assuming L/D of 9.0 and sfc of 1.2. These results are considered tentative but enable a way forward for further detail optimisation.

Fig.5.5 shows the low-speed performance assuming attached flow over the wing using suitable LE and TE devices. Ground effect will be favourable but has not been included. We have given a chart assuming an appropriate value of C_{Do}. The main inference is that limiting the AoA to 12° or 14°, the take-off Mach number is 0.39 or 0.36. This suggests that to operate with the SR401 planform, we will need to design-in vortex-lift at the expense of L/D much in the same manner as Concorde has always done. **Fig.5.6** shows the trends assuming vortex lift is present. Essentially we can get 15 to 20% more (non-linear) lift at 12° and 14°. This corresponds to take-off at Mach 0.35 and 0.33. Intrinsically this is a safer and manageable situation although more engine thrust is required because of lower L/D.

To generalise the sizing aspect (W/S) further, **Fig.5.7** has been derived. This shows Low-Speed (Take-off or Landing) Mach number plotted against Range achieved for different wing loadings and Rp variations (for Mach 2, L/D and sfc variations). Such a graph is obviously highly dependent on planform and is indicative of several avenues for future work to improve performance i.e. reduce the take-off speed and extend the range. For example, we may need to change or revise the planform to increase the subsonic lift-curve slope without penalising the supersonics. Incorporation of limited variable geometry in the configuration could be useful. An alternative would be to exploit flow control to enhance L/D. Reducing sfc would, of course, help greatly.

6. SR301 (Larger Strike Aircraft)

We now discuss the SR301 planform aimed at an aircraft with a notional MTOW of 400,000 lb, W/S = 54 and a payload of 49,000 lb. The designed wing (neutral stability) for Mach 2 and its predicted aerodynamic characteristics (forces, moments and spanwise loadings) are in **Fig.6.1**.

For the wing at this design point, **Fig.6.2** shows the characteristics through the Mach number range using results from linear theory. Verification of selected (key) points is with Euler. As before, the difficulty of predicting supersonic L/D is noted. Estimates suggest that it is of the order 8.0 at Mach 2 close to projected trends of **Fig.1.3**. We need to understand the parametric effects of L/D and for this planform have taken a range of values (7.5 to 9.0) at Mach 2.0.

Fig.6.3 shows the preliminary estimates of MTOW against Range using the Breguet Range formulae. We vary combinations of L/D (7.5, 8.0, 8.5 & 9.0) and sfc (1.2 & 1.25). Also shown are WOE, Wfuel (total & consumed) and Wp. In deriving the graphs, the empty weight fraction WOE/MTOW has been allowed to vary as function of MTOW (Ref.8) but biased towards MTOW weight of 392,000 lb aircraft. With MTOW increasing, the empty weight factor reduces slightly. The payload is kept at 48,760 lb.

The estimated MTOW and WOE trends are summarised in **Fig.6.4**. We note that an aircraft of 392,000 lbs will have a range of about 5500 nm assuming L/D of 9.0 and sfc of 1.2. These results are considered tentative but enable a way forward for further detail optimisation. It is interesting to compare with similar results for SR401 planform based on **Fig.5.4** as depicted in **Fig.6.5**. It is inferred that the heavier SR 301 offers a better payload and range capability.

Fig.6.6(a-b) shows the low-speed performance assuming two flow situations, without or with vortex lift. **Fig.6.6(a)** assumes attached flow over the wing using suitable LE and TE devices. Ground effect will be favourable but has not been included. We have given a chart assuming an appropriate value of C_{Do}. The main inference is that limiting the AoA to 12° or 14°, the take-off Mach number is 0.32 or 0.29. This suggests that to operate with the SR301 planform, we will need to design-in vortex-lift at the expense of L/D much in the same manner as Concorde has always done. **Fig.6.6(b)** shows the trends with vortex lift present. Again, we can get 15 to 20% more (non-linear) lift at AoA 12° and 14°. This corresponds to take-off at Mach 0.30 and 0.27. Intrinsically this is a safer and manageable situation although more engine thrust is required (because of lower L/D available with vortex lift).

To generalise the sizing aspect (W/S) further, **Fig.6.7** has been derived. This shows Low-Speed (Take-off or Landing) Mach number plotted against Range achieved for different wing loadings and Rp variations (for Mach 2, L/D and sfc variations).

It is interesting to compare the trends for SR301 against those for the smaller aircraft SR401, **Fig.5.7**. Note that SR301 trends with lower OEW/MTOW ratio confirm higher range capabilities. Such graphs are obviously highly dependent on planforms and indicative of several avenues for future work to improve performance i.e. reduce the take-off speed and extend the range. For example, we may need to change or revise the planform to increase the subsonic lift-curve slope without penalising the supersonics. Incorporation of limited variable geometry in the configuration could be useful. An alternative would be to exploit flow control to enhance L/D. Reducing sfc would help greatly.

7. FURTHER WORK

So far, one comparative exercise reported here has shown the capability of assessing planforms suitable for long range aircraft. Several ideas on improving performance have emerged and provide the encouragement for continuing the studies. Arrow Wings (Refs.28-30) hold the promise of offering still higher aerodynamic performance (see **Fig.7.1**), providing the aero-elastic / structural problems can be dealt with as in the Joined-Wing layout. Related work is in Ref.25 on Mach 2 aircraft. We need to capitalize on this and a long "shopping list" for future work can be arrived at e.g. wing sweep optimisation (particularly TE sweep), experiments at low, high speeds.

Configuration aspects such as wing body+nacelles integration need to be considered in detail. The performance needs to re-visited in terms of optimising the range / sizing / power-plant "loop". Suitable general and useful works on Supersonic Technology are Refs.31-32.

We also need to consider off-design performance including lateral and directional characteristics. Aero-elastics and structural loadings need to be addressed.

8. CONCLUDING REMARKS

With advances in technologies of controls, propulsion, and flow control, there is emphasis on re-visiting the long-range military scenario.

Results of studies illustrate that the potential of "cranked delta" layout, with further improvement of L/D, possibly using flow control appropriately.

From this preliminary analysis, the larger 400,000 lb MTOW aircraft offers the greater potential for development in terms of range and low speed performance.

Typical results presented demonstrate the flexibility and potential of the techniques for direct and inverse design. Further work needs to be continued in assessing structural and flow control implications. We are only at the starting post and a sizeable, interesting work programme remains!

Capability for study of several geometric variables of configurations is offered in a timely sense. Data for detail design of wind tunnel models and possibly a flight demonstrator can be enabled. An understanding of control laws arises. The potential and limitations of the aircraft in meeting a given design envelope can be assessed.

Several areas for continued work have emerged.

REFERENCES

1. NANGIA, R.K., "Pilot Document Introducing all Aspects of Work Accomplished under USAF-EOARD Contract SPC-024051", RKN/AERO/REPORT/2004-10 – Part 1, Issue 1, 2004.

2. NANGIA, R.K., "High Aspect Ratio Unconventional Joined-Wing Configurations Incorporating Laminar Flow", RKN/AERO/REPORT/2004-10 – Part 2, Issue 1, 2004.

3. NANGIA, R.K., "Planform Effects on High Aspect Ratio Unconventional Joined-Wing Configurations Incorporating Laminar Flow", RKN/AERO/REPORT/2004-10 – Part 3, Issue 1, 2004.

4. NANGIA, R.K., "High Aspect Ratio Lambda-Wing Configurations Incorporating Laminar Flow", RKN/AERO/REPORT/2004-10 – Part 4, Issue 1, 2004.

5. NANGIA, R.K., "Integration of Over-Surface Scarfed Intakes on Aircraft with High Aspect Ratio Wings (e.g. Sensor-Craft)", RKN/AERO/REPORT/2004-10 – Part 5, Issue 1, 2004.

6. NANGIA, R.K., "Towards Design of Long-Range Supersonic Military Aircraft", RKN/AERO/REPORT/2004-10 – Part 6, Issue 1, 2004. *This Report*.

7. NANGIA, R.K., "Configuration & Aerodynamic Design Studies of Joined-Wing High Aspect Ratio Sensor-Craft Concept", RKN/Aero/Report/2002-10, June 2002, (USAF-EOARD Contract SPC-01-4087).

8. WLEIZEN, R. & VEITCH, L., "Quiet Supersonic Platform Program", AIAA-2002-0143, 2002.

9. KOMADINA, S, DRAKE, A, BRUNER, S., "Development of a Quiet Supersonic Aircraft with Technology Applications to Military & Civil Aircraft", AIAA 2002-0519.

10. KROO, I. et al, "Natural Laminar Flow for Quiet and Efficient Supersonic Aircraft", AIAA-2002-0146, See also DARPA www 2000.

11. TILMANN, C.P. Presentation at 21st Applied Aerodynamics / Fluid Dynamics Meeting, Orlando, 23-26 June 2003.

12. SARIC, W.S. & REED, H.L., "Supersonic Laminar Flow Control on Swept Wings", AIAA-2002-0771, Reno, NV, Jan 2002.

13. HARRIS. R.V., "The Potential for a New Era of Supersonic & Hypersonic Aviation", Proceedings of European ACTES Symposium, Strasbourg, Nov. 1989.

14. THIBERT, J.J., "The Aerodynamics of Future Supersonic Transport Aircraft", RTO- EN-4, 1998

15. JENKINSON et al, "Civil Jet Aircraft Design", Arnold, 1999.

16. LOWRIE, B., "Future SST Propulsion Optimisation", Proceedings of European ACTES Symposium, Strasbourg, Nov. 1989.

17. NANGIA, R.K., "Low Speed Performance Optimisation of Advanced SCT With Different Types of LE Devices", EAC, Proceedings: "The Supersonic Transport of Second Generation", EAC'94, Toulouse, Oct. 1994.

18. NANGIA, R.K. & MILLER, A.S. "Vortex Flow Dilemmas & Control on Wing Planforms for High Speeds", RTO AVT Symposium, Loen, Norway, May 2001.

19. NANGIA, R.K., "The Design of "Manoeuvrable" Wings using Panel Methods, Attained Thrust & Euler Codes", ICAS-92.

20. NANGIA, R.K. & GREENWELL, D.I., "Wing Design of Oblique Wing Combat Aircraft", ICAS 2000-1.6.1, 2000.

21. NANGIA, R. K. & GALPIN, S.A., "Towards Design of High-Lift Krueger Flap Systems with Mach & Reynolds No. Effects for Conventional & Laminar Flow Wings", CEAS European Forum, Bath, UK, 1995.

22. NANGIA, R. K. & GALPIN, S.A., "Prediction of LE & TE Devices Aerodynamics in High-Lift Configurations with Mach & Reynolds No. Effects", ICAS-1996-2.7.6..

23. NANGIA, "Design of Conventional & Unconventional Wings for UAV's", RTA-AVT Symposium, "UV for Aerial & Naval Military Operations", Ankara, Turkey, Oct. 2000.

24. NANGIA, R.K., PALMER, M.E. & DOE, R.H., "A Study of Supersonic Aircraft with Thin Wings of Low Sweep", AIAA-2002-0709, January 2002.

25. NANGIA, R.K., PALMER. M.E., "Unconventional Joined-Wing Concept for Supersonic Aircraft", RTO-AVT-99, Paper 25, Brussels, April 2003.

26. GUPTA, K.K. & MEEK, J.L., "Finite Element Multidisciplinary Analysis", AIAA, 2000.

27. NANGIA, R.K., "Developing an Inverse Design Method using 3-D Membrane Analogy", Future Paper.

28. KUCHEMANN, D. "The Aerodynamic Design of Aircraft", Pergamon.

29. JONES, R.T., "Wing Theory", Princeton.

30. KULFAN, B.M., " Reynolds Number Considerations for Supersonic Flight", AIAA 2002-2038, 32nd AIAA Fluid Dyn. Conf. & Exhibit, St Louis, Missouri, USA, 2002.

31. ACTES, Proceedings: The European Symposium on Future Supersonic, Hypersonic Transportation Systems", Strasbourg, Nov 1989.

32. EAC, Proceedings: "The Supersonic Transport of Second Generation", EAC'94, Toulouse, Oct. 1994.

LIST OF SYMBOLS & ABBREVIATIONS

AoA	α, Angle of Attack
AR	Aspect Ratio
b	= 2 s, Wing span
c	Local Wing Chord
c_{av}	Average Chord of Wing
C_D	= Drag Force /(q S), Drag Coefficient
C_{D0}	Friction Drag Coefficient
C_L	= Lift Force/(q S), Lift Coefficient
C_m	= Pitching Moment/(q S c_{av}), Pitching Moment Coeff
C_p	Coefficient of Pressure
CG	Centre of Gravity
LE	Leading Edge
LEF	Leading Edge Flap
M	Mach Number
OEW	Overall Empty weight
q	= 0.5 ρ V^2, Dynamic Pressure
Re	Reynolds Number, based on c_{av}
s	Wing semi-span
S	Wing Area
S_S	Suction Parameter
SST	Supersonic Transport (e.g. ESCT, SCT, HSCT)
TE	Trailing Edge
TEF	Trailing Edge Flap
V	Airstream Velocity
x,y,z	Orthogonal Co-ordinates, x along body-axis
x_{ac}	Location of aerodynamic centre on x-axis
x_{cp}	Location of centre of pressure along x-axis
α	=AoA, Angle of Attack, ref. to body-axis
λ	Taper Ratio
Λ	LE Sweep Angle
ρ	= Air Density
η	= y/s, Non-dimensional spanwise Distance

Key Attributes/Features

- Intercontinental range
- Responsiveness
- Survivability (speed, altitude, standoff)
- High Sortie Generation Rate
- Multi-targeted payload

FIG. 1.1 LONG-RANGE SUPERSONIC STRIKE AIRCRAFT, MANNED or UNMANNED

57.7 ft
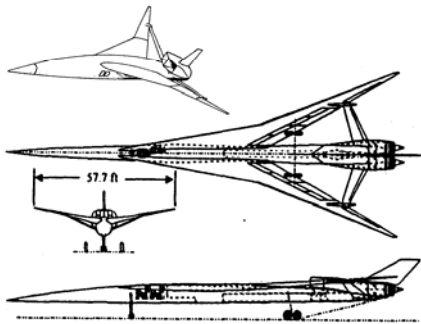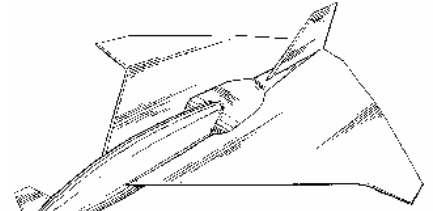
POSSIBLE LOW SONIC-BOOM JOINED-WING LAYOUT

McDonnell Douglas HSCT

Tupolev 244

ESCT

Lockheed SR-71

SupersonicTypes

Sukhoi T-4

ESRP

Tupolev 144

XB-70

F.S. 1621.2

DARPA QSP Project

Rockwell B-1

Boeing 733

US-

FIG. 2.1 SUPERSONIC CONFIGURATIONS, CIVIL & MILITARY

Virtual Control Surfaces
·Survivable Flight Control

Fluidic Thrust Vectoring
·Survivable Flight Control

Leading Edge Separation Control
·Active surface
·Active Flow Control
·Takeoff/landing

Laminar Flow on Swept Wings Using DREs

Mitigate shock-induced separations for supersonic inlet integration

FIG. 1.2 POSSIBLE TECHNOLOGY APPLICABLE

Transonic

Long-Term GOAL

Goal

Large 250

L/D

Feasible with 20000 lb payload

Douglas SCR

HSCT

Lockheed SCR

small 100 seats

Concorde

XB-70

SR-71

B-58

Mach Number

FIG. 1.3 POSSIBLE L/D IMPROVEMENTS, Based on DARPA WORK

14

FIG. 2.3 DESIGN APPROACHES & AERODYNAMIC
POTENTIAL FOR AIRCRAFT CLASSES

FIG. 2.2 AIRCRAFT CLASSIFICATION BY SPEED REGIME

ESCT
5500nm

Note payload Critical as
SIZE decreases

Concorde
3500 nm

Derived
Concorde
4000nm

FIG. 2.4 SST WEIGHT BREAKDOWN

Mach 2.0

Typical range 5500nm

RESERVES :
4 % block-fuel
+ 30 min. hold
+ 240 nm diversion
+ 2 × 10 min. at
V_c = 250 / 200 Kt

MACH 2.05 CRUISE
+ DESCENT

SUBSONIC
CLIMB +
M = 0.95
CRUISE

SUPER
-SONIC
CLIMB

540 nm | 4960 nm | 240 nm

FUEL
BURNT : 19 % | 7 % | 64 % | 10 % | = 100 %

WEIGHT
BREAKDOWN

100 % FUEL CAPACITY	179 t
EQUIPED EMPTY WEIGHT	137 t
PAYLOAD (250 pax.)	24 t
T.O. GROSS WEIGHT	340 tons

$\frac{Fuel}{Payload}$ = 7.46

$\frac{Payload}{TOGW}$ = 7.06%
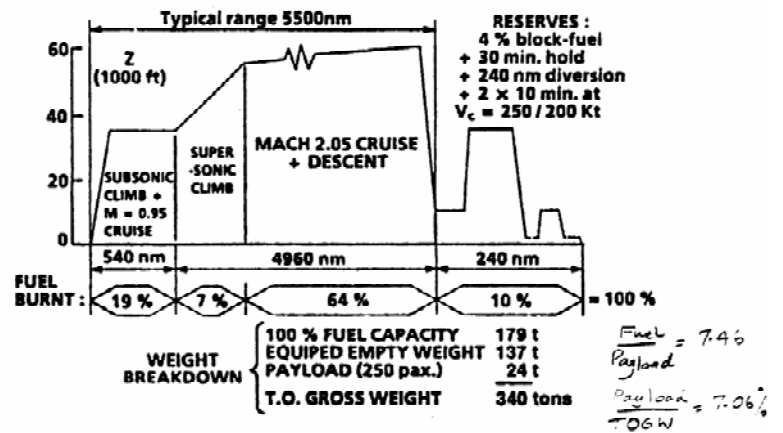
FIG. 2.5 WEIGHT BREAKDOWN FOR 5500 NM
FLIGHT, Ref. Thibert
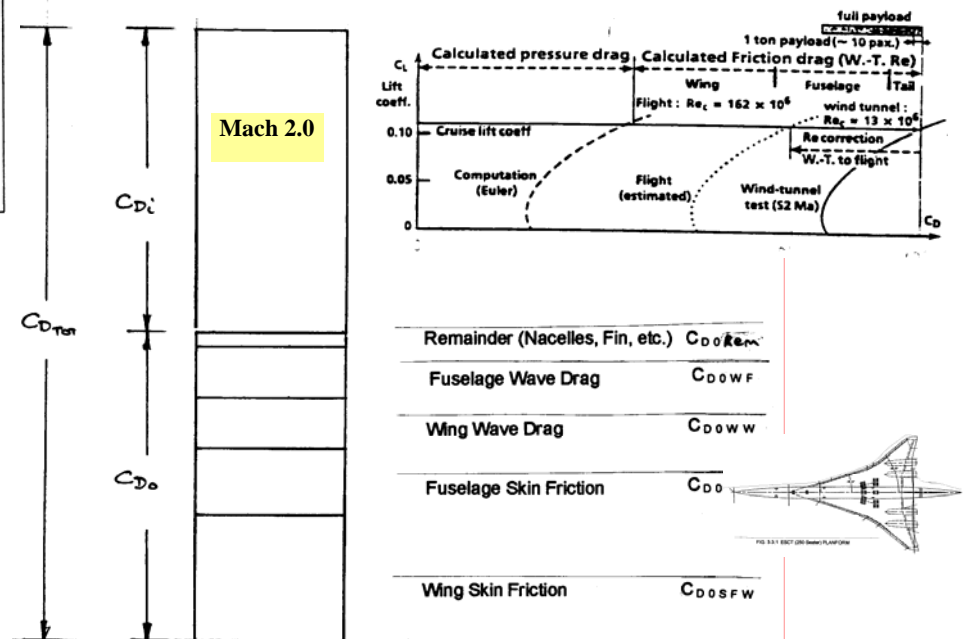
FIG. 2.6 SUPERSONIC DRAG, DESIGN
ISSUES & SPECIAL CHARACTERISTICS

15

FIG. 2.7 Mission Diagram

- M2.0-2.5 Cruise at Best Altitude
- Accel/ Climb to M2.0-2.5
- Decel/ Descend to 10kft
- M# 2.0-2.5
- Combat Zone:
  • Drop A/G Weapons
  • 180° Mil Pwr
- 20 min Loiter at
- Mil Pwr Accel and Climb to M2.0-2.5 Cruise M#
- Mission
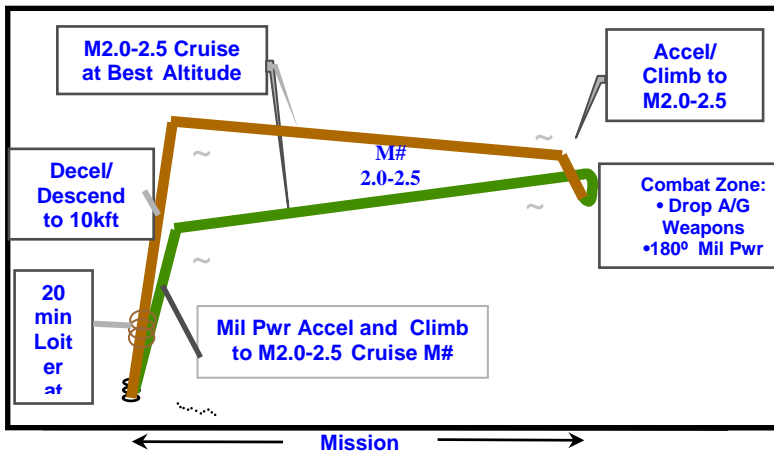
Warm-up, Taxi, Takeoff Allowance: 20 Minutes Idle + Max Pwr Takeoff to 0.3M
Landing Reserves: 20 Minutes Loiter at 10,000 ft + 5% Internal Fuel
Payload: 20,000 lbs

FIG. 2.7 POSSIBLE MILITARY SUPERSONIC MISSION

Optimum Fan Pressure Ratio
Turbine Entry Temperature 1600°K, 2420°F
Maximum Compressor Delivery Temperature 850°K, 1070°F
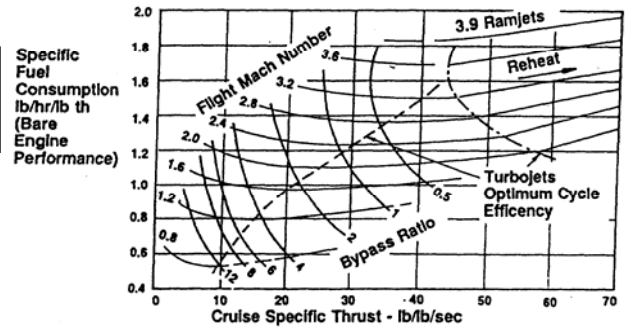
FIG. 3.1 TRENDS OF SFC WITH MACH no (LOWRIE)

$W_{payload}/MTOW$ – Range (nm)

CONCORDE TYPE
Likely Trend with improvements
Definite Point
+10% +30% +50%

MTOW – Range (nm)
+50% +30% +10%
Definite Point
CONCORDE TYPE
Likely Trend
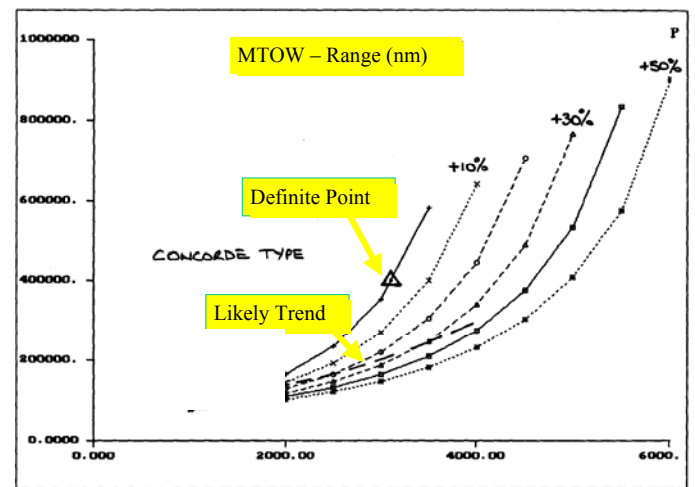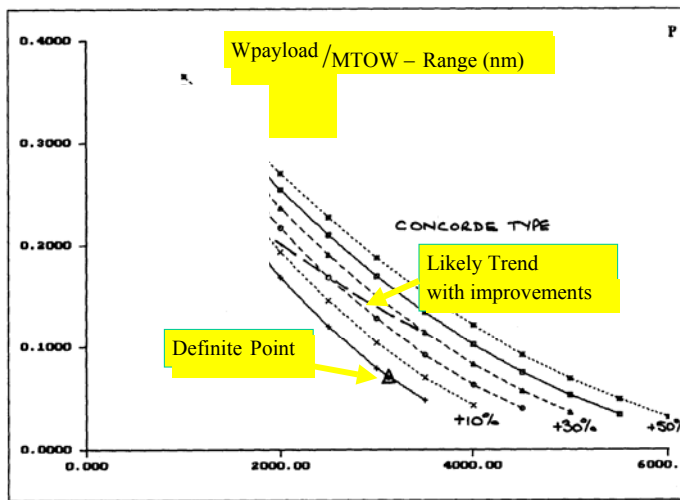
FIG. 3.2 PARAMETERS FROM BREGUET Eqn. PLOTTED AGAINST RANGE, Mach 2 AIRCRAFT BASED ON IMPROVING CONCORDE TECHNOLOGY

$W_{pay} * Range/ W_{fuel}$ – Range

CONCORD
250 SEAT
SUBSONIC
100 SEAT
Likely
Definite
+10% +30% +50%
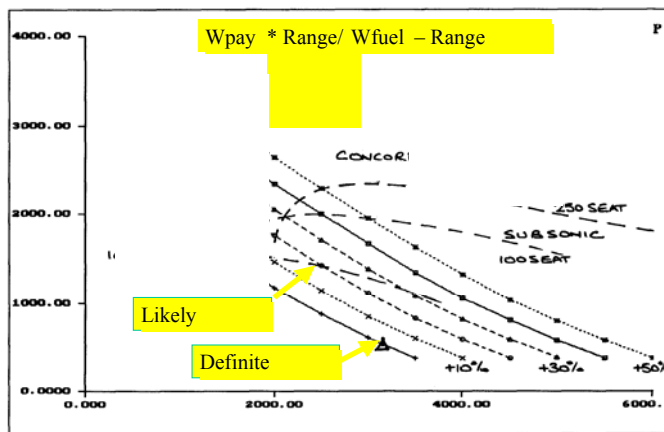
FIG. 4.1 POSSIBLE PLANFORMS FOR INITIAL WORK IN RELATION TO OTHER SUPERSONIC AIRCRAFT

SR301 SR401
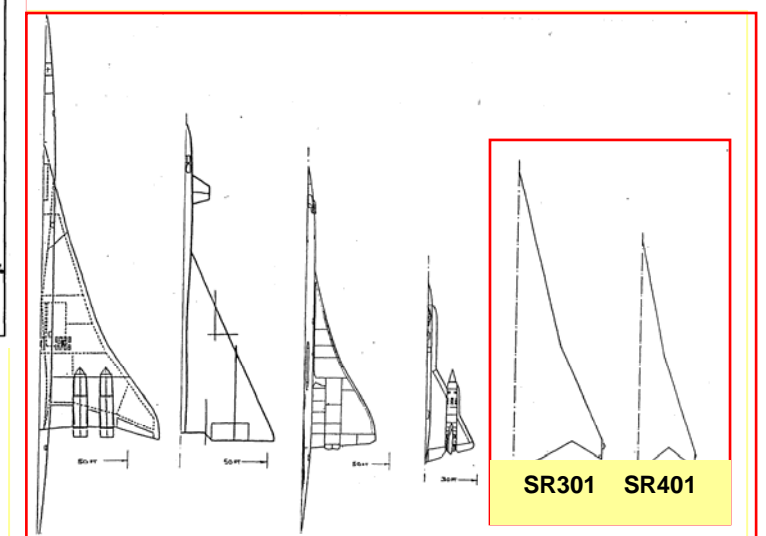
750000	534700	400000	172000	392000	250000	W lb
9000	6298	4250	1800	7270	3720	S ft²
138	105	85	55.6	101.5	66	b ft
83	90	94	96	54+	67+	W / S

16
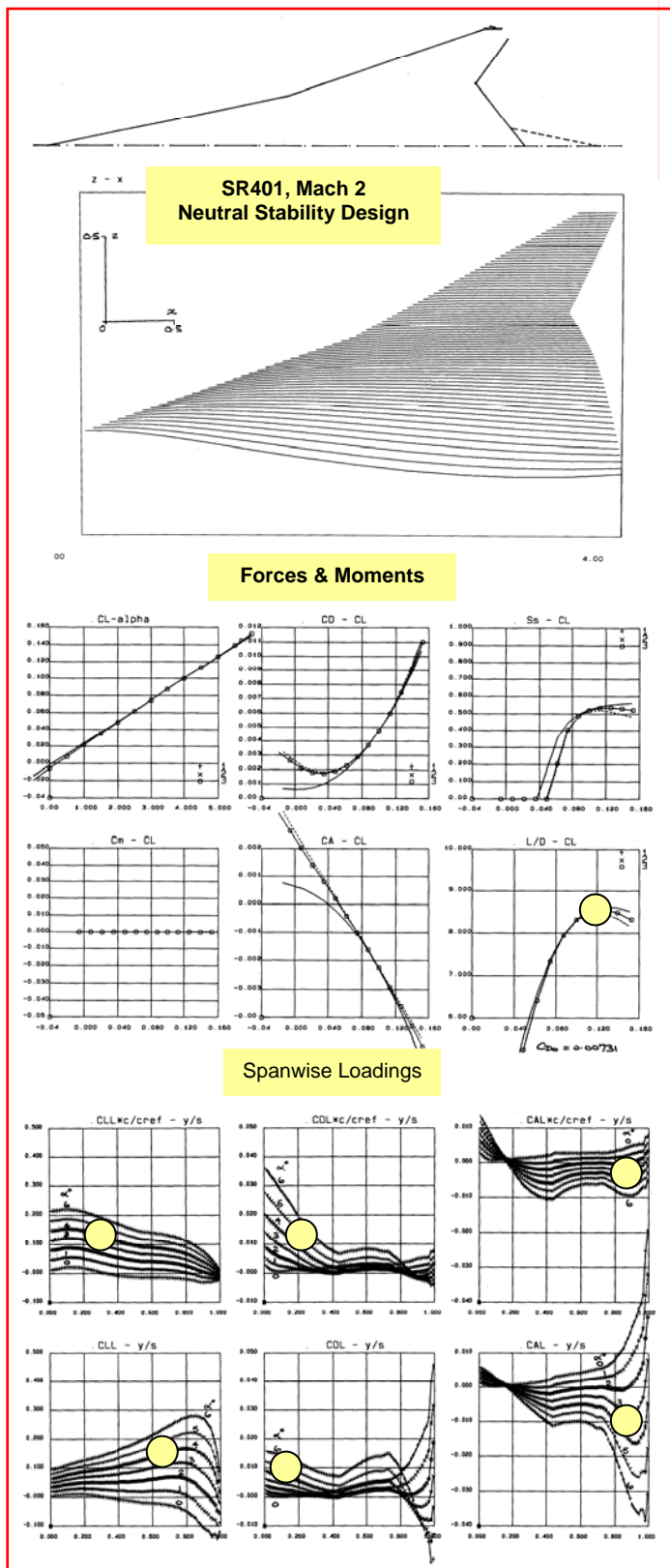
FIG. 5.1 SR401, DESIGNED FOR Mach 2 & PREDICTED AERODYNAMIC CHARACTERISTICS AT MACH 2
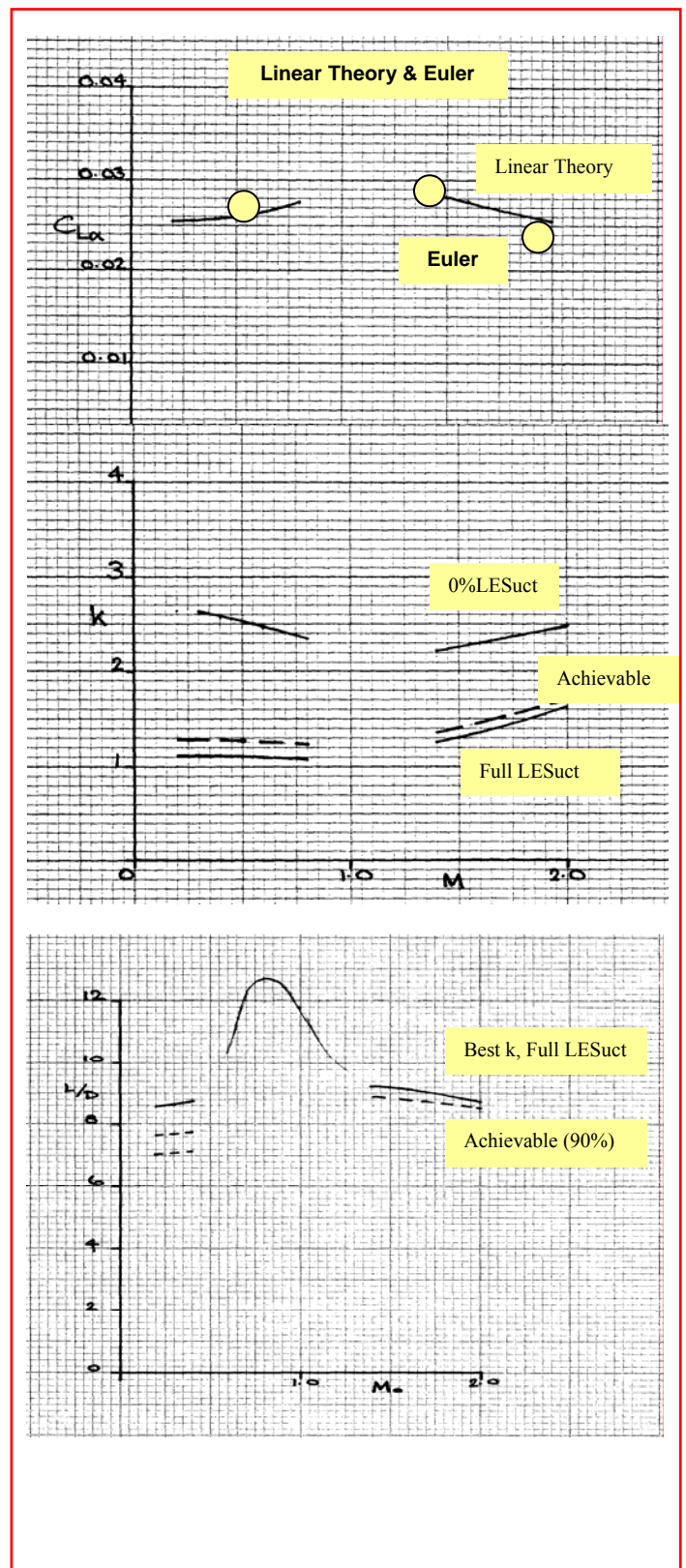
FIG. 5.2 SR401, DESIGNED FOR Mach 2 & PREDICTED AERODYNAMIC CHARACTERISTICS THROUGH MACH NUMBER RANGE

Weights (lb) – Range (nm)
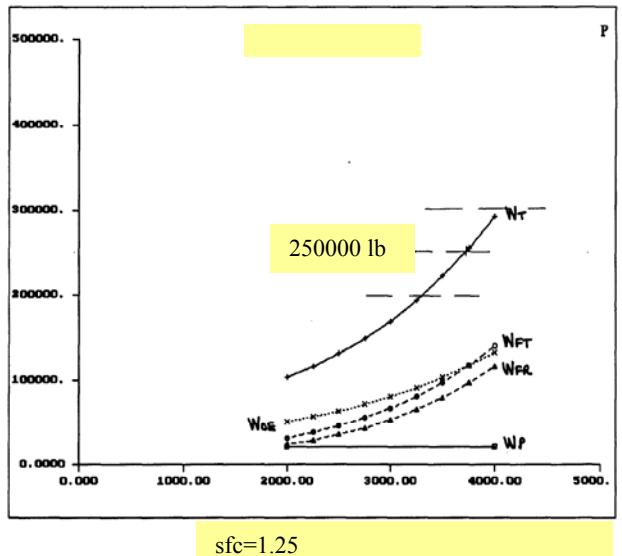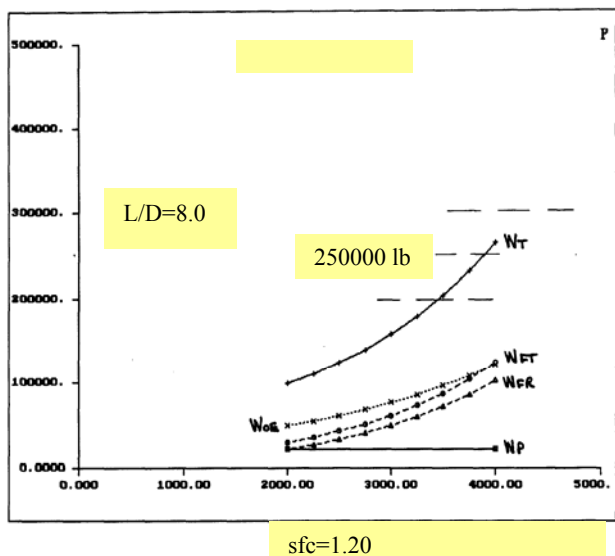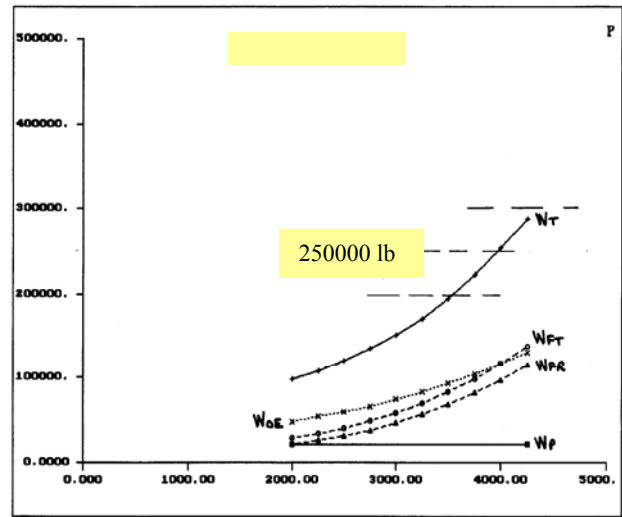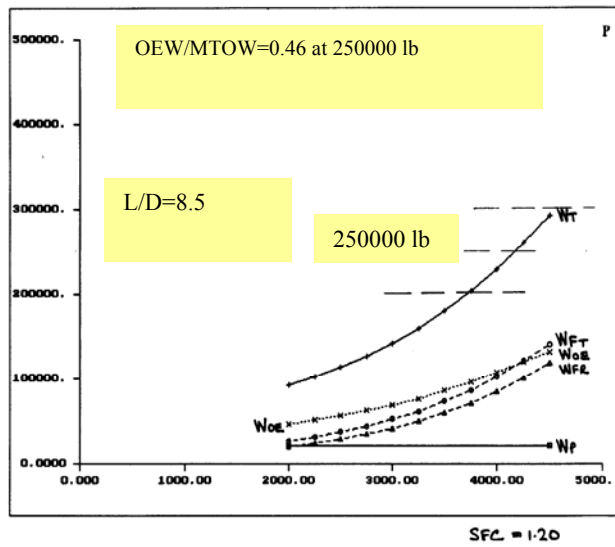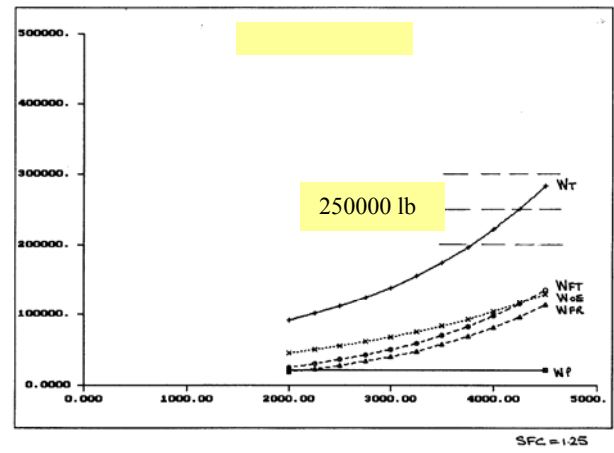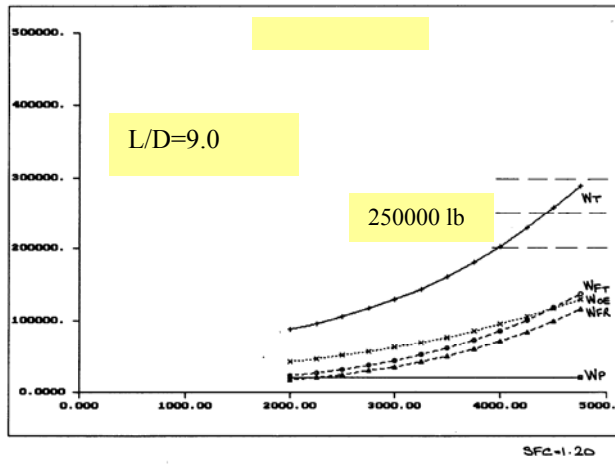
FIG. 5.3 MTOW, OEW, WP, WF – RANGE WITH L/D & SFC VARIATION
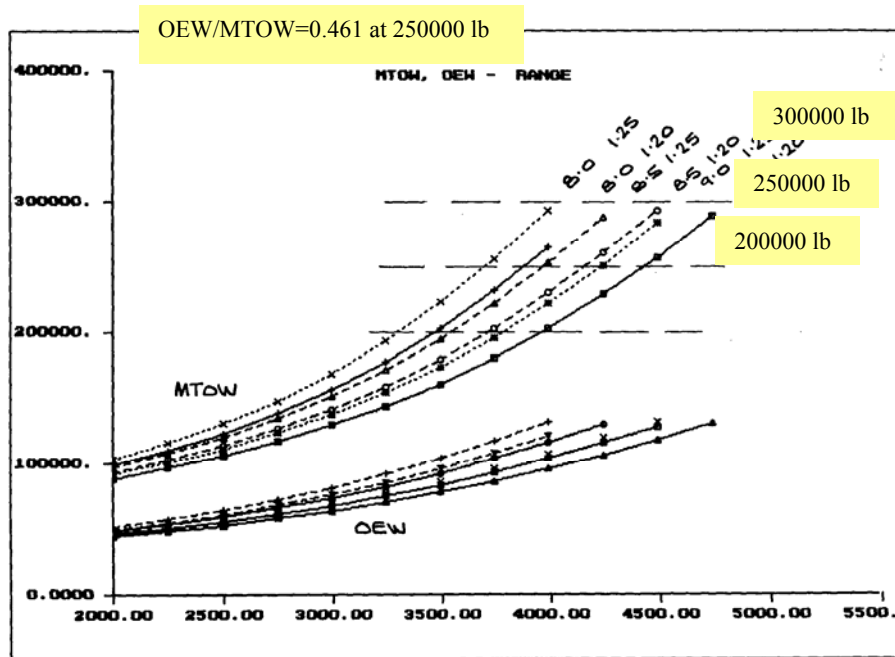
FIG. 5.4 SUMMARY, MTOW & OEW - RANGE, SFC & L/D VARIATIONS
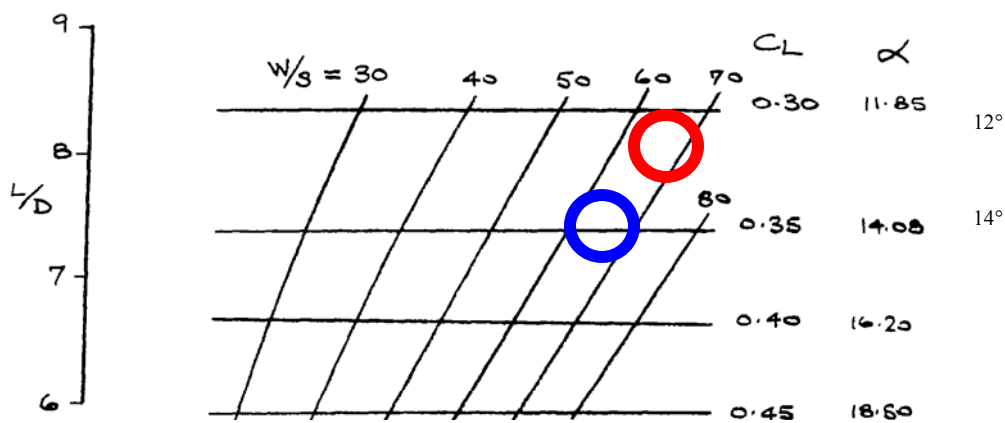
FIG. 5.5 LOW-SPEED PERFORMANCE, NO VORTEX LIFT
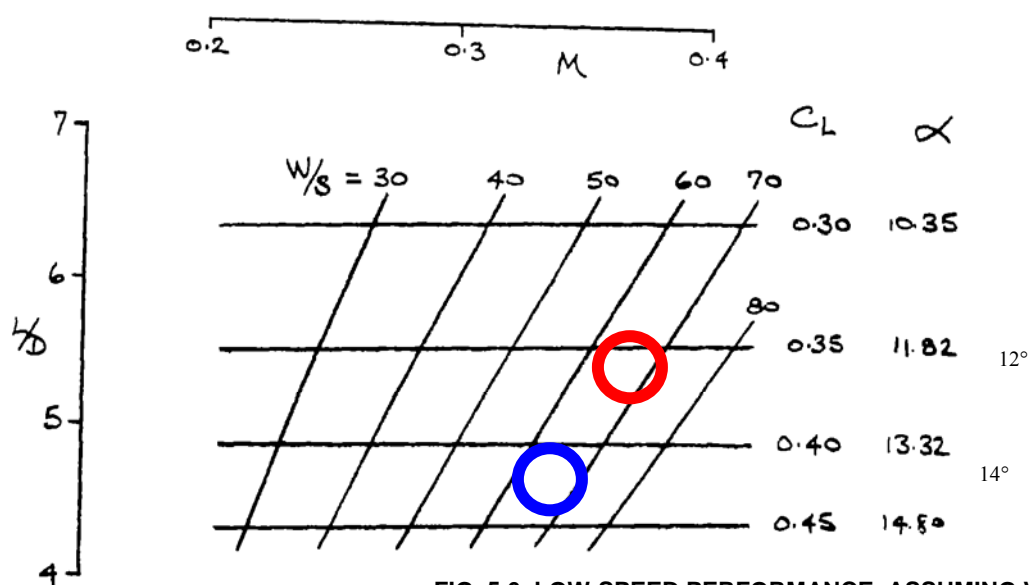
FIG. 5.6 LOW-SPEED PERFORMANCE, ASSUMING VORTEX LIFT
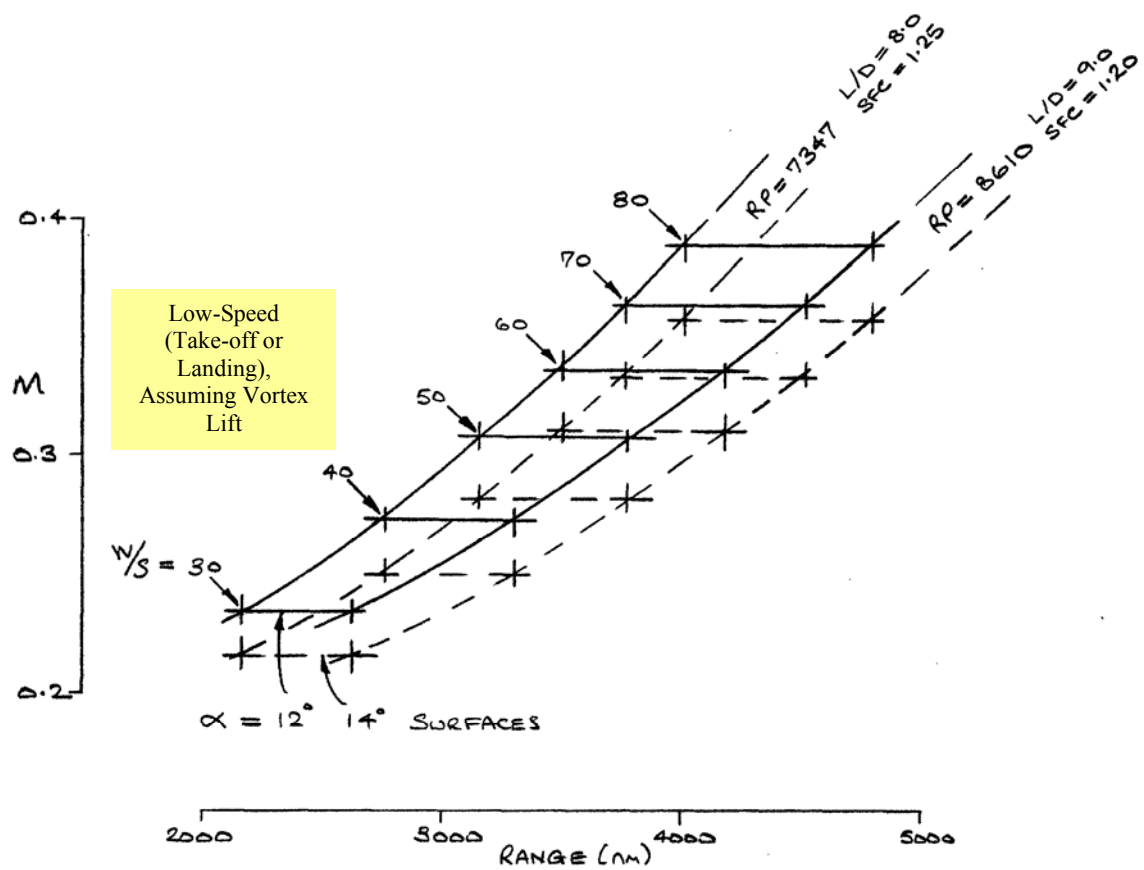
FIG. 5.7 TAKE-OFF MACH NUMBER PLOTTED AGAINST RANGE
ACHIEVED FOR DIFFERENT WING LOADINGS AND RP VARIATIONS.

SR301, Mach 2 Neutral Stability Design

Forces & Moments

Spanwise Loadings

FIG. 6.1 SR301, DESIGNED FOR Mach 2 & PREDICTED AERODYNAMIC CHARACTERISTICS AT MACH 2

Linear Theory & Euler

Linear Theory

Euler

0%LESuct

Achievable

Full LESuct

Best k, Full LESuct

Achievable (90%)
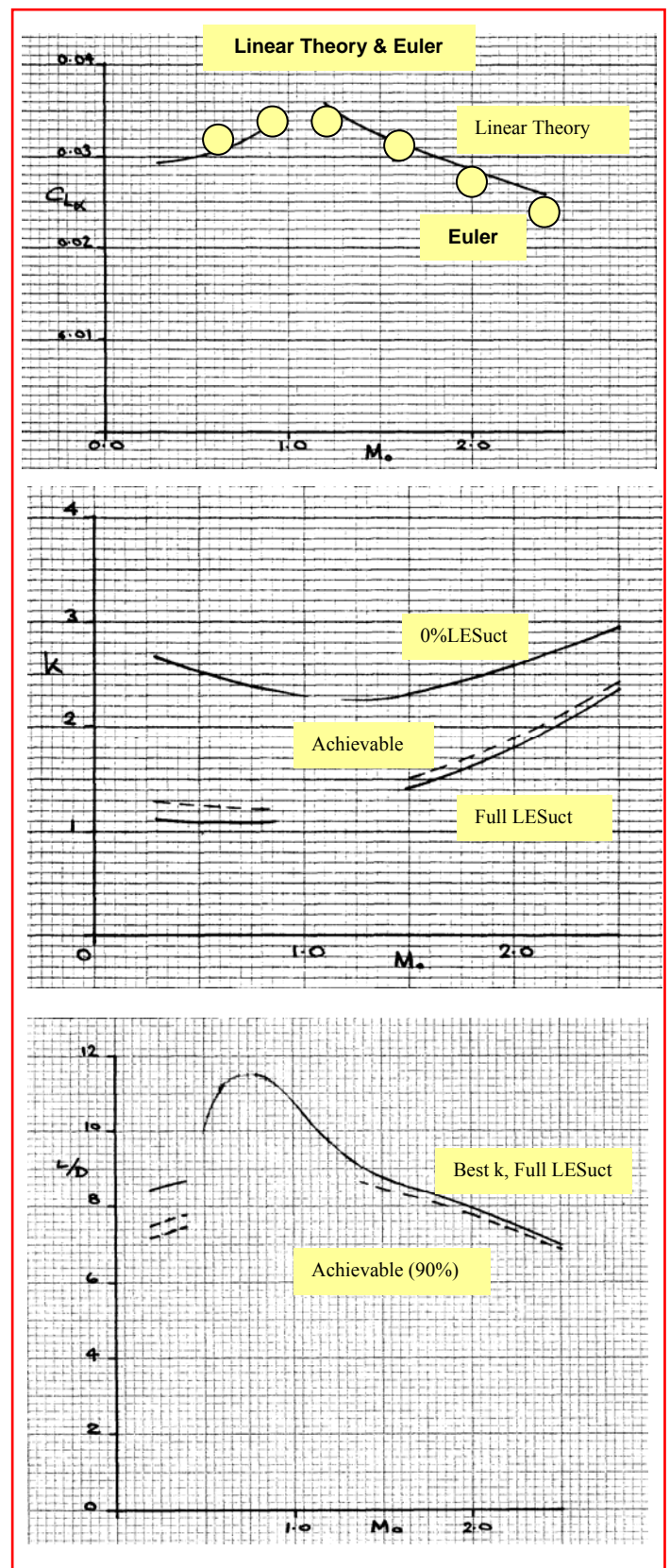
FIG. 6.2 SR301, DESIGNED FOR Mach 2 & PREDICTED AERODYNAMIC CHARACTERISTICS THROUGH MACH NUMBER RANGE
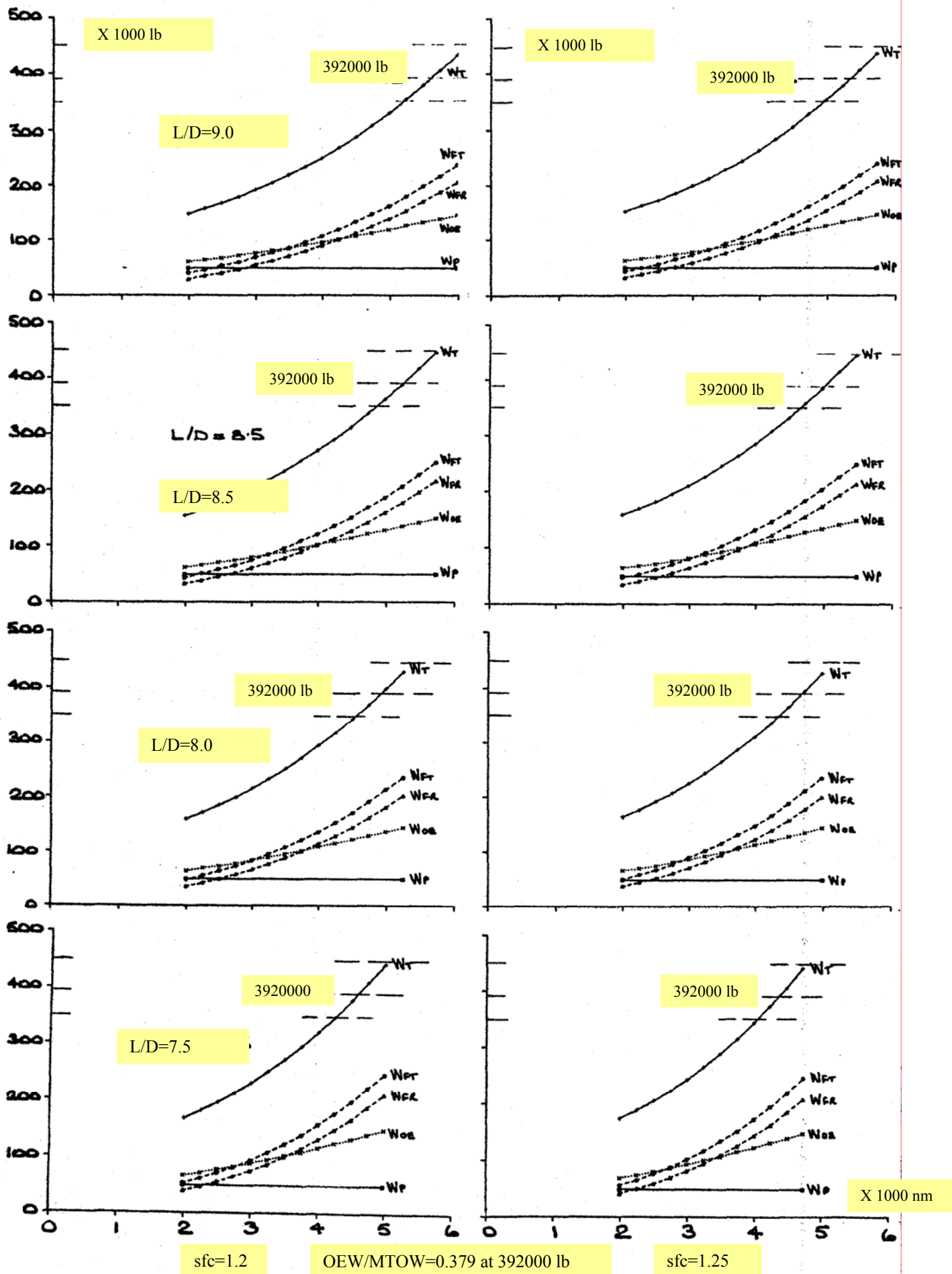
FIG. 6.3 SR301, MTOW, OEW, WP, WF (x 1000 lb) – RANGE (x1000 nm) WITH L/D & SFC VARIATION

22

FIG. 6.4 SUMMARY SR301, MTOW & OEW (x 1000 lb – RANGE (x 1000 nm) , SFC & L/D VARIATIONS

OEW/MTOW=0.379 at 392000 lb

FIG. 6.5 SUMMARY SR401, MTOW & OEW (x 1000 lb – RANGE (x 1000 nm) , SFC & L/D VARIATIONS (For Comparisons)

OEW/MTOW=0.461 at 250000 lb
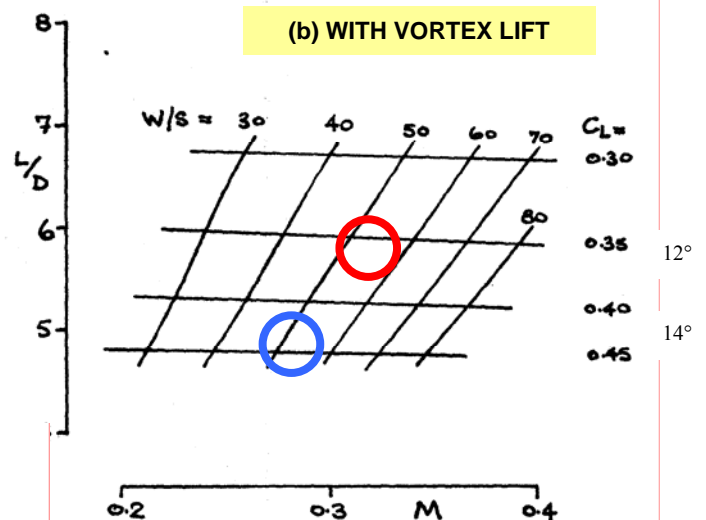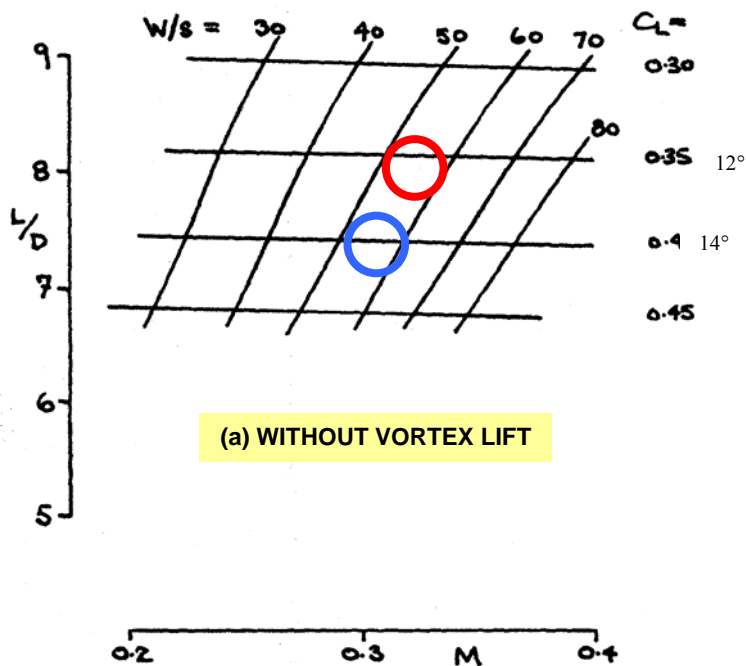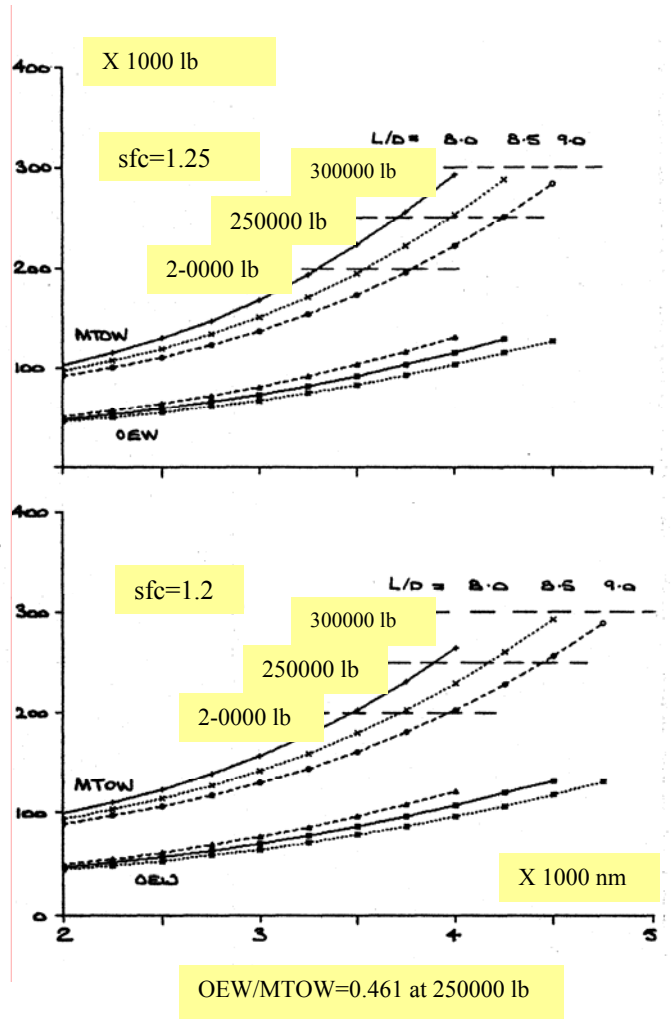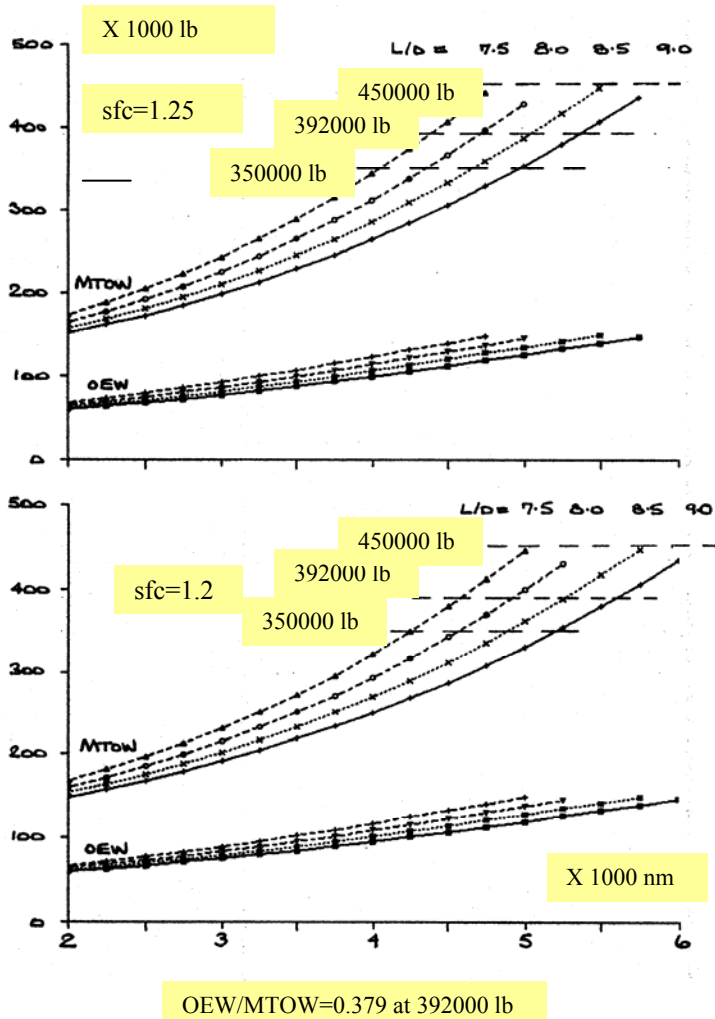
FIG. 6.6 LOW-SPEED PERFORMANCE, SR301, WITH OR WITHOUT VORTEX LIFT

FIG. 6.7 SR301, TAKE-OFF MACH NUMBER PLOTTED AGAINST RANGE ACHIEVED FOR DIFFERENT WING LOADINGS AND RP VARIATIONS.

Range (nm)

FIG. 5.7 SR401, TAKE-OFF MACH NUMBER PLOTTED AGAINST RANGE ACHIEVED FOR DIFFERENT WING LOADINGS AND RP VARIATIONS (For Comparison)

Range (nm)

Idealized minimum drag due to lift for arrow wings.
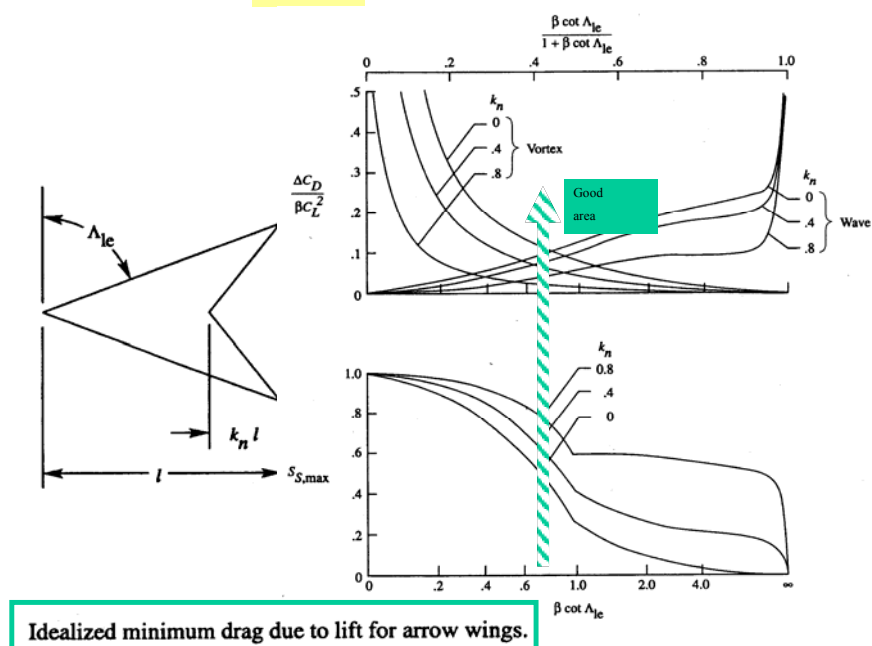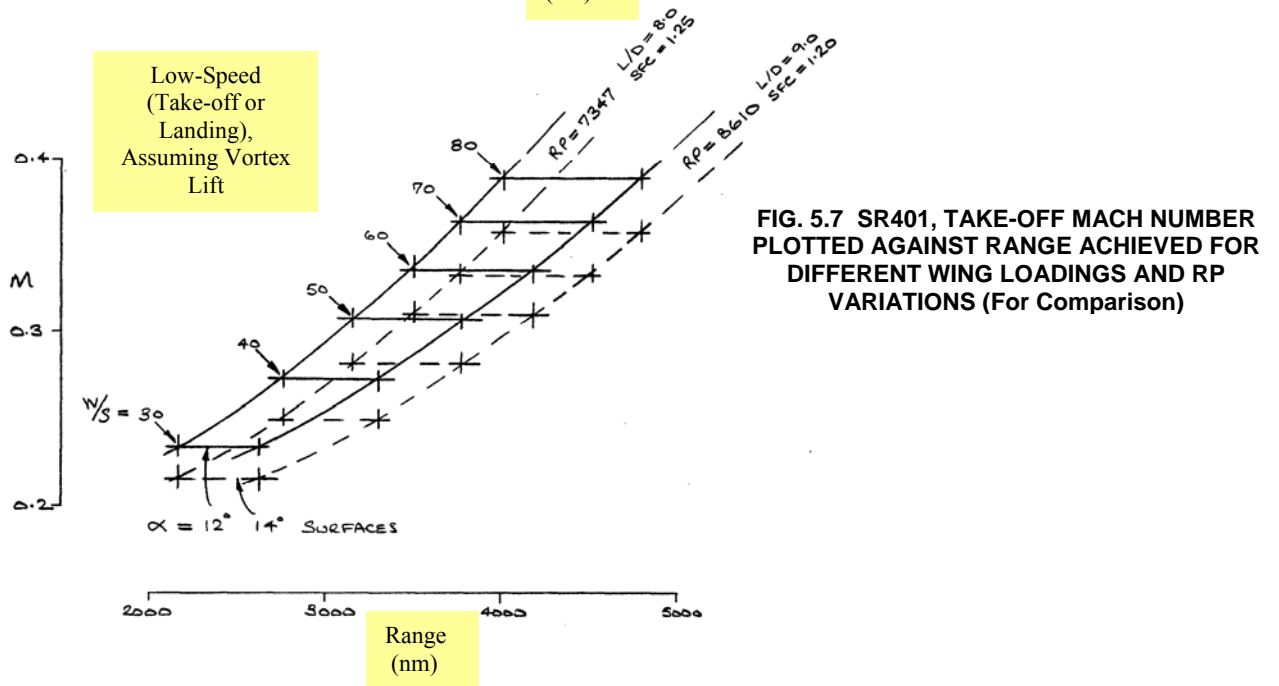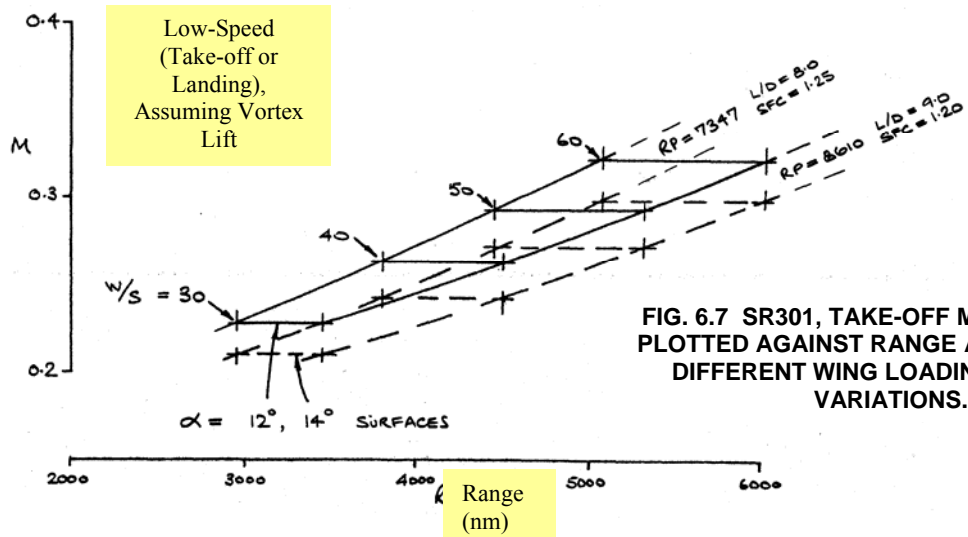
FIG. 7.1 ARROW WINGS, Wave-DRAG & Lift-Induced DRAG

24

INTEGRATION OF OVER-SURFACE SCARFED INTAKES ON AIRCRAFT WITH HIGH ASPECT RATIO WINGS
(e.g. Sensor-Craft)

Dr. R. K. Nangia

For reasons of survivability, different intake types and location options are being considered. Future aircraft, particularly unmanned, will have substantially "widened" flight envelopes (higher "g", α and ß over Mach, altitude and CL ranges). Integration of such intakes (usually heavily and negatively scarfed) in flying vehicles and obtaining high efficiency and performance then become very important issues. Flow control needs can be identified.

To replace the AWACS aircraft, a proposal is for a HALE-UAV sensor-craft. Such craft take advantage of high aspect ratio (AR) as well as enclosing an antenna in the aircraft diamond wing layout. The aircraft carry a high proportion of fuel and "loiter" at high altitudes for a few days. This implies a wide C_L - altitude capability and need for extreme efficiency.

This report is concerned with design studies on scarfed intakes that can be integrated with different types of aircraft but more particularly with high AR sensor-craft. Several examples are given. Implications of typical flight envelope on Intake design aspects have been mentioned. The techniques developed, can be adapted to more complex intake shapes as well as integration with aircraft layouts.

The potential benefits to the military user are considered to be significant and include: reduced life cycle costs, improved operability, improved reliability and maintainability, enhanced performance, enhanced survivability, reduced complexity and weight, and reduced environmental impact.

Further work has been proposed in several areas.

This report is Part 5 of a series of six relating to high AR, long endurance surveillance aircraft, laminar flow, integrated intakes and long range supersonic military aircraft.

Consulting Engineers
Nangia Aero Research Associates
WestPoint, 78 Queens Road, Clifton
Bristol BS8 1QX, UK

The Investigation which is the subject of this report was initiated by
USAF - EOARD, 223/231 Old Marylebone Road, London, NW1 5TH, UK
and was carried out under the terms of Contract SPC-024051

DISTRIBUTION LIST

1	Mr. W. Donaldson	USAF-EOARD, London NW1 5TH, UK
1	Mr. C. Remillard	Chief, AFRL/VAAA; Bldg 45
		2130 8th Street, WPAFB, Ohio, USA 45433-7542
1	Mr. D. Multhopp	Technical Area Lead, AFRL/VAAA; Bldg 45
		2130 8th Street, WPAFB, Ohio, USA 45433-7542
2	Dr. C. P. Tilmann	Sr. Aerospace Engineer, AFRL/VAAA; Bldg 45
		2130 8th Street, WPAFB, Ohio, USA 45433-7542
1	Mr. William Fields	Tech Area Lead, AFRL/VAAA; Bldg 45
		2130 8th Street, WPAFB, Ohio, USA 45433-7542
1	Dr. K. P. Iwanski	Aerospace Engineer, AFRL/VAAA; Bldg 45
		2130 8th Street, WPAFB, Ohio, USA 45433-7542
1	Mr. Larry Leavitt	Head, Configuration Aerodynamics Branch
		NASA Langley Research Center, Mail Stop 499
		Hampton, VA 23681-2199
1	Dr. James Luckring	Configuration Aerodynamics Branch
		NASA Langley Research Center, Mail Stop 286
		Hampton, VA 23681-2199
1	Mr. John Perdzock	Head, SensorCraft Integrating Concept Office, AFRL/VAC; Bldg 45
		2130 8th Street, WPAFB, Ohio, USA 45433-7542
1	Dr. Maxwell Blair	AFRL/VASD; Bldg 146
		2210 Eighth Street
		Wright-Patterson AFB OH 45433-7531
1	Dr. Keith Numbers	AFRL/VAA, Long Range Strike Integrating Concept Office
1	Mr. D. Adamczak	Sr. Aerospace Engineer, AFRL/VAAA; Bldg 45
		2130 8th Street, WPAFB, Ohio, USA 45433-7542
1	Dr. Michael OL	Research Engineer, AFRL/VAAA Bldg 45
		2130 8th Street, WPAFB, Ohio, USA 45433-7542
2	Dr. R.K. Nangia	Nangia Aero Research Associates
		WestPoint, 78-Queens Road, Clifton
		BRISTOL BS8 1QX, UK.

CONTRACTUAL DECLARATIONS

"The Contractor, Dr. R. K. Nangia, hereby delcares that, to the best of its knowledge and belief, the technical data delivered herewith under Contract No.SPC-024051 is complete, accurate, and complies with all requirements of the contract.

DATE: **March 2004**   **Name and Title of Authorized Official:**   **Dr R K Nangia**

"I certify that there were no subject inventions to declare as defined in FAR 52.227-13, during the performance of this contract."

DATE: **March 2004**   **Name and Title of Authorized Official:**   **Dr R K Nangia**

CONTENTS

SUMMARY

DISTRIBUTION LIST

CONTRACTUAL DECLARATIONS

CONTENTS

1. INTRODUCTION & BACKGROUND

2. INTAKE INTEGRATION PROCESS & GENERAL FEATURES

3. INTAKE DESIGN METHODS

4. INTAKES WITH NEGATIVE SCARF, -30 & -60 deg.

5. SINGLE FUSELAGE LAYOUT WITH A CENTRAL INTAKE

6. TWIN FUSELAGE LAYOUT WITH TWIN INTAKES

7. SUMMARISING MASS FLOW RATIO CAPABILITY FOR VARIOUS INTAKES

8. CONCLUDING REMARKS, FUTURE WORK

ACKNOWLEDGEMENTS
REFERENCES
LIST OF SYMBOLS & ABBREVIATIONS
FIGURES   1.1-5, 2.1-5, 4.1-5, 5.1-2, 6.1-2 and 7.1 (20 Total)

1. INTRODUCTION & BACKGROUND

The work discussed in this report relates specifically to the integration of over-surface intakes on aircraft with high Aspect Ratio (AR) wings. This report is Part 5 of a series of six, Refs.1 to 6, relating to high AR, long endurance surveillance aircraft, laminar flow, integrated intakes and long range supersonic military aircraft. This work follows previous work funded by USAF-EOARD under seeding Contract SPC-01-4087 which was reported in Ref.7.

For reasons of survivability, different intake shapes and location options are being considered (**Fig.1.1**). Future aircraft particularly those that are unmanned will have substantially "widened" flight envelopes (higher "g", α and ß over Mach, altitude and C_L ranges). Integration of such intakes (usually heavily and negatively scarfed) in flying vehicles, whilst obtaining high efficiency and performance, then becomes a very important issue. The need for flow control is to be identified. Flying wings and Blended Wing Body (BWB) configurations also feature such intakes.

Over-surface intakes have associated problems, such as coping with variable thickness viscous layers (over the surface). Off-design sensitivity can be compromised. Consequently there is a continued emphasis on diverter-less / bump intakes with and without flow control.

High Aspect Ratio Sensor-Craft

A proposal is to replace the AWACS aircraft with a HALE-UAV (Refs.8 to 10). Such craft may take advantage of high aspect ratio (AR) as well as enclosing an antenna in a diamond shaped joined-wing planform, based on the ideas of Wolkovitch (Refs.11 and 12). Joined-wing HALE aircraft (Sensor-Craft) carry a high proportion of fuel and "loiter" at high altitudes for a few days in each flight. This implies a wide C_L - altitude capability (Refs.13 to 17) as shown in **Figs.1.2-1.3.** This gives an idea of Altitude and Weight relationships during a typical mission. **Fig.1.4** shows the Mach number and C_L relationships (C_L based on the front wing area). Take-off is near C_L of 0.95 at Mach 0.2 (Re 1.4×10^6/ft), whilst landing is at C_L of 0.7 at Mach 0.15 (Re 1.0×10^6/ft). The Mach 0.6 cruise C_L varies from 1.58 to 0.88 (Re 0.44×10^6/ft to 0.35×10^6/ft). It is interesting to reflect that on conventional aircraft the cruise C_L values are near 0.5 and take-off and landing C_L values near 0.8 to 1.2 (all at very high Re). Sensor-craft values are very different from the conventional!

Sizing & Configuration Integration

The main sizing drivers are the integration of a "rhombic" planform antenna and fuel tank volume for the payload-range relationships. The cruise Mach number is "high" subsonic. The low-speed near-field performance is more akin to that of a (very) high aspect ratio wing glider. Take-off and landing phases are critical.

The design demands obviously "conflict" and this has led to work towards suitable layouts and propulsion integration. The sensor aircraft as envisaged in **Fig.1.3**, is subject to a demanding flight envelope (mission profile). At present, the design is relatively "fluid". Joined-wings of varying layouts arise. The sensor craft has to cruise and loiter (very high L/D) for substantial periods and needs to carry a large percentage of its all-up-weight (AUW) as fuel. The high aspect-ratio wings (sweep about +/- 35°) therefore need to be fairly thick (15-20% t/c streamwise). This implies emphasis on efficient aerodynamic and structural loading. A particularly critical aspect is the design of the wing juncture and LE / TE design. Many geometry parameters arise e.g. wing tip sweep, dihedral / anhedral, implying substantial computations. The "diamond" shapes offer useful survivability "compliance".

At the outset, there are several aspects that need to be considered, e.g.

- Type of spanwise loadings and design of "cruise" wing camber and twist including trim considerations at low speeds and with different C_L levels. The TE geometry may need to be varied.

- Due to a large C_L variation (fuel usage), the attitude varies and off-design becomes important. There is a need to sustain 2g+

- Integration of intakes in single- or twin- fuselage layouts. S-ducts may need to be incorporated for reasons of survivability.

- "Reasonable" off-design performance of airframe and intakes is to be ensured in situations such as sideslip and cross-winds during landing and take-off.

- Roll, Pitch and Yaw Stability levels and the determination of Control laws for the aircraft and propulsion system.

Previous papers (Refs.13 to 17) have addressed the aspects related to "high-speed" wing design. However, intakes and fuselages were not included.

Two propulsion integration options are shown in **Fig.1.5**. One layout depicts a single fuselage with a central over-wing scarfed intake whilst the other represents a twin-fuselage arrangement with twin over-wing, raked and scarfed, intakes. To a first order, the intake scarf angle is the more dominant parameter.

2. INTAKE INTEGRATION PROCESS & GENERAL FEATURES

For a fully integrated design, there are many aspects that interplay and the design process is iterative, **Fig.2.1**. In particular the lip flow separations at low and high speeds play a very important role in controlling the quality of air (flow distortion) supplied at the engine-face. **Fig.2.2** shows the order of complexity in design of intakes ranging from simple axi-symmetric to highly scarfed, survivable, and over-surface intakes (based on discussions in Refs.18 and 19).

The engine demand varies throughout the flight envelope, depending on several factors that include flight attitude, acceleration etc. **Fig.2.3** sketches the effect of Mass Flow Ratio (MFR) and angle of attack (AoA, α) on the onset of External or Internal lip flow separation. MFR is defined as the ratio A_o / A_C where A_o is the intake onset flow capture area and A_C is the intake highlight area. In the case of swept and scarfed intakes, the definition of highlight area is arbitrary. Mean engine face Mach number (MEF) is frequently used to define the internal flow conditions.

Fig. 2.4 sketches the MFR, AoA and geometry effects on the flow regions. Large changes occur due to introducing scarf.

Fig.2.5 shows the zero-speed effects on a scarfed intake. High local velocities occur on the downstream lip and these are likely to lead to flow separation.

Typical objectives of propulsion integration include seeking answers to aspects such as:

- Can very "high" (negative) scarf angles be incorporated into intakes without any undue aerodynamic penalties (engine and / or vehicle) at high or low speeds. Associated aspects are diverter design, S-ducts etc.
- Is the intake / ground performance adequate, particularly at very low speeds.
- To confirm reduced ground vortex strengths with negative scarf. This concerns debris ingestion.
- To highlight and stimulate aspects for further analysis and development e.g. need for flow control, variable geometry or smart structures.

3. INLET DESIGN METHODS

The principles of intake design follow the well-established fundamentals of Refs.18 and 19. The design methodology is as follows.

A given intake geometry is evaluated in terms of attached flow limits (function of M, Re, AoA, ß, aerofoil t/c, r/c, etc.). Geometry changes, required to achieve a desired performance, are determined (using modes and transpiration techniques) and then applied to the given geometry. The re-designed geometry is then re-evaluated (a stage of an iterative loop). This method has been successfully applied to several 3-D intakes including Circular, Rectangular (Unswept and Swept) and "survivable" types.

The design methodology "sits above" the aerodynamic prediction methods. Panel Codes, Full Potential, Euler and Navier-Stokes can be all used. The accuracy attained by the design process is dependent upon the solver used. Euler codes are more expensive in grid formation and cpu usage (cf. panel codes). Panel codes offer a great flexibility in preliminary design stages.

Panel Codes

Panel codes (surface singularity methods) are well established and form an important part of the designer's inventory. These have been developed over the last 25 years and have reached a reasonable level of maturity. Various first and second order codes are available e.g. PMARC, VSAERO, PANAIR and QUADPAN (in USA). Most of these methods produce very similar results for Mach numbers less than about 0.8. Flow compressibility effects are based on the Prandtl-Glauert approximation. The surface of the configuration is overlaid by panels of surface singularities e.g. doublet and sources. A matrix of influence coefficients, relating the effects of each panel on all others is then formed. This matrix is then solved with respect to the boundary conditions and onset flow parameters.

The boundary condition can be set up in different ways. In Neumann or "direct" type formulation, the normal velocity is applied directly, balancing the velocities due to singularities placed on the surface panel network. In the "Dirichlet Potential formulation", the solution assumes zero potential inside a closed body and this implies an "indirect" compliance of zero normal velocity across a surface. The propulsion effects (engine-face, mass flows) are handled with a matrix of source singularity panels.

Once the strengths of the flow singularities are known, velocities, pressures, forces and moments can be calculated. In general, the wake geometries are pre-specified. Some methods allow relaxation of wakes in an iterative manner.

Good descriptions of the underlying principles are given in standard texts (e.g. Katz & Plotkin, "Low Speed Aerodynamics").

Inverse Codes

The inverse approaches can be used with any of the aerodynamic prediction codes. Various methodologies have been pioneered throughout the world e.g. NASA Langley C-DISC. Such codes are usually applied in the final stages to help in fine-tuning and tailoring of flow parameters, e.g. velocities or pressure distributions. We have been developing a research code in-house. As far as the current work programme is concerned, these methods have not needed to be exploited. One would expect their use when more detailed integration aspects are to be dealt with. It is planned, eventually, to publish a paper on the methodology (Ref.20).

Over the years, we have used the design methodology above to aid intake design, evaluation and integration (Refs.21 to 30) on military and civil aircraft. The evaluation / design approach can help in optimising an intake design in a short time-scale. Wind tunnel models of selected designs can then be manufactured for final validation. The evaluation method can be used to define the test series, ensuring that only "areas of interest" (Mach, α, ß, etc.) are tested during limited and expensive tunnel occupancy.

We look next at Sensor-Craft intakes from the point of view of achieving a first-order design intake. The process will in turn highlight problem areas and the need for flow control. It is obviously prudent to begin with isolated intakes. The starting point is cruise geometry with AoA effects. Once a reasonable geometry has been obtained, we can then focus on off-design (e.g. side-slip) and zero speed aspects.

4. INTAKES WITH NEGATIVE SCARF, -30 & -60 deg.

The Sensor-Craft layout indicated a special cross-section for the intake. The top lip width is much lower than that for the lower lip. This led to consideration of a selection of geometries as shown in **Fig.4.1.** The main parameters varied are scarf, lip geometry and contraction ratio (CR).

Emphasis is on flight Mach numbers up to 0.6. The engine face Mach number is varied between 0.2 and 0.6 to simulate an appropriate demand and thus varying the MFR.

Intakes with -30 deg. Scarf

Fig.4.2 refers to the -30° Scarf intake Configuration. A-30. Chordwise distributions of local Mach number and C_P are shown at nine stations along the semi-perimeter. Note that the critical region, as expected, is at the top lip. Also shown are the predicted boundaries (AoA = 0° and 3°.) for the onset of external and internal flow separations at the lip, as the Engine face Mach number varies. This then allows a band of operation to be derived.

Intakes with -60 deg. Scarf Showing Control Over Design Process

Fig.4.3 refers to the -60° Scared intake Configuration. A-60. Chordwise distributions of local Mach number and C_P are shown at nine stations along the semi-perimeter. Note that the critical region, as expected, is at the top lip. This can also be inferred from the plot of peak Mach number (inner and outer surface). Also shown are the predicted boundaries (AoA = 0° and 3°.) for the onset of external and internal flow separations at the lip, as the Engine face Mach number varies. The effect of AoA is slightly adverse. This process in turn allows an estimation of the MFR band of operation as a function of free stream flight Mach number.

Fig.4.4 refers to the -60° Scarfed intake Configuration. B-60. Chordwise distributions of local Mach number and C_P are shown at nine stations along the semi-perimeter. As before, the critical region is at the top lip, confirmed from the plot of peak Mach number (inner and outer surface). Flow separation Boundaries demonstrate control over design process.

Fig.4.5 refers to the -60° Scarfed intake Configuration. C-60. Chordwise distributions of local Mach number and C_P are shown at nine stations along the perimeter. The critical region is at the top lip as also inferred from the plot of peak Mach number (inner and outer surface). Flow separation Boundaries are shown.

5. SINGLE FUSELAGE LAYOUT WITH A CENTRAL INTAKE

Typical geometry of an intake incorporated into a single, central fuselage is shown in **Fig.5.1**. The bottom lip of the intake forms the center section of the dihedral, swept back, front wing. The bottom intake lip, therefore, has an "apex", dihedral and sweep. The top and sides of the intake effectively represent an over-wing intake. Note that at this stage we are mainly interested in the intake flow and the effects of sweep and scarf. The main requirement is to model the intake and the front, centre wing section, as emphasised in **Fig.5.2**. The effects of the wing outboard of the intake need to be assessed in future work.

For M = 0.6 (freestream) and MEF = 0.5 (Engine Face)**,** Chordwise distributions of local Mach number (M_L) and C_P are shown at stations around the semi-perimeter in **Fig.5.2**. The critical region as expected is at the top lip. This can also be inferred from the plot of peak M_L (inner and outer surface), **Fig.5.2**.

Flow separation boundaries are shown in **Fig.5.2** for AoA 0°. At M = 0.4, for example, the engine can operate in the range 0.1 < MEF < 0.5 without either external or internal flow separations occurring at any point around the intake perimeter. However, typical engine idle is MEF 0.3 and so external separation will occur during in-flight shutdown. If the engine flow demands were increased, such that MEF = 0.6 at M = 0.4, internal flow separation would occur.

At zero forward speed (start of Take-off roll), with MEF = 0.5, very high M_L occur on the top, rearmost lip. This area may require some form of variable geometry.

6. TWIN FUSELAGE LAYOUT WITH TWIN INTAKES

Fig.6.1 shows the derived geometry of one of a pair of intakes for the twin fuselage layout. The intake is swept and raked, effective diagonal scarf is equivalent to 64.42 deg. The design Mach number is 0.6 and the engine face MEF is 0.5. An isolated intake is considered here with the most leading corner denoted by A.

For a range of M (0.6, 0.5 & 0.4) and MEF = 0.5 (Engine Face)**,** Chordwise distributions of local Mach number (M_L) and C_P are shown at stations around the perimeter in **Fig.6.2**. The critical region as expected is at the top lip. At "off-design" conditions, e.g. M = 0.4, high suctions arise on the top lip inner surface. Note the easing of C_P and M_L as the design point is reached. At the design condition, M = 0.6, MEF = 0.5, the intake is well behaved, **Figs.6.1**and **6.2**.

The flow separation bands are shown in **Fig.6.1**. These are slightly more limited than those for the single, centerline intake, **Fig.5.2**. For these offset, over-wing intakes, one further complexity is expected to be the presence of spanwise flows and boundary layer growth at the intake locations. This will need to be addressed.

7. SUMMARISING MASS FLOW RATIO CAPABILITY FOR VARIOUS INTAKES

Fig.7.1 shows a first-order summary for 3 types of intakes. Boundaries for internal flow separation at MEF = 0.5 are displayed alongside boundaries for external separation arising at MEF = 0.3 at AoA = 0° and 3°. Such relationships offer the possibility of matching the cruise requirements to the low-speed characteristics. Need for passive or active flow control is highlighted. One option will be incorporating variable lip geometry either with hinges or using smart structures (see Ref.31), applied to intake lips.

It is implied that reasonable intake lip flows will mean less flow distortions at the engine face via a S-shaped diffuser duct. Flow control on that is however another story and internal flow control (active and passive) may well be required.

8. CONCLUDING REMARKS, FUTURE WORK

For reasons of survivability, different intake types and location options are being considered. Future aircraft particularly those that are unmanned will have substantially "widened" flight envelopes (higher "g", α and β over Mach, altitude and CL ranges). Integration of such intakes (usually heavily and negatively scarfed) in flying vehicles and obtaining high efficiency and performance then become very important issues. Flow control needs can be identified.

One of replacement options for the AWACS aircraft, is a remotely-controlled UAV sensor-craft. Such craft take advantage of high aspect ratio (AR) as well as enclosing an antenna in the aircraft diamond planform. Such aircraft carry a large proportion of fuel and "loiter" at high altitudes for a few days in each flight. This implies a wide C_L - altitude capability and need for extreme efficiency.

This report has been concerned with design studies on scarfed intakes that can be integrated with different types of aircraft but more particularly with high AR sensor-craft. Typical options are single or twin layouts. Implications of envisaged flight envelope on Intake design and integration aspects have been mentioned.

An understanding is offered of effects on intake performance, lip flow separation, due to variation of several major geometry and flow parameters.

Although aspects need to be studied in further, several inferences have arisen e.g. the effective contraction ratio needed for cruise and the need to trade-off against low-speed field performance. This process highlights the need for flow control, variable geometry or smart structures applied to intake lips to cope with off-design behaviour. More generally:

- The techniques developed, can be adapted to more complex configurations of intakes and aircraft layouts.
- The technologies mentioned include novel integration concepts (vehicle, intake/engine/nozzle/exhaust) which may need to use improved materials, advanced design methodologies and integrated controls.
- The potential benefits to the military user are considered to be significant and include: reduced life cycle costs, improved operability, improved reliability and maintainability, enhanced performance, enhanced survivability, reduced complexity and weight, and reduced environmental impact.
- Techniques mentioned enable simulation prior to any flight tests, thus implying large savings in costs.

ACKNOWLEDGEMENTS

REFERENCES

1. NANGIA, R.K., "Pilot Document Introducing all Aspects of Work Accomplished under USAF-EOARD Contract SPC-024051", RKN/AERO/REPORT/2004-10 – Part 1, Issue 1, 2004.

2. NANGIA, R.K., "High Aspect Ratio Unconventional Joined-Wing Configurations Incorporating Laminar Flow", RKN/AERO/REPORT/2004-10 – Part 2, Issue 1, 2004.

3. NANGIA, R.K., "Planform Effects on High Aspect Ratio Unconventional Joined-Wing Configurations Incorporating Laminar Flow", RKN/AERO/REPORT/2004-10 – Part 3, Issue 1, 2004.

4. NANGIA, R.K., "High Aspect Ratio Lambda-Wing Configurations Incorporating Laminar Flow", RKN/AERO/REPORT/2004-10 – Part 4, Issue 1, 2004.

5. NANGIA, R.K., "Integration of Over-Surface Scarfed Intakes on Aircraft with High Aspect Ratio Wings (e.g. Sensor-Craft)", RKN/AERO/REPORT/2004-10 – Part 5, Issue 1, 2004. *This Report*.

6. NANGIA, R.K., "Towards Design of Long-Range Supersonic Military Aircraft", RKN/AERO/REPORT/2004-10 – Part 6, Issue 1, 2004.

7. NANGIA, R.K., "Configuration & Aerodynamic Design Studies of Joined-Wing High Aspect Ratio Sensor-Craft Concept", RKN/Aero/Report/2002-10, June 2002, (USAF-EOARD Contract SPC-01-4087).

8. JOHNSON, F. P., "Sensor Craft : Tomorrow's Eyes and Ears of the Warfighter," AIAA-2001-4370, Aug. 2001. *See www.afrlhorizons.com /Briefs/Mar01/SN0001.html*

9. Aerospace America, Dec. 01, pp 50.

10. TYLER, C., SCHWABACHER & CARTER, D., "Comparison of Computational and Experimental Studies for a Joined-Wing Aircraft", AIAA 2002-0702, January 2002.

11. WOLKOVITCH, J., "The Joined Wing: An Overview", J. of Aircraft, Vol 23, pp. 161-178, March 1986.

12. WOLKOVITCH, J., "A Second Look at the Joined Wing", Proc. of NVVL Symposium "Unconventional Aircraft Concepts", Delft Uni. Press, 1987.

13. NANGIA, R.K., PALMER, M.E. & TILMANN, C.P., "Towards Design of Unconventional High Aspect Ratio Joined-Wing Type Aircraft Configurations", RAeS Conference – "A 2020 Vision", April 2002, London UK.

14. NANGIA, R.K., PALMER, M.E. & TILMANN, C.P., "Towards Design & Optimisation of Unconventional High Aspect Ratio Joined-Wing Type Aircraft Configurations", CEAS / RAeS Conference, June 2002, London UK.

15. NANGIA, R.K., PALMER, M.E. & TILMANN, C.P., "On Design of Unconventional High Aspect Ratio Joined-Wing Type Aircraft Configurations", Paper 25R2, ICAS 2002, Toronto, Canada.

16. NANGIA, R.K., PALMER, M.E. & TILMANN, C.P., "Unconventional High Aspect Ratio Joined-Wing Aircraft With Aft- & Forward- Swept Wing-Tips", AIAA -2003, Aerospace Sciences Meeting , Reno, NV, USA.

17. NANGIA, R.K., PALMER, M.E., " Exploiting Unconventional Joined-Wing Concept For Subsonic & Supersonic Aircraft", Paper for RTO-AVT-099, Brussels, April 2003.

18. GOLDSMITH, E.L. & SEDDON. J.E.,, "Practical Intake Aerodynamic Design", Blackwell, 1993.

19. SEDDON, J.E. &. GOLDSMITH, E.L., "Intake Aerodynamics", Blackwell, 1989.

20. NANGIA, R.K., "Development of an Inverse Design Method for 3-D Intakes using 3-D Membrane Analogy", Future Paper.

21. NANGIA, R.K. & PALMER, M.E., "Application of Subsonic First-Order Panel Methods for Prediction of Inlet & Missile Aerodynamics Interactions with Airframe", AGARD, CP-498, Paper 25, 1991.

22. NANGIA, R.K., PALMER, M.E. & HODGES, J., "Flow Separation Prediction on Inlets with Mach & Reynolds Number Effects in Subsonic Flight", ICAS-96-6.10.3, September 1996, Sorrento, Italy.

23. NANGIA, R.K., PALMER, M.E. & MARTIN, P.G., "Flow Separation Prediction on 3-D Inlets with Mach & Reynolds Number Effects in Subsonic Flight", RAeS - IMechE Conference "Engine-Airframe integration", October 1996, Bristol, UK.

24. NANGIA, R.K., PALMER, M.E. & HODGES, J., "Modelling of 3-D Aircraft Inlets at "Zero" Speed (& Low Speeds with Cross-wind) & Flow Separation Prediction", RAeS - IMechE Conference "Verification of Design Methods by Test & Analysis", November 1998, London, UK.

25. NANGIA, R.K., PALMER, M.E. & HODGES, J., "Addressing the 'Zero Speed' & Low-Speed Aspects of 3-D Aircraft Intakes, Modelling With & Without Ground Effect, In Presence of Cross-wind & Lip-flow Separation Prediction", CEAS 7th European Propulsion Forum "Aspects of Engine / Airframe Integration", March 1999, Pau, France.

26. NANGIA, R.K. & PALMER, M.E., "Negatively Scarfed Inlets for Acoustic Reduction, Aerodynamic Performance Assessment", AIAA 2000-0354, January 2000.

27. NANGIA, R.K. & PALMER, M.E., "Inlets with Negative Scarf for Acoustic Reduction, Aerodynamic Performance Assessment at Transonic Speeds", AIAA 2000-4409, August 2000.

28. NANGIA, R.K. & PALMER, M.E., "Application of Negative Scarf to Inlet Design for Acoustic Reduction, Aerodynamic Assessment at Subsonic & Transonic Speeds", ICAS 2000.

29. NANGIA, R.K. & PALMER, M.E., "Inlets with Negative Scarf for Acoustic Reduction, Aerodynamic Performance Assessment at Transonic Speeds", 18th Applied Aerodynamics Meeting, AIAA 2000-4409, August 2000, Colorado, USA.

30. NANGIA, R.K. & PALMER, M.E., "Application of Negative Scarf to Inlet Design for Acoustic Reduction, Aerodynamic Assessment at Subsonic & Transonic Speeds", ICAS 22nd Congress, Harrogate, UK, Aug. 2000.

31. REY, N.M. et al, "Shape Memory Alloy Actuation for Variable Area Fan nozzle", Vol 4332, Proceedings of SPIE, 5-8 March 2001, Newport Beach, USA.

LIST OF SYMBOLS & ABBREVIATIONS

A_C	Intake Highlight Area
A_o	Intake Onset Flow Capture Area
AoA	α, Angle of Attack
AR	Aspect Ratio
b	$= 2 s$, Wing span
c	Local Wing Chord
c_{av}	Wing Mean Chord
C_D	$= D/(q\,S)$, Drag Coefficient
C_L	$= CL = L/(q\,S)$, Lift Coefficient
C_p	Coefficient of Pressure
CR	Contraction Ratio
D	Drag Force
L	Lift Force
LE	Leading Edge
M	Mach Number
MEF	M_E, Mean Mach Number at Engine Face
MFR	Mass Flow Ratio
ML	Local Surface Mach Number
q	$= 0.5\,\rho\,V^2$, Dynamic Pressure
Re	Reynolds Number, based on c_{av}
s	Wing semispan
S	Wing Area
TE	Trailing Edge
V	Velocity
Λ	LE Sweep Angle
η	$= y/s$, Non-dimensional spanwise Distance
ρ	Air Density

FIG. 1.1 OVER-SURFACE INTAKES
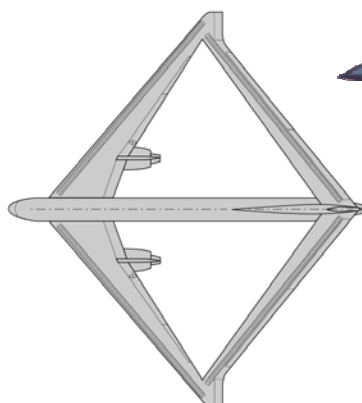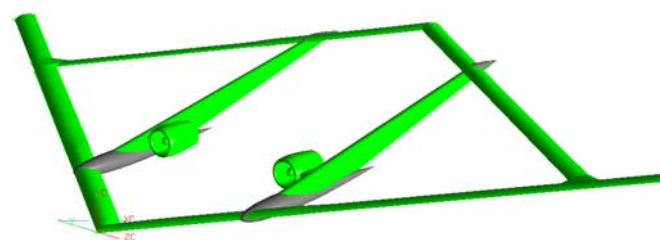
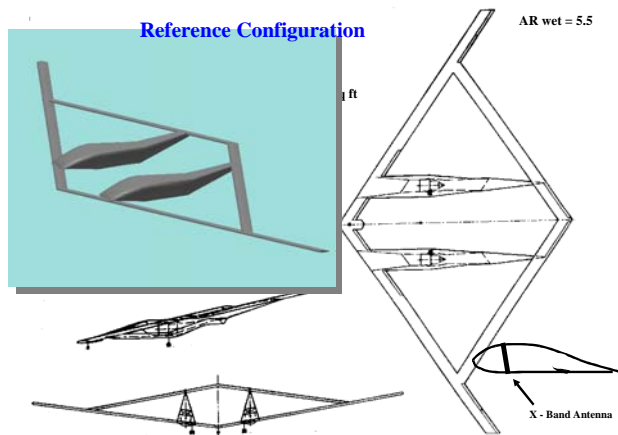

FIG. 1.2 POSSIBLE INTAKE LAYOUTS ON
JOINED WING AIRCRAFT

Reference Configuration

AR wet = 5.5

X - Band Antenna

Mission profile and requirements

Loiter
40-80 hr 65 k ft

W_TO

Loiter
1 hr @ SL

3000 nm   3000 nm

Mission Segments

1. Engine Start & Warm-up
2. Taxi
3. Takeoff
4. Climb & Accelerate to Cruise
5. Cruise out 3000
6. Loiter
7. Return Cruise
8. Descend
9. Loiter at Sea Level
10. Landing, Taxi, Shutdown

Cruise Radius: 3000 nm

Loiter: 65 Kft for 40 - 80 hr (at 3000 nm range)

Payload: 4000 lb Field Length: 5350 ft over 50 ft Obstacle (SLS)

Control: 20 kt cross-wind on takeoff and landing

W/S range of interest: 30 - 60

T/W range of interest: .30 - .50

FIG. 1.3 REFERENCE SENSOR-CRAFT & MISSION

Altitude - ft

Mach 0.6, CL=0.88 Re=0.35mil/ft

CRUISE

Mach 0.6, CL=1.59 Re=0.4 mil/ft

Mach 0.15 CL=0.7 Re=1.1mil/ft

LAND   TAKE-OFF

Mach 0.2 CL=0.95 Re=1.4mil/ft

Weight - lb

CL

TAKE-OFF Re=1.4mil/ft

CRUISE, Re=0.44mil/ft

LANDING Re=1.1mil/ft

CRUISE, Re=0.35mil/ft

Mach no
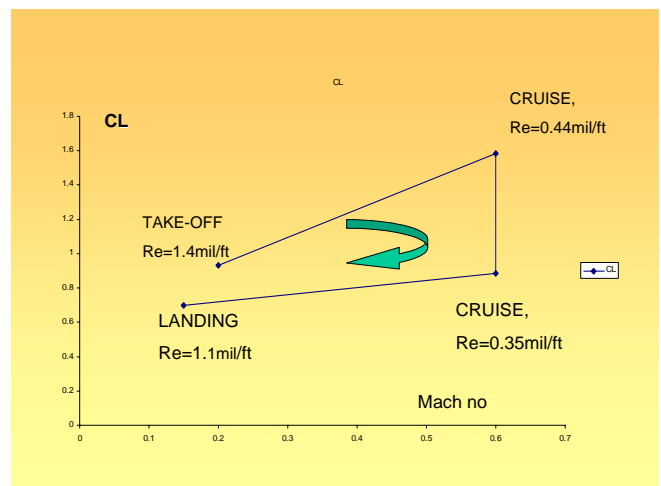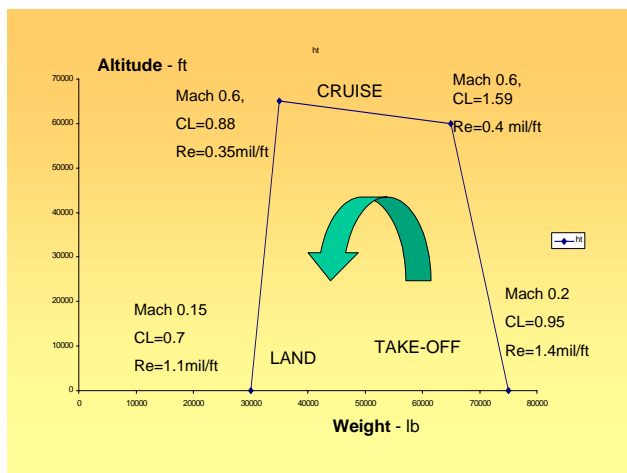
FIG. 1.4 SENSOR-CRAFT , POSSIBLE FLIGHT ENVELOPE

Twin Fuselage intakes

Central Fuselage intake
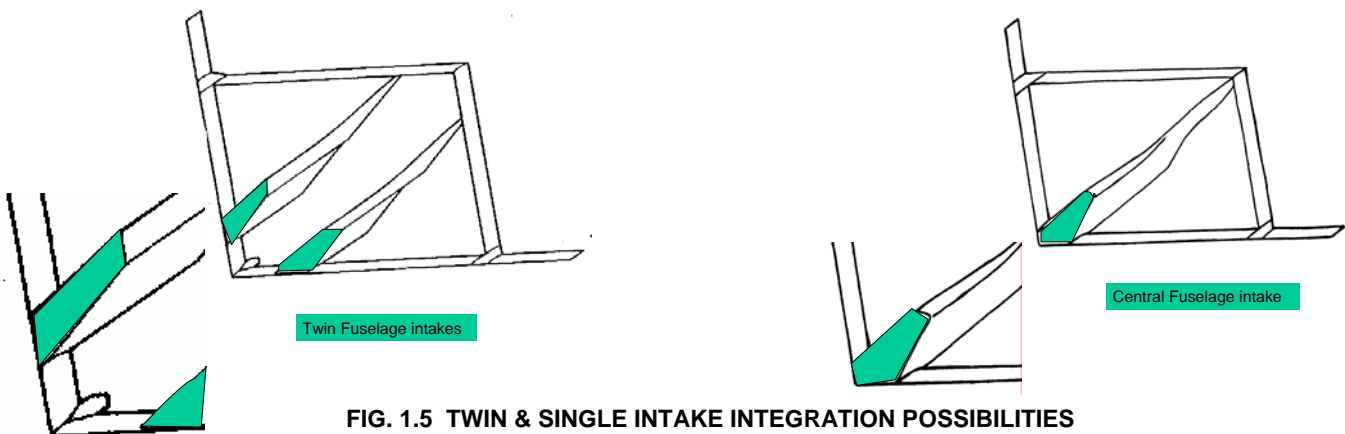
FIG. 1.5 TWIN & SINGLE INTAKE INTEGRATION POSSIBILITIES

Low Speed → Design Process

High Speed

Installed Effects

Ground Effects

Inlet Geometry

M_o, α, Re Capability — NO / YES

M_o, β, Re Capability — NO / YES
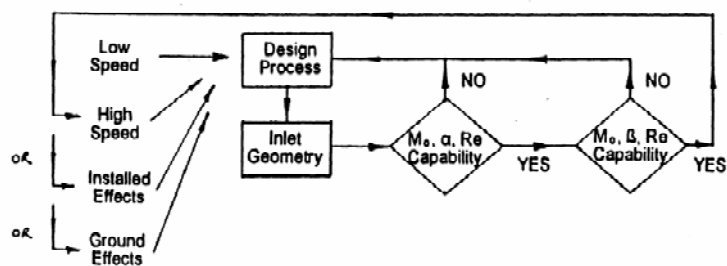
FIG. 2.1 AN ITERATIVE INLET DESIGN PROCESS

COMPLEXITY

Configuration   engine-face   Complexity Level

M, MFR variation

high suction

M, α & MFR

Geometry, M, α, β & MFR

Geometry, Scarf, M, α, β & MFR

forward-swept corner

Geometry, Scarf, Installation M, α, β & MFR
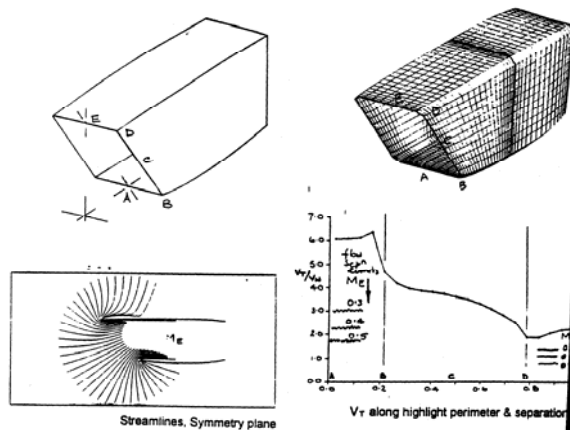
critical area (high suction)

FIG. 3 ORDER OF COMPLEXITY, INLET DESIGN
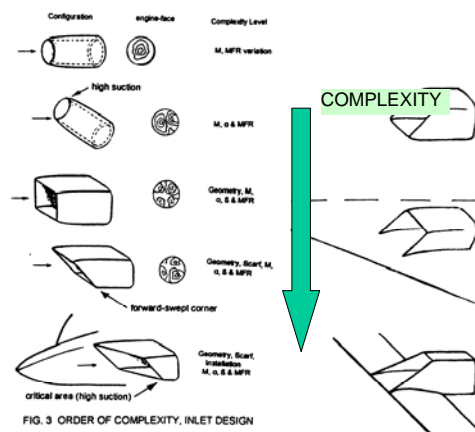
FIG. 2.2 ORDER OF INTAKE DESIGN COMPLEXITY

16

FIG. 2.3 EFFECT OF MFR & AOA, ONSET OF EXTERNAL & INTERNAL LIP FLOW SEPARATION

FIG. 2.4 UNSCARFED, SCARFED & SURVIVABLE TYPE 3-D INTAKES, SKETCHING MFR, AoA & GEOMETRY EFFECTS

Streamlines, Symmetry plane V_T along highlight perimeter & separation

FIG. 2.5 "ZERO-SPEED" EFFECTS ON A SCARFED INTAKE

ISOLATED INTAKES, Different lip shapes

A, 30deg

A, 60deg   B, 60deg   C, 60deg

FIG. 4.1 TYPICAL -30 & -60 deg. SCARFED INTAKES CONSIDERED, DIFFERENT CONTRACTION RATIOS

17

Cp & Mach Chordwise Distbns.   Possible Flow Separation Onset, AoA 0 deg   AoA 3 deg.

FIG. 4.2 -30 deg. SCARF INTAKE
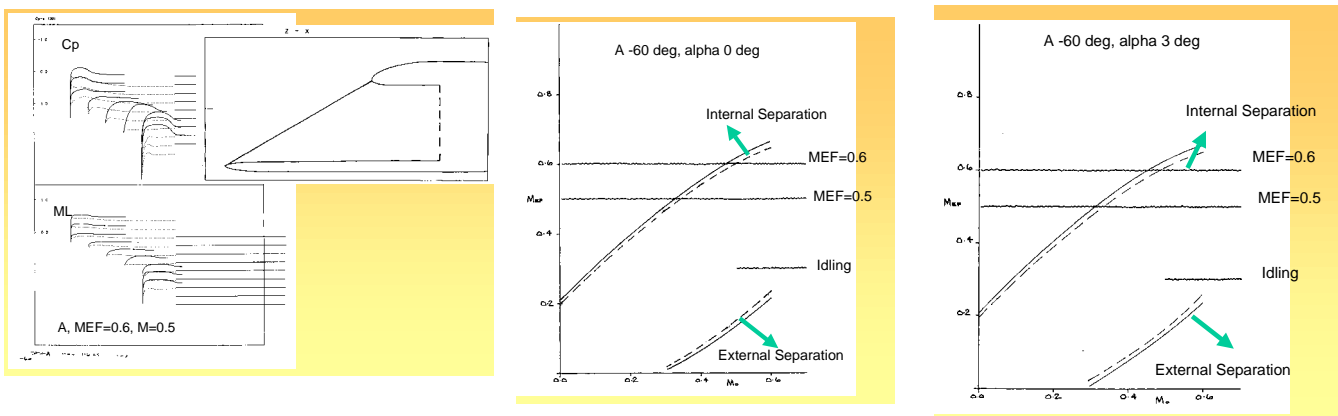
Cp & Mach Chordwise Distbns.   Flow Separation Onset, AoA 0 deg.   AoA 3 deg.
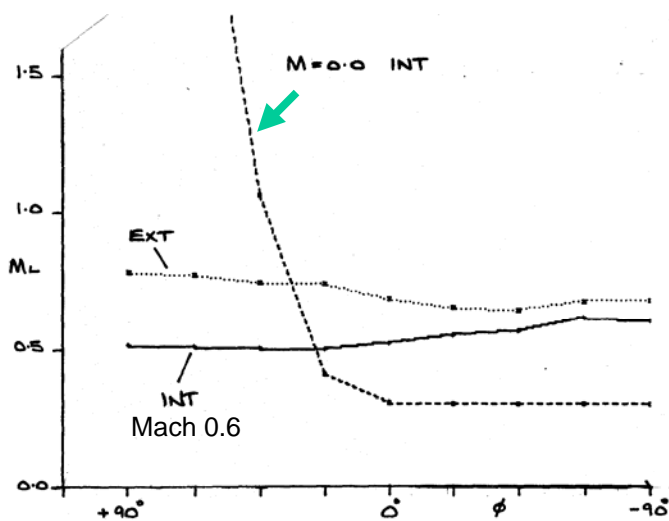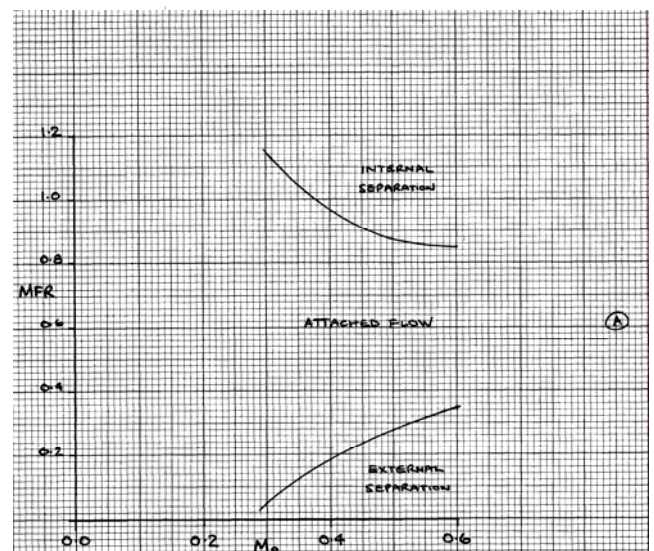
Peak Mach No Variation along Perimeter   MFR & Flight Mach Boundaries

FIG. 4.3 -60 deg. SCARF. INTAKE-A

B, MEF=0.6, M=0.5

Peak Mach no. Variation along Perimeter

C, MEF=0.6, M=0.5
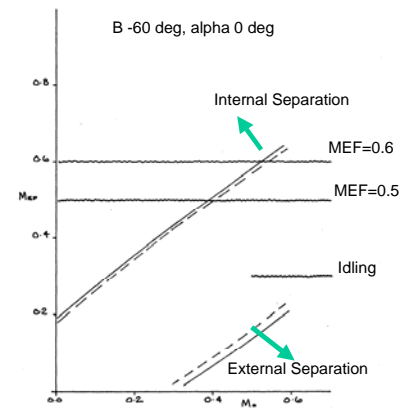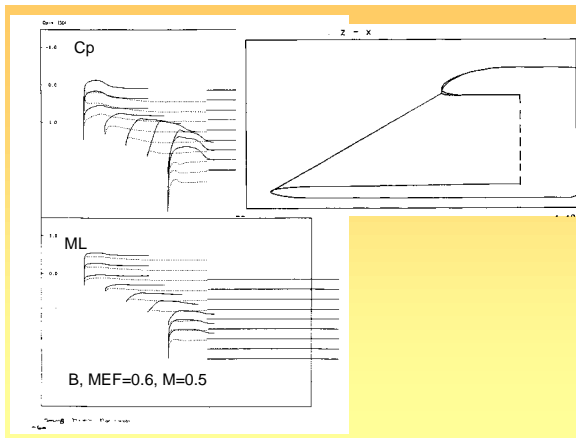
FIG. 4.4 -60 deg. SCARF INTAKE-B
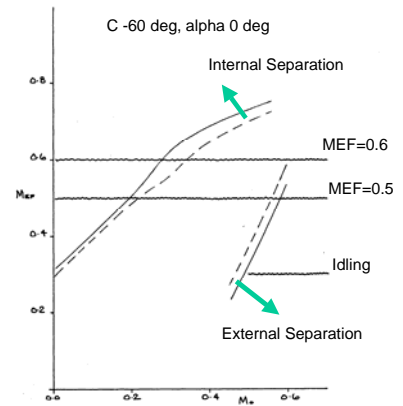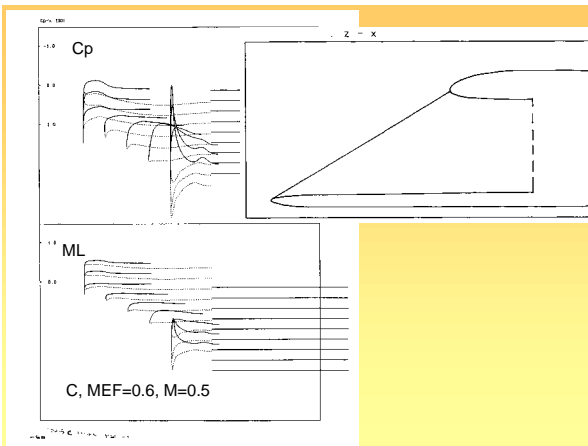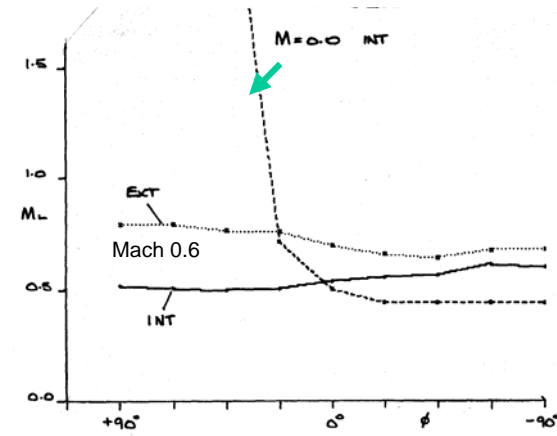
FIG. 4.5 -60 deg. SCARF INTAKE-C
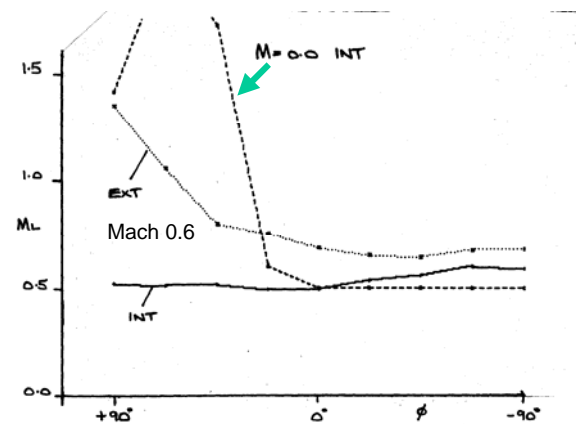
Central Intake Integration
& Modelling
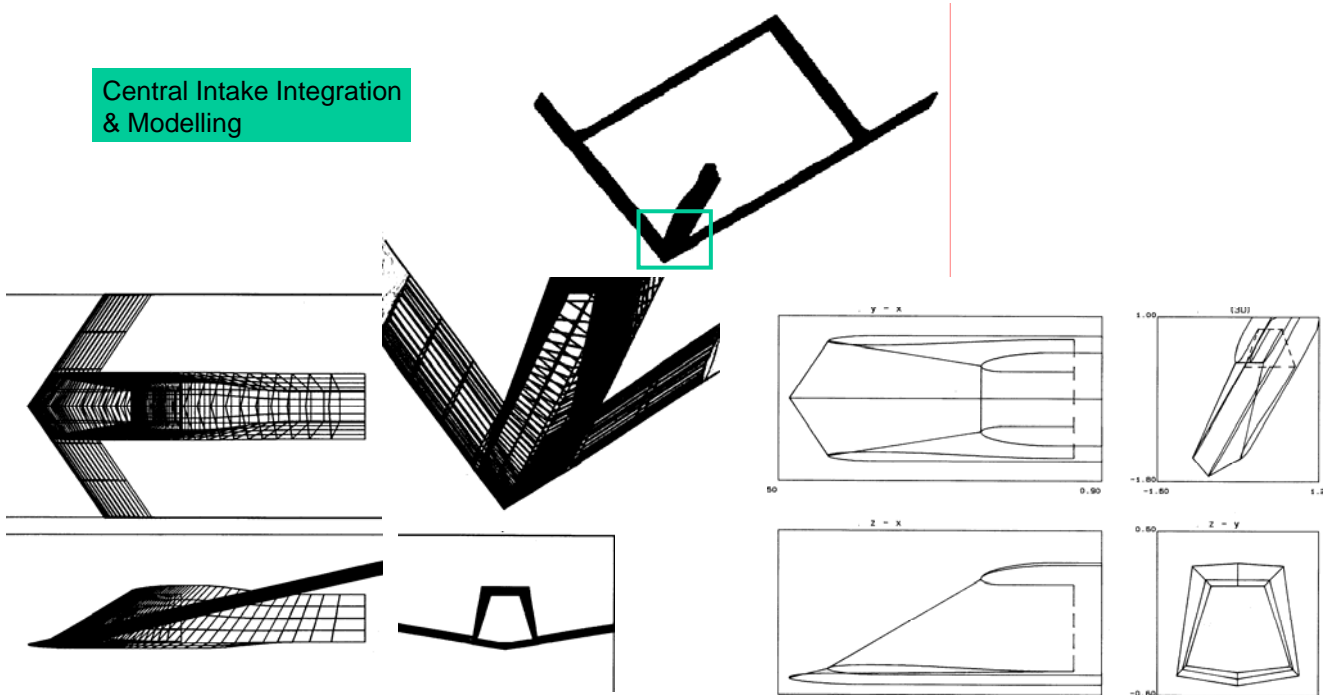
FIG. 5.1 DETAIL OF CENTRAL INTAKE MODELLING

Cp

ML

Central, MEF=0.5, M=0.6
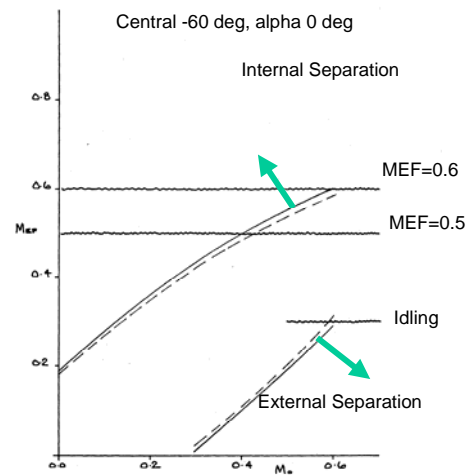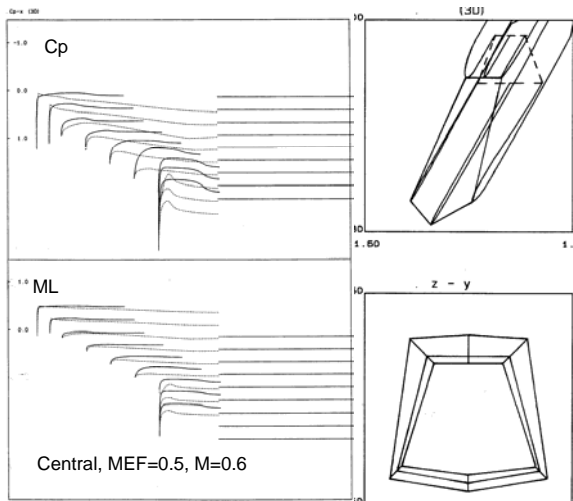
Peak Cp & Mach no. Chordwise Distbns.

Central -60 deg, alpha 0 deg

Internal Separation

MEF=0.6

MEF=0.5

Idling

External Separation

Flow Separation Onset, AOA 0 deg.

M = 0.0   M$_{EF}$ = 0.5

EXT

Mach 0.6

INT

TOP

BOTTOM

+90°   0°   φ   -90°

**FIG. 5.2 CENTRAL INTAKE.
SCARF -60 deg.**

3-D Survivable Intake –64.42 deg, alpha 0 deg

Peak ML - phi

M = 0.0 int

ext

M = 0.6

int

+90	+45		−45	−90	−135		−225	−270
TOP			BOTTOM				TOP	
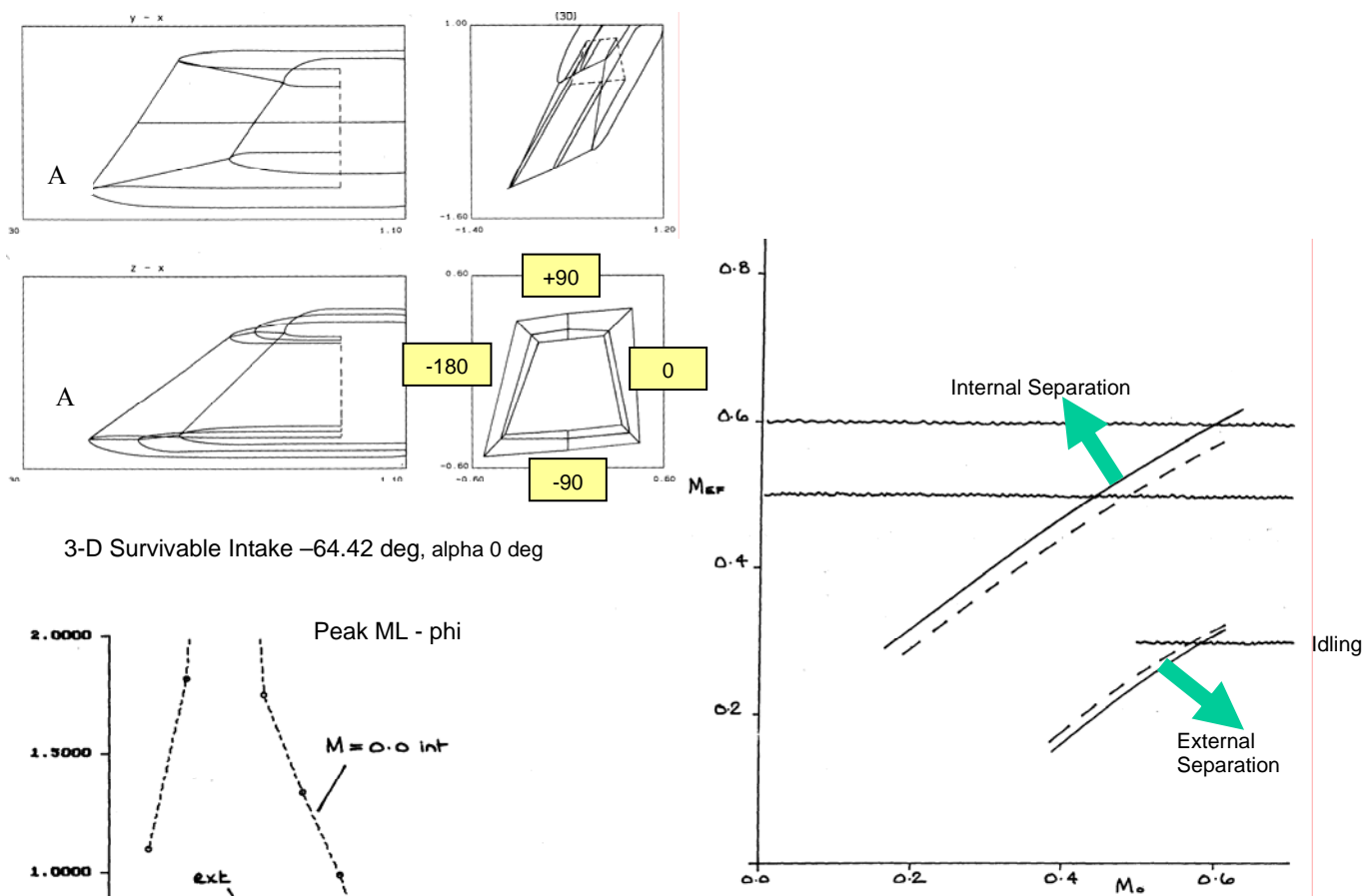
FIG. 6.1 TWIN INTAKE. SCARF -64.42 deg., DESIGNED FOR M=0.6, MEF=0.5

Internal Separation

Idling

External Separation

Cp Distbn

ML Distbn
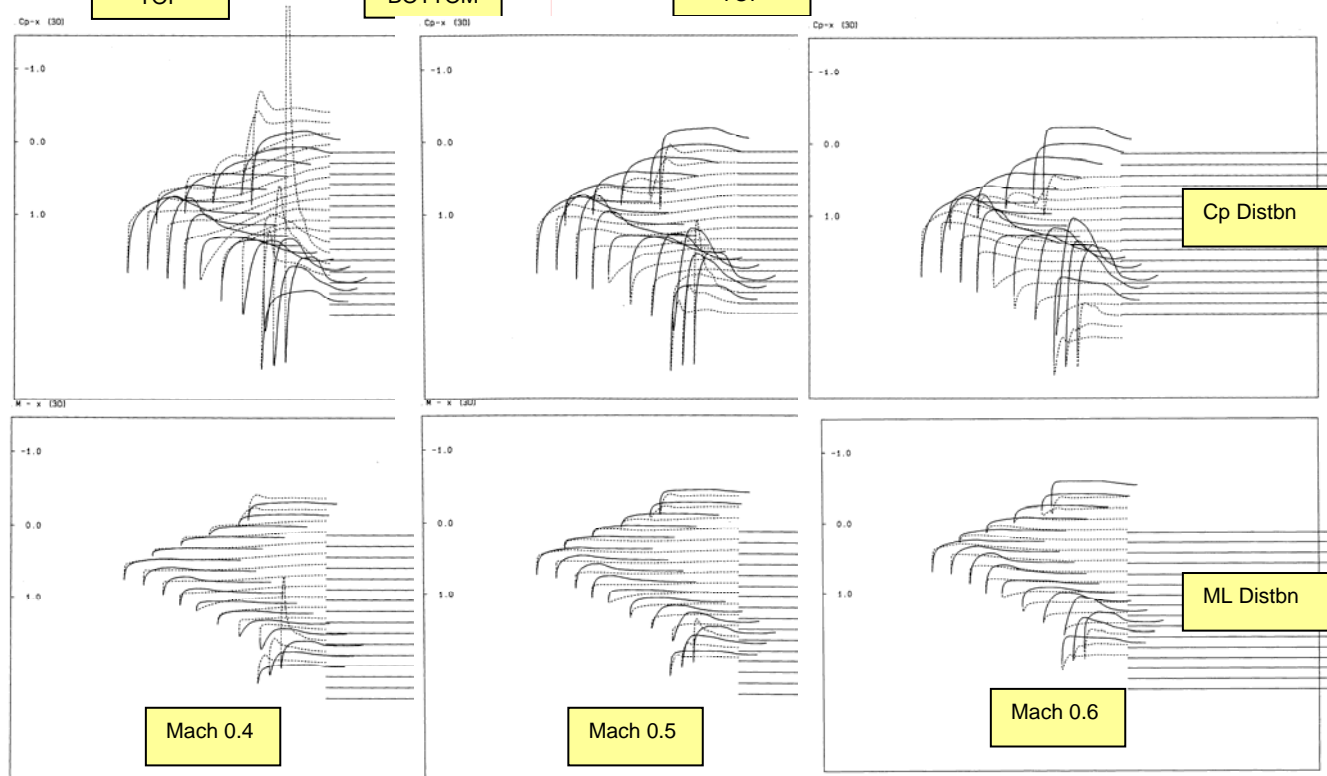
Mach 0.4

Mach 0.5

Mach 0.6

FIG. 6.2 TWIN INTAKE. SCARF -64.42 deg. "OFF-DESIGN" & DESIGN CASES
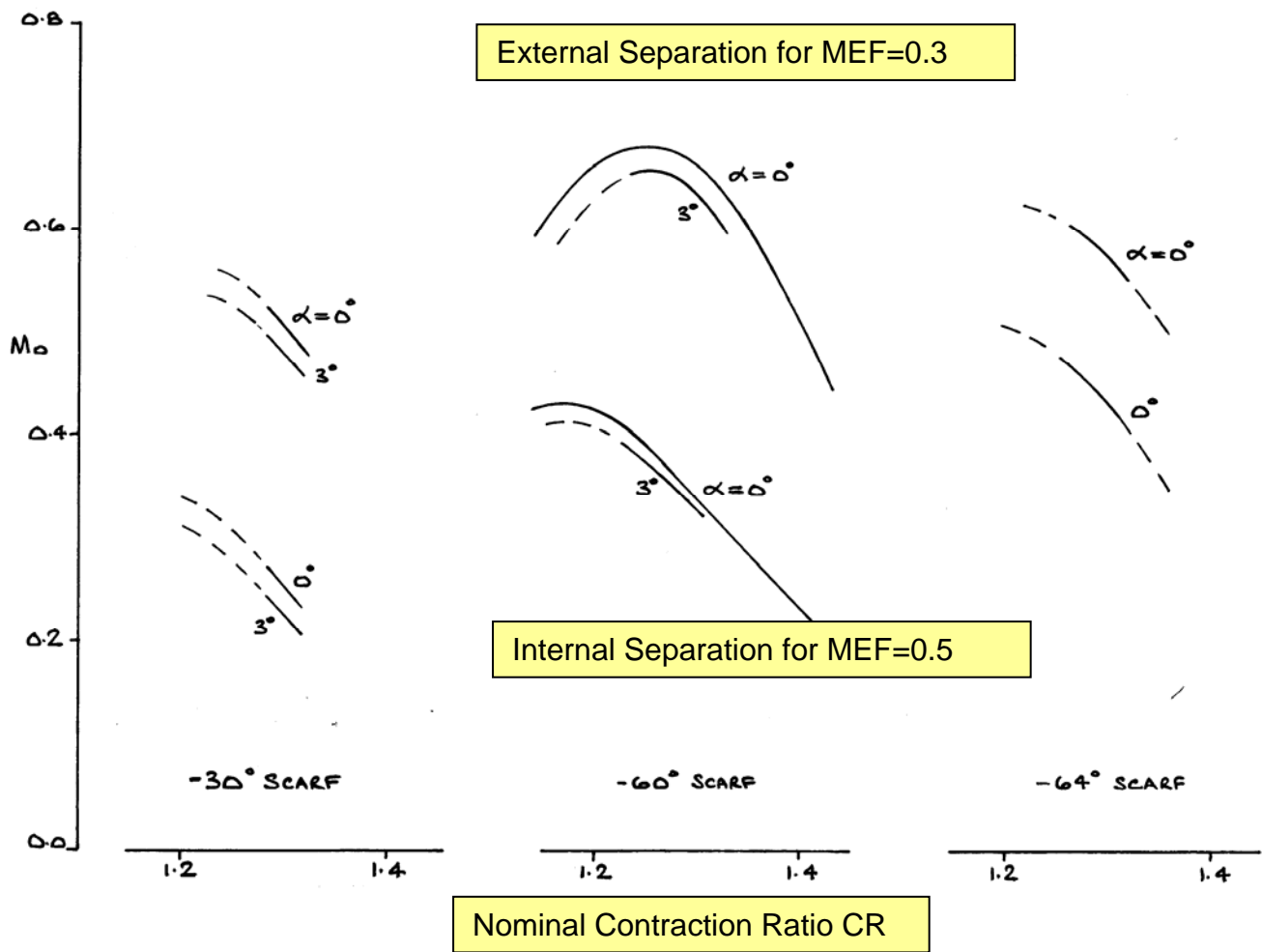M = 0.4, 0.5 & 0.6, MEF = 0.5

21

FIG. 7.1 SUMMARISING FLIGHT MACH NO CAPABILITY AGAINST
CONTRACTION RATIO, FOR DIFFERENT INTAKES